

VOLUME 79

Time
JULY 17, 1975

NUMBER 15

JPCHAX

THE JOURNAL OF

PHYSICAL

CHEMISTRY

PUBLISHED BIWEEKLY BY THE AMERICAN CHEMICAL SOCIETY

THE JOURNAL OF PHYSICAL CHEMISTRY

BRYCE CRAWFORD, Jr., *Editor*
STEPHEN PRAGER, *Associate Editor*
ROBERT W. CARR, Jr., **FREDERIC A. VAN-CATLEDGE**, *Assistant Editors*

EDITORIAL BOARD: C. A. ANGELL (1973-1977), F. C. ANSON (1974-1978), V. A. BLOOMFIELD (1974-1978), J. R. BOLTON (1971-1975), L. M. DORFMAN (1974-1978), H. L. FRIEDMAN (1975-1979), E. J. HART (1975-1979), W. J. KAUZMANN (1974-1978), R. L. KAY (1972-1976), D. W. McCLURE (1974-1978), R. M. NOYES (1973-1977), J. A. POPLE (1971-1975), B. S. RABINOVITCH (1971-1975), S. A. RICE (1969-1975), F. S. ROWLAND (1973-1977), R. L. SCOTT (1973-1977), A. SILBERBERG (1971-1975), J. B. STOTHERS (1974-1978), W. A. ZISMAN (1972-1976)

AMERICAN CHEMICAL SOCIETY, 1155 Sixteenth St., N.W., Washington, D.C. 20036

Books and Journals Division

D. H. MICHAEL BOWEN *Director*

CHARLES R. BERTSCH *Head, Editorial Processing Department*
BACIL GUILEY *Head, Graphics and Production Department*
SELDON W. TERRANT *Head, Research and Development Department*

©Copyright, 1975, by the American Chemical Society. Published biweekly by the American Chemical Society at 20th and Northampton Sts., Easton, Pa. 18042. Second-class postage paid at Washington, D.C., and at additional mailing offices.

All manuscripts should be sent to *The Journal of Physical Chemistry*, Department of Chemistry, University of Minnesota, Minneapolis, Minn. 55455.

Additions and Corrections are published once yearly in the final issue. See Volume 78, Number 26 for the proper form.

Extensive or unusual alterations in an article after it has been set in type are made at the author's expense, and it is understood that by requesting such alterations the author agrees to defray the cost thereof.

The American Chemical Society and the Editor of *The Journal of Physical Chemistry* assume no responsibility for the statements and opinions advanced by contributors.

Correspondence regarding accepted copy, proofs, and reprints should be directed to Editorial Processing Department, American Chemical Society, 20th and Northampton Sts., Easton, Pa. 18042. Department Head: CHARLES R. BERTSCH. Associate Department Head: MARIANNE C. BROGAN. Assistant Editors: CELIA B. McFARLAND, JOSEPH E. YURVATI.

Advertising Office: Centcom, Ltd., 50 W. State St., Westport, Conn. 06880.

Business and Subscription Information

Send all new and renewal subscriptions *with payment* to: Office of the Controller, 1155 16th Street, N.W., Washington, D.C. 20036. Subscriptions should be renewed promptly to avoid a break in your series. All correspondence and telephone calls regarding

changes of address, claims for missing issues, subscription service, the status of records, and accounts should be directed to Manager, Membership and Subscription Services, American Chemical Society, P.O. Box 3337, Columbus, Ohio 43210. Telephone (614) 421-7230. For microfiche service, contact ACS Microfiche Service, 1155 16th St. N.W., Washington, D.C. 20036. Telephone (202) 872-4444.

On changes of address, include both old and new addresses with ZIP code numbers, accompanied by mailing label from a recent issue. Allow four weeks for change to become effective.

Claims for missing numbers will not be allowed (1) if loss was due to failure of notice of change in address to be received before the date specified, (2) if received more than sixty days from date of issue plus time normally required for postal delivery of journal and claim, or (3) if the reason for the claim is "issue missing from files."

Subscription rates (hard copy or microfiche) in 1975: \$20.00 for 1 year to ACS members; \$80.00 to nonmembers. Extra postage \$4.50 in Canada and PUAS, \$5.00 other foreign. Supplementary material (on microfiche only) available on subscription basis, 1975 rates: \$15.00 in U.S., \$19.00 in Canada and PUAS, \$20.00 elsewhere. All microfiche airmailed to non-U.S. addresses; air freight rates for hard-copy subscriptions available on request.

Single copies for current year: \$4.00. Rates for back issues from Volume 56 to date are available from the Special Issues Sales Department, 1155 Sixteenth St., N.W., Washington, D.C. 20036.

Subscriptions to this and the other ACS periodical publications are available on microfilm. For information on microfilm write Special Issues Sales Department at the address above.

THE JOURNAL OF PHYSICAL CHEMISTRY

Volume 79, Number 15 July 17, 1975

JPCA 79(15) 1483-1624 (1975)

ISSN 0022-3654

Self-Exchange of Carbon Monoxide behind Reflected Shock Waves A. F. Bopp, R. D. Kern, Jr.,* and B. V. O'Grady	1483 ■
Dissociation of Molecular Hydrogen in Gas Discharges of Moderate Pressure. The Role of Vibro-Rotational Excitation Pio Capezzuto, Francesco Cramarossa,* Riccardo d'Agostino, and Ettore Molinari	1487
Primary Steps in the Reactions of Organic Disulfides with Hydroxyl Radicals in Aqueous Solution M. Bonifačić, K. Schäfer, H. Möckel, and K.-D. Asmus*	1496
One-Electron Transfer Equilibria and Redox Potentials of Radicals Studied by Pulse Radiolysis Dan Meisel* and Gideon Czapski	1503
Ionic Aggregation of the Solvated Electron with Lithium Cation in Tetrahydrofuran Solution Bradley Bockrath and Leon M. Dorfman*	1509
Electron Scavenging and Trapping in γ -Irradiated Organic Glasses T. Ito, K. Fueki,* and Z. Kuri	1513
γ Radiolysis of Isobutyrate Salts R. S. Marshall, B. M. Tolbert, and W. C. Gottschall, Jr.*	1517
Triboluminescence and Associated Decomposition of Solid Methanol Graham J. Trout, Douglas E. Moore,* and John G. Hawke	1519
Aqueous Solutions of Azoniaspiroalkane Halides. I. Enthalpies of Solution, Dilution, and Transfer David P. Wilson and Wen-Yang Wen*	1527
Heats of Mixing Aqueous Electrolytes. XII. The Reciprocal Salt Pair Na^+ , Li^+ Cl^- , SO_4^{2-} R. H. Wood,* Danne E. Smith, H. K. W. Chen, and P. T. Thompson	1532
Heats of Mixing Aqueous Electrolytes. XIII. The Reciprocal Salt Pair Na^+ , Mg^{2+} Cl^- , SO_4^{2-} R. F. Srna and R. H. Wood*	1535
Heats of Mixing Aqueous Electrolytes. XIV. Charge-Asymmetric Mixtures of Three Salts at Constant Equivalent per Kilogram. Lithium Chloride-Sodium Chloride-Magnesium Chloride R. H. Wood* and M. V. Falcone	1540 ■
Thermal Pressure Coefficient and Internal Pressure of 2,2-Dimethylpropane George A. Few and Maurice Rigby*	1543
Thermochemical Isotope Effects. III. Hydrogen-Deuterium Exchange between Methanol and Water at 25° Gary L. Bertrand* and Thomas E. Burchfield	1547 ■
Thermodynamics of Ion-Exchange Equilibria in Mixed Solvents Adel M. El-Prince* and Kenneth L. Babcock	1550
Self-Association in Lactams as a Function of the Ring Size G. Montaudo, S. Caccamese,* and A. Recca	1554
Optical Probes in Polyelectrolyte Studies. I. Acid-Base Equilibria of Dansylated Copolymers of Maleic Anhydride and Alkyl Vinyl Ethers Ulrich P. Strauss* and Gorazd Vesnaver	1558
Foaminess of Binary and Ternary Solutions Sydney Ross* and Gary Nishioka	1561
Physical Studies of Homologous <i>trans</i> -4-Ethoxy-4'- <i>n</i> -alkanoyloxyazobenzenes. Calorimetry Craig L. Hillemann, Gerald R. Van Hecke,* S. Robert Peak, John B. Winther, Martin A. Rudat, David A. Kalman, and Martha L. White	1566

Isocyanate Formation from Adsorbed Carbon Monoxide and Ammonia or Hydrazine on Vanadium, Iron, and Nickel	R. W. Sheets and G. Blyholder*	1572
Relation between Amounts of Chemisorbed Water and Carbon Dioxide on Zinc Oxide	Tetsuo Morimoto* and Kunimitsu Morishige	1573
Zeolite Crystallization Kinetics Related to Dissolution Rates of Quartz Reactant	R. A. Cournoyer, W. L. Kranich, and L. B. Sand*	1578
Oxygen Exchange between C ¹⁸ O ₂ and "Acidic" Oxide and Zeolite Catalysts	J. B. Peri	1582
Investigations on the Growth of the Zeolite Type NaY	Hartmut Kacirek and Hans Lechert*	1589
Crystallographic Evidence for Hydrolysis in Zeolites. The Structure of Hydrated Partially Cobalt(II)-Exchanged Zeolite A	Paul E. Riley and Karl Seff*	1594 ■
The Insignificance of Second Coordination Sphere Interactions in Cobalt-59 Nuclear Magnetic Resonance Relaxation	K. L. Craighead and R. G. Bryant*	1602
Conductance of the Alkali Halides. XIII. Cesium Bromide, Lithium-7 Chloride, and Lithium-7 Iodide in Dioxane-Water Mixtures at 25°	Charles F. Mattina and Raymond M. Fuoss*	1604 ■
Electrical Conductivity of the Molten Bismuth Chloride-Aluminum Chloride, Tellurium Chloride-Aluminum Chloride, and Potassium Chloride-Tellurium Chloride Systems	Finn W. Poulsen and Niels J. Bjerrum*	1610
Temperature Dependence of the Diffusion Coefficient of ¹⁴ CO ₂ in Dilute HCl	J. G. Hawke* and I. White	1614
Photodissociation of Ketene at 313 nm	Vaclav Zabransky and Robert W. Carr, Jr.*	1618

COMMUNICATIONS TO THE EDITOR

Influence of Lower Alcohols on the Pfeiffer Effect of Tris(1,10-phenanthroline)zinc(II) Sulfate-Cinchonine Hydrochloride and <i>l</i> -Strychnine Hydrosulfate Systems in Water	Katsuhiko Miyoshi, Koro Sakata, and Hayami Yoneda*	1622
---	--	------

■ Supplementary and/or miniprint material for this paper is available separately, in photocopy or microfiche form. Ordering information is given in the paper.

* In papers with more than one author, the asterisk indicates the name of the author to whom inquiries about the paper should be addressed.

AUTHOR INDEX

Asmus, K.-D., 1496	Falcone, M. V., 1540	Möckel, H., 1496	Seff, K., 1594
Babcock, K. L., 1550	Few, G. A., 1543	Molinari, E., 1487	Sheets, R. W., 1572
Bertrand, G. L., 1547	Fueki, K., 1513	Montaudo, G., 1554	Smith, D. E., 1532
Bjerrum, N. J., 1610	Fuoss, R. M., 1604	Moore, D. E., 1519	Srna, R. F., 1535
Blyholder, G., 1572	Gottschall, W. C., Jr., 1517	Morimoto, T., 1573	Strauss, U. P., 1558
Bockrath, B., 1509	Hawke, J. G., 1519, 1614	Morishige, K., 1573	Thompson, P. T., 1532
Bonifačić, M., 1496	Hillemann, C. L., 1566	Nishioka, G., 1561	Tolbert, B. M., 1517
Bopp, A. F., 1483	Ito, T., 1513	O'Grady, B. V., 1483	Trout, G. J., 1519
Bryant, R. G., 1602	Kacirek, H., 1589	Peak, S. R., 1566	Van Hecke, G. R., 1566
Burchfield, T. E., 1547	Kalman, D. A., 1566	Peri, J. B., 1582	Vesnaver, G., 1558
Caccamese, S., 1554	Kern, R. D., Jr., 1483	Poulsen, F. W., 1610	Wen, W.-Y., 1527
Capezzuto, P., 1487	Kranich, W. L., 1578	Recca, A., 1554	White, I., 1614
Carr, R. W., Jr., 1618	Kuri, Z., 1513	Rigby, M., 1543	White, M. L., 1566
Chen, H. K. W., 1532	Lechert, H., 1589	Riley, P. E., 1594	Wilson, D. P., 1527
Cournoyer, R. A., 1578	Marshall, R. S., 1517	Ross, S., 1561	Winther, J. B., 1566
Craighead, K. L., 1602	Mattina, C. F., 1604	Rudat, M. A., 1566	Wood, R. H., 1532, 1535, 1540
Cramarossa, F., 1487	Meisel, D., 1503	Sakata, K., 1622	Yoneda, H., 1622
Czapski, G., 1503	Miyoshi, K., 1622	Sand, L. B., 1578	Zabransky, V., 1618
d'Agostino, R., 1487		Schäfer, K., 1496	
Dorfman, L. M., 1509			
El-Prince, A. M., 1550			

THE JOURNAL OF PHYSICAL CHEMISTRY

Registered in U. S. Patent Office © Copyright, 1975, by the American Chemical Society

VOLUME 79, NUMBER 15 JULY 17, 1975

Self-Exchange of Carbon Monoxide behind Reflected Shock Waves^{1a,b}

A. F. Bopp, R. D. Kern, Jr.,* and B. V. O'Grady

Department of Chemistry, University of New Orleans,^{1c} New Orleans, Louisiana 72122 (Received January 20, 1975)

Publication costs assisted by the National Science Foundation

The exchange reaction, $^{13}\text{C}^{16}\text{O} + ^{12}\text{C}^{18}\text{O} \rightleftharpoons ^{13}\text{C}^{18}\text{O} + ^{12}\text{C}^{16}\text{O}$ (k_1, k_{-1}), was investigated in order to assess the importance of reactant vibrational excitation and its effect upon the isotopic switching rate. A shock tube equipped to record infrared emission was used to select two reaction environments; one in which the vibrational equilibration of CO was established in a very short time after shock arrival (8% CO, 11% H₂, 80% Ne, 1% Ar) and one in which equilibration was about six times slower (8% CO, 20% Kr, 72% Ar). The rate of exchange was studied with a shock tube connected to a time-of-flight mass spectrometer over the temperature range 2900–4650 K. The time dependence for product formation was observed to be linear and there was no discernible difference in the exchange rate constants from either mixture. The rate constants from this work were combined with the tabular data of Lifshitz reported in a previous single pulse shock tube study which employed an argon diluent over the temperature range of 2000–2650 K. The results are represented by one Arrhenius line from 2000 to 4650 K; namely $k_b = 10^{12.58 \pm 0.07} \exp(-55,470 \pm 980/RT)$ cm³ mol⁻¹ sec⁻¹. The observation times spanned by the shock tube experiments were all in the region where vibrational equilibration was attained prior to the production of measurable amounts of exchange products. It was necessary to assume that the rate constants obtained from the Kr–Ar mixture could be extrapolated along the combined Arrhenius line to lower temperatures (~2100 K) in order to propose that the rate of self-exchange is not solely dependent upon the vibrational energy content of the reactants. However, this indirect conclusion is supported directly by experiments which utilized mercury photosensitization to populate $v = 2-9$ levels in carbon monoxide and which failed to induce exchange in a $^{12}\text{C}^{18}\text{O}$, $^{13}\text{C}^{16}\text{O}$, Kr, Ar mixture at room temperature.

Introduction

Shock tube investigations of the exchange of a variety of diatomic and small polyatomic molecules with themselves and with deuterium have yielded kinetic results which have posed a stiff challenge with regard to the formulation of acceptable mechanisms. A large number of these experiments have been performed by Professor Bauer and his colleagues utilizing the single pulse shock tube technique (SPST).² In all of their reports they have rejected the single-step, four-center exchange intermediate and the atomic mechanism for the good reason that their experimental rate laws contained order dependencies and activation energies which were not consistent with the predictions of either the bimolecular or atomic mechanism. They proposed the vibrational excitation mechanism (VEX) which states that the exchange takes place exclusively by collisions of molecules

in a critical vibrational energy manifold with molecules containing lesser amounts of vibrational energy.

The reservoir of information concerning high-temperature gas-phase exchange reactions was increased by workers employing dynamic sampling techniques which revealed the nonlinear time dependence associated with product formation in several exchange systems. In some of these reports ($\text{C}_2\text{H}_2 + \text{C}_2\text{D}_2$,³ $\text{CD}_4 + \text{HCl}$,⁴ and $\text{HBr} + \text{D}_2$)⁵ arguments were made for an atomic mechanism. However, in a key reaction, $\text{H}_2 + \text{D}_2$, the dynamic results⁶ were shown to be consistent with the rate law developed by SPST⁷ when the SPST data were corrected for a quadratic time dependence with respect to HD production.

All but one of the small molecules studied have extremely short vibrational relaxation times when compared to typical exchange reaction times. The exception is carbon

monoxide whose vibrational relaxation time may be appreciably varied by the choice of inert gas diluent⁸ and it was the intent of this investigation to record the rate of self-exchange in reaction environments which were significantly different with regard to the vibrational energy content of the reactant molecules. Also of interest was the comparison of the results herein with those obtained in a previous SPST report in which all of the runs were performed in an argon diluent.⁹

There have been few attempts to experimentally show that molecules which are vibrationally excited but translationally cold will participate in the exchange process. Bauer using laser excitation obtained questionable evidence for the contribution of excited H₂ to the H₂, D₂ exchange. The extent of reaction taking place on the surface was considerable.¹⁰ In a more complex system the reaction of CH₂N₂ with HCl was used to produce chemically activated CH₃Cl which in turn exchanged with D₂.¹¹

Polanyi has shown that CO may be readily excited to the $\nu = 2-9$ vibrational levels by mercury photosensitization.¹² Lifshitz has suggested that in the ¹³C¹⁶O, ¹²C¹⁸O system exchange occurs via CO excited to the $\nu = 7-9$ levels.⁹ In the present work an attempt was made to promote exchange in the carbon monoxide system at room temperature by photolyzing ¹²C¹⁸O, ¹³C¹⁶O mixtures saturated with mercury vapor with radiation from low-pressure mercury lamps.

Experimental Section

The complementary shock tube facility used in this work has been described previously.¹³ Recent improvements include the replacement of the oscillographic raster display upon which was recorded the signals from the four velocity gauges with a set of three 10-MHz digital counters which are controlled by signals from a gating circuit. A fourth 10-MHz counter is triggered on and off by the signal from the velocity gauge located closest to the time-of-flight mass spectrometer (TOF) inlet nozzle and the signal generated by the triggering of the first mass spectral recording oscilloscope. Knowledge of this interval greatly improves the determination of time zero for the reaction.

To study the vibrational relaxation, a number of gases were purified and tested. Matheson CP carbon monoxide (99.5%) was treated by flowing the gas through a liquid nitrogen trap in order to remove any condensable impurities. Linde hydrogen, argon, and helium (99.5%), Matheson Research Grade krypton (99.995%), and Matheson Research Grade Ne-1% Ar mixture were used without further purification. For the exchange work, isotopic carbon monoxide, ¹²C¹⁸O (100 ml) and ¹³C¹⁶O (250 ml), were obtained from Stohler Isotopic Chemicals and were analyzed on the TOF. From mass spectral peak heights, the composition of each of these gases was determined: (1) ¹²C¹⁸O: 12.4% CO(28), 0.7% CO(29), 86.0% CO(30), 1.0% CO(31), and (2) ¹³C¹⁶O: 1.0% CO(28), 94.0% CO(29), 4.6% CO(30), and 0.4% CO(31). These gases were used without further purification because of the aforementioned sample sizes.

Mixtures were prepared by flowing the gas into 5-l. (2 l. for the exchange experiments) Pyrex storage bulbs to a predetermined pressure. After each component was added, the entire gas handling system was heated under vacuum prior to the introduction of the next constituent. The reactant gas pressures were measured with a Wallace-Tiernan 0-10 in. water differential pressure gauge while the diluent pressure was read from a 0-400 in. water differential gauge. All mixtures were allowed to mix for at least 16 hr.

TABLE I: CO Relaxation Mixtures

Mixture	Percentage composition					
	CO	H ₂	He	Ne	Ar	Kr
R1	6				94	
R2	6	3			91	
R3	8	11		80	1	
R4	8				72	20
R5	8		34	58	1	

The compositions of the mixtures for the relaxation experiments are listed in Table I. The variance of the average molecular weight of the mixtures was limited by the excessive driver pressures required to attain high temperatures with low molecular diluents and by TOF multiplier saturation experienced with diluents composed mainly of krypton and argon.

Two mixtures were used to study the exchange rate and were composed of the diluents for R3 and R4. The percent composition for each of the exchange mixture were as follows: E1 8.02 CO (0.55, 3.70, 3.71, 0.06), 11.24 H₂, 0.83 Ar, and 79.91 Ne; E2 8.01 CO (0.55, 3.69, 3.71, 0.06), 20.18 Kr, and 71.79 Ar. The numbers in parentheses refer to the individual CO isotopes, listed in order of increasing m/e , from 28 to 31. Prior to shocking these samples, a complete mass spectrum was taken of each mixture and each was found to have an impurity level below background. Before every experiment, the oxygen content of the test gas was compared to background. Runs in which the oxygen level was greater than 30 ppm were not used. Hydrogen was employed as the driver in all experiments.

The infrared emission of CO passing through a slit set at 0.5 mm and an interference filter (Infrared Industries, centered at 5.05 μ with ± 0.10 - μ bandpass at half-peak height) was monitored behind reflected shock waves by a Texas Instruments liquid nitrogen cooled indium antimonide detector. The detector output was amplified (Control and Computing Devices, Model LAB-25) and then fed to a Tektronix 531A oscilloscope for photographic record and also to two Biomation 610B transient recorders which were triggered in parallel. One recorder was set to sample at 0.2- μ sec intervals allowing an accurate determination of shock wave arrival while the other recorder setting was varied from 0.5 to 2 μ sec in order to record most efficiently the growth of the infrared emission signal at a particular temperature. The detector signal was digitized by the recorders and output via a Pivan Data Systems Model B103 interface to a 33 ASR Teletype equipped with a paper tape punch. The paper tape records were read and stored on the computing facility, DecSystem 10, for reduction at a more convenient time.

Four oscilloscopes displayed the mass spectra for photographic record at TOF sampling intervals of 20, 25, or 30 μ sec in order to maximize the number of spectra available during the course of the reaction. Experiments with temperatures as low as 2000 K were performed but product formation was not detectable until temperatures exceeded 2900 K. The low average molecular weight of E1 made the attainment of temperatures greater than 3715 K an extremely difficult task. When the driver pressure exceeded 20 psig, the pressures in the TOF rose to unacceptable levels and the mechanical pumps for the shock tube were subjected to pressures far in excess of atmospheric. In con-

TABLE VII: Landau-Teller Parameters Determined from the Relaxation Mixtures^a

Mixture	A	B
R1	58.87 ± 16.24	0.44 ± 1.20
R2	27.38 ± 36.60	(-1.14 ± 2.69)
R3	50.41 ± 9.81	2.01 ± 0.74
R4	77.65 ± 9.14	1.98 ± 0.68
R5	54.34 ± 6.95	2.07 ± 0.52

^a Units of $P\tau$ are atm μ sec.

trast to these difficulties, a temperature of 4650 K was easily achieved in E2 with a driver pressure of 9 psig.

Mixture E2 (180 Torr) saturated with mercury vapor was irradiated in a Rayonet photoreactor fitted with 254-nm low-pressure mercury lamps for periods of 1–24 hr. The reactants were contained in a 1 cm × 20 cm Suprasil tube. After irradiation the mixture was analyzed with the TOF mass spectrometer.

Results

The infrared emission records for the relaxation of carbon monoxide were fit to the equation

$$1 - I/I_\infty = \exp(-kt)$$

where I and I_∞ are the observed values of the emission intensity and k is the pseudo-first-order rate constant for relaxation. The data were converted to the standard Landau-Teller form

$$\ln P\tau = AT^{-1/3} - B$$

The values of the reflected shock zone pressures P (atm), the relaxation times τ (μ sec), and the corresponding temperatures are listed in Tables II–VI for each of the mixtures R1–R5 and are available on microfilm (see paragraph at end of text regarding supplementary material). The Landau-Teller coefficients and their standard deviations as calculated from a least-squares procedure are presented in Table VII. The relaxation times for mixtures R3 and R4 differed by a constant factor of about 6 throughout the temperature range covered, 1800–3000 K. Hence, these two diluents were chosen for the exchange reaction TOF runs; R3 would provide the environment for short relaxation times for CO compared to the relatively longer times required in R4 for CO to attain vibrational equilibration.

In the exchange experiments, the peak heights corresponding to m/e 28, 29, 30, and 31 were measured. The mole fraction of $^{13}\text{C}^{18}\text{O}$, f_{31} , was computed on a total carbon monoxide basis

$$f_{31} = 31/(28 + 29 + 30 + 31)$$

where the numbers correspond to the respective mass peak heights. The data were fit to the following equation

$$\ln \frac{f_{\text{eq}} - f_0}{f_{\text{eq}} - f_t} = k_m t$$

where the subscripts eq, 0, and t refer to the mole fraction at equilibrium, at time zero, and at times during the course of the reaction, respectively. The growth of the product, $^{13}\text{C}^{18}\text{O}$, was observed to be linear. Attempts to determine the individual orders of the components were not made due to the limited amount and expense of the isotopic reactants. In mixture E1, the dissociation of H_2 was calculated⁶ to be less than 0.1% during the observation time at the

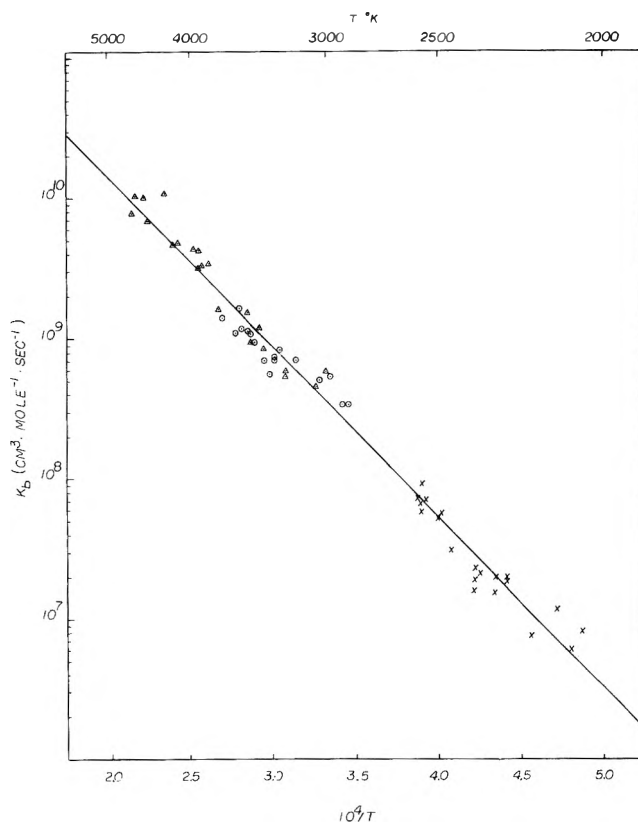


Figure 1. Arrhenius plot of self-exchange data: O, mixture E1; Δ , E2; X, ref 9, Table II.

highest temperature recorded, 3714 K. The reactions of hydrogen atoms with carbon monoxide are unfavorable with respect to endothermicity and rate. The rate constants k_m from E1 and E2 were converted using the rate law determined by Bar-Nun and Lifshitz⁹

$$k_b = k_m/([\text{CO}]^{0.45}[\text{M}]^{0.55})$$

where $[\text{M}]$ refers to the total gas concentration. The values for the rate constants are listed in miniprint in Tables VIII and IX (see paragraph at end of text regarding supplementary material). An Arrhenius plot revealed considerable overlap for the data and, in fact, the rate constants for E1 and E2 may be represented by

$$k_b = 10^{12.50 \pm 0.16} \exp[-(54,130 \pm 2500)/RT] \text{ cm}^3 \text{ mol}^{-1} \text{ sec}^{-1}$$

Furthermore, these rate constants may be combined with the data found in ref 9, Table II, to yield an Arrhenius line spanning a 2700 K temperature range

$$k_b = 10^{12.58 \pm 0.07} \exp[-(55,470 \pm 890)/RT] \text{ cm}^3 \text{ mol}^{-1} \text{ sec}^{-1}$$

All of the results are plotted in Figure 1.

In the photolysis experiments, irradiation of mixture E2 for periods of up to 24 hr produced less than 3% conversion of $^{13}\text{C}^{16}\text{O}$ into $^{13}\text{C}^{18}\text{O}$.

Discussion

The fact that the rate constants derived from E1, the fast relaxation environment, and E2, the relatively slow relaxation mixture, can be combined with the rate constants reported by Lifshitz in an argon diluent suggests that the

TABLE VIII
RATE CONSTANTS FOR EXCHANGE IN THE H_2 - Ne SYSTEM (E1)

T	[CO] $\times 10^6$ mole-cm ⁻³	[M] $\times 10^6$ mole-cm ⁻³	k_a $\times 10^{-3}$ sec ⁻¹	k_b $\times 10^{-8}$ cm ³ -mole ⁻¹ -sec ⁻¹
2091	.205	2.57	.779	.539
2917	.199	2.49	.274	.343
2983	.208	2.60	.450	.559
3044	.204	2.55	.418	.510
3046	.205	2.56	.418	.508
3186	.210	2.60	.603	.737
3286	.212	2.65	.724	.892
3322	.210	2.63	.625	.741
3323	.208	2.60	.592	.709
3352	.223	2.78	.511	.572
3384	.217	2.71	.614	.705
3467	.218	2.73	.854	.975
3475	.234	2.93	1.04	1.11
3504	.210	2.63	.971	1.15
3551	.217	2.72	1.04	1.20
3575	.219	2.73	1.45	1.66
3597	.218	2.73	.974	1.11
3714	.217	2.72	1.23	1.41

TABLE IX
RATE CONSTANTS FOR EXCHANGE IN THE Kr - Ar SYSTEM (E2)

T °K	[CO] $\times 10^6$ mole-cm ⁻³	[M] $\times 10^6$ mole-cm ⁻³	k_a $\times 10^{-3}$ sec ⁻¹	k_b $\times 10^{-8}$ cm ³ -mole ⁻¹ -sec ⁻¹
3015	.201	2.52	.464	.599
3068	.188	2.35	.342	.452
3285	.184	2.30	.441	.598
3290	.190	2.38	.410	.538
3395	.186	2.32	.637	.805
3419	.197	2.46	.953	1.21
3485	.184	2.30	.711	.962
3510	.194	2.43	1.21	1.55
3738	.213	2.67	1.37	1.63
3829	.190	2.38	2.61	3.40
3879	.194	2.43	1.81	2.32
3928	.197	2.46	2.52	3.18
3951	.193	2.41	3.32	4.29
3955	.194	2.42	2.38	3.04
4122	.197	2.46	2.77	3.76
4155	.197	2.46	2.70	3.69
4266	.201	2.51	8.76	10.9
4466	.201	2.52	5.34	6.86
4509	.198	2.48	8.14	10.2
4611	.206	2.58	11.60	14.4
4651	.205	2.57	6.41	7.79

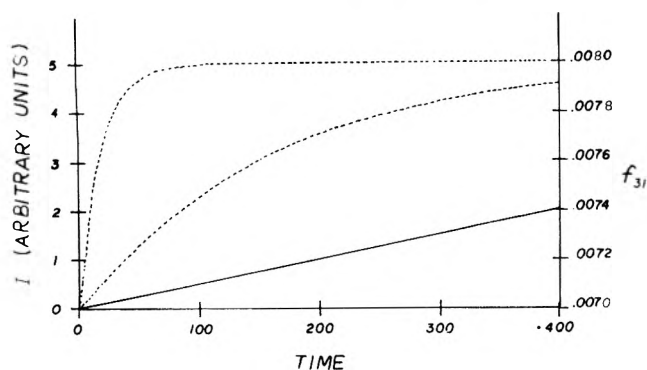


Figure 2. Uppermost curves represent emission intensity profiles of CO in mixtures R3 and R4, respectively, at 2100 K. Lower solid line represents mole fraction of exchange product formed at 2100 K. The time scale is microseconds.

rate of self-exchange is independent of the identity of the inert gas collision partner. This conclusion is not surprising since the rate of exchange was in all experiments observed under the condition of vibrational equilibration. The situation may be summarized in Figures 2 and 3.

In Figure 2 is plotted the amount of f_{31} formed at 2100 K according to the rate law reported by the SPST workers and the rate constants reported herein. The conversion

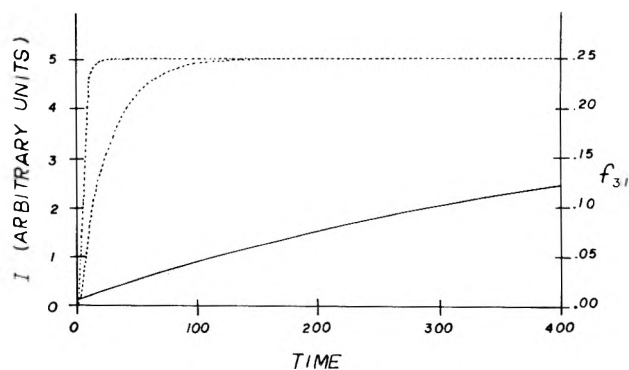


Figure 3. Same as Figure 2 except at 3700 K.

level corresponds to a peak height which is not detectable in the TOF experiments. Superimposed on the figure are the vibrational relaxation profiles observed for R3 and R4 at 2100 K. They are appreciably different. If the rate constants obtained for E1 and E2 can be extrapolated to 2100 K, then it may be concluded that the rate of self-exchange does not depend solely upon the vibrational energy content of CO and there must be a significant contribution from translational energy of CO to the exchange process. It is unfortunate that at those temperatures, where the exchange conversion is detectable by the TOF, the relaxation times for E1 and E2 are short compared to the conversion time. This condition is depicted in Figure 3 in which the temperature is 3700 K.

Lifshitz, from the activation energy of 76 kcal mol⁻¹ obtained in his experiments, has suggested that vibrational levels $v = 7-9$ may be responsible for the atom switching reaction.⁹ The lower activation energy from the combined results reported here would reduce these critical levels to $v = 5-7$. In the photolysis experiment 3% conversion of ¹³C¹⁶O into ¹³C¹⁸O would have been readily observed. This corresponds to the formation of approximately 7×10^{10} molecules cm⁻³ sec⁻¹ over 24 hr. The photon flux in the photoreactor is approximately 10^{16} photons cm⁻³ sec⁻¹.¹⁴ After allowing for losses in the system due to reflection from the walls of the reaction vessel, insufficient mercury vapor for the complete absorption of radiation and the small proportion of molecules which are excited to $v = 7-9$, it is apparent that at least 10% exchange should have been observed if vibrational levels $v < 9$ dominate the exchange reaction.

The argument against the critical importance of vibrational energy and the applicability of VEX to this particular exchange is based on conclusions which have been drawn indirectly from the shock tube work. However, the Hg photosensitization results provide direct support for this contention. Photosensitization using metal atoms to selectively excite vibrational levels in reactant molecules may prove to be a convenient way of testing VEX. Recently it has been shown that sodium atoms can be used to excite H₂ to $v = 3$,⁴ and these are the critical levels proposed by Bauer to be responsible for exchange in H₂, D₂ mixtures.⁷ Experiments by one of us (BVOG) on this and analogous systems are in progress.

The reasons presented by Bar-Nun and Lifshitz ruling out the one-step, bimolecular intermediate and the atomic mechanism remain valid. It is pleasing to note the agreement of the kinetic data over a truly wide temperature range that was obtained by the diverse methods of the SPST and TOF dynamic sampling technique.

Acknowledgments. The assistance of Mr. David Willbanks with the TOF shock tube experiments is greatly appreciated.

Supplementary and Miniprint Material Available. Tables II–VI, containing $P\tau$ values for mixtures R1–R5, will appear following these pages in the microfilm edition of this volume of the journal. Photocopies of the supplementary material and full-sized photocopies of the miniprinted material (Tables VIII and IX) from this paper only or microfiche (105 × 148 mm, 24× reduction, negatives) containing all of the supplementary material for the papers in this issue may be obtained from the Journals Department, American Chemical Society, 1155 16th St., N.W., Washington, D.C. 20036. Remit check or money order for \$4.00 for photocopy or \$2.50 for microfiche, referring to code number JPC-75-1483.

References and Notes

- (1) (a) Paper presented at 168th National Meeting of American Chemical Society, Philadelphia, Pa., April, 1975. (b) Support of this work by National Science Foundation, Grant No. GP-33949, is gratefully acknowledged. (c) Formerly Louisiana State University in New Orleans.
- (2) D. Lewis and S. H. Bauer, *J. Am. Chem. Soc.*, **90**, 5390 (1968). Contains references to previous work.
- (3) I. D. Gay, G. B. Kistiakowsky, J. V. Michael, and H. Niki, *J. Chem. Phys.*, **43**, 1720 (1965).
- (4) R. D. Kern and G. G. Nika, *J. Phys. Chem.*, **76**, 2809 (1972).
- (5) R. D. Kern and G. G. Nika, *J. Phys. Chem.*, **78**, 2549 (1974).
- (6) R. D. Kern and G. G. Nika, *J. Phys. Chem.*, **75**, 1615 (1971).
- (7) S. H. Bauer and E. Ossa, *J. Chem. Phys.*, **45**, 434 (1966).
- (8) B. Stevens, "Collisional Activation in Gases", Vol. 3, "The International Encyclopedia of Physical Chemistry and Chemical Physics", Pergamon Press, Oxford, 1967, Topic 19.
- (9) A. Bar-Nun and A. Lifshitz, *J. Chem. Phys.*, **51**, 1826 (1969).
- (10) S. H. Bauer, D. M. Lederman, E. R. Resler, and E. R. Fisher, *Int. J. Chem. Kin.*, **5**, 93 (1973).
- (11) T. Baer and S. H. Bauer, *J. Am. Chem. Soc.*, **92**, 4773 (1970).
- (12) G. Karl, P. Kruss, and J. C. Polanyi, *J. Chem. Phys.*, **46**, 224 (1967).
- (13) J. M. Brupbacher and R. D. Kern, *J. Phys. Chem.*, **77**, 1329 (1973).
- (14) G. Griffin, private communication.
- (15) D. A. Jennings, W. Braun, and H. P. Broida, *J. Chem. Phys.*, **59**, 4305 (1973).

Dissociation of Molecular Hydrogen in Gas Discharges of Moderate Pressure. The Role of Vibro-Rotational Excitation

Pio Capezzuto, Francesco Cramarossa,* Riccardo d'Agostino, and Ettore Molinari

Centro di Studio per la Chimica dei Plasmi del C.N.R., Istituto di Chimica Generale ed Inorganica, Università di Bari, 70126 Bari, Italy
(Received December 16, 1974)

The dissociation of molecular hydrogen has been studied in radiofrequency gas discharges operated at power levels of 1–10 cal sec⁻¹ cm⁻³, in the pressure range 5–40 Torr, and at H₂ flow rates up to 60 l. (STP)/min. The degree of dissociation of H₂ has been evaluated calorimetrically and the experimental results have been compared with different theories of molecular dissociation in plasmas. It is shown that under the conditions prevailing in these experiments the dominating mechanism involves the participation of vibro-rotationally excited molecules, the population of which is maintained, by the radiofrequency fields, at levels substantially higher than those corresponding to the kinetic gas temperature.

Introduction

Radiofrequency (35 MHz) gas discharges, operated at power levels of the order of 1–10 cal sec⁻¹ cm⁻³, have recently been utilized in this laboratory as chemical reactors for a number of homogeneous and heterogeneous reactions. These reactions include the synthesis of HCN from CH₄ and N₂,^{1,2} the synthesis of acetylene from CH₄,³ and the heterogeneous reduction of metal oxides (CuO, NiO, PbO, ZnO) in a hydrogen plasma.⁴

The pressure range investigated was between 5 and 40 Torr with a maximum of 75 Torr in the reduction of metal oxides. Spectroscopic investigations of the discharges have also been carried out with the aim of evaluating vibrational and rotational temperatures of emitting species (N₂, N₂⁺, C₂, CN) under plasma conditions similar to those utilized in kinetic studies.^{5–7} The general conclusions derived from this work can be summarized as follows. In the pressure range and at the power levels utilized in these experiments, plasma conditions are intermediate between those of "ther-

mal" plasmas and those of "cold" plasmas. Remarkable disequilibrium exists between electronic, vibrational, rotational, and kinetic temperatures, the latter being in the range 700–2000°K. Excited vibrational and rotational levels are populated well above equilibrium and this can be regarded as the main cause of the high rates observed for the dissociation of molecular species. This point of view allowed a rationalization to be made of the kinetic data collected for the above-mentioned reactions. A review of this work can be found in ref 8. In spite of the remarkable uncertainties involved in the evaluation of plasma characteristics and of the somewhat indirect derivation of rate constants for the dissociation of species such as H₂, N₂, and CH₄, the picture that emerged was that these plasmas were too "cold" to account for a purely thermal dissociation of these species and that electron temperatures were also too small to account for a mechanism of dissociation by direct electron impact.

A dissociation mechanism, which gives due consideration

to the contribution of excited vibro-rotational levels to the overall rate of dissociation of molecular species, has therefore been discussed.² The evidence accumulated in favor of this mechanism is rather indirect and the aim of the present work was therefore to investigate a process of molecular dissociation directly, under conditions corresponding to the "intermediate" state of the plasma.

Rates of thermal dissociation of molecular hydrogen have been measured or calculated up to sufficiently high gas temperatures,^{9,10} while rates of dissociation by direct electron impact have been calculated in ref 11 as a function of the electron temperature T_e .

Experimental rates of hydrogen dissociation in an electric discharge can therefore be analyzed with respect to both these mechanisms and the mechanism involving the contribution of vibro-rotationally excited molecules.

The main difficulty in performing experiments on the dissociation of molecular hydrogen in gas discharges, operated at the power levels, gas flow rates, and in the pressure range utilized in these experiments, resides in the evaluation of the concentration of atomic hydrogen. Methods reported in the literature for the quantitative determination of H atoms would be of little use under these conditions. E.g., a hot wire calorimeter technique would not be applicable under many of the experimental conditions explored, as a consequence of the rapid melting of the wire which is subject to a very intense enthalpy flux. Under the "mildest" experimental conditions, apart from the interference of pick-up of the rf field, the complexity of data reduction would make these measurements quite inaccurate. This difficulty has however been circumvented by resorting to the experimental arrangement described below.

Experimental Section

Apparatus. The calorimetric discharge reactor utilized in these experiments is illustrated in Figure 1. The inner tube was of quartz with inner radius $r_T = 2.25$ cm and wall thickness $d = 0.25$ cm. The outer tube ($\phi_{ext} = 7$ cm) was of Pyrex and was provided with water inlets and outlets at different axial positions. Separation of the calorimetric water jacket into different sections was accomplished by means of O rings. All the water outflowing from a lower section was conveyed to a mercury thermometer (divisions of 0.1°) and returned to the next upper section. The bottom of the discharge tube was fitted to a double wall copper pipe, also divided into sections.

Water was pumped through the water jacket at a constant and metered rate (1–3 l./min). The power transferred from the generator to the gas and from the gas to the cooling water can be measured, in each section of the calorimetric jacket, from the temperature rise, as read by the various thermometers in series, and from the measured flow of the water.

The temperature of the gas leaving the copper pipe was measured by means of a thin thermocouple immersed in the gas. The system was connected by a 2-in. vacuum valve to a rotary pump with a pumping speed of $2 \text{ m}^3/\text{min}$ and by a 0.5-in. valve to a second rotary pump with a pumping speed of $0.45 \text{ m}^3/\text{min}$. This arrangement provides a fine regulation of the pressure within the discharge system.

UPP hydrogen from the tank was utilized without further purification.

The gas flow rate was regulated by means of needle valves and read on calibrated flowmeters or rotameters. (The range of gas flow rates was between 0.1 and 60 l.

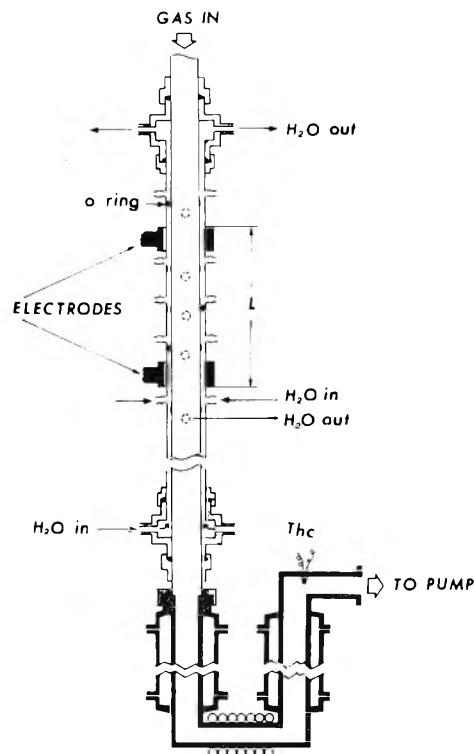


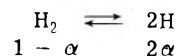
Figure 1. A scheme of the calorimetric discharge reactor.

(STP)/min.) The 35 MHz, 10 kW, power generator (supplied by STEL of Massy, France) was capacitively coupled to the discharge by means of two sleeve electrodes of copper 3.6 cm high positioned at fixed separation $L = 24$ cm, including the electrode height.

The generator is equipped with meters to read d.c. plate voltage (0–5 kV), d.c. plate intensity (0–2.5 A), and grid intensity (0–2 A).

In Figure 2 the d.c. plate voltage V_p has been plotted as a function of total power W_T collected in the calorimetric system, for various pressures, at a fixed flow rate of 10 l. (STP)/min. The product $V_p I_p / 2$ vs. W_T has been plotted in Figure 3, for a variety of experimental conditions. The least-squares slope of the straight line is 0.93 ± 0.04 , pointing to a good coupling of the generator to the discharge. The power dissipated as visible radiation has been evaluated by injecting a sufficient amount of china ink into the flowing water of the calorimeter. This power was found to be always less than 1% of total.

Calorimetric Evaluation of the Extent of Hydrogen Dissociation. If α is the extent of dissociation of molecular hydrogen according to



one has $\alpha = [\text{H}]/(2N - [\text{H}])$, with $N = P/RT_g$, where P = pressure, T_g = kinetic gas temperature, and R = gas constant.

The enthalpy of the discharged gas, H (cal mol⁻¹), referred to 1 mol of inlet H_2 , can be expressed with good approximation as follows:

$$H = \alpha D_{\text{H}_2} + [\bar{C}_{p_{\text{H}_2}}(1 - \alpha) + \bar{C}_{p_{\text{H}}}2\alpha](T_g - 298) \quad (1)$$

where D_{H_2} (cal mol⁻¹) = enthalpy of dissociation of H_2 (104×10^3) and $\bar{C}_{p_{\text{H}_2}}$ and $\bar{C}_{p_{\text{H}}}$ (cal mol⁻¹ K⁻¹) = mean

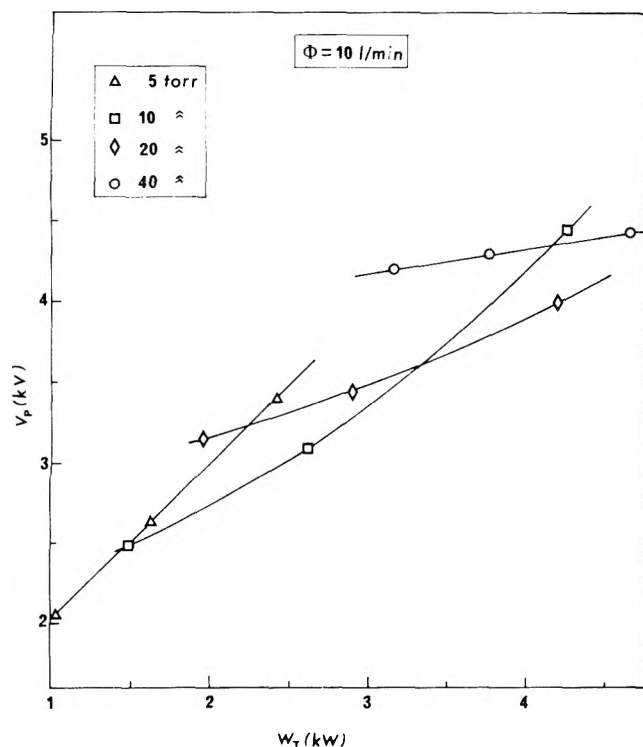


Figure 2. The d.c. plate voltage vs. total power collected in the calorimetric system, for various pressures and at a fixed gas flow rate.

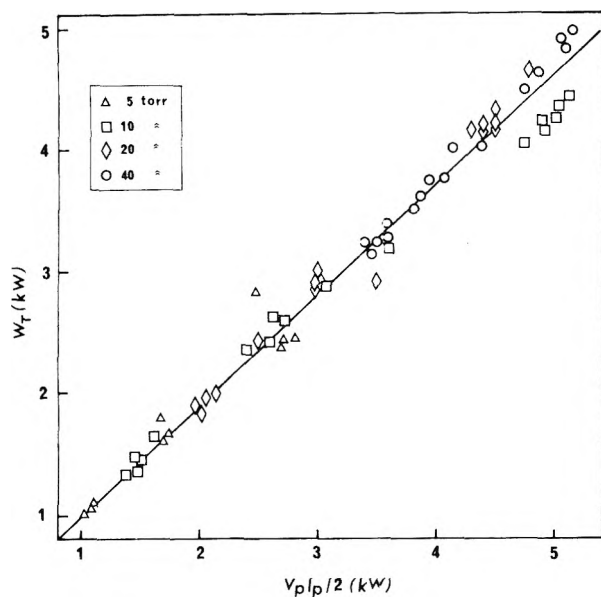


Figure 3. Total power collected in the calorimetric system vs. $V_p l_p / 2$, for different experimental conditions.

specific heats at constant pressure of molecular and atomic hydrogen, respectively, in the temperature interval $T_g \pm 298^\circ\text{K}$.

The enthalpy flux associated to the stream of the discharged gas will be given by ΦH (cal sec^{-1}), with Φ (mol sec^{-1}) = molar flow rate of the inlet gas.

In any volume element of the reactor, the following energy balance will hold:

$$dW = dW_w + \Phi dH \quad (2)$$

where W is the electrical power transferred to the discharge, W_w is the power transferred by the gas to the reac-

tor walls and collected by the streaming water, and ΦdH is the enthalpy increase of the flowing gas in the volume element.

In Figure 4 the power collected by the water jacket has been plotted as function of the axial distance l , measured in the direction of the water flow (i.e., in the opposite direction of gas flow), at a fixed gas flow rate of 0.1 l./min for different pressures and power input.

The circles on the figure mark the position of the O rings and the zero of the abscissae corresponds to the position of the lower O ring (see Figure 1). The point at $l = -30$ cm gives the power collected in the copper section of the calorimeter, i.e., up to the beginning of the quartz tube. A length l_0 is defined as the abscissa corresponding to the intersection between the straight line connecting the points at $l = -30$ cm and $l = 0$, and that connecting the points within the electrodes.

At a flow rate of 0.1 l. (STP)/min the term ΦdH in eq 2 can be neglected under all experimental conditions, and the curves of Figure 4 represent the axial profile of the electric power input to the gas. l_0 has been taken as the beginning of the intense electric field.

One appreciates from the figure that the field remains constant up to the upper electrode and then decreases, extending for a few centimeters above this electrode. An extension of the field below the lower electrode is observable with decreasing pressure and increasing power. The curves at 0.1 l./min have been taken as base lines for our calculations.

In Figure 5 the power collected by the water jacket has been plotted as a function of the axial distance, at a fixed power input of 4.18 kW and at flow rates between 0.1 and 60 l. (STP)/min. This figure shows that all the curves merge to a common point corresponding to the upper end of the electric field and to the total power input utilized. Starting from this common point, deviation from the base line of 0.1 l./min becomes increasingly important with increasing the axial distance in the direction of the gas flow and with increasing flow rate. The difference between the ordinate of any one of these curves and that of the base line, at any value of l gives the enthalpy flux associated with the gas at that particular point:

$$W(\Phi, l) - W(0.1, l) = \Phi H(l) \quad (3)$$

as follows from eq 2. At $l = l_0$, one has from eq 1 and 3:

$$[W(\Phi, l_0) - W(0.1, l_0)] / \Phi = H(l_0) = \alpha(l_0) D_{\text{H}_2} + \{ \bar{C} p_{\text{H}_2} [1 - \alpha(l_0)] + \bar{C} p_{\text{H}} 2\alpha(l_0) \} [T_g(l_0) - 298] \quad (4)$$

$\alpha(l_0)$ can therefore be derived from the experiments by means of eq 4 once the gas temperature $T_g(l_0)$ is known. This requires an additional equation which can be derived from a detailed energy balance, as discussed in Appendix B.

Experimental Results. Values of $\alpha(l_0)$ as a function of the gas flow rate have been plotted in Figure 6a-d, at pressures of 5, 10, 20, and 40 Torr, respectively, and at three different values of W_T .

Values of $\alpha(l_0)$ at low flow rates are affected by large errors, as an immediate consequence of the large error involved in the evaluation of $W(\Phi, l_0) - W(0.1, l_0)$ at small Φ 's. At large Φ 's the error on α becomes acceptable.

The data of Figure 7, derived from Figure 6, give a clear picture of the observed dependence of $\alpha(l_0)$ on power density (W) ($\text{cal cm}^{-3} \text{sec}^{-1} = W_T / \pi r_T^2 L$) and pressure, at a

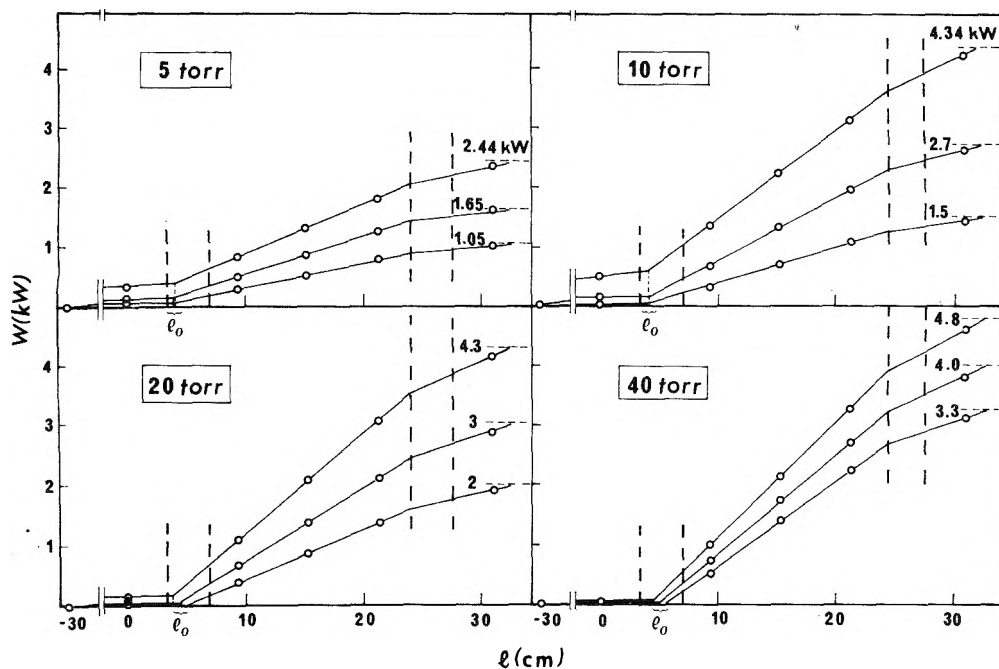


Figure 4. Power collected in the calorimetric system vs. the axial distance measured in the direction of the water flow, for a fixed gas flow rate of 0.1 l./min, at different pressures and total power input. The zero of the abscissae corresponds to the position of the O ring set below the lower electrode.

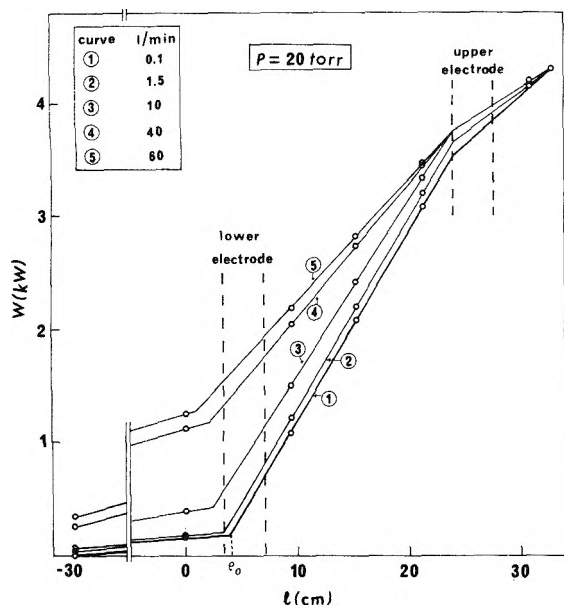


Figure 5. Power collected in the calorimetric system vs. the axial distance measured in the direction of the water flow, at a fixed power input of 4.18 kW, but at variable gas flow rates.

constant flow rate of 10 l. (STP)/min. The dependence of the calculated gas temperature $T_g(l_0)$ on pressure, power density, and flow rate is illustrated by the data of Figure 8.

Discussion

In order to rationalize the experimental observations reported above, it is necessary to define a model of the discharge as a chemical reactor, where hydrogen molecules are dissociated, as a consequence of the energy transfer from the field, and where hydrogen atoms recombine both in the gas phase and on the reactor walls. The easiest model to deal with is that of a radially uniform plasma extending up

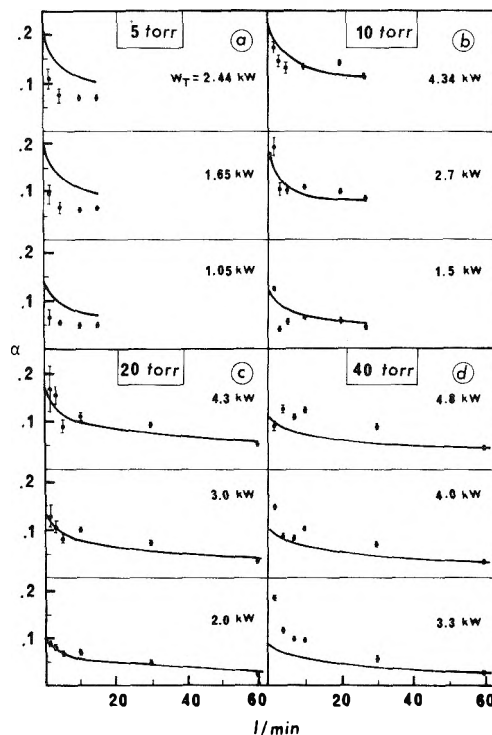


Figure 6. Observed and calculated values of $\alpha(l_0)$ as a function of the gas flow rates, at different pressures and total power input. The curves refer to the calculated values.

to the reactor walls. This is, however, a rather severe approximation in that, in the pressure range investigated, the plasma column is more or less constricted, according to conditions. Plasma constriction increases with increasing pressure and decreasing power input.

The experimental values of $\alpha(l_0)$ derived in the preceding section represent, therefore, *radially averaged* values of this quantity, which should actually exhibit a marked radi-

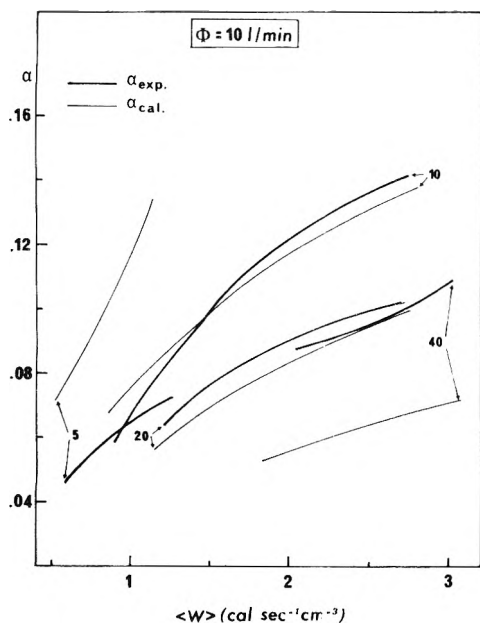


Figure 7. Observed and calculated values of $\alpha(l_0)$ as a function of the power density at 5, 10, 20, and 40 Torr and fixed gas flow rate.

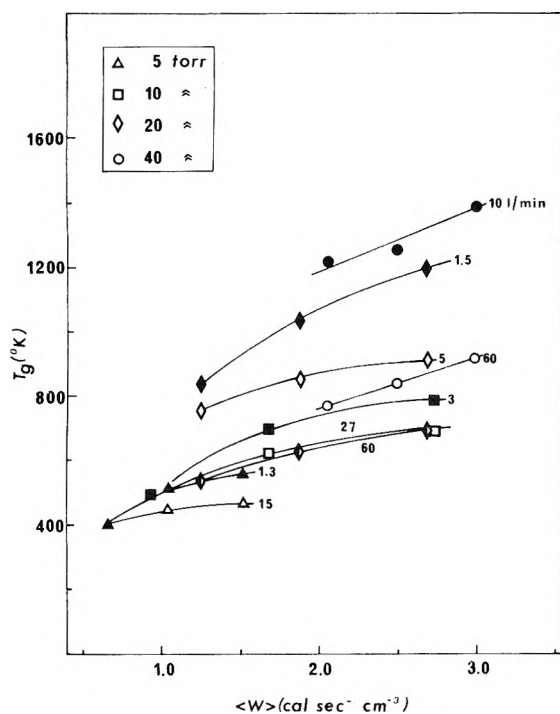


Figure 8. Calculated values of the kinetic gas temperature $T_g(l_0)$ as a function of the power density, at different pressures and gas flow rates.

al profile. A rather abrupt fall of α , beyond the luminous central column of the discharge, is in fact to be expected.

The real situation of the discharge will however be considered after discussion of a simplified, radially uniform model.

Model Discharge. (a) *Rate Expression.* Two extreme rate expressions will be considered, one corresponding to a *plug flow* reactor, the other to a *stirred tank* reactor. Inspection of the data of Figure 5 shows quite clearly that the enthalpy flux associated with the gas stream is an increasing function of the axial length. The largest contribution to

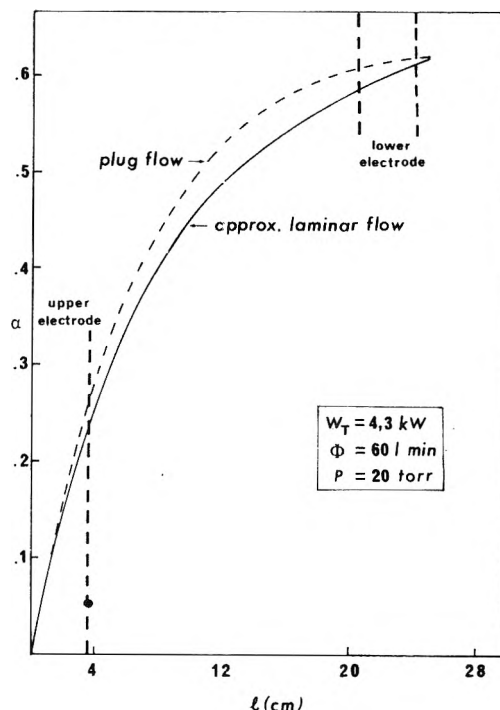


Figure 9. Representative profile of α within the reactor, calculated according to eq 5 (plug flow) and eq 6 (approximate laminar flow).

the enthalpy results from the first term in eq 1 and α is therefore increasing along the reactor axis. The existence of an *axial* profile of α is incompatible with the existence of complete back mixing, i.e., the reactor cannot be treated as a stirred tank. It has however been pointed out in ref 2 that the rate expression of the stirred tank, when made *parametric in the axial length l* , can often be utilized to approximate the kinetics of a *laminar flow* reactor, with the great advantage of a very simple mathematical expression. The rate expression for a *plug flow* is given by

$$\frac{4N}{(2N - [H])^2} \Phi \frac{d[H]}{r_T^2 dl} = k_D [H_2] - \{k' [H] + k'' (N - [H]) [H]^2 + k''' [H]^3\} \quad (5)$$

For an *approximately laminar flow* (stirred tank, parametric in l measured in the direction of the gas flow) the rate expression can be written as

$$\frac{2N}{(2N - [H])} \frac{\Phi}{r_T^2 l} = k_D [H_2] - \{k' [H] + k'' (N - [H]) [H]^2 + k''' [H]^2\} \quad (6)$$

with k_D = pseudo-first-order rate constant for H_2 dissociation within the discharge; k' = first-order rate constant corresponding to the heterogeneous process of atom recombination at the walls. The analytical expression for k' is derived in Appendix A. k'' = rate constant for trimolecular recombination: $H + H + H_2 = H_2 + H_2$; k''' = rate constant for triatomic recombination: $H + H + H = H_2 + H$.

Values of the different constants have been taken from the literature already quoted in ref 2.

On the assumption that all the power delivered by the field to the gas is utilized for the dissociation of molecular hydrogen, one can write

$$k_D [H_2] = 2 \langle W \rangle / 104 \times 10^3 \quad (7)$$

The concentration of atomic hydrogen can be derived from either eq 5 or 6, if the gas temperature T_g is known. The experimental determination of T_g is a complex problem; T_g can however be evaluated as shown in Appendix B.

(b) *Comparison with the Experimental Results.* In Figure 9 representative profiles of α calculated according to eq 5 or 6, at a fixed flow rate of 60 l. (STP)/min, have been reported. A comparison between the two profiles shows that values of α are somewhat higher when use is made of the plug flow expression, but they converge to a common value at the end of the reactor. The experimental data have been compared with values of α obtained from eq 6, which is much easier to use.

The continuous curves of Figures 6a–d connect the calculated values, which have also been plotted as thick lines in Figure 7. The agreement appears satisfactory at 10 and at 20 Torr, while calculated values are higher than the experimental ones at 5 Torr and smaller at 40 Torr. There are a number of uncertainties in the values of constants utilized in the model: the values of γ for H-atom recombination on quartz are not accurate and reported values can differ by as much as a factor of 5. The temperature dependence of γ is also uncertain. These uncertainties are reflected in the values of k' (Appendix A). Values of k''' have been taken, in accordance with ref 11, as $10k''$, but a value of $3k''$ could not be ruled out.⁹

Table I summarizes the results obtained at 5 and 40 Torr when different values of k' or k'' are used. Although the experimental points at 5 and 40 Torr might fall within the above-mentioned uncertainties, it should be remarked that an improved agreement at 5 Torr, which can be obtained using higher values of k' , would make the disagreement much stronger at all other pressures. It should be remembered, at this stage, that the plasma is progressively constricted with increasing pressure. The radially uniform model should therefore be more appropriate to describe the real situation at 5 Torr rather than at 40. One very important consequence of the constriction is that the plasma is surrounded by an annulus of gas at a much lower temperature than the hot core. This has a profound influence on k' , and the transport of atoms to the walls is strongly reduced, thus increasing the concentration of the atoms quite appreciably. This point has been discussed in ref 3. These considerations might therefore suggest a possible explanation of the low values calculated at 40 Torr.

Mechanism of H₂ Dissociation. If one considers the agreement between calculated and observed values of α as satisfactory, at least above 10 Torr, it follows that the approximation utilized in the calculation, namely, $2 \langle W \rangle / 104 \times 10^3 = k_D[\text{H}_2]$, should provide acceptable values for the rate of dissociation of molecular hydrogen.

These rates can therefore be compared as already mentioned in the Introduction, with rates calculated on the basis of either a mechanism of thermal dissociation, or of dissociation by direct electron impact. Rate constants for the thermal process can be calculated up to 10,000°K from the corresponding rate constants for atom recombination⁹ and the known values of the equilibrium constants.¹⁰ This comparison shows that, in the pressure range investigated, it is impossible to attain the observed values of $k_D[\text{H}_2]$, at any temperature. A purely thermal mechanism is therefore unable to account for the observed rates and should be ruled out completely. For a mechanism of molecular dissociation by direct electron impact, $\text{H}_2 + e = 2\text{H} + e$, the rate of atom production can be written as¹¹

TABLE I: Influence on the Calculated Values of α of the Variation in the Values of the Constants k''' and k'

ϕ , l./min	k'''	k'	α_{calcd}	$\alpha_{\text{exp t}}$	
1.3	5 Torr		$W_T = 1.5 \text{ kW}$		
	$10k''$	324	0.165	0.115	
	$3k''$	324	0.183		
	$10k''$	616	0.096		
	15	$10k''$	344		0.099
		$3k''$	344		0.104
$10k''$		710	0.059		
1.5	40 Torr		$W_T = 4.0 \text{ kW}$		
	$10k''$	544	0.092	0.149	
	$3k''$	544	0.098		
	$10k''$	887	0.060		
	60	$10k''$	435		0.040
		$3k''$	435		0.044
$10k''$		760	0.028		

$$d[\text{H}]/dt = k_e' n_e [\text{H}_2] = k_e [\text{H}] \quad (8)$$

with n_e = number density of the electrons and $k_e' =$

$$(8/\pi m_e)^{1/2} (kT_e)^{-3/2} \int_0^\infty \epsilon \sigma_D(\epsilon) \exp(-\epsilon/kT_e) d\epsilon \quad (9)$$

where T_e = electron temperature, ϵ = electron energy, m_e = mass of electron, and $\sigma_D(\epsilon)$ = cross section for H₂ dissociation by direct electron impact, a function of ϵ . In the derivation of eq 9, a Boltzmann distribution of electron energies has been assumed. Evaluation of the integral in eq 9 is possible once $\sigma_D(\epsilon)$ is known and values of k_e' have been determined as a function of kT_e in ref 11. In order to compare our rates of dissociation with those calculated according to eq 8 and 9, it is necessary to evaluate both n_e and T_e under various experimental conditions.

Values of the characteristic electron energy $\epsilon_k = kT_e$ can be derived from the literature as function of the reduced field E/N ,¹² with E (V cm⁻¹) = field intensity and $N = P/RT_g$.

According to the results reported in Figure 5, which indicate that the rate of energy dissipation is essentially constant and the results of Figure 3, which show that $W_T \simeq V_p J_p / 2$, one can assume a uniform field within the electrodes and equate E to $V_p / (\sqrt{2}L)$. The electron concentration n_e can be evaluated from the relationship¹³

$$\langle W \rangle = \frac{n_e e^2 E^2}{m_e} \frac{\nu_m}{\nu_m^2 + \omega^2} \quad (10)$$

where ν_m = frequency of elastic collisions of the electron, ω = applied radiofrequency (35 MHz), and e = electronic charge. ν_m is a unique function of ϵ_k and can be taken from the literature.¹²

One can therefore calculate the rate of formation of the H atoms from eq 8 by means of the $k_e'(T_e)$ function as given in ref 11, and compare these rates with those derived from the expressions $k_D[\text{H}_2] = 2 \langle W \rangle / 104 \times 10^3$, utilized in the present calculations.

In Figure 10 the ratio k_e/k_D has been plotted as a function of the power density $\langle W \rangle$, at 5, 10, 20, and 40 Torr and at different flow rates. The figure shows beyond any doubt that the contribution of the mechanism of dissociation by direct electron impact (eq 8) becomes smaller with increasing pressure, decreasing power density, and, above 10 Torr,

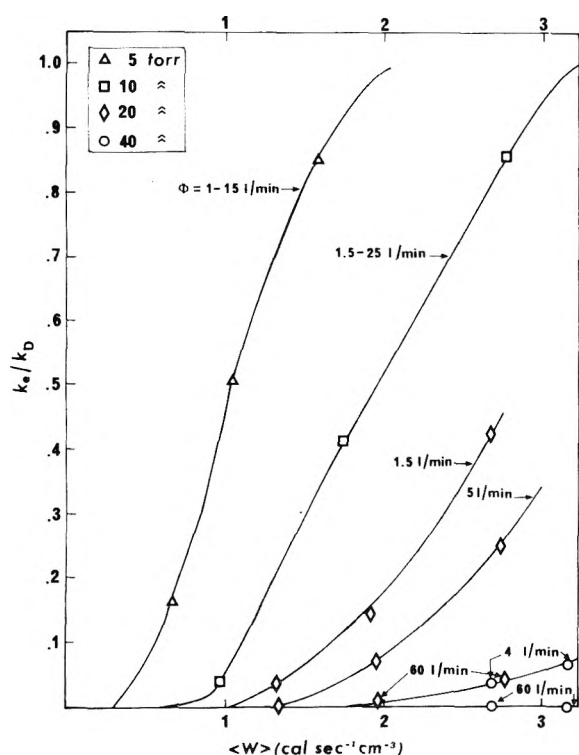


Figure 10. k_a/k_D ratio as a function of the power density, at different pressures and gas flow rates.

also with increasing flow rate. This behavior is the consequence of the form of the $k_e'(T_e)$ function and of the dependence of T_e on E/N . The separation of the curves at different flow rates resides in the fact that T_g , hence N , depends appreciably on the flow rate, above 10 Torr (see Figure 8).

It is also apparent from Figure 10 that the transition from a situation in which the mechanism of dissociation by direct electron impact predominates, to a situation in which a different mechanism should be invoked, is gradual. Direct dissociation can be considered as dominating below about 2–3 Torr, in full agreement with the results of ref 11, while, at 40 Torr and 60 l./min, the contribution of this mechanism is reduced to zero.

Thermal dissociation has been ruled out completely, while the mechanism of dissociation by direct electron impact is seen to give only a partial contribution to the observed rates of dissociation. A different mechanism of dissociation, which should dominate in the pressure region corresponding to the "intermediate" state of our plasmas, must therefore be operative. The mechanism suggested in ref 2 will now be discussed.

In order to simplify the problem, we shall make the assumption of a quasicontinuum of vibro-rotational levels of equal weight between the zero energy level and the dissociation limit of the molecule and write a Boltzmann distribution of the molecules among these levels.

As already mentioned in the Introduction, spectroscopic investigations of N_2 and $N_2 + H_2 + CH_4$ plasmas,⁵⁻⁷ operated at the power levels and in the pressure range of the present experiments, have shown the presence of Boltzmann distributions characterized by vibrational and rotational temperatures in the neighborhood of 4,000°K, while T_g never exceeded 2,000°K.

This distribution will be characterized by a unique vibro-

rotational temperature T_ξ :

$$d[H_2(\xi)]/[H_2] = \exp(-\xi/RT_\xi) d\xi/RT_\xi \quad (11)$$

where ξ is the energy of the level. One should now consider that dissociation can take place from any one of the vibro-rotationally excited levels. The rate of atom production from the set of excited molecules with energies between ξ and $\xi + d\xi$ will be given by

$$dV_D(\xi) = 2k_D(\xi)N d[H_2(\xi)] \quad (12)$$

If one makes use of the naive idea that the relative kinetic energy between the excited molecule and the third body must supply the energy difference between the dissociation energy D_{H_2} and the energy ξ of the vibro-rotational level, one writes

$$k_D(\xi) = k_D^0 \exp[-(D_{H_2} - \xi)/RT_g] \quad (13)$$

The overall rate of atom production is obtained by integration of eq 12 after substitution from eq 11 and 13, and, for T_ξ sufficiently higher than T_g , one has

$$V_D = k_D[H_2] = 2k_D^0 N[H_2] \times \int_0^{D_{H_2}} \exp[-(D_{H_2} - \xi)/RT_g] \exp(-\xi/RT_\xi) (d\xi/RT_\xi) = 2k_D^0 N[H_2] \left(\frac{T_g}{T_\xi - T_g} \right) \exp(-D_{H_2}/RT_\xi) \quad (14)$$

Equation 14 is essentially of the Arrhenius type, in which the gas temperature T_g has, however, been substituted by the characteristic temperature T_ξ , which defines the distribution function of the vibro-rotationally excited molecules. To a first approximation one could take for k_D^0 the appropriate crude collision value, i.e., one assumes that the collision diameter is independent of ξ . However, even on the basis of a purely collisional model, a change of k_D^0 with ξ is expected. In fact the bond length of H_2 in its ground vibrational state ($v = 0$) is 0.74 Å, whereas at $v = 14$ the bond length is about 3.5 Å. This would cause a tenfold increase between $k_D^0(v = 0)$ and $k_D^0(v = 14)$. k_D^0 should in any case be expressed as an increasing function of ξ . A convenient form is

$$k_D^0(\xi)/k_D^0(0) = \exp B\xi \quad (15)$$

Equation 13 then becomes

$$k_D(\xi) = 2k_D^0(0) \exp B\xi \exp[-(D_{H_2} - \xi)RT_g] \quad (16)$$

and eq 14 is transformed into

$$k_D[H_2] = 2k_D^0(0) \exp BD_{H_2} \exp(-D_{H_2}/RT_\xi) \times \left(\frac{T_g}{T_\xi - T_g + RBT_\xi T_g} \right) N[H_2] \quad (17)$$

The mechanism outlined above involves therefore, like a purely thermal mechanism, a bimolecular encounter between heavy particles, but takes into consideration the nonequilibrium distribution of the vibro-rotational levels. This distribution is characterized by a vibro-rotational temperature $T_\xi \gg T_g$. T_ξ will be a function of the effectiveness with which the field energy is transferred to vibrational and rotational modes. This, in turn, depends on the distribution of electron energies and on the functional relation between the cross sections for vibrational and rotational excitation and the electron energy.

The distribution function of the vibro-rotational energy will, eventually, be determined by the loss mechanism con-

nected with the transfer of vibrational and rotational energy to translational modes or to the reactor wall. These loss mechanisms are functions of the gas composition (H/H_2) and of the gas temperature T_g .

In order to calculate the rate of dissociation according to eq 17, one therefore needs the vibro-rotational temperature T_ξ and the constant B , which determines the dependence of the collision cross section on the vibro-rotational energy ξ . B is unfortunately unknown and T_ξ can not be derived, for H_2 , from simple spectroscopy measurements.

For an order of magnitude calculation, one can assign to B a value which makes the ratio $k_D^0(v=14)/k_D^0(v=0) \simeq 10$, according to crude collision theory. T_ξ can then be derived, by trial and error, from eq 17 by equating this expression to $k_v[H_2]$, where $k_v = k_D - k_e$.

k_v represents therefore the contribution of the vibro-rotational mechanism of dissociation to the overall dissociation constant k_I .

This calculation shows that T_ξ steadily decreases from about 3400°K, at 5 Torr, to about 3100°K, at 40 Torr, and therefore gives values of T_ξ which are reasonable for H_2 , under the discharge conditions prevailing in the experiments. T_ξ is lowered by only about 400°K, when the ratio $k_D^0(v=14)/k_D^0(v=0)$ is increased by a factor 10.

The fact that the vibro-rotational contribution to the mechanism of dissociation might become predominant, under the present experimental conditions, appears to be supported by the following considerations. In our experiments the characteristic energies of the electron, kT_e , range from 1 to 3 eV; cross sections for vibrational excitation are by far the largest of all inelastic collisions in hydrogen, in the range of electronic energies 0–10 eV.¹² The consequence is that the main fraction of the energy input to the gas is actually utilized for vibrational excitation.

Conclusions

Two points deserve further comments, one in connection with the use of eq 7, the other with the derivation of eq 17.

In view of the fact that eq 7 is utilized both in the theoretical calculation of α and in its derivation from the experimental data (eq 4 in conjunction with eq 3 of Appendix B), it might be questioned whether or not calculated and observed values of α will always be brought into coincidence by this procedure. In other words the coincidence might be a fictitious one. Let us consider, for simplicity, the situation for $\Phi \rightarrow 0$. For any value of $\langle W \rangle$ a value of α can be derived from the system of eq 1 and 3 of Appendix B, together with the corresponding value of T_g . On the other hand, the solution of the system of eq 4 and B3 yields the "experimental" values of α and T_g . These values can however coincide with the theoretical ones for a *unique value* only of the observable of eq 4. In conclusion, the reported agreement is real; when calculated and observed values of α and T_g coincide, within the already mentioned uncertainties, the procedure adopted is consistent and eq 7 acceptable ($p \geq 10$ Torr). The noncoincidence of observed and calculated values (e.g., at 5 Torr) implies, on the contrary, that $k_D[H_2] < 2\langle W \rangle / 104 \times 10^3$ and eq B1 and B2 must be modified consequently. The evaluation of α , T_g , and of the corresponding rate of dissociation becomes in this case quite involved and these quantities will depend on the particular model of the plasma utilized in the calculation.

In the type of plasma utilized in the present experiments, the fractional energy input to ionization, electronic excitation, or elastic collisions is below 1%. Use of eq 7

would therefore be entirely justified, in the absence of appreciable excitation of vibrational and rotational modes. In presence of v-r excitation, a fraction of the power might indeed be lost for the dissociation process, as a consequence of partial transfer of internal energy to the reactor walls.¹⁴ Use of eq 7 would in this case lead to calculated values of α higher than the observed ones. The situation at 5 Torr might indeed be attributed to wall losses; v-r energy transport is in fact favored by low pressures and by the radial expansion of the plasma column. At higher pressures, and with contracted plasma column, these losses are reduced and eq 7 apparently becomes a reasonable approximation to the actual rates of dissociation. The k_e/k_D ratios of Figure 10 should therefore be somewhat in defect at 5 Torr; however, the decrease of the contribution of k_e to k_D with increasing the pressure, flow rate, and with decreasing $\langle W \rangle$ is well outside the uncertainties involved in the estimate of the actual rates of dissociation.

It is worth mentioning, in this connection, that results very similar to those of Figure 10 have recently been obtained for CO_2 dissociation, under similar discharge conditions.¹⁵ Rates of CO_2 dissociation can be measured and a direct comparison between calculated and observed rates has been possible in this case.

The other point to be examined concerns our derivation of eq 17. The starting point is eq 11. A Boltzmann distribution has been assumed for the populations of vibrational and rotational levels, as suggested by previous spectroscopic measurements. For a non-Boltzmann distribution, eq 11 should evidently be substituted by the actual distribution; integration would then lead to a rate expression different from eq 17.

Equation 13 has been derived using a classical hard sphere collision approach: the relative kinetic energy of the colliding particles must provide the energy difference $D_{H_2} - \xi$. In the classical collision model the preexponential term cannot be evaluated a priori (steric factor P). In the present case the preexponential term contains a classical hard sphere $k_D^0(0)$ and the unknown dependence of this quantity on the vibrational level. The preexponential term does therefore contain our ignorance about the detailed mechanism of dissociation.

The problem of the a priori calculation of rates of thermal dissociation of diatomic molecules is a much more complex one. This problem has been tackled by a number of authors,^{16–20} with different approaches and partial success. It would however be well outside the scope of the present work to adapt these treatments to the complex situation of our plasma. The most that can be expected from eq 17 is to give a sufficiently correct functional dependence of the rate of dissociation on pressure and T_ξ . In the case of CO_2 dissociation, it can be shown¹⁵ that an increasing fraction of the energy pumped by the electric field into the vibrational system of this molecule is utilized for the dissociation process when the pressure is increased. This closely corresponds to the situation illustrated by Figure 10 and can be rationalized on the basis of eq 17.

Acknowledgment. The authors wish to thank Mr. V. Colaprico for his technical assistance.

Appendix A

The first-order rate constant k' accounts for the losses of H atoms by heterogeneous recombinations at the reactor walls and is given by

$$k' = (2/r_T)(k\delta)/(k + \delta) \quad (\text{A1})$$

where, $k = (1/4)v_H\gamma$, with v_H = random velocity of the hydrogen atoms at the gas temperature T_g and γ = the recombination coefficient of H on quartz, a function of the reactor wall temperature T_w . $\delta = \text{Sh } D_H/2r_T$, with Sh = Sherwood's number for cylindrical geometry, D_H = diffusion coefficient of hydrogen atoms in H-H₂ mixtures at T_g .

The term $(k\delta)/(k + \delta)$ represents the rate constant for a first-order heterogeneous recombination of atoms in the presence of limitation by diffusion.²¹ The dependence of the Sherwood's number on flow conditions is given by its functional dependence on the Schmidt and Reynold's numbers. Values of Sherwood's number for the flow conditions utilized in the experiments have been calculated according to ref 22. They range from 3.7, at low rates, to about 13, at the highest flow rates used in the experiments, and depend on whether the flow is laminar or plug. This leads to a significant variation in the values of k' , i.e., of atom losses at the reactor wall with the flow rate and type of flow.

The wall temperature has been evaluated as follows: if W_L (cal sec⁻¹) is the power collected by the cooling water within the discharge region of length L , one can write the following energy balance:

$$W_L = (\lambda_{qz}/d)(T_w - T_{H_2O})2\pi r_T L \quad (\text{A2})$$

with λ_{qz} (cal cm⁻¹ sec⁻¹ °K⁻¹) = thermal conductivity of quartz (3×10^3 as given by the manufacturer), and T_{H_2O} = temperature of the water in the calorimetric jacket. Values of γ as a function of wall temperature have been taken from ref 23, while values of D_H from ref 24.

Appendix B

When a steady state concentration of hydrogen atoms is reached within the reactor (small gas flow rates or high values of the axial length in the direction of the gas flow), either eq 5 or 6 take the form

$$2\langle W \rangle / 104 \times 10^3 = k_D [H_2] = k' [H] + k'' \{ (N - [H]) \} [H]^2 + k''' [H]^3 \quad (\text{B1})$$

All the quantities of eq B1 are rather complex functions of the gas temperature T_g and a second equation is therefore needed to sort out the two unknowns $[H]$ and T_g . The second equation can be derived from an energy balance, under steady state conditions. The power W_w transferred from the gas to the reactor walls, in any volume element within the reactor, is equal, at steady state, to the power received from the field W (eq 2 with $\Phi dH = 0$).

The power released by gas at the reactor walls is the sum of two terms: (a) the energy released by the heterogeneous recombination of the atoms; (b) the contribution of thermal conduction from the gas at T_g to the walls at T_w . One can therefore write

$$\langle W \rangle = \langle W_w \rangle = k' [H] 52 \times 10^3 + (2/r_T) h (T_g - T_w) \quad (\text{B2})$$

where $h = \text{Nu}\lambda/2r_T$, with Nu = Nusselt's number and λ (cal cm⁻¹ sec⁻¹ °K⁻¹) = thermal conductivity of the H-H₂ mixture at T_g .

The system of eq B1 and B2 can be solved, by trial and error procedures, and the values of $[H]$ and T_g derived as solution of this system. From (B1) and (B2) one obtains

$$52 \times 10^3 \{ k'' (N - [H]) [H]^2 + k''' [H]^3 \} = (2/r_T) h (T_g - T_w) \quad (\text{B3})$$

On the assumption that, at $l = l_0$, axial concentration profiles of $[H]$ are sufficiently flat, eq B3 can be utilized in connection with eq 4 to derive $\alpha(l_0)$ and $T_g(l_0)$ from the experimental data. The values of $\alpha(l_0)$ and $T_g(l_0)$ reported in Figures 7-9 have been obtained by this method. The problem becomes remarkably more complex if, instead of the steady state eq B1, the kinetic eq 5 or 6 have to be utilized in order to derive $[H]$ and T_g . This is, however, the problem which has to be solved in order to compare the experimental data with the values of $\alpha(l_0)$ derived from the theoretical model of the discharge. A concentration profile will develop along the reactor axis, together with the corresponding temperature profile and detailed calculation becomes very involved.

A reasonable approximation is to use eq 5 or 6 at the constant temperature, which is obtained by coupling one of these equations with the energy balance equation

$$\langle W \rangle = k' [H] 52 \times 10^3 + (2/r_T) h (T_g - T_w) + \langle \Phi H(l_0) \rangle \quad (\text{B4})$$

List of Symbols

d	= quartz tube thickness, cm
e	= electron charge
h	= heat transfer coefficient, cal sec ⁻¹ °K ⁻¹
k	= $(1/4)v_H\gamma$, cm sec ⁻¹ (see Appendix A)
k'	= first-order rate constant for heterogeneous recombination of atoms, sec ⁻¹
k''	= rate constant for homogeneous trimolecular recombination of atoms, cm ⁶ mol ⁻² sec ⁻¹
k'''	= rate constant for homogeneous triatomic recombination of atoms, cm ⁶ mol ⁻² sec ⁻¹
k_D^0	= Arrhenius preexponential factor according to crude collision theory, cm ³ mol ⁻¹ sec ⁻¹
k_D	= pseudo-first-order rate constant for hydrogen dissociation, sec ⁻¹
k_e'	= rate constant for direct electron impact dissociation, cm ³ sec ⁻¹
k_v	= $k_D - k_e$ (see text)
m_e	= electron mass, g
n_e	= electron concentration, cm ⁻³
r_T	= inner radius of the discharge reactor, cm
B	= constant which accounts for the dependence of the preexponential factor on the vibro-rotational energy
$\bar{c}_{p_{H_2, H}}$	= mean specific heat of H ₂ and H, respectively, cal mol ⁻¹ °K ⁻¹
D_{H_2}	= dissociation energy of H ₂ , cal mol ⁻¹
E	= electric field, V cm ⁻¹
I_p	= d.c. current intensity of the plate circuit, A
L	= electrode separation, including electrode height, cm
N	= total number of mole per unit volume, mol cm ⁻³
Nu	= Nusselt's number
P	= total pressure, atm
Sh	= Sherwood's number
T_e	= electron temperature, °K
T_g	= translational temperature
T_v	= vibro-rotational temperature, °K
T_{H_2O}	= temperature of the cooling water jacket, °K
T_w	= temperature of the reactor inner walls, °K
W	= electric power transferred to the gas, cal sec ⁻¹ or kW
$\langle W \rangle$	= power density, cal cm ⁻³ sec ⁻¹ , (= $W_T/\pi r_T^2 L$)
α	= degree of dissociation of H ₂

δ	= $ShD_H/2r_T$, cm sec^{-1} , (see Appendix A)
γ	= recombination coefficient of H atoms on quartz walls
ϵ	= electron energy, eV
ϵ_k	= characteristic energy of electrons, eV, ($= kT_e$)
λ_{qz}	= thermal conductivity of quartz, $\text{cal cm}^{-1} \text{sec}^{-1} \text{ } ^\circ\text{K}^{-1}$
λ	= thermal conductivity of H-H ₂ mixtures, $\text{cal cm}^{-1} \text{sec}^{-1} \text{ } ^\circ\text{K}^{-1}$
ν_m	= frequency of elastic collision of electrons, sec^{-1}
σ_D	= cross section for H ₂ dissociation by direct electron impact, cm^2
ω	= frequency of the electric field, sec^{-1}
Φ	= gas molar flow rate, mol sec^{-1}
l	= axial distance, cm
l_0	= distance which marks the beginning of the intense electric field, cm
H	= enthalpy of the discharged gas, referred to 1 mol of inlet gas, cal mol^{-1}
k	= Boltzmann constant, $\text{erg } ^\circ\text{K}^{-1} \text{ molecule}^{-1}$
D_H	= diffusion coefficient of hydrogen atoms in a mixture of H-H ₂ , $\text{cm}^2 \text{sec}^{-1}$

References and Notes

- (1) P. Capezzuto, F. Cramarossa, G. Ferraro, P. Maione, and E. Molinari, *Gazz. Chim. Ital.*, **103**, 1153 (1973) (English translation).
- (2) P. Capezzuto, F. Cramarossa, R. d'Agostino, and E. Molinari, *Gazz. Chim. Ital.*, **103**, 1169 (1973) (English translation).
- (3) P. Capezzuto, F. Cramarossa, P. Maione, and E. Molinari, *Gazz. Chim. Ital.*, **103**, 891 (1973) (English translation).
- (4) P. Capezzuto, F. Cramarossa, P. Maione, and E. Molinari, *Gazz. Chim. Ital.*, **104**, 1109 (1974) (English translation).
- (5) F. Cramarossa, G. Ferraro, and E. Molinari, *J. Quant. Spectrosc. Radiat. Transfer*, **14**, 419 (1974).
- (6) F. Cramarossa and G. Ferraro, *J. Quant. Spectrosc. Radiat. Transfer*, **14**, 159 (1974).
- (7) F. Cramarossa, G. Ferraro, and E. Molinari, manuscript in preparation.
- (8) E. Molinari, *Pure Appl. Chem.*, **39**, 343 (1974).
- (9) V. H. Shui, J. P. Appleton, and J. C. Keck, *Symp. (Intl.) Combust.*, [Proc.], **13th**, 21 (1971).
- (10) (a) "JANAF Tables of Thermochemical Data", The Dow Chemical Co, Midland, Mich., 1964; (b) M. Capitelli, E. Ficocelli, and E. Molinari, *Centro Studio Chimica Plasmica C.N.R.*, Bari, 1972.
- (11) A. T. Bell, *Ind. Eng. Chem., Fundam.*, **11**, 209 (1972).
- (12) H. S. W. Massey, "Electronic and Ionic Impact Phenomena", Vol. 2, Clarendon Press, Oxford, 1969.
- (13) G. Francis, "Ionization Phenomena in Gases", Butterworths, London, 1960.
- (14) A. Kh. Mnatsakanyan and G. V. Naidis, *Teplotiz. Vys. Temp.*, **11**, 932 (1973).
- (15) P. Capezzuto, F. Cramarossa, R. d'Agostino, and E. Molinari, to be submitted for publication.
- (16) D. L. S. Mc Elwain and H. O. Pritchard, *Symp. (Intl.) Combust.*, [Proc.], **13th**, 37 (1971); *J. Am. Chem. Soc.*, **92**, 5027 (1970).
- (17) V. H. Shui, J. P. Appleton, and J. C. Keck, *Symp. (Intl.) Combust.*, [Proc.], **13th**, 21 (1971).
- (18) L. S. Polak in "Reaction under Plasma Conditions", Vol. 2, M. Venugopalan, Ed., Wiley, New York N.Y., 1971, p 141.
- (19) H. S. Johnston and J. Birk, *Acc. Chem. Res.*, **5**, 327 (1972).
- (20) N. G. Valance and J. Lin, *Physica*, **52**, 620 (1971); J. Lin, *ibid.*, **62**, 369 (1972).
- (21) D. A. Frank-Kamanetskii, "Diffusion and Heat Transfer in Chemical Kinetics", Plenum Press, New York, N.Y., 1969.
- (22) C. O. Bennett and J. E. Myers, "Momentum Heat and Mass Transfer", McGraw-Hill, New York, N.Y., 1962.
- (23) B. J. Wood and H. Wise, *J. Phys. Chem.*, **66**, 1049 (1962).
- (24) J. T. Vanderslice, S. Weisman, E. A. Mason, and R. J. Fallon, *Phys. Fluids*, **5**, 155 (1962).

Primary Steps in the Reactions of Organic Disulfides with Hydroxyl Radicals in Aqueous Solution

M. Bonifačić, K. Schäfer, H. Möckel, and K.-D. Asmus*

Hahn-Meitner-Institut für Kernforschung Berlin GmbH, Bereich Strahlenchemie, 1 Berlin 39, West Germany (Received February 18, 1975)

Publication costs assisted by Hahn-Meitner-Institut Berlin GmbH

Interaction of hydroxyl radicals with the sulfur bridge of simple aliphatic disulfides leads to an electron transfer ($\text{RSSR}^{\cdot+} + \text{OH}^-$) or OH^{\cdot} attachment with about equal probability. $\text{RSSR}^{\cdot+}$ radical ions show optical absorption with $\lambda_{\text{max}} \approx 420 \text{ nm}$ and extinction coefficients of $\epsilon \approx 2 \times 10^3 \text{ M}^{-1} \text{ cm}^{-1}$. Chemically they act as oxidants in their reaction with $\text{Fe}(\text{CN})_6^{4-}$, $\text{Fe}_{\text{aq}}^{2+}$, RSOH , etc. The rate constants for electron transfer processes to $\text{RSSR}^{\cdot+}$, e.g., from $\text{Fe}_{\text{aq}}^{2+}$, and for the neutralization process $\text{RSSR}^{\cdot+} + \text{OH}^-$, seem to depend on the effective electron density at the sulfur bridge. In the absence of reducing agents the radical cations decay by a diffusion-controlled bimolecular process. The chemical fate of the OH^{\cdot} adduct radical depends on the pH of the solution and the structure of the aliphatic groups of the disulfide. In acid solution protons assist S-S bond breaking and rearrangement to thiols and RSO^{\cdot} radicals. The same products are formed in very basic solutions probably via SN2 substitution of RS^- by OH^- . In neutral solutions the formation of RS^{\cdot} radicals and sulfenic acid, RSOH , prevails. Noticeable yields of C-S bond rupture products have only been observed for the *tert*-butyl compound. This is indicated by the formation of isobutene and trisulfides.

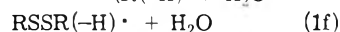
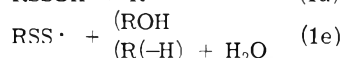
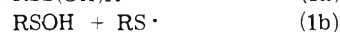
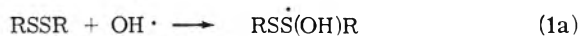
Introduction

Several studies have shown that ion pair formation plays an important role during the oxidation of sulfur containing organic compounds by hydroxyl radicals. From thioethers, for example, relatively long-lived $(\text{R}_2\text{S})_2^{\cdot+}$ radical ions were

observed.¹⁻³ $\text{RSSR}^{\cdot+}$ radical ions formed in the reaction of disulfides with OH^{\cdot} radicals were identified by means of pulse radiolysis conductivity experiments.⁴ The existence of these species was also indicated by steady-state γ radiolysis studies of aqueous solutions of various disulfides.⁵

Quantitative analysis of the pulse radiolysis conductivity

data showed that approximately half of the $\text{OH}\cdot$ radicals yielded transient $\text{RSSR}\cdot^+$ radical ions while the remainder apparently react via nonionic intermediates.⁴ Possible reaction routes include addition of the $\text{OH}\cdot$ radical to the sulfur bridge or a dissociative capture⁴⁻⁷



Some of the radicals could be identified directly by ESR experiments.^{7,8} $\text{RSO}\cdot$, for example, was found to be formed to a considerable extent in acid solutions ($\text{pH} < 6$),⁷ and trapping experiments indicated $\text{RS}\cdot$ radical formation particularly in neutral and slightly basic solutions.^{7,8} Radicals with unpaired spin located on carbon atoms, $\text{RSSR}(-\text{H})\cdot$, produced by hydrogen abstraction, could be observed during the oxidation of disulfides containing carboxyl groups.⁷ Cleavage of a C-S bond leading to $\text{RSS}\cdot$ radicals has been discussed in liquid phase photolysis of some compounds where the remaining alkyl fragment can be resonance stabilized (e.g., *tert*-butyl).^{9,10} The latter process could also be responsible for the formation of trisulfides which were found in the γ radiolysis of cystine and penicillamine solutions.^{6a,b} Other stable products identified in steady-state radiolysis of disulfide solutions were thiols and sulfonic acids.^{5,6}

The present work is concerned with physical and chemical properties of the $\text{RSSR}\cdot^+$ radical ions of some simple aliphatic disulfides (dimethyl-, diethyl-, diisopropyl-, and di-*tert*-butyl disulfide). In addition pulse radiolysis and γ radiolysis experiments were carried out to determine the yield of formation of stable products and the destruction of RSSR as a function of pH in order to establish an overall mechanism for the primary steps of disulfide oxidation.

Experimental Section

Commercially available disulfides were purified to >99% by fractional distillation. Nitrous oxide was bubbled through a freshly prepared Cr^{2+} solution to remove traces of oxygen. All other chemicals were of analytical grade and were used without further treatment.

Solutions were generally prepared from triply distilled, N_2O saturated ($2.6 \times 10^{-2} M$) water and up to $2 \times 10^{-3} M$ disulfide (the latter depending on solubility). Under these conditions all hydrated electrons generated simultaneously with $\text{OH}\cdot$ radicals during the irradiation are quantitatively converted to $\text{OH}\cdot$ radicals via $\text{N}_2\text{O} + e_{\text{aq}}^- \rightarrow \text{N}_2 + \text{OH}\cdot + \text{OH}^-$ prior to a possible reaction with RSSR .

The pulse radiolysis technique and the evaluation of the experimental data have already been described.¹¹ Experiments were carried out using electron pulses of 0.5–3- μsec duration from a 1.6-MeV Van de Graaff generator. The absorbed dose per microsecond pulse was ca. 700 rads which is equivalent to a yield of $4 \times 10^{-6} M$ $\text{OH}\cdot$ radicals (in N_2O saturated aqueous solutions 5.5 $\text{OH}\cdot$ radicals are formed per 100 eV absorbed energy).

The steady-state γ radiolysis experiments were carried out with a ^{60}Co source of ca. 1500 Ci and an absorbed dose rate of 1.2×10^5 rads/hr.

Quantitative analysis of thiols was achieved by either measuring the RS^- absorption in basic solutions (at a $\text{pH} >$

pK of RSH) spectrophotometrically on a Zeiss RPK 20A instrument or gas chromatographically. For the latter the RSH produced during the irradiation was extracted from the aqueous solution with small volumes of suitable organic solvents (CS_2 , CHCl_3 , CCl_4) and thereby concentrated by a factor of 20–40. The organic phase was then gas chromatographed on an SE 30, Porapak P-S, or Carbowax 20 M column, depending on the retention times of the components. The gas chromatograph used was a Varian 2860 with FID. The yield of disulfide destruction was determined in the same way. Neutral aqueous solutions could also be investigated by direct injection onto an SE 30 column. Isobutene was identified on a Porapak P-S column by comparison with an authentic sample. *tert*-Butyl trisulfide was analyzed on both an SE 30 and Carbowax 20 M and identified by comparison with a sample synthesized according to a procedure by Westlake, Laquer, and Smyth.²⁰ Further details of the analytical techniques are presented separately.¹²

All experiments refer to room temperature.

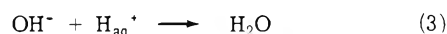
Results and Discussion

1. *Rate Constants for $\text{RSSR} + \text{OH}\cdot$.* The reaction of organic disulfides with hydroxyl radicals occurs essentially in diffusion-controlled processes. The respective values of $k(\text{OH}\cdot + \text{RSSR})$ for the disulfides investigated in this study are listed in Table I. The rate constant obtained by direct observation of the formation of one of several primary products, $\text{RSSR}\cdot^+$, was found to be identical with the overall rate constant derived from competition studies between RSSR and SCN^- for the $\text{OH}\cdot$ radical. As will be shown later only ca. half of the $\text{OH}\cdot$ radicals yield $\text{RSSR}\cdot^+$ while the remainder reacts via nonionic pathways. The results therefore indicate that the rate-determining step for the formation of the transient products is the primary interaction of the $\text{OH}\cdot$ radical with the disulfide.

2. *Optical Absorption of $\text{RSSR}\cdot^+$.* One of the important intermediates in the oxidation of simple aliphatic disulfides has been shown to be the radical cation which is formally produced by an electron transfer



This has been demonstrated by pulse radiolysis conductivity experiments.⁴ Figure 1a shows a typical conductivity-time trace from a pulsed, N_2O -saturated solution of $5 \times 10^{-4} M$ $(\text{C}_2\text{H}_5)_2\text{S}_2$ at pH 4.0. Under these conditions the reaction of the disulfide with $\text{OH}\cdot$ radicals is complete within the pulse (ca. 1 μsec). Immediately after the pulse a decrease in conductivity is observed. This is a result of reaction 2 and subsequent neutralization



i.e., of the effective replacement of a highly conducting proton by a less conducting disulfide radical cation (such conductivity-time curves and the corresponding kinetics have been discussed in a previous paper⁴).

Simultaneous tracing of the optical absorption at 420 nm as a function of time also indicates the formation of a transient species (Figure 1b). Its spectrum taken from the absorption immediately after the pulse (Figure 1c) has a maximum at 420 nm. Very similar results were obtained for the other three disulfides investigated in the present study. All of the 420-nm absorptions decay to their prepulse values.

Another optical absorption is generally found in the uv region around 300 nm. It is stable on the microsecond and

TABLE I: Rate Constants for the Reaction of Disulfides with Hydroxyl Radicals

RSSR	$k(\text{OH}\cdot + \text{RSSR}), M^{-1} \text{sec}^{-1}$
$(\text{CH}_3)_2\text{S}_2$	$(1.7 \pm 0.3) \times 10^{10}$
$(\text{C}_2\text{H}_5)_2\text{S}_2$	$(1.4 \pm 0.5) \times 10^{10}$
$(i\text{-C}_3\text{H}_7)_2\text{S}_2$	$(2.0 \pm 1.0) \times 10^{10}$
$(t\text{-C}_4\text{H}_9)_2\text{S}_2$	$(6.5 \pm 1.5) \times 10^9$

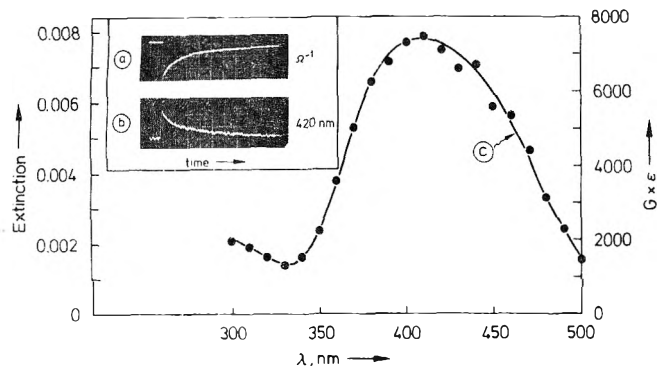


Figure 1. (a) Conductivity-time curve of a pulse-irradiated N_2O -saturated solution of $5 \times 10^{-4} M$ $(\text{C}_2\text{H}_5)_2\text{S}_2$ at pH 4; time scale 100 μsec /large division; dose 1000 rads. (b) Optical absorption-time curve at 420 nm: same solution, time scale: 50 μsec /large division. (c) Optical absorption spectrum of $(\text{C}_2\text{H}_5)_2\text{S}_2\cdot^+$.

millisecond time scale. No specific assignment was possible, however, since the absorption is very small and uncharacteristic.

The 420-nm absorption is assigned to the $\text{RSSR}\cdot^+$ radical ion on account of its kinetic similarity with the conductivity signal and on the basis of kinetic salt effect experiments. The rate of decay of the 420-nm absorption is influenced by the addition of high concentrations of a radiolytically inactive salt (0.3–0.5 M NaClO_4) at various pH values. In slightly acid solution where the decay is of second order (see below) the first half-life of the transient absorption decreases with increasing ionic strength (Table II) indicating a bimolecular reaction of two species with a charge of the same sign. In basic solutions the rate of decay becomes pseudo-first order, the half-life being dependent on the OH^- concentration. Addition of NaClO_4 now leads to an increase in $t_{1/2}$ as is expected for reaction of the OH^- ion with a positively charged species. A quantitative analysis of the kinetic salt effect is not planned owing to the complex nature of the overall oxidation mechanism (as will be discussed later). Qualitatively, however, the results clearly imply that the transient 420-nm absorption may be assigned to the $\text{RSSR}\cdot^+$ radical ion. It is interesting to note that this radical cation absorbs at nearly the same wavelength as the radical anion $\text{RSSR}\cdot^-$ which results from the one-electron reduction of disulfides.¹³

3. Yields. Absolute yields of $\text{RSSR}\cdot^+$ formed during the oxidation of disulfides have been determined by pulse radiolysis conductivity measurements.⁴ Table III contains values of $G(\text{RSSR}\cdot^+)$ and the corresponding fraction of $\text{OH}\cdot$ radicals leading to $\text{RSSR}\cdot^+$ for solutions of disulfide $>10^{-4} M$ at pH ≈ 4 . At this RSSR concentration scavenging of the hydroxyl radicals is complete, i.e., the yield of $\text{RSSR}\cdot^+$ as measured conductometrically and optically is independent of the solute concentration. For $(t\text{-Bu})_2\text{S}_2$

TABLE II: Effect of Ionic Strength on the Decay of the $\text{RSSR}\cdot^+$ Absorption at 420 nm in Acid and Basic Solutions^a

RSSR	$[\text{NaClO}_4], M$	pH	$t_{1/2, 420 \text{ nm}}, \mu\text{sec}$
$(\text{CH}_3)_2\text{S}_2$		4.2	50.6
	0.45	4.5	41.8
		9.2	10.6
$(\text{C}_2\text{H}_5)_2\text{S}_2$	0.35	9.2	21.6
		4.5	69.2
	0.42	4.8	58.0
$(i\text{-C}_3\text{H}_7)_2\text{S}_2$		9.0	24.5
	0.50	9.1	28.6
		4.1	71.5
$(t\text{-C}_4\text{H}_9)_2\text{S}_2$	0.43	4.2	62.5
		10.0	13.0
	0.45	10.0	24.3
		4.0	114.0
	0.45	4.2	85.0
		10.6	32.2
	0.45	10.7	50.5

^a $t_{1/2}$ taken at the same dose.

TABLE III: Yields, Wavelength of Maximum Absorption, and Maximum Extinction Coefficients of $\text{RSSR}\cdot^+$ Radical Ions

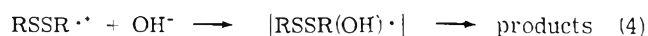
RSSR	$G(\text{RSSR}\cdot^+)$ ^a	% of $\text{OH}\cdot$	$\lambda_{\text{max, RSSR}\cdot^+}, \text{nm}$	$\epsilon_{\text{max, RSSR}\cdot^+}, M^{-1} \text{cm}^{-1}$
$(\text{CH}_3)_2\text{S}_2$	3.1	56	440	$(1.8 \pm 0.2) \times 10^3$
$(\text{C}_2\text{H}_5)_2\text{S}_2$	3.0	55	420	$(1.8 \pm 0.2) \times 10^3$
$(i\text{-C}_3\text{H}_7)_2\text{S}_2$	3.1	56	410	$(2.0 \pm 0.2) \times 10^3$
$(t\text{-C}_4\text{H}_9)_2\text{S}_2$	2.3 ^b	42 ^b	410	$(2.1 \pm 0.5) \times 10^3$

^a Determined by pulse radiolysis conductivity measurements. The yields given in ref 3 are somewhat lower since measurements were done at concentrations where $G(\text{RSSR}\cdot^+)$ was not yet independent of the disulfide concentration. ^b Measured at ca. $10^{-4} M$ $(t\text{-Bu})_2\text{S}_2$ (saturated solution).

complete scavenging of $\text{OH}\cdot$ radicals could not be achieved owing to the too low solubility ($\leq 10^{-4} M$). The concentration dependence of the radical cation yield is, however, similar to the other disulfides. It can thus be concluded that a similar fraction, about 55%, of the $\text{OH}\cdot$ radicals leads to $\text{RSSR}\cdot^+$ ions in the case of the *tert*-butyl compound also.

From the knowledge of the yields it is possible to calculate the extinction coefficients of $\text{RSSR}\cdot^+$ from the optical absorptions. The respective ϵ values together with the wavelengths of maximum absorptions of the $\text{RSSR}\cdot^+$ ions are also listed in Table III.

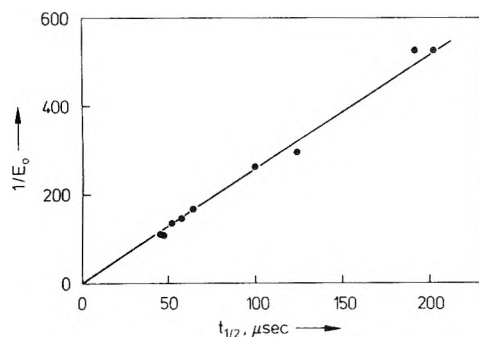
$G(\text{RSSR}\cdot^+)$ is found to be independent of pH in the acid and neutral range (corrections for the reaction $e_{\text{aq}}^- + \text{H}_{\text{aq}}^+$ which competes with $\text{N}_2\text{O} + e_{\text{aq}}^-$ at pH < 3 and leads to a decrease in $G(\text{OH}\cdot)$ have been taken into account). The observed decrease in G value with increasing OH^- ion concentration in basic solutions is attributed to the neutralization reaction



4. Decay Kinetics. The $\text{RSSR}\cdot^+$ radical ion decays by a second-order process in acid and neutral solution. This is demonstrated in Figure 2 where the reciprocal initial ex-

TABLE IV: Rate Constants for the Bimolecular Decay, the Neutralization, and Electron-Transfer Processes of $\text{RSSR}^{\cdot+}$

RSSR	$2k_2, M^{-1} \text{sec}^{-1}$	$k_{\text{RSSR}^{\cdot+} + \text{OH}^-}, M^{-1} \text{sec}^{-1}$	$k_{\text{Fe}(\text{CN})_6^{4-} + \text{RSSR}^{\cdot+}}, M^{-1} \text{sec}^{-1}$	$k_{\text{Fe}_{\text{aq}}^{2+} + \text{RSSR}^{\cdot+}}, M^{-1} \text{sec}^{-1}$
$(\text{CH}_3)_2\text{S}_2$	$(6.0 \pm 0.5) \times 10^9$	$(1.8 \pm 0.1) \times 10^9$	$(1.5 \pm 0.2) \times 10^{10}$	$(5.2 \pm 0.3) \times 10^6$
$(\text{C}_2\text{H}_5)_2\text{S}_2$	$(4.6 \pm 0.2) \times 10^9$	$(8.75 \pm 0.1) \times 10^8$	$(1.0 \pm 0.2) \times 10^{10}$	$(2.1 \pm 0.3) \times 10^6$
$(i\text{-C}_3\text{H}_7)_2\text{S}_2$	$(4.3 \pm 0.2) \times 10^9$	$(3.9 \pm 0.3) \times 10^8$	$(1.6 \pm 0.1) \times 10^{10}$	$(1.3 \pm 0.1) \times 10^6$
$(t\text{-C}_4\text{H}_9)_2\text{S}_2$	$(3.4 \pm 0.1) \times 10^9$	$\approx 3 \times 10^7$	$(1.2 \pm 0.2) \times 10^{10}$	$(5.4 \pm 0.6) \times 10^5$

**Figure 2.** Plot of reciprocal initial extinctions at 420 nm at various doses against first half-lives of $\text{RSSR}^{\cdot+}$. N_2O saturated $2 \times 10^{-4} M$ $(\text{C}_2\text{H}_5)_2\text{S}_2$, pH 4.05.

tinctions of the transient at 420 nm at various doses in N_2O -saturated solutions $2 \times 10^{-4} M$ $(\text{C}_2\text{H}_5)_2\text{S}_2$ (pH 4.05) are plotted against the corresponding first half-lives. The straight line obtained passes through the origin as is expected for a second-order process. Since the extinction coefficient is known (Table III), the bimolecular rate constant can be derived from the slope of this curve. The $2k_2$ values listed in Table IV indicate that the rates of reaction are essentially determined by the diffusion of the reactants. $2k_2$ is found to be independent of pH. One of the most probable processes responsible for the decay of the optical absorption is the disproportionation reaction of two radical cations

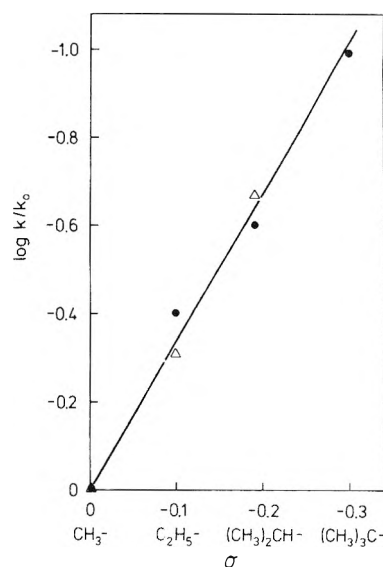


This process also explains the longer lifetime of the conductivity signal compared with the optical signal at 420 nm. Reaction 5 does not yield a noticeable change in conductivity since two singly charged ions are replaced by one doubly charged species. The decay of the conductivity signal is therefore not to be attributed to a reaction of $\text{RSSR}^{\cdot+}$ but to a secondary reaction of RSSR^{2+} .

In basic solution the half-life for the decay of the 420-nm absorption becomes increasingly shorter with increasing pH, and at $[\text{OH}^-] \gg [\text{RSSR}^{\cdot+}]$ the decay becomes pseudo-first order with $t_{1/2}$ decreasing proportionally with OH^- ion concentration. The rate constants for the neutralization (eq 4) are listed in Table IV.

It is interesting to note that k is generally lower than might be expected for a merely diffusion-controlled process. The highest value is found for the reaction of $(\text{CH}_3)_2\text{S}_2^{\cdot+}$ with OH^- and k then decreases for the ethyl, isopropyl, and *tert*-butyl radical cation.

Figure 3 (triangles) shows a plot of $\log k/k_0$ as a function of the Taft parameter σ .¹⁴ The term k_0 here represents the fastest rate constant, i.e., for the reaction of OH^- with the dimethyl radical cation, $(\text{CH}_3)_2\text{S}_2^{\cdot+}$, and σ describes the inductive +I effect of the aliphatic substituents R^{15} in the di-

**Figure 3.** Plot of $\log k/k_0$ vs. Taft's σ parameter: (Δ) $\text{RSSR}^{\cdot+} + \text{OH}^-$; (\bullet) $\text{Fe}_{\text{aq}}^{2+} + \text{RSSR}^{\cdot+}$.

sulfides. The obtained proportionality between $\log k/k_0$ and σ indicates that the rate constant for the neutralization of $\text{RSSR}^{\cdot+}$ by OH^- is to a certain extent controlled by the effective positive charge density at the sulfur bridge. Since the electron-donating effect increases from the methyl to the *tert*-butyl group ($\text{CH}_3 < \text{C}_2\text{H}_5 < (\text{CH}_3)_2\text{CH} < (\text{CH}_3)_3\text{C}$) the net positive charge is expected to be highest for the $(\text{CH}_3)_2\text{S}_2^{\cdot+}$ and lowest for the $((\text{CH}_3)_3\text{C})_2\text{S}_2^{\cdot+}$ radical ions. In addition structural effects may contribute to the observed changes in k , since steric hindrance also increases parallel to the inductive effect.

In agreement with these considerations the lowest value of k is found for the neutralization of the $(t\text{-Bu})_2\text{S}_2^{\cdot+}$ radical ion. The experimental value of $k \approx 3 \times 10^7 M^{-1} \text{sec}^{-1}$ ($\log k/k_0 = -1.78$) is, however, found to be three to four times smaller than would be expected from the Taft plot, but since the relatively slow neutralization process in this case is difficult to separate from the simultaneously occurring second-order decay, k could therefore not be determined with the same accuracy as for the other compounds.

5. Oxidation Reactions of $\text{RSSR}^{\cdot+}$. A number of radical cations from sulfur containing organic compounds, e.g., thioethers, were found to be oxidants.³ Similar properties have now been also observed for the $\text{RSSR}^{\cdot+}$ radical ions. For example, in γ -irradiated N_2O -saturated solutions of high concentrations of RSSR and comparatively low concentration of $\text{Fe}(\text{CN})_6^{4-}$ or Fe^{2+} , i.e., where the oxidizing OH^{\cdot} radicals quantitatively reacted with the disulfide, considerable yields of $\text{Fe}(\text{CN})_6^{3-}$ and Fe^{3+} could still be detected. This certainly suggests the formation of oxidants

other than OH· radicals in the irradiated solutions. Pulse radiolysis experiments directly show that RSSR·⁺ are involved in the electron transfer processes



Figure 4a shows the absorption-time curve at 420 nm from a pulsed N₂O-saturated solution of $1 \times 10^{-3} \text{ M}$ (C₂H₅)₂S₂ and $2 \times 10^{-5} \text{ M}$ Fe(CN)₆⁴⁻ (pH 4.4). The signal is seen to decrease to about half of its initial value which is expected if Fe(CN)₆⁴⁻ is oxidized only by RSSR·⁺. The extinction coefficient of Fe(CN)₆³⁻ at this wavelength ($\epsilon_{420} 1.025 \times 10^3 \text{ M}^{-1} \text{ cm}^{-1}$) is approximately half of that of RSSR·⁺. The decay kinetics are of pseudo-first order with the half-life linearly dependent on the Fe(CN)₆⁴⁻ concentration. The bimolecular rate constants for reaction 6 derived from these experiments are listed in Table IV. They indicate essentially diffusion-controlled electron transfer processes.

Figure 4b shows the decay of the 420-nm absorption of (CH₃)₂S₂⁺ in the presence of ferrous ions in a pulsed N₂O-saturated solution of $5 \times 10^{-3} \text{ M}$ (CH₃)₂S₂ and $6.4 \times 10^{-3} \text{ M}$ FeSO₄. (Since Fe²⁺ ions react fairly slowly with OH· radicals,¹⁶ $k = 3 \times 10^8 \text{ M}^{-1} \text{ sec}^{-1}$, the latter are quantitatively scavenged by the disulfide.) Simultaneous tracing at 305 nm (Figure 4c) shows a fast initial rise in absorption due to tailing of the RSSR·⁺ absorption at this wavelength followed by a slow increase showing the formation of Fe³⁺ ions in reaction 7 ($\epsilon_{\text{Fe}^{3+}, 305 \text{ nm}} 2201 \text{ M}^{-1} \text{ cm}^{-1}$). Both the decay at 420 nm and the slow increase at 305 nm are first-order processes, the half-life being inversely proportional to the Fe²⁺ concentration. The bimolecular rate constants thus derived for reaction 7 are also listed in Table IV.

It can be seen that the electron transfer process from Fe²⁺ to RSSR·⁺ is not diffusion controlled and further that the rate constants significantly decrease in going from the methyl to the *tert*-butyl compound. A similar dependence has been discussed already for the neutralization reaction RSSR·⁺ + OH⁻. Accordingly $\log k/k_0$ was plotted against Taft's σ values where k is the rate constant for RSSR·⁺ + Fe²⁺ and k_0 refers to the methyl compound. The linear relationship also obtained in this case (Figure 3, circles) indicates that the effective charge at the sulfur bridge of the radical cation is an important rate-controlling factor. As the electron density at the positive center increases from the methyl to the *tert*-butyl compound, the rate of electron transfer from Fe²⁺ to RSSR·⁺ is expected to decrease.

6. Formation of Thiols. One of the stable products which could be identified under certain conditions in irradiated aqueous solutions of disulfides were the corresponding thiols, RSH. They are detectable, however, only at low and high pH. The yields measured, for example, in γ -irradiated N₂O-saturated solutions of $4 \times 10^{-4} \text{ M}$ (C₂H₅)₂S₂ are shown in Figure 5 (circles). (The conversion of RSSR was kept to less than 10%.) Similarly no RSH is found in irradiated neutral solutions of diisopropyl and di-*tert*-butyl disulfide, whereas $G(i\text{-C}_3\text{H}_7\text{SH}) = 2.3$ (pH 0) and 3.5 (pH 13.5), and $G(t\text{-C}_4\text{H}_9\text{SH}) = 2.6$ (pH 0) and 1.5 (pH \approx 13) is measured for acid and basic solutions.

At high pH the formation of thiols could be observed directly by means of pulse radiolysis owing to the strong optical absorption of the stable RS⁻ ions in the uv. Figure 6, for example, shows the extinction at 245 nm for a pulse-irradiated N₂O-saturated solution of $2 \times 10^{-4} \text{ M}$ (*i*-C₃H₇)₂S₂ as a function of pH. Very similar curves are obtained for the other disulfides. The S-shaped curves seem essentially

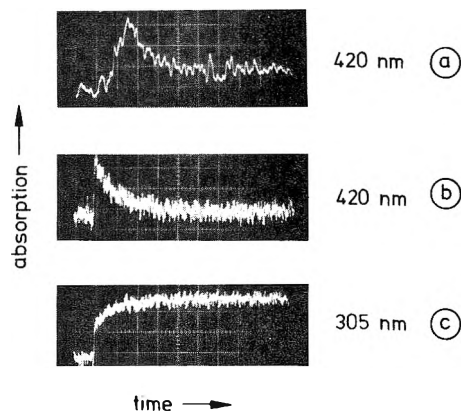


Figure 4. (a) Absorption-time curve at 420 nm of a pulsed N₂O saturated solution of $1 \times 10^{-3} \text{ M}$ (C₂H₅)₂S₂ and $2 \times 10^{-5} \text{ M}$ Fe(CN)₆⁴⁻ (pH 4.4); time scale 5 $\mu\text{sec}/\text{cm}$; dose 900 rads. (b) Absorption-time curve at 420 nm of a pulsed N₂O saturated solution of $5 \times 10^{-3} \text{ M}$ (C₂H₅)₂S₂ and $6.4 \times 10^{-3} \text{ M}$ FeSO₄ (pH 3.6); time scale 50 $\mu\text{sec}/\text{cm}$; dose 600 rads. (c) Absorption-time curve at 305 nm, same solution and conditions as b.

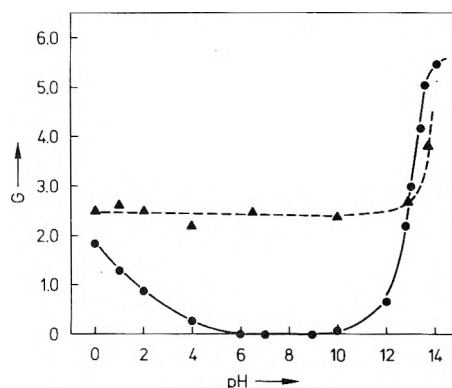


Figure 5. Yield of RSH formation (●) and RSSR destruction (▲) as function of pH in γ -irradiated N₂O-saturated solutions of $4 \times 10^{-4} \text{ M}$ (C₂H₅)₂S₂.

to describe the dissociation reaction



because the half-values at pH 10.7, 11.7, and 10.8 for (CH₃)₂S₂, (C₂H₅)₂S₂, and (*i*-C₃H₇)₂S₂, respectively, are in the same range as the pK values of RSH of 11.0, 10.6, and 10.7.¹⁷ Since in the γ -radiolysis experiments no significant thiol yields are detectable below pH 12 the pulse experiments suggest that thiols primarily formed at pH <12 might undergo secondary reactions. The experiments do not however allow a definite conclusion to be reached as to whether thiols are also formed at pH below their pK values, or direct reduction of disulfides to thiols is only possible where the thiol anion, RS⁻, is the stable form.

The rate constant for the thiol formation from (CH₃)₂S₂ was determined pulse radiolytically from the buildup of the 250-nm absorption (Figure 7a). The kinetics are found to be of pseudo-first order with the half-life of the formation decreasing linearly with increasing OH⁻ ion concentration. Figure 7b shows a plot of the apparent first-order rate constant as a function of [OH⁻]. The reaction involving the hydroxyl ion is attributed to the dissociative process



(RS(OH)₂· = hydrated RSO⁻). From the slope of Figure 7b

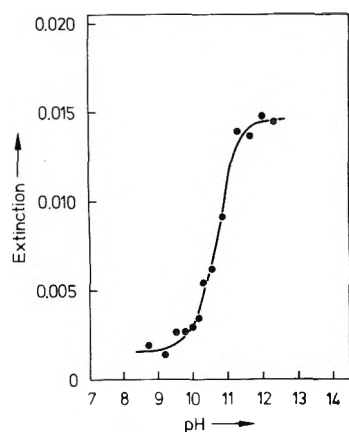


Figure 6. Extinction of RS^- at 245 nm (normalized to a dose of 1000 rads) as a function of pH from pulsed N_2O -saturated solutions of $2 \times 10^{-4} M$ ($i-C_3H_7$) $_2S_2$.

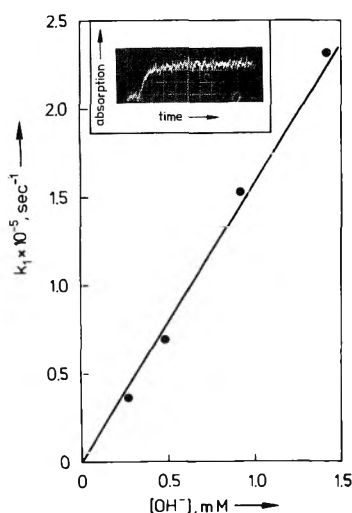
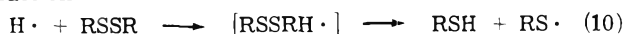


Figure 7. (a) Absorption-time curve at 250 nm of a pulsed N_2O -saturated solution of $2 \times 10^{-4} M$ $(CH_3)_2S_2$ at pH 10.7: time scale 20 $\mu sec/cm$; dose 950 rads. (b) First-order rate constant for the 250-nm buildup as a function of OH^- concentration.

the bimolecular rate constant $k_9 = (1.5 \pm 0.1) \times 10^8 M^{-1} sec^{-1}$ is derived.

The yields of RS^- calculated both from the γ and pulse experiments at high pH (13–14) correspond to $G(RS^-) = G(OH\cdot) = 5.5$, which means that the reaction of hydroxyl radicals, i.e., of O^- at this pH ($pK_{OH} = 11.9$) leads quantitatively to the formation of thiols. On the acid side similarly high yields could not be attained within the investigated range of $pH \geq 0$. The fact that e_{aq}^- in acid solutions reacts with H_{aq}^+ rather than N_2O thereby forming $H\cdot$ atoms should have no influence on the yield of RSH since the reaction



also leads to the production of thiols.¹⁸ The results shown in Figure 6 indicate that a plateau in $G(RSH)$ has not yet been reached at pH 0.

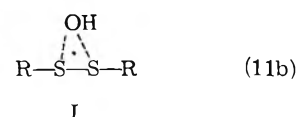
7. Destruction of Disulfides and Formation of Other Stable Products. The overall yield for the destruction of disulfides is shown for $(C_2H_5)_2S_2$ in Figure 5 (triangles). $G(-RSSR)$ is found to be essentially constant at $G = 2.4$. Since the disulfides are attacked by $OH\cdot$ radicals at a concentration corresponding to $G = 5.5$ this means that part of the $RSSR$ is regenerated during the overall process. Only at

high pH (>13) is the yield for $RSSR$ destruction seen to increase. Similarly $G(-RSSR) = 2.0$ is found for neutral solutions of $(i-C_3H_7)_2S_2$, and the yield is also increasing at $pH >13$.

A somewhat different mechanism seems to occur with the *tert*-butyl compound. $G(-RSSR) = 1.9$ is found without a noticeable change at high pH. In addition, appreciable yields of isobutene ($G \approx 0.8$) and trisulfides, $RSSSR$, $G(\approx 0.3)$ could be detected (neutral solution). For the other disulfides no pure hydrocarbons and sulfur compounds containing more than two sulfur atoms are formed.

8. Oxidation Mechanism. Considering the present results together with the previous findings by pulse radiolysis conductivity measurements⁴ and by ESR experiments⁷ it is evident that the oxidation of disulfides by hydroxyl radicals cannot be described by a simple reaction mechanism. At least some of the possible reaction pathways given in eq 1 a–f and 2 must occur simultaneously. Reactions 1d–f may, however, be excluded since no significant yields of aliphatic chains, alcohols, and olefins (except for the *tert*-butyl compound) could be detected, and no evidence also exists for a C-type radical.⁷

Looking at the remaining pathways, it appears that at least reactions 1b and 1c would require some activation energy since they involve bond breaking and rearrangement of atoms. The rate constant for the reaction of $RSSR$ with $OH\cdot$ radicals is found, however, to be in the range of a diffusion-controlled process. It is suggested therefore that the interaction of hydroxyl radical with the sulfur bridge leads to an electron transfer or $OH\cdot$ attachment



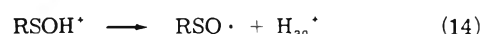
with about equal probability, independent of pH. Radical I, the existence of which is also suggested in the recent ESR study,⁷ would then break apart via two major routes



depending on the pH of the solution.

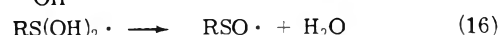
From the ESR and γ -radiolysis experiments it would appear that in neutral solution I primarily decays via reaction 12a leading to $RS\cdot$ radicals and sulfenic acid whereas in acid and basic solutions the decay to thiols, RSH , and $RSO\cdot$ radicals predominates.

The thiol formation in acid solution can be explained by a proton catalyzed decay of I:



The proton could interact with the free electron pair of the sulfur thereby assisting S–S bond breaking. $RSOH\cdot^+$ is a protonated $RSO\cdot$ radical and probably loses its proton immediately.

In basic solutions where thiol anions, RS^- , are stable the reaction



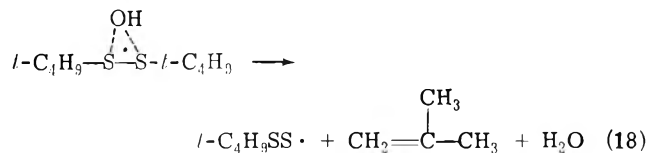
could easily occur via an SN2/substitution of RS⁻ by OH⁻.

At very high pH where O⁻ is the predominant form of the hydroxyl radical (pK_{OH} = 11.9) the RS⁻ formation might even occur via a dissociative capture



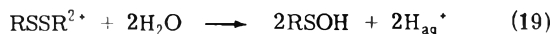
In the intermediate pH range the decay of I into RS⁻ radicals and sulfenic acid prevails (eq 11b and 12a).

In case of (*t*-C₄H₉)₂S₂ the relative stability of the *tert*-butyl fragment is thought to be responsible for the possibility of C-S bond rupture. The overall process



leads to the formation of isobutene and RSS⁻ radicals which then could combine with RS⁻ radicals to form trisulfides.

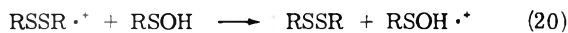
The fate of the radical cation RSSR^{·+} also depends on the pH of the solution. In the neutral and acid range disproportionation (eq 5) could primarily lead to a doubly charged ion which is likely to react with the solvent



to yield sulfenic acid and protons. The RSSR²⁺ might even break apart into two RS⁺ prior to reaction with water.

In basic solution RSSR^{·+} is neutralized by OH⁻ ions to form the hydroxyl addition radical I which then further decays.

Another reaction of RSSR^{·+} which has to be taken into account in the intermediate pH range is



followed by the deprotonation of RSOH^{·+} to RSO⁻. Several observations indicate such a reaction. (I) Sulfenic acid is known to be an efficient radical scavenger and to be easily oxidized,¹⁹ and RSSR^{·+} has now been established as an oxidant. (II) Both reactants (RSSR^{·+} and RSOH) are present at about equal concentration and the process is therefore expected to be of second order. In addition, reaction 20 would not show a kinetic salt effect. As mentioned earlier attempts to quantitatively analyze the ionic strength effect experiments failed on the basis of the RSSR^{·+} + RSSR^{·+} reaction (eq 5) alone. (III) Reaction 20 also leads to the desired liberation of one proton per RSSR^{·+} ion. (IV) It also explains the ESR finding that significant yields of RSO⁻ radicals are formed even in neutral solutions⁷ (where no RSH is detectable). In slightly basic solutions where RSSR^{·+} is neutralized and not available for reaction with RSOH, no RSO⁻ could be identified.

The yield of RSSR destruction shows that a considerable fraction of the disulfide initially attacked by the OH radical is regenerated during the overall process. This is

achieved via reactions 5 and 20, and by combination of RS⁻ radicals.

It must finally be pointed out, however, that the different decay modes of radical I in the various pH ranges cannot with certainty be considered as rigorously quantitative. Thus thiols might also be formed to a certain extent within the intermediate pH range without being detectable. RSH is known to undergo "repair" reactions with radicals, e.g.



and would also react with C radicals if the latter were formed. In addition thiols could be oxidized, e.g.



All these possible reactions are difficult to detect since they essentially lead to the regeneration of RSSR. Though reactions 11-20 best describe the experimental results they should therefore only be considered to represent the predominant pathways.

References and Notes

- (1) G. Meissner, A. Henglein, and G. Beck, *Z. Naturforsch. B*, **22**, 13 (1967).
- (2) (a) B. C. Gilbert, D. K. C. Hodgeman, and R. O. C. Norman, *J. Chem. Soc., Perkins Trans. 2*, 1748 (1973); (b) B. C. Gilbert, J. P. Larkin, and R. O. C. Norman, *ibid.*, 272 (1973).
- (3) M. Bonifačić, H. Möckel, D. Bahnmann, and K.-D. Asmus, *J. Chem. Soc., Perkins Trans. 2*, in press.
- (4) H. Möckel, M. Bonifačić, and K.-D. Asmus, *J. Phys. Chem.*, **78**, 282 (1974).
- (5) (a) T. C. Owen, A. C. Wilbraham, J. A. Roach, and D. R. Ellis, *Radiat. Res.*, **50**, 234 (1972); (b) T. C. Owen and A. C. Wilbraham, *ibid.*, **50**, 253 (1972); (c) T. C. Owen and D. R. Ellis, *ibid.*, **53**, 24 (1973).
- (6) (a) J. W. Purdie, *J. Am. Chem. Soc.*, **89**, 226 (1967); (b) *Can. J. Chem.*, **47**, 1029 (1969); (c) *ibid.*, **47**, 1037 (1969); (d) *ibid.*, **49**, 725 (1971).
- (7) B. C. Gilbert, H. A. H. Laue, R. O. C. Norman, and R. C. Sealy, *J. Chem. Soc., Perkins Trans. 2*, submitted for publication.
- (8) W. A. Armstrong and W. G. Humphreys, *Can. J. Chem.*, **45**, 2589 (1967).
- (9) D. Grant and J. Van Wazer, *J. Am. Chem. Soc.*, **86**, 3012 (1964).
- (10) G. W. Byers, H. Gruen, H. G. Giles, H. N. Scott, and J. A. Kampmeier, *J. Am. Chem. Soc.*, **94**, 1016 (1972).
- (11) (a) A. Henglein, *Allg. Prakt. Chem.*, **17**, 296 (1966); (b) G. Beck, *Int. J. Radiat. Phys. Chem.*, **1**, 361 (1969); (c) K.-D. Asmus, *ibid.*, **4**, 417 (1972).
- (12) J. Beyrich and H. Möckel, to be submitted for publication.
- (13) (a) G. E. Adams, G. S. McNaughton, and B. D. Michael in "Excitation and Ionization", G. Scholes and G. R. A. Johnson, Ed., Taylor and Francis, London, 1967; (b) M. Z. Hoffman and E. Hayon, *J. Am. Chem. Soc.*, **94**, 7950 (1972).
- (14) (a) R. W. Taft, Jr., *J. Am. Chem. Soc.*, **74**, 2729, 3120 (1952); **75**, 4231 (1953); (b) E. S. Gould in "Mechanismus und Struktur in der organischen Chemie", Verlag Chemie, Weinheim, 1962.
- (15) The σ values quoted here refer to the effect of only a single aliphatic group. It might be expected, however, that the effect of two R groups only differs by a constant factor.
- (16) See L. M. Dorfman and G. E. Adams, *Natl. Stand. Ref. Data Ser., Natl. Bur. Stand.*, No. 46, (1973), and references cited therein.
- (17) (a) W. Karmann, A. Granzow, G. Meissner, and A. Henglein, *Int. J. Radiat. Phys. Chem.*, **1**, 395 (1969); (b) J. P. Danehy and C. J. Noel, *J. Am. Chem. Soc.*, **82**, 2511 (1960); (c) M. M. Kreevoy, E. T. Harper, R. E. Duvell, H. S. Wilgus, and L. T. Ditsch, *ibid.*, **82**, 4899 (1960).
- (18) M. Z. Hoffman and E. Hayon, *J. Am. Chem. Soc.*, **94**, 7950 (1972).
- (19) (a) P. Koelewijn and H. Berger, *Recl. Trav. Chim. Pay-Bas*, **91**, 1275 (1972); (b) N. Kharasch, S. J. Potempa, and H. L. Wehrmeister, *Chem. Rev.*, **39**, 269 (1946).
- (20) H. E. Westlake, Jr., H. L. Laquer, and C. P. Smyth, *J. Am. Chem. Soc.*, **72**, 436 (1950).

One-Electron Transfer Equilibria and Redox Potentials of Radicals Studied by Pulse Radiolysis¹

Dan Meisel*

Radiation Research Laboratories and Department of Chemistry, Mellon Institute of Science, Carnegie-Mellon University, Pittsburgh, Pennsylvania 15213

and Gideon Czapski

Department of Physical Chemistry, The Hebrew University, Jerusalem, Israel (Received December 16, 1974)

Publication costs assisted by Carnegie-Mellon University and the U.S. Atomic Energy Commission

The pulse radiolysis technique is utilized for measurements of the equilibrium constants for electron transfer between the durosemiquinone radical anion and oxygen, menadione, and indigodisulfonate. These equilibrium constants are in turn used for calculations of one-electron redox potentials for these systems. Each of these equilibrium constants was determined experimentally and independently and found to be self-consistent. Only for the reactions of the semiquinone radical ions with oxygen could the electron transfer reaction be followed directly. For the reactions between the various quinone-semiquinone systems substantial indirect evidence is presented that these equilibria are achieved rapidly. In those cases equilibrium constants were determined from studies of the effect of quinone concentrations on the relative yields of the semiquinones. A method for distinguishing between kinetic competition and equilibrium is outlined and its usefulness is emphasized. The DQ|DQ⁻ (DQ = duroquinone) and IDS|IDS⁻ (IDS = indigodisulfonate) systems were employed as reference couples as the redox potentials for these systems are either available in the literature (IDS|IDS⁻) or may be calculated from available data (DQ|DQ⁻). Taking E_7^1 , the redox potential for the first one-electron reduction step at pH 7, of DQ|DQ⁻ as -0.235 V or of IDS|IDS⁻ as -0.247 V both yield $E_7^1 = -0.325$ V for the O₂|O₂⁻ system (1 atm of O₂) and $E_7^1 = -0.20$ V for the menadione system.

Introduction

The experimental determination of redox potentials of short-lived radicals has been the aim of considerable effort ever since Michaelis^{2a} presented his approach to the problem of two consecutive single steps of electron transfer redox reactions. The conventional potentiometric titration technique may be used for calculating such redox potentials provided that the buildup of the intermediates formed during the titration is sufficiently high to affect the titration curve. This technique has been used to calculate the one-electron redox potentials for several systems using the procedure suggested by Michaelis^{2a} or Elema.^{2b} For most of these systems (cf. ref 3 and references cited therein) the effect of the semiquinonoidic form on the titration curve was observed only at highly acidic or highly basic aqueous solutions. Half-wave potentials for many quinone|semiquinone systems were measured by polarography in aprotic solvents⁴⁻⁸ where the semiquinone is rather stable. In such aprotic solvents O₂⁻ is also very long lived and Peover⁹ was able to measure the half-wave potential of the O₂|O₂⁻ system. It was shown that the energy of the first unoccupied orbital as well as solvation energy are major factors affecting the redox potentials of these systems.^{6,10}

In spite of the wealth of information regarding these potentials in aprotic solvents, very few measurements have been performed in aqueous solutions at near neutral pH. This, undoubtedly, is the result of the short lifetimes of the radicals in aqueous solutions. Results from the polarographic pulse radiolysis technique¹¹ are in certain instances indicative of the electrochemical behavior of short-lived radicals but the irreversible nature of the polarographic

waves in the short time range limits its usage. The work of Patel and Willson¹⁴ established the existence of equilibrium between some semiquinone radical ions and O₂ but no redox potentials were calculated since appropriate reference one-electron redox potentials were not available.

In this study we have tried to establish a method for measuring single electron redox potentials for several quinones and for the O₂|O₂⁻ systems. Under all conditions used in this study all the semiquinone radicals were found to transfer an electron to oxygen.

Experimental Section

The computer-controlled pulse radiolysis facilities of the Radiation Research Laboratories of the Carnegie-Mellon University²⁹ were used in this study. The solutions flowed through either a 2-cm or a 0.5-cm optical-path Spectrosil cell, the latter being used for solutions containing the highly absorbing indigodisulfonate dye. It was verified by changing both the flow rate and the rate of pulsing of the Van de Graaff that no observable accumulation of radiation products or depletion in the original solutes occurred. By inserting light filters in the light path it was verified that no appreciable photochemical reactions occurred as the result of irradiation by the pulsed 450-W Osram Xe lamp. For time scales longer than 0.4 msec the unpulsed mode of the lamp was used. No effect of the lamp pulsing on yields and kinetics was observed in the entire time range.

The 2.8-MeV electron pulses of 0.5–1.5- μ sec pulse width from the Van de Graaff gave total concentration of radicals of 0.5–2 μ M. The total yield of the radicals never exceeded

10% of the lowest concentration of the solutes used. However, initial concentrations of solutes were corrected for depletion due to their reaction with the radicals whenever this effect exceeded 3%. No difficulties were encountered in measuring yields of radicals with $G\epsilon = 3.5 \times 10^3 \text{ mol}/100 \text{ eV } M^{-1} \text{ cm}^{-1}$, using the computer averaging option. The secondary emission dose monitor was calibrated against N_2O saturated 10^{-2} M KSCN solution assuming $G(\text{SCN}_2^-) = 6.0 \text{ molecules}/100 \text{ eV}$ and $\epsilon_{480}(\text{SCN}_2^-) = 7600 \text{ M}^{-1} \text{ cm}^{-1}$. Kinetic analysis was carried out on a 9830A Hewlett-Packard calculator using a least-squares best fit program.

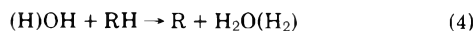
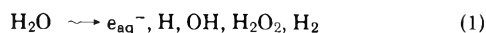
When 2-propanol was used as OH and H scavenger $G_{\text{red.}} = 6.2$ was assumed, allowing for 10% yield of the relatively unreactive $\text{CH}_2\text{CHOHCH}_3$. When HCO_2^- replaced 2-propanol $G_{\text{red.}} = 6.6$ was assumed. The use of the alcohol greatly accelerated the solution of the quinones but might complicate the analysis of the results due to formation of alcoholic peroxy radicals. Therefore, 2-propanol was used in all deaerated solutions while HCO_2^- was used whenever oxygen was present.

All substances used were of the highest commercially available purity. Freshly prepared solutions were flushed with the desired gas for at least 15 min. Extra pure nitrogen was used for deaeration. Four different oxygen-nitrogen mixtures were used: 0.96%, 9.6%, dry air, and 100% oxygen. The concentration of O_2 in saturated solutions under 1 atm of O_2 was taken as $1.25 \times 10^{-3} \text{ M}$ and Henry's law was assumed. Water was distilled and the vapor passed with oxygen through a silica oven. Solutions were buffered to pH 7 using 5 mM phosphate unless otherwise stated. Extinction coefficients were corrected for loss of absorption by the parent substrate.

The ^{60}Co γ source (Gammacell 220) has a dose rate of $6.7 \times 10^{17} \text{ eV } g^{-1} \text{ min}^{-1}$ and samples were irradiated for 1 min in a specially designed cell which enables deaerated solutions to be measured in the Cary 13 spectrophotometer several minutes after irradiation. The in situ radiolysis ESR technique was described in great detail.³⁰

Results and Discussion

A. Characterization of the Radicals. Two semiquinone radical ions and one quinoidic dye were tested for their possible electron transfer to oxygen. These were the semiquinones of duroquinone (DQ^-), menadione (MQ^-), and indigodisulfonate (IDS^-). On irradiating deaerated solutions containing 10^{-2} M of OH and H scavengers (HCO_2^- or 2-propanol designated RH) and 10^{-4} M of the quinone, the spectrum observed is that of the corresponding semiquinone radical ion which is formed by the sequence of reactions 1–5. Reactions 1–4 are completed at the end of



the pulse under our experimental conditions. The rate of reaction 5 was measured previously^{14–16} for both CO_2^- and $(\text{CH}_3)_2\text{COH}$ radicals. This reaction is over in less than 10 μsec under our experimental conditions. The spectra of DQ^- and MQ^- radicals were observed in the present study (Figures 1a and 1b); and are very similar to those obtained

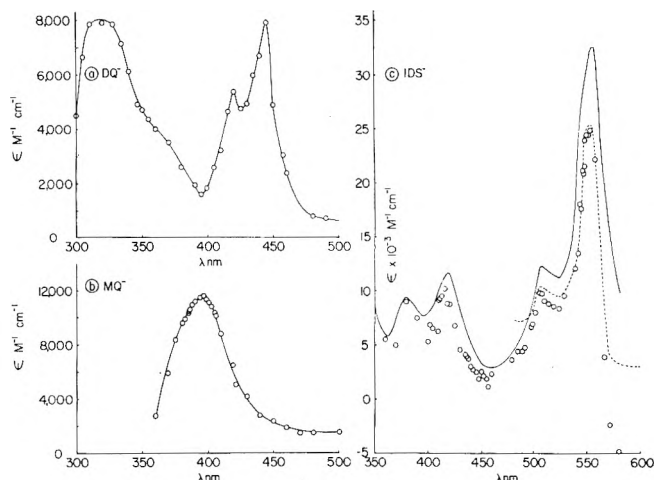


Figure 1. Optical spectra of the semiquinones used in this study obtained on pulse irradiation of deaerated solutions at pH 7 containing 10^{-2} M NaHCO_2 and (a) 10^{-4} M DQ^- , (b) 10^{-4} M MQ^- , (c) $5 \times 10^{-5} \text{ M}$ IDS^- (1- μsec pulse, $\sim 0.3 \text{ krad}$). Points in c are observed extinction coefficients; solid line shows ϵ corrected for bleaching of the dye; dashed line is ΔOD obtained in the ^{60}Co γ source experiment at pH 11.8 normalized at $\lambda 555 \text{ nm}$.

by Patel and Willson.¹⁴ At pH 7 equilibrium 3 is shifted to the right, i.e., both MQH and DQH are fully ionized.

The spectrum for IDS^- is shown in Figure 1c. The points in this figure give the observed spectrum. Correction for the loss of the parent dye gives the solid line shown in that figure. When the same solution at pH 11.8 (phosphate-NaOH buffer) was irradiated in a ^{60}Co γ source the blue color of the oxidized form nearly entirely disappeared and the solution turned red. That red color persisted for several hours. No attempt was made to calculate the extinction coefficient of the absorbing red intermediate since the various acid-base forms of both the oxidized and fully reduced forms along with the various oxidation-reduction equilibria considerably complicate such a calculation. However, the shape of the spectrum in the region where such complications are relatively small is shown by the dashed line in Figure 1c to closely resemble that of the spectrum obtained by pulse radiolysis.

The ESR spectra for DQ^- and MQ^- radicals obtained by the in situ radiolysis technique using similar solutions to those employed in the pulse experiments are shown in Figures 2a and 2d. The one for IDS^- is shown in Figure 2e. Unfortunately too many line overlaps render any detailed analysis of the IDS^- spectrum impractical. The same ESR spectrum for IDS^- was obtained several minutes after irradiation at pH 11.8. This finding, combined with the data presented by Preisler et al.,¹⁷ undoubtedly indicates that the red intermediate observed on reductive titration¹⁸ of the indigodisulfonate dye in the pH range of 11–12.5 is the semiquinone of that dye, identical with the one observed by pulse radiolysis. The optical characteristics and the ESR parameters for these semiquinones are given in Table I. References are cited therein for comparison purposes. The g factor and hyperfine splittings of DQ^- are similar to those reported previously¹⁹ in alkaline alcohol media. The assignment of the splitting for MQ^- may be compared to those reported for naphthosemiquinone.²⁰ The nonequivalency of the protons at positions 5, 6, 7, and 8 was enough to cause line broadening but resolution under our experimental conditions was not enough to obtain the different splittings.

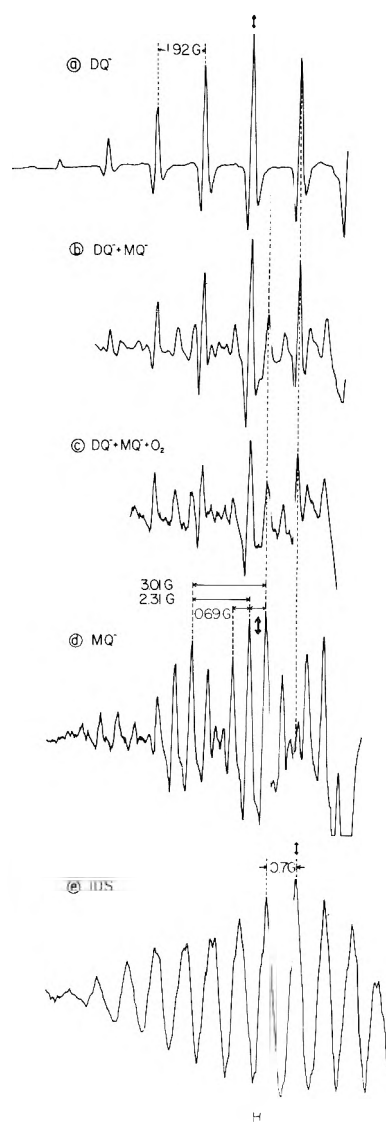
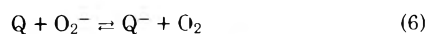


Figure 2. ESR spectra of the semiquinones used obtained on irradiations of solutions containing 10^{-2} M NaHCO₂ and (a) 10^{-4} M DQ, pH 7, deaerated; (b) 10^{-4} M DQ + 10^{-4} M MQ, pH 7 deaerated; (c) same as in b + 1.2×10^{-4} M O₂; (d) 10^{-4} M MQ, pH 7, deaerated; (e) 10^{-4} M IDS, pH 11.8, deaerated. The double arrows indicate the spectra center. Dashed lines represent the ESR lines where $[DQ^{\bullet}]/[MQ^{\bullet}]$ could be estimated. The right end of the figures was limited by the silica signal.

B. Electron Transfer from Q⁻ to Oxygen. On saturating solutions of 10^{-4} M Q and 10^{-2} M NaHCO₂ with 9.6% O₂ in N₂, absorption of the semiquinone radical ion decayed in a first-order reaction which was at least an order of magnitude faster than that observed in the absence of O₂. Such an example is shown in the computer processed oscillogram presented in Figure 3. This decay is attributed to the relaxation of reaction 6 toward equilibrium. The competition of



O₂ for the primary radicals, e_{aq}⁻ and CO₂⁻ in our case, was reflected in the decrease of the initial absorption of Q⁻ as compared to its initial absorption in the absence of O₂. Since reactions 7 and 8 as well as 1-5 are completed before

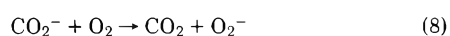


TABLE I: Optical and ESR Characteristics of the Semiquinone Radicals Examined in this Study

Q ⁻	λ_{max} , nm	ϵ_{max} , M ⁻¹ cm ⁻¹	g factor	Hyperfine splitting constants
DQ ⁻	445 (440 ^a)	7.5×10^3 (7.6×10^3 ^a)	2.00438 (2.0055 ^c)	$a_{(CH_3)}^H = 1.92$ G (1.987 G ^c)
MQ ⁻	395 (390 ^a)	1.19×10^4 (1.25×10^4 ^a)	2.00416	$a_{CH_3}^H = 3.01$ G $a_3^H = 2.31$ G $a_5^H = a_6^H = a_7^H = a_8^H = 0.69$ G
IDS ⁻	555 (555 ^b)	3.3×10^4	2.0039	~0.7 G (unassigned)

^a Reference 14. ^b Reference 17. ^c Reference 19.

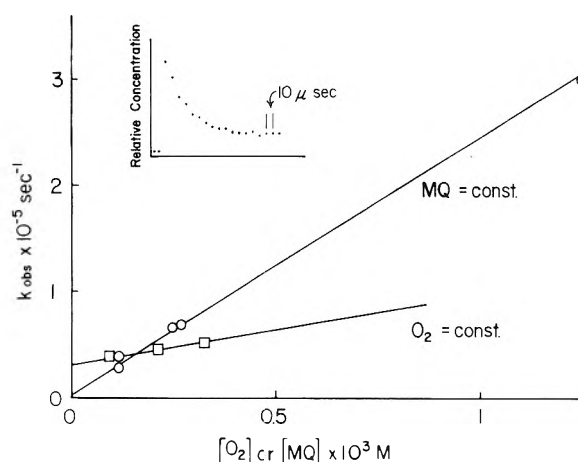


Figure 3. Kinetics of the reaction of MQ⁻ + O₂ solutions of 10^{-2} M NaHCO₂ at pH 7 and (O) [MQ] = 10^{-4} M = constant, (□) [O₂] = 1.2×10^{-4} M = constant. Insert shows computer processed oscillogram for the decay of MQ⁻ in solutions of 10^{-4} M MQ + 10^{-2} M NaHCO₂ at pH 7, saturated with 9.6% O₂ in N₂. 10 μsec per point.

any appreciable decay of Q⁻ takes place, these reactions should not affect the equilibrium concentration of the radicals. The only reaction of Q⁻ under our experimental conditions is the electron transfer to oxygen (reaction 6). This is evident from the findings that the residual absorption spectra and the ESR lines observed at the end of their decay in the presence of oxygen are the same as those obtained in the absence of oxygen. Furthermore, the quantitative analysis of kinetics and yields, presented later, is in accordance with the assumption that equilibrium 6 is achieved. Similar conclusions were derived by Patel and Willson.¹⁴

The independence of the observed first-order rate constant, k_{obsd} , for the decay of Q⁻, on dose in the range of 0.2-2 krad, and its dependence on both [Q] and [O₂] (cf. Figure 3), are in agreement with equation 9, which is as ex-

$$k_{obsd} = k_6[Q] + k_{-6}[O_2] \quad (9)$$

pected from reaction 6. Due to the low value of k_6 , its determination from Figure 3 is liable to have a large experimental error.

The equilibrium constant, K_6 , was determined from the residual absorption of the semiquinone radical ion assuming

$$\frac{[Q^-]_{eq}}{[O_2^-]_{eq}} = \frac{A_{eq}}{A_0 - A_{eq}} \quad (10)$$

Since

$$[O_2^-]_{eq} = [Q^-]_0 - [Q^-]_{eq} \quad (11)$$

where A is the absorbance and the indexes 0 and eq represent $[O_2] = 0$ and equilibrium conditions, respectively.

The equilibrium constants along with the rate constants involved are summarized in Table II. Each of these equilibrium constants was calculated from three different concentrations of oxygen and two of Q . Our value for K_6 for DQ^-/O_2 is twice that determined previously.¹⁴ The high concentration of alcohol and acetone present in the previous study might have caused this difference either by direct effect on the free energy of reaction 6 or by interference of the reaction of the alcoholic radicals with oxygen.

The electron transfer rate from IDS^- to oxygen was slower than that of the other semiquinones. Higher $[O_2]$ were thus necessary in order to achieve equilibrium 6. This forced us also to increase the concentration of the dye thus reducing the sensitivity of our measurements, as the dye itself strongly absorbs at the same region where the semiquinone does. However, using 10^{-4} M indigodisulfonate and two concentrations of oxygen (1.2×10^{-4} and 2.5×10^{-4} M) we could estimate K_6 for this system by measuring the equilibrium of IDS^- at λ 415 nm ($\Delta\epsilon = 9000$ M⁻¹ cm⁻¹).

C. Equilibrium between the Quinones-Semiquinones Systems. The equilibrium reaction between duroquinone and menadione and their semiquinone radical ions was measured in deaerated solutions containing 0.1 M 2-propanol



The effect of the quinones concentration on the semiquinones yield was studied by following the absorption at both 395 and 440 nm. The absorption at 395 nm increased on increasing $[MQ]$ and holding $[DQ]$ constant, while the absorption at 440 nm decreased (Figure 4a). The reverse behavior was found when $[MQ]$ was kept constant and $[DQ]$ was changed. No transfer reaction from one semiquinone radical ion to the other quinone could be observed directly.

Two possible assumptions may explain these results: (i) a kinetic competition between the two quinones for the primary radicals (e_{aq}^- and $(CH_3)_2\dot{C}OH$); (ii) the $[Q]$ effect on equilibrium 12 which is rapidly achieved.

If assumption i is valid reaction 12 must be so slow to reach equilibrium, that the radicals decay beforehand. If, on the other hand, assumption ii is correct the fact that no electron transfer could be detected must mean that either reaction 12 is very fast or the value of K_{12} is very similar to the ratio of the rate constants for the competition between the two quinones on the primary radicals. The results presented hereafter indicate that assumption ii is the correct one and that equilibrium 12 is rapidly achieved.

In case that the curves in Figure 4a represent equilibrium state eq 13 should hold

$$\frac{1}{A_{eq} - A_j} = \left(1 + K_{12} \frac{[DQ]}{[MQ]}\right) \frac{1}{A_i - A_j} \quad (13)$$

where A_j and A_i are the absorbances of semiquinone j or i in the absence of the other and A_{eq} is the absorbance of both semiquinone radical ions at equilibrium. Equation 13 assumes that under conditions of full scavenging of the primary radicals $[Q^-]_i + [Q^-]_j$ is constant and that the Beer-Lambert law is obeyed. No complexation of any of the species involved is expected under the concentrations used in this study as was verified for the DQ^{21} and IDS^{17} sys-

TABLE II: Equilibrium and Rate Constants Determined Experimentally in this Study (all Values at pH 7)

	DQ	MQ	IDS
K_6	4.6×10^{-2a} (2.3×10^{-2c})	0.16^a	2.9×10^{-2a}
$k_6, M^{-1} sec^{-1}$	1.0×10^{7a}	3.8×10^{7a}	9×10^{5a}
$k_{-6}, M^{-1} sec^{-1}$	2.2×10^{8b}	2.4×10^{8b}	3×10^{7b}
K_{12}	0.32^a $\left(\frac{K_6(DQ)}{K_6(MQ)} = 0.29\right)$		
K_{14}			1.8^a $\left(\frac{K_6(DQ)}{K_6(IDS)} = 1.6\right)$

^a Experimentally determined. ^b Calculated from K_6 and k_6 .
^c Reference 14.

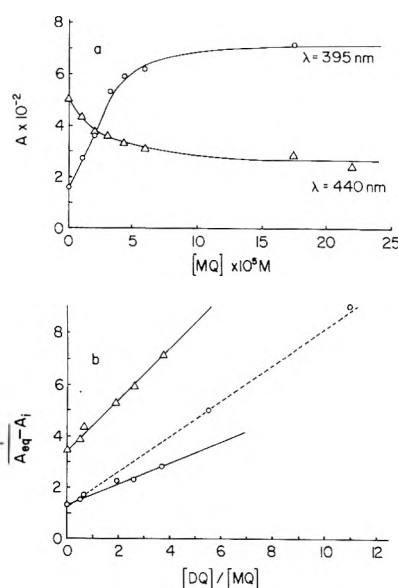
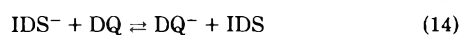


Figure 4. MQ^- and DQ^- yields in deaerated solutions containing 0.1 M *i*-PrOH at pH 7. $[DQ] = 1 \times 10^{-4}$ M = constant, $[MQ]$ variable: (a) absorption vs. $[MQ]$ at λ 395 and 440 nm; (b) equilibrium constant derivation according to eq 13. The dashed line in b represents incomplete equilibrium.

tems. Figure 4b shows that the linear relation expected from eq 13 is obeyed and the intercepts of the lines in that figure give the experimentally measured difference in the extinction coefficients at both wavelengths. Competition of MQ and DQ for e_{aq}^- and $(CH_3)_2\dot{C}OH$ would yield an equation similar to eq 13 where the ratio of the rate constants will replace K_{12} . The ratio of the rate constants of the reactions of e_{aq}^- and of $(CH_3)_2\dot{C}OH$ with the quinones was measured previously and verified by us to be ~ 1 . However, the slope in the lines of Figure 4b yields a value of 0.32 which indicates assumption ii to be correct, thus we measure the equilibrium constant K_{12} . Two points in Figure 4b, at the lower $[MQ]$, are displayed on the dashed line the slope of which gives a value of 0.6. These points might represent an incomplete transformation from the initial state to the equilibrium one, since under these low $[MQ]$ reaction 12 is not fast enough.

A strong indication that the value calculated from Figure 4b is K_{12} , the equilibrium constant, is obtained from the other values for K_6 presented in Table II. The fact that the experimentally measured value for $K_{12} = 0.32$ is very similar to the ratio of the independently measured values of K_6 for MQ and DQ, which is 0.29, is very reassuring. Furthermore, when a solution $10^{-4} M$ in each of the quinones was saturated with 9.6% O_2 in N_2 the observed residual absorptions of the semiquinones yield $K_{12} = 0.29$ was calculated using eq 13. Under these conditions at the end of the reaction of the semiquinones with O_2 , equilibrium 12 should be reached if not directly then through the corresponding reactions 6. Actually equilibrium 12 is achieved directly long before reactions 6 are over. The ratio of MQ^-/DQ^- ESR signal is three times higher in presence of O_2 than in its absence (see Figure 1b,c). From the lowest value of $[MQ]$ in Figure 4b where the equilibrium is reached we can roughly estimate $k_{12} \sim 1.5 \times 10^9 M^{-1} \text{sec}^{-1}$ very near the diffusion-controlled limit.

We have also studied the electron transfer from IDS^- to DQ and the respective equilibrium 14. In this system the



yield of the two semiquinones was recorded at several different wavelengths where the two radicals have different relative extinction coefficients. Some of our experimental results are given in Table III. K_{14} was calculated using the corresponding rearranged eq 13. Similar to the MQ-DQ system, also here, no electron transfer could be observed directly and the question arises whether the constancy of the value calculated as K_{14} is the equilibrium constant of reaction 14 or a competition ratio. Again the value of K_{14} is very close to the ratio of K_6 for DQ to K_6 for IDS (see Table II). However, this might incidentally be the case also if K_{14} is very close to the competition ratio. To verify this possibility we saturated solution containing $5 \times 10^{-5} M$ IDS, $1 \times 10^{-4} M$ DQ, and $10^{-2} M$ in $NaHCO_2$ with 9.6% O_2 - N_2 mixture and followed the decay of the absorption at both 445 and 550 nm, the absorption maxima of DQ^- and IDS^- , respectively. Results of that experiment are shown in Figure 5. For comparative examination the decay of each one of the semiquinones in the presence of oxygen is also displayed, all of them on the same time scale (10 μsec per point). It is obvious from these results that the reaction of IDS^- with O_2 is much slower than that of DQ^- . However, when a mixture of both semiquinones is allowed to react with oxygen, IDS^- decays much faster than in the absence of DQ^- . Actually, both DQ^- and IDS^- decay at the same rate. No dose effect on the decay rate was found on increasing the dose from 0.15 to 1.7 krad (Figures 5c and 5d). This obviously indicates that no effective radical-radical reaction is involved in that decay. We take these results as a proof for the existence of equilibrium 14 in the absence of oxygen. The DQ in the mixed experiments acts as a mediator for the transfer of one electron from the dye semiquinone to the oxygen. It is interesting to note that while IDS is often used as a mediator for electron transfer measurements, DQ is used here as the mediating agent.

D. One-Electron Redox Potentials Calculations. The equilibria constants for electron transfer from DQ^- , MQ^- , and IDS^- to O_2 as well as between IDS^- and MQ^- to DQ were determined here independently. Their values are presented in Table II and are all self-consistent with each other as the respective ratios of K_6 equal K_{12} and K_{14} . Therefore, we will proceed with the calculation of the one-

TABLE III: Determination of Equilibrium Constant between $IDS|IDS^-$ and $DQ|DQ^-$ Systems

$[DQ]$, μM	$[IDS]$, μM	λ , nm	$(A - A_{IDS^-}) / (A_{DQ} - A)$ ^a	K_{14}
62	50	550	2.27	1.82
		505	2.13	1.69
		445	2.44	1.96
		415	2.04	1.61
93	50	550	3.33	1.78
		505	3.33	1.78
137	50	550	5.13	1.89
		505	5.00	1.82
29	100	550	5.90	1.75
43	100	550	4.55	1.95
49	150	550	0.62	1.89
		505	0.41	1.25
70	150	550	1.12	2.38
		505	0.83	1.72
		445	1.18	2.50
		415	0.71	1.52

$$K = 1.8 \pm 0.3$$

^a A , A_{IDS^-} , and A_{DQ} are absorbances obtained on pulse irradiation of the corresponding solution, the solution in absence of DQ, and the solution in absence of IDS, respectively.

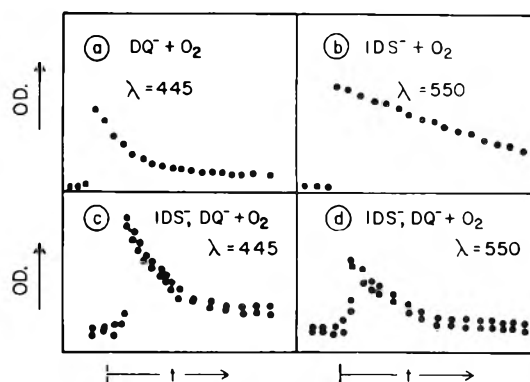


Figure 5. Reaction of DQ^- , IDS^- , and their mixture with O_2 . Time scale 10 μsec per point. All solutions at pH 7 containing $10^{-2} M$ $NaHCO_2$ and $1.2 \times 10^{-4} M$ O_2 : (a) $10^{-4} M$ DQ, 0.15 krad; (b) $5 \times 10^{-5} M$ IDS, 0.15 krad; (c and d) $10^{-4} M$ DQ + $5 \times 10^{-5} M$ IDS, upper curves 0.15 krad lower curves 1.7 krad. Curves were shifted for clarity.

electron redox potentials of the systems. Two reference couples were included in our study, i.e., the $DQ|DQ^-$ and $IDS|IDS^-$ systems. The method for the calculation of the redox potential of $DQ|DQ^-$ has been outlined by us previously.²² For such calculations one has to know essentially the value of the two-electron redox potential, and the semiquinone formation constant, K_{15} .



In order to estimate redox potentials at different pH's one has to know also all the pK_a 's of the various species involved. Once all these parameters are known, one can calculate the two one-electron redox potentials for the system using

$$E_{m_i} = (E_i^1 + E_i^2)/2 \quad (16)$$

and

$$E_i^1 - E_i^2 = 0.059 \log K_{15}' \quad (17)$$

where E^1 and E^2 are the half-cell redox potentials for the first and second reduction steps, respectively, when the ratio of the total concentrations of the oxidized to reduced forms is 1 and E_m is similarly the two-electron redox potential. The index i specifies the pH to which those potentials refer. K_{15}' is defined by

$$K_{15}' = [Q^-]_T^2/[Q][Q^{2-}]_T \quad (18)$$

where $[Q^-]_T$ and $[Q^{2-}]_T$ are the total concentrations of the semiquinone and the hydroquinone ionized and un-ionized. E^1 , E^2 , E_m , and K_{15}' are all pH dependent. The values for the DQ system thus calculated are $E_7^1 = -0.235$ and $E_7^2 = 0.355$ V.

In order to gain confidence in the values of the redox potentials determined here, we thought it worthwhile to choose another independent reference and the indigodisulfonate seemed suitable. The electrochemical behavior, including the one-electron redox potentials of the indigodisulfonate dye (IDS), was the subject of a detailed study by Preisler et al.¹⁷ Using the conventional potentiometric titration technique along with the analysis of the titration curves suggested by Elema^{2b} they were able to determine the redox potentials of the IDS|IDS⁻ and IDS⁻|IDS²⁻ couples of that dye and their pH dependence. Since K_{14} determined above matches closely the potential difference between DQ|DQ⁻ and IDS|IDS⁻ systems each of these references will give the same value for the redox potentials of the rest of the systems. The values for the one-electron redox potentials are summarized in Table IV. These values were calculated using eq 19 where ΔE_7^1 is the potential dif-

$$\Delta E_7^1 = 0.059 \log K_{(pH 7)} \quad (19)$$

ference for the first reduction step between the reference and the system under consideration at pH 7 and K is the observed equilibrium constant for the electron transfer between those systems at that pH. E_7^2 , the second reduction step, was calculated from the two-electron reduction redox potential, E_{m7} , using eq 16. Two values are included for the oxygen. The first one is the single redox potential of the oxygen electrode under 1 atm oxygen pressure, which is the commonly used electrochemical definition for the oxygen standard state. The other one refers to the oxygen at 1 M activity as the standard state and was included for convenience in making comparisons between those systems. The value reported here is very similar to the corresponding half-wave potential determined recently²³ polarographically. The pH dependence of the various potentials involved in the O₂ and the DQ systems is shown in Figure 6. Included in that figure is also the dependence of the redox potentials on pH for the benzoquinone (BQ) calculated as indicated previously.²² For the DQ and BQ systems the dashed line in Figure 6 describes the dependence of $-pK_{15}'$ on pH. Obviously BQ⁻ and DQ⁻ are thermodynamically stable species at high pH's while O₂⁻ must decay at any reasonable pH.

Conclusions

The pulse radiolysis technique is shown here to be a useful technique for determination of redox potentials of short-lived radicals. However, a careful examination must be made to ensure establishment of equilibrium. Previous studies^{12,13} claiming to measure redox potentials of short-lived radicals are incorrect since in the first place they used two-electron potentials as references and secondly it is very unlikely that equilibrium was established in those systems.

TABLE IV: Single Step Oxidation-Reduction Potentials for the Systems Studied

Q	pK_r^a pK_o^a	pK_3	E_{m7}, V	E_7^1, V	E_7^2, V
DQ	$pK_{r1} = 11.3^b$ $pK_{r2} = 12.7^c$	5.1^e	0.060^h	-0.235	0.355
MQ		4.4^f		-0.203	
IDS	$pK_{r1} = 7.5^d$ $pK_{r2} = 12.3^d$ $pK_{o1} = 12.3^d$ $pK_{o2} = 12.7^d$	13.9^d	-0.125^d	-0.247^d	-0.003^d
O ₂	$pK_{r1} = 11.8$	4.8^g	0.27^i (1 atm O ₂) 0.355 (1 M O ₂)	-0.325 (1 atm O ₂) -0.155 (1 M O ₂)	0.865 0.865

^a pK_r and pK_o are ionization constants of the reduced and oxidized species, respectively. ^b Reference 26. ^c Reference 27. ^d Reference 17. ^e References 24 and 25. ^f Reference 14. ^g Reference 18. ^h Reference 3. ⁱ Reference 31.

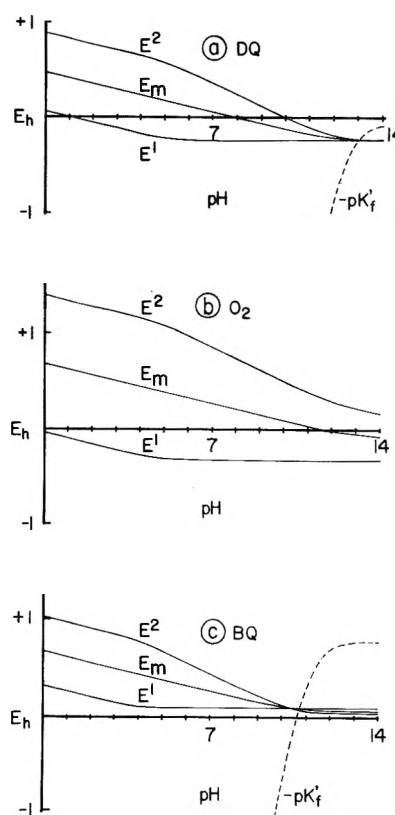


Figure 6. Dependence of E_h on pH for (a) DQ|DQ⁻|DQ²⁻ (b) O₂|O₂⁻|O₂²⁻; and (c) BQ|BQ⁻|BQ²⁻ systems. Dashed lines are $-pK_{15}'$, the semiquinone formation constant. Ordinates' units are in volts for the potentials.

Once a reaction of the radical with an acceptor is observed it should be verified that the only reaction is an electron transfer reaction which leads to a measurable equilibrium state. The rate constants measured in such a case are the sum of the forward and backward reactions rather than one of them. If a direct reaction is not observed one can still measure the equilibrium constant by studying the effect of concentrations. In that case, it should be verified if that effect is kinetic competition or on equilibrium.

The method presented here has already been applied to

the measurement of redox potentials correlating them with spin density distribution in radicals and radiosensitization efficiencies.³² Correlation between two-electron redox potentials and any parameter involving one-electron transfer, such as rates of electron transfer or the energy of the first unoccupied orbital, reflects in effect the correlation between the two- and the one-electron transfer if such a correlation exists.

References and Notes

- (1) Supported in part by the U.S. Atomic Energy Commission.
- (2) (a) L. Michaelis, *J. Biol. Chem.*, **96**, 703 (1932); (b) B. Elema, *ibid.*, **100**, 149 (1933).
- (3) W. M. Clark, "Oxidation-Reduction Potentials of Organic Systems", Williams and Wilkins, Baltimore, Md., 1960.
- (4) L. Edsberg, D. Eichlin, and J. Gavis, *Anal. Chem.*, **25**, 798 (1953).
- (5) I. M. Kolthoff and T. B. Reddy, *J. Electrochem. Soc.*, **108**, 980 (1961).
- (6) M. E. Peover, *J. Chem. Soc.*, 4540 (1962).
- (7) S. Wawzonek, R. Berkey, W. Blaka, and E. Runner, *J. Electrochem. Soc.*, **103**, 456 (1956).
- (8) E. Mueller and W. Dilger, *Chem. Ber.*, **106**, 1643 (1973).
- (9) M. E. Peover and B. S. White, *Electrochim. Acta*, **11**, 1061 (1966).
- (10) M. E. Peover, *Nature (London)*, **193**, 475 (1962).
- (11) (a) J. Lilie, G. Beck, and A. Henglein, *Ber. Bunsenges. Phys. Chem.*, **75**, 458 (1971); (b) M. Grätzel and A. Henglein, *ibid.*, **77**, 2 (1973), and the three following papers.
- (12) P. S. Rao and E. Hayon, *Biochem. Biophys. Res. Commun.*, **51**, 468 (1973).
- (13) P. S. Rao and E. Hayon, *J. Am. Chem. Soc.*, **96**, 1287, 1295 (1974).
- (14) K. B. Patel and R. L. Willson, *J. Chem. Soc., Faraday Trans. 1*, **69**, 814 (1973).
- (15) P. S. Rao and E. Hayon, *J. Phys. Chem.*, **77**, 2753 (1973).
- (16) P. S. Rao and E. Hayon, *Nature (London)*, **243**, 344 (1973).
- (17) P. W. Preisler, E. S. Hill, R. G. Loeffel, and P. A. Shaffer, *J. Am. Chem. Soc.*, **81**, 1991 (1959).
- (18) P. A. Shaffer and P. W. Preisler, *Ind. Eng. Chem. News*, **11**, 236 (1933).
- (19) B. Venkatoraman, B. G. Segal, and G. K. Fraenkel, *J. Chem. Phys.*, **30**, 1006 (1959).
- (20) G. Vincow and G. K. Fraenkel, *J. Chem. Phys.*, **34**, 1333 (1961).
- (21) L. Michaelis, M. P. Schubert, R. K. Reber, J. A. Kuck, and S. Granick, *J. Am. Chem. Soc.*, **60**, 1678 (1938).
- (22) Y. I. Ilan, D. Meisel, and G. Czapski, *Isr. J. Chem.*, **12**, 891 (1974).
- (23) J. Chevalet, F. Rouelle, L. Gierst, and J. P. Lambert, *Electroanal. Chem. Interface Electrochem.*, **39**, 201 (1972).
- (24) R. L. Willson, *Chem. Commun.*, 1249 (1971).
- (25) P. S. Rao and E. Hayon, *J. Phys. Chem.*, **77**, 2274 (1973).
- (26) J. H. Baxendale and H. R. Hardy, *Trans. Faraday Soc.*, **49**, 1140 (1953).
- (27) J. H. Baxendale and H. R. Hardy, *Trans. Faraday Soc.*, **49**, 1433 (1953).
- (28) D. Behar, G. Czapski, J. Rabani, L. M. Dorfman, and H. A. Schwartz, *J. Phys. Chem.*, **74**, 3209 (1970).
- (29) L. K. Patterson and J. Lilie, *Int. J. Radiat. Phys. Chem.*, **6**, 129 (1974).
- (30) K. Eiben and R. W. Fessenden, *J. Phys. Chem.*, **75**, 1186 (1971).
- (31) L. E. Bennett, *Prog. Inorgan. Chem.*, **18**, 27 (1973).
- (32) D. Meisel and P. Neta, submitted to *J. Am. Chem. Soc.*

Ionic Aggregation of the Solvated Electron with Lithium Cation in Tetrahydrofuran Solution¹

Bradley Bockrath and Leon M. Dorfman*

Department of Chemistry, The Ohio State University, Columbus, Ohio 43210 (Received September 9, 1974; Revised Manuscript Received April 30, 1975)

Publication costs assisted by the Energy Research and Development Administration

Aggregation of the solvated electron with lithium cation in tetrahydrofuran forms an ion pair which has been investigated by the pulse radiolysis method. The ion pair (Li^+, e_s^-) has a near-infrared absorption band with λ_{max} 1180 nm and a molar extinction coefficient of $2.28 \times 10^4 \text{ M}^{-1} \text{ cm}^{-1}$ at the maximum. Absolute rate constants have been determined for reactions of this species with anthracene, biphenyl, and dibenzylmercury. These reactivities are compared with the reactivities of (Na^+, e_s^-) and e_s^- in THF solution.

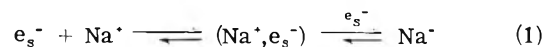
Introduction

Aggregation of the solvated electron with alkali metal cations forms a variety of species in a number of weakly polar liquids. The sodium cation-electron pair, (Na^+, e_s^-), has been observed in diglyme^{2,3} and in tetrahydrofuran.⁴ The species Na^- , formed by reaction of two solvated electrons with sodium cation, has been observed in ethylenediamine⁵⁻⁷ and in tetrahydrofuran.^{8,9} The ion pairs (K^+, e_s^-) and (Cs^+, e_s^-) in tetrahydrofuran have recently been reported.¹⁰ Optical absorption spectra have been determined. The kinetics^{4,7,10,11} of both the formation of such species and the reactions they undergo have been studied.

In some solvents, the optical absorption spectrum of the solvated electron is very greatly altered upon ion pair formation. Thus, the absorption maximum for (Na^+, e_s^-) in THF is 890 nm⁴ compared with a maximum at 2120 nm for e_s^- in THF,^{12,13} corresponding to a change of 0.8 eV in the transition energy. Rate constants for the attachment of the

electron to various substrates are substantially diminished^{4,11} upon ion pair formation with sodium cation.

The reactions involved in this pairing



are by no means unique to sodium cation. To obtain a broader knowledge of alkali metal-electron pairing, information has been obtained about the pairing of the solvated electron with lithium cation in THF. The results have been obtained by pulse radiolysis of THF solutions of various dissociative lithium salts. We report here the optical absorption spectrum of the species (Li^+, e_s^-) as well as rate constants for the attachment of this species to anthracene and to biphenyl.

Experimental Section

The source of the electron pulse, as in our earlier studies,¹⁴ was a Varian V-7715A electron linear accelerator, de-

livering 3–4-MeV electrons at a pulse current of about 300 mA for pulse duration of 100–1500 nsec and about 600 mA for pulse duration less than 80 nsec. Electron pulses of 200- to 800-nsec duration were used in this work. The transient optical absorptions in the region from 600 to 1100 nm were observed using an RCA 7102 photomultiplier which has S-1 spectral response. Our infrared detector,¹³ a solid state diode employing a diffused junction of indium antimonide, manufactured by Barnes Engineering Co., was used for observation in the region from 900 to 2000 nm. The 10–90% rise time of the electronic detection systems is 80 nsec for the infrared detector and considerably less for the RCA 7102 photomultiplier. A Bausch and Lomb grating monochromator, Type 33-86-25, $f/3.5$ was used. Corning filters were selected to eliminate second-order components from the analyzing light beam. Our standard reaction cells,¹⁴ with high-purity silica windows and a cell length of 20.0 mm, were used with a double pass of the analyzing light beam.

The THF was purified first by refluxing under argon, for several hours, a solution containing benzophenone and excess sodium metal. The solvent was then distilled through a glass-bead-packed column, the middle fraction being retained. It was then degassed and vacuum distilled into a storage bulb containing a mirror of freshly distilled potassium. Solvent was vacuum distilled from this bulb into the reaction cells just prior to the runs. Pulse radiolysis experiments with this pure solvent show only the spectrum of the solvated electron itself.^{12,13}

Anthracene and biphenyl (Aldrich) were zone refined, with a nominal purity of at least 99.9%. Dibenzylmercury (Alfa Inorganics) was recrystallized from ethanol, dried under vacuum, and stored in the dark until used. Lithium perchlorate (Alpha Products, 99.5%) was found, in our analysis for potassium by atomic absorption, to contain only 0.001% K by weight. Lithium bromide (Matheson Coleman and Bell, purity nominally >99%) was found, in our assay, to contain 0.01% K by weight. Lithium chloride (Baker, purity nominally 99.8%) contains, according to the manufacturer's assay, 0.005% K and 0.002% Na. These salts were used as supplied after thorough drying under vacuum. Lithium tetraphenylboron was prepared from sodium tetraphenylboron (Fisher reagent grade) and lithium chloride by cation exchange.¹⁵ The freshly prepared salt was recrystallized three times by addition of cyclohexane to a dichloroethane solution. Solutions of lithium tetraphenylboron become discolored when exposed to the atmosphere. Precautions were taken to reduce contact with the atmosphere by conducting the preparation and recrystallization in a glove bag filled with argon and storing the salt under vacuum until immediately before weighing on a pan balance and transfer to the reaction cell.

Results and Discussion

Optical Absorption Spectrum of (Li^+, e_s^-) . The transient absorption band which we assign to the lithium cation-solvated electron ion pair, (Li^+, e_s^-) , was obtained by measuring the optical density, at different wavelengths, immediately after an electron pulse in THF solutions of several dissociative lithium salts. The data are shown in Figure 1. The data combined in Figure 1 were obtained in separate experiments using either LiCl, LiBr, or LiClO₄ as the added salt. The salt concentration was sufficiently high so that the ion pairing reaction, $e_s^- + \text{Li}^+$, was essentially complete at the end of the electron pulse. This was readily

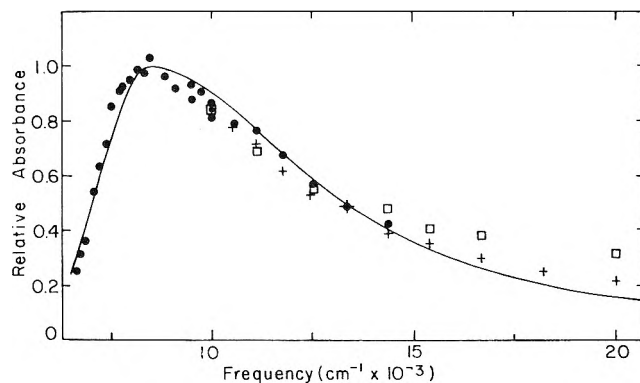
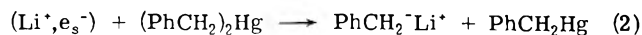


Figure 1. Spectrum of (Li^+, e_s^-) in THF at 25° obtained in solutions of: ●, LiClO₄ (0.035 *F*); □, LiCl (0.064 *F*); and +, LiBr (0.12 *F*). The absorption maximum is at 1180 nm with a molar extinction coefficient of 22,800 at the maximum and width at half-height of 6270 cm^{-1} . The line is calculated using a gaussian curve on the low-energy side of the maximum and a lorentzian curve on the high-energy side, and is not a best fit for the experimental points.

verified by observations in the near-infrared which showed that e_s^- is not present after the pulse because of this effective scavenging. It may be readily seen that, when the optical densities obtained from the separate solutions of the three salts are normalized to the absorption maximum, the data define a common absorption band with the maximum at 1180 nm. Since the same band is obtained from the three lithium salts it is evident that the anion does not play a role in the formation of this transient which is indicated to be (Li^+, e_s^-) . It should be noted that in pure THF^{12,13} only the band corresponding to the solvated electron, with maximum at 2120 nm, is seen. In short, the "blank" for these runs contains no hint of a band at 1180 nm which is thus produced solely by addition of the various lithium salts. Moreover, an atomic absorption analysis of a THF solution of LiClO₄ (0.035 *F*) showed a potassium content of only 0.04 ppm, consistent with the salt concentration, and indicating no potassium contamination from unknown sources.

Further scavenger experiments indicate that this transient is composed of both the lithium cation and a solvated electron. When dibenzylmercury was used to scavenge the band at 1180 nm, formed in lithium perchlorate solutions, a new band with a maximum at 330 nm appeared. This new species is identified as benzyl lithium since the absorption band corresponds to that reported¹⁶ for $\text{PhCH}_2^-\text{Li}^+$. Under our experimental conditions, this band could have arisen only by the reaction:



This conclusion is well founded for several reasons. First, we have previously established that, in irradiated THF solutions of dibenzylmercury, the solvated electron is the precursor of free benzyl anion.¹⁷ Secondly, the absorption spectrum of $\text{PhCH}_2^-\text{Li}^+$ is readily distinguished from that of PhCH_2^- or that of PhCH_2^- paired with other alkali metal cations,¹⁸ since the absorption maximum differs in the case of sodium cation and presumably also for potassium cation. Finally it was shown that no significant amount of e_s^- could react directly with dibenzylmercury. To ensure that the solvated electron reacted only with lithium cation, the solution was made with lithium perchlorate (0.028 *F*) in rather large excess over dibenzylmercury (2.5×10^{-4} *M*). Observation of the band at 1180 nm under these conditions shows only decay, as expected. Thus we may confidently

TABLE I: Optical Absorption Spectrum of the Solvated Electron and Its Lithium Ion Pair in THF Solution

Species	Absorption maximum, nm	Transition energy, eV	Shift from e_s^- , eV	Width at half-height, cm^{-1}
e_s^-	2120 ^a	0.58		3450
(Li^+, e_s^-)	1180	1.04	0.46	6270
(Na^+, e_s^-)	890 ^b	1.39	0.81	7000
(K^+, e_s^-)	1125 ^c	1.10	0.52	6000
(Cs^+, e_s^-)	1400 ^c	0.88	0.30	5000

^a Data taken from ref 12. ^b Data taken from ref 4. ^c Data taken from ref 10.

rule out formation of benzyl lithium by the reaction sequence $e_s^- + (\text{PhCH}_2)_2\text{Hg}$ followed by $\text{PhCH}_2^- + \text{Li}^+$. Reaction 2 thus seems well established, providing assurance that the benzyl lithium precursor, with λ_{max} 1180 nm, is in fact (Li^+, e_s^-) .

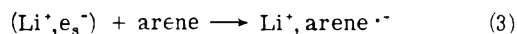
Table I contains a comparison of the optical transition energies for the absorption bands of the solvated electron itself, the lithium–electron pair, the sodium–electron pair, and recent data for the potassium–electron pair and cesium–electron pair,¹⁰ all in THF. The change in transition energy for the solvated electron induced by pairing with lithium ion is considerably less than that induced by pairing with sodium ion. If this shift in transition energy is taken as an indication of the strength of the coupling in the ion pair, the relative effect for Li^+ and Na^+ is difficult to rationalize only on the basis of the ionic radii of the bare alkali metal cations. If ionic radius was the dominant parameter in determining the change in transition energy, the smaller lithium ion might be expected to induce the greater shift. Our contrary observation suggests that solvation of the alkali metal cation is the important phenomenon which determines the interionic distance in the pair; in short, we are dealing with a solvent-separated pair.

Any meaningful evaluation of the role of the solvent would require knowledge of the number and the geometric arrangement of solvent molecules in at least the first solvation shell. Such detailed microscopic information is lacking. Attention has, however, been drawn to the role of the solvent with these ions on the basis of other macroscopic properties. The limiting conductance^{15,19} of Li^+ in THF solution was found to be lower¹⁵ than that of Na^+ , a fact attributed to the relative size of the solvation shell of THF molecules bound to the metal cations. Of the two ions, Li^+ apparently has the larger solvation shell. The effect on the spectrum, which we observe and which we interpret as stronger coupling of the electron by sodium cation, may be rationalized similarly on the basis that Li^+ is solvated to a greater degree than Na^+ in the ion pair, (M^+, e^-) , just as for the free ion in solution. A greater degree of solvation, together with the lesser effect of effective nuclear charge for Li^+ than for Na^+ , would reduce the coulombic attraction between the cation and the electron in the pair.

The shape of the absorption band of (Li^+, e_s^-) conforms reasonably well to the same shape function as does the band for e_s^- and for (Na^+, e_s^-) , namely, a gaussian curve on the low-energy side and a lorentzian curve on the high-energy side of the maximum. The fit of the data in the region to the right of the band maximum in Figure 1 does not appear to be quite as close as for other cases. The total band-

width at half-height, for the five spectra in THF, is also compared in Table I. All the metal cation-paired species have a considerably broader band, on a wave number scale, than does e_s^- .

The molar extinction coefficient of (Li^+, e_s^-) at the band maximum was found to be $2.28 \times 10^4 M^{-1}$. This value was determined, as before,⁴ by using aromatic compounds to scavenge the transient species:



The extent of growth or decay, after the electron pulse, of optical density at any given wavelength, depends upon the relative values of the extinction coefficient of (Li^+, e_s^-) and of $\text{Li}^+, \text{arene}^{\cdot -}$. At wavelengths for which the extinction coefficients of these two species are equal, neither growth nor decay is observed. With anthracene as the scavenger, this wavelength of equivalence was found to be 720 nm, which happens to correspond to an absorption peak of anthracene ion. With biphenyl as scavenger the wavelength of equivalent extinction coefficients was found to be 675 nm. The extinction coefficient of (Li^+, e_s^-) was then obtained from the two sets of data by using the known extinction coefficients of sodium anthracenide²⁰ and sodium biphenylide²⁰ in THF, 10,000 and 12,500 $M^{-1} \text{cm}^{-1}$ at the absorption peak, respectively. Good agreement was obtained, the average value being $2.28 \times 10^4 M^{-1} \text{cm}^{-1}$.

The oscillator strength of the 1180-nm band was determined from the equation

$$f = 4.32 \times 10^{-9} (1.065 W_{1/2}^G + 1.511 W_{1/2}^L) \epsilon_{\text{max}} \quad (4)$$

where $W_{1/2}^G$ and $W_{1/2}^L$ are the portions of the half-width on the gaussian and lorentzian side, respectively. This gives a value of $f = 0.90$ for the band of (Li^+, e_s^-) , which is similar to the value found for other one-electron species, namely, e_s^- in THF¹³ ($f = 0.85$) and (Na^+, e_s^-) in THF⁴ ($f = 1.0$), as well as for e_s^- in a variety of liquids.

The optical absorption data thus indicate that ion pairing of e_s^- in THF induces a shift in the absorption to higher transition energies. The magnitude of the shift depends upon the specific cation involved, being greater for sodium than for lithium. The absorption band for e_s^- is considerably broadened by cation pairing, and the extinction coefficient reduced, while the oscillator strength remains roughly the same.

Reaction Kinetics of (Li^+, e_s^-) . Table II contains absolute rate constants for elementary reactions of (Li^+, e_s^-) with three different substrates. Two are examples of electron attachment to aromatic compounds, reaction 3, and one of a dissociative electron attachment, reaction 2. Values of the rate constants for analogous reactions of e_s^- and of (Na^+, e_s^-) have been included for comparison.

These rate constants were determined in each case by observing the decay in the absorption at 1000 nm in the absence as well as in the presence of appropriate concentrations of the added reactants. This wavelength is near the absorption maximum of (Li^+, e_s^-) , but sufficiently far removed from the absorptions arising from the products (either the corresponding aromatic radical anions or benzyl lithium) so that there is no spectral overlap. In the absence of added substrate, the decay of (Li^+, e_s^-) in LiClO_4 solutions (0.03 to 0.06 F) followed a first-order rate law with a half-life of about 3 μsec . In the presence of anthracene (0.46 and $1.0 \times 10^{-4} M$) and of dibenzylmercury (1.3 and $2.4 \times 10^{-4} M$) the decay was again first order with a half-

TABLE II: Absolute Rate Constants for Reactions of (Li⁺, e_s⁻), (Na⁺, e_s⁻), and e_s⁻ in THF Solution at 25° (M⁻¹ sec⁻¹ × 10⁻¹⁰)

Reactant	(Li ⁺ , e _s ⁻)	(Na ⁺ , e _s ⁻)	e _s ⁻
Anthracene	2.65		
Biphenyl	1.00	0.55 ^a	11.0 ^a
Dibenzylmercury	1.8	0.79 ^b	2.7 ^b

^a Data taken from ref 4. ^b Data taken from ref 17.

life reduced to less than 300 nsec. The rate constant for the reaction was then evaluated from the pseudo-first-order constant and each substrate concentration. The rate constants in Table II are the average of the two determinations at the indicated substrate concentrations. The separate values agree to within ±15%. The uncertainty of the rate constant values in Table II is ±20%. In the case of biphenyl, k_3 was obtained in an experiment using lithium tetraphenylboron as the dissociative salt.

These attachment rate constants for (Li⁺, e_s⁻) are all close to the diffusion-controlled limit judging from the approximate value for k_{diff} calculated from the Smoluchowski equation.^{21,22}

$$k_{diff} = \frac{2RT}{3\eta} \frac{(r_a + r_b)^2}{r_a r_b} \quad (5)$$

where η , the viscosity, is¹⁹ 4.61×10^{-3} P, and r_a and r_b are the interaction radii, which are taken, as an approximation, to be equal. We thus estimate $k_{diff} = 1.4 \times 10^{10} M^{-1} sec^{-1}$, quite comparable to the experimental values.

Two properties of the rate constants for the metal cation-coupled species, compared with those for e_s⁻, are noteworthy. First, the values for (M⁺, e_s⁻) are somewhat lower. Secondly, there is a difference in selectivity; the ratio $k_{Ph_2}/$

$k_{(PhCH_2)_2Hg}$ is less than unity for (M⁺, e_s⁻), while it is 4 for e_s⁻.

Acknowledgment. We are indebted to Mr. Ed Ray for maintaining the electron linear accelerator and the electronic detection equipment. We are grateful to Dr. James Gavlas for performing the atomic absorption analyses.

References and Notes

- (1) This work was supported by the U.S. Atomic Energy Commission under Contract No. AT(11-1)-1763.
- (2) J. G. Kloosterboer, L. J. Gilling, R. P. H. Rettschnick, and J. D. W. Van-Voorst, *Chem. Phys. Lett.*, **8**, 462 (1971).
- (3) G. Ramme, M. Fisher, S. Claesson, and M. Szwarc, *Proc. R. Soc., Ser. A*, **327**, 467 (1972).
- (4) B. Bockrath and L. M. Dorfman, *J. Phys. Chem.*, **77**, 1002 (1973).
- (5) S. Matalon, S. Golden, and M. Ottolenghi, *J. Phys. Chem.*, **73**, 3098 (1969).
- (6) M. G. DeBacker and J. L. Dye, *J. Phys. Chem.*, **75**, 3092 (1971).
- (7) J. L. Dye, M. G. DeBacker, J. A. Eyre, and L. M. Dorfman, *J. Phys. Chem.*, **76**, 839 (1972).
- (8) G. A. Salmon and W. A. Seddon, *Chem. Phys. Lett.*, **24**, 366 (1974).
- (9) M. T. Lok, F. J. Tehan, and J. L. Dye, *J. Phys. Chem.*, **76**, 2975 (1972).
- (10) G. A. Salmon, W. A. Seddon, and J. W. Fletcher, *Can. J. Chem.*, **52**, 3259 (1974).
- (11) M. Fisher, G. Ramme, S. Claesson, and M. Szwarc, *Proc. R. Soc., Ser. A*, **327**, 481 (1972).
- (12) L. M. Dorfman, F. Y. Jou, and R. Wageman, *Ber. Bunsenges. Phys. Chem.*, **75**, 681 (1971).
- (13) F. Y. Jou and L. M. Dorfman, *J. Chem. Phys.*, **58**, 4715 (1973).
- (14) W. D. Felix, B. L. Gall, and L. M. Dorfman, *J. Phys. Chem.*, **71**, 384 (1967).
- (15) D. N. Bhattacharyya, C. L. Lee, J. Smid, and M. Szwarc, *J. Phys. Chem.*, **69**, 608 (1965).
- (16) R. Waack and M. A. Doran, *J. Am. Chem. Soc.*, **85**, 1651 (1963).
- (17) B. Bockrath and L. M. Dorfman, *J. Am. Chem. Soc.*, **96**, 5708 (1974).
- (18) B. Bockrath and L. M. Dorfman, *J. Am. Chem. Soc.*, in press.
- (19) C. Carvajal, K. J. Toile, J. Smid, and M. Szwarc, *J. Am. Chem. Soc.*, **87**, 5548 (1965).
- (20) J. Jagur-Grodzinski, M. Feld, S. L. Yang, and M. Szwarc, *J. Phys. Chem.*, **69**, 628 (1965).
- (21) M. Smoluchowski, *Z. Phys. Chem.*, **92**, 129 (1917).
- (22) P. Debye, *Trans. Electrochem. Soc.*, **82**, 265 (1942).

Electron Scavenging and Trapping in γ -Irradiated Organic Glasses

T. Ito, K. Fueki,* and Z. Kuri

Department of Synthetic Chemistry, Faculty of Engineering, Nagoya University, Chikusa-ku, Nagoya, Japan (Received February 10, 1975)

Publication costs assisted by Nagoya University

A study has been made of electron scavenging and trapping in γ -irradiated organic glasses at 77 K. Experimental data are presented on the concentration dependences of the yields of biphenyl anions and trapped electrons produced in five glassy matrices containing biphenyl. A kinetic model is developed for analysis of the experimental data, which includes three competitive processes: geminate ion-electron recombination, the electron trapping in the matrix, and electron scavenging by a scavenger. Values of kinetic parameters derived from such analysis are reported. The present model can reasonably account for the observed concentration dependences of the yields of biphenyl anions and trapped electrons. However, there remains some discrepancy between the calculated and observed yields of trapped electrons at the higher biphenyl concentrations.

Introduction

It is well known that the yield of trapped electrons in irradiated organic glasses decreases in the presence of an electron scavenger.¹ At present, mechanisms of electron scavenging and trapping in organic glasses are not very clear, however. The mechanisms of electron scavenging proposed to date may be classified as (1) competition between scavenging of mobile¹ or shallowly trapped² electrons by scavenger and stably trapping of electrons in the matrix and (2) tunneling of stably trapped electrons to scavenger.³ Most previous studies on this subject, however, have been focused on only either the yield of trapped electrons or that of radical ions (or radicals) produced by electron scavenging.

In the present work we have measured by means of optical absorption techniques both the yields of biphenyl anions and trapped electrons produced in 3-methylhexane, triethylamine, diisopropylamine, 2-methyl-*n*-amylamine, and 2-methyltetrahydrofuran glasses γ -irradiated at 77 K. To analyze the experimental data we have developed a model in which Schuler's scavenging function⁴ has been modified to be applicable to electron scavenging in irradiated organic glasses. The present model is essentially empirical, but implies the physical picture of electron diffusion in spurs. The diffusion of electrons in organic glasses may be either hopping of electrons or tunneling of electrons between shallow traps. Using this model we have calculated the concentration dependences of the yields of biphenyl anions and trapped electrons and determined values of parameters involved in the modified scavenging function. A discussion is given on the total ion yield and electron trapping efficiency in γ -irradiated organic glasses at 77 K.

Experimental Section

2-Methyl-*n*-amylamine (2MAA), diisopropylamine (DIPA), and triethylamine (TEA) were Tokyo Kasei guaranteed reagents and purified as previously described.⁵ Aldrich 2-methyltetrahydrofuran (MTHF) was purified by passage through a column of activated Silica Gel followed by distillation. Tokyo Kasei 3-methylhexane (3MHx) was purified by washing with concentrated sulfuric acid and water followed by distillation. The middle fraction was degassed and treated with sodium blocks and distilled under

vacuum on a freshly prepared sodium mirror. Tokyo Kasei ultrapure grade biphenyl was used without further purification. Solutions containing biphenyl at various concentrations were transferred to quartz optical absorption cells (optical path length 5 mm) and the samples were irradiated by ⁶⁰Co γ -rays at 77 K in the dark. The total dose was usually 2.6×10^{18} eV g⁻¹. Optical absorption measurements were carried out at 77 K with a Hitachi Model 323 recording spectrophotometer. The *G* value of biphenyl anions was determined from the measured optical density assuming an extinction coefficient of 3.7×10^4 M⁻¹ cm⁻¹ at 408 nm.¹ The *G* value of trapped electrons in a pure matrix was obtained by ESR measurements and those in matrices containing biphenyl were determined from the optical density at a specified wavelength of trapped electron absorption relative to that in the pure matrix.

Kinetic Model

As regards the fate of electrons produced by ionization in organic glasses, three processes are generally considered: (1) recombination with matrix cations, (2) trapping in the matrix to form stable trapped electrons, and (3) scavenging by electron scavenger present. If one applies Schuler's scavenging function⁴ to electrons in organic glasses and regards electron traps in the matrix as a kind of electron scavenger, the yields of trapped electrons (e_t^-) and products (P) arising from electron scavenging are given by

$$G(P)_s = \frac{\alpha[S]}{\alpha[S] + \beta[T]} \left[G_{ft} + G_{rt} \frac{\sqrt{\alpha[S] + \beta[T]}}{1 + \sqrt{\alpha[S] + \beta[T]}} \right] \quad (1)$$

$$G(e_t^-)_s = \frac{\beta[T]}{\alpha[S] + \beta[T]} \left[G_{ft} + G_{rt} \frac{\sqrt{\alpha[S] + \beta[T]}}{1 + \sqrt{\alpha[S] + \beta[T]}} \right] \quad (2)$$

where [S] and [T] are the concentrations of scavenger molecules and electron traps, respectively. α and β correspond to the efficiencies of electron scavenging by the scavenger and of electron trapping by the matrix, respectively. G_{ft}

and G_{gi} represent the yields of free and geminate ions, respectively. When $[S] = 0$, eq 1 and 2 reduce to

$$G(P)_0 = 0$$

$$G(e_t^-)_0 = G_{ft} + G_{gi} \frac{\sqrt{\beta[T]}}{1 + \sqrt{\beta[T]}} \quad (3)$$

where $G(e_t^-)_0$ is the yield of trapped electrons observed in the absence of electron scavenger. If an approximation $G_{ft} = 0$ is made for electrons in the matrix at 77 K, G_{gi} is taken as equal to G_t . Equation 3 is then written as

$$G(e_t^-)_0 = G_t \frac{\sqrt{\beta[T]}}{1 + \sqrt{\beta[T]}}$$

or

$$\beta[T] = \{G(e_t^-)_0/[G_t - G(e_t^-)_0]\}^2 \quad (4)$$

Also, eq 1 and 2 are expressed as

$$G(P)_S = G_t \frac{\alpha[S]}{\alpha[S] + \beta[T] + \sqrt{\alpha[S] + \beta[T]}} \quad (5)$$

$$G(e_t^-)_S = G_t \frac{\beta[T]}{\alpha[S] + \beta[T] + \sqrt{\alpha[S] + \beta[T]}} \quad (6)$$

Assuming an appropriate value for G_t , one can readily determine $\beta[T]$ from eq 4 and obtain curves of $G(P)_S$ or $G(e_t^-)_S$ vs. scavenger concentration from eq 5 or 6 with the properly chosen values of the parameters α and $\beta[T]$. It should be stressed that although there are two adjustable parameters, G_t and α , in the present model, two sets of experimental data, $G(P)_S$ and $G(e_t^-)_S$, must simultaneously be accounted for, so the choice of values of the parameters cannot be very arbitrary.

Results and Discussion

The results of the experiments and model calculations are given in Figures 1–6 and Table I. Figures 1–3 show the dependences on the biphenyl concentration of the yields of biphenyl anions and trapped electrons in TEA, DIPA, and 2MAA, respectively. In these figures, the experimental data points are shown as solid and open circles, which represent, respectively, the biphenyl anion and trapped electron. Solid lines show curves calculated from the present model, which fit best to the experimental data. Values of the parameters yielding such best curves are listed in Table I.

Knowledge of the total ion yield G_t is of considerable importance for an understanding of fundamental processes in irradiated organic glasses, but at present little is known about G_t in organic glasses. In gases, the W value can be determined accurately and the values of G_t are close to 4.3 for large polyatomic molecules.⁶ The values of G_t have been reported as 4–5 for liquids.^{7–11} The values of G_t obtained in the present work on the organic glasses are about 4 as given in Table I. These values of G_t are close to those in gases and liquids. The results of the calculations with G_t less than 4 are also shown in Figure 1. When making curves calculated with G_t less than 4 fit to the experimental data at high biphenyl concentrations, the curves do not fit the experimental data at low biphenyl concentrations. We could make the calculated trapped electron yield fit the observed one by properly choosing a value of the parameter α , but in this case the calculated biphenyl anion yield deviates very much from the observed one. We note that the G_t values obtained here are extrapolated from considerably lower observed values.

The reactivity parameter α corresponds to the ratio of

TABLE I: Kinetic Parameters for Electrons in γ -Irradiated Organic Glasses at 77 K

Matrix	$G(e_t^-)_0$	G_t	$\beta[T]$	α, M^{-1}	C, M	K, M^{-1}
TEA	0.53	4.0	0.023	30	7.7×10^{-4}	230
3MHx	0.87	4.0	0.077	50	1.5×10^{-3}	230
DIPA	0.97	4.2	0.090	70	1.3×10^{-3}	180
2MAA	2.1	4.0	1.2	250	4.8×10^{-3}	120
MTHF	2.6	4.2	1.9	350	5.4×10^{-3}	90

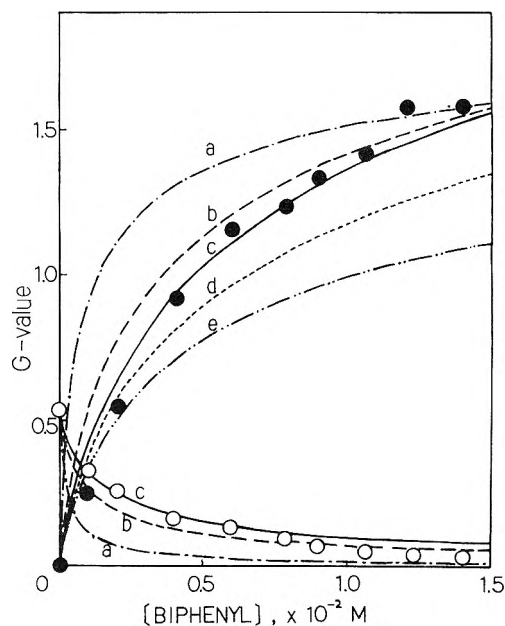


Figure 1. Plots of $G(Ph_2^-)$, ●, and $G(e_t^-)$, ○, vs. concentration of biphenyl in TEA: (a) $G_t = 2.0$, $\alpha = 1 \times 10^4 M^{-1}$; (b) $G_t = 3.0$, $\alpha = 90 M^{-1}$; (c) $G_t = 4.0$, $\alpha = 30 M^{-1}$; (d) $G_t = 3.0$, $\alpha = 50 M^{-1}$; (e) $G_t = 2.0$, $\alpha = 125 M^{-1}$.

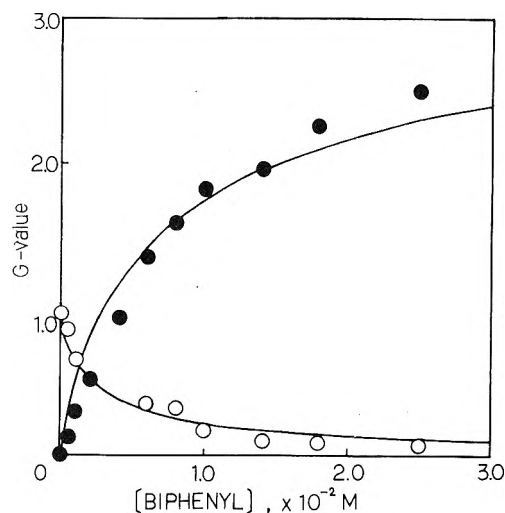


Figure 2. Plots of $G(Ph_2^-)$, ●, and $G(e_t^-)$, ○, vs. concentration of biphenyl in DIPA. Curves were calculated with $G_t = 4.2$ and $\alpha = 70 M^{-1}$.

the rate constant for electron scavenging by biphenyl to the rate for geminate ion–electron recombination and represents the efficiency of electron scavenging by biphenyl in the individual matrix. It is seen in Table I that the value of

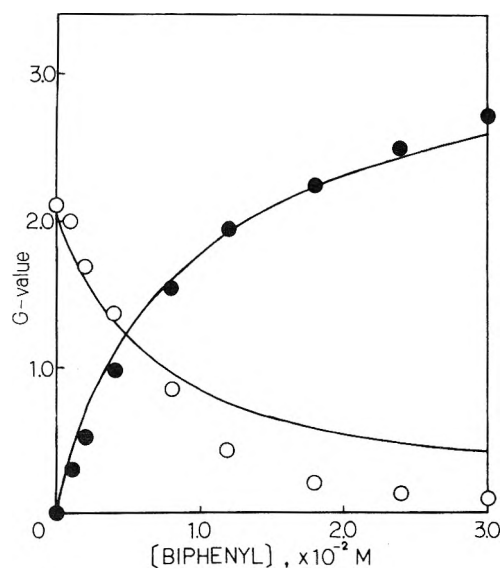


Figure 3. Plots of $G(\text{Ph}_2^-)$, \bullet , and $G(e_1^-)$, \circ , vs. concentration of biphenyl in 2MAA. Curves were calculated with $G_t = 4.0$ and $\alpha = 250 \text{ M}^{-1}$.

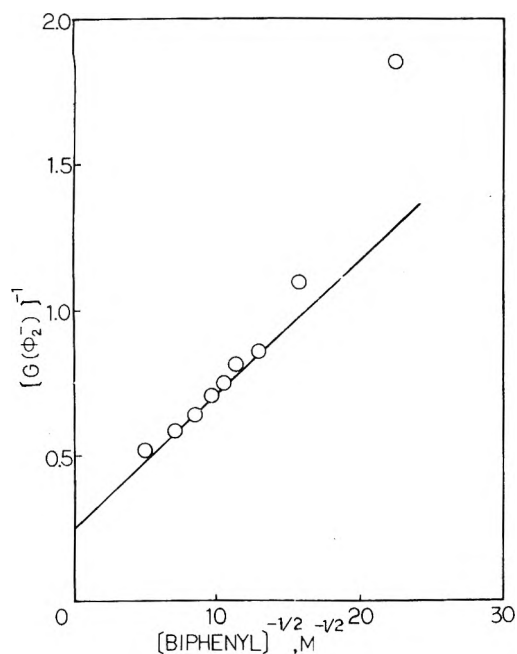


Figure 4. Plot of $G(\text{Ph}_2^-)^{-1}$ vs. $[\text{Ph}_2]^{-1/2}$ for TEA. The straight line shows Schuler's plot with $G_t = 4.0$ and $\alpha = 30 \text{ M}^{-1}$.

α increases with increase in matrix polarity, although TEA and 3MHx are reversed in their order.

It is seen in Figures 1–3 that the agreement between the calculated curve and the experimental data for the trapped electron yield becomes worse at higher biphenyl concentrations. This might indicate that a fraction of trapped electrons have recombined with positive ions by tunneling via aromatic solute molecules such as biphenyl before optical measurements are made.¹² Miller³ considers that electron scavenging occurs by tunneling of trapped electrons to scavenger molecules because the observed trapped electron yield decreases exponentially with the scavenger concentration. This implies that mobile electrons become trapped once in the matrix and then the trapped electrons tunnel to scavenger molecules. This mechanism seems to work for

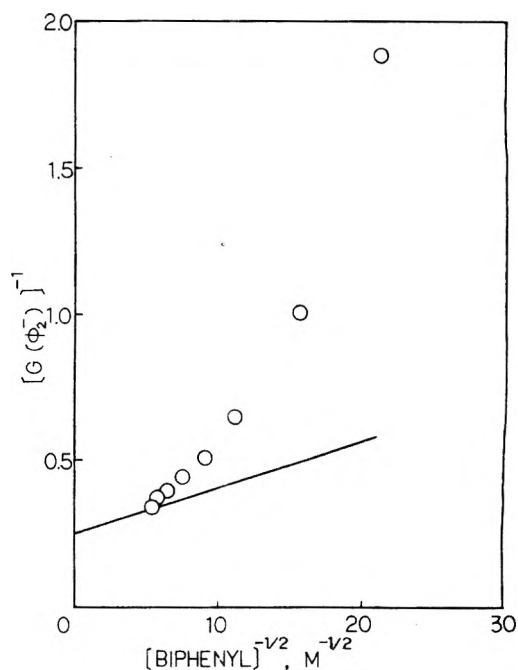


Figure 5. Plot of $G(\text{Ph}_2^-)^{-1}$ vs. $[\text{Ph}_2]^{-1/2}$ for 2MAA. The straight line shows Schuler's plot with $G_t = 4.0$ and $\alpha = 250 \text{ M}^{-1}$.

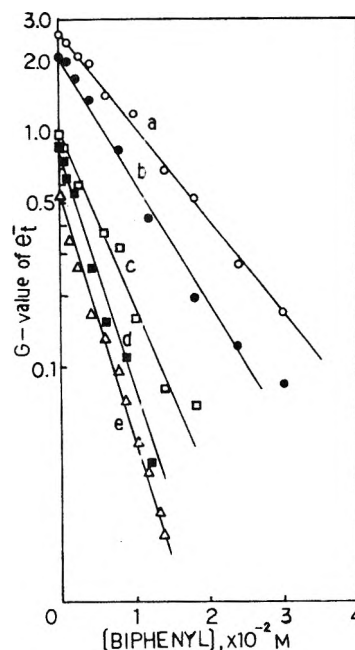


Figure 6. Plots of $\log G(e_1^-)$ vs. concentration of biphenyl: (a) MTHF, (b) 2MAA, (c) DIPA, (d) 3MHx, (e) TEA.

polar matrices such as alcohols and ethers since the scavengable electron yields are nearly equal to the trapped electron yields in these matrices, but does not seem to work satisfactorily for nonpolar or slightly polar matrices such as hydrocarbons or tertiary amines in which the trapped electron yields are considerably lower than the scavengable electron yields. In the latter case, the ion–electron recombination must be explicitly taken into account.

The parameter C in Table I was obtained by dividing $\beta[T]$ by α . This parameter provides a measure of the relative efficiency of electron trapping in a matrix, that is, it is the scavenger concentration at which the efficiency of elec-

tron scavenging by scavenger is equal to that of electron trapping in the matrix. It is seen in Table I that the value of C is in the increasing order for TEA, 3MHx, DIPA, 2MAA, and MTHF which is about the order of matrix polarity. This indicates that a small amount of electron scavenger has a large effect on the yield of trapped electrons in nonpolar or slightly polar matrices such as 3MHx or TEA. To see how much the present experimental data deviate from original Schuler's scavenging function for electrons in liquids, we have made plots of $G(\text{Ph}_2^-)^{-1}$ vs. $[\text{Ph}_2]^{-1/2}$ for TEA and 2MAA, which are shown in Figures 4 and 5, respectively. The straight line in these figures represents eq 5 with $\beta[\text{T}] = 0$, i.e., the assumption that electron trapping is negligible and with the values of G_t and α given in Table I. It is seen in Figure 4 that the experimental data fit the calculated straight line only over a limited range of biphenyl concentration. This result indicates that electron trapping in the TEA matrix effectively competes with electron scavenging by biphenyl at the lower concentrations. Figure 5 illustrates that the experimental data for 2MAA do not fit the calculated straight line over the entire range of biphenyl concentration studied. This indicates that the efficiency of electron trapping in the 2MAA matrix is so high that the electron trapping process cannot be neglected in this matrix.

We have shown that the present model can account for the concentration dependence of the biphenyl anion yield over the entire range of biphenyl concentration as well as that of the trapped electron yield at the lower biphenyl concentrations. However, there remains some discrepancy between the calculated and observed yields of trapped electrons at the higher biphenyl concentrations for all the matrices listed in Table I. Some mechanism other than that assumed in the present model seems to be required to account for this discrepancy. Tunneling of a fraction of deeply trapped electrons to positive ions via the biphenyl molecules may be responsible for the observed trapped electron yields which are lower than expected from the present model. We have tried to make plots of $\log G(e_t^-)$ vs. $[\text{Ph}_2]$, which are shown in Figure 6. The experimental data points fit rather well a straight line for each matrix. This suggests the necessity of taking into account the disappearance of a

fraction of deeply trapped electrons by the tunneling mechanism,³ at least, at higher biphenyl concentrations. From the slope of the straight line in Figure 6 we have obtained the reactivity parameter K defined as

$$G(e_t^-) = G(e_t^-)_0 \exp(-K[S]) \quad (7)$$

where $G(e_t^-)_0$ represents $G(e_t^-)$ observed in the absence of biphenyl and $[S]$ is the concentration of biphenyl (M). Values of K are given in Table I. It is seen in Table I that the value of K decreases with increase in matrix polarity. This trend in K with matrix polarity is opposite to that in α . Such a relation between K and α implies that the rate of reaction of electrons with biphenyl decreases with increasing matrix polarity, but the rate of geminate ion-electron recombination also decreases with increasing matrix polarity much more than does the reaction rate.

Recent pulse radiolysis studies of trapped electrons in hydrocarbon glasses at low temperatures have shown that the decay of electrons is more rapid in the presence of biphenyl and this decay is accompanied by an increase in biphenyl anion yield.^{13,14} To substantiate the validity of the present model, it would be necessary to reconcile it with pulse radiolysis observations.

References and Notes

- (1) (a) W. H. Hamill in "Radical Ions", E. T. Kaiser and L. Kevan, Ed., Wiley-Interscience, New York, N.Y., 1968, Chapter 9; (b) J. E. Willard in "Fundamental Processes in Radiation Chemistry", P. Ausloos, Ed., Wiley, New York, N.Y., 1968, Chapter 9; (c) L. Kevan in "Advances in Radiation Chemistry", Vol. 4, M. Burton and J. L. Magee, Ed., Wiley-Interscience, New York, N.Y., 1974, pp 181-305.
- (2) H. B. Steen, *J. Chem. Phys.*, **61**, 3387 (1974).
- (3) J. R. Miller, *J. Chem. Phys.*, **56**, 5173 (1972).
- (4) P. P. Infelta and R. H. Schuler, *J. Phys. Chem.*, **76**, 987 (1972).
- (5) S. Noda, K. Fueki, and Z. Kuri, *Can. J. Chem.*, **50**, 2699 (1972).
- (6) G. G. Meisels, *J. Chem. Phys.*, **41**, 51 (1964).
- (7) J. M. Warman, K.-D. Asmus, and R. H. Schuler, *J. Phys. Chem.*, **73**, 931 (1969).
- (8) J. M. Warman and S. J. Rzed, *J. Chem. Phys.*, **52**, 485 (1970).
- (9) N. H. Sagert, J. A. Reid, and R. W. Robinson, *Can. J. Chem.*, **47**, 2655 (1969).
- (10) M. Tanaka and K. Fueki, *J. Phys. Chem.*, **77**, 2524 (1973).
- (11) R. K. Wolff, J. E. Aldrich, T. L. Penner, and J. W. Hunt, *J. Phys. Chem.*, **79**, 210 (1975).
- (12) B. Brocklehurst, *Chem. Phys.*, **2**, 6 (1973).
- (13) J. T. Richards and J. K. Thomas, *J. Chem. Phys.*, **53**, 218 (1970).
- (14) N. V. Klasson, H. A. Gilis, and G. G. Teather, *J. Phys. Chem.*, **76**, 3847 (1972).

γ Radiolysis of Isobutyrate Salts

R. S. Marshall, B. M. Tolbert, and W. C. Gottschall, Jr.*

Chemistry Department, University of Colorado, Boulder, Colorado 80302 and Chemistry Department, University of Denver, Denver, Colorado 80210 (Received January 30, 1975)

Publication costs assisted by the University of Denver

Isobutyric- I - ^{14}C acid was prepared from $\text{Ba}^{14}\text{CO}_3$ via a Grignard reaction. Eight isobutyrate- I - ^{14}C salts were prepared by treating hydroxides or carbonates with isobutyric- I - ^{14}C acid. The salts were irradiated in vacuo with γ radiation from a ^{137}Cs source. $^{14}\text{CO}_2$ from the salts was quantitatively measured by an ionization chamber method and $G(^{14}\text{CO}_2)$ values were calculated. Initial $G(^{14}\text{CO}_2)$ values for sodium, potassium, calcium, strontium, barium, nickel(II), copper(II), and zinc isobutyrate- I - ^{14}C are 0.34, 1.2, 1.5, 1.1, 1.9, 0.48, 0.48, and 1.3, respectively.

Introduction

A moderate amount of information has been published on the γ radiolysis of salts and chelates,¹⁻⁵ with Johnson's book⁴ representing the outstanding compilation to date. Although one might expect a correlation between cation electronic properties and rates of decomposition for a given ligand or anion, this does not appear to be the case. Thus, for example, cation ionization potential, radius, charge density, and polarizability do not correlate with observed stabilities nor do macroscopic properties of the crystals such as density, melting point, temperature of thermal decomposition, or free volume.

This study was undertaken to obtain additional facts concerning cation effects on radiation stability. We felt that combining known cation properties and macroscopic properties from an organic moiety would furnish a fresh look at the stability question. Despite considerable interest in the solid state reactions, mechanisms have been poorly understood and theories or postulates have not endured. Ultimately it was hoped that by finding known parameters that would correlate with $G(\text{CO}_2)$ values, a better understanding of radiation stability or at least radiation-induced decarboxylation mechanisms could be obtained.

$^{14}\text{CO}_2$ evolution is studied in this series because the carboxyl position is readily labeled with ^{14}C , the acidic nature of CO_2 simplifies analytical techniques, and because CO_2 has been shown to be the major product in the parent acid^{6,7} and in these salts in the course of this study.

Experimental Section

Syntheses. Isobutyric- I - ^{14}C acid was prepared by a Grignard⁸ reaction using J. T. Baker reagent grade magnesium powder, Eastman Kodak White Label isopropyl iodide, Mallinkrodt analytical reagent absolute ethyl ether, barium carbonate- ^{14}C from New England Nuclear, and Baker and Adamson reagent grade sulfuric acid. Eastman Kodak White Label isobutyric acid was added to the distillation flask and the isobutyric- I - ^{14}C acid was distilled twice before use. A specific activity of $6.85 \pm 0.09 \mu\text{Ci}/\text{mmol}$ was determined for this acid.

Sodium isobutyrate- I - ^{14}C was prepared by titration of the acid with Baker reagent grade sodium hydroxide.

Potassium isobutyrate- I - ^{14}C was prepared by titration of the acid with Baker reagent grade potassium hydroxide.

Calcium isobutyrate- I - ^{14}C was prepared by allowing the acid to react with Baker and Adamson reagent grade calcium oxide.

Strontium isobutyrate- I - ^{14}C was prepared by allowing the acid to react with Merck technical grade strontium oxide.

Barium isobutyrate- I - ^{14}C was prepared by allowing the acid to react with Baker and Adamson reagent grade barium hydroxide monohydrate.

Nickel(II) isobutyrate- I - ^{14}C was prepared by allowing the acid to react with Merck reagent grade $\text{NiCO}_3 \cdot 2\text{Ni}(\text{OH})_2 \cdot 4\text{H}_2\text{O}$. The nickel(II) isobutyrate- I - ^{14}C was extracted with hot distilled water and filtered twice through fritted glass funnels.

Copper(II) isobutyrate- I - ^{14}C was prepared by allowing the acid to react with J. T. Baker reagent grade copper(II) carbonate. The copper(II) isobutyrate- I - ^{14}C was extracted with USP 95% ethanol and filtered twice through fritted glass funnels.

Zinc(II) isobutyrate- I - ^{14}C was prepared by allowing the acid to react with J. T. Baker reagent grade zinc carbonate. The zinc(II) isobutyrate was extracted with a 50/50 mixture of distilled water and USP 95% ethanol and filtered twice through fritted glass funnels.

Irradiation. All salts were dried on a vacuum line at less than 30μ of mercury for 12 hr or more before use. All samples were weighed into Pyrex tubing capillaries of $1.75 \pm 0.5 \text{ mm}$ i.d. with a wall thickness of $0.2 \pm 0.1 \text{ mm}$ and length of $10 \pm 2 \text{ cm}$. Drybox techniques were required for the hygroscopic salts and all salts were redried in a vacuum desiccator for at least 12 hr, at 30μ of mercury or less before sealing under a vacuum of $20 \pm 10 \mu$ of mercury.

Replicate samples were irradiated in the University of Colorado cesium-137 γ source calibrated at $2.77 \times 10^{19} \text{ eV g}^{-1} \text{ hr}^{-1}$ with a Fricke Dosimeter for doses ranging from 1.3 to $6.7 \times 10^{21} \text{ eV g}^{-1}$.

Analytical Procedure. Samples were analyzed via basically the same procedure discussed previously⁵ using the same type of set up. The ionization chambers used with the Cary vibrating reed electrometer were calibrated frequently and the specific activities of the salts determined by combustion with this set up yielded values within 2% of those calculated. Experimental points from the measured CO_2 yields were plotted and generally gave good straight

* Address correspondence to this author at the Department of Chemistry, University of Denver, Denver, Colo. 80210.

TABLE I: Sodium Isobutyrate

eV/g $\times 10^{-21}$	% ¹⁴ CO ₂	G(CO ₂)
1.43	0.086	0.33
1.43	0.094	0.36
2.76	0.16	0.33
3.98	0.24	0.33
3.98	0.26	0.33

TABLE II: Potassium Isobutyrate

eV/g $\times 10^{-21}$	% ¹⁴ CO ₂	G(CO ₂)
1.32	0.33	1.2
1.32	0.30	1.1
4.20	0.86	0.98
4.20	0.90	1.0
5.36	1.1	0.94
5.36	1.2	1.0

TABLE III: Calcium Isobutyrate

eV/g $\times 10^{-21}$	% ¹⁴ CO ₂	G(CO ₂)
1.56	0.85	1.5
1.56	0.81	1.5
3.37	1.5	1.3
4.70	1.8	1.1
6.04	2.2	1.0
6.04	2.4	1.1

TABLE IV: Strontium Isobutyrate

eV/g $\times 10^{-21}$	% ¹⁴ CO ₂	G(CO ₂)
1.35	0.63	1.1
1.35	0.65	1.1
2.72	1.1	0.91
2.58	1.1	0.94
3.97	1.0	0.60
4.36	1.4	0.74

TABLE V: Barium Isobutyrate

eV/g $\times 10^{-21}$	% ¹⁴ CO ₂	G(CO ₂)
1.77	1.4	1.9
3.12	2.2	1.4
3.12	2.2	1.4
4.50	2.8	1.2
4.50	2.8	1.2

lines from the slope of which the initial $G(\text{CO}_2)$ values listed were determined. In all cases blanks were run in identical fashion and gave CO₂ yields less than 1% of those determined for irradiated samples.

Results and Discussion

Tables I-VIII present the data for the eight isobutyrate salts investigated. Table IX is a compilation of initial $G(\text{CO}_2)$ values for the isobutyrate with acetate values included for comparison.

Except for the sodium salt, all the isobutyrate salt

TABLE VI: Nickel(II) Isobutyrate

eV/g $\times 10^{-21}$	% ¹⁴ CO ₂	G(CO ₂)
2.04	0.38	0.48
2.04	0.37	0.47
3.34	0.48	0.37
3.34	0.55	0.42
4.20	0.76	0.47
4.20	0.63	0.39
6.19	0.65	0.27
6.19	0.73	0.31

TABLE VII: Copper(II) Isobutyrate

eV/g $\times 10^{-21}$	% ¹⁴ CO ₂	G(CO ₂)
1.34	0.30	0.58
1.34	0.26	0.49
3.32	0.61	0.48
3.32	0.61	0.48
4.64	0.64	0.36
4.64	0.88	0.49
5.83	1.1	0.47
5.83	1.1	0.47

TABLE VIII: Zinc Isobutyrate

eV/g $\times 10^{-21}$	% ¹⁴ CO ₂	G(CO ₂)
1.82	0.87	1.2
1.82	0.99	1.4
3.26	1.6	1.2
3.26	1.7	1.3
4.58	2.2	1.2
4.58	2.2	1.2
6.55	3.1	1.2
6.55	3.1	1.2

TABLE IX: G Values for Irradiated Isobutyrate and Acetate Salts

Cation	Isobutyrate G(CO ₂)	Acetate G(CO ₂)
Na	0.34	0.48
K	1.2	0.56
Ca	1.5	1.3
Sr	1.1	0.91
Ba	1.9	1.5
Ni(II)	0.48	0.10
Cu(II)	0.48	0.17
Zn	1.3	0.36

$G(\text{CO}_2)$ values are higher than the corresponding acetate salt values. This fact is in accord with observations that secondary carboxylic acids have higher $G(\text{CO}_2)$ values than primary carboxylic acids of similar molecular weight.⁹

The acetate values were included because one might anticipate similarity with this more studied, more simple aliphatic acid and in fact similar decomposition mechanisms for the parent acids have been shown.^{10,11}

The mechanism consistent with these findings and as-

sumed operable in the radiation decomposition of isobutyrate salts, despite their decreased radiation sensitivity compared to parent acid, is that postulated for the acid.¹¹

The cation $G(\text{CO}_2)$ trends within periodic groups for isobutyrate and acetate salts are consistent and can be summarized as $\text{K} > \text{Na}$, $\text{Ba} > \text{Ca} > \text{Sr}$, and $\text{Zn} > \text{Cu} > \text{Ni}$ and it should be noted that $G(\text{NO}_2^-)$ for the nitrates follows the same trend.^{1,12} An all inclusive listing of cations according to decreasing G values, however, reveals no consistent correlation in accord with previous results.⁴ From these observations, it appears that γ radiation stability of salts depends to some extent upon electronic properties of the cation but that the predominant factor is some property of the salt as a whole.

References and Notes

- (1) J. Cunningham, *J. Phys. Chem.*, **65**, 628 (1961).
- (2) E. R. Johnson and J. Forten, *Discuss. Faraday Soc.*, **31**, 238 (1961).
- (3) C. J. Hochanadel, *Radiat. Res.*, **15**, 546 (1961).
- (4) E. R. Johnson, "Radiation Induced Decomposition of Inorganic Molecular Ions", Gordon & Breach, New York, N.Y., 1970.
- (5) W. C. Gottschall and B. M. Tolbert, *Adv. Chem. Ser.*, **No. 81**, 1 374 (1968).
- (6) S. V. Choi and J. E. Willard, *J. Phys. Chem.*, **66**, 1041 (1962).
- (7) M. A. Sweeney, UCRL No. 9983, 1962.
- (8) H. Gilman, "Organic Syntheses", Vol. 1, Wiley, London, 1941.
- (9) A. J. Swallow, "Radiation Chemistry of Organic Compounds", Pergamon Press, New York, N.Y., 1960.
- (10) P. B. Ayscough and J. P. Oversby, *Trans. Faraday Soc.*, **67**, 1365 (1971).
- (11) H. Rush, Masters Thesis, University of Colorado, Boulder, Colo., 1962.
- (12) J. Cunningham and H. G. Heal, *Trans. Faraday Soc.*, **67**, 1365 (1971).

Triboluminescence and Associated Decomposition of Solid Methanol

Graham J. Trout, Douglas E. Moore*¹

Department of Pharmacy, The University of Sydney, New South Wales 2006, Australia

and John G. Hawke

School of Chemistry, Macquarie University, New South Wales 2113, Australia (Received May 30, 1974; Revised Manuscript Received January 2, 1975)

An investigation of the phase change induced decomposition of methanol has been carried out. The decomposition is initiated by the cooling of solid methanol through the $\beta \rightarrow \alpha$ transition at 157.8 K, producing the gases hydrogen, carbon monoxide, and methane. The passage through this λ transition causes the breakup of large crystals of β -methanol into crystallites of α -methanol and is accompanied by light emission as well as decomposition. The emitted light exhibits the properties of gas discharge triboluminescence, being accompanied by, and apparently produced by, electrical discharges through methanol vapor in the vicinity of the solid. The light has a spectrum similar to that produced by an electrical discharge through methanol vapor at low pressure. The potential differences needed to produce the electrical breakdown of the methanol vapor apparently arise from the disruption of the long hydrogen bonded chains of methanol molecules present in crystalline methanol. Charge separation following crystal deformation is a characteristic of substances which exhibit gas discharge triboluminescence; solid methanol has been found to emit such luminescence when mechanically deformed in the absence of the $\beta \rightarrow \alpha$ transition. As expected for an electrical discharge phenomenon it has been found that the characteristics of the discharges are affected by the nature and pressure of the gas above the methanol. The decomposition products are not produced directly by the breaking up of the solid methanol but from the vapor phase methanol by the electrical discharges. That gas phase decomposition does occur has been confirmed by observing that the vapors of $\text{C}_2\text{H}_5\text{OH}$, CH_3OD , and CD_3OD decompose on being admitted to a vessel containing methanol undergoing the $\beta \rightarrow \alpha$ phase transition. The composition of the gas evolved from methanol and deuterated methanols has been explained using reactions occurring on electron impact in mass spectrometry.

Introduction

The decomposition of methanol to the gases hydrogen, methane, and carbon monoxide has been found to accompany the freezing of large volumes of methanol with liquid air.² During such treatment the methanol would undergo a liquid-solid phase transition (175.37 K) followed by a solid-solid phase transition (157.8 K). Further work has revealed that the latter $\beta \rightarrow \alpha$ solid phase transition is intimately associated with the decomposition and that there is an accompanying emission of light.³

The $\beta \rightarrow \alpha$ phase transition in methanol has been reported to produce crystal breakdown⁴ and the destruction of crystals both organic and inorganic is frequently accompanied by the emission of light known as triboluminescence.⁵ The light appears as a series of flashes or pulses of varying intensity. These light pulses have long been known to be associated with electrical discharges in or around the crystal being strained, and the detection of such discharges may be used to distinguish triboluminescence and crystal-luminescence.⁶

Much recent work has been concerned with the alkali halides which exhibit gas discharge triboluminescence. As expected for an electrical discharge, Meyer and Polly⁷ found that the duration and intensity of the light pulses depend upon the nature and pressure of the gas around the crystal. Potential differences set up between new crystal faces may occur when crystals fracture leading to an electric discharge.⁵ However a study of the effect of impact load on the triboluminescence of the alkali halides revealed that light emission occurs with low impact forces where no fracture of the crystal can be seen.⁷ It was postulated that the triboluminescence was not due to electrical discharges between fracture planes but rather that the potential differences arose from the formation and movement of charged dislocations in the pure plastic transport of material. In further consideration of the dislocation mechanism Meyer and Polly⁸ have shown that fracture is neither a necessary condition for triboluminescence in the alkali halides nor even a sufficient condition. However other workers^{9,10} have found that triboluminescence does not occur without fracture. Cracking may be necessary to produce a space through which charge neutralization can occur by gas breakdown and discharge, although dislocation rather than cracking produces the charge separation itself. Relatively little work has been done recently on the large known number of organic triboluminescent crystals. Sucrose, the most studied, has been found to exhibit gas discharge type luminescence.¹¹ It has been reported¹² that light emission from sucrose occurs only on crystal rupture although as with the alkali halides it is possible that dislocation motion is involved.

Light is also observed when crystals are subjected to thermal shock,¹³ annealing, polymorphic transitions, and thermal decomposition.¹⁴ All such phenomena involve a disruption or change in the state of strain of crystals with the movement of dislocations, suggesting that the light emissions may also be triboluminescent in nature. The light emission observed from solid methanol appeared to be an example of such a process and therefore a further investigation of the phenomenon and the associated decomposition was carried out.

Experimental Section

Materials. Methanol was purified by the following procedure. BDH Analar methanol (2.5 l) containing 20 g of 2,4-dinitrophenylhydrazine and 10 ml of hydrochloric acid (to remove carbonyl compounds) was distilled through a 25 mm × 1 m jacketed column packed with 6-mm single turn Fenske helices, with a reflux ratio of 40 to 1. The middle 80% was retained and distilled again with added calcium hydride (3 g). The first 10% was distilled off slowly over a period of 15 hr and then 800 ml of purified methanol was collected. All operations were carried out under nitrogen. The container of purified methanol was attached to a vacuum system, cooled with solid CO₂-acetone bath, and pumped on for 30 min. The vessel was kept under vacuum and used as a reservoir from which purified methanol could be obtained as required by vacuum distillation. The density D_4^{20} of the purified methanol was measured to be $791.3 \pm 0.1 \text{ kg m}^{-3}$ in good agreement with the literature value¹⁵ of 791.42.

Deuterated methanols CH₃OD and CD₃OD (E. Merck), certified to be of at least 99% isotopic purity, were used without further purification.

Gases used were supplied by Commonwealth Industrial

Gases (Sydney) and were found by mass spectrometry to be 99+% pure. The nitrogen used was high-purity oxygen-free nitrogen containing less than 10 ppm oxygen.

Glassware was cleaned before use by treatment with boiling nitric and sulfuric acids (1:1), followed by numerous rinsings with doubly distilled water, and oven dried.

Low Temperature Baths. To provide reasonably constant low temperatures intermediate between those attainable with solid CO₂ (193 K) and liquid N₂ (77 K) a number of "slush-baths" were used according to the recipe of Rondeau.¹⁶ The temperatures were achieved as follows with mixtures of partially frozen liquid with liquid N₂

isooctane (2,2,4-trimethylpentane)	166 K
1-propanol	146 K
<i>n</i> -pentane	143 K
isopentane	113 K

Apparatus. All handling of methanol samples and analysis of decomposition products was performed in a Pyrex glass vacuum system equipped with Pirani and Penning (Edwards) gauges and connected to an A.E.I. MS10 mass spectrometer. A choice of porous Metrosil plugs which functioned as molecular leaks, or a direct inlet, permitted analysis of gas mixtures containing from 10⁻¹⁰ to 10⁻⁵ mol of gas. The mass spectrometer was calibrated with known amounts of each gas encountered and found to have a linear response over its entire working range.

The light detecting and measuring apparatus was based on an E.M.I 9661 B photomultiplier tube which was fitted into a light-tight housing with a shutter. The output from the photomultiplier was fed into the input amplifier of an Ekco N624A ratemeter, and/or an Ekco N530C automatic scaler, so that the photomultiplier operated as a photon or pulse counter. The light detecting circuit was operated at 940 V, resulting in a sensitivity of 1000 A lumen⁻¹ and a count rate from the dark current of 400 sec⁻¹. The response of the photon counter was found to be linear by using a light source at varying distances from the photomultiplier. A Keithley Model 610B electrometer was used for voltage, current, and capacitance measurements, and a Tektronix 564 storage oscilloscope for pulse recording.

Results

As reported previously³ decomposition of methanol is found to accompany successive transitions through the $\beta \rightarrow \alpha$ solid phase transition at 157.8 K. This was established in controlled cooling experiments, using an isooctane slush bath (166 K) to produce the high-temperature β form which could then be converted to the α form by further cooling with a liquid air bath. Direct cooling of liquid methanol with liquid air also produces decomposition if a critical sample size is exceeded in a given flask. This can be explained in terms of the direct formation of α -methanol at the outer parts of the flask while some β -methanol is produced in the center due to slower cooling arising from the low thermal conductivity of solid methanol. Michel¹⁷ has found that methanol always spontaneously crystallizes below 145 K and that pure methanol has two reproducible rates of freezing. The faster rate occurs only when the methanol is supercooled to below the λ transition, this possibly being the direct liquid to α -solid transition, while the slower rate corresponds to the normal liquid to β -solid transition.

Kinetics of Gas Evolution. The rate of gas evolution obtained on cooling β -methanol with liquid air, as shown in Figure 1, is basically similar to that found previously³ for

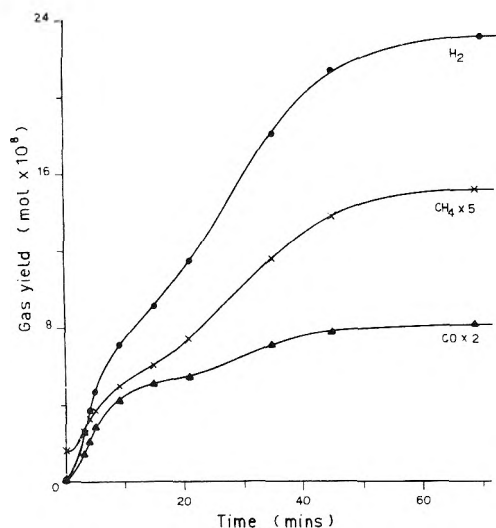


Figure 1. Evolution of H₂, CH₄, and CO obtained on cooling β -methanol with liquid air. Time is measured from the commencement of the liquid air cooling.

direct liquid air freezing of larger volumes of methanol, with the notable difference that decomposition starts almost immediately as the liquid air cooling begins. The results in Figure 1 show an initial evolution of gas before cooling with liquid air, with the exception of fresh methanol samples having no previous history of decomposition. The gas is rich in methane, reported to be difficult to remove from frozen methanol.¹⁸ By addition of CH₄ to frozen CH₃OH and CD₃OD we have confirmed that methane remains strongly adsorbed onto solid methanol at 83 K.

Luminescence Accompanying Decomposition. When viewed in the dark, no light is observed on freezing methanol with an isooctane slush bath; on further cooling with a liquid air bath, flashes of white light superimposed on a lesser background glow can be seen to come from the methanol. The light first appeared near the circumference of the methanol surface and moved inward with time. Ten minutes after cooling began most of the light came from a 2 cm diameter area in the center of the methanol surface. Several minutes later the light flashes became more random occurring from many points over the whole surface, and continued with diminishing intensity for about 40 min. Gaseous decomposition products accompanied the light emission. After the reaction was complete, the liquid air bath was removed and further light was observed as the solid methanol warmed.

A photomultiplier was set up in the apparatus shown in Figure 2 to seek a correlation between the amount of light emitted and the gas yield. The results of a series of freezings and coolings (Figure 3) show a linear relation between total number of light pulses and H₂ yield. The results were similar, irrespective of whether the gaseous products were removed from or retained in the vessel as they were produced, i.e., the gases, once formed, have little subsequent effect on the light emitting process. Not only is the total light yield from a freezing and cooling closely related to the total gas yield, but also the kinetics of the production of gas and light correspond. Many of the larger light pulses from solid methanol emit more than 10⁷ photons, as expected from triboluminescent emission rather than chemiluminescence. Meyer and Polly⁷ observed light flashes of 3 × 10⁴ photons from alkali halides in which triboluminescence was

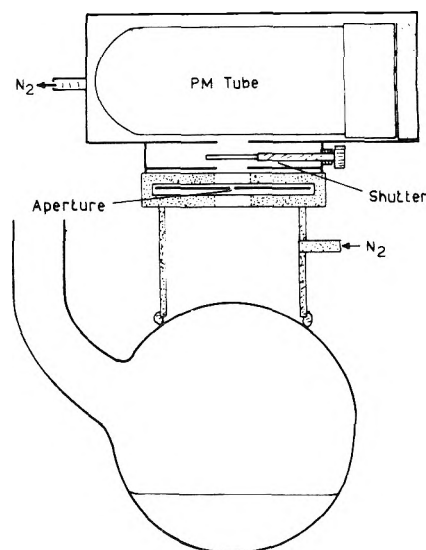


Figure 2. Apparatus for measuring the emitted light.

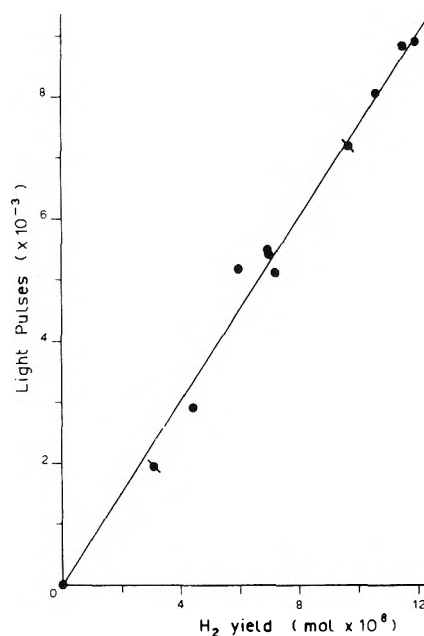


Figure 3. Relationship between the number of emitted light pulses and the yield of hydrogen gas. The points marked \bullet were obtained with the reaction vessel opened to the vacuum system.

induced by a needle impinging on the crystal surface.

Electrical Effects Accompanying Light Emission and Gas Evolution. Thiessen¹⁹ has reported that a plate placed above a substance which is mechanically abraded acquires a negative potential directly proportional to the amount of abrasion. The mechanical changes develop potential differences in the substance, leading to an emission of electrons. For this purpose we constructed the stainless steel vessel shown in Figure 4. Cooling the empty vessel with an isooctane slush bath or with liquid air produced no change in the potential of the central electrode.

Approximately 13 ml of purified methanol was distilled into the vessel. As expected, when frozen directly with liquid air, neither light, decomposition, nor significant voltage change was observed. Solid β -methanol was then prepared using the isooctane slush bath. No voltage change accom-

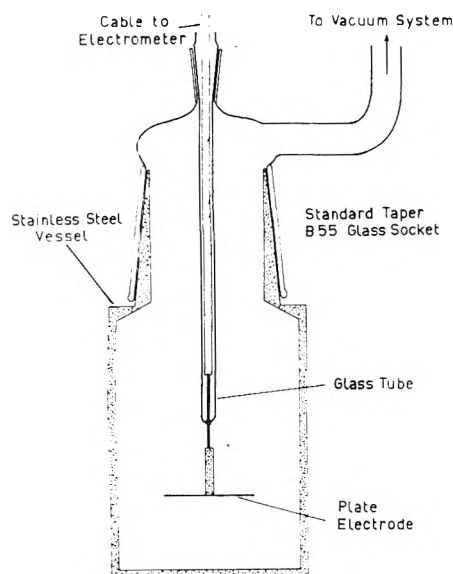


Figure 4. Apparatus for measuring electrical effects accompanying the phase transitions of methanol.

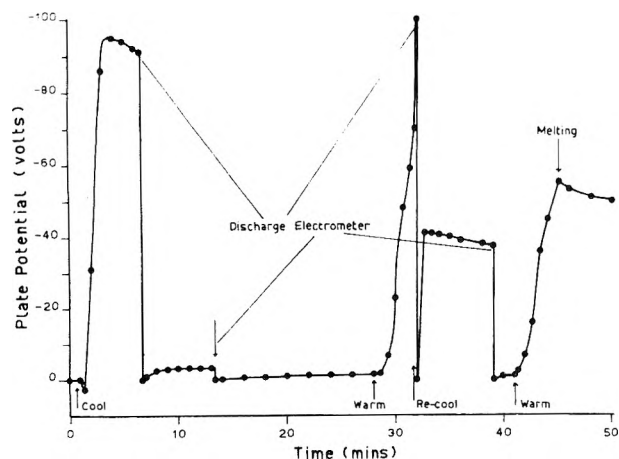


Figure 5. Potential changes observed on cooling and warming solid β -methanol.

panied this freezing. When the isooctane bath was replaced by the liquid air bath, light emission and decomposition occurred, as found in glass vessels previously. Figure 5 shows the changes in potential of the central plate electrode. The slow fall of the potential from 95 V is due to current leakage through the high but finite resistance of the electrometer. The gas yield was only about 2×10^{-8} mol. After the reaction was complete the gas was pumped away and the liquid air bath removed. A further increase in negative potential occurred, accompanied by the evolution of about 1×10^{-8} mol of H_2 , CH_4 , and CO (Figure 5). The cycle could be repeated provided no melting of solid occurred. All gas observed on warming was evolved from the solid methanol and could not be attributed to the release of gas trapped in the solid. The data are summarized in Table I.

The negative potential produced on the central electrode was independent of whether the metal vessel was electrically isolated or connected to earth, indicating that negatively charged species, presumably electrons, were being emitted by the solid methanol. The electrical discharge was observed as individual pulses of 20 to 25 mV measured across a 10^7 ohm resistor, and occurred at the same time as the

TABLE I: Gas Evolution from Solid Methanol in Cooling and Warming Cycles

	Gas yield, mol $\times 10^8$		
	H_2	CH_4	CO
Cooling	1.2	0.15	0.5
Warming 1	0.5	0.07	0.2
Warming 2	0.1	0.05	0.05

light pulses. The electrical pulses and the gas production were shown to begin at the same time by connecting a fast response Penning vacuum gauge to the vessel via a liquid air trap.

A linear relationship was found between the H_2 yield and the number of electrical pulses³ further indicating the close correlation between the emission of electrons and the observed decomposition. The similarity of the cooling and warming curves and the gas composition indicates that the mechanism of decomposition is similar in both cases. Small samples of liquid methanol frozen directly with liquid air produce no decomposition or electrical pulses on warming, suggesting that the $\alpha \rightarrow \beta$ transition is not responsible for the decomposition on warming, although we are not able to establish conclusively whether the β solid is formed in the warming stage of the cycle. Although λ transitions can superheat, α -methanol has been observed to do so by only 2° .²⁰

Relationship between Light Emission and Electrical Pulses. The apparatus of Figure 4 was not amenable to simultaneous light and electrical measurement. However, following the method of Belyaev, Nabatov, and Martysh-ev,²¹ an aerial (the bared end of a coaxial cable) placed next to the glass vessel of Figure 2 was able to detect the electromagnetic radiation associated with the electrical discharges. The aerial and the photomultiplier were connected via amplifiers to the two channels of an oscilloscope whereby it was established that the light and electrical pulses occurred simultaneously.

Effect of Cooling Rates on Decomposition. Wick¹³ has observed that uranyl nitrate crystals fracture and emit triboluminescence on being dropped into liquid air. In view of this possibility, solid β -methanol at 166 K was cooled slowly with a 1-propanol slush bath (146 K). A time lag of 30 min was observed before gas evolution with accompanying light and electrical discharges began. The fact that decomposition did begin when the cooling was slow indicates that the $\beta \rightarrow \alpha$ transition, rather than thermal shock, was responsible. A faster rate of cooling with an isopentane slush bath (113 K) resulted in a time lag of 2 min and a slower contraction of the light flashes to the center of the flask (15 min compared to 10 min for liquid air cooling).

A controlled warming experiment confirmed that the $\alpha \rightarrow \beta$ transition on warming is not responsible for any decomposition. A sample of methanol which had been frozen at 166 K and then cooled to 83 K was warmed to 143 K. Gas evolution accompanied by light flashes began after the n -pentane bath was raised and continued for about 20 min. After the gas production had ceased, no further decomposition or light emission was observed when the n -pentane slush bath was replaced by an isooctane bath at 166 K.

Variable Decomposition Behavior. There is another aspect of the effect of cooling rates on the decomposition of β -methanol. It was found that similar volumes of methanol

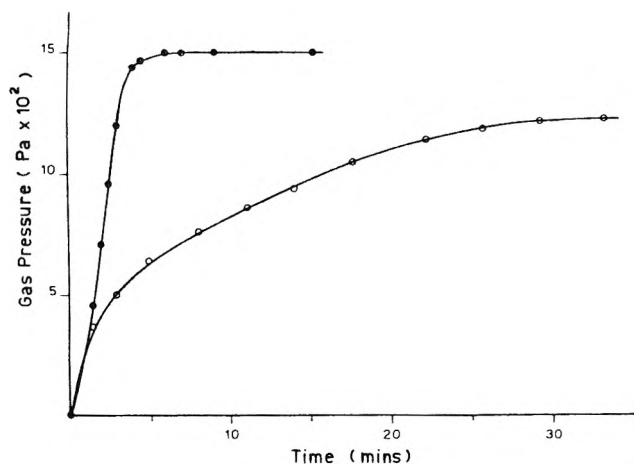


Figure 6. Variable decomposition behavior. Total gas evolved as a function of time from long duration type (flask 1, O) and short duration type (flask 2, ●). Time is measured from the commencement of cooling with liquid air.

from the same reservoir of purified methanol distilled into different, but apparently similar, flasks had somewhat different decomposition behavior. Within each flask with identical treatment, the behavior is consistent but there is a variation in the time course of reaction and composition of product from flask to flask. In Figure 6 experiments 1 and 2 represent extremes of behavior for the wide variety of flasks studied. The composition of the total gas evolved is shown in Table IV and it can be seen that the ratio $\text{CO}:\text{H}_2$ is significantly higher in flask 2 than flask 1, an increase which may be due to the faster rate of reaction.

The possibility of impurity was tested by distilling a sample of methanol from one vessel to another under vacuum and observing the decomposition behavior on freezing. The pattern observed was a function of the vessel, and not the sample of methanol. Other experiments in which small quantities of water were introduced into a flask containing purified methanol showed that the decomposition behavior is affected very little by up to 9.5 mol % water. This can be contrasted with earlier experiments² in which direct liquid air freezing of methanol containing 3 mol % water produced a glass and little decomposition. In other words, impurities which markedly affect the freezing of methanol when rapid rates of cooling are used have little effect on the growth of β -methanol when frozen slowly, and do not much alter the nature of the $\beta \rightarrow \alpha$ transition or the phenomena accompanying it.

We can only attribute the different behavior from flask to flask to differences in the manner in which methanol froze at 166 K in spite of identical treatment. Typically, in flask 1 (and similar flasks) the methanol froze slowly (30 min) to crystals 4–5 mm in length. In flask 2 (and similar flasks) the freezing was complete in 10 min and small crystals (2–3 mm) resulted. However, all samples of β -methanol exhibited decomposition on cooling.

Following the measurements of Staveley and Gupta²⁰ and Kelley²² regarding the supercooling of β -methanol, we suggest that the larger crystals supercool to a greater extent thereby extending the time course of the triboluminescence phenomenon. The different freezing patterns are possibly a result of variation in the glass surface of the flasks which enhance nucleation to varying extents.

More rapid freezing does affect the subsequent decompositions on cooling, as shown by experiments in which the

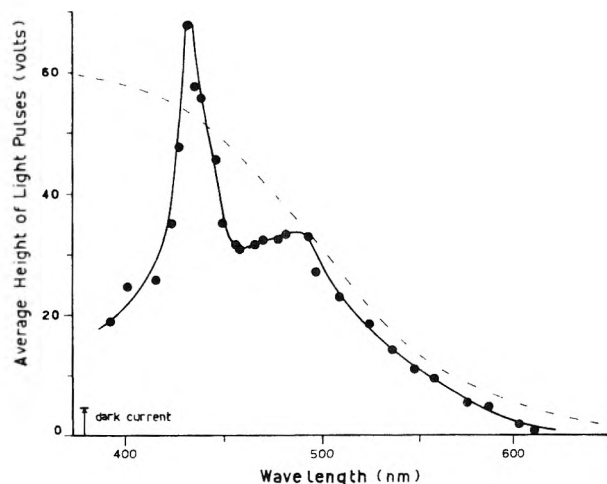


Figure 7. Spectrum of light emitted from cooling β -methanol. The dashed curve represents the spectral response of the photomultiplier.

methanol in a flask (type 1) was frozen rapidly with a continuously agitated isooctane slush bath. On cooling the resulting small crystals, light emission and gas evolution occurred but to about half the extent observed after normal freezing.

Spectral Distribution of the Light. A Schott VERIL S-60 variable line interference filter suitably positioned in front of the aperture in the light pulse counting apparatus (Figure 2) enabled the light pulse height to be observed as a function of wavelength (Figure 7). The pulse height (average of at least 30 pulses) for any given wavelength varied little during the course of the cooling and the same spectrum was obtained irrespective of whether the product gases were allowed to accumulate in the vessel or were pumped away as formed. The spectrum of Figure 7 is not corrected for a varying quantum efficiency of the photomultiplier. The qualitative nature of the spectrum is little altered by the correction, the significant features being the peaks at 430 and 485 nm.

Koliubin²³ has observed the emission spectrum of flowing methanol vapor at pressures as low as 50 Pa. The spectra were found to vary with flow rate and pressure, but in all cases the bands and lines of CH, OH, CO, H_2 , H, C_2 , and C_1 were observed. Of these, OH and C_1 are in the uv region, beyond the range of the interference filter. We obtained a spectrum by a Tesla coil discharge across a tube containing methanol vapor distilled off the solid at 166 K, the spectrum being recorded on Kodak 2475 film through the interference filter. The resolution of the spectrum did not permit identification of all the band systems described by Koliubin,²³ but correlated well with the spectrum of the light emitted on the cooling of solid β -methanol.

Triboluminescence of Solid Methanol. Methanol has not been recorded as one of the many triboluminescent substances known⁵ but this can be ascertained by observing whether mechanical pressure alone can cause solid methanol to emit light.

An apparatus was constructed in which methanol frozen in a glass tube could be broken up by rotating a stainless steel trepanning arm into its surface under vacuum. The arm was forced into the solid methanol at the rate of 0.5 mm per revolution. The gas yield was low, the average per revolution being 1×10^{-9} mol, with the H_2/CH_4 ratio of 11 ± 1 and H_2/CO ratio of 2.2 ± 0.8 , i.e., within the limits of

TABLE II: Effect of Added Argon

Argon pressure, Pa	0	3.5	3.9	24
No. of light flashes	9000	6600	8100	24,400
H ₂ yield, mol × 10 ⁸	12.0	4.4	4.5	2.2
CH ₄ yield, mol × 10 ⁸	1.05	0.40	0.40	0.15
CO yield, mol × 10 ⁸	2.75	0.91	0.88	0.2
Duration of reaction, min	48	23	20	13

those found previously for phase transition induced breakdown. Breaking up α -methanol at 83 K in the vicinity of a probe from the oscilloscope showed that electrical discharges accompanied the decomposition. Any light emission which may have occurred was too faint for visual observation. When the temperature of the solid methanol was raised to 113 K the gas yield on crushing increased sixfold, and light flashes could be seen.

The increased triboluminescent activity at the higher temperature is unusual. Polly et al.²⁴ have found that triboluminescent activity is sensibly independent of temperature, up to a temperature at which the increasing conductivity of the solid under investigation causes the triboluminescent intensity to decrease. In the case of methanol, however, there is a considerable increase in vapor pressure between 83 and 113 K. If the gas and light is produced by electrical discharges occurring between freshly fractured surfaces, then the increase in gas yield from 83 to 113 K is expected. Attempts to break up β -methanol at 166 K failed as the methanol always melted on contact with the crushing arm.

Effect of Gas Phase Additives. Gas discharge type triboluminescence is affected by the nature and pressure of the gas in the vicinity of the site of light emission.⁷ In the following experiments the gas space above cooling β -methanol was filled with (i) a permanent gas, such as argon, helium, oxygen, methane, or hydrogen; or (ii) an organic vapor such as the deuterated methanols, CH₃OD or CD₃OD, or ethanol.

(i) *Permanent Gases.* The addition of argon reduced the duration of the triboluminescence (Table II) but the electrical and light pulses were more frequent and smaller in size. The product gas contained a lower proportion of CO, particularly in the initial stages. These results are consistent with a mechanism in which energy transfer occurs between methanol and argon excited by electrical discharge. CH₃OH⁺ is the only ion formed when this mechanism applies.²⁵ The increase in number of light pulses is consistent with a reduction in breakdown potential caused by low pressures of argon. The above observations are similar to those made by Meyer and Polly⁷ with the alkali halides and sugar.

After the light emission and gas evolution had ceased in the presence of argon, the vessel was evacuated. Light emission and gas evolution began again after 25 min. A further admission of Ar had the same effect as before. In a similar experiment, the vessel was left for 6 hr before evacuating. Nevertheless, the triboluminescent process recommenced and continued for 40 min evolving 8.5×10^{-8} mol of gas. Thus Ar appears to inhibit the processes leading to decomposition. When the above experiments were performed using He in place of Ar, the same effects were observed although He was more efficient, e.g., 2 Pa of He was as effective as 4 Pa of Ar in stopping the reaction in 20 min. Helium also caused the electrical and light pulses to increase in size while occurring with the same frequency in comparison with the control.

TABLE III: Ethanol Decomposition in Solid and Vapor Phases

	Gas yield, mol × 10 ¹⁰				
	H ₂	CH ₄	CO	C ₂ H ₄	C ₂ H ₆
Ethanol decomposing on cooling glass → crystal					
Ethanol decomposing over cooling methanol	600	130	130	15	6
Cooling methanol decomposing alone	600	60	80	0	0

While it is known that added gases markedly lower the temperature of solid–solid transformations of finely divided solids by physical adsorption,²⁶ the more probable explanation for the observed behavior is based on an increase in thermal conductivity of the solid. The thermal conductivity of a powder increases in proportion to the pressure and conductivity of the gas occupying the spaces between the solid particles.²⁷ If solid methanol undergoing the $\beta \rightarrow \alpha$ transition is assumed to be powder-like due to cracking and fissuring, then its effective thermal conductivity would be increased by the introduction of argon or helium. Thus the regions of methanol furthest from the liquid air bath cool more quickly and reach a lower final temperature. Removing the Ar or He has the same effect as lowering the coolant level in the external bath or increasing the flow of N₂ over the top of the flask, i.e., the central regions of the methanol are warmed and the mechanical changes and triboluminescence recommence. The difference in efficacy of Ar and He can be attributed to a difference in thermal conductivity. Of the other gases tested, methane and oxygen (low thermal conductivity) affected the reaction in a similar way to argon, while hydrogen (high thermal conductivity) was similar to helium.

All the above observations indicate that the mechanical changes in solid methanol are affected by the thermal conductivity of the gas occupying the spaces between the particles varying the apparent thermal conductivity of the solid. When methanol was cooled with an isopentane slush bath (113 K) addition of argon caused the number of electrical and light pulses to increase but there was no effect on reaction duration.

(ii) *Organic Vapors.* A vessel containing degassed liquid CH₃OD at 193 K was opened for 15 min to a vessel containing frozen methanol which was then cooled with liquid air. The hydrogen evolved from the cooling CH₃OH was found to contain 5% HD and 0.3% D₂ and the methane contained 3% CH₃D. On subsequent freezings and coolings in which the CH₃OD distilled into the flask was intimately mixed with the CH₃OH, no HD or D₂ could be detected, indicating that the mass of CH₃OD transferred was very small. On repeating the experiment with CD₃OD in place of CH₃OD, the D₂ yield was found to be fivefold larger. Thus exchange of D and H between the hydroxyl functions of the methanol is of negligible importance. Also some 25% of the methane was CD₄ while no CH₃D was detected.

The nature of the gas produced in these experiments is

TABLE IV: Major Gaseous Decomposition Products of Methanol

	Typical long duration CH ₃ OH		Typical short duration CH ₃ OH		CH ₃ OD		CD ₃ OD		Electric discharge in CH ₃ OH			Radiolysis of CH ₃ OD, ^a %
	mol × 10 ⁸	% ^e	mol × 10 ⁸	%	mol × 10 ⁸	%	mol × 10 ⁸	%	% ^a	% ^b	% ^c	
H ₂	8.3	73.5	16.2	69	3.6	40			58.3	66.2	73.3	49.8
HD					2.3	26						39
D ₂					0.3	3.4	3.2	69				0.2
CH ₄	1.1	9.5	1.2	5	0.4	4.4			10.6	1.4	15.5	2
CH ₃ D					0.25	2.7						
CHD ₃												
CD ₄							0.44	9.5				
CO	1.9	17	6.0	26	2.1	23.5	1.0	21.5	19.8	28.5	10.8	9
C ₂ H ₄										8.3		

^a Results in glow discharge, ref 30. ^b Results with explosive electric discharge, ref 31. ^c Results from ozonizer type apparatus, ref 32. ^d Reference 33. ^e Yield expressed as percentage of total gaseous products found.

consistent with what would be produced by an electric discharge through a mixture of CH₃OH and CH₃OD or CD₃OD vapors. Substances other than methanol should be decomposed in this context, e.g., ethanol.

Some decomposition has been observed on freezing large volumes of ethanol with liquid air, although the amount of gas produced is much smaller than from methanol,² as shown in Table III. There is no λ transition in ethanol to explain the decomposition. Ethanol, unlike methanol, readily forms a clear glass on being frozen with liquid air. If the coolant level falls the ethanol glass at the surface changes to a mass of opaque white crystals. It appears that gas evolution accompanies this glass to crystal transition since a number of small electric discharges were detected. No light could be seen with the naked (dark adjusted) eye. Also shown in Table III is the composition of the gas evolved when some ethanol vapor (from degassed liquid ethanol at 193 K) was admitted to a vessel containing cooling β -methanol. The production of ethane and ethylene in particular verify that the ethanol vapor added is decomposed by the electrical discharges which accompany the $\beta \rightarrow \alpha$ phase transition in methanol.

Decomposition of Deuterated Methanols. Samples of CH₃OD (freezing point 173 K) and CD₃OD (freezing point 169 K) were frozen with an isooctane slush bath (166 K) and outgassed. On subsequent cooling with liquid air, light flashes, electrical discharges, and decomposition occurred. The products were within the range of compositions produced by CH₃OH (Table IV) but for fully deuterated methanol reveal very little about the details of the reaction other than to show that the decomposition proceeds in CD₃OD as in CH₃OH. Also given in Table IV are the comparable yields of the major gaseous products obtained by various investigators for electric discharge²⁸⁻³⁰ or radiation-induced³¹ decomposition of methanol vapor. There seems to be a correlation between electric discharge decomposition and the phase transition decomposition.

Of the condensable products possible from the decomposition of methanol, we have detected only traces of formaldehyde and ethylene glycol using chromotropic acid,³² while the CO₂ yield was less than 1% of the total gas. There was no detectable ethylene, acetylene, or ethane in the product gas.

Discussion

The $\beta \rightarrow \alpha$ transition in solid methanol involves changes in secondary coordination from an orthorhombic to a

monoclinic crystal form.⁴ The hypothesis that the resulting crystal breakdown causes the decomposition of methanol and light emission by means of electrical discharges is supported by the observation that all three phenomena occur when solid methanol is mechanically deformed. The light and electrical emissions exhibit the characteristics of gas discharge triboluminescence.

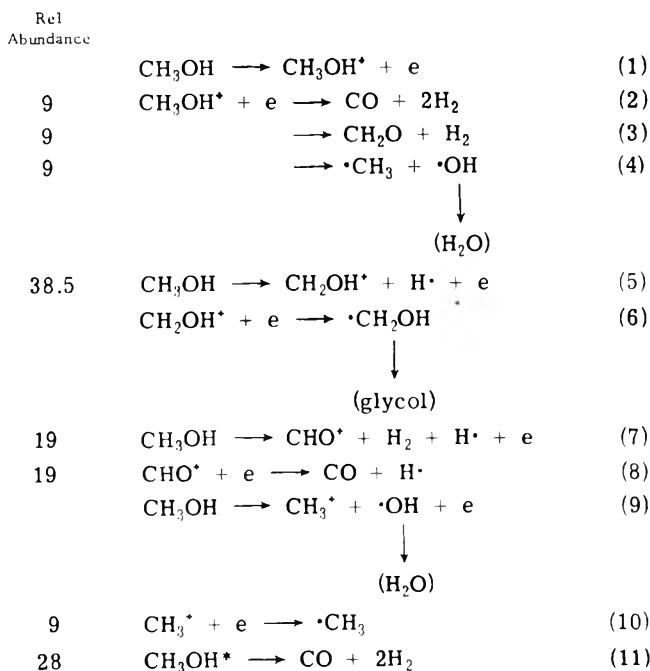
The most commonly proposed triboluminescence excitation mechanism is triboelectrification,³³ the source of which is the separation of electrical charges caused by contact potential differences. The structural properties of the methanol $\beta \rightarrow \alpha$ transition are those of a displacive transformation³⁴ involving orientational changes in the infinite parallel hydrogen-bonded chains of methanol molecules.⁴ Although the transition can occur rapidly, supercooling of the high temperature form is possible.²⁰ The orientational changes apparently rupture the hydrogen bond chains thus causing crystals of the β phase to break into crystallites of the α phase. The resulting charge separation appears analogous to the effects of plastic deformation in the alkali halides,³⁵ where an applied stress has been shown to induce the motion of charged imperfections producing a voltage pulse on suitably placed electrodes.

The extended time course of the triboluminescence in methanol is attributed to the low temperature of the coolant baths used. Strains induced by the phase transition are released in a random fashion. However the solid methanol continues to cool at a rate which can be influenced by the presence of an inert gas such as argon or helium and the movement of the dislocations to reduce the strain becomes more difficult. By 83 K very little movement is possible and thus the light and electrical emission and decomposition ceases. The trapped strains are released on warming with further energy emission and decomposition. This phenomenon is probably similar to that called annealing luminescence or stress-induced thermoluminescence by Johnson and Daniels.¹⁴ The mechanism of delayed light production is therefore considered to be the same as that of prompt triboluminescence. The rate at which strain is released increases with increasing temperature.

Mechanism of the Phase Transition Decomposition of Methanol. A mechanism of the decomposition of methanol is shown in Scheme I, proposed on the following basis.

Mass spectrometry of methanol³¹ indicates that the main ions formed by electron impact are CH₃OH⁺, CH₂OH⁺, CHO⁺, and CH₃⁺ (reactions 1, 5, 7, and 9). It might be expected that ion-molecule reactions would not be common

Scheme I: Reaction Scheme for Methanol Decomposition



in the phase transition induced decomposition where the process appears to be due to a series of short duration (ca. 1 μsec) electric discharges at less than 0.1 Pa. From the spectrum of the light emitted by an electric discharge through methanol vapor the radicals CH_3 , OH , and H are known to be present. Uv irradiation of solid methanol and subsequent electron spin resonance measurements have shown that excited methanol can also produce the radicals CH_2OH , CHO , and CH_3O .³⁶

We propose therefore that the ions formed by reactions 1, 5, 7, and 9 are neutralized to excited molecules and radicals which may further decompose. The formyl radical dissociation (reaction 8) is as suggested by Johnsen.³⁷ Three pathways have been proposed for the decomposition of excited methanol: (a) Poma and Nesti³⁰ from electrical discharge work found the products to be carbon monoxide and hydrogen (reaction 2); (b) Baxendale and Sedgwick³¹ from studies of the γ radiolysis of methanol vapor suggest formaldehyde and hydrogen (reaction 3); (c) Theard and Burton¹⁸ also from radiolysis experiments suggest that dissociation of excited methanol molecules produces methyl radicals and hence methane (reaction 4).

Taking the relative abundances of the ions found in the mass spectrum of CH_3OH^+ ³¹ as CH_3OH^+ 28%, CH_2OH^+ 38.5%, CHO^+ 19%, and CH_3^+ 9%, and assuming reactions 2, 3, and 4 to occur equally, the predicted composition of gaseous products is 73% H_2 , 17% CO , and 10% CH_4 , in good agreement with that found for the long duration (type 1) decomposition of solid methanol.

In the shorter duration (type 2) decompositions the gas produced has more CO and less CH_4 . Here the gas production is more rapid and perhaps under these more intense conditions, the formation of excited methanol molecules by direct excitation becomes a significant source of decomposition. Poma and Bassi²⁹ have found for the decomposition induced by an intense explosive discharge that reaction 11 predominates. If we assume that half of the CO comes from the decomposition of directly excited molecules then the gas produced would have the composition 71% H_2 , 22% CO ,

and 7% CH_4 , in reasonable agreement with the observations.

The mechanism suggested above for CH_3OH can be extended to apply to CH_3OD , with the assumption that reaction 3 gives 80% HD and 20% D_2 by analogy with the results of Porter and Noyes³⁸ (in the photolysis of CD_3OH , the hydrogen yield comprised 80% HD and 20% H_2). Also, the H atoms are assumed to abstract a H or D atom with equal facility from CH_3OD to give H_2 and HD in the ratio 3:1. A D atom behaves similarly. The gas produced by this series of reactions would have the composition 40% H_2 , 28% HD , 3% D_2 , 22% CO , and 7% CH_4 . The excellent agreement with the composition found experimentally (Table IV) is perhaps fortuitous.

Conclusion

The mechanism of the decomposition and light emission have no features which can be regarded as unique to methanol. The crystal breakdown accompanying the $\beta \rightarrow \alpha$ transition is said to be one of the characteristics of such displacive transformations.³⁴ Thus other triboluminescent organic crystals having adequate vapor pressure might be expected to decompose somewhat on undergoing a displacive transformation or on being mechanically broken up. In fact it appears that decomposition should be a characteristic feature of the gas discharge triboluminescence of organic materials. What is perhaps surprising in regard to methanol is that despite a very small heat for the $\beta \rightarrow \alpha$ transition (710 J mol^{-1}), the triboluminescence has greater intensity than comparable phenomena, such as observed in the mechanical crushing of sucrose. A relatively large amount of energy thus appears to be stored as strain energy in the methanol undergoing the solid phase transition. The extent of the decomposition is however very small ($<10^{-5}\%$ for mechanical breakdown) so that unless the triboluminescence is observed under high vacuum conditions with direct access to a mass spectrometer, the decomposition products may not be detected.

References and Notes

- (1) Author to whom correspondence should be addressed.
- (2) G. J. Trout and J. G. Hawke, *J. Phys. Chem.*, **73**, 3521 (1969).
- (3) G. J. Trout, D. E. Moore, and J. G. Hawke, *Nature (London), Phys. Sci.*, **235**, 174 (1972).
- (4) K. J. Tauer and W. N. Lipscombe, *Acta Crystallogr.*, **5**, 606 (1952).
- (5) G. Wolff, G. Gross, and I. N. Stranski, *Z. Elektrochem.*, **56**, 420 (1952).
- (6) V. A. Garten and R. B. Head, *Nature (London)*, **209**, 705 (1966).
- (7) K. Meyer and F. Polly, *Phys. Status Solidi*, **8**, 441 (1965).
- (8) K. Meyer and F. Polly, *Ber. Bunsenges. Phys. Chem.*, **69**, 24 (1965).
- (9) L. M. Belyaev and V. V. Nabatov, *Sov. Phys. Crystallogr. (Engl. Transl.)*, **8**, 744 (1963).
- (10) L. M. Belyaev and Yu. N. Martyshev, *Phys. Status Solidi*, **34**, 57 (1969).
- (11) H. Longchambon, *Bull. Soc. Fr. Mineral. Cristallogr.*, **48**, 130 (1925).
- (12) G. Alzetta, I. Chudacek, and R. Scarmozzino, *Phys. Status Solidi A*, **1**, 775 (1970).
- (13) F. G. Wick, *J. Opt. Soc. Am.*, **29**, 407 (1939).
- (14) N. M. Johnson and F. Daniels, *J. Chem. Phys.*, **34**, 1434 (1961).
- (15) A. Weissberger, E. S. Proskauer, J. A. Riddick, and E. E. Toops, "Technique of Organic Chemistry", Vol. 7, "Organic Solvents", 2nd ed, Interscience, New York, N.Y., 1955.
- (16) R. E. Rondeau, *J. Chem. Eng. Data*, **11**, 124 (1966).
- (17) J. Michel, *Bull. Soc. Chim. Belg.*, **48**, 105 (1939).
- (18) L. M. Theard and M. Burton, *J. Phys. Chem.*, **67**, 59 (1963).
- (19) P. A. Thiessen, *Abh. Deut. Akad. Wiss. Berlin, Kl. Chem., Geol., Biol.*, **5**, 15 (1965).
- (20) L. A. K. Staveley and A. K. Gupta, *Trans. Faraday Soc.*, **45**, 50 (1949).
- (21) L. M. Belyaev, V. V. Nabatov, and Yu. N. Martyshev, *Sov. Phys. Crystallogr. (Engl. Transl.)*, **7**, 464 (1963).
- (22) K. K. Kelley, *J. Am. Chem. Soc.*, **51**, 180 (1929).
- (23) A. A. Koliubov, *Bull. Acad. Sci. USSR, Phys. Ser. (Engl. Transl.)*, **22**, 747 (1958).
- (24) F. Polly, D. Obrikat, and K. Meyer, *Krist. Tech.*, **2**, 425 (1967).
- (25) V. Cermak and Z. Herman, *Coll. Czech. Chem. Commun.*, **30**, 169 (1965).
- (26) H. Forestier and J.-P. Kiehl, *C. R. Acad. Sci.*, **230**, 2288 (1950).

- (27) R. G. Deissler and J. S. Boegli, *ASME Trans.*, **80**, 1417 (1958).
 (28) E. G. Linder and A. P. Davis, quoted by G. Glocker and S. C. Lind, "The Electrochemistry of Gases and Other Dielectrics", Wiley, New York, N.Y., 1939, p 200.
 (29) G. Poma and G. Bassi, *Gazz. Chim. Ital.*, **51**, 71 (1921).
 (30) G. Poma and A. Nesti, *Gazz. Chim. Ital.*, **51**, 80 (1921).
 (31) J. H. Baxendale and R. D. Sedgwick, *Trans. Faraday Soc.*, **57**, 2157 (1961).
 (32) C. E. Bricker and H. R. Johnson, *Ind. Eng. Chem. Anal. Ed.*, **17**, 400 (1945).
 (33) S. DePaoli and O. P. Strausz, *Can. J. Chem.*, **48**, 3756 (1970).
 (34) M. J. Bueger in "Phase Transformations in Solids", R. Smoluchowski, J. E. Mayer, and W. A. Wey, Ed., Wiley, New York, N.Y., 1951, p 183.
 (35) F. R. N. Nabarro, "Theory of Crystal Dislocations", Clarendon Press, Oxford, 1967, p 595.
 (36) P. J. Sullivan and W. S. Kosk, *J. Am. Chem. Soc.*, **85**, 384 (1963).
 (37) R. H. Johnson, *J. Phys. Chem.*, **65**, 2144 (1961).
 (38) R. P. Porter and W. A. Noyes, *J. Am. Chem. Soc.*, **81**, 2307 (1959).

Aqueous Solutions of Azoniaspiroalkane Halides. I. Enthalpies of Solution, Dilution, and Transfer

David P. Wilson and Wen-Yang Wen*

Jeppson Laboratory, Chemistry Department, Clark University, Worcester, Massachusetts 01610 (Received February 5, 1975)

Publication costs assisted by the National Science Foundation

Enthalpies of solution of azoniaspiroalkane halides, $(\text{CH}_2)_n\text{N}^+(\text{CH}_2)_m\text{X}^-$ ($n = 4, 5, \text{ or } 6$ and $\text{X} = \text{Br}$; for $n = 5$, $\text{X} = \text{Cl}$ and I also), in H_2O have been measured calorimetrically in dilute solution at 25° . For the three bromide salts the enthalpies of solution were also measured in D_2O at 25° . Apparent molal heat contents and enthalpies of transfer obtained are compared with those of the corresponding tetraalkylammonium halides, and the results are discussed in terms of the cation structure (particularly with respect to the presence or absence of flexible alkyl chains). Forming closed loops from the alkyl chains in tetraalkylammonium ions seem to alter their thermodynamic properties greatly and weaken their hydrophobic interactions with water considerably.

Introduction

Azoniaspiroalkane halides have so far been of interest to synthetic organic chemists and workers in the pharmacology field. As a group of curariform-type muscle relaxants, they have been found to inhibit certain enzyme activity, and attempts have been made to correlate the antienzymatic activity of the ions with their structure.¹⁻³

There seem to be rather few reports on the physical properties of solutions of these compounds in the literature. The surface tensions of aqueous solutions of some of the halides have been reported by Thomas and Clough.⁴ The apparent molal volumes at infinite dilution for a few iodides were determined by Barlow et al.⁵ with a pycnometric method on dilute aqueous solutions at 25° . In their NMR line width study of ^{79}Br nuclei in aqueous solutions of various ammonium, phosphonium, and sulfonium salts, Forsen and his coworkers have included azoniaspiro[4.4]nonane bromide.⁶ Lowe and Rendall⁷ reported viscosity and density, as well as conductance measurements of dilute solutions of some "monocyclic" quaternary ammonium iodides.

We are interested in solutions of this type of salt primarily in connection with the studies on solutions of tetraalkylammonium salts. Aqueous solutions of symmetrical tetraalkylammonium salts show many interesting properties which are now being actively investigated in various laboratories.⁸⁻¹⁰ As pointed out by Friedman¹¹ and others,¹² we have to consider the following factors for a better understanding of properties of solutions containing large tetraalkylammonium ions: (i) flexibility of alkyl chains, (ii)

nonspherical shape of the cations, and (iii) penetration of the anion into the space between the alkyl chains.

The flexibility of alkyl chains in a large tetraalkylammonium ion would be greatly reduced if these alkyl chains are linked to form loops. Since these azoniaspiro ions have no terminal methyl group, comparison of the solution properties of these salts with tetraalkylammonium salts of corresponding molecular size is expected to reveal differences between flexible alkyl chains and relatively inflexible methylene groups forming loops.

In this communication we report our experimental results on the enthalpies of solution and dilution of some of the halides in H_2O and D_2O at 25° .

Experimental Section

1. *Materials.* The general methods for preparing some of the azoniaspiroalkane halides $(\text{CH}_2)_n\text{N}^+(\text{CH}_2)_m\text{X}^-$ were introduced by von Braun and coworkers¹³ in 1906 and expanded in his later articles.¹⁴ We have modified some of the recently improved methods for synthesizing these compounds by Blicke and Hotelling,¹⁵ and by Thomas and his coworkers.^{16,17} For convenience we shall use abbreviated names for these compounds, denoting only the halide and the number of carbon atoms in each ring. For example, a spiro quaternary ammonium halide, $\text{C}_{12}\text{H}_{24}\text{NBr}$, will be called "6.6 bromide" in place of its IUPAC name of 7-azoniaspiro[6.6]tridecane bromide or its common name, 1,1-spirobi(hexamethyleniminium bromide). Our method of synthesis may be summarized as follows.

Reagent grade α,ω -dihaloalkane (0.1 mol) was allowed to

react with equimolar cyclic amine (having the same number of methylene groups as the dihaloalkane) in water or 2-propanol containing 0.1 mol of NaOH. After evaporation to dryness, the crude product was extracted and precipitated with chloroform and purified by Soxhlet extractions with methyl ethyl ketone followed by several recrystallizations from 2-propanol and absolute ethanol. (Some variations are necessary for synthesis of different compounds. For details, see ref 18.)

Yields of the reaction, melting point, results of analysis, and solid densities obtained for the five compounds are given.

(a) $(\text{CH}_2)_4\text{N}^+(\text{CH}_2)_4\text{Br}^-$, "4.4 bromide" (5-azoniaspiro[4.4]nonane bromide): final yield, 8.0 g (39%), mp 269–270° (dec), lit. 250–252°,^{15–17} 261–262°,¹⁶ 261.5–262°.⁵ Anal. $\text{C}_8\text{H}_{16}\text{N}$, 61.23; Br, 38.70; $d = 1.40$ g/ml.

(b) $(\text{CH}_2)_5\text{N}^+(\text{CH}_2)_5\text{Br}^-$, "5.5 bromide" (6-azoniaspiro[5.5]undecane bromide): final yield, 15.0 g (64%), mp 331–332°, lit. 300°,⁵ 304°,¹⁷ 309°,¹⁶ 311–312°,¹⁵ 335–336°.⁴ Anal. $\text{C}_{10}\text{H}_{20}\text{N}$, 65.67; Br, 33.96; $d = 1.34$ g/ml.

(c) $(\text{CH}_2)_5\text{N}^+(\text{CH}_2)_5\text{Cl}^-$, "5.5 chloride" (6-azoniaspiro[5.5]undecane chloride): final yield, 5.4 g (28%), mp 350–351° (dec), lit. 310–311°.¹⁵ Anal. $\text{C}_{10}\text{H}_{20}\text{N}$, 81.27; Cl, 18.65; $d = 1.15$ g/ml.

(d) $(\text{CH}_2)_5\text{N}^+(\text{CH}_2)_5\text{I}^-$, "5.5 iodide" (6-azoniaspiro[5.5]undecane iodide): final yield, 8.0 g (28%), mp 253–255°, no literature value available. Anal. $\text{C}_{10}\text{H}_{20}\text{N}$, 53.17;³⁹ I, 44.91; $d = 1.54$ g/ml.

(e) $(\text{CH}_2)_6\text{N}^+(\text{CH}_2)_6\text{Br}^-$, "6.6 bromide" (7-azoniaspiro[6.6]tridecane bromide): final yield, 8.1 g (31%), mp 284.5–285.5°, lit. 281–282°.¹⁵ Anal. $\text{C}_{12}\text{H}_{24}\text{N}$, 69.32; Br, 30.47; $d = 1.37$ g/ml.

The salts were analyzed gravimetrically for the total amount of cations and anions. The cation analysis followed the procedure of Flaschka and Barnard,¹⁹ where the quaternary ammonium ion was precipitated in neutral solution as the tetraphenylboron salt by addition of a twofold excess of purified 3% sodium tetraphenylboron reagent. The anion analysis followed the standard silver halide gravimetric procedure. Triplicate determinations on the cation and anion agreed to within 0.2%. Proton magnetic resonance spectra were taken to check the purity of the compounds and to see if any side reaction such as polymerization occurred in the ring closure process. Densities of the solid compounds were determined by a flotation method similar to that described by Wulff and Heigl.²⁰ The solvents used to form mixtures were benzene and carbon tetrachloride.

Deuterium oxide was obtained from the Stohler Isotope Chemicals, Inc. and used without further purification. Its proton content after experiment was checked with a high-resolution NMR spectrometer indicating that the D_2O content was 99.7% or higher.

2. *Calorimeter.* A constant-temperature environment or isoperibol calorimeter used has been described previously.^{21,22} The calorimeter with some recent modifications¹⁸ was standardized by measuring the heat of solution and neutralization of tris(hydroxymethyl)aminomethane (THAM) in excess 0.103 *m* HCl. The average heat of solution at 25° for seven runs was –7118.0 cal/mol with 95% confidence level of ± 7.3 cal/mol (1 cal = 4.1840 J). This result compares favorably with other values reported, particularly the most recent ones.^{23–27} The main sources of error in the calorimetric experiment were the heats of breaking the glass bulbs containing samples and the error in the measurements of the temperature rise, ΔT , depending on

TABLE I: Enthalpies of Solution of Azoniaspiroalkane Halides in H_2O at 25°^a

$\text{C}_8\text{H}_{16}\text{NBr}$ (4.4 Br)		$\text{C}_{10}\text{H}_{20}\text{NBr}$ (5.5 Br)	
$10^2 m_s^{1/2}$	$\Delta\bar{H}_s$	$10^2 m_s^{1/2}$	$\Delta\bar{H}_s$
(0)	1097 ± 10	(0)	2150 ± 10
5.43	1121 ± 6	5.12	2171 ± 7
8.20	1133 ± 7	8.39	2175 ± 9
10.44	1132 ± 9	11.40	2170 ± 10
13.46	1126 ± 9	14.69	2158 ± 11
17.69	1112 ± 9	17.69	2143 ± 11
21.85	1091 ± 10	20.60	2125 ± 12
26.16	1064 ± 10	23.51	2108 ± 12
31.97	1022 ± 10	27.03	2085 ± 12
35.18	998 ± 10	30.08	2061 ± 13
41.57	945 ± 10	34.15	2029 ± 13
47.42	895 ± 10	36.69	2008 ± 13
55.02	824 ± 10	41.33	1967 ± 14
		43.47	1948 ± 14
		48.67	1898 ± 14
		54.80	1840 ± 14
$\text{C}_{12}\text{H}_{24}\text{NBr}$ (6.6 Br)		$\text{C}_{12}\text{H}_{24}\text{NI}$ (6.6 Br)	
$10^2 m_s^{1/2}$	$\Delta\bar{H}_s$	$10^2 m_s^{1/2}$	$\Delta\bar{H}_s$
(0)	3813 ± 14	28.12	3738 ± 23
3.49	3830 ± 14	31.91	3720 ± 23
3.56	3828 ± 14	32.57	3713 ± 23
5.46	3843 ± 18	37.13	3683 ± 23
6.11	3837 ± 16	41.50	3665 ± 24
7.53	3840 ± 20	41.71	3647 ± 24
10.67	3821 ± 21	49.86	3610 ± 24
14.55	3803 ± 21	54.08	3573 ± 24
18.95	3776 ± 22	59.32	3531 ± 25
22.50	3762 ± 22	62.62	3511 ± 25
$\text{C}_{10}\text{H}_{20}\text{NCl}$ (5.5 Cl)		$\text{C}_{10}\text{H}_{20}\text{NI}$ (5.5 I)	
$10^2 m_s^{1/2}$	$\Delta\bar{H}_s$	$10^2 m_s^{1/2}$	$\Delta\bar{H}_s$
(0)	–1268 ± 15	(0)	4960 ± 20
3.90	–1256 ± 10	3.04	5007 ± 19
6.76	–1234 ± 11	5.13	4976 ± 23
10.13	–1236 ± 12	7.57	4990 ± 24
13.57	–1234 ± 12	10.30	4974 ± 26
16.56	–1240 ± 13	13.17	4962 ± 26
20.73	–1253 ± 13	17.71	4938 ± 27
24.13	–1267 ± 13	21.45	4916 ± 27
28.20	–1286 ± 13	27.22	4873 ± 28
33.74	–1318 ± 13	30.19	4851 ± 29
37.84	–1340 ± 13	34.17	4818 ± 29
		37.80	4786 ± 29

^a m_s = moles of salt per 1000 g of H_2O ; $\Delta\bar{H}_s$ is the enthalpy of solution in calories per mole.

the tolerances of the resistance elements of the Wheatstone bridge. The heats of bulb breaking ranged from 0 to 0.012 cal for bulb sizes from 0.25 to 1.5 ml. After many runs, the blank heats of bulb opening could be estimated to a precision of ± 0.003 cal. The error in the estimation of ΔT is about $\pm 0.1\%$ which is the primary source of random error for large samples.

Results

Enthalpies of solution and apparent molal heat contents of azoniaspiroalkane halides in H₂O at 25° and some of the bromides in D₂O at 25° are tabulated in Tables I–III. For additive enthalpies of solution, where consecutive samples are introduced into solution and the individual enthalpy values recorded, the uncertainty in the enthalpy of solution for the *i*th consecutive sample bulb is

$$\delta_i = \left\{ \sum_{j=1}^i \left[\left(0.001 + \frac{0.003}{Q_j} \right) \Delta \bar{H}_s(m_j) \right]^2 \right\}^{1/2}$$

where Q_j is the experimental heat change on dissolution and $\Delta \bar{H}_s(m_j)$ is the molar enthalpy of solution. The above uncertainty determines the errors of the data reported in Tables I–IV.

The low-concentration enthalpy data have been extrapolated to infinite dilution using the Debye–Hückel limiting law. The apparent molal heat contents, $\phi_L(m)$, at concentration *m* is given by

$$\phi_L(m) = \Delta \bar{H}_s(m) - \Delta \bar{H}_s(1/\infty)$$

TABLE II: Apparent Molal Heat Contents of Azoniaspiroalkane Halides in H₂O at 25°

$m^{1/2}$	ϕ_L , cal/mol				
	4.4 Br ^a	5.5 Br ^a	6.6 Br ^b	5.5 Cl ^b	5.5 I ^c
0	0	0	0	0	0
0.05	23	21	23	22	22
0.10	36	23	17	34	18
0.15	26	7	-15	31	-8
0.20	4	-21	-42	18	-37
0.25	-25	-52	-67	-3	-71
0.30	-61	-87	-89	-28	-109
0.35	-99	-128	-115	-56	-151
0.40	-140	-172	-143		-198
0.45	-182	-218	-171		
0.50	-227	-264	-205		
0.55	-273		-243		
0.60			-283		

^a Average errors of data for the salt are about 15 cal/mol. ^b Average errors of data for the salt are about 20 cal/mol. ^c Average errors of data for the salt are about 25 cal/mol.

where $\Delta \bar{H}_s(1/\infty)$ is the molar enthalpy of solution of a salt at infinite dilution.

Discussion

1. *Apparent Molal Heat Contents in Water.* Our results for the azoniaspiroalkane halides are plotted in Figures 1 and 2 together with those of selected alkali halides²⁸ and tetraalkylammonium halides.^{29,30}

According to Levine and Wood³⁰ the effect of pair-wise interactions on the heat content per mole of salt may be summarized as follows. At low concentrations the deviation from the Debye–Hückel limiting law stems from both the like and oppositely charged interactions. As the concentration increases, the effect of oppositely charged interaction is reduced and the effect of the like-charged interaction is increased.

Comparison of our results with those of the tetraalkylammonium halides seems to reveal the following trends. (i) In the concentration range studied, ϕ_L for 4.4 Br and 6.6 Br decrease with the concentration increase much faster than those of corresponding Et₄NBr and Pr₄NBr, respectively. (ii) Below 0.09 *m*, the decreasing order of ϕ_L for the spiro bromides is 4.4 > 5.5 > 6.6, but above 0.09 *m* the order is 6.6 > 4.4 > 5.5. For tetraalkylammonium bromides, the decreasing order of ϕ_L is Me₄NBr > Pr₄NBr > Et₄NBr for concentrations below 0.04 *m*, but it changes to Pr₄NBr > Me₄NBr > Et₄NBr for concentrations above 0.04 *m* and below 1.4 *m*.³⁰ (iii) The higher concentration (above 1.2 *m*) behavior of ϕ_L for R₄N⁺X⁻ is “regular” depending on the size of the cation (Bu₄N⁺ > Pr₄N⁺ > Et₄N⁺ > Me₄N⁺). The ϕ_L curve crossover of 6.6 Br with 5.5 Br at about 0.1 *m* suggests that the trend for ϕ_L at higher concentrations may similarly become “regular”. It is suspected that when 4.4 Br and 5.5 Br curves crossover as eventually do their tetraalkylammonium counterparts at higher concentrations, the crossover may not take place until much higher concentrations.

Aside from these details, the ϕ_L values of our three spiro bromides are close to each other and considerably lower (more negative) than those of the corresponding tetraalkylammonium bromides, presumably due to the “wrong shape” of these spiro ions as far as the surrounding water structure is concerned. In addition to the shape, the smaller size of the spiro ions should also contribute to their solu-

TABLE III: Enthalpies of Solution and Apparent Molal Heat Contents of Azoniaspiroalkane Bromides in D₂O at 25°^a

$10^2 m'^{1/2}$	4.4 Br		5.5 Br			6.6 Br		
	$\Delta \bar{H}_s$	ϕ_L	$10^2 m'^{1/2}$	$\Delta \bar{H}_s$	ϕ_L	$10^2 m'^{1/2}$	$\Delta \bar{H}_s$	ϕ_L
0	1550 ± 10	0	0	2576 ± 15	0	0	4225 ± 15	0
5.14	1572 ± 6	22	3.64	2596 ± 12	20	3.74	4240 ± 13	15
8.55	1577 ± 8	27	5.78	2592 ± 15	16	5.90	4245 ± 16	20
12.53	1569 ± 8	19	9.06	2590 ± 16	14	8.52	4245 ± 18	20
16.36	1556 ± 9	6	12.52	2572 ± 16	-4	11.46	4240 ± 19	15
20.36	1545 ± 9	-5	17.26	2549 ± 17	-27	14.64	4214 ± 20	-11
24.54	1510 ± 9	-40	23.06	2514 ± 17	-62	21.21	4179 ± 20	-46
29.18	1472 ± 9	-78	27.03	2485 ± 17	-91	23.68	4164 ± 21	-61
34.08	1428 ± 10	-122	34.79	2420 ± 17	-156	28.87	4130 ± 22	-95
37.22	1400 ± 10	-150				32.60	4107 ± 22	-118
42.02	1355 ± 10	-195				36.64	4077 ± 23	-148

^a m' = moles of salt per 55.51 mol of D₂O. $\Delta \bar{H}_s$ is the enthalpy of solution in calories per mole. ϕ_L is the apparent molal heat content in calories per mole.

TABLE IV: Ionic Enthalpies of Transfer from H₂O to D₂O at 25°

Ion	ΔH_{tr} , kcal/mol	Ion	$\Delta \bar{H}_{tr}$, kcal/mol
(CH ₂) ₄ N ⁺ (CH ₂) ₄	0.36 ± 0.02	(C ₂ H ₅) ₄ N ⁺	0.21 ^a
(CH ₂) ₅ N ⁺ (CH ₂) ₅	0.34 ± 0.02	(C ₃ H ₇) ₄ N ⁺	-0.05 ^a
(CH ₂) ₆ N ⁺ (CH ₂) ₆	0.32 ± 0.02	(C ₄ H ₉) ₄ N ⁺	-0.23 ^a
(CH ₃) ₄ N ⁺	0.43 ^a	Br ⁻	0.09 ^a

^a From ref 33.

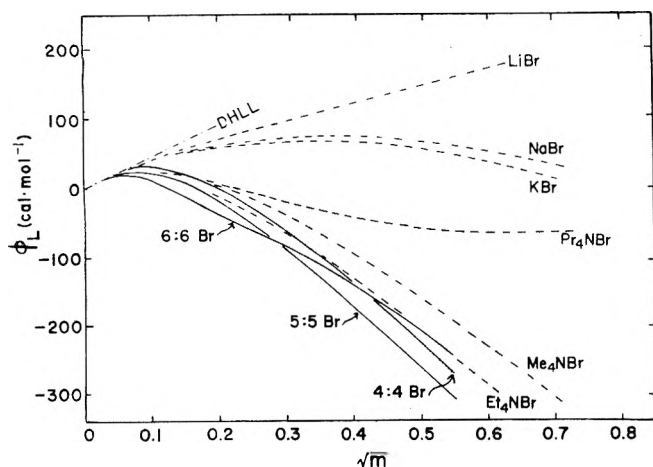


Figure 1. Apparent molal heat contents of the azoniaspiroalkane bromides in H₂O at 25° compared with those of some alkali bromides and tetraalkylammonium bromides.

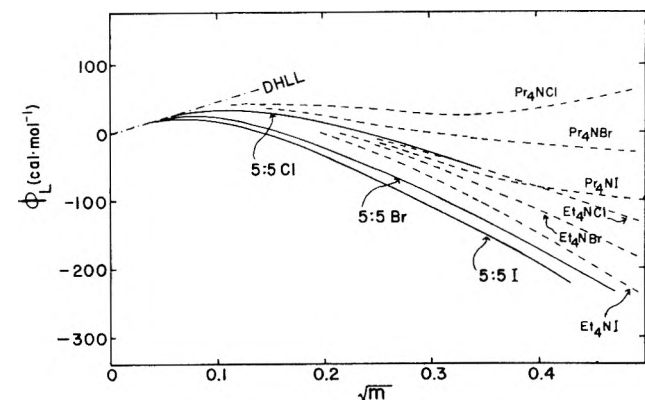


Figure 2. Apparent molal heat contents of 5:5 halides in H₂O at 25° compared with those of some tetraalkylammonium halides.

tion properties. Our recent experimental results³¹ show that the apparent molal volumes at infinite dilution of 4.4 cation and 6.6 cation in water are about 85% of those of Et₄N⁺ ion and Pr₄N⁺ ion, respectively. We also found that the difference in apparent molal volumes at infinite dilution between Pr₄NBr and 6.6 Br is about 10.5 ml/mol greater than the corresponding difference between Et₄NBr and 4.4 Br. It means that the apparent molal volume per methylene or methyl group is larger when the group is farther away from the charged nitrogen center. This seems to provide some indication of the flexibility of the alkyl chains in the larger tetraalkylammonium ion. Since the terminal groups should be most flexible, they are expected to make a substantial contribution to the excess in apparent molal volumes.³¹

In a related way, the apparent molal heat content of a larger tetraalkylammonium ion is expected to be influenced by the swaying terminal methyl groups, since the flexible alkyl chains can fit into the surrounding water structure more easily than the relatively inflexible methylene groups connected to form a tight ring.

2. *Enthalpy of Transfer.* The thermodynamic functions for the transfer of a salt at infinite dilution from one solvent to another reflect differences in solvation, work of cavity formation, dipole interaction, etc. One term which contributes significantly to the enthalpy of solvation in a highly structured solvent is that due to changes in the solvent structure induced by the presence of the solute species. For a transfer process between two aqueous media differing primarily by degree of structuredness, such as D₂O ← H₂O,^{32,33} this effect may be the primary contribution to the enthalpy of transfer. Krishnan and Friedman³⁴ have studied the enthalpies of transfer of sodium *n*-alkylsulfonates from water to heavy water and water-alcohol mixtures as a function of the length of the alkyl chains. Their results illustrated clearly the strong interaction between the hydration regions near the chains and the terminal methyl groups.

The molal enthalpies of transfer for the azoniaspiroalkane bromides can be obtained from the enthalpies of solution in H₂O and D₂O given in Tables I and III. If we assume a value of 0.09 kcal/mol for the enthalpy of transfer of Br⁻ ion from H₂O to D₂O as reported by Krishnan and Friedman,³² then we can obtain the ionic enthalpies of transfer at infinite dilution for the cations. The values obtained are given in Table IV together with those of tetraalkylammonium ions.³²

Based on the ratio of Walden product in D₂O to that in H₂O, Kay and Evans³⁵ concluded that Et₄N⁺ ion has very little effect on the structure of water, Me₄N⁺ ion has structure breaking effect, while Pr₄N⁺ ion and Bu₄N⁺ ions have structure enhancing effect. These interpretations are consistent with the results on the enthalpy of transfer reported by Krishnan and Friedman.³² If we compare our enthalpy of transfer data with those of tetraalkylammonium ions, the $\Delta \bar{H}_{tr}$ values of our spiro ions are all greater than that of Et₄N⁺ ion and less than that of Me₄N⁺ ion.

Levine and Wood³⁰ have plotted $\phi_L(D_2O) - \phi_L(H_2O)$ against aquamolality m' for the R₄NBr series. Their plots are compared with our plots for the spiro compounds in Figure 3. Three curves for the spiro bromides are seen to cluster below the R₄NBr curves. The curve for our 6.6 Br (which is the highest among the three spiro compounds) turns lower than that of Me₄NBr, leading to a dubious implication that it is a water-structure breaker, if we are to follow the frequently used argument based on the sign and trend of heats of transfer from H₂O to D₂O. We are puzzled by this "structure breaking" implication for the (CH₂)₆N⁺(CH₂)₆ ion, because our recent studies on apparent molal heat capacities and viscosities of the salt indicate that 6.6 ion is definitely a structure maker.³¹

Caution should be exercised in any structural interpretation which relies solely on the enthalpy of transfer data at one temperature. In their recent studies of bolaform electrolytes in H₂O and D₂O, Burns and Verrall³⁶ found that $\Delta \bar{H}_{tr}(D_2O \leftarrow H_2O)$ values are small positive for all of the solutes investigated. This would classify the solutes as structure breakers. However, their $\Delta C_{p(tr)}(D_2O \leftarrow H_2O)$ values are relatively large positive, which would classify the solutes as structure makers.

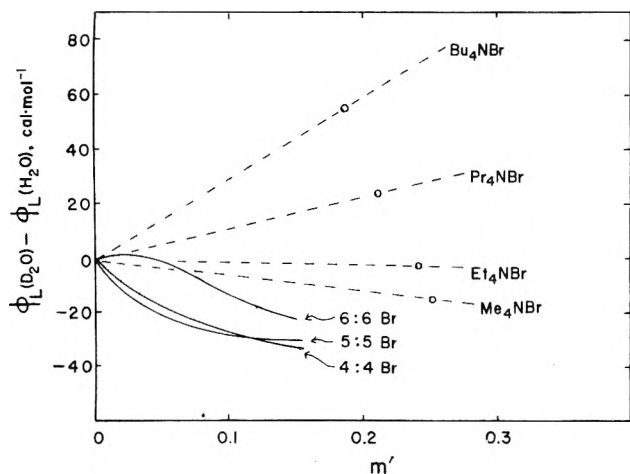


Figure 3. $\phi_L(H_2O) - \phi_L(D_2O)$ for the azoniaspiroalkane bromides at 25° compared with those of tetraalkylammonium bromides.

In an interesting study, Philip and Jolicoeur³⁷ used the scaled-particle theory to investigate the solvent isotope effects. Their conclusion should be taken as a timely warning for our simple interpretations. "In the $D_2O \leftarrow H_2O$ transfer functions of inert solutes, departure from hard-sphere behavior can be attributed to two possible sources: a solute geometrical effect and a local solvent molecular reorientational (structural) effect; the latter does not seem dominant in any of the cases examined here."

For this reason and others,³⁸ it is important to study various properties of the solutes by different techniques, and we are currently engaging in the measurements of apparent molal volumes and heat capacities, viscosities, free energies, as well as some nuclear magnetic properties of these azoniaspiroalkane halides in solutions.

In conclusion, our experiments show that forming closed loops from the alkyl chains in tetraalkylammonium ions has a great effect upon the thermodynamic properties, particularly those which have been regarded as characteristic of aqueous tetraalkylammonium salts. The hydrophobic interaction with the solvent water is weakened considerably for the azoniaspiroalkane ions presumably due to their "wrong shape", lack of swaying terminal methyl groups, and flexible alkyl chains.

Acknowledgments. It is our great pleasure to acknowledge the financial support of the National Science Founda-

tion. Acknowledgment is also made to the donors of the Petroleum Research Fund, administered by the American Chemical Society.

References and Notes

- (1) I. B. Wilson, *J. Biol. Chem.*, **197**, 215 (1952).
- (2) F. Bergmann and A. Shimoni, *Biochem. Biophys. Acta*, **10**, 49 (1953).
- (3) B. D. Roufogalis and J. Thomas, *J. Pharm. Pharmacol.*, **22**, 649 (1970).
- (4) J. Thomas and D. Clough, *J. Pharm. Pharmacol.*, **15**, 167 (1963).
- (5) R. B. Barlow, B. M. Lowe, J. D. Pearson, H. M. Rendall, and G. M. Thompson, *Mol. Pharmacol.*, **7**, 357 (1971).
- (6) H. Wennerström, B. Lindman, and S. Forsen, *J. Phys. Chem.*, **75**, 2936 (1971).
- (7) B. M. Lowe and H. M. Rendall, *Trans. Faraday Soc.*, **67**, 2318 (1971); **68**, 2191 (1972).
- (8) F. Franks, "Effects of Solutes on the Hydrogen Bonding in Water" in "Hydrogen-Bonded Solvent Systems", A. K. Covington and P. Jones, Ed., Taylor & Francis, London, 1968, p 41.
- (9) W.-Y. Wen, "Aqueous Solutions of Symmetrical Tetraalkylammonium Salts" in "Water and Aqueous Solutions", R. A. Horne, Ed., Wiley, New York, N.Y., 1972, Chapter 15, p 613.
- (10) W.-Y. Wen, *J. Solution Chem.*, **2**, 253 (1973).
- (11) P. S. Ramanathan, C. V. Krishnan, and H. L. Friedman, *J. Solution Chem.*, **1**, 237 (1972).
- (12) R. W. Kreis and R. H. Wood, *J. Phys. Chem.*, **75**, 2319 (1971).
- (13) J. von Braun, C. Muller, and E. Beschke, *Berichte*, **39**, 4337 (1906).
- (14) J. von Braun, *Berichte*, **49**, 966 (1916); **56**, 1994 (1923).
- (15) F. F. Blicke and E. B. Hotelling, *J. Am. Chem. Soc.*, **76**, 5099 (1954).
- (16) J. Thomas, *J. Med. Pharm. Chem.*, **3**, 45 (1961).
- (17) B. D. Roufogalis and J. Thomas, *J. Pharm. Pharmacol.*, **20**, 153 (1968).
- (18) D. P. Wilson, Ph.D. Thesis, Clark University, 1974.
- (19) H. Flaschka and A. J. Barnard, Jr., *Adv. Anal. Chem. Instrum.*, **1**, 24 (1960).
- (20) P. Wulf and A. Heigl, *Z. Phys. Chem. A*, **153**, 187 (1931).
- (21) R. B. Cassel and W.-Y. Wen, *J. Phys. Chem.*, **76**, 1369 (1972).
- (22) R. B. Cassel, Ph.D. Thesis, Clark University, 1971.
- (23) R. J. Irving and I. Wadso, *Acta Chem. Scand.*, **18**, 195 (1964).
- (24) S. R. Gunn, *J. Phys. Chem.*, **69**, 2902 (1965).
- (25) I. Petersson, *Acta IMEKO, Proc. Int. Meas. Conf.*, **4th**, **2**, 337 (1968).
- (26) M. V. Kilday and E. J. Prosen, Abstracts, 26th Annual Calorimetry Conference, Orono, Maine, 1971.
- (27) J. D. Navratil and F. L. Oetting, Abstracts, 27th Annual Calorimetry Conference, Park City, Utah, 1972.
- (28) V. B. Parker, *Natl. Stand. Ref. Data. Ser., Natl. Bur. Stand.*, **No. 2** (1965).
- (29) S. Lindenbaum, *J. Phys. Chem.*, **70**, 814 (1966).
- (30) A. S. Levine and R. H. Wood, *J. Phys. Chem.*, **77**, 2390 (1973).
- (31) Unpublished results of W.-Y. Wen, A. LoSurdo, C. Jolicoeur, and J. Boileau. Details will be published shortly.
- (32) C. V. Krishnan and H. L. Friedman, *J. Phys. Chem.*, **74**, 2356 (1970).
- (33) C. Jolicoeur and G. Lacroix, *Can. J. Chem.*, **51**, 3051 (1973).
- (34) C. V. Krishnan and H. L. Friedman, *J. Solution Chem.*, **2**, 37 (1973).
- (35) R. L. Kay and D. F. Evans, *J. Phys. Chem.*, **69**, 4216 (1965); **70**, 366, 2325 (1966).
- (36) J. A. Burns and R. E. Verrall, *J. Solution Chem.*, **2**, 489 (1973).
- (37) P. R. Philip and C. Jolicoeur, *J. Solution Chem.*, **4**, 105 (1975).
- (38) H. S. Frank, "Structural Models", in "Water, A Comprehensive Treatise", Vol. 1, F. Franks, Ed., Plenum Press, New York, N.Y., 1972, p 527, footnote.
- (39) The low percentage of cation analysis reported here was due to the difficulties encountered in filtering the fine colloidal precipitates formed with the sodium tetraphenylboron reagent. The 5.5 iodide prepared is believed to be better than 99% pure.

Heats of Mixing Aqueous Electrolytes. XII. The Reciprocal Salt Pair $\text{Na}^+, \text{Li}^+ || \text{Cl}^-, \text{SO}_4^{2-}$

R. H. Wood,* Danne E. Smith, H. K. W. Chen,

Department of Chemistry, University of Delaware, Newark, Delaware 19711

and P. T. Thompson

Department of Chemistry, Swarthmore College, Swarthmore, Pennsylvania 19081 (Received June 21, 1974; Revised Manuscript Received February 27, 1975)

Publication costs assisted by the National Science Foundation

The heats of mixing aqueous solutions of all combinations of the reciprocal salt pair $\text{Na}^+, \text{Li}^+ || \text{Cl}^-, \text{SO}_4^{2-}$ have been measured at 25°. In one set of experiments, the initial solutions had the same molal ionic strength ($I = 1, 3, \text{ or } 6 \text{ mol/kg}$). In another set of experiments, the initial solutions had the same number of equivalents per kilogram of solvent ($E = 1, 3, \text{ or } 6 \text{ mol/kg}$). For charge-asymmetric mixtures, the magnitude of constant E mixings is about the same as that of the constant I mixings. Young's cross-square rule is quite accurate at $I = 3 \text{ mol/kg}$ and $E = 3$ and 6 mol/kg , marginal at I and $E = 1$ and fails definitely at $I = 6 \text{ mol/kg}$. The constant E mixing process is preferred because the cross-square rule holds at higher concentrations. The predictions of the cross-square rule based on both constant I and constant E mixings are surprisingly accurate at these high concentrations in view of the fact that sodium and sulfate as well as lithium and sulfate ions have rather strong interactions.

Introduction

According to Young's cross-square rule,¹ for a reciprocal salt pair, the sum of the heats of mixing involving a common ion equals the sum of the heats of mixing not involving a common ion. This rule has been shown to be quite accurate in predicting heats of mixing aqueous solutions of charge-symmetric electrolytes.¹⁻³ For charge-asymmetric mixtures appropriate weighting factors should be used for constant ionic strength mixings.⁴ Wood and Ghamkhar⁵ suggested that for charge-asymmetric mixtures, mixing at a constant number of equivalents per kilogram of water (E) might be preferred to mixing at constant molal ionic strength (I), especially at higher electrolyte concentrations (>0.2 ional). Reilly and Wood⁶ recently measured the heats of mixing of aqueous solutions of the reciprocal salt pair $\text{Mg}^{2+}, \text{Na}^+ || \text{Cl}^-, \text{Br}^-$ at both constant E and constant I . Their results indicated the accuracy of Young's rule for both types of mixing even at very high concentrations ($I, E = 6 \text{ mol/kg}$). The heat of mixing with a common ion was lower for the constant E mixings indicating the potential usefulness of the constant E mixing process. The present investigation was undertaken in order to study the relative advantages of the E concentration scale when strong cation-anion interactions are present.

Experimental Section

Because the complete experimental procedures and results for both the constant I ⁷ and constant E ⁸ mixings have been given elsewhere, only a brief description will be given here. The solutions were prepared from reagent grade salts and deionized distilled water. All impurities recorded for these salts were less than 0.1%. The sodium salts were dried under vacuum for 24 hr at 100°. Lithium chloride was dried under vacuum for 24 hr at 200°. The lithium sulfate used for the constant ionic strength runs was dried under vacuum at 200° for 24 hr.⁹ The lithium sulfate used in the con-

stant equivalents per kilogram measurements was standardized by conductance measurements on solutions that were diluted to 0.1 m . The conductance of 0.1 m lithium sulfate was first determined by drying two separate samples at 500° in silica crucibles for 15 hr.^{10,11} Solutions with $m = 0.1000 \text{ mol/kg}$ were prepared from these samples and the conductivity measured at $25 \pm 0.02^\circ$. The conductivity for $m = 0.1000 \text{ mol/kg}$ Li_2SO_4 is $141.63 \pm 0.04 \text{ g mol}^{-1} \text{ ohm}^{-1} \text{ cm}^{-1}$. The conductance cell was calibrated using potassium chloride standards.

The pH was adjusted to 9 for the sulfate solutions and to 8 for the chlorides by the addition of negligible amounts ($\ll 0.1\%$) of NaOH or LiOH.

The mixings at constant E were measured with a LKB batch microcalorimeter.¹² The calorimeter and the experimental procedure have been described in detail elsewhere.^{6,13}

The calorimeter used for the constant ionic strength mixings⁷ consisted of a 250-ml Dewar flask with magnetic stirring which was immersed in a constant temperature bath. A 20-ml solution pipet occupied the center of the flask. A 2000-ohm thermistor was used to detect the temperature changes and an electrical heater was used for standardization. The calorimeter had an accuracy of about $\pm 0.4\% \pm 0.003 \text{ cal}$ for a single experiment.

The calorimeter was checked by measuring the heat of dilution of 12 m urea with satisfactory agreement with literature values. The average of five runs when corrected to a final molality $m = 0.78 \text{ mol/kg}$ was $\Delta H^{\text{ex}} = \Delta\phi_L = 466.1 \text{ cal/mol}$ with a standard deviation of the average of 1.2. The data of Hamilton and Stokes¹⁴ yield a calculated value of 465.6 cal/mol. The results are consistent with those of Egan and Luff¹⁵ but are about 1% lower than the results of Guckler and Pickard.¹⁶

Treatment of Data and Results

The treatment of the data is the same as that used previously.⁶ The constant I mixings consisted of mixing two

solutions of the same molal ionic strength ($I = \frac{1}{2} \sum_i m_i Z_i^2$). The change in enthalpy for this process ($\Delta_m H$) is represented by the equation

$$\Delta_m H / n_w M_w = y_A y_B I^2 (RTh_0^I + (y_B - y_A) RTh_1^I + \dots) \quad (1)$$

where y_A is the ionic strength fraction of salt A, y_B is the ionic strength fraction of salt B, $\Delta_m H$ is the change in enthalpy (in calories), and $n_w M_w$ is the weight of water (in kg). The quantity RTh_0^I is a measure of the magnitude of the heat of mixing at $y = 0.5$ and the quantity RTh_1^I is a measure of the skew in the heat of mixing.

Similarly the enthalpy of mixing of two solutions of the same equivalents per kilogram ($E = \frac{1}{2} \sum_i m_i |Z_i|$) is given by the equation

$$\Delta_m H / n_w M_w = y_A' y_B' E^2 (RTh_0^E + (y_B' - y_A') RTh_1^E + \dots) \quad (2)$$

where y_A' is the equivalent fraction of salt A, etc. The individual experimental measurements at a given I or E were fit by least-squares procedures to eq 1 or 2. The results are given in Table I. Tests showed that in all but a few borderline cases a higher term in eq 1 or 2 was not necessary to fit the data within the experimental precision. Between four and seven experimental points were measured for each mixing. The range of y_A covered was 0.1 to 0.25 and 0.75 to 0.9 while the range of y_A' covered was about 0.25 to 0.75.

Discussion

Because some of the present results involve supersaturated solutions of Na_2SO_4 (I and $E = 6$ mol/kg), it is useful to have more than the usual number of checks on the accuracy of the data. The data for the Li_2SO_4 - Na_2SO_4 mixing at constant I can be compared with the data at constant E . For instance, both the $E = 2$ mol/kg and $I = 3$ mol/kg mixings involve solutions which are 1 m . For this reason, the constant E mixing results can be recalculated as constant I mixings. When calculated values of RTh_0^I were plotted vs. I , the initial results did not lie on a smooth curve. It appeared that the original $I = 6$ mol/kg heat of mixing was too high.⁷ When this mixing was remeasured (see Table I footnote *d*) with the LKB calorimeter, the results did lie on a smooth curve within the experimental error. The 2 mol/kg solution is slightly supersaturated ($m_{\text{sat}} = 1.96$ mol/kg). If crystallization occurred before opening the pipet, the results would be too high as observed.

For LiCl - NaCl mixtures, Stern and Anderson¹⁷ found $RTh_0 = 83.6, 57.8$, and 32.0 cal kg mol⁻²; $RTh_1 = 6.3, 12.2$, and 12.3 cal kg mol⁻² at ionic strengths of 1, 3, and 6 mol/kg. In addition, for this same salt pair, Wu, Smith, and Young² reported $RTh_0 = 84.6$ cal kg mol⁻² and $RTh_1 = 6.6$ cal kg mol⁻² at $I = 1$ mol/kg. The agreement with the present results is satisfactory. For the NaCl - Na_2SO_4 mixing, Wu, Smith, and Young report $RTh_0 = -27.1$ cal kg mol⁻² and $RTh_1 = 3.0$ cal kg mol⁻² which is in good agreement with the present results. The present results for NaCl - Na_2SO_4 mixtures at $I = 1, 3$, and 6 mol/kg lie on a smooth curve with the data of Smith at $I = 0.2, 0.5, 2$, and 5¹⁸ mol/kg.

For charge symmetric mixtures, Wu, Smith, and Young² derived an exact thermodynamic relationship between the difference in the two mixings without a common ion (the cross mixings) and the excess heat contents (ϕ_L) of the four salts. This relationship depends on the fact that 50/50 mixtures of the two salts without a common ion give identi-

cal solutions. For constant E mixings, the derivation is essentially unchanged and the results are

$$\begin{aligned} \Delta_m H(\text{Li}_2\text{SO}_4\text{-NaCl}, y' = 1/2) / n_w M_w + \\ (E/4)[\phi_L(\text{Li}_2\text{SO}_4, E) + 2\phi_L(\text{NaCl}, E)] = \\ \Delta_m H(\text{Na}_2\text{SO}_4\text{-LiCl}, y' = 1/2) / n_w M_w + \\ (E/4)[\phi_L(\text{Na}_2\text{SO}_4, E) + 2\phi_L(\text{LiCl}, E)] \quad (3) \end{aligned}$$

where $\phi_L(\text{Li}_2\text{SO}_4, E)$ is the excess enthalpy (cal/mol of Li_2SO_4) of pure Li_2SO_4 at a concentration E and the enthalpies of mixing are calculated at the same E and $y' = 1/2$. For constant I mixings, the derivation takes account of the fact that, for constant ionic strength solutions, the mixture of LiCl and Na_2SO_4 at $y(\text{Na}_2\text{SO}_4) = 3/5$ is the same solution as the mixture of NaCl with Li_2SO_4 at $y(\text{Li}_2\text{SO}_4) = 3/5$. The resulting equation is

$$\begin{aligned} \Delta_m H(\text{Li}_2\text{SO}_4\text{-NaCl}, y_A = 3/5) / n_w M_w + \\ (I/5)[\phi_L(\text{Li}_2\text{SO}_4, I) + 2\phi_L(\text{NaCl}, I)] = \\ \Delta_m H(\text{Na}_2\text{SO}_4\text{-LiCl}, y_A = 3/5) / n_w M_w + \\ (I/5)[\phi_L(\text{Na}_2\text{SO}_4, I) + 2\phi_L(\text{LiCl}, I)] \quad (4) \end{aligned}$$

When these equations are used to check if the heats of the two cross mixings are consistent with the heats of dilution,¹⁹ the agreement is quite satisfactory. For instance, the right- and left-hand sides of eq 3 are 160 ± 4 and 156 ± 4 cal/kg at $E = 1$ mol/kg, 263 ± 13 and 291 ± 10 ²⁰ cal/kg at $E = 3$ mol/kg, and 1184 ± 26 and 1194 ± 26 cal/kg at $E = 6$ mol/kg. Similarly, the right- and left-hand sides of eq 4 are 130 ± 4 and 132 ± 3 cal/kg at $I = 1$ mol/kg, 266 ± 8 and 269 ± 10 cal/kg at $I = 3$ mol/kg, and 652 ± 18 and 622 ± 17 cal/kg at $I = 6$ mol/kg. The estimated errors are based on 5 cal/mol for H^{ex} of NaCl and LiCl and 10 cal/mol for Na_2SO_4 and Li_2SO_4 .

In the present results, the skew terms in Table I (RTh_1^I or RTh_1^E) are no longer always small compared to the parabolic term (RTh_0). The same result was found for the other charge-asymmetric reciprocal salt pair that has been measured.⁶ The increase in skew for charge-asymmetric mixtures is expected since all triplet interactions contribute to skew. For charge-symmetric mixtures only triplets involving three ions of the same sign contribute to the skew term.

If the pairwise interactions are the most important terms, it would be expected that RTh_0^E for the Na_2SO_4 - Li_2SO_4 mixing at some concentration, E , would be close to $RTh_0^I (= RTh_0^E)$ for NaCl - LiCl at the same E . This is because both mixings involve the same sodium ion and lithium ion concentrations. The results in Table I show that the values of RTh_0 are within 20% of each other at $E = 1, 3$, and 6 mol/kg, and thus that the Na-Na, Na-Li, and Li-Li interactions are the most important.

Wood and Ghamkhar⁵ suggested that for charge-asymmetric mixtures the constant E mixings would, to a first approximation, cancel the oppositely charged pairwise interactions in a common-ion mixture and, thus, the heat of mixing at constant E normally would be smaller than the heat of mixing at constant I . Reilly and Wood⁶ found that RTh_0 for the common ion, charge-asymmetric mixtures in the system Mg^{2+} , $\text{Na}^+||\text{Cl}^-$, Br^- were much smaller for constant E than for constant I mixing.

The results for the Na_2SO_4 - NaCl and Li_2SO_4 - LiCl mixings in Table I show that RTh_0 for the constant E mixings are of the same order of magnitude as the RTh_0 for the constant I mixings.

TABLE I: Enthalpy of Mixing at Constant Ionic and Equivalent Strength
(A) Constant Ionic Strength Mixes

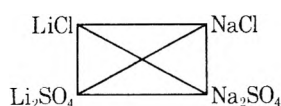
Salt pair	$I = 1$ mol/kg		$I = 3$ mol/kg		$I = 6$ mol/kg	
	RTh_0^I , cal kg mol ⁻²	RTh_1^I , cal kg mol ⁻²	RTh_0^I , cal kg mol ⁻²	RTh_1^I , cal kg mol ⁻²	RTh_0^I , cal kg mol ⁻²	RTh_1^I , cal kg mol ⁻²
Na ₂ SO ₄ (A)–Li ₂ SO ₄ (B)	48.7(7) ^a	4(1)	34.3(4)	5.8(7)	20(1) ^d	-5(3)
NaCl(A)–LiCl(B)	82.5(8)	6(1)	59(2)	13(2)	34(2)	14(2)
Na ₂ SO ₄ (A)–NaCl(B)	-26.6(9)	+2.1(15)	-13.7(3)	+4.9(5)	-7.2(2)	+4.5(3)
Li ₂ SO ₄ (A)–LiCl(B)	-26(5)	+8(8)	-26.0(1)	+1.3(2)	-34.4(3)	+3.0(5)
$\Sigma \square^b$ (weighted)	72(5)		49(2)		10(2)	
Na ₂ SO ₄ (A)–LiCl(B)	61.6(12)	-6(2)	6.0(3)	3.4(5)	-22.9(8)	8(1)
Li ₂ SO ₄ (A)–NaCl(B)	18.3(16)	-11(3)	43(2)	-8(3)	41.2(3)	-4.2(4)
$\Sigma \times^c$	80(2)		49(2)		18.3(9)	

(B) Constant Equivalents per Kilogram of Solvent Mixes

Salt pair	$E = 1$ mol/kg		$E = 3$ mol/kg		$E = 6$ mol/kg	
	RTh_0^E , cal kg mol ⁻²	RTh_1^E , cal kg mol ⁻²	RTh_0^E , cal kg mol ⁻²	RTh_1^E , cal kg mol ⁻²	RTh_0^E , cal kg mol ⁻²	RTh_1^E , cal kg mol ⁻²
Na ₂ SO ₄ (A)–Li ₂ SO ₄ (B)	106(5)	14(15)	49.5(16)	12(10)	34.0(11)	8(4)
NaCl(A)–LiCl(B)	82.5(8)	6(1)	59(2)	13(2)	34(2)	14(2)
Na ₂ SO ₄ (A)–NaCl(B)	-21.1(7)	2(2)	-7.0(4)	1(1)	17.0(12)	2(3)
Li ₂ SO ₄ (A)–LiCl(B)	4.7(10)	3(3)	13.2(4)	3(1)	19.9(2)	0.1(6)
$\Sigma \square^b$	172(5)		115(3)		105(3)	
Na ₂ SO ₄ (A)–LiCl(B)	258(2)	12(6)	127(3)	22(8)	71(2)	5(7)
Li ₂ SO ₄ (A)–NaCl(B)	-77(2)	-28(6)	-10.7(8)	-18(2)	32(2)	-7(6)
$\Sigma \times^c$	181(3)		116(3)		103(3)	

^a The number in parentheses expresses the 95% confidence limits of the least significant digit; i.e., 48.7 ± 0.7 becomes 48.7(7). This estimate does not include any systematic errors. ^b For constant E mixings this is the sum around the square. For constant I mixings it is the weighted sum around the square (eq 5). ^c This is the sum of the cross terms in eq 5 and 6. ^d The raw data for this point do not appear in ref 7 or 8. Measurements with the LKB calorimeter gave the following results: (weight Na₂SO₄ solution), (weight Li₂SO₄ solution), ($\Delta_m H$): 1.989 g, 6.525 g, 0.748 cal; 3.214 g, 4.603 g, 1.014 cal; 5.583 g, 1.977 g, 0.933 cal. The ionic strength of the solutions was 5.961 mol/kg.

All of the mixings in a reciprocal salt pair can be represented by the diagram



where the common ion mixtures are represented by the sides of the square, and the mixings without a common ion are represented by the cross terms. Young and coworkers^{1,2} suggested that the sum of the terms around the square ($\Sigma \square$) should be equal to the sum of the two cross terms ($\Sigma \times$) and this is now known as Young's cross-square rule. Numerous measurements have shown that this rule usually gives quite accurate predictions for excess free energies,²¹⁻²⁵ heats,¹⁻⁴ and volumes.²⁶⁻²⁸ For charge-asymmetric mixtures at constant ionic strength, Reilly and Wood²⁹ showed that a weighted cross-square rule should be used. For the present reciprocal salt pair, the weighted cross-square rule is

$$RTh_0^I(\text{LiCl}-\text{Na}_2\text{SO}_4) + RTh_0^I(\text{NaCl}-\text{Li}_2\text{SO}_4) = \\ RTh_0^I(\text{NaCl}-\text{Na}_2\text{SO}_4) + RTh_0^I(\text{LiCl}-\text{Li}_2\text{SO}_4) + \\ (4/5)RTh_0^I(\text{NaCl}-\text{LiCl}) + (6/5)RTh_0^I(\text{Na}_2\text{SO}_4-\text{Li}_2\text{SO}_4) \quad (5)$$

The results in Table I show that the cross-square rule is

quite accurate at $I = 3$, marginal at $I = 1$, and definitely fails at $I = 6$ mol/kg.

For charge asymmetric mixings at constant E , Reilly and Wood⁶ showed that the unmodified cross-square rule is appropriate. The equation is

$$RTh_0^E(\text{LiCl}-\text{Na}_2\text{SO}_4) + RTh_0^E(\text{NaCl}-\text{Li}_2\text{SO}_4) = \\ RTh_0^E(\text{NaCl}-\text{Na}_2\text{SO}_4) + RTh_0^E(\text{LiCl}-\text{Li}_2\text{SO}_4) + \\ RTh_0^E(\text{NaCl}-\text{LiCl}) + RTh_0^E(\text{Na}_2\text{SO}_4-\text{Li}_2\text{SO}_4) \quad (6)$$

The results in Table I showed that the cross-square rule is quite accurate at $E = 3$ and 6 and marginal at $E = 1$ mol/kg.

The cross-square rules are expected to fail as the concentration increases because of larger contributions from higher order interactions which are expected to be strong in this system. Davies³⁰ concludes from the available conductivity and transport numbers that both sodium sulfate and lithium sulfate are somewhat ion paired. This indicates strong attractive forces between lithium or sodium and sulfate ions. The present data, although limited, indicate that the cross-square rule at constant E is obeyed to higher concentrations than is the rule at constant I .

In some respects, it is very surprising that the cross-square rule works at all in this system. Both NaCl–Na₂SO₄ and NaCl–BaCl₂ mixings show very anomalous behavior at the low ionic strengths, $I = 0.05$ – 0.2 ³¹ mol/kg. In particular,

a large amount of skew is found, which shows that triplet terms are important even at these low concentrations. It may be that the anomalous behavior at low concentrations is due to long-range electrostatic forces between the ions and that as the concentration of ions increases the shielding of these forces by the high local concentration of ions makes the effective force between ions of much shorter range and thus the properties of the solutions much more regular. Recent experimental results on NaCl–Na₂SO₄ and NaCl–BaCl₂³¹ and theoretical results³² on charge-asymmetric mixtures show that the behavior of RTh_0 and RTh_1 is much more regular at concentrations above $I = 0.1$ mol/kg. The interactions responsible for the low concentration anomalies could also be responsible for the slight failure of the cross-square rule at I and $E = 1$ mol/kg.

Although the amount of data is limited, it still appears that the constant E mixing process is advantageous at high concentrations. For the present system, the common-ion mixings are not much smaller at constant E but the cross-square rule does hold at higher concentrations when constant E mixings are used.

Acknowledgments. The authors are grateful to the Office of Saline Water U.S. Department of the Interior, and the National Science Foundation for support of this work.

References and Notes

- (1) T. F. Young, Y. C. Wu, and A. A. Krawetz, *Discuss. Faraday Soc.*, **24**, 27, 77, 80 (1957).
- (2) Y. C. Wu, M. B. Smith, and T. F. Young, *J. Phys. Chem.*, **69**, 1868, 1873 (1965).
- (3) R. H. Wood and R. W. Smith, *J. Phys. Chem.*, **69**, 2974 (1965).
- (4) R. H. Wood and H. L. Anderson, *J. Phys. Chem.*, **70**, 992 (1966).
- (5) R. H. Wood and M. Ghamkhar, *J. Phys. Chem.*, **73**, 3959 (1969).
- (6) P. J. Reilly and R. H. Wood, *J. Phys. Chem.*, **76**, 3474 (1972).
- (7) H. K. W. Chen, M.S. Thesis, University of Delaware, June, 1971.
- (8) D. E. Smith, M.S. Thesis, University of Delaware, May, 1973.
- (9) Duval, "Inorganic Thermogravimetric Analysis", Elsevier, New York, N.Y., 1953, pp 60, 91–92.
- (10) G. Akerlof, *J. Am. Chem. Soc.*, **48**, 1160 (1926).
- (11) Kitajima, *J. Chem. Soc. Jpn.*, **55**, 199 (1934).
- (12) LKB—Produkter A B, Fack, 161 25 Bromma 1, Sweden, Model 10700-2.
- (13) I. Wadso, *Acta. Chem. Scand.*, **22**, 927 (1968).
- (14) D. Hamilton and R. H. Stokes, *J. Solution Chem.*, **1**, 223 (1972).
- (15) E. P. Egan and B. B. Luff, *J. Chem. Eng. Data*, **11**, 192 (1966).
- (16) F. T. Gucker, Jr., and H. B. Pickard, *J. Am. Chem. Soc.*, **62**, 1464 (1940).
- (17) J. H. Stern and C. W. Anderson, *J. Phys. Chem.*, **68**, 2528 (1964).
- (18) M. B. Smith, Ph.D. Dissertation, University of Chicago, Chicago, Ill., 1942.
- (19) P. T. Thompson, D. E. Smith, and R. H. Wood, *J. Chem. Eng. Data*, **19**, 386 (1974).
- (20) The limits of error are only rough estimates so the slight disagreement in one consistency check is probably not significant.
- (21) Y. C. Wu, R. M. Rush, and G. Scatchard, *J. Phys. Chem.*, **72**, 4048 (1968); **73**, 2047, 4434 (1969).
- (22) A. K. Covington, T. H. Lilley, and R. A. Robinson, *J. Phys. Chem.*, **72**, 2759 (1968).
- (23) R. A. Robinson, A. K. Covington, and C. P. Bezboruah, *J. Chem. Thermodyn.*, **2**, 431 (1970).
- (24) R. F. Platford, *J. Chem. Thermodyn.*, **3**, 319 (1971).
- (25) R. A. Robinson and R. F. Platford, *J. Solution Chem.*, **1**, 167 (1972).
- (26) H. E. Wirth, R. Lindstrom, and J. Johnson, *J. Phys. Chem.*, **67**, 2339 (1963).
- (27) H. E. Wirth and W. L. Mills, *J. Chem. Eng. Data*, **13**, 102 (1968).
- (28) H. E. Wirth and A. LoSurdo, *J. Chem. Eng. Data*, **13**, 226 (1968).
- (29) P. J. Reilly and R. H. Wood, *J. Phys. Chem.*, **73**, 4292 (1969).
- (30) C. W. Davies, "Ion Association", Butterworths, Washington, D.C., 1962, p 169.
- (31) R. B. Cassel and R. H. Wood, *J. Phys. Chem.*, **78**, 1924 (1974).
- (32) H. L. Friedman and C. V. Krishnan, *J. Phys. Chem.*, **78**, 1927 (1974).

Heats of Mixing Aqueous Electrolytes. XIII. The Reciprocal Salt Pair Na^+ , $\text{Mg}^{2+}||\text{Cl}^-$, SO_4^{2-}

R. F. Srna and R. H. Wood*

Department of Chemistry, University of Delaware, Newark, Delaware 19711 (Received June 21, 1974; Revised Manuscript Received February 27, 1975)

Publication costs assisted by the National Science Foundation

The heats of mixing aqueous solutions of all combinations of the reciprocal salt pair Na^+ , $\text{Mg}^{2+}||\text{Cl}^-$, SO_4^{2-} have been measured at 25°. In one set of experiments, the initial solutions had the same molal ionic strength ($I = 1, 3, \text{ or } 6$ mol/kg). In another set of experiments, the initial solutions had the same number of equivalents per kilogram of solvent ($E = 1, 3, \text{ or } 6$ mol/kg). The cross-square rule does not hold for this system at any concentration studied. For constant I mixings, the sum of the cross terms is about 10% higher than the sum of the square terms. For constant E mixings, the sum of the cross terms is about 20% higher than the sum of the square terms. The failure of the cross-square rule is due to the strong attractive forces between the magnesium and sulfate ions. Rough calculations based on an ion-pairing model are able to predict the signs and magnitude of some of the results.

Introduction

According to Young's cross-square rule for a reciprocal salt pair² the sum of the heats of mixing involving a common ion equals the sum of the heats of mixing not involving a common ion. This rule has been shown to be quite ac-

curate in predicting heats of mixing aqueous solutions for charge-symmetric mixtures.^{2,3} For charge-asymmetric mixtures, appropriate weighting factors should be used for constant ionic strength mixings (constant I).⁴ For mixings in which the two solutions contain the same number of equivalents per kilogram of water (constant E) the cross-

square rule holds without weighting factors.⁵ Wood and Ghamkhar suggested that mixings at constant equivalents per kilogram (E) might be preferred to mixing at constant molal ionic strengths (I) when charge-asymmetric mixtures at high concentrations are involved.⁶ Studies of the reciprocal salt pairs Na^+ , $\text{Mg}^{2+}||\text{Cl}^-$, Br^- ⁵ as well as the salt pair Na^+ , $\text{Li}^+||\text{Cl}^-$, SO_4^{2-} ⁷ at both constant E and constant I have shown that constant E mixings are preferred at higher concentrations. One of the surprising results of these studies is that for constant E mixings the cross-square rule holds even at $E = 6$ mol/kg.

The present investigation was undertaken to see if the cross-square rule would still hold in a system with two divalent ions and with much stronger interactions between two of the ions (Mg^{2+} and SO_4^{2-}). The system was also of interest from a practical standpoint because it contains all of the major components of seawater. The results of this investigation show that in this system the interactions are so strong that the cross-square rule no longer holds (I or $E = 1$ to 6 mol/kg).

Experimental Section

Only a brief description of the experimental procedures will be given here because they have been given in detail elsewhere.⁸ The sodium sulfate solutions were prepared by weight from ACS grade sodium sulfate after drying in a vacuum oven for 3 days at 125°. Carl Fisher analysis indicated less than 0.003% water in the salt dried by this method. The pH of these solutions was between 6.5 and 7.0. Supersaturated solutions ($m = 1.96$ mol/kg or larger at 25°) were maintained at 60° until the solution was needed. A stock solution of magnesium chloride was made from ACS grade $\text{MgCl}_2 \cdot 6\text{H}_2\text{O}$ and standardized with an EDTA solution using the technique described by Schwartzbach.⁹ Since the pH of all MgCl_2 solutions was acidic (approximate pH 5.7) small amounts of 0.1 mol/kg NaOH solution (less than 0.025 mol %) were added to adjust the final pH of the solutions to 6.5–7. Magnesium sulfate solutions were prepared from Fisher Certified salt and standardized by titration with EDTA. The 3 mol/kg solution is slightly supersaturated so it was stored at 60°. The pH was adjusted to 6.5–7.0 using negligible amounts (less than 0.1%) of 0.1 N HCl. A stock solution of reagent grade sodium chloride was titrated with silver nitrate using Fajan's method. The pH of the solution was between 6.5 and 7.0. The preparation and standardization of all solutions was carried out with an accuracy of 0.1% or better. In all cases the impurities in the salts were negligible (less than 0.05%).

The 250-ml isothermal dewar calorimeter^{7,8} and the LKB Model 10700-2 batch microcalorimeter used in this research have been described previously.^{5,10} The dewar calorimeter was used for all $I = 1$ and 3 mol/kg mixings, all $E = 1$ mol/kg mixings and the $E = 3$ mol/kg NaCl– MgSO_4 mixing. The LKB calorimeter was used for all other experiments and for one duplicate of the $I = 3$ mol/kg Na_2SO_4 – MgCl_2 mixing. The dewar calorimeter was checked by measuring the heat of dilution of urea ($m = 12.00$ mol kg^{-1}) to a final concentration of 0.060 mol kg^{-1} . The results of three runs were 0.5% \pm 0.3% lower than the results of Gucker and Pickard¹¹ and about 0.5% higher than the results of Hamilton and Stokes¹² and Eagen and Luff.¹³

In using the LKB calorimeter, the cells were rinsed and dried with a stream of nitrogen and then filled by weight using plastic disposable syringes. With the more viscous solutions as many as three separate mixes were necessary to

assure complete mixing. The calorimeter was calibrated electrically after each experimental run. When using supersaturated solutions, the warm solutions were transferred by weight into the calorimeter cell. The cell was allowed to equilibrate for 15–30 min and this equilibration was monitored by the heat flow sensor in the calorimeter. The cell contents occasionally crystallized but this was easily detectable as an exothermic break in the equilibration curve. The accuracy of these supersaturated runs is somewhat lower than normal because of the short equilibration times.

The pH of all solutions was adjusted to 6.5–7.0 in order to reduce the heat effects due to hydrolysis of both Mg^{2+} and SO_4^{2-} . In this pH range the amount of MgOH^+ plus HSO_4^- is at a minimum.^{8,14} Several measurements of the pH change during the mixing process indicated that it was typically less than 0.2 pH units. Calculations indicate that the heat effects due to changes in hydrolysis of either Mg^{2+} or SO_4^{2-} are small compared to the experimental error.

Results and Discussion

The treatment of the data is the same as that used previously.^{5,7} The constant I mixings consisted of mixing two solutions of the same molal ionic strength ($I = (\frac{1}{2})\sum_i m_i Z_i^2$). The change in enthalpy for this process ($\Delta_m H$) is represented by the equation

$$\Delta_m H^{\text{ex}}/W = y_A y_B I^2 (RTh_0^I + (y_B - y_A)RTh_1^I + (y_B - y_A)^2 RTh_2^I) \quad (1)$$

where y_A is the ionic strength fraction of salt A, y_B is the ionic strength fraction of salt B, $\Delta_m H$ is the change in enthalpy (in calories), and W is the weight of water (in kg). The quantity RTh_0^I is a measure of the skew in the heat of mixing.

Similarly the enthalpy of mixing two solutions of the same number of equivalents per kilogram ($E = (\frac{1}{2})\sum_i m_i |Z_i|$) is given by⁵

$$\Delta_m H^{\text{ex}}/W = y_A' y_B' E^2 (RTh_0^E + (y_B' - y_A')RTh_1^E + (y_B' - y_A')^2 RTh_2^E) \quad (2)$$

where y_A' is the equivalent fraction of salt A, etc. The individual experimental measurements at a given I or E were least-squares fit to eq 1 or 2. The results are given in Table I and shown in Figures 1–4. If the RTh_2 in eq 1 and 2 is unnecessary to fit the data, then the plots in Figures 1–4 should be straight lines with intercept at $y = 0.5$ (or $y_B - y_A = 0$) equal to RTh_0 and slope equal to $-2RTh_1$. This follows from the fact that $y_B - y_A = 1 - 2y_A$. An F test at 95% confidence level indicated that RTh_2 was not necessary to fit the mixings with a common ion except for $E = 3$ mol/kg Na_2SO_4 with MgSO_4 and $E = 1$ mol/kg MgCl_2 with MgSO_4 which were borderline cases. Since these were borderline cases, only two parameters were used for all of the common ion mixings. An F test showed that, for the two mixtures without a common ion (MgSO_4 with NaCl and Na_2SO_4 with MgCl_2), RTh_2 is necessary to fit the data at nine of the twelve concentrations. This is also seen in the curvature of the plots in Figures 1 and 2. For this reason RTh_2 terms were used in fitting all of the mixtures without a common ion.

Eight points were eliminated from the least-squares fits because they deviated from the rest of the data by an amount greater than twice the standard deviation or because their elimination drastically reduced the standard deviation of the fit.

TABLE I: Enthalpies of Mixing in the System Na^+ , $\text{Mg}^{2+}||\text{Cl}^-$, SO_4^{2-} at 25°
(A) Constant Molal Ionic Strength Mixings

Salt pair	$I = 1 \text{ mol/kg}$			$I = 3 \text{ mol/kg}$			$I = 6 \text{ mol/kg}$		
	RTh_0^I ^a	RTh_1^I	RTh_2^I	RTh_0^I	RTh_1^I	RTh_2^I	RTh_0^I	RTh_1^I	RTh_2^I
$\text{Na}_2\text{SO}_4(\text{A})-\text{NaCl}(\text{B})$	-26.6(9) ^{b,c}	2(2)		-13.7(3) ^c	4.9(5)		-7.2(2) ^c	4.5(3)	
$\text{MgSO}_4(\text{A})-\text{MgCl}_2(\text{B})$	0.0(1)	-4.4(1)		-7.9(6)	-0.4(8)		7.1(2)	1.0(6)	
$\text{MgCl}_2(\text{A})-\text{NaCl}(\text{B})$	172(1) ^{d,c}	-12(1)		113.6(6) ^{d,e}	-18(2)		62.0(3) ^e	-18(1)	
$\text{Na}_2\text{SO}_4(\text{A})-\text{MgSO}_4(\text{B})$	98.6(9)	6(1)		70.9(8)	9(1)		28.6(3)	7(1)	
$\Sigma \square^e$	236(2)			157(1)			87.4(5)		
$\text{MgSO}_4(\text{A})-\text{NaCl}(\text{B})$	58(2)	-12(3)	-4(3)	73(1)	-17.0(6)	2.0(8)	52(1)	-13(1)	-11(5)
$\text{Na}_2\text{SO}_4(\text{A})-\text{MgCl}_2(\text{B})$	197(2)	-11(3)	-16(4)	97(1)	2(2)	-8(3)	45.5(3)	4.7(9)	0(3)
$\Sigma \times^h$	255(3)			170(2)			98(1)		

(B) Constant Equivalents per Kilogram of Solvent Mixings

	$E = 1 \text{ mol/kg}$			$E = 3 \text{ mol/kg}$			$E = 6 \text{ mol/kg}$		
	RTh_0^E ^a	RTh_1^E	RTh_2^E	RTh_0^E	RTh_1^E	RTh_2^E	RTh_0^E	RTh_1^E	RTh_2^E
$\text{Na}_2\text{SO}_4(\text{A})-\text{NaCl}(\text{B})$	-21.1(7) ^f	2(2)		-7.0(4) ^f	1(1)		17(1) ^f	2(3)	
$\text{MgSO}_4(\text{A})-\text{MgCl}_2(\text{B})$	20.0(4)	-2.7(6)		4.2(1)	0.5(5)		35(1)	3(2)	
$\text{MgCl}_2(\text{A})-\text{NaCl}(\text{B})$	105(1) ^e			53.9(5) ^e			12.0(3) ^e	-12(1)	
$\text{Na}_2\text{SO}_4(\text{A})-\text{MgSO}_4(\text{B})$	175.5(9)	12(1)		85(3)	16(8)		32(4)	8(13)	
$\Sigma \square^i$	279(2)			136(3)			96(4)		
$\text{MgSO}_4(\text{A})-\text{NaCl}(\text{B})$	-50(3)	-57(5)	-19(7)	26(2)	-35(3)	-5(3)	50(2)	-29(5)	-8(17)
$\text{Na}_2\text{SO}_4(\text{A})-\text{MgCl}_2(\text{B})$	383(2)	-6(1)	-29(2)	143.7(9)	10(2)	-6(4)	60.9(9)	8(3)	8(8)
$\Sigma \times^j$	333(4)			169(2)			110(2)		

^a The units of RTh_0^I , RTh_1^I , RTh_2^I , RTh_0^E , RTh_1^E , and RTh_2^E are cal kg mol⁻² and 1 cal = 4.184 J. ^b The number in parentheses is the estimated 95% confidence limit of the last digit, i.e., -26.6(9) is -26.6 ± 0.9. ^c Results from the M.S. Thesis of H. K. W. Chen, University of Delaware, Newark, Del., June 1971. See also ref 7. ^d Results from R. H. Wood, J. D. Patton, and M. Ghamkhar, *J. Phys. Chem.*, 73, 346 (1969). ^e Results from ref 5. ^f Results from the M.S. Thesis of D. E. Smith, University of Delaware, Newark, Del., May 1973. See also ref 7. ^g The sum of the terms around the square, i.e., the right-hand side of eq 3. ^h The sum of the cross terms, i.e., the left-hand side of eq 3. ⁱ The sum of the terms around the square, i.e., the right-hand side of eq 4. ^j The sum of the cross terms, i.e., the left-hand side of eq 4.

The errors in the measurements are in many cases larger than what would be expected from the standpoint of the precision which should be attainable using the dewar and LKB calorimeter (±0.3%). Sometime after these experiments were performed, it was found that the electrical calibration supply of the LKB calorimeter was occasionally varying by as much as 1 or 2%. The experiments involving supersaturated solutions, sodium sulfate (m above 1.96 mol/kg) and magnesium sulfate (m above 2.98 mol/kg), were necessarily performed with equilibration times that were shortened and thus their accuracy was somewhat lower. Precipitation of MgSO_4 occurred after a 1–4 ml mixing of MgCl_2 with MgSO_4 at $E = 6 \text{ mol/kg}$. Thus, it was not experimentally possible to get meaningful data at the extremes of y_A for this mixture.

The two cross mixings can be checked for thermodynamic consistency with the heat contents of the component pure electrolytes using a relationship similar to those derived previously.^{2,7} The most likely reason for the failure of this consistency check is an error in the heat of dilution of magnesium sulfate. The results indicate that the reported values¹⁵ for the apparent molal heat content of magnesium sulfate are too high by 200 ± 50 cal/mol at $m = 0.25\text{--}1.5$ mole/kg and too high by 50 cal/mol at 3 mol/kg.

It had previously been suggested for charge asymmetric mixtures that RTh_0 for constant E mixings would be less than RTh_0 for constant I mixings.⁶ However, this generali-

zation did not hold for the Li^+ , $\text{Na}^+||\text{Cl}^-$, SO_4^{2-} system⁷ and Table I shows that it does not hold for the present system. If anything the constant I mixings have smaller values of RTh_0 .

The cross-square rule with the weighting factors for the present system is

$$RTh_0^I(\text{MgSO}_4-\text{NaCl}) + RTh_0^I(\text{Na}_2\text{SO}_4-\text{MgCl}_2) = \\ (5/6)RTh_0^I(\text{Na}_2\text{SO}_4-\text{NaCl}) + (7/6)RTh_0^I(\text{MgSO}_4-\text{MgCl}_2) + \\ (5/6)RTh_0^I(\text{MgCl}_2-\text{NaCl}) + (7/6)RTh_0^I(\text{MgSO}_4-\text{Na}_2\text{SO}_4) \quad (3)$$

where the weighting factors are derived from the general equations of Reilly and Wood.^{4,16} For constant E mixings the cross-square rules of Wu, Smith, and Young should hold without any weighting factors.⁵ The equation is

$$RTh_0^E(\text{MgSO}_4-\text{NaCl}) + RTh_0^E(\text{Na}_2\text{SO}_4-\text{MgCl}_2) = \\ RTh_0^E(\text{Na}_2\text{SO}_4-\text{NaCl}) + RTh_0^E(\text{MgSO}_4-\text{MgCl}_2) + \\ RTh_0^E(\text{MgCl}_2-\text{NaCl}) + RTh_0^E(\text{MgSO}_4-\text{Na}_2\text{SO}_4) \quad (4)$$

The calculated sums of the cross and square terms given in Table I show that the cross-square rule does not hold at any concentration studied for either constant I (eq 3) or constant E (eq 4) mixings. The sum of the cross terms is about 10% too high for constant I mixings and about 20% too high for constant E mixings.

The present measurements were undertaken because it

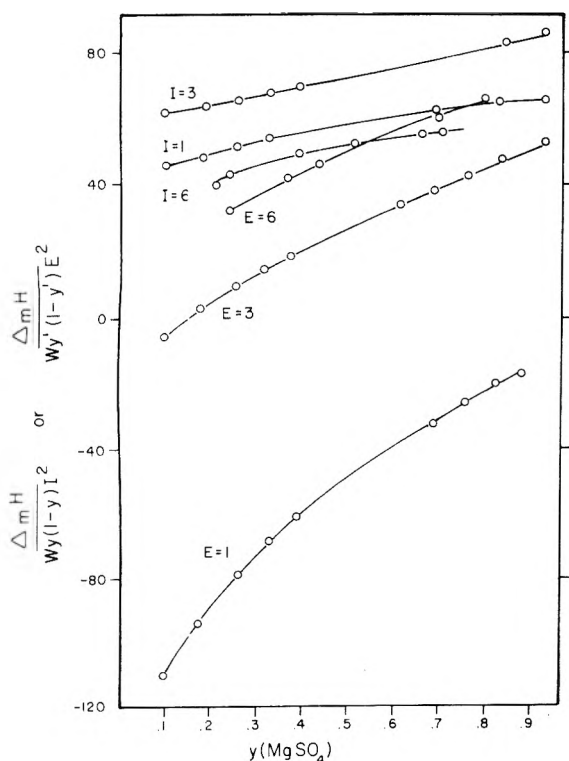


Figure 1. Reduced heat of mixing for the MgSO_4 - NaCl mixtures is plotted as a function of the ionic strength fraction (y) or equivalent fraction (y') of MgSO_4 . The reduced heat of mixing is $\Delta_m H / y(1-y)I^2$ cal kg mol^{-2} for constant I mixings (see eq 1) and $\Delta_m H / y'(1-y')E^2$ cal kg mol^{-2} for constant E mixings (see eq 2).

was felt that a system containing magnesium sulfate would present a very severe test to the cross-square rule. Previous results had shown that the cross-square rule is amazingly accurate even at very high concentrations. It holds within experimental error for the Na^+ , $\text{Mg}^{2+}||\text{Cl}^-$, Br^- system up to I or $E = 6$ mol/kg⁵ and for the Li^+ , $\text{Na}^+||\text{Cl}^-$, SO_4^{2-} system it is quite accurate up to $I = 3$ or $E = 6$ mol/kg.⁷

The most probable explanation for the failure of the cross-square rule for this system is the very large attractive forces between some of the ions. Very strong ion pairing ($K_{\text{assoc}} \approx 2 \times 10^2$) has been found in magnesium sulfate solutions by a variety of techniques.¹⁴ The strong attractive forces between Mg^{2+} and SO_4^{2-} should also lead to large triplet and even quadruplet terms at the high concentrations studied here. An analysis of terms that contribute errors to the cross-square rule for charge-asymmetric mixtures at constant I indicates that the cross-square rule is valid if only pairwise terms are important; i.e., if triplets and higher terms are negligible.¹⁷ For the cross-square rule at constant E , errors can be caused either by quadruplet terms or (most probably) by failure of the assumption that the activity coefficients of the ions do not vary appreciably with small changes in the ionic strengths.

Wu, Rush, and Scatchard have investigated the free energy of the Na^+ , $\text{Mg}^{2+}||\text{Cl}^-$, SO_4^{2-} system.¹⁸ They concluded that the unweighted cross-square rule held within experimental error. The actual data show an average difference of 8% between the sum of the cross terms and the sum of the square terms (constant I mixings) for both the weighted and unweighted cross-square rule. This is about the same error as found in the present study. Thus it is possible that the free energy of the Na^+ , $\text{Mg}^{2+}||\text{Cl}^-$, SO_4^{2-}

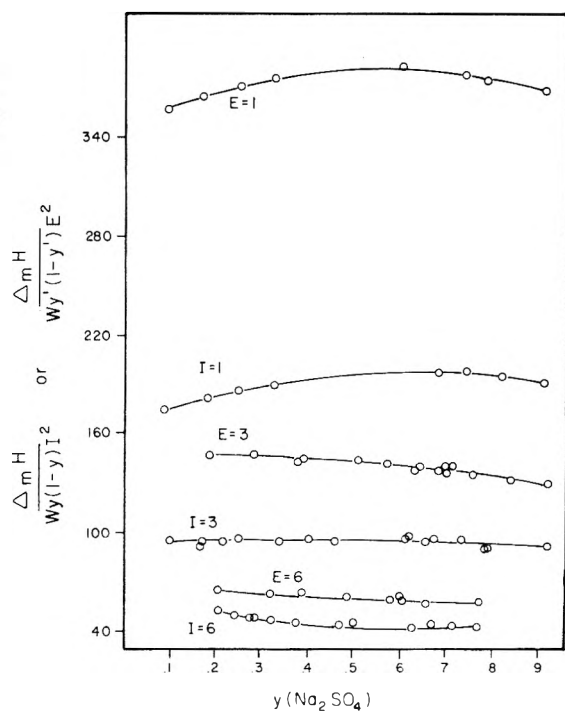


Figure 2. Reduced heat of mixing for the Na_2SO_4 - MgCl_2 mixtures is plotted as a function of the ionic strength fraction (y) or equivalent fraction (y') of Na_2SO_4 . The reduced heat of mixing is $\Delta_m H / y(1-y)I^2$ cal kg mol^{-2} for constant I mixings (see eq 1) and $\Delta_m H / y'(1-y')E^2$ cal kg mol^{-2} for constant E mixings (see eq 2).

system does not obey the cross-square rule and that the relative deviations from the rule are about the same for both heats and free energies.

In previous results a close correspondence between the magnitude of heat (RTh_0) and free energy (RTg_0) terms has been observed.^{19,20} This is no longer true for the present system. In about half of the results RTg_0 is not of the same sign as RTh_0 . In addition Table I shows that the skew terms in the heats of mixing at constant ionic strength are appreciable. Values of RTh_1 which are 20% of RTh_0 are common. The free energy measurements of Wu, Rush, and Scatchard did not detect skew terms in any of the mixtures.

Some of the unusual features of the present results can be explained in a qualitative way by considering the heat involved in forming or dissociating magnesium sulfate ion pairs. Assuming that, at these high concentrations, the stoichiometric equilibrium constant for forming MgSO_4 ion pairs is about 10^{21} and the heat of association is about 0.5 kcal/mol²² the expected shape and magnitude of the various curves can be calculated. For each mixing experiment this calculation involves using the stoichiometric equilibrium constant to calculate the number of MgSO_4 ion pairs in the initial and final solutions. The effect of ion pairing on the heat of mixing is then calculated from the heat of ion pairing and the change in the number of ion pairs during the experiment. For instance, when Na_2SO_4 and MgCl_2 are mixed, a large number of MgSO_4 ion pairs are formed. The result is that RTh_0 for all of these mixings is large and positive both at constant E and at constant I . In addition to the large value for RTh_0 detailed calculations show that appreciable contributions from RTh_2 are expected. The largest RTh_2 values measured in this work are for this mixture at I and $E = 1$ mol/kg (see Figure 2). The relative

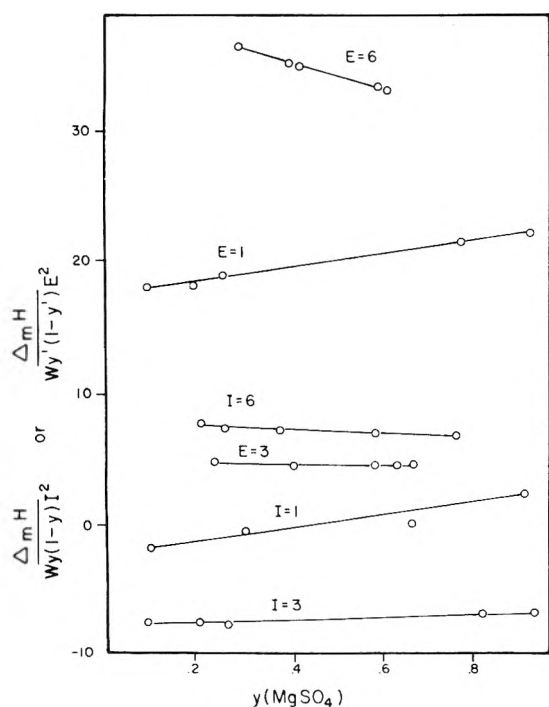


Figure 3. Reduced heat of mixing for the $\text{MgSO}_4\text{-MgCl}_2$ mixtures is plotted as a function of the ionic strength fraction (y) or equivalent fraction (y') of MgSO_4 . The reduced heat of mixing is $\Delta_m H / y(1-y)I^2$ W cal kg mol^{-2} for constant I mixings (see eq 1) and $\Delta_m H / y'(1-y')E^2$ W cal kg mol^{-2} for constant E mixings (see eq 2).

order of magnitude of both RTh_0 and RTh_2 at $I = 1$ mol/kg are predicted from the above ion pairing constants.

When magnesium sulfate and sodium chloride are mixed, the ion pairs already present in the magnesium sulfate solution are diluted and the amount of ion pairing is reduced. Detailed calculations show that this ought to give substantial negative contributions to RTh_0 at E and $I = 1$ mol/kg (-53 and -30 cal kg mol^{-2}) and rather small negative contributions at higher concentrations (-13 to -3 cal kg mol^{-2}). Of the experimental values in Table I only the $E = 1$ mol/kg value is negative. Evidently there is some other effect which leads to positive values of RTh_0 for this system. The detailed calculations also predict very large and negative values of RTh_1 for this system. The predicted values are higher than the experimental ones (Table I) by 20–100% but the more negative skews at lower concentrations and the more negative skews for constant E mixings are correctly predicted. In addition the calculation predicts negative values for RTh_2 and all but one of the values in Table I are negative.

For the common ion mixtures involving magnesium sulfate (MgSO_4 with MgCl_2 and MgSO_4 with Na_2SO_4) calculations show that a few more ion pairs ought to be formed in the final solution. The expected effect is small (2–36 cal kg mol^{-2}) so it is difficult to tell if it is present. Most but not all of the mixings have positive RTh_0 's as predicted. The reason for these small contributions is that the heat effects are not a great deal larger than the heat effects found for systems in which large amounts of ion pairing do not occur. Undoubtedly, this is also why the ion-pairing approach does not give more quantitative predictions of these effects and why it cannot distinguish between a fairly wide range of association constants and heats of association. However, the rough agreement found for the predictions of the ion-pairing model indicates that the strong attractive forces be-

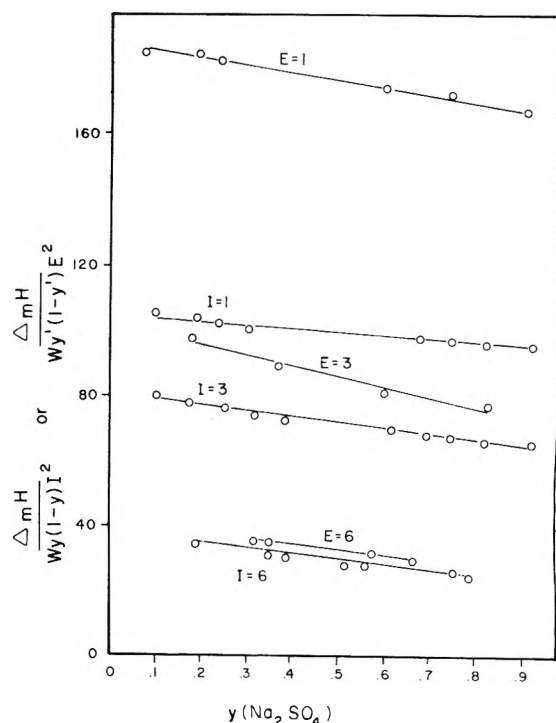


Figure 4. Reduced heat of mixing for the $\text{Na}_2\text{SO}_4\text{-MgSO}_4$ mixtures is plotted as a function of the ionic strength fraction (y) or equivalent fraction (y') of Na_2SO_4 . The reduced heat of mixing is $\Delta_m H / y(1-y)I^2$ W cal kg mol^{-2} for constant I mixings (see eq 1) and $\Delta_m H / y'(1-y')E^2$ W cal kg mol^{-2} for constant E mixings (see eq 2).

tween Mg^{2+} and SO_4^{2-} are indeed responsible for some of the unusual effects observed in this system. It is interesting to note that similar effects have also been observed in charge-symmetric mixtures where strong ion pairing is thought to be present.²³

Acknowledgment. The authors are grateful to the Office of Saline Water, U.S. Department of the Interior, and the National Science Foundation for the support of this work.

References and Notes

- (1) Taken in part from the Ph.D. Thesis of R. F. Srna, University of Delaware, June, 1972.
- (2) (a) T. F. Young, Y. C. Wu, and A. A. Krawetz, *Discuss. Faraday Soc.*, **24**, 27, 77, 80 (1957); (b) Y. C. Wu, M. B. Smith, and T. F. Young, *J. Phys. Chem.*, **69**, 1868, 1873 (1965).
- (3) (a) R. H. Wood and R. W. Smith, *J. Phys. Chem.*, **69**, 2974 (1965); (b) R. H. Wood and H. L. Anderson, *ibid.*, **70**, 992 (1966).
- (4) P. J. Reilly and R. H. Wood, *J. Phys. Chem.*, **73**, 4292 (1969).
- (5) P. J. Reilly and R. H. Wood, *J. Phys. Chem.*, **76**, 3474 (1972).
- (6) R. H. Wood and M. Ghamkhar, *J. Phys. Chem.*, **73**, 3959 (1969).
- (7) R. H. Wood, D. E. Smith, H. K. W. Chen, and P. T. Thompson, *J. Phys. Chem.*, **79**, 1532 (1975).
- (8) R. F. Srna, Ph.D. Thesis, University of Delaware, Newark, Del., June 1972.
- (9) G. Schwartzbach, "Complexometric Titrations", London, Interscience, New York, N.Y., 1957.
- (10) LKB-Produktor AB, Fack, 161 25 Bromma 1, Sweden.
- (11) F. J. Gucker, Jr., and H. B. Pickard, *J. Am. Chem. Soc.*, **62**, 1464 (1940).
- (12) D. Hamilton and R. H. Stokes, *J. Solution Chem.*, **1**, 223 (1972).
- (13) E. P. Eagen and B. B. Luff, *J. Chem. Eng. Data*, **11**, 192 (1966).
- (14) L. Sillen and A. E. Martell, *Chem. Soc., Spec. Publ.*, **No. 17** (1967) No. 25 (1971).
- (15) V. B. Parker, D. D. Wagman, and W. H. Evans, *Natl. Bur. Stand. Tech. Note*, **No. 270-6** (1971).
- (16) During the course of this work a new cross-square rule was found which also can be derived from the general equations of Reilly and Wood.⁴ The new cross-square rule is

$$\Delta_m H(\text{Na}_2\text{SO}_4\text{-MgCl}_2, y = \frac{1}{2}) + \Delta_m H(\text{MgSO}_4\text{-NaCl}, y_{\text{MgSO}_4} = \frac{2}{3}) = (\frac{2}{3})\Delta_m H(\text{Na}_2\text{SO}_4\text{-NaCl}, y = \frac{1}{2}) + (\frac{1}{3})\Delta_m H(\text{MgSO}_4\text{-MgCl}_2, y = \frac{1}{2}) + (\frac{2}{3})\Delta_m H(\text{MgCl}_2\text{-NaCl}, y = \frac{1}{2}) + (\frac{1}{3})\Delta_m H(\text{MgSO}_4\text{-Na}_2\text{SO}_4, y = \frac{1}{2})$$

- If the data in Table I are used to test this cross-square rule the results are slightly further off than eq 3. There may be a series of cross-square rules that can be predicted from the general equations but it does not look as if this is the reason for the failure of the rule.
- (17) L. D. Cerankowski (Ph.D. Thesis, Princeton University, Princeton, N.J., 1969) has shown that if the mixing is charge symmetric then triplet terms do not cause errors in the cross-square rule.
- (18) Y. C. Wu, R. M. Rush, and G. Scatchard, *J. Phys. Chem.*, **72**, 4048 (1968); **73**, 2047, 4433, 4434 (1969); **74**, 3786 (1970). These authors use an unweighted cross-square rule which also holds within experimental error. No derivation of the unweighted rules is given.
- (19) A. K. Covington, T. F. Lilley, and R. A. Robinson, *J. Phys. Chem.*, **72**, 2759 (1968).
- (20) R. H. Wood and P. J. Reilly, *Annu. Rev. Phys. Chem.*, **21**, 387 (1970).
- (21) D. R. Kester and R. M. Pytkowicz, *Limnol. Oceanog.*, **13**, 670 (1968), determined a stoichiometric association constant = 10.2 ± 0.5 at an ionic strength of 0.67. This is also about the value expected from a consideration of the low concentration value (ref 14) and normal activity coefficients.
- (22) R. M. Izatt, D. E. Eatough, J. J. Christensen, and C. H. Barthol, *J. Chem. Soc. A*, 47 (1969), found an enthalpy of association for MgSO_4 of +0.5 kcal/mol. More recent determinations are by J. W. Larson, *J. Phys. Chem.*, **74**, 3392 (1970), $\Delta H = 1.3$ kcal/mol; H. K. J. Powell, *J. Chem. Soc. Dalton Trans.*, 1947 (1973), $\Delta H = 1.4$ kcal/mol; D. R. Kester and R. M. Pytkowicz, *Geochim. Cosmochim. Acta*, **34**, 1039 (1970), $\Delta H = -2.7$ kcal/mol at $I = 0.67$. The use of the more recent values for ΔH would not change the conclusions found in the present work.
- (23) J. S. Falcone, Jr., and R. H. Wood, *J. Solution Chem.*, **4**, 239 (1974).

Heats of Mixing Aqueous Electrolytes. XIV. Charge-Asymmetric Mixtures of Three Salts at Constant Equivalents per Kilogram. Lithium Chloride–Sodium Chloride–Magnesium Chloride

R. H. Wood* and M. V. Falcone

Department of Chemistry, University of Delaware, Newark, Delaware 19711 (Received June 21, 1974; Revised Manuscript Received February 27, 1975)

The heats of mixing aqueous solutions of lithium chloride, sodium chloride, and magnesium chloride with each other have been measured at 25°. The solutions to be mixed had equal concentrations expressed as equivalents per kilogram of water ($E = 1, 3, \text{ and } 6 \text{ mol/kg}$). The heat of forming a three salt mixture by mixing magnesium chloride with a mixture of a sodium chloride and lithium chloride was also measured at $E = 1, 3, \text{ and } 6 \text{ mol/kg}$. These results were compared with the prediction based on the results from two salt mixings and the equations of Reilly and Wood for constant E mixings. The predicted heats are not too far off at $E = 1$ (10% low), rather poor at $E = 3$ (30% low), and way off at $E = 6 \text{ mol/kg}$. Previous measurements of three salt mixtures at constant ionic strength showed similar differences from the predicted values. Predictions of the heats of mixing solutions which contain three cations (or three anions) are a more stringent test of the predictive equations than predictions of the heats of mixing reciprocal salt mixtures.

Introduction

In a previous paper of this series, Wood and Ghamkhar¹ suggested that heats of mixing at constant equivalents of salt per kilogram of water might be more easy to predict than heats of mixing at constant ionic strengths. Following up on this suggestion, Reilly and Wood² measured all of the heats of mixing of the reciprocal salt pair $\text{Mg}^{2+}, \text{Na}^+||\text{Cl}^-, \text{Br}^-$ and showed that Young's cross-square rule held quite accurately both for constant ionic strength mixtures $I = 1, 3, \text{ or } 6 \text{ mol/kg}$ and constant equivalents per kilogram of solvent mixtures $E = 1, 3, \text{ or } 6 \text{ mol/kg}$. Recently measurements showed that for the $\text{Li}^+, \text{Na}^+||\text{Cl}^-, \text{SO}_4^{2-}$ system the cross-square rule was accurate at higher concentrations for constant E mixings³ whereas neither of the cross-square rules holds accurately for the $\text{Na}^+, \text{Mg}^{2+}||\text{Cl}^-, \text{SO}_4^{2-}$ system at I or $E = 1, 3 \text{ or } 6 \text{ mol/kg}$.⁴ Reilly and Wood derived equations for predicting the properties of any mixture of electrolytes. One set of equations was based on constant E mixings,² in contrast to previous equations which were based on constant ionic strength mixings.⁵ The present paper reports a test of the constant E equations on

mixtures of three cations; lithium, sodium, and magnesium with a common anion, the chloride ion.

Experimental Section

All solutions were made with reagent grade salts and deionized distilled water. Two different sets of stock solutions were prepared. The first set was analyzed by gravimetric titration with standard silver nitrate using dichlorofluorescein indicator. Duplicate analyses agreed to $\pm 0.1\%$ or better. The second set was analyzed by diluting the sample to approximately 0.1 N and measuring its conductance at 25.0°. The concentration of the stock solution was then back calculated from the equivalent conductivities given by Harned and Owen⁶ and densities given by Harned and Owen⁶ or Dunn.⁷ Conductivities were measured to 0.02% using a general radio impedance comparator in a bridge similar to that of Janz and McIntire.⁸ The cell was standardized with 0.1 demal KCl. The pH's of all stock solutions were between 6.0 and 7.0 so no adjustments were necessary. All experimental solutions were prepared to an accuracy of 0.1% by weight dilution. There was no significant difference between results with different stock solutions.

The LKB 10700-2 batch calorimeter⁹ which is similar to the calorimeter described by Wadsö¹⁰ was used for all measurements. All heats are in units of calories (4.184 J = 1 cal) and the temperature was 25.0°. Normally the two compartments were washed with distilled water and dried in a stream of nitrogen before adding (by weight) the new reagents. Previous experiments have shown that when this technique is used, the heat of mixing the reagents is higher (by about 200 ± 200 μcal) presumably because of the heat of wetting the walls.¹¹ To reduce this uncertainty, the following technique was used:¹² 5 ml of one of the reagents was added to the 4-ml compartment (weighing the exact amount). The mixing procedure was initiated so that this solution wet down the walls of the whole vessel and then was poured back into the 4-ml compartment. Some of the solution remained in the 2-ml side and this was removed as completely as possible and weighed. The difference in weight is then the weight of reagents on the 4-ml side plus the weight of reagent clinging to the walls on the 2-ml side. The weight of water clinging to the walls on the 2-ml side was measured in separate experiments and found to be 0.020 ± 0.002 g. The second reagent was then transferred by weight into the 2-ml compartment and after temperature equilibration the heat of mixing was measured. Using this technique the heat of friction was reduced to 7 ± 20 μcal. The experiments in which this procedure was used are easily identified in Table I by the fact that the 2-ml compartment contains approximately 2 g of one reagent and 0.020 g of the other reagent.

Results and Discussion

The results of the experiments on two salt mixtures are given in Table I (see paragraph at end of text regarding supplementary material). The heat of mixing two salt solutions at constant $E = (1/2)\sum_i m_i |Z_i|$ was represented by the equation²⁻⁴

$$\Delta_m H = -q = W y_{A'}(1 - y_{A'})E^2 [RTh_0^E + (1 - 2y_{A'})RTh_1^E] \quad (1)$$

where W is the weight of solvent (in kg), $y_{A'}$ is the equivalent fraction of the salt with the highest formula weight (component A), and RTh_0^E are coefficients for constant E mixings similar to those for constant ionic strength mixings.¹³ In an actual experiment where the initial solutions in compartments I and II contain both salts, the experimental heat, $q(\text{expt})$, is given by

$$q(\text{expt}) = q_f - q_I - q_{II} \quad (2)$$

where q_f , q_I , and q_{II} are heats calculated by eq 1 for the final solution and the initial solutions in compartments I and II. The values of RTh_0^E and RTh_1^E obtained by a least-squares technique are reported in Table II along with the estimated 95% confidence limits of the data. Table II also gives the results of previous measurements by other investigators. The agreement with previous results is excellent in all cases.

Table III reports the change in enthalpy per kilogram of solvent, $\Delta H/W$, when a $MgCl_2$ solution is mixed with a solution containing NaCl and LiCl to form a final solution which has equivalent fractions of Li^+ , Na^+ , and Mg^{2+} equal to $y_{Li'}$, $y_{Na'}$, and $y_{Mg'}$. All solutions contain E equivalents per kilogram of solvent.

The values of $\Delta H/W$ (calcd) are the heats of reaction predicted by the equation of Reilly and Wood² for the enthalpy of constant E mixtures. The equation is

TABLE II: Values of RTh_0^E and RTh_1^E for Two Salt Mixtures

Salt pair ^a	E , ^b mol kg ⁻¹	RTh_0^E , cal kg mol ⁻²	RTh_1^E , cal kg mol ⁻²
NaCl(A)-LiCl(B)	1	85.0(14) ^f	7(4)
		84.6 ^c	
		83.6 ^d	6 ^d
	3	82.5 ^c	6 ^c
		58(3)	12(10)
		57.8 ^d	12 ^d
6	59.2 ^e	13 ^e	
	31(3)	11(12)	
	32 ^d	12 ^d	
MgCl ₂ (A)-NaCl(B)	1	34 ^e	14 ^e
		104.6(11)	-9(3)
	3	105.1 ^e	
		52.0(11)	-13(3)
	6	53.9 ^e	
		12.7(14)	-13(5)
MgCl ₂ (A)-LiCl(B)	1	12.0 ^e	-12 ^e
		+2.6(6)	
	3	-2.0(2)	+1.2(5)
		-8(3)	0 ^h
	6		

^a Component A is the salt with the higher formula weight. ^b Concentration in equivalents per kg of water (units of $E = \frac{1}{2}\sum_i m_i |Z_i|$ are moles/kg). For instance $E = 1$ mol/kg for a solution containing 1 mol of NaCl per kg of water and $E = 1$ mol/kg for a solution containing 0.5 mol of $MgCl_2$ per kg of water. ^c Reference 17. ^d J. H. Stern and C. W. Anderson, *J. Phys. Chem.*, 68, 2528 (1964). ^e H. K. W. Chen, M.S. Thesis, University of Delaware, 1971. ^f The numbers in parentheses are the estimated 95% confidence limits of the last digit. Thus 85.0(14) is 85.0 ± 1.4 . ^g Reference 2. ^h This coefficient was set to zero because it was zero well within the 95% confidence limits.

$$H^{ex}/W = \sum_{M,X} y_M y_X (H_{MX}^{ex}/W) + RTE^2 \sum_{M < N, Y} y_M y_N y_X h_{M,N}^{X,Y} + RTE^2 \sum_{X < Y, N} y_N y_X y_Y h_{X,Y}^{N} \quad (3)$$

where W is the weight of solvent (in kilograms), H_{MX}^{ex} is the excess enthalpy (in calories) of a solution of pure MX at a concentration E , y_M' is the equivalent fraction of cation M ($y_M' = m_M |Z_M| / (\sum_N m_N |Z_N|)$), the sums are over cations M and N with anions X and Y, and a sum with $M < N$ means that each h term is taken only once; i.e., either h_{MN}^X or h_{NM}^X but not both. The term $h_{M,N}^{X,Y}$ is just h_0^E in eq 1 for the mixture of MX with NX at constant E .

To apply eq 3 to the experiments in Table III one starts with

$$\Delta H = H_f^{ex} - H_i^{ex} \quad (4)$$

where eq 2 is used to calculate H_i^{ex} and H_f^{ex} , the excess enthalpies of the initial and final solutions. The result for H_i^{ex} is

$$H_i^{ex} = \{y_{Li'}/(y_{Li'} + y_{Na'})\}(H_{LiCl}/W) + \{y_{Na'}/(y_{Li'} + y_{Na'})\}(H_{NaCl}/W) + RTE^2 \{y_{Li'} y_{Na'}/(y_{Li'} + y_{Na'})^2\} h_{LiNa}^{Cl} (y_{Li'} + y_{Na'}) + y_{Mg'} (H_{MgCl_2}/W) \quad (5)$$

since the initial solution of LiCl and NaCl contains $y_{Li'}$ + $y_{Na'}$ kg of water and has equivalent fractions of $y_{Li'}/(y_{Li'} + y_{Na'})$ and $y_{Na'}/(y_{Li'} + y_{Na'})$, respectively. The first term in eq 5 is for the LiCl-NaCl mixture and the second term is

TABLE III: Test of Prediction of Three-Salt Mixtures for (Li, Na)Cl^a with MgCl₂

y_{Li}'	y_{Na}'	y_{Mg}'	$-\Delta H/W$ (expt), ^a cal kg ⁻¹	$-\Delta H/W$ (calcd), cal kg ⁻¹
$E = 1 \text{ mol kg}^{-1}$				
0.2195	0.4464	0.3340	12.25	11.61
0.2154	0.4309	0.3536	12.17	11.82
0.1143	0.2379	0.6478	13.28	12.06
0.1144	0.2344	0.6512	12.90	11.91
0.2322	0.1069	0.6609	4.16	3.68
0.2278	0.1066	0.6656	4.13	3.71
0.2497	0.2559	0.4944	9.01	8.24
0.2521	0.2512	0.4967	9.52	8.06
0.2500	0.2434	0.5066	8.74	7.92
$E = 3 \text{ mol kg}^{-1}$				
0.2526	0.2537	0.4937	37.08	24.26
0.2540	0.2551	0.4909	37.09	23.76
$E = 6 \text{ mol kg}^{-1}$				
0.2582	0.2350	0.5069	7.81	-52.82
0.2613	0.2390	0.4998	8.16	-52.54

^a The values of $\Delta H/W$ are the changes in enthalpy per kilogram of solvent for the process of mixing a LiCl-NaCl solution with a MgCl₂ solution to form a final solution with equivalent fractions y_{Li}' , y_{Na}' , and y_{Mg}' . The concentration of all solutions is E mol/kg.

for the initial MgCl₂ solution. Similarly eq 3 is used to calculate H_i^{ex} and both H_i^{ex} and H_i^{ex} are substituted into eq 4. After some simplification the result is

$$\Delta H/W = RTE^2[y_{Li}'y_{Mg}'h_{LiMg}^{Cl} + y_{Na}'y_{Mg}'h_{NaMg}^{Cl} + \{(y_{Li}'y_{Na}' - y_{Li}'y_{Na}')/(y_{Li}' + y_{Na}')\}h_{LiNa}^{Cl}] \quad (6)$$

This equation shows that the heat of mixing the three salts is predicted from the properties of the three mixtures containing two salts. It is similar to equations derived for constant ionic strength mixtures of three cations.^{14,15}

A comparison of the experimental enthalpy, $\Delta H/W$ (expt), with the predicted enthalpy, $\Delta H/W$ (calcd), in Table III shows that at the lowest concentration, $E = 1$ mol/kg, the predicted enthalpies are about 10% lower than the experimental enthalpy indicating that the predicted equations are quite useful at this concentration, but not exact. At $E = 3$ mol/kg the discrepancy is larger. The predicted enthalpy is about 30% lower than the experimental enthalpy. At the highest concentration, $E = 6$ mol/kg, the predicted enthalpies are high by a factor of 7 and of the wrong sign. The predictive equations are not useful at this concentration.

Wood, Ghamkhar, and Patton¹⁵ made a similar test of the constant ionic strength equations for charge-asymmetric mixtures of three cations with a common anion. The predictions were quite good at ionic strength of 0.5 and 1.0 mol/kg. At an ionic strength of 3 mol/kg the predictions of four out of five mixtures were off by 20–50% with a fifth mixture being off 200%. Evidently, both predictive equations begin to fail at ionic or equivalent strengths of 3 mol/kg. With the limited data available, it is not possible to tell if one equation has a slight advantage.

The accuracy of the predictive equations depends on the

type of mixing process to which they are applied. Reilly and Wood² tested both the constant E and constant I equations using mixtures of two cation and two anions. In this case, the equations reduced to Young's cross-square rule,^{16,17} although in the case of constant I mixings appropriate weighting factors must be used.⁵ For comparison we will use the system investigated by Reilly and Wood, Na⁺, Mg²⁺||Cl⁻, Br⁻. This system contains salts that are either similar or identical with the ones used in this investigation.¹⁸ Reilly and Wood found that Young's cross-square rule holds quite accurately for both constant I and constant E mixings even at I or $E = 6$ mol/kg. Evidently, the three cation mixtures are a much more stringent test of the equations. This result is expected. For constant E mixings an examination of the equations^{5,19} shows that failure of the cross-square rule can be due to quadruplet or higher terms. For predictions of mixtures of three cations, the failure can be due to triplet interactions (specifically interactions of three cations).

Acknowledgment. The support of the Office of Saline Water, U.S. Department of the Interior, and the National Science Foundation is gratefully acknowledged. The authors are indebted to Bruce Cassel and James Falcone, Jr., for helpful discussions.

Supplementary Material Available. Table I, containing experimental data for common-ion mixings, will appear following these pages in the microfilm edition of this volume of the journal. Photocopies of the supplementary material from this paper only or microfiche (105 × 148 mm, 24× reduction, negatives) containing all of the supplementary material for the papers in this issue may be obtained from the Journals Department, American Chemical Society, 1155 16th St., N.W., Washington, D.C. 20036. Remit check or money order for \$4.00 for photocopy or \$2.50 for microfiche, referring to code number JPC-75-1540.

References and Notes

- R. H. Wood and M. Ghamkhar, *J. Phys. Chem.*, **73**, 3959 (1969).
- P. J. Reilly and R. H. Wood, *J. Phys. Chem.*, **76**, 3474 (1972).
- R. H. Wood, D. E. Smith, H. K. W. Chen, and P. T. Thompson, *J. Phys. Chem.*, **79**, 1532 (1975).
- R. F. Srna and R. H. Wood, *J. Phys. Chem.*, **79**, 1535 (1975).
- (a) P. J. Reilly and R. H. Wood, *J. Phys. Chem.*, **73**, 4292 (1969); (b) P. J. Reilly, R. H. Wood, and R. A. Robinson, *ibid.*, **75**, 1305 (1971).
- H. S. Hamed and B. B. Owen, "The Physical Chemistry of Electrolyte Solutions", 3rd ed, Reinhold, New York, N.Y., 1958.
- L. A. Dunn, *Trans. Faraday Soc.*, **62**, 2348 (1966).
- G. J. Janz and J. D. E. McIntire, *J. Electrochem. Soc.*, **108**, 272 (1961).
- LKB-Produktter AB, Fack, 161 25 Bromma 1, Sweden.
- I. Wadsö, *Acta. Chem. Scand.*, **22**, 927 (1968).
- A. S. Levine, Ph.D. Thesis, University of Delaware, Newark, Del., June, 1971.
- J. S. Falcone, A. S. Levine, and R. H. Wood, *J. Phys. Chem.*, **77**, 2137 (1973).
- H. L. Friedman, *J. Chem. Phys.*, **32**, 1351 (1960).
- R. H. Wood and H. L. Anderson, *J. Phys. Chem.*, **70**, 1877 (1966).
- R. H. Wood, M. Ghamkhar, and J. D. Patton, *J. Phys. Chem.*, **73**, 4298 (1969).
- T. F. Young, Y. C. Wu, and A. A. Krawetz, *Discuss. Faraday Soc.*, **24**, 27, 77, 80 (1957).
- Y. C. Wu, M. B. Smith, and T. F. Young, *J. Phys. Chem.*, **69**, 1868, 1873 (1965).
- The systems Li⁺, Na⁺||Cl⁻, SO₄²⁻ and Na⁺, Mg²⁺||Cl⁻, SO₄²⁻ have recently been measured (see preceding papers^{3,4}). These systems were not used for this comparison because they contain salts which are usually considered to be ion paired.
- L. D. Cerankowski, Ph.D. Thesis, Princeton University, Princeton, N.J., May, 1969.

Thermal Pressure Coefficient and Internal Pressure of 2,2-Dimethylpropane

George A. Few and Maurice Rigby*

Chemistry Department, Queen Elizabeth College, Campden Hill, London W8 7AH, England (Received January 27, 1975)

Direct measurements have been made of the thermal pressure coefficient, $(\partial P/\partial T)_V$, for liquid 2,2-dimethylpropane (neopentane) at densities near to the coexistence curve in the temperature range from -15 to $+85^\circ$. Other values of $(\partial P/\partial T)_V$ have been derived from the *PVT* data of Dawson et al. from 65° to the critical temperature 160.6° . These data have been used to obtain the internal pressure $(\partial U/\partial V)_T$, along the coexistence curve from triple point to critical point. The results have been compared with those for other simple liquids using the principle of corresponding states.

The thermal pressure coefficient, $(\partial P/\partial T)_V$, and the internal pressure, $(\partial U/\partial V)_T$, provide a useful basis for understanding the nature of the liquid state.² They are related by the thermodynamic equation of state

$$P = T(\partial P/\partial T)_V - (\partial U/\partial V)_T \quad (1)$$

and may also be considered in terms of the van der Waals equation of state

$$P = \frac{nRT}{V - nb} - a \left(\frac{n}{V}\right)^2 \quad (2)$$

or its generalized form

$$P = \frac{nRT}{V} f_1 \left(\frac{n}{V}\right) - f_2 \left(\frac{n}{V}\right) \quad (3)$$

Equations 2 and 3 both require that pressure-temperature isochores should be linear, i.e., that the thermal pressure coefficient should be a function of density only. Although this is not precisely true, it proves to be a good approximation for most liquids at densities fairly near to the coexistence curve. The molecular interpretation³ of eq 2 and 3 associates the first term on the right-hand side, and hence the thermal pressure coefficient, with the effects of intermolecular repulsive interactions, as represented by a hard sphere model. The second term, corresponding to the internal pressure, describes the effects of intermolecular attractions, necessary to maintain the high density of the liquid state, but having little effect on the geometrical structure.

In the original van der Waals equation the contribution due to the repulsive interactions was given by an inaccurate representation of the hard sphere equation of state. There have been several investigations⁴ using more accurate hard sphere expressions, together with the original attractive energy term, and these have proved to give remarkably good qualitative equations of state. An extension to mixed fluids⁵ has been particularly successful.

The relationship between the thermal pressure coefficient and the hard sphere equation of state has been pointed out previously,⁶ but there seems to have been no systematic study for a variety of liquids over an extended range of temperature. Recently data have been presented for the thermal pressure coefficient of the heavier inert gases over most of the liquid range,⁷ and in this paper we supplement these results with measurements of the thermal pressure coefficient of 2,2-dimethylpropane (neopentane) at densities near to the coexistence curve from -15 to $+85^\circ$. These data have been combined with results derived from *PVT* studies by Dawson et al.¹ to give the thermal pressure coefficient of neopentane from a temperature near

to the triple point up to the critical point. This then permits a comparison between the results for the inert gases and for the pseudospherical, globular molecule, neopentane, over the whole liquid range.

Experimental Section

Direct measurements of thermal pressure coefficients may conveniently be made using an apparatus of the type described by Hildebrand⁸ and subsequently used by several other workers.^{9,10} We have used a glass cell of the general appearance shown in Figure 1. The sample liquid is confined to the cell by mercury and the presence of the mercury-liquid interface is established electrically using contacts sealed through the glass. By adjusting the pressure and temperature of the cell, the mercury surface can be brought to the pointer at Q and sets of isochoric *P-T* data can be obtained. The cell is placed in a pressure vessel, and pressures up to about 35 atm were applied from a nitrogen cylinder. The pressures were measured using a Texas Instruments Model 44 Bourdon tube pressure gauge, with an estimated error not exceeding 0.002 atm. Temperatures were measured using a Hewlett-Packard 2801A quartz thermometer, with a Model 2850B sensor which was sealed through the lid of the pressure vessel. Most of the space in the pressure vessel was filled with liquid toluene, acting as a heat transfer fluid, and the thermometer probe was positioned in the toluene, close to the cell. The pressure vessel was placed in a thermostat tank which could operate over the temperature range -20 to $+85^\circ$.

Since neopentane is gaseous at room temperature, the sample cell was filled at a reduced temperature, and quickly transferred to the previously cooled pressure vessel, which was then closed. A moderate nitrogen pressure was then applied, after which the vessel could be stored at room temperature.

A series of runs was made after a single filling. Each run consisted of a set of about six *P-T* points covering a rising pressure range of about 10–15 atm, followed by a similar set with the pressure being decreased. After changes in the pressure, suitable times were allowed to elapse for the avoidance of errors due to adiabatic heating or cooling. When a particular isochore had been studied, the temperature was raised by 10–15 K, without increasing the pressure. The liquid then expanded to an extent sufficient to displace some of the sample. On cooling, a new isochore could then be investigated.

The sets of *P-T* data were always linear within the experimental error. No systematic changes were observed be-

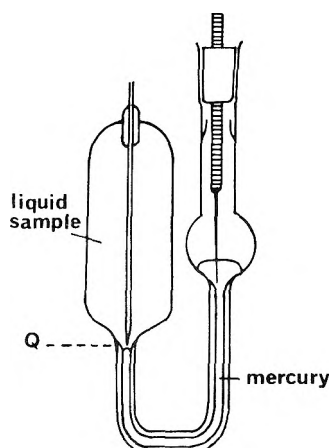


Figure 1. The thermal pressure cell. Q is the position of the liquid/mercury interface.

tween the sets obtained with rising and falling temperatures. The slopes of the experimental P - T data were obtained by a least-squares analysis. This "experimental" value of the thermal pressure coefficient, γ_{expt} , was then corrected to allow for the compressibility and thermal expansivity of the glass, using the equation⁹

$$\gamma_V = \gamma_{\text{expt}} \left[1 + \frac{\alpha_g}{\alpha} - \frac{\gamma_{\text{expt}} \beta_g}{\alpha} \right]$$

where γ_V is the corrected value, α and α_g are the thermal expansivities of the sample liquid and of the glass, and β_g is the compressibility of glass.

The isochoric P - T line was extrapolated back to the saturated vapor pressure curve. The intersection temperature was then used to determine the density of the sample, from a knowledge of the molar volume of the liquid on the coexistence curve. The latter data were not available for neopentane below 65°, except for a single value at 0°. We have confirmed the latter value, and have measured the coefficient of thermal expansion, $1/V(\partial V/\partial T)_P$, directly in the temperature range from -10 to +30°. The dilatometer used was closely based on that described by Orwoll and Flory,⁹ and operated under a constant total pressure of about 2 atm. Data could thus be obtained at temperatures above the normal boiling point. The method of operation was very similar to that described by the previous workers. The observed values of the coefficient of expansion are believed to be accurate to about 0.5-1%.

Material. The 2,2-dimethylpropane was of commercial grade, supplied by the Matheson Co. Its purity was stated to be better than 99%, with *n*-butane as the principal impurity. In view of the similarity between the physical properties of *n*-butane and 2,2-dimethylpropane it seems unlikely that the impurity would have a detectable effect on the results. The samples were carefully degassed before use, by means of two or three freeze-pump-thaw cycles.

Results and Discussion

Some preliminary results were first obtained using benzene. In these experiments a slightly different cell was used, and the total volume of benzene and the confining mercury was held constant. The benzene used was supplied by British Drug Houses Ltd. with a purity not less than 99.8%. The sample was carefully dried and degassed before use. The results of these measurements are shown in Table I. The thermal pressure coefficients are quoted for the tem-

TABLE I: Thermal Pressure Coefficients for Benzene

$T, ^\circ\text{C}$	$\gamma_V, \text{bar K}^{-1}$	$T, ^\circ\text{C}$	$\gamma_V, \text{bar K}^{-1}$
22.8	12.6 ₂	52.9	10.6 ₇
32.9	11.9 ₂	62.2	9.9 ₇
42.3	11.2 ₆	69.7	9.5 ₇
48.3	10.8 ₂	81.8	8.8 ₄

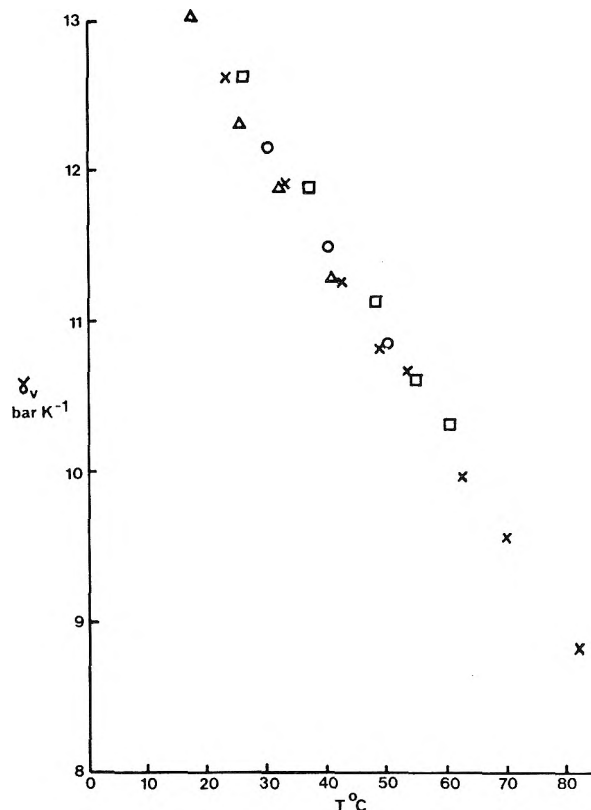


Figure 2. Thermal pressure coefficient results for benzene: (X) this work; (Δ) ref 8; (O) ref 8; (\square) ref 10.

peratures on the coexistence curve corresponding to the density studied. The results are compared with those of previous workers⁸⁻¹⁰ in Figure 2. It may be seen that the available data are somewhat scattered, with a spread of around 2%, and that the results obtained in this work lie within the range of values found previously. We have found no data above 60° to permit comparison at the higher temperatures.

In Table II we summarize the thermal pressure results obtained for 2,2-dimethylpropane. In Table III results are given at regular temperature intervals, and include values obtained by graphical interpolation of the PVT data in ref 1. In addition we have reported the measured coefficients of thermal expansion, and the derived values of the molar volumes. The molar volumes between 30 and 65° are based on a corresponding states correlation. They are believed to be accurate to 0.3%. The thermal pressure coefficients are shown in Figure 3, where it may be seen that our directly measured values are in good agreement with the indirect values from ref 1. In the region of overlap, our results lie within about 0.1 bar K^{-1} of the other data.

Using the results in Table III the internal pressure, $(\partial U/\partial V)_T$, of neopentane along the coexistence curve for most of

TABLE II: Thermal Pressure Coefficients for 2,2-Dimethylpropane

$T, ^\circ\text{C}$	$\gamma_v, \text{bar K}^{-1}$	$T, ^\circ\text{C}$	$\gamma_v, \text{bar K}^{-1}$
-16.0	8.5 ₄	39.4	5.3 ₉
-2.7	7.6 ₅	49.8	4.8 ₉
8.0	7.0 ₄	59.5	4.4 ₈
99.3	7.0 ₂	62.5	4.3 ₈
17.1	6.5 ₄	71.4	3.9 ₇
30.0	5.8 ₇	84.1	3.4 ₄
38.8	5.4 ₁		

TABLE III: Smoothed Data for 2,2-Dimethylpropane

$T, ^\circ\text{C}$	$\gamma_v, \text{bar K}^{-1}$	$\alpha_p \times 10^3, \text{bar}^{-1}$	$\bar{V}, \text{cm}^3 \text{mol}^{-1}$
-15	8.4 ₇	1.8 ₀	114.4
-10	8.1 ₃	1.8 ₃	115.4
0	7.5 ₃	1.8 ₉	117.2
10	6.9 ₂	1.9 ₆	119.9
20	6.3 ₂	2.0 ₅	122.3
30	5.8 ₇	2.1 ₇	124.9
40	5.3 ₆		127.2 ^a
50	4.8 ₈		130.0
60	4.4 ₄		132.8
70	4.0 ₁		136.4
80	3.6 ₃		140.1
85	3.4 ₃		142.1
70 ^b	4.1 ₂		136.4
90 ^b	3.2 ₉		144.2
100 ^b	2.9 ₀		149.2
120 ^b	2.1 ₆		161.3
135 ^b	1.6 ₃		175.1
150 ^b	1.1 ₀		199.8
160.6 ^b	.4 ₉		311.3

^aData between 30 and 70° from corresponding states interpolation. Above 70° from ref 1. ^bValues from ref 1.

the liquid range was calculated. These data are shown as a function of molar volume in Figure 4, and it is seen that the internal pressure decreases with increasing molar volume. The relationship between the configurational internal energy and the internal pressure² implies that, throughout the liquid range, neopentane has a structure which is sufficiently expanded that the attractive intermolecular forces are dominant. This behavior seems to be typical of most simple fluids. The reverse situation has been reported for only a few liquids,² at densities near to the triple point. It seems probable that this behavior is found only in liquids which have an extended liquid range, such as the normal alkanes, but there do not seem to be sufficient data available to test this hypothesis thoroughly.

A convenient basis for a corresponding states comparison of thermal pressure coefficient data may be achieved using the quantity $\bar{V}\gamma_v/R$, as a function of reduced temperature or density. As may be seen from a comparison of eq 1 and 2 this term is the equivalent of the van der Waals hard sphere compressibility factor, and so may perhaps be associated with the repulsive intermolecular forces. In Figure 5 we show the results for the heavier inert gases, together with our results for neopentane, as a function of the reduced temperature. In addition we have included values for

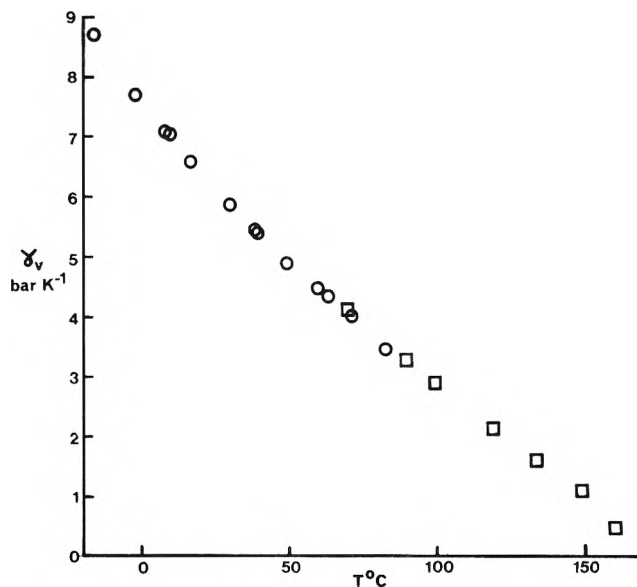


Figure 3. Thermal pressure coefficients of 2,2-dimethylpropane: (O) this work; (□) from PVT data of ref 1.

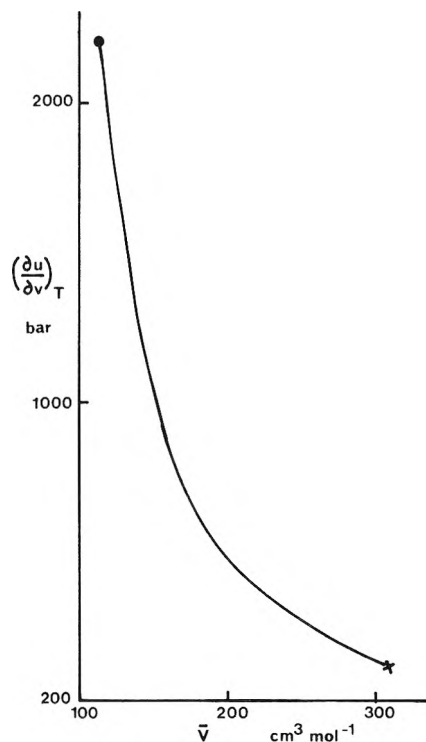


Figure 4. The internal pressure of liquid 2,2-dimethylpropane along the coexistence curve: (●) triple point; (×) critical point.

another globular molecule, carbon tetrachloride, for which there are data at lower reduced temperatures. It is seen that the inert gases are in good corresponding states with each other, and that the results for neopentane and carbon tetrachloride lie significantly above the inert gas values. The two globular molecules show similar behavior, as might be expected from their acentric factors, which are almost identical. Thus despite the approximately spherical shape of the globular molecules there is a marked difference in the effect of the repulsive interactions. This pre-

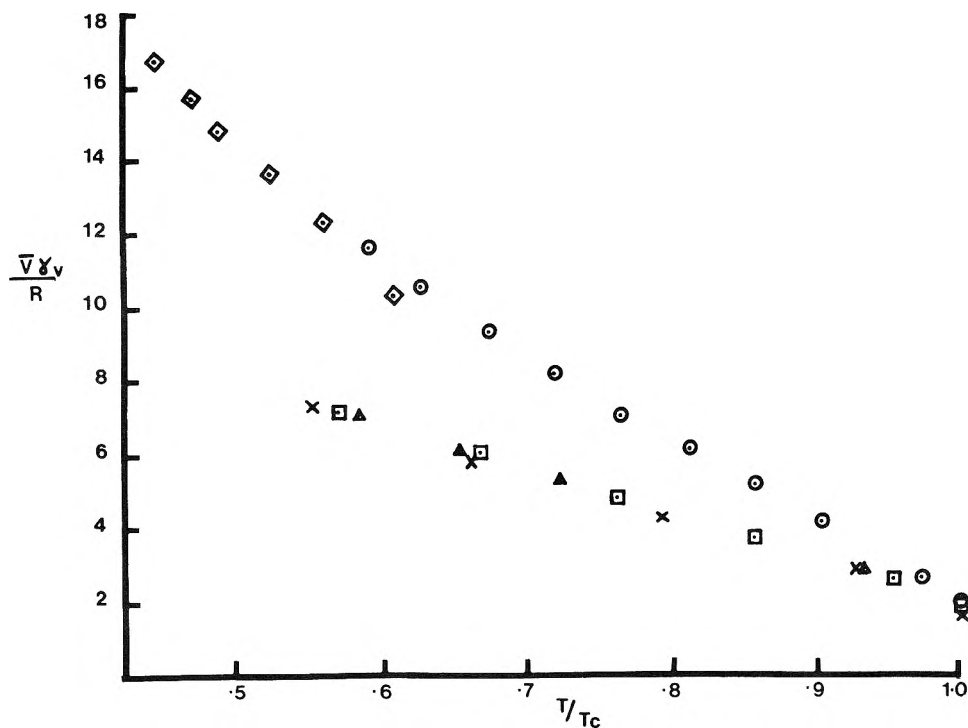


Figure 5. Reduced thermal pressure coefficients for the heavier inert gases and for 2,2-dimethylpropane: (O) $C(CH_3)_4$; (X) Ar ref 7; (□) Kr ref 7; (△) Xe ref 7; (◇) CCl_4 from ref 12.

sumably reflects the nonconformality of the intermolecular potential energy functions for the inert gases and the globular molecules, with a consequently different dependence of density on reduced temperature. If the corresponding states comparison is made as a function of reduced density, a similar distinction is again seen between the inert gases and the globular molecules. This suggests that the relationship between the critical volume and the hard core molecular volume is different for the two classes of molecules. This again implies nonconformality of the intermolecular potential functions. A more detailed analysis of the role of molecular shape and intermolecular repulsive forces on the thermal pressure coefficient will be presented subsequently.

Acknowledgment. We thank the Science Research Council for the award of a research studentship to G.A.F., and

for an equipment grant for the purchase of the pressure gauge.

References and Notes

- (1) P. P. Dawson, I. H. Silberberg, and J. J. McKetta, *J. Chem. Eng. Data*, **18**, 7 (1973).
- (2) J. H. Hildebrand and R. L. Scott, "The Solubility of Nonelectrolytes", 3rd ed, Dover Publications, New York, N.Y., 1964, Chapter 5.
- (3) M. Rigby, *Quart. Rev. Chem. Soc.*, **24**, 416 (1970).
- (4) E. A. Guggenheim, *Mol. Phys.*, **9**, 199 (1965); H. C. Longuet-Higgins and B. Widom, *ibid.*, **8**, 549 (1964).
- (5) N. S. Snider and T. M. Herrington, *J. Chem. Phys.*, **47**, 2248 (1967).
- (6) E. B. Smith, *J. Chem. Phys.*, **36**, 1404 (1962).
- (7) W. B. Streett and L. A. K. Staveley, *J. Chem. Phys.*, **50**, 2302 (1969).
- (8) W. Westwater, H. W. Frantz, and J. H. Hildebrand, *Phys. Rev.*, **31**, 135 (1928).
- (9) R. A. Orwoll and P. J. Flory, *J. Am. Chem. Soc.*, **89**, 6814 (1967).
- (10) G. A. Allen, G. Gee, D. Mangaraj, D. Sims, and G. J. Wilson, *Polymer*, **1**, 467 (1960); U. Bianchi, G. Agabio, and A. Turturro, *J. Phys. Chem.*, **69**, 4392 (1965).
- (11) V. Mathot and A. Desmyter, *J. Chem. Phys.*, **21**, 782 (1953).
- (12) H. Benninga and R. L. Scott, *J. Chem. Phys.*, **23**, 1911 (1955).

Thermochemical Isotope Effects. III. Hydrogen-Deuterium Exchange between Methanol and Water at 25°

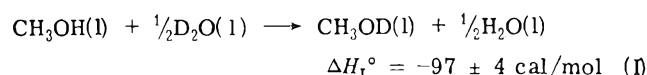
Gary L. Bertrand* and Thomas E. Burchfield

Department of Chemistry, University of Missouri—Rolla, Rolla, Missouri 65401 (Received March 24, 1975)

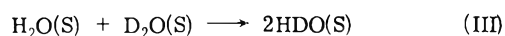
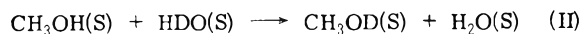
Publication costs assisted by the University of Missouri—Rolla

Enthalpies of solution of small amounts of D₂O and CH₃OD in mixtures of methanol and water at 25° have been interpreted in terms of the equilibrium (CH₃OH + HDO = CH₃OD + H₂O). The enthalpy of this reaction appears to vary from -100 cal/mol in methanol to -200 cal/mol in water. Approximations are introduced to account for this variation. "Best" estimates of the equilibrium constant are 0.6 in methanol and 0.6-0.7 in water.

In a recent paper,¹ we reported the standard enthalpy for hydrogen-deuterium exchange between pure water and pure methanol.



Since a large amount of the present research on exchange reactions involves liquid solutions rather than vapor phase or pure liquids, we have studied the exchange in liquid mixtures of methanol and water, and we have attempted to apply calorimetric methods to the determination of both the equilibrium constant and the enthalpy of exchange. The exchange equilibrium is obviously more complex than is indicated by (I) because of the species HDO. To minimize the complications of multiple equilibria, we have worked at low concentrations of deuterium, so that our measurements are best considered in terms of process II,



with very small contributions from (III), in which (S) indicates that the solvent is a methanol-water mixture. By extrapolating to zero concentration of deuterium, the contributions of process III have been removed. As a first approximation, the equilibrium constant and enthalpy change for (II) might be assumed to be independent of composition, as was done in a study of process III in aqueous solutions.² However, in this study we find that the equilibrium constant and/or the enthalpy of exchange vary with composition, particularly in solutions containing less than 0.5 mol fraction methanol. Consideration of the effects of solution nonideality on the exchange process allows development of approximations which provide estimates of the equilibrium constant and enthalpy of exchange in methanol-water mixtures.

Experimental Section

Materials. Stohler Isotope Chemicals methanol-*d* (99% isotopic purity) and heavy water (99.8% isotopic purity) were used without further purification. Methanol was Matheson Coleman and Bell Spectroquality reagent. Conductivity water was prepared in an all-glass still (Corning Model AG-1a). Gas chromatograms of methanol and methanol-*d* showed no detectable impurities.

Solvent mixtures were prepared by weight in amounts sufficient for experiments with both isotopic isomers of the solutes, and experiments with a given mixture were performed within 6 hr of preparation to minimize the effects of solvent variation due to preparation and evaporation.

Calorimetry. The calorimeter and calorimetric procedures have been described.³ Thermometric readout is now recorded with a Hewlett-Packard 7127A strip chart recorder with a 17505A module, normally used with a sensitivity of 0.5 mV full-scale. Electrical heating can be monitored either by the one-potential method using a Leeds and Northrup K-3 potentiometer, or by the two-potential method using a Keithley 160 digital multimeter.

Solute samples were approximately 3 ml, except in two cases in which 13-ml samples were used. The deuterium concentration ranged from 0.005 to 0.05 atom fraction of exchangeable protons. All measurements were completely within the range 25.0 ± 0.1°. In some cases, the deuterated compound produced an endotherm at a composition at which the parent compound produced an exotherm. To determine whether this reversal introduced errors because of differences in heat leakage, some measurements on the deuterated compound were performed with simultaneous electrical heating to produce an apparent exotherm. No differences could be detected between the results of the two types of measurements.

Results

Calorimetric measurements usually involved the addition of two successive increments of solute in a solvent mixture of some initial methanol composition, X_m^0 , as given in Table I. The volumes of solute and solvent for measurements with isotopic isomers were closely matched so that the range of compositions covered with each addition would be very similar. This raw data will appear in the microfilm edition of this volume of the journal.⁴ Molar enthalpy effects were extrapolated back to zero addition of solute, and thus to zero deuterium content and/or the initial solvent composition. For methanol and water as solutes, the observed molar enthalpy increments are "apparent partial molar excess enthalpies" as described by Taylor and Bertrand.⁵ These were divided by the square of the average mole fraction of the other component and this parameter was extrapolated (linear with mole fraction) to the initial solvent composition to obtain the partial molar excess enthalpies (\bar{L}_m, \bar{L}_w) of methanol and water listed in Table

TABLE I: Partial Molar Excess Enthalpies and Heats of Solution (cal/mol) in the Methanol-Water System at 25°

X_m^0	$-\bar{L}_w$	$-\bar{L}_m$	$(\Delta\bar{H}_{DD}^0)^S$	$(\Delta\bar{H}_{MD}^0)^S$
0.0000	0	1746 ^a	+31.5 ^b	-1635 ^a
0.0500	9.9	(1372) ^c	+9.4	
0.1000	41.8	(991)	-32.7	
0.1500	89.0	(664)	-86.7	
0.5000	(281)	104.0		-36.6
0.7000	(357)	55.5		-9.1
0.8000	(442)	28.6		+2.5
0.9000	(570)	7.7		+11.3
1.0000	718 ^d	0	-904 ^a	+3 ^a

^a G. L. Bertrand and W. C. Duer, *J. Am. Chem. Soc.*, in press.

^b W. C. Duer and G. L. Bertrand, *J. Chem. Phys.*, **53**, 3020 (1970).

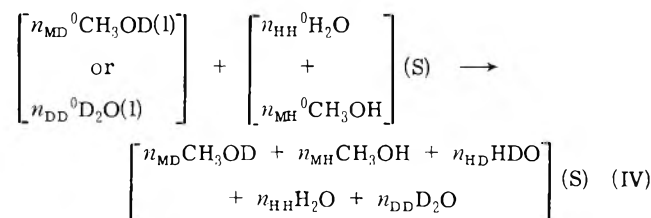
^c Values in parentheses were obtained by combination of partial molar excess enthalpies determined in this work with smoothed values of the excess enthalpy of the methanol-water system. See text.

^d E. L. Taylor and G. L. Bertrand, *J. Solution Chem.*, **3**, 479 (1974).

I. The relative partial molar enthalpies of the other component, given in parentheses, were obtained by combining our data with the smoothed excess enthalpy data of Benjamin and Benson.⁶ A similar extrapolation procedure was used for the deuterated compounds, along with a simple extrapolation of the observed molar enthalpy effect vs. atom fraction of deuterium, and a more sophisticated treatment based on the exchange equilibrium using preliminary results of this study. All three extrapolation methods gave very similar results and the average values are given in Table I as $(\Delta\bar{H}_{MD}^0)^S$ and $(\Delta\bar{H}_{DD}^0)^S$ for CH₃OD and D₂O, respectively. These values are considered to have a precision of about (0.5% + 0.2 cal/mol). Because of possible solvent and solute impurities, the absolute accuracy of these values is impossible to assess, but we feel that the above index of precision will give a reasonable approximation to the accuracy of the difference between the molar enthalpy effects for isotopic pairs.

Discussion

Interpretation of the Calorimetric Process. The calorimetric process is assumed to be



with either $n_{MD}^0 = 0$ or $n_{DD}^0 = 0$. Kwart, Kuhn, and Banister⁷ have shown that this system comes to equilibrium within 2 min (and thus within the time period of the calorimetric measurement), with no further changes over a 6-hr period. The amounts of the various species in the equilibrium mixture are related to the measured quantities (n_{HH}^0 , n_{MH}^0 , n_{DD}^0 , and n_{MD}^0) by the stoichiometric relations

$$n_{MD}^0 + 2n_{DD}^0 = n_{MD} + n_{HD} + 2n_{DD} \quad (1a)$$

$$n_{DD}^0 + n_{HH}^0 = n_{DD} + n_{HH} + n_{HD} \quad (1b)$$

$$n_{MD}^0 + n_{MH}^0 = n_{MD} + n_{MH} \quad (1c)$$

and the equilibrium constants (which may be composition dependent)

$$K_{II}^S = \frac{n_{MD}n_{HH}}{n_{MH}n_{HD}} \quad \text{and} \quad K_{III}^S = \frac{(n_{HD})^2}{n_{HH}n_{DD}} \quad (2)$$

With methanol-*d* as solute ($n_{DD}^0 = 0$), the enthalpy change for (IV) can be written

$$\Delta H_{MD}^S = -(n_{HD} + 2n_{DD})\Delta H_{II}^S - n_{DD}\Delta H_{III}^S + n_{MD}^0(\bar{H}_{MD}^S - \bar{H}_{MD}^{MD}) \quad (3)$$

With D₂O as solute ($n_{MD}^0 = 0$), the enthalpy change for (IV) is

$$\Delta H_{DD}^S = n_{MD}\Delta H_{II}^S + (1/2)(n_{HD} + n_{MD})\Delta H_{III}^S + n_{DD}^0(\bar{H}_{DD}^S - \bar{H}_{DD}^{DD}) \quad (4)$$

To eliminate the contribution of reaction III, we consider the limiting expressions as the atom fraction of deuterium approaches zero, with the following definitions

$$(\Delta H_{DD}^0)^S = \lim_{n_{DD}^0 \rightarrow 0} (\Delta H_{DD}^S/n_{DD}^0) \quad \text{and} \quad (\Delta H_{MD}^0)^S = \lim_{n_{MD}^0 \rightarrow 0} (\Delta H_{MD}^S/n_{MD}^0) \quad (5)$$

$$f_{MD} = (1 - f_{MH}) = \lim_{(n_{MD}^0, n_{DD}^0) \rightarrow 0} n_{MD}^0 / (n_{MD}^0 + 2n_{DD}^0) \quad (6)$$

Further simplification can be gained by considering results of two earlier investigations:

$$(\bar{H}_{MD}^{MH} - \bar{H}_{MD}^{MD}) = 3 \pm 1 \text{ cal/mol}^1$$

$$\Delta H_{II}^{HH} + (\bar{H}_{DD}^{HH} - \bar{H}_{DD}^{DD}) = 31.5 \text{ cal/mol}^2 \quad (7)$$

This latter result is obtained by applying eq 4 to the standard enthalpy of solution of D₂O in H₂O. The standard enthalpies of solution of CH₃OD and D₂O in mixtures of methanol and water then become

$$(\Delta H_{MD}^0)^S = (f_{MD} - 1)\Delta H_{II}^S + (\bar{H}_{MD}^S - \bar{H}_{MD}^{MH}) + (3 \text{ cal/mol}) \quad (8a)$$

$$(\Delta H_{DD}^0)^S = 2f_{MD}\Delta H_{II}^S + 2(\bar{H}_{HD}^S - \bar{H}_{HD}^{HH}) - (\bar{H}_{HH}^S - \bar{H}_{HH}^{HH}) + (31.5 \text{ cal/mol}) \quad (8b)$$

$$f_{MD} = K_{II}^S X_m^0 / (X_w^0 + K_{II}^S X_m^0) \quad (9)$$

Equations 8-9 are quite general, though K_{II}^S and ΔH_{II}^S may vary with composition.

Approximation for Enthalpy Effects. The most obvious difficulty of eq 8 lies in the evaluation of the partial molar enthalpies of the deuterated species, which cannot be measured directly. A reasonable approximation here is to assume that the enthalpy of transfer of the deuterated species (MD or HD) from a state of infinite dilution in the pure undeuterated liquid (MH or HH) to a state of infinite dilution in the mixed solvent (S) will parallel the enthalpy of transfer of the undeuterated species (MH or HH) from its pure state to the mixed solvent:

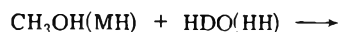
$$(\bar{H}_{\text{MD}}^{\text{S}} - \bar{H}_{\text{MD}}^{\text{MH}}) \approx \alpha(\bar{H}_{\text{MH}}^{\text{S}} - \bar{H}_{\text{MH}}^{\text{MH}}) = \alpha\bar{L}_{\text{m}}^{\text{S}} \quad (10\text{a})$$

$$(\bar{H}_{\text{HD}}^{\text{S}} - \bar{H}_{\text{HD}}^{\text{HH}}) \approx \beta(\bar{H}_{\text{HH}}^{\text{S}} - \bar{H}_{\text{HH}}^{\text{HH}}) = \beta\bar{L}_{\text{w}}^{\text{S}} \quad (10\text{b})$$

Then, if α and β are independent of composition

$$\Delta H_{\text{II}}^{\text{S}} = \Delta H_{\text{II}}^{\text{MH}} + (\alpha - 1)\bar{L}_{\text{m}}^{\text{S}} - (\beta - 1)(\bar{L}_{\text{w}}^{\text{S}} - \bar{L}_{\text{w}}^{\text{MH}}) \quad (11)$$

To obtain an independent relationship between α and β , eq 7 is applied to reaction I to yield



Combination of the enthalpy change for this reaction with eq 10 gives

$$\Delta H_{\text{II}}^{\text{HH}} + 1746(\alpha - 1) = \Delta H_{\text{II}}^{\text{MH}} - 718(\beta - 1) = -110 \pm 4 \text{ cal/mol (12)}$$

using the limiting values of the partial molar excess enthalpies of methanol and water. Equation 12 allows estimation of α and β from the limiting values of the enthalpy of reaction II in methanol and in water.

To evaluate the enthalpy of reaction II in methanol or in water, approximations for the composition dependence of K_{II}^{S} are necessary. The simplest approach is to assume that the equilibrium constant does not vary with composition over limited ranges of composition, either in methanol-rich solutions or in water-rich solutions, giving two equilibrium constants, $K_{\text{II}}^{\text{MH}}$ and $K_{\text{II}}^{\text{HH}}$.

Approximation A for K_{II}^{S} . If the equilibrium constant is assumed to be independent of composition for solutions rich in methanol ($K_{\text{II}}^{\text{MH}}$) and for solutions rich in water ($K_{\text{II}}^{\text{HH}}$), our data for the standard enthalpies of solution of CH_3OD and D_2O can be treated with eq 8–12 through a reiterative process to obtain the “best” values of the experimental parameters. $K_{\text{II}}^{\text{MH}}$ and $\Delta H_{\text{II}}^{\text{MH}}$ were evaluated from the standard enthalpy of solution of methanol-*d* in mixtures of methanol and water ranging from the equimolar mixture to pure methanol, while $K_{\text{II}}^{\text{HH}}$ and $\Delta H_{\text{II}}^{\text{HH}}$ were evaluated from the standard enthalpy of solution of D_2O in mixtures ranging from pure water to $X_{\text{m}}^0 = 0.15$; starting with the approximation $\alpha = \beta = 1$, and converging. This treatment leads to $K_{\text{II}}^{\text{MH}} = 0.6 \pm 0.1$; $\Delta H_{\text{II}}^{\text{MH}} = -104 \pm 9 \text{ cal/mol}$; $\alpha = 1.065$ and $K_{\text{II}}^{\text{HH}} = 0.6 \pm 0.1$; $\Delta H_{\text{II}}^{\text{HH}} = -223 \pm 26 \text{ cal/mol}$; $\beta = 1.008$. The uncertainties given are statistical standard deviations, assuming no uncertainty in α and β . In the reiterative procedure, $K_{\text{II}}^{\text{MH}}$ and $\Delta H_{\text{II}}^{\text{MH}}$ were observed to be independent of the values of α and β , so that the uncertainties for these parameters are comparable to the “marginal” uncertainties used by Drago.⁸ The agreement between the equilibrium constants determined for the two sets of data appears to justify the assumption that the equilibrium constant does not change within a given set of data. However, it should also be noted that the uncertainties in these equilibrium constants are so large as to be of little practical use. Values of $\Delta H_{\text{II}}^{\text{S}}$ vs. X_{m}^0 calculated with approximation A are given in Table II, along with smoothed values at intermediate compositions, and deviations between observed and calculated values.

Approximation B for K_{II}^{S} . The enthalpy change for reaction II appears to be rather strongly dependent on composition in the methanol–water system. This raises the

TABLE II: Estimates of Thermodynamic Parameters for Reaction II at 25°

X_{m}^0	Approximation A ^a ($K_{\text{II}} = 0.6$)		Approximation B ^b		
	$-\Delta H_{\text{II}}^{\text{S}}$, cal/mol	δ , ^c cal/mol	K_{II}^{S}	$-\Delta H_{\text{II}}^{\text{S}}$, cal/mol	δ , ^c cal/mol
0.00	223 ± 26		0.70	198 ± 10	
0.05	199	-0.2	0.68	179	-0.3
0.10	174	-0.1	0.65	159	-0.3
0.15	152	-1.0	0.64	142	-1.1
0.20	(136)		(0.62)	(130)	
0.30	(122)		(0.61)	(119)	
0.40	(117)		(0.61)	(114)	
0.50	114	0.0	0.60	112	+0.2
0.60	(112)		(0.60)	(110)	
0.70	110	-1.2	0.60	108	-0.9
0.80	108	+1.8	0.60	106	+1.7
0.90	106	+0.1	0.60	103	-0.1
1.00	104 ± 9		0.59	101 ± 5	

^a Values calculated with eq 11 for $\alpha = 1.065$, $\beta = 1.008$. ^b Values calculated with eq 11 and 14 for $\alpha = 1.050$, $\beta = 1.013$. ^c Deviations (calcd - obsd) between observed values of $(\Delta H_{\text{DD}}^{\text{S}})^{\text{S}}$ or $(\Delta H_{\text{MD}}^{\text{S}})^{\text{S}}$ and values calculated with eq 8–11 and the indicated approximation for K_{II}^{S} .

question of whether the equilibrium constant might also be composition dependent. Bell⁹ and others have discussed the compensating effects of enthalpy and entropy which make the Gibbs free energy, and thus the equilibrium constant, rather insensitive to changes which might cause large changes in enthalpy and entropy. Complete compensation will lead to an equilibrium constant which is independent of composition, as was found in approximation A. At the other extreme, complete lack of compensation will lead to

$$RT \ln (K_{\text{II}}^{\text{S}}/K_{\text{II}}^{\text{MH}}) = -(\Delta H_{\text{II}}^{\text{S}} - \Delta H_{\text{II}}^{\text{MH}}) \quad (13)$$

In applying this approximation to our data, we have found that eq 13 is almost identical with a possibly more basic approximation for isotope exchange equilibria in solution

$$K_{\text{x}}^{\text{S}} = (K_{\text{x}}^{\text{stat}}) e^{-\Delta H_{\text{x}}^{\text{S}}/RT} \quad (14)$$

in which $K_{\text{x}}^{\text{stat}}$ is the statistical equilibrium constant based on a completely random distribution of exchangeable protons and deuterons, with $K_{\text{II}}^{\text{stat}} = 0.5$. In applying the ideal solution approximation to reaction III in mixtures of H_2O and D_2O at 25°, Duer and Bertrand² found $K_{\text{III}} = 3.8$, $K_{\text{III}}^{\text{stat}} = 4$, $\Delta H_{\text{III}} = 31.5 \text{ cal/mol}$, in very good agreement with eq 14. Equation 14 reduces the number of experimental parameters to three: $\Delta H_{\text{II}}^{\text{MH}}$, α , and β ; and these are related by eq 11 and 12 to a quantity which is independent of the exchange equilibrium in solution. However, since the relationship between eq 13 and 14 for this system may be purely fortuitous. Approximation B should be considered as a two-parameter treatment, with $K_{\text{II}}^{\text{MH}}$ and $\Delta H_{\text{II}}^{\text{MH}}$ as independent parameters.

To determine these parameters, a reiterative procedure was used, starting with the values of α , β , and $\Delta H_{\text{II}}^{\text{MH}}$ from approximation A, using eq 8–13 to obtain the “best” solution of these values for this entire set of data. The results of this calculation are given in Table II, and are seen to be quite similar to the results of approximation A.

Conclusions

While the agreement of results calculated with two approximations for the composition dependence of the equilibrium constant for reaction II appears to be quite good, it must be remembered that the form of the enthalpy approximation, eq 10, is the same in both cases. The choice of this approximation is, of course, completely arbitrary. However, relationships of this general form are expected for simple nonexchanging ideal associated solutions. Also, the results of Bertrand and Duer¹ show the standard heats of solution of methanol and methanol-*d*, as well as those of ethanol and ethanol-*d*, to be roughly parallel over a variety of nonexchanging solvents, with proportionality constants (similar to α and β) of 1.03 to 1.05. This comparison fails in the case of pyridine as solvent, in which experimental difficulties were encountered. Isotope effects on the standard heats of solution of chloroform and chloroform-*d*¹⁰ show similar trends with proportionality constants of 1.00 to 1.03. This comparison appears to fail for acetone and acetone-*d*₆,¹⁰ through keto-enol tautomerism is known to be a complicating factor in this case. Other approximations for the enthalpy effect were attempted, with roughly the same results as with eq 10, but in these cases the convergence of the solution was not nearly as satisfactory. Until theoretical and experimental techniques are greatly improved, eq 10 represents a state-of-the-art approximation for calorimetric investigations of uncatalyzed isotope exchange reactions in solution.

Independent determinations of the distribution of protons and deuterons in the methanol-water system may resolve the question of composition dependence of the equilibrium constant for isotope exchange in this system. By

considering both a composition-independent equilibrium constant and one reasonable form of composition dependence, we feel that we have established the limitations of possible values for the thermodynamic parameters of this exchange reaction.

Supplementary Material Available. Raw calorimetric data (Table III) will appear following these pages in the microfilm edition of this volume of the Journal. Photocopies of this material from this paper only, or microfiche (105 × 148 mm, 24× reduction, negatives) containing all material for the papers in this issue, may be obtained from the Journals Department, American Chemical Society, 1155 Sixteenth Street, N.W., Washington, D.C. 20036. Remit check or money order for \$4.00 for photocopy or \$2.50 for microfiche, referring to code number JPC-75-1547.

References and Notes

- (1) W. C. Duer and G. L. Bertrand, *J. Am. Chem. Soc.*, in press.
- (2) W. C. Duer and G. L. Bertrand, *J. Chem. Phys.*, **53**, 3020 (1970).
- (3) (a) G. L. Bertrand, R. D. Beaty, and H. A. Burns, *J. Chem. Eng. Data*, **13**, 436 (1968); (b) E. L. Taylor, M.S. Thesis, University of Missouri—Rolla, 1969; (c) T. E. Burchfield and G. L. Bertrand, *J. Solution Chem.*, **4**, 205 (1975).
- (4) See the paragraph at the end of the text regarding supplementary material.
- (5) E. L. Taylor and G. L. Bertrand, *J. Solution Chem.*, **3**, 479 (1974).
- (6) L. Benjamin and G. C. Benson, *J. Phys. Chem.*, **67**, 858 (1963).
- (7) H. Kwart, L. P. Kuhn, and E. L. Bannister, *J. Am. Chem. Soc.*, **76**, 5998 (1954).
- (8) F. L. Slejko, R. S. Drago, and D. G. Brown, *J. Am. Chem. Soc.*, **94**, 9210 (1972).
- (9) R. P. Bell, "The Proton in Chemistry", Cornell University Press, Ithaca, N.Y., 1959.
- (10) W. C. Duer and G. L. Bertrand, *J. Am. Chem. Soc.*, **96**, 1300 (1974).

Thermodynamics of Ion-Exchange Equilibria in Mixed Solvents¹

Adel M. El-Prince*² and Kenneth L. Babcock

Department of Soils and Plant Nutrition, University of California, Berkeley, California 94720

(Received October 16, 1974; Revised Manuscript Received April 22, 1975)

Publication costs assisted by the University of California

Gaines and Thomas³ thermodynamic treatment of ion-exchange equilibria is extended to mixed solvents. Another solvent term is added to Gibbs-Duhem equation, mixed solvent and aqueous standard states are chosen, and, by integration along special paths, expressions for solid phase activity coefficients and thermodynamic equilibrium constants are set up for ion-exchange equilibria in water-organic mixtures. For uni-univalent exchange with low ionic strength, these expressions undergo simplification. Relative to the mixed solvent standard state, one ends with the well-known recipe used for ion exchange in aqueous media. On the other hand, relative to the aqueous standard state, medium effect terms become highly significant.

Introduction

The abstract thermodynamic treatment of ion-exchange equilibria has a certain resemblance to that of Vanselow,³ who suggested treating the heteroionic form of the ion exchanger (containing both competing species A and B) as a

"solid solution" of the components AE and BE (E symbolizes a structural unit of the exchanger). In contrast to Vanselow who equated the activities of the solid components AE and BE to their mole fraction in the solid, Argersinger et al.⁴ expressed solid phase activity coefficients in terms of

measurable quantities. These authors considered the ion exchanger as a binary component phase (AE and BE) and by integrating the Gibbs–Duhem equation they obtained expressions for the thermodynamic equilibrium constant and the solid phase activity coefficients. Gaines and Thomas⁵ suggested a much more rigorous treatment by taking into account the changes in solvent content, i.e., they considered the ion exchanger as a three component phase, namely, AE, BE, and adsorbed water. More detailed and critical discussions of these treatments have been given by Babcock,⁶ Holm,⁷ and Helmy and Peinemann.⁸

Despite a considerable amount of work^{9–15} on ion exchange in mixed solvents, there is no rigorous solution for the thermodynamic problem. Gupta^{15a,b} adapted a semi-empirical approach. He considered Gaines and Thomas' equation derived for aqueous systems as a model, and then the various terms were corrected, using the appropriate activity coefficients. Starobinets¹² showed that Gupta's equation was not quantitatively successful and he suggested a correction. At the same time Gupta^{15c-e} corrected his equation by including organic solvent activity integral terms. However, the consideration of ion exchange in aqueous–organic solvent systems, on the above basis, must involve the addition of another solvent term in the Gibbs–Duhem equation, choosing of the standard states, and, finally, integration on an isothermal surface. Below we shall do that.

List of Symbols

Regardless of solvent, the ion-exchange process can be represented by the equation



where A and B are the ions involved in the exchange process (1), Z is the valency, and E refers to an equivalent of the ion exchanger. The thermodynamic equilibrium constant K_t may be written as

$$K_t = N_B^{Z_A} M_A^{Z_B} \gamma_A^{Z_B} f_B^{Z_A} / N_A^{Z_B} M_B^{Z_A} \gamma_B^{Z_A} f_A^{Z_B} \quad (2)$$

and the selectivity coefficient K_s as

$$K_s = N_B^{Z_A} M_A^{Z_B} / N_A^{Z_B} M_B^{Z_A} \quad (3)$$

and the corrected selectivity coefficient K_c as

$$K_c = K_s (\gamma_A^{Z_B} / \gamma_B^{Z_A}) \quad (4)$$

so that

$$K_t = K_c (f_B^{Z_A} / f_A^{Z_B}) \quad (5)$$

where

$$N_i = Z_i n_i / (Z_A n_A + Z_B n_B) \quad (6)$$

Moreover

$$\begin{aligned} d\mu'_A &= RT d \ln f_A N_A \\ d\mu'_B &= RT d \ln f_B N_B \\ d\mu'_w &= RT d \ln a_w \end{aligned} \quad (7)$$

where N_A = equivalent fraction of component AE in ion exchanger (solid phase); M_A = molality of component A; n_A = number of moles of component AE in solid phase; m_i = number of moles of component i in liquid phase; l_i = number of moles of component i in gas phase; γ_i = activity coefficient of ion i in liquid phase; f_A = activity coefficient of component AE in solid phase; μ'_A = chemical potential

of component AE in solid phase; a_i = activity of component i ; X_s = mole fraction of organic solvent in liquid phase; \bar{n}_i = number of moles of component i in the solid phase per "exchange equivalent" of the ion exchanger; single, double, and triple primes refer to solid phase, liquid phase, and gas phase, respectively.

Ion Exchanger as a Quaternary Component Phase

We write the Gibbs–Duhem equation for the ion exchanger phase as

$$n_A d\mu'_A + n_B d\mu'_B + n_w d\mu'_w + n_s d\mu'_s = 0 \quad (8)$$

Substituting eq 6 and 7 into eq 8 gives

$$\begin{aligned} N_A d \ln (N_A f_A)^{Z_B} + N_B d \ln (N_B f_B)^{Z_A} + \\ Z_A Z_B (d\eta_w + d\eta_s) = 0 \end{aligned} \quad (9)$$

where

$$d\eta_i = \bar{n}_i d \ln a_i \quad (10)$$

Since $dN_A = -dN_B$, eq 9 reduces to

$$\begin{aligned} (Z_A - Z_B) dN_B + N_A d \ln f_A^{Z_B} + N_B d \ln f_B^{Z_A} + \\ Z_A Z_B (d\eta_w + d\eta_s) = 0 \end{aligned} \quad (11)$$

From eq 5 we have

$$d \ln K_c + d \ln f_B^{Z_A} - d \ln f_A^{Z_B} = 0 \quad (12)$$

Eliminating $d \ln f_B^{Z_A}$ from (12) and (11) gives

$$\begin{aligned} d \ln f_A^{Z_B} = (Z_B - Z_A) dN_B + N_B d \ln K_c - \\ Z_A Z_B (d\eta_w + d\eta_s) \end{aligned} \quad (13)$$

Eliminating $d \ln f_A^{Z_B}$ from (12) and (11) gives

$$\begin{aligned} d \ln f_B^{Z_A} = (Z_B - Z_A) dN_B - N_A d \ln K_c - \\ Z_A Z_B (d\eta_w + d\eta_s) \end{aligned} \quad (14)$$

We define the path of integration as shown in Figure 1. The curve $a_s Q_s b_s$ represents an isotherm determined at constant total molality M_0 ($M_0 = M_A + M_B$), and constant solvent composition X_s . The result of integrating eq 13 and 14 along $a_s Q_s b_s$ is

$$\begin{aligned} \ln f_A^{Z_B} = (Z_B - Z_A) N_B + N_B \ln K_c - \\ \int_0^{N_B} \ln K_c dN_B - Z_A Z_B \int_{a_s}^{Q_s} (d\eta_w + d\eta_s) + \\ \ln f_A^{Z_B}(a_s) \end{aligned} \quad (15a)$$

$$\begin{aligned} \ln f_B^{Z_A} = (Z_A - Z_B) N_A - N_A \ln K_c + \\ \int_{N_B}^1 \ln K_c dN_B + Z_A Z_B \int_{Q_s}^{b_s} (d\eta_w + d\eta_s) + \\ \ln f_B^{Z_A}(b_s) \end{aligned} \quad (15b)$$

$$\begin{aligned} \ln K_t = (Z_A - Z_B) + \int_0^1 \ln K_c dN_B + Z_A Z_B \times \\ \int_{a_s}^{b_s} (d\eta_w + d\eta_s) + \ln [f_B^{Z_A}(b_s) / f_A^{Z_B}(a_s)] \end{aligned} \quad (15c)$$

It is now necessary to define the standard states of the various components in order to evaluate K_c and the last terms in eq 15a–c. For the water we choose the reference states so that the activity of the water in each phase is the same, i.e., we select $\mu''_w{}^0$ so that $a''_w = 1$ for pure water and make $\mu'_w{}^0 = \mu''_w{}^0 = \mu'''_w{}^0$. For the organic solvent we choose a similar standard state. For the other components

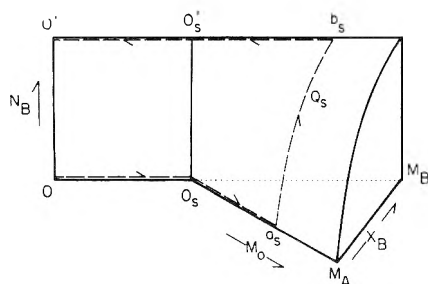


Figure 1. Path of integration.

we have two different choices. As long as the composition of the mixed solvent remains fixed it is convenient to choose the standard state of infinite dilution in a solvent of this unvarying composition. When, on the other hand, it is desired to compare activity coefficients in different solvents or solvent mixtures of different composition, a single common reference state must be chosen. The best choice, at least for mixed solvents of which water is a component, appears to be the customary aqueous standard state.

A. Standard State of Infinite Dilution in the Mixed Solvent. In this case the activity coefficients of the ions in the external solution go to unity as the solute content approaches zero in the mixed solvent. We refer to such activity coefficients by the symbol γ' and to the selectivity coefficient corrected for such activity coefficients by K'_c , i.e.

$$K'_c = K_s(\gamma'_A{}^{Z_B}/\gamma'_B{}^{Z_A}) \quad (16)$$

For the solid phase we choose the reference states as the monion solid in equilibrium with an infinitely dilute solution of that ion, in the mixed solvent, i.e., for $N_A = 1$ and $M_0 = 0$, $f'_A = 1$ and for $N_B = 1$ and $M_0 = 0$, $f'_B = 1$.

The solid phase activity coefficients at a_s and b_s (Figure 1) are to be determined as follows. For isothermal equilibrium between the pure B solid and gas phase we have for the pressure term

$$V' dP = n_B d\mu'_B + n_w d\mu_w + n_s d\mu_s \quad (17)$$

$$V''' dP = l_w d\mu_w + l_s d\mu_s \quad (18)$$

Eliminating dP from eq 17 and 18 and using eq 6 and 7 gives

$$d \ln f_B{}^{Z_A} = Z_A Z_B (d\xi_w + d\xi_s) \quad (19)$$

where

$$d\xi_i = [(\bar{v}/\tau_i) - \bar{n}_i] d \ln a_i \quad (20)$$

$\bar{v} = V'/(Z_A n_A + Z_B n_B)$ is the equivalent volume of the monion solid wetted with water and organic solvent and $\tau_i = V'''/l_i$ is the molar volume of component i (water or organic solvent) in the vapor phase in equilibrium with the monion solid wetted with water and organic solvent.

Following the path of integration $b_s \rightarrow 0'_s$ in Figure 1, eq 19 gives

$$\ln f'_B{}^{Z_A}(b_s) = Z_A Z_B \int_{0'_s}^{b_s} (d\xi_w + d\xi_s) \quad (21)$$

An entirely similar expression holds for $f'_A(a_s)$, i.e.

$$\ln f'_A{}^{Z_B}(a_s) = Z_A Z_B \int_{0_s}^{a_s} (d\xi_w + d\xi_s) \quad (22)$$

Substitution into eq 15a-c gives the desired equations

$$\begin{aligned} \ln f'_A{}^{Z_B} &= (Z_B - Z_A)N_B + N_B \ln K'_c - \int_0^{N_B} \ln K'_c dN_B \\ &- Z_A Z_B \int_{a_s}^{Q_s} (d\eta_w + d\eta_s) + Z_A Z_B \int_{0_s}^{a_s} (d\xi_w + d\xi_s) \end{aligned} \quad (23a)$$

$$\begin{aligned} \ln f'_B{}^{Z_A} &= (Z_A - Z_B)N_A - N_A \ln K'_c + \int_{N_B}^1 \ln K'_c dN_B \\ &+ Z_A Z_B \int_{Q_s}^{b_s} (d\eta_w + d\eta_s) + Z_A Z_B \int_{0'_s}^{b_s} (d\xi_w + d\xi_s) \end{aligned} \quad (23b)$$

$$\begin{aligned} \ln K'_t &= (Z_A - Z_B) + \int_0^1 \ln K'_c dN_B + Z_A Z_B \times \\ &\int_{a_s}^{b_s} (d\eta_w + d\eta_s) + Z_A Z_B \int_{0'_s}^{b_s} (d\xi_w + d\xi_s) - \\ &Z_A Z_B \int_{0_s}^{a_s} (d\xi_w + d\xi_s) \end{aligned} \quad (23c)$$

As one may expect, the above equations reduce identically to those of Gaines and Thomas⁵ if the organic solvent terms ($d\eta_s$ and $d\xi_s$) are dropped and to those of Argersinger et al.⁴ if both organic solvent and water terms are dropped.

B. Standard State of Infinite Dilution in Water. In this case the activity coefficients of the ions in the external solution refer to unity as the solute content approaches zero in water. We refer to such activity coefficients by the symbol γ'' and to the selectivity coefficient corrected for such activity coefficients by K''_c , i.e.

$$K''_c = K_s(\gamma''_A{}^{Z_B}/\gamma''_B{}^{Z_A}) \quad (24)$$

For the solid phase we choose the reference states as the monion solid in equilibrium with an infinitely dilute solution of that ion, in water, i.e., for $N_A = 1$ and $a_w = 1$, $f''_A = 1$ and for $N_B = 1$ and $a_w = 1$, $f''_B = 1$.

The solid phase activity coefficients at a_s and b_s (Figure 1) are to be determined as follows. It is clear that eq 19 holds, and by integration along $b_s \rightarrow 0'_s$ in Figure 1 we find

$$\ln f_B{}^{Z_A}(b_s) = Z_A Z_B \int_{0'_s}^{b_s} (d\xi_w + d\xi_s) + \ln f_B{}^{Z_A}(0'_s) \quad (25)$$

similarly

$$\ln f_A{}^{Z_B}(a_s) = Z_A Z_B \int_{0_s}^{a_s} (d\xi_w + d\xi_s) + \ln f_A{}^{Z_B}(0_s) \quad (26)$$

To evaluate $f_B{}^{Z_A}(0'_s)$ we integrate eq 19 along the path $0'_s \rightarrow 0$ in Figure 1 to get

$$\ln f_B{}^{Z_A}(0'_s) = Z_A Z_B \int_{0'}^{0'_s} (d\xi_w + d\xi_s) \quad (27)$$

similarly

$$\ln f_A{}^{Z_B}(0_s) = Z_A Z_B \int_0^{0_s} (d\xi_w + d\xi_s) \quad (28)$$

Substitution into eq 15a-c gives the desired equations

$$\ln f''_A{}^{Z_B} = \ln f'_A{}^{Z_B} + \ln f_A{}^{0Z_B} \quad (29a)$$

$$\ln f''_B{}^{Z_A} = \ln f'_B{}^{Z_A} + \ln f_B{}^{0Z_A} \quad (29b)$$

$$\ln K_t = \ln K'_t + \ln (\gamma_A{}^{0Z_B}/\gamma_B{}^{0Z_A}) + \ln (f_B{}^{0Z_A}/f_A{}^{0Z_B}) \quad (29c)$$

where the first terms on right-hand side are given by eq 23a-c and

$$\begin{aligned} \ln f_A^{0Z_B} &= Z_A Z_B \int_0^{0s} (d\xi_w + d\xi_s) \\ \ln f_B^{0Z_A} &= Z_A Z_B \int_0^{0's} (d\xi_w + d\xi_s) \end{aligned} \quad (30)$$

Equations 29a-c are written in the above forms to show that the quotients (f''/f') and (K_s/K'_s) are constants for any particular solvent compositions. The quantity γ^0 or f^0 characteristic of the two standard states is called by Owen^{16,17} the primary medium effect.

As previously mentioned, Gupta^{15a} derived an equation for the thermodynamic equilibrium constant referred to the aqueous standard state, for uni-univalent ion exchange. Comparing Gupta's equation with eq 29c shows that the latter can be rewritten as

$$\begin{aligned} \ln K_t &= \ln K_G + \int_{a_s}^{b_s} d\eta_s + \int_{0's}^{b_s} d\xi_s + \int_{0's}^{0's} d\xi_s - \\ &\quad \int_{0's}^{a_s} d\xi_s - \int_0^{0s} d\xi_s \end{aligned} \quad (31)$$

where K_G is the thermodynamic equilibrium constant which has been derived by Gupta. The other terms on right-hand side are a result of another solvent term in Gibbs-Duhem equation. Starobients¹² showed that Gupta's equation was not quantitatively successful. He went further and claimed the applicability of the equation

$$\ln K_t = \ln K_G + \ln (\bar{f}_{B^+}^0 / \bar{f}_{A^+}^0) \quad (32)$$

where the last term is that of Gibbs-Donnan equation. Equation 32 is different from eq 31 and there is no reason to believe in its validity. At the same time Gupta^{15c-e} corrected his equation by including organic solvent activity integral terms. The corrected equation and eq 29c become identical if the (\bar{v}/τ_i) terms in the latter are neglected.

Uni-Univalent Exchange with Low Ionic Strength

When the ion-exchange process in aqueous-organic mixtures involves two 1-1 electrolytes with low ionic strength ($M_0 < 0.1$), the equations which have been derived to calculate thermodynamic equilibrium constants and solid phase activity coefficients undergo simplification. For instance, the integrals $\int_{0's}^{a_s}$ and $\int_{0's}^{b_s}$ in eq 23a-c are not expected to contribute much. This will be particularly so if the ionic strength is low ($M_0 < 0.1$). The \bar{v}/τ_i terms are comparatively small compared to \bar{n}_i terms, so that

$$d\xi_w + d\xi_s \approx -(d\eta_w + d\eta_s) \quad (33)$$

Furthermore, the influence of $<0.1 M$ electrolyte on water activities in mixed solvent will be very small compared to the influence of the organic solvent on water activity, so that

$$d \ln a_s \approx -[(1 - X_s)/X_s] d \ln a_w \quad (34)$$

Substitution of eq 10 and 34 into 33 gives

$$d\xi_w + d\xi_s \approx -(d\eta_w + d\eta_s) \approx -d\phi \quad (35)$$

where

$$d\phi = [(1 - K_w^s)\bar{n}_w] d \ln a_w \quad (36)$$

and

$$K_w^s = \bar{n}_s(1 - X_s)/\bar{n}_w X_s \quad (37)$$

Finally, the integral \int_0^1 can be resolved to

$$\begin{aligned} \int_0^1 \ln K'_c dN_B &= \int_0^1 \ln K_s dN_B + \\ &\quad \int_0^1 \ln (\gamma'_{\pm AY} / \gamma'_{\pm BY})^2 dN_B \end{aligned} \quad (38)$$

Since by Harned's rule¹⁸ the activity coefficient ratio in the mixed solvent is the same in water, and since in water for 1-1 electrolytes and dilute solutions the ratio is almost exactly unity, the last integral in eq 38 vanishes.

Summing up, we rewrite eq 23a-c as follows

$$\ln f'_A \approx N_B \ln K_s - \int_0^{N_B} \ln K_s dN_B - \int_{a_s}^{Q_s} d\phi \quad (39a)$$

$$\ln f'_B \approx -N_A \ln K_s + \int_{N_B}^1 \ln K_s dN_B + \int_{Q_s}^{b_s} d\phi \quad (39b)$$

$$\ln K'_t \approx \int_0^1 \ln K_s dN_B + \int_{a_s}^{b_s} d\phi \quad (39c)$$

When the ionic strength is low ($M_0 < 0.1$) and the composition (X_s) is constant one may expect the activity of water will not change much by going from $M_{AY} < 0.1$ to $M_{BY} < 0.1$. Consequently the $\int d\phi$'s terms in eq 39a-c are expected not to contribute much and may be ignored. Consequently we end with the well-known recipe for the calculation of thermodynamic equilibrium constants and solid phase activity coefficients for ion-exchange equilibria in aqueous media.

Following the same assumptions which have been used to obtain eq 39a-c from eq 23a-c one may approximate eq 29a-c by

$$\ln f''_A \approx N_B \ln K_s - \int_0^{N_B} \ln K_s dN_B - \int_0^{0s} d\phi \quad (40a)$$

$$\ln f''_B \approx -N_A \ln K_s + \int_{N_B}^1 \ln K_s dN_B - \int_{0's}^{0's} d\phi \quad (40b)$$

$$\begin{aligned} \ln K_t &\approx \int_0^1 \ln K_s dN_B + 2 \ln (\gamma^0_{\pm AY} / \gamma^0_{\pm BY}) - \\ &\quad \int_{0's}^{0's} d\phi + \int_0^{0s} d\phi \end{aligned} \quad (40c)$$

In order to test the validity of eq 40c adsorption isotherms and solvent uptake data are collected for the Na → Cs exchange on Wyoming montmorillonite in water-dioxane mixtures. The details of the experimental procedure are given elsewhere¹ and the results are presented in Table I.

In the calculation of the second term on the right-hand side of eq 40c we employed data for the transfer free energies of NaCl and CsCl from water to 20% (w/w) dioxane¹⁹ and also assumed a linear relationship between $2 \ln (\gamma^0_{\pm NaCl} / \gamma^0_{\pm CsCl})$ and the reciprocal of the dielectric of the water-dioxane mixtures.^{20,21} In the calculation of the third and the fourth terms we used Vierk's²² data for the activity of water in water-dioxane mixtures.

TABLE I: Calculation of the Various Terms of the Thermodynamic Equilibrium Constant Relative to the Aqueous Standard State (Eq 40c) for Na-Cs Exchange on Wyoming Montmorillonite in Four Compositions of Water-Dioxane Mixtures at 25°

X_D	$\int_0^1 \ln K_s \frac{dN_{cs}}{dN_{cs}}$	$2 \ln \left(\frac{\gamma_{\pm NaCl}^0}{\gamma_{\pm CsCl}^0} \right)$	$\int_0^{0_s} d\phi - \int_0^{0_s'} d\phi$	$\ln K_t$
0.00 ^a	1.83	0.000	0.000	1.83
0.05	3.487	-0.065	-1.596	1.83
0.10	3.783	-0.118	-1.812	1.85
0.30	4.183	-0.562	-1.852	1.77

^a R. G. Gast, *Soil Sci. Soc. Am. Proc.*, **36**, 14 (1972).

The results in Table I show that the thermodynamic equilibrium constant is independent of the solvent composition which indicates the validity of eq 40c for the complete description of uni-univalent exchange in mixed solvents with low ionic strength. Also it is evident that the $\int d\phi$'s terms in eq 40c are significant and cannot be ignored depending on the water activity in the liquid phase, the swelling of the exchanger phase, and whether the organic solvent "salted in" (i.e., $K_w^s > 1$) or "salted out" (i.e., $K_w^s < 1$) of the exchanger phase.

References and Notes

- (1) Taken in part from the Ph.D. dissertation submitted by A. M. El-Prince to the Graduate Division of the University of California, Berkeley.
- (2) Address correspondence to this author at the Department of Agronomy, Virginia Polytechnic Institute and State University, Blacksburg, Va. 24061.
- (3) A. P. Vanselow, *Soil Sci.*, **33**, 95 (1932).
- (4) W. J. Argersinger, A. W. Davidson, and O. D. Bonner, *Trans-Kansas Acad. Sci.*, **53**, 404 (1950).
- (5) G. L. Gaines and H. C. Thomas, *J. Chem. Phys.*, **21**, 714 (1953).
- (6) K. L. Babcock, *Hilgardia*, **34**, 417 (1963).
- (7) L. W. Holm, *Ark. Kemi*, **10**, 151 (1956).
- (8) A. K. Helmy and N. Peinemann, *Geoderma*, **6**, 69 (1971).
- (9) G. J. Moody and J. D. E. Thomas, *Analyst*, **93**, 557 (1968).
- (10) J. L. Pauley, D. D. Vietti, C. C. Ou-Yang, D. A. Wood, and R. D. Sherrill, *Anal. Chem.*, **41**, 2047 (1969).
- (11) R. B. Barrett and J. A. Marinsky, *J. Phys. Chem.*, **75**, 85 (1971).
- (12) G. L. Starobinets, A. B. Chizhevskaya, and L. I. Sevast'yanov, *Russ. J. Phys. Chem.*, **45**, 1767 (1971).
- (13) R. Smits, P. Van Den Winkel, D. L. Massart, J. Julliard, and J. P. Morel, *Anal. Chem.*, **45**, 339 (1973).
- (14) (a) R. G. Fessler and H. A. Strobel, *J. Phys. Chem.*, **67**, 2562 (1963); (b) K. A. Boni and H. A. Strobel, *Z. Phys. Chem.*, (Frankfurt am Main), **87**, 169 (1973).
- (15) (a) A. R. Gupta, *J. Phys. Chem.*, **69**, 341 (1965); (b) M. R. Ghatge, A. R. Gupta, and J. Shankar, *Indian J. Chem.*, **3**, 287 (1965); (c) A. R. Gupta, *J. Phys. Chem.*, **75**, 1152 (1971); (d) D. Nandon, A. R. Gupta, and J. Shankar, *Indian J. Chem.*, **10**, 285 (1972); (e) D. Nandon, A. R. Gupta, and J. Shankar, *Indian J. Chem.*, **11**, 655 (1973).
- (16) B. B. Owen, *J. Am. Chem. Soc.*, **54**, 1758 (1932).
- (17) R. A. Robinson and R. H. Stokes, "Electrolyte Solutions", Butterworths, London, 1970, p 351.
- (18) H. S. Harned, *J. Phys. Chem.*, **66**, 589 (1962).
- (19) H. P. Benetto and D. Feakins in "Hydrogen-Bonded Solvent Systems", A. K. Covington and P. Jones, Ed., American Elsevier, New York, N.Y., 1969, p 71.
- (20) R. G. Bates, in ref 19.
- (21) H. Harned and B. B. Owen, "The Physical Chemistry of Electrolyte Solutions", Reinhold, New York, N.Y., 1943, p 118.
- (22) A. L. Vierk, *Z. Anorg. Chem.*, **261**, 283 (1950).

Self-Association in Lactams as a Function of the Ring Size

G. Montaudo, S. Caccamese,* and A. Recca

Institute of Industrial Chemistry of the University, Catania, Italy (Received June 26, 1974; Revised Manuscript Received April 3, 1975)

Vapor pressure osmometer (VPO) measurements in benzene at 37° have been used to estimate the association equilibrium constants (K_a) for 17 lactams and related compounds. Remarkably, our measurements reveal a strong dependence of K_a on the lactam ring size, the smaller rings being the most associated and the larger rings showing little association. A drastic drop in K_a is also observed in comparison of the unsubstituted lactams with those methyl substituted in the ring. A rationalization of these effects is offered. As expected, *N*-methyl lactams are found to be much less associated than the corresponding *N*-hydrogen lactams.

It is well known that association through hydrogen bonding exists in amides, lactams, and proteins, and the subject has stimulated widespread and continued interest.¹

Several spectroscopic studies have shown that the associated species are cyclic dimers for lactams having the amide group in the cis form, while a chain dimer and a small fraction of higher oligomers is involved in the case of trans amide groups.² For three lactams (compounds 4, 8 and 9 in Table I), association constant (K_a) values and thermodynamic parameters were determined in CCl₄ solutions over a wide concentration range from ir examination of the inten-

sity of the bands associated with "free" and "bonded" NH stretching.³⁻⁵ Other polar solvents such as chloroform which bear hydrogen atoms capable of competing with the amide NH in binding the carbonyl oxygen, usually are not used in experimentation.⁶ However, NMR attempts to measure the self-association and solvation enthalpies for γ -butyrolactam and δ -valerolactam in chloroform were recently reported.^{7,8} 2-Pyridone, an unsaturated analog of lactams, is found to be much more associated than the above two lactams by vapor pressure osmometry (VPO) measurements in benzene.⁹

From the literature survey,¹⁻⁹ however, one is forced to conclude that there is a lack of reliable K_a values for the overall series of lactams, measured with a single technique and in one solvent.

In our opinion, the latter information is relevant to the purpose of correlating the hydrogen-bonding ability of the amide group to structural factors. We have therefore measured the apparent molecular weights of 17 compounds (Table I) in benzene at 37° and have derived a single, reliable value of K_a for each compound in the range of concentration studied.

Our results show that the degree of association in lactams is a regular function of the ring size, and reveal the extreme sensitivity of the amide hydrogen-bonding ability to apparently minor structural factors.

K_a Determinations

We used a simple treatment¹⁰ modified according to our VPO procedure. The only assumption here is that the equilibrium involves only monomer and dimer, and this allows us to derive the following equations. By definition, the average numerical molecular weight \bar{M}_n is

$$\bar{M}_n = \frac{\sum N_i M_i}{\sum N_i} \quad (1)$$

where N_i is the mole number of the i th species and M_i is its molecular weight. In our case, the apparent molecular weight M_a is

$$M_a = \frac{N_1 M_1 + N_2 M_2}{N_1 + N_2} \quad (2)$$

If m is the formal molar concentration and b_1 and b_2 are the molarity of monomer and dimer, respectively, at equilibrium one always has

$$m = b_1 + 2b_2 \quad (3)$$

Combining eq 2 and 3 and assuming $r = M_1/M_a$

$$b_2 = m(1 - r) \quad (4)$$

Since $K_a = b_2/b_1^2$, and assuming $\gamma = 2r - 1$, one can write

$$K_a = (1 - \gamma)/2m\gamma^2 \quad (5)$$

so that K_a can be obtained as the slope in a plot of $1/\gamma$ vs. $2m\gamma$. This plot has the advantage of yielding a straight line with a known intercept of 1.

In Table I are reported the K_a values determined by least-squares minimization and all the necessary data.

The standard deviations in K_a are in the order of 5–10% and are calculated according to the usual statistical methods.¹¹ Because of the good straight line relationship in eq 5, it appears unlikely that the eventual existence of open chain oligomers in lactams with $n \geq 9$ would affect the conclusions drawn from our data.

All measurements were carried out in benzene at 37°. A series of preliminary measurements in chloroform convinced us that no reliable and quantitative K_a data could be obtained in this solvent under our conditions. As a general trend, we noticed a marked decrease of the degree of association in chloroform with respect to benzene; our figures range among K_a values of $1-50 M^{-1}$ for all compounds in Table I, except for compound 16 ($K_a = 823 \pm 7$ in chloroform at 37°).

Discussion

The K_a data reported in Table I reveal several inter-

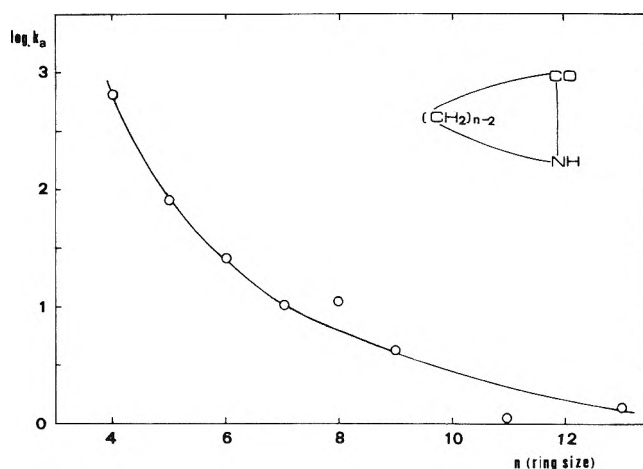
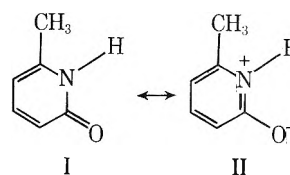


Figure 1. Dependence of K_a in lactams as a function of the ring size.

esting features of the self-association phenomenon in lactams.

As expected, the four tertiary amides examined (compounds 5, 7, 12, and 17) show a negligible amount of association independent of their ring size. On the contrary, the degree of association in lactams is a regular function of the ring size. This remarkable result is observed in Figure 1, where the K_a values are plotted against the size of the respective lactam.

Attempts to rationalize this result lead us to consider that the hydrogen-bonding strength in amides increases parallel to the acidity of the NH group and the basicity of the CO group.^{12,13} Accordingly, compound 16 (Table I) exists almost exclusively in the dimeric form, due to the strong polarization of the NH and CO groups induced by the resonance structure II.



Ring strain plausibly produces a similar polarization effect in smaller lactams, resulting in their high association. Also the drastic drop observed in the K_a values by comparing the unsubstituted lactams (compounds 1 and 4) with those bearing methyl substituents in the rings (compounds 2, 3, and 6) can be explained by this hypothesis. In fact, those methyl substituents influence the amide system by electron-donating inductive effect, reducing therefore the degree of polarization of the NH and CO groups in the corresponding lactams.

In evaluating our results, the effects found here appear simple and straightforward: a strong relation exists between the hydrogen-bonding ability of the amide group and structural factors which might appear of minor importance (ring size and inductive effects). It should be remarked that, because of the relevance of the amide hydrogen-bonding phenomena, these findings may exceed their interest in the specific lactams field and may prove of more general interest and utility.

Experimental Section

Materials. Analytical grade benzene was refluxed over

TABLE I: Association Constants Derived from Molecular Weight Measurements

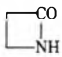
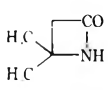
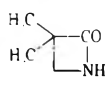
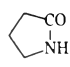
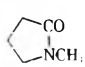
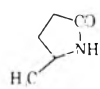
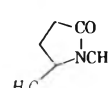
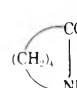
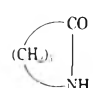
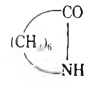
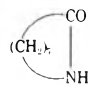
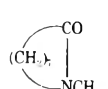
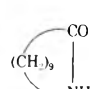
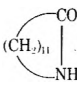
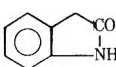
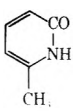
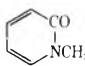
No.	Compound	Concn, <i>M</i>	M_2/M_1^a	Monomer ^b fraction	K_{12} , M^{-1}
1		0.0105	1.583	0.263	643 ± 63 ^c
		0.0280	1.731	0.155	
		0.0304	1.744	0.147	
2		0.0061	1.187	0.684	39.2 ± 1.8
		0.0497	1.454	0.375	
		0.0647	1.485	0.347	
		0.0700	1.489	0.343	
		0.0859	1.518	0.318	
3		0.0105	1.362	0.468	54.1 ± 16.2
		0.0292	1.438	0.391	
		0.0334	1.426	0.402	
4		0.0104	1.262	0.585	81.7 ± 8.6
		0.0280	1.396	0.432	
		0.1060	1.653	0.210	
		0.1160	1.694	0.213	
5		0.0600	1.142	0.752	2.8 ± 0.4
		0.0820	1.162	0.721	
		0.1340	1.198	0.669	
6		0.0129	1.123	0.657	34.1 ± 2.3
		0.0168	1.208	0.540	
		0.0247	1.297	0.542	
		0.0393	1.386	0.444	
		0.0649	1.447	0.382	
		0.0795	1.492	0.341	
7		0.0510	1.131	0.769	3.2 ± 0.4
		0.0604	1.124	0.779	
		0.0665	1.140	0.754	
8		0.0135	1.263	0.583	27.2 ± 4.3
		0.0187	1.238	0.616	
		0.0570	1.379	0.451	
		0.0752	1.455	0.374	
9		0.0158	1.095	0.826	10.4 ± 1.3
		0.0239	1.162	0.721	
		0.0347	1.192	0.678	
10		0.0192	1.167	0.714	11.2 ± 1.5
		0.0284	1.181	0.693	
		0.0447	1.223	0.635	
		0.0566	1.284	0.558	
11		0.0204	1.059	0.887	4.3 ± 0.3
		0.0374	1.093	0.830	
		0.0425	1.107	0.807	
		0.0573	1.159	0.726	
		0.0650	1.165	0.743	
		0.0905	1.202	0.663	
12		0.0217	1.089	0.836	4.1 ± 0.6
		0.0285	1.121	0.783	
		0.0433	1.135	0.761	
		0.0656	1.163	0.719	
13		0.0146	1.018	0.964	0.8 ± 0.2
		0.0245	1.030	0.942	
		0.0334	1.030	0.941	
		0.0410	1.029	0.943	

TABLE I (Continued)

No.	Compound	Concn, <i>M</i>	M_2/M_1^a	Monomer ^b fraction	K_a, M^{-1}
14		0.0411	1.054	0.898	1.4 ± 0.2
		0.0496	1.055	0.895	
		0.0604	1.073	0.864	
		0.0805	1.100	0.824	
		0.0865	1.084	0.845	
15		0.0100	1.137	0.758	17.9 ± 2.7
		0.0282	1.199	0.668	
		0.0329	1.236	0.618	
		0.0543	1.312	0.524	
		0.0704	1.390	0.439	
16		0.0479	1.865	0.072	2059 ± 129
		0.0589	1.882	0.062	
		0.1210	1.917	0.043	
17		0.0456	1.055	0.895	1.3 ± 0.1
		0.0731	1.070	0.868	
		0.0915	1.092	0.831	
		0.1010	1.092	0.832	
		0.1200	1.101	0.816	
		0.1450	1.135	0.762	

^a This ratio ($1/r$) is obtained taking in account that $r = \Delta R_{\text{obsd}}/\Delta R_{\text{calc}}$. ^b This value identifies γ . In fact from simple substitution in eq 3-5 (see text) $\gamma = b_1/m$. ^c Standard deviation (see text).

sodium wire and stored over molecular sieves. Stock solvent was the same for all series of measurements. All solutions were made up by weight. Pure commercial lactams (Schuchardt) were purified by recrystallizations from benzene when solids, or by distillation at reduced pressure when liquids. The propiolactams were prepared and purified according to the literature.

Molecular Weights Determinations. Molecular weights were determined in benzene using a Mechrolab 301 A vapor pressure osmometer. Measurements were carried out at 37.0° over the concentration range of about 0.01–0.1 *M*.

Calibration of the osmometer was made with benzene solutions of saccharose octacetate (puriss. Fluka) and frequently checked, from the relation $\Delta R_{\text{obsd}} = Km$. The value of K , 364 ΩM^{-1} , remained constant ± 0.5 for all series of measurements.

References and Notes

- (1) S. N. Vinogradov and R. H. Linneli, "Hydrogen Bonding", Van Nostrand-Reinhold, New York, N.Y., 1971.
- (2) H. E. Hallam and C. M. Jones, *J. Mol. Struct.*, **1**, 413, 425 (1968).
- (3) H. E. Afsprung, S. D. Christian, and J. D. Worley, *Spectrochim. Acta*, **20**, 1415 (1964).
- (4) R. C. Lord and T. J. Porro, *Z. Elektrochem.*, **64**, 672 (1960).
- (5) M. Tsuboi, *Bull. Chem. Soc. Jpn.*, **24**, 75 (1951).
- (6) W. Klemperer, M. W. Cronyn, A. H. Maki, and G. C. Pimentel, *J. Am. Chem. Soc.*, **76**, 5846 (1954).
- (7) L. F. Blackwell, P. D. Buckley, K. W. Jolley, and I. D. Watson, *Aust. J. Chem.*, **25**, 67 (1972).
- (8) J. M. Purcell, H. Susi, and J. R. Cavanaugh, *Can. J. Chem.*, **47**, 3655 (1969).
- (9) M. H. Krackov, C. M. Lee, and H. G. Mautner, *J. Am. Chem. Soc.*, **87**, 892 (1965).
- (10) B. C. Barton and C. A. Kraus, *J. Am. Chem. Soc.*, **73**, 4561 (1951).
- (11) See ref 1, p 280.
- (12) N. Kulevsky and W. Reineke, *J. Phys. Chem.*, **72**, 3339 (1968).
- (13) N. Kulevsky and P. M. Froehlich, *J. Am. Chem. Soc.*, **89**, 4839 (1967).

Optical Probes in Polyelectrolyte Studies. I. Acid-Base Equilibria of Dansylated Copolymers of Maleic Anhydride and Alkyl Vinyl Ethers¹

Ulrich P. Strauss*² and Gorazd Vesnaver

School of Chemistry, Rutgers University, New Brunswick, New Jersey 08903 (Received January 20, 1975)

Hydrolyzed 1-1 maleic anhydride copolymers of methyl and butyl vinyl ethers which had been chemically tagged with small moieties of an optical probe were investigated over their primary ionization regions by potentiometric titration and absorption spectroscopy. For comparison, the optical probe which was 1-dimethylamino-5-(β -aminoethyl)sulfonamidonaphthalene was similarly studied in its free state. For the methyl copolymer the apparent pK_{acid} values of its dicarboxylate groups and of the dimethylamino groups of the probes maintained a constant small difference as they increased with increasing degree of dissociation, α , indicating that both types of groups experience the same local pH determined by the electrostatic potential of the polyion. In the case of the butyl copolymer both pK_{acid} values pass through a maximum as the macromolecule undergoes a transition from a compact to a random coil conformation. However, the difference between the pK_{acid} values at low α was much larger than for the methyl copolymer. The difference decreased with increasing α and attained the value observed for the methyl copolymer at the completion of the conformational transition. These results are interpreted in terms of changes in the local solvent environment surrounding the probe.

Introduction

Despite the intensive effort devoted in recent years to the study of proton equilibria of acid-base groups on polyelectrolytes, our understanding of these equilibria is still incomplete.^{3,4} It has become increasingly clear that the long-range electrostatic interactions between such groups alone cannot always be held accountable for the characteristic variations in acid strength with changing degree of ionization and that other factors frequently play an important role.⁵⁻¹² Such factors include specific binding of counterions,^{5,8} conformational changes,^{6,10} neighboring group interactions,^{9,11,12} and alteration of the solvent structure by the intense electrical field around the macroion.^{7,8}

In order to elucidate the contributions of these factors, it is necessary to supplement the conventional potentiometric titration technique with methods which can provide more detailed information about the immediate molecular environment of the polyelectrolyte. A promising approach in this direction might involve the attachment of an optical probe to the macromolecule by means of a covalent linkage. As the optical probe one would choose a molecule whose spectroscopic behavior is sensitive to one or more of the environmental properties one wishes to observe such as the local pH, solvent polarity, and viscosity as well as features relating specifically to the conformational state of the polymer.

The results of such studies might also be of value in the interpretation of data obtained with protein-probe conjugates.¹³⁻¹⁷ The synthetic polyelectrolytes into which various types of complexities can be built by chemical means in a step-wise fashion should serve as useful model systems for examining probe responses under conditions more clearly defined than are obtainable with the less easily modifiable protein conjugates.

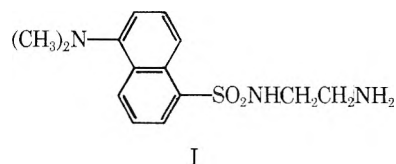
Two polyelectrolytes likely to be useful for this purpose are the alternating 1-1 methyl and butyl vinyl ether copolymers of maleic anhydride.^{10,18} They differ in that the first behaves as a normal randomly coiled macroion over its whole range of ionization while the second exists at low de-

grees of dissociation in a compact state stabilized by hydrophobic forces and undergoes a conformational transition to the random coil form as the degree of dissociation is increased. An optical probe which appears to be suitable for our purpose and which has been successfully employed in protein studies is the 1-dimethylaminonaphthalene-5-sulfonyl (dansyl, DNS) group.^{13,15} This group is readily attachable to our macromolecules by the reaction of the primary amino group of dansyl(β -aminoethyl)amide with an anhydride group of the copolymers. The extent of dansylation of the copolymers should be small to minimize possible alterations of the polyelectrolyte properties by the probe.

In this paper we present absorption spectra obtained with these copolymer-probe conjugates as well as with the free dansyl(β -aminoethyl)amide in order to compare the acid-base behavior of the dimethylamino groups of the probe with that of the dicarboxylate groups of the polyacids.

Experimental Section

Materials. Specially purified grade 1-dimethylaminonaphthalene-5-sulfonyl chloride, obtained from Pierce Chemical Co. as a 10% solution in acetone, was allowed to react with freshly distilled ethylenediamine. The desired product, 1-dimethylamino-5-(β -aminoethyl)sulfonamidonaphthalene (I) (dansyl(β -aminoethyl)amide), was separated



from reagents and by-products, recrystallized several times from ethanol-water mixtures, and dried under reduced pressure. The melting point was 149-151°, in good agreement with that reported by Seiler and Wiechmann whose detailed procedure for the preparation and purification of I was followed.¹⁹

The methyl vinyl ether-maleic anhydride copolymer (HMVEMA) was obtained from GAF Corp. (their sample Gantrez An 139). It was purified by repeated precipitations from tetrahydrofuran (THF) into ethyl ether. The *n*-butyl vinyl ether-maleic anhydride copolymer (HBVEMA) was our laboratory sample B-II, the preparation and properties of which have been reported previously.¹⁰

The probe I was chemically attached to the copolymers according to the following procedures. To 0.37 g of HMVEMA dissolved in 3 ml of THF 2 ml of 0.106 M solution of I in THF was added dropwise. The reaction mixture was stirred for 24 hr at room temperature and for 1 hr at 50°. It was then poured at room temperature into excess ethyl ether in which the copolymer is insoluble but in which the unreacted probe I is soluble. The dansylated copolymer was purified by repeated precipitations from THF into ethyl ether followed by exhaustive dialysis of its aqueous solution against water. No fluorescence was detectable in the final change of external water which had been dialyzed for 2 days against the internal copolymer solution. The copolymer solution was then passed through a column of purified Dowex 50 ion-exchange resin in the hydrogen ion form and stored at 4°. The conjugate of I and the butyl copolymer was prepared and purified by the same procedure except that the starting solutions were 0.27 g of HBVEMA in 1.8 ml of THF and 1.33 ml of 0.106 M solution of I in THF.

The fraction of dicarboxylate groups which is dansylated, to be denoted by *g*, was calculated from absorbance measurements in aqueous solution with the assumption that the extinction coefficient of the bound probe at the isobestic point at λ 304 m μ is equal to that of the free probe. The values of *g* obtained in this way were 0.070 for the methyl and 0.055 for the butyl copolymer.

THF and ethyl ether were refluxed over calcium hydride, distilled, and stored under nitrogen. Water was triple distilled. Electrolytes were reagent grade and used without further purification.

Preparation of Solutions. Modified universal buffer mixtures ranging in pH between 1.8 and 11.0 were prepared by titration with 0.2 N NaOH of a solution being 0.04 M each in phosphoric, acetic, and boric acids.²⁰ Solutions of constant probe concentration with different pH's were then prepared by adding to a given volume of a stock solution of I equal volumes of the different buffer solutions (or of aqueous HCl solutions for pH values below the range accessible with the buffers). The blank solutions needed for the spectroscopic measurements were prepared in the same manner by using pure water instead of the stock solution of I. The same procedure was followed in preparing buffered solutions of equal concentrations of I in 0.5 M NaCl. Solutions of equal concentrations of the dansylated copolymers at various pH values in water and in 0.5 M NaCl were similarly prepared using NaOH or HCl but omitting buffers other than the polyacids themselves.

Methods. Absorption spectra were recorded at 25.0° with a Cary 14 spectrophotometer. The pH was measured at the same temperature with a Radiometer Model 26 pH meter.

Results and Discussion

Free Probe. Absorption spectra of 7.09×10^{-5} M 1-dimethylamino-5-(β -aminoethyl)sulfonamidonaphthalene (I) obtained at various pH values are shown in Figure 1 where the optical density, *A*, is given as a function of the wave-

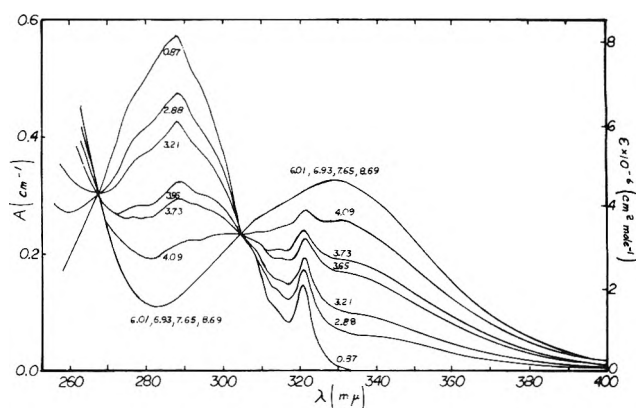


Figure 1. Absorption spectra of 7.09×10^{-5} M 1-dimethylamino-5-(β -aminoethyl)sulfonamidonaphthalene solutions in modified universal buffer mixtures (see text). Curves are labeled with appropriate pH values. Ordinate scale on left-hand side gives the optical density, *A*, and applies to all curves. Ordinate scale on right-hand side allows the two outside curves to be read as decadic extinction coefficients, ϵ , of the two forms with the dimethylamino group in protonated and unprotonated states in units of $\text{cm}^2 \text{mol}^{-1}$.

length, λ . The results exhibit isobestic points at 268 and 304 m μ and can be resolved quantitatively into contributions from spectra of two species of I differing in the protonation state of the dimethylamino group. The curves corresponding to the highest and lowest pH values in Figure 1 represent the spectra of the unprotonated and protonated forms, respectively. If read with the ordinate scale on the right-hand side, these curves give the decadic extinction coefficients, ϵ , of the two forms in units of $\text{cm}^2 \text{mol}^{-1}$. These spectra are similar to, but not identical with, the spectra reported for DNS acid and DNS amide.²¹

These results follow very closely the relation

$$\text{p}K_d = \text{pH} + \log [y/(1 - y)] \quad (1)$$

with $\text{p}K_d = 3.5 \pm 0.1$, where K_d is the acid dissociation constant of the $(\text{CH}_3)_2\text{N}$ group of I and *y* is the fraction of these groups in the protonated form. When the ionic strength was raised to 0.5 M with NaCl, the absorbances could again be resolved into additive contributions from protonated and unprotonated forms whose extinction coefficients were identical with those obtained in the absence of NaCl. However, the value of $\text{p}K_d$ was raised to 3.9 ± 0.1 . This raise may be ascribed to a reduction, due to Debye-Hückel shielding, of the electrostatic force of the protonated primary amino group of I on the acid-base equilibrium of the $(\text{CH}_3)_2\text{N}$ group. A $\text{p}K_d$ of 3.9 has been reported for DNS amide,²¹ which supports these findings.

Dansylated Methyl Copolymer. The degree of dissociation of the carboxylate groups of the polyacid may be expressed by the relation

$$\alpha = \{[(\text{NaOH}) + (\text{H}^+) - (\text{OH}^-)]/C_p\} + yg \quad (2)$$

where (NaOH) is the molarity of added base, (H^+) and (OH^-) are molarities of free hydrogen and hydroxyl ion, respectively, determined from the pH together with potentiometric titrations of appropriate blank solutions, and C_p is the polymer concentration in monomoles per liter. (One monomole contains one maleic acid and one alkyl vinyl ether residue.) The last term in eq 2 accounts for the protons abstracted by the conjugated probe. Defined in this way, α may range from 0 to 2. Because of the large differ-

ences in the successive pK 's of the dicarboxylate groups, the following relation is useful for the range $0 < \alpha < 0.9$.

$$pK_1^a = \text{pH} + \log [(1 - \alpha)/\alpha] \quad (3)$$

where K_1^a is the apparent first dissociation constant of a diprotic acid residue. As is well known, pK_1^a is not constant with varying α and may be divided into two contributions as follows:

$$pK_1^a = pK_1^0 + \frac{1}{RT \ln 10} \left(\frac{\partial G_{\text{ion}}}{\partial \alpha} \right) \quad (4)$$

where pK_1^0 is the limiting value of pK_1^a as α approaches zero and the second term on the right-hand side accounts for the electrostatic and other possible excess contributions to the free energy of dissociation.

Similarly, one would not expect the pK_d , defined by eq 1, of the attached probe to be constant. Absorption spectra obtained with 1.22×10^{-3} monomolar aqueous solutions of the dansylated methyl copolymer at various pH values show that the extinction coefficients of the protonated and unprotonated forms of the probe are not affected by the attachment to the copolymer, at least over the wavelength range from 300 to 380 $m\mu$.²² The fraction of protonated probe, y , could then be determined as a function of pH from the spectra. The values of pK_d calculated by eq 1 are compared with the values of pK_1^a as a function of α in Figure 2. In the same figure are also shown values of pK_d and pK_1^a calculated from similar results obtained in 0.5 M NaCl solutions.

For each of the two solvent systems the pK_1^a and pK_d curves are seen to run parallel, indicating that the primary dissociation of the dicarboxylate groups and the dissociation of the dimethylammonium groups are affected in the same manner by the changes in the condition of the polyion with increasing α .²³ These findings may be viewed as evidence that both types of groups experience approximately the same local pH which, in turn, is controlled by the electrostatic potential near the macroion. Thus, for the methyl copolymer over the dissociation range $0 < \alpha < 1$ this potential appears to be the sole factor responsible for the last term in eq 4. Other possible causes for deviations from constancy of pK values, such as conformational changes, hydrogen bonding, specific counterion binding, and changes in the solvent structure, would be expected to be more specific and to affect the behavior of the two types of groups in different ways. This conclusion is consistent with previous results which show that in the primary dissociation region of the methyl copolymer solvation effects are small,¹⁸ specific counterion binding is negligible,²⁴ and potentiometric titration data follow the predictions of electrostatic theoretical treatments.^{9,25}

Dansylated Butyl Copolymer. As with the methyl copolymer, absorption spectra obtained with the butyl copolymer in 1.79×10^{-3} monomolar solutions in water and in 0.5 M aqueous NaCl solutions indicated that the extinction coefficients between 300 and 380 $m\mu$ of the acidic and basic forms of the probe were not affected by attachment to the copolymer. The pK_d and pK_1^a values, determined as described for the methyl copolymer, are shown as functions of α in Figure 3. The pK_1^a values obtained in the absence of salt are seen to go through a maximum with increasing α . This maximum has been reported previously and attributed to a conformational transition from a compact state stabilized by hydrophobic forces to a random coil charac-

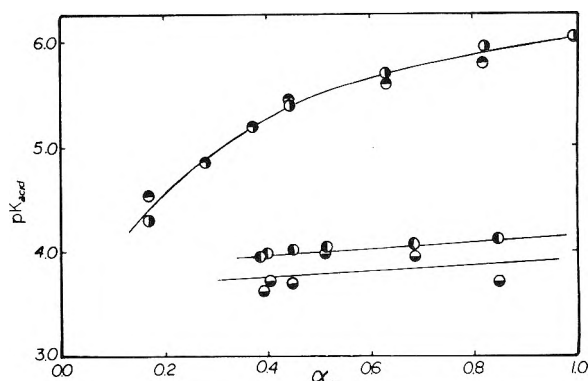


Figure 2. Apparent pK_{acid} values of HMVEMA and attached probe: (●) pK_1^a in water; (○) pK_d in water; (■) pK_1^a in 0.5 M NaCl; (□) pK_d in 0.5 M NaCl.

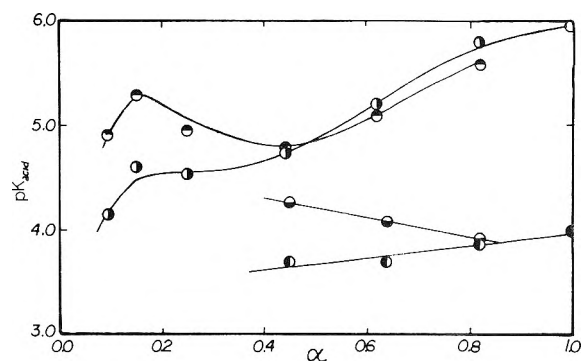


Figure 3. Apparent pK_{acid} values of HBVEMA and attached probe. Symbols as in Figure 2.

teristic of nonhydrophobic polyions.¹⁰ The initial steeply rising portion of the pK_1^a curve has been ascribed to strong electrostatic interactions among the ionized carboxyl groups in the tightly coiled state. As α increases the electrostatic repulsions cause the coil to expand causing a decrease in pK_1^a until the conversion to the random coil form is complete when the pK_1^a increases again but less steeply than in the compact form. In contrast to the behavior exhibited by the methyl copolymer, the pK_d curve does not run parallel to the pK_1^a curve at low α . The maximum in the pK_d curve, while located at the same value of α as the pK_1^a maximum, is extremely shallow, indeed almost nondiscernible. The pK_d and pK_1^a curves become parallel only in the range of α corresponding to the random coil form.

The nonparallelity of the pK curves makes it impossible to account for the protonation equilibria at low α entirely in terms of electrostatic effects. A possible explanation for the observed behavior may be that when the polyion is in the compact state the probe molecules find themselves in the nonpolar environment of the pendant butyl groups; compared with water this environment would favor the neutral basic form of the dimethylamino group over the ionic acidic form and thereby counteract the electrostatic forces favoring the latter. The same argument would not apply to the carboxylate groups for which the acidic form is neutral and the basic form ionic. In fact, if the carboxylate groups were to extend into the environment of the butyl groups, the effects of the hydrocarbon environment would reinforce the electrostatic acid-weakening effect. However, such a location of the carboxylate groups should raise the

value of pK_1^0 relative to that of the methyl or ethyl copolymer. The evidence so far, while not conclusive, shows no such variation in pK_1^0 values.^{9,10}

In the 0.5 M NaCl solutions the butyl copolymer exhibits insolubility in the region of α where the maximum in the pK curves would be expected. However, the conformational transition occurs at higher α than it does in water, and the initial separation of the pK_1^a and pK_d curves and their mutual convergence as the end of the transition region is approached resemble these features observed in the absence of excess electrolyte and may be explained similarly.

We have seen that in the compact conformation of the butyl copolymer the electrostatic forces due to the negative carboxylate groups and the environmental influence of the nonpolar butyl groups exerted opposing effects on the $(CH_3)_2NH^+$ groups of the probe, the former being acid weakening and the latter acid strengthening. One may speculate that if we were dealing with a compact polycation instead of a polyanion the electrostatic and nonpolar environmental effects would reinforce one another, both acting to increase the acid strength of the probe. Such an effect has indeed been reported for dansylated bovine serum albumin for which the value of pK_d of the conjugated probe was found to be 2.3 units lower than that of the free probe.¹⁵ Moreover, denaturation with 8 M urea reduced the pK_d lowering to 0.9 units, a result which could also be predicted from our findings with the butyl copolymer by assuming that the denaturation changes the protein molecule from its native compact to a random coil form, thereby both weakening the electrostatic effects and destroying the nonpolar environmental influence of the hydrophobic groups. It is noteworthy that these protein results were originally interpreted quite differently.

These conclusions demonstrate the utility of the synthetic hydrophobic polyacids both as model compounds for

proteins and as a means for gauging the response of conjugated optical probes to environmental changes.

References and Notes

- (1) Support of this research by the United States Public Health Service (Grant No. GM 12307) is gratefully acknowledged.
- (2) Author to whom correspondence should be addressed.
- (3) G. S. Manning, *Annu. Rev. Phys. Chem.*, **23**, 117 (1972).
- (4) R. W. Armstrong and U. P. Strauss, *Encycl. Polym. Sci. Technol.*, **10**, 781 (1969).
- (5) L. M. Gross and U. P. Strauss in "Chemical Physics of Ionic Solutions", B. E. Conway and R. G. Barradas, Ed., Wiley, New York, N.Y., 1966, pp 361-389.
- (6) M. Nagasawa and A. Holtzer, *J. Am. Chem. Soc.*, **86**, 538 (1964).
- (7) G. S. Manning and A. Holtzer, *J. Phys. Chem.*, **77**, 2206 (1973).
- (8) U. P. Strauss in "Polyelectrolytes", E. Selegny, Ed., Ridel, Dordrecht, Holland, 1974, pp 79-85.
- (9) A. W. Schultz and U. P. Strauss, *J. Phys. Chem.*, **76**, 1767 (1972).
- (10) P. L. Dubin and U. P. Strauss, *J. Phys. Chem.*, **74**, 2842 (1970).
- (11) S. Lifson, *J. Chem. Phys.*, **26**, 727 (1957).
- (12) R. A. Markus, *J. Phys. Chem.*, **58**, 621 (1954).
- (13) G. Weber, *Biochem. J.*, **51**, 155 (1952).
- (14) I. M. Klotz and J. Ayers, *J. Am. Chem. Soc.*, **79**, 4078 (1957).
- (15) I. M. Klotz and H. F. Fiess, *Biochim. Biophys. Acta*, **38**, 57 (1960).
- (16) R. F. Steiner and H. Edelhoch, *Chem. Rev.*, **62**, 457 (1962).
- (17) G. M. Edelman and W. O. McClure, *Acc. Chem. Research*, **1**, 65 (1968).
- (18) A. J. Begala and U. P. Strauss, *J. Phys. Chem.*, **76**, 254 (1972).
- (19) N. Sella and M. Wiechmann, *Prog. Thin-Layer Chromatogr. Relat. Methods*, **1970**, **1**, 95-144 (1970).
- (20) H. T. S. Britton, "Hydrogen Ions", van Nostrand, New York, N.Y., 1932, p 225.
- (21) D. Lagunoff and P. Ottolenghi, *C. R. Trav. Lab. Carlsberg*, **35**, 63 (1965).
- (22) At wavelengths below 300 m μ there are small deviations from the spectra of the free probe probably due to light scattering of the copolymer. Since the calculations of γ were based on the absorbances at 340 m μ where the spectra of free and bound probe were identical, these deviations should not affect our results.
- (23) In the absence of excess salt the values of pK_1^a and pK_d overlapped and therefore only one curve was drawn through both sets of data. This overlap is probably fortuitous and results from the near equality of the intrinsic pK values.
- (24) U. P. Strauss and A. Rosengart, unpublished results.
- (25) Previously presented evidence indicates that factors other than the electrostatic potential are involved for this polycation over the range $1 < \alpha < 2$,⁹ but a probe with a pK_d about three units higher than the one used here would be needed to study this α region.

Foaminess of Binary and Ternary Solutions

Sydney Ross* and Gary Nishioka

Chemistry Department, Rensselaer Polytechnic Institute, Troy, New York 12181 (Received November 13, 1974)

Homogeneous solutions containing two or three components exhibit increasing foaminess at concentrations near the critical-solution point and plait point, respectively. However on separating the phases that occur on the inhomogeneous side of these critical or plait points, one of the liquid phases is found to act as a defoamer for the other liquid phase. These two contrary effects are traced to two different manifestations of surface activity in the vicinity of the critical point, namely, adsorption (in the one-phase region) and spontaneous spreading (in the two-phase region).

Introduction

A continuous range of amphipathic solutes, such as an homologous series of soaps or a series of block copolymers of varying hydrophile-lipophile balance, offers a striking foam phenomenon. If two adjacent members of a series are separately mixed with a constant amount of solvent at a

constant temperature, the total amount of one member will be dissolved whereas the excess of the other member will be present as a separate phase. The phenomenon in question is the action of the undissolved material as a defoamer, whereas its immediately adjacent neighbor acts as a profoamer in the solvent selected. The phenomenon is suffi-

ciently general to be found in various situations. Thus at a certain HLB number on the Atlas scale,¹ two adjacent members of the series of nonionic emulsifiers that is registered by I.C.I. (America) under the trade names of Spans and Tweens display an abrupt transition from defoaming to profoaming in aqueous solution, exactly where the demarcation occurs between insolubility and solubility in water. The same effect can also be observed in a block copolymer, of which polyethylene oxide constitutes the hydrophilic moiety and poly(dimethylsiloxane) constitutes the lipophilic moiety: the hydrophilic members of the series are insoluble in toluene and act as defoamers in aromatic solvents; but when the lipophilic moiety is sufficiently increased to make the compound soluble in toluene, it acts as a profoamer. A third example of essentially the same effect can be observed with a single solute if its solubility changes markedly with temperature. Sodium stearate, for example, is insoluble in cold water but is much more soluble in hot water; the solution is foamy at high temperatures but is defoamed (unless the stearate is solubilized by another solute) at low temperatures. Schwartz and Reid² refer to an essentially similar effect observed with a block copolymer containing poly(ethylene oxide), a substance that, in water, always confers a retrograde solubility with temperature to any compound of which it forms a part. At temperatures below its cloud point the solute is a profoamer, whereas it becomes a defoamer at temperatures where cloudiness appears. Pluronics of the Wyandotte Co. behaves in the same way in aqueous solution below and above the cloud point temperature of each one.

The explanation of the remarkable contrast in behavior of two compounds that differ only slightly in chemical composition and are so nearly alike in all their properties except degree of solubility in a particular solvent resides in their different degrees of dispersion in the medium. The insoluble compound retains enough interaction with the medium to spread as an insoluble layer on its surface. This property meets the requirements of a defoaming agent:³ namely, that it be insoluble in the foamy liquid and that it be able to spread spontaneously over the surface of the liquid films. By the mere mechanical action of the spreading liquid and its attendant viscous drag of underlying substrate, the foam films are ruptured.³ In the soluble compound a relatively slight change in the hydrophile-lipophile balance of the molecule causes the solute to interact more strongly with the medium so that its degree of dispersion is brought down to the ultimate molecule, which is what is implied by observing that it is rendered soluble in the medium. However the interaction is not strong enough to give the dissolved molecules the lowest possible free energy attainable; they can attain still lower free-energy levels by adsorption at a surface or by micellization. This behavior is precisely that of a surface-active solute. The foaminess of the solution, which is now to be observed, has the same origin as that of a soap solution; it can be traced to adsorption of the solute at the liquid surface, to the attendant surface-tension lowering, and to the Marangoni effect.³

The present authors, recalling the above defoaming-profoaming phenomena that are associated with an amphipathic solute or a related series of such solutes as the point of solubility is reached, reasoned that a similar effect might accompany the transition from two phases to one phase in multicomponent systems, even where amphipathic structure in the solute is not recognized. Conventional amphi-

pathic solutes such as soaps and synthetic detergents are perhaps not unique in displaying surface activity. Certainly a solute whose molecular structure is planned to be amphipathic by a balancing of hydrophilic and lipophilic elements is thereby assured of any required degree of interaction with the solvent; but other solutes may well exist that have the requisite degree of interaction for surface activity although their molecular structure does not proclaim their amphipathy even to experienced chemists. The surface activity of a solute is primarily the result of a relatively weak interaction with the solvent, which must of course still be sufficient to dissolve the solute but need not be greater than the least degree necessary to do so. A propensity toward phase separation might therefore be a general guide to surface-active behavior. Indeed a prescient but passing and incidental remark made by Langmuir could have been seized at the time by an alert investigator to stimulate something like the present series of experimental researches and so anticipate our findings by 50 years. Langmuir wrote:⁴ "Undoubtedly, in mutually saturated liquids, especially near the critical temperature, the conditions are favorable for orientation and segregation of the molecules in the liquids." This hint was not taken up by anyone, so far as we are aware, nor did we ourselves notice it until after most of our work had been done.

The foregoing reasoning suggests that surface activity and hence foaminess might be found in two-component and three-component systems that display critical points and plait points, respectively. The critical-solution point of a two-component system is reached by raising or lowering the temperature, and the plait point of a three-component system is reached by adding a cosolvent to the immiscible liquids. For both kinds of system we have found, with examples selected only because the materials were readily available, that the foaminess did occur as projected. Presumably the effects are general behavior of all such systems. The results reported here may be taken as typical of what to expect on passing back and forth from the two-phase to the one-phase region of the phase diagram (see Figures 3-5).

Experimental Section

Sources of Materials. See Table I for the sources of materials used in this study.

Apparatus and Procedure. The foam stabilities were measured with the dynamic foam meter shown in Figure 1. Nitrogen gas was bubbled through 25 or 50 cm³ of a suitable liquid at measured rates V/t cm³/sec (V is gas volume, t is time) and the steady-state volume v_0 of foam was read. The ratio $v_0 t/V = \Sigma$ is almost independent of V/t and may be used as a measure of foaminess.⁵ Σ is, for example, about 6 sec for 1% aqueous 1-butanol; about 140 sec for 0.04% solution of egg albumen at pH 4.8.

Solutions were foamed in a column 70 cm high with a diameter of 3 cm. Temperature was controlled by means of an oil circulating from a thermostat. The cooling of the oil as it passed through the jacketed column was counteracted by heating tapes wound in a wide spiral around the outside of the apparatus. Thermocouples placed inside the oil jacket allowed proper adjustment of the current in the heating tapes to ensure uniformity of temperature throughout the column. The temperature of the foamed solution was read directly by a thermocouple placed inside the sample space of the foam meter. The sample temperatures were stable to within 0.2°.

TABLE I

Benzene	C_6H_6	Fisher Chemicals	Certified Reagent Grade
Diisobutyl- carbinol	$[(CH_3)_2-CHCH_2]_2-CHOH$	Union Carbide	Industrial Grade
Ethanol (absolute)	CH_3CH_2OH	U.S. Industrial Chemicals	Reagent Grade
Ethylene glycol	$HOCH_2CH_2OH$	Fisher Chemicals	Certified Reagent Grade
Ethylene glycol monobutyl ether	$C_6H_{14}O_2$	Fisher Chemicals	Certified Reagent Grade

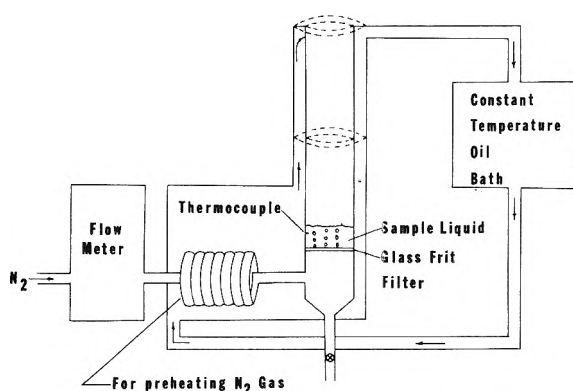


Figure 1. Dynamic foam meter, equipped for temperature control of entering gas and of the entire foam column. Not shown is the heating tape used to counteract thermal losses of the oil in the upper portions of the column.

Mixtures were prepared of 10, 20, 30, 35, 40, and 50 wt % diisobutylcarbinol in ethylene glycol. The foaminess of each composition was measured at different temperatures ranging from 20 to 90°. The clear-point temperature of each solution was also observed in order to determine the binodal curve and the critical-solution point.

Solutions of 20, 30, and 40 wt % ethylene glycol monobutyl ether in water were also prepared and foaminess at temperatures from 20 to 90° was determined for each solution. Published information^{6,7} stated that this system exhibited a lower as well as an upper critical solution temperature, i.e., mutual solubility occurs below a certain temperature (see Figure 2).

To study the three-component systems (benzene-ethanol-water and ethylene glycol-1-butanol-water) 80 solutions of varying composition (based on weight percent) were prepared for each system. Mixtures in the two-phase region were also prepared for the ethylene glycol-butanol-water system, the two phases were separated, and foam stability at 20° was measured for each of the conjugate solutions.

Results

Results for the two-component system diisobutylcarbinol + ethylene glycol are reported in Figure 3 as interpolated lines of equal foam stability (*isaphroic* lines, from *aphros* the Greek word for foam) superimposed on the phase diagram. The isaphroic lines center about the critical-solu-

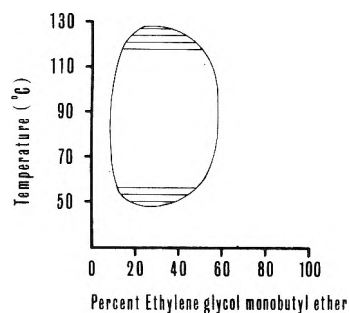


Figure 2. Phase diagram of the two-component system, ethylene glycol monobutyl ether-water, showing upper and lower critical-solution temperatures.

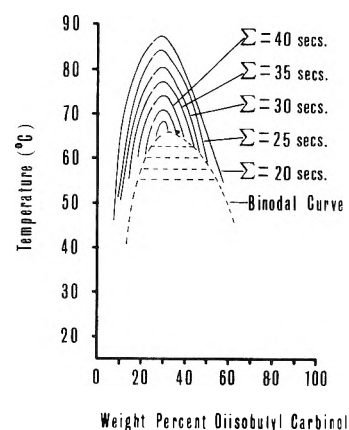


Figure 3. Phase diagram and interpolated isaphroic lines of the two-component system, diisobutylcarbinol-water, showing maximum foaminess near the critical-solution temperature.

tion point as a maximum and decrease in value the farther they are from it. Solutions of composition falling within the two-phase region of the diagram do not foam.

To decide a point of theoretical importance, namely, whether the vapor condensed from the foamy solution is of lower or higher surface tension than the liquid remaining, the 20% diisobutylcarbinol in ethylene glycol solution was partially distilled at reduced pressure at 70°. The measured surface tensions, designated σ , show that the condensed vapor has a lower surface tension than the remaining liquid: σ of condensed vapor at 70° = 23.6 dyn/cm; σ of remaining liquid at 70° = 38.3 dyn/cm. The surface tension of the volatile component of the solution is therefore less than that of the residual liquid, which could produce Marangoni effects at temperatures high enough for vapor fractionation. These solutions therefore would be capable of foaming during distillation.⁸ However at atmospheric pressure and at the temperatures of our foam tests, the liquids are too involatile for this mechanism to serve as the cause of the observed foam stability. The observed foam stabilization arises from adsorption of solute at the interface, and the surface activity thus postulated is of the kind we have been discussing in this paper.

We found that homogeneous solutions of the glycol ether-water system do not foam at compositions and temperatures very close to the lower critical-solution point (see Figure 2). This lack of foam stability may stem from the very reason that determines the existence of a lower critical-solution point. Francis⁹ speculated that aqueous systems containing glycol ethers have a lower critical-solution

point because at a critical temperature a chemical reaction (dehydration) occurs, which then produces two immiscible liquids. The insolubility is not produced by gradual changes in the intermolecular forces, leading finally to phase separation, but by an abrupt chemical change of one of the components of the system. Hence for solutions close to but cooler than the lower critical point there is no reason to expect increased adsorption or its consequent stabilization of foam. These solutions near their upper critical-solution point were not tested for foaminess due to experimental difficulty.

A lower critical-solution point is also exhibited by solutions of heavy liquids containing light hydrocarbons that are near their critical temperature (the highest temperature at which the liquid can exist). Presumably the light hydrocarbons exhibit a retrograde solubility with temperature due to acquired gaseous behavior. Foaminess has been reported¹⁰ for solutions of light hydrocarbon in dimethylformamide at high pressures, but only below a certain temperature. We could not investigate this system experimentally as our foam meter is not suited to run at higher pressures, but it is likely that increased adsorption for these gas-like solutions would occur beneath the lower critical-solution point, so that foaming would be expected.

Foam stabilities ($\Sigma \geq 5$ sec) at 20° for three-component systems are shown in Figures 4 and 5 for the benzene-ethanol-water system and the ethylene glycol-1-butanol-water system, respectively. The data are reported as interpolated isaphroic curves. Superimposed on these graphs are the binodal curves^{11,12} and tie lines for these systems. Solutions of composition falling within the two-phase region of each diagram do not foam. No plait-point data were available for these systems at 20° but its approximate position on the binodal curve can be observed by eye.

Discussion of Results

From these diagrams one notices a maximum of foaming at the plait point, with a gradual decrease in foaming of solutions in the one phase region with increasing distance from the plait point, and an absence of foam within the two phase region. For each system, compositions on one side of the binodal curve foamed while those on the other side did not. In the ethylene glycol-2-butanol-water system, the composition at the aqueous extremity of the tie line foamed while its conjugate composition at the organic extremity did not. Addition of small portions of the organic phase to the foaming aqueous phase produced a nonfoaming system, showing that the organic phase acts to defoam its aqueous conjugate. This result explains the absence of foam within the two-phase region; mixtures within this region contain an intrinsically foamable solution along with its inhibitor.

The explanation of the defoaming action of one conjugate solution on the other is to be found in their relative surface and interfacial tensions near the critical point, where the interfacial tension between the conjugates approaches zero and the two surface tensions approach equality. The former effect is found to precede the latter. The spreading coefficient of A on B is defined as

$$S = \sigma_B - (\sigma_A + \sigma_{A/B}) \quad (1)$$

where σ_A , σ_B , and $\sigma_{A/B}$ designate the surface tensions of A, B, and the interfacial tension of A/B, respectively. As $\sigma_{A/B}$ approaches zero more rapidly than σ_A becomes equal to σ_B , the value of S in the vicinity of the critical point is nearly approximated by

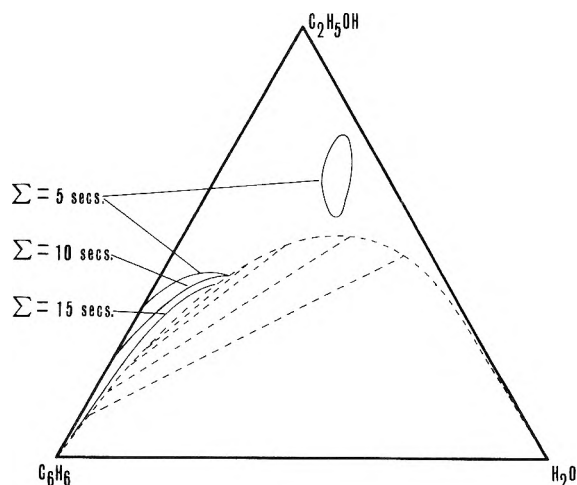


Figure 4. Phase diagram and interpolated isaphroic lines of the three-component system, ethanol-benzene-water, at 20°.

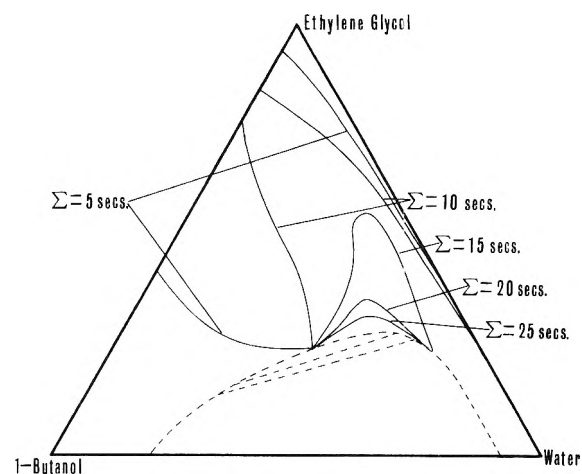


Figure 5. Phase diagram and interpolated isaphroic lines of the three-component system, ethylene glycol-butanol-water, at 20°.

$$S = \sigma_B - \sigma_A \quad (2)$$

If A and B represent the two conjugate solutions, then S is positive when $\sigma_B > \sigma_A$ and S is negative when $\sigma_A > \sigma_B$; i.e., the solution with the lower surface tension will spread spontaneously on the surface of its conjugate. The behavior is exactly what is required of a foam inhibitor. Conjugate solutions that lie farther from the critical point do not behave in this way and such two-phase mixtures would not be defoamed.

The current literature on foaming problems that occur during fractionation or distillation of liquids emphasizes the surface-tension relation of solutions containing volatile constituents, and even promulgates a dogmatic rule of thumb, as follows. If the loss of volatile constituents causes the surface tension of the remaining solution to increase, then anticipate a foam problem; if the loss of volatile constituents causes the surface tension to decrease, then no foam problem need be feared.⁸ So runs the dictum, which is based on the mechanism of bubble stabilization by the Marangoni effect, resulting from local changes in surface tension.

The normal behavior of liquids is such that, in general, involatility and high surface tension go together; so that,

although exceptions exist (the polysiloxanes being the best known of these exceptions), the usual behavior of solutions leads to the surface tension of the remaining solution being higher after the loss of its more volatile constituents. According to the rule cited above, that should lead to foaming within a fractionation tower. However it does not always do so in practice. The incidence of the surface-tension properties that one is warned against is therefore more to be taken as an alert to a situation that is potentially rather than necessarily troublesome. The converse conclusion, namely, that a reduction of the surface tension of the remaining solution after the loss of some of the more volatile constituents can be interpreted as an all-clear signal for the nonoccurrence of foaming, is indeed corroborated by the small body of existing data on the subject. The evidence pertaining to the foregoing rule is that it is inconclusive when it proffers a positive warning about an impending foam problem, and conclusive only when it indicates a safety signal. The relative frequency of receiving the inconclusive positive warning is, however, much higher than the frequency with which one will receive an "all-clear".

The usefulness of the rule is much reduced by the lack of surface tension data under conditions of temperature and varying concentrations within the column. These data are not readily obtained by laboratory measurements, requiring special equipment suitable for conditions prevailing inside the column.

A more useful and more far-reaching rule is to be obtained from the present work. Foaming of a solution reaches its maximum under conditions of temperature and concentration where a transition into two separate liquid phases is imminent. Two-component systems show maximum foam stability at the temperature and composition of the critical point, but only as long as the system is maintained as a homogeneous one-phase solution. Should the slightest degree of phase separation occur, one of the separated liquid phases acts as a defoamer for its foamy conjugate. When the two conjugate liquid phases are in contact with each other the system cannot sustain a stable foam, *even though the more volatile constituent has a lower surface tension than the less volatile constituent*. Here is a case, therefore, where the former rule about surface tensions would sound an unnecessary alert: an additional factor that the rule does not provide for has supervened and overturned its prediction.

Three-component systems show maximum foam stability at a given temperature at compositions near that of the plait point, but again only when the system is a homogeneous single phase. As before, the slightest degree of separation of liquid phases produces a conjugate solution that can defoam its foamy conjugate. It is highly probable that polycomponent systems would behave in a similar way, and show a maximum foam stability where separation of phase is imminent, and also show defoaming action once the slightest degree of phase separation occurs.

In the light of these conclusions some prior observations of foams are seen to be more significant. It has been pointed out,¹⁴ for instance, that saturated solutions are as incapable of sustaining a stable foam as are pure liquids, whereas on diluting them with solvent the solutions may

show foam stability. The only guarantee that a solution is saturated is to have excess insoluble phase present, and so it is likely that the reported tests of foam stability were conducted on heterogeneous systems, which as we now have reason to suspect, would thereby have included their own defoaming agents. The separated phase, even though solid, may still be an effective defoamer. Fatty acids, for example, even in their solid crystalline form, disintegrate on a water surface and spread over it, and hydrophobic solids form a useful part of many commercial defoamers.

Another prior set of observations is also of interest. Bolles, in a discussion of the design of bubble caps,¹⁵ suggested three different aqueous solutions that can be used to provide suitable standard foams at room temperature for testing such equipment. His list consists of (a) 2-propanol, 800 ppm; (b) methyl isobutyl ketone, 200 ppm; (c) 1-butanol, 1% by volume. In some of these standard solutions the concentration specified is just within the solubility limit, thus confirming the present contention that maximum foaming occurs near the conditions of phase separation. In another publication¹⁰ Bolles describes a foaming problem encountered in the industrial-scale separation of propylene from dimethylformamide. Although no phase diagram is given, various statements in this report suggest that the abrupt decrease of the foam stability with increasing temperature between 51 and 54°F might be due to the separation of a liquid phase acting as a defoamer to its foamy conjugate solution. In general in extractive distillation, in which a solvent is introduced, troublesome foaming is so common an occurrence that in the design of extractive-distillation columns excess capacity is always built in; experience has indicated that a foaming problem is likely to arise. We point out as significant that in those solutions phases appear and disappear at various stages inside the column; therefore, a knowledge of the phase diagram of the systems to be treated in an extractive-distillation process is the best guide to locate potential sources of troublesome foam.

Acknowledgment. The authors gratefully acknowledge support from Fractionation Research Inc., South Pasadena, Calif.

References and Notes

- (1) P. Becher, "Emulsions, Theory and Practice", Reinhold, New York, N.Y., 1965.
- (2) E. G. Schwarz and W. G. Reid, *Ind. Eng., Chem.*, **56**, 26 (1964); printed in "Chemistry and Physics of Interfaces", Vol. 1, S. Ross, Ed., American Chemical Society Special Publications, Washington, D.C., 1965, pp 65-71.
- (3) S. Ross, *Chem. Eng. Prog.*, **63** (9), 41 (1967).
- (4) I. Langmuir, *Colloid Symp. Monogr.*, **3**, 62 (1925).
- (5) J. J. Bikerman, *Trans. Faraday Soc.*, **34**, 634 (1938).
- (6) A. W. Francis, *Adv. Chem. Ser.*, No. **31**, 209 (1961).
- (7) "International Critical Tables", Vol. III, McGraw-Hill, New York, N.Y., 1929, p 390.
- (8) F. J. Zuiderweg and A. Harmens, *Chem. Eng. Sci.*, **9**, 89 (1958).
- (9) A. W. Francis, "Liquid-Liquid Equilibriums", Interscience, New York, N.Y., 1963, pp 11-15.
- (10) W. Bolles, *Chem. Eng. Prog.*, **63** (9), 48 (1967).
- (11) W. D. Bancroft and S. C. Hubbard, *J. Am. Chem. Soc.*, **64**, 349 (1942).
- (12) K. Matsumoto and S. Sone, *J. Pharm. Soc. Jpn.*, **76**, 475 (1956).
- (13) S. Ross and V. D. Papanu, unpublished report.
- (14) J. J. Bikerman, "Foams", Springer-Verlag, New York, N.Y., 1973, p 99.
- (15) W. L. Bolles in "Design of Equilibrium Stage Processes", B. D. Smith, Ed., McGraw-Hill, New York, N.Y., 1963, Chapter 14, p 480.

Physical Studies of Homologous *trans*-4-Ethoxy-4'-*n*-alkanoyloxyazobenzenes. Calorimetry

Craig L. Hillemann,^{1a} Gerald R. Van Hecke,* and (in part) S. Robert Peak, John B. Winther,^{1b} Martin A. Rudat,^{1b} David A. Kalman,^{1b} and Martha L. White

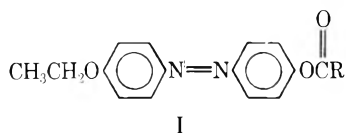
Department of Chemistry, Harvey Mudd College, Claremont, California 91711 (Received November 15, 1974; Revised Manuscript Received April 2, 1975)

Publication costs assisted by Harvey Mudd College

Calorimetric data are presented for the homologous *trans*-4-ethoxy-4'-*n*-alkanoyloxyazobenzenes. The extensive solid state polymorphism exhibited by this series is discussed in terms of free energy-temperature diagrams. Trends in the nematic-isotropic temperature and entropy data are discussed within the framework of current theories.

1. Introduction

As pointed out recently by van der Veen et al. very few calorimetric studies of homologous mesomorphic compounds have been reported.^{2a} With the view of providing such calorimetric data, some time ago we began to study the homologous nematogens *trans*-4-ethoxy-4'-*n*-alkanoyloxyazobenzenes (I) first reported by Vorländer.^{2b} Sub-



sequent to our beginning these studies Neff et al. reported a polymorphism in the solid state of the heptanoate homolog.^{3,4} Solid state polymorphism occurs frequently in this homologous series as will be discussed. McCaffrey and Castellano reported the synthesis and transition temperatures for the acetate to octanoate homologs but no calorimetric data.⁵ This paper will be the first in a series reporting the results of various physical measurements for this homologous series from pentanoate to tetradecanoate. Here we present the calorimetric data and discuss the results in light of some current theories of the nematic mesophase.

2. Experimental Section

Preparation of trans-4-Ethoxy-4'-n-alkanoyloxyazobenzenes. The pentanoate, hexanoate, and heptanoate esters obtained from Eastman Organic Chemicals were used after three recrystallizations from ethanol. The other esters were prepared from *p*-(*p'*-ethoxyphenylazo)phenol and the respective acyl chlorides. The compounds proved to be the *trans* isomer when checked by the uv spectrum technique of Neff et al. The acyl chlorides were prepared by refluxing the respective carboxylic acids with thionyl chloride and subsequent vacuum distillation. In a typical ester synthesis 8.26 mmol of the acyl chloride was added slowly by syringe to 2.00 g (8.26 mmol) of the *p*-(*p'*-ethoxyphenylazo)phenol dissolved in 15 ml of ice-cold pyridine in a flask flushed with nitrogen. After several hours the mixture was added to 100 ml of ice-cold, 1 M H₂SO₄, collected, washed with 200 ml of cold water, and subsequently recrystallized three times from ethanol. Final yields were about 45% with about 90% recovery per recrystallization.

Preparation of p-(*p'*-Ethoxyphenylazo)phenol. East-

man *p*-phenetidine (50.0 g, 0.365 mol, used without further purification) was added to 150 ml of 6 *F* hydrochloric acid, the resulting mixture cooled to 0° by the addition of ice, and a sodium nitrite solution (27.5 g in 750 ml of water, 0.398 mol) was added in small portions. After each addition the solution was checked with potassium iodide-starch paper to indicate the end point. The resulting diazonium chloride was added slowly to an ice bath-cooled phenolate solution prepared by the addition of 34.5 (0.365 mol) of phenol to 38.5 g (0.365 mol) of sodium carbonate in 350 ml of water. The golden-yellow product was acidified to pH 7 and extracted into chloroform. After drying with magnesium sulfate and removal of ether, the product was recrystallized from benzene. Recrystallized yield was 41.2 g (0.17 mol or 46.6%).

*Anal.*⁶ Pentanoate (calcd for C_xH_yN₂O₃: C, 69.90; H, 6.81. Found C, 70.07; H, 7.71). Hexanoate (calcd: C, 70.53; H, 7.12. Found C, 71.02; H, 7.45). Heptanoate (calcd: C, 71.15; H, 7.41. Found C, 71.66; H, 7.85). Octanoate (calcd: C, 71.70; H, 7.67. Found C, 72.21; H, 7.55). Nonanoate (calcd: C, 72.21; H, 7.92. Found C, 72.03; H, 7.93). Decanoate (calcd: C, 72.68; H, 8.15. Found C, 72.03; H, 8.12). Undecanoate (calcd: C, 73.12; H, 8.36. Found C, 72.15; H, 8.40). Dodecanoate (calcd: C, 73.54; H, 8.56. Found C, 73.16; H, 8.88). Tridecanoate (calcd: C, 73.92; H, 8.75. Found C, 73.48; H, 8.78). Tetradecanoate (calcd: C, 74.28; H, 8.92. Found C, 74.33; H, 9.10).

Microscopy. The mesophases were identified and transition temperatures measured by the use of a Bausch and Lomb Dynoptic polarizing microscope equipped with a Nikon photographic attachment and a modified Koeffler hot stage.⁷ The temperature calibration was accomplished by use of Aldrich zone-refined (99.9%+) melting point standards. The thermometric accuracy was estimated to be at least ±0.1°.

Calorimetric Measurements. The phase transition enthalpies and temperatures were determined using a Perkin-Elmer DSC-1B differential scanning calorimeter. The temperature was calibrated using the same standards as above. The instrument constant was determined using Alfa Inorganics m5n indium powder assuming a heat of fusion of 6.80 cal/g.⁸ The heats of transition were obtained by photocopying, cutting, and weighing, or planimetry of the peak areas. The following technique was used to determine the peak shape for area measurement. The initial and final

TABLE I: Transition Temperatures, Enthalpies, and Derived Entropies for 4-Ethoxy-4'-*n*-alkanoyloxyazobenzenes

Ester	Transition ^a	Temp ref ^b	M ^c	Temp, K		$\Delta\bar{H}$, kJ mol ⁻¹	$\Delta\bar{S}$, J mol ⁻¹ K ⁻¹
				V ^c	Present		
Pentanoate	K _{III} → N	T4	351	352	352.02 ± 0.09	33.2 ± 1.1	94 ± 3
	N → I	T7	399	398	400.2 ± 0.1	0.88 ± 0.03	2.19 ± 0.07
Hexanoate	K _{III} → N ^e	T4	341	343	339.11 ± 0.05	37.3 ± 0.8	108 ± 3
	K _I → N ^f	T6			345.08 ± 0.25	29.8 ± 0.7	88 ± 2
	N → I	T7	400	399	401.6 ± 0.1	1.13 ± 0.06	2.82 ± 0.15
Heptanoate	K _{III} → N	T4	337	341	333.74 ± 0.17	<i>d</i>	<i>d</i>
	K _I → N	T6			338.74 ± 0.11	23.1 ± 1.8	68 ± 5
	N → I	T7	390	391	392.3 ± 0.1	0.91 ± 0.02	2.33 ± 0.06
Octanoate	K _{III} → N	T4	360	360	358.95 ± 0.21	48.1 ± 1.4	134 ± 4
	N → I	T7	391	391	392.8 ± 0.1	1.11 ± 0.03	2.82 ± 0.08
Nonanoate	K _{III} → K _{II} ^g	T1			333.92 ± 0.38	13.7 ± 0.3	38 ± 1
	K _{II} → K _I	T3			342.7 ± 1.0	<i>d</i>	<i>d</i>
	K _{II} → N	T5			343.26 ± 0.10	28.8 ± 1.8	84 ± 5
	K _I → N ^h	T6		345	345.46 ± 0.20	27.7 ± 1.6	80 ± 5
	N → I	T7		385	387.7 ± 0.1	0.93 ± 0.03	2.39 ± 0.06
Decanoate	K _{III} → K _{II} ⁱ	T1			~337	<i>d</i>	<i>d</i>
	K _{II} → K _I	T3			~343	<i>d</i>	<i>d</i>
	K _{III} → N	T4			344.56 ± 0.10	45.8 ± 1.3	133 ± 4
	K _{II} → N ^j	T5			346.92 ± 0.06	32.1 ± 0.7	93 ± 2
	K _I → N ⁱ	T6		348	348.6 ± 0.2	<i>d</i>	<i>d</i>
	N → I	T7		386	386.1 ± 0.1	1.10 ± 0.03	2.85 ± 0.09
Undecanoate	K _{II} → K _I ⁱ	T3			~348	<i>d</i>	<i>d</i>
	K _{II} → N	T5			350.44 ± 0.10	31.9 ± 0.9 ^k	91 ± 3
	K _I → N ⁱ	T6	351	352.2 ± 0.2			
	N → I	T7		382	383.1 ± 0.1	0.98 ± 0.05	2.56 ± 0.12
Dodecanoate	K _{II} → N	T5			352.35 ± 0.12	38.9 ± 0.6 ^k	110 ± 2
	K _I → N ⁱ	T6		354	353.8 ± 0.3		
	N → I	T7		381	382.5 ± 0.1		
Tridecanoate	K _{II} → N	T5		351	355.80 ± 0.07	41.7 ± 0.8 ^k	117 ± 2
	K _I → N ⁱ	T6			356.5 ± 0.3		
	N → I	T7		378	379.7 ± 0.1		
Tetradecanoate	K _{II} → N	T5			357.80 ± 0.09	43.2 ± 0.9 ^k	121 ± 2
	K _I → N ⁱ	T6		356	358.3 ± 0.3		
	N → I	T7		376	379.4 ± 0.1		

^a Notation of Verbit ref 10: K = crystal, N = nematic, I = isotropic. ^b Temp ref code refers to the transitions depicted in Figure 1. T6 means temperature of point 6, the K_I → N transition Figure 1. ^c M is data of McCaffrey and Castellano, ref 5; V is data of Vorländer, ref 2b. ^d Value not reported for lack of suitable resolution or reproducibility of DSC curves. ^e DSC: previously melted and cooled to 320 K for 15 min. ^f DSC: previously allowed to stand at room temperature for more than 9 hr. ^g DSC: previously allowed to stand at 312 K for 2 hr. ^h DSC: previously allowed to stand at 336 K for 15 min. ⁱ Temperatures determined by microscope; by DSC event could not be observed or not resolved. ^j DSC: the ester was previously allowed to stand at 343 K for 30 min. Under these conditions no formation of K_I was detectable. ^k Values reported are for two transitions.

baselines were respectively extrapolated to the initial transition temperature and to the final transition temperature. The effect of the heat capacity variation occurring between these temperatures was estimated by then drawing a line joining the intersections just defined above. The precision estimates were calculated on the basis of repetitive runs and samples.

Several esters, as will be discussed, possess crystal modifications which are thermodynamically unstable relative to other crystal forms near their melting points. The rate of crystal-crystal transformation, though usually slow in the solid phase, is rapid in the presence of the liquid nematic, often resulting in an endotherm-exotherm-endotherm DSC thermogram. The enthalpy of fusion of the less stable crystal is calculated by summing the areas of the endotherm peaks and subtracting the area corresponding to the exotherm. The more stable crystal can be exclusively obtained by heating the ester at such a temperature as to melt

the less stable but not the more stable crystal modification. Its enthalpy of fusion can then be easily determined from a single endothermic DSC peak.

3. Results

The combined results of the microscopic and calorimetric studies are presented and correlated with previous data in Table I. Each homolog exhibits only an enantiotropic nematic mesophase. However, considerable polymorphism is exhibited in the solid state by most of the homologs, and before further discussion of general trends, the peculiarities of each homolog will be delineated.

4-Ethoxy-4'-n-pentanoyloxyazobenzene (Pentanoate). Our transition temperatures agree to within implied experimental uncertainty of literature values. The pentanoate is one of two homologs that do not show solid state polymorphism. Figure 1 presents an idealized free energy diagram capable of describing the many phases observed for these

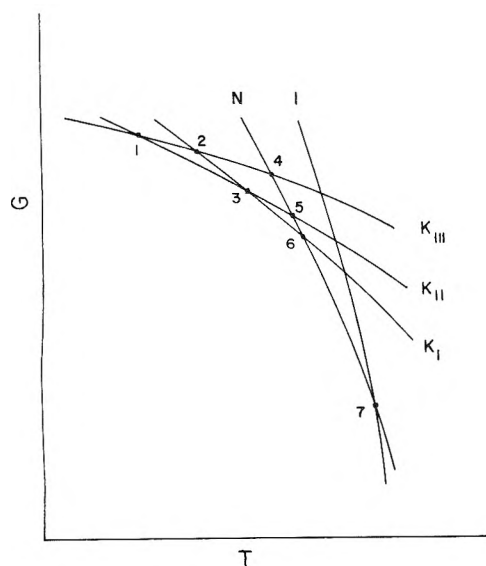


Figure 1. Idealized free energy-temperature diagram. Slopes and temperature differences are exaggerated for clarity. The notation of Verbit (ref 10) is used.

compounds.⁹ Neff et al. used a diagram similar to Figure 1 to explain the anomalous melting of the heptanoate ester. Here for pentanoate the observed phase transitions would be described by lines K_{III} , N , and I and their temperature intersection points T_4 and T_7 .¹⁰ Calling the crystal K_{III} is not arbitrary since there is a trend in the types of crystal-line phases observed in the series as will be discussed later.

4-Ethoxy-4'-n-hexanoyloxyazobenzene (Hexanoate). The nematic-isotropic transition temperature reasonably well agrees with literature values, our value being slightly higher. Hexanoate shows two crystal forms and in Figure 1 the appropriate free energy lines are K_{III} , K_I , N , and I . With reference to Table I, no well-defined temperature for the $K_{III} \rightarrow K_I$ transition can be reported since the K_I crystal form is thermodynamically stable relative to K_{III} from its melting point to below room temperature, at which point the rate of conversion is even too slow to be studied microscopically. The literature values for the crystal-nematic temperature appear to be for $K_I \rightarrow N$. Striking evidence for the existence of two crystals is provided by DSC. When the K_{III} crystal is initially present the DSC curves usually appear as in Figure 4. At slow heating rates (less than $2.5^\circ/\text{min}$) this endothermic-exothermic behavior is often observed since at such rates the nematic phase obtained from $K_{III} \rightarrow N$ can be superheated past T_4 (Figure 1) with accompanying $N \rightarrow K_I$ and then $K_I \rightarrow N$ at T_6 . Not infrequently, however, $K_{III} \rightarrow N$ is solely observed. Since the exothermic-endothermic phenomenon is never observed for heating rates greater than $2.5^\circ/\text{min}$, McCaffrey and Castellano could not have been expected to see the conversions at their $10^\circ/\text{min}$ heating rate even if K_{III} were present.

4-Ethoxy-4'-n-heptanoyloxyazobenzene (Heptanoate). The nematic-isotropic transition temperatures agree well with the literature. Heptanoate exhibits two crystal forms of the same appearance as hexanoate. For the heptanoate ester K_{III} is evidently the thermodynamically stable form at room temperature. The behavior of this compound was first discussed by Neff et al. The observation of the endothermic-exothermic DSC curve (of the type depicted in Figure 4) is also dependent on heating rate.

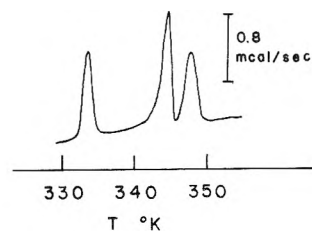


Figure 2. A first heating DSC curve obtained at $2.5^\circ/\text{min}$ for 4-ethoxy-4'-n-nonanoyloxyazobenzene.

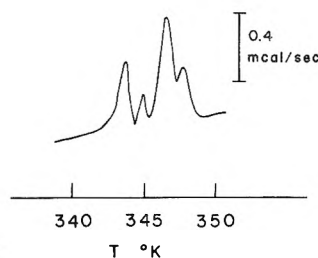


Figure 3. A heating DSC curve obtained at $1.25^\circ/\text{min}$ for 4-ethoxy-4'-n-nonanoyloxyazobenzene.

4-Ethoxy-4'-n-octanoyloxyazobenzene (Octanoate). Octanoate is the other member of this series that exhibits only one crystal form. The transition temperatures agree well with the literature, though again our nematic-isotropic temperature is slightly higher. The free energy diagram is the same as that for pentanoate: K_{III} , N , and I .

4-Ethoxy-4'-n-nonanoyloxyazobenzene (Nonanoate). The nematic-isotropic transition temperature is not in good agreement with Vorländer, his value being almost 3° lower, perhaps indicating purity differences. On the other hand, nonanoate exhibits the most complex solid state polymorphism observed in this series. Three crystal modifications have been observed microscopically and resolved by DSC experiments. The free energy diagram is given by all lines in Figure 1. The usefulness, if not the necessity, of such a diagram to assist the understanding of these systems is demonstrated in sorting out the observed DSC behavior, examples of which are given in Figures 2 and 3. Figure 2 is a first heating curve obtained at $2.5^\circ/\text{min}$. The endothermic events observed are, in order of increasing temperature, $K_{III} \rightarrow K_{II}$, $K_{II} \rightarrow K_I$, and $K_I \rightarrow N$. Agreement of the transition temperatures determined microscopically and by DSC is excellent. Different curves can result since the extent of the interconversion of crystal forms is dependent on sample treatment. Here also the kinetics of interconversion are rapid enough to watch microscopically. The explanation of the DSC curve in Figure 3 obtained at $1.25^\circ/\text{min}$ is, in order of increasing temperature, $K_{II} \rightarrow K_I$, unconverted $K_{III} \rightarrow N$, unconverted $K_{II} \rightarrow N$, and finally $K_I \rightarrow N$. Thus in this experiment the system, which can exist in several metastable states at the same time because of kinetic factors, started initially as a mixture of K_{III} and K_{II} which simply followed possible free energy paths through transitions marked T_3 , T_4 , T_5 , and T_6 in Figure 1. Ready explanation of the variety of DSC curves obtained and microscopic transitions observed would be difficult at best without Figure 1. The reported crystal-nematic transition of Vorländer appears to be that for $K_I \rightarrow N$ which is plausible for only visual observation.

4-Ethoxy-4'-n-decanoyloxyazobenzene (Decanoate).

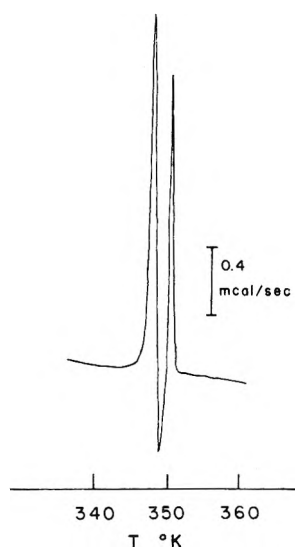


Figure 4. A heating DSC curve obtained at 2.5°/min for 4-ethoxy-4'-*n*-decanoyloxyazobenzene.

The nematic-isotropic transition temperature is in excellent agreement with literature. Decanoate also exhibits three crystalline modifications which can be clearly discerned microscopically. However, the kinetics of transformation between these phases make the dynamic experiment, DSC, more difficult to sort out in contrast to nonanoate results. Figure 4 shows a DSC curve reminiscent of those observed for hexanoate and heptanoate. Here the explanation is analogous to that for the previous cases. However, if the heating rate is slowed down quite different DSC curves are obtained for decanoate compared to the lower homologs as might well be expected. Figure 5 shows the result of one run at 0.625°/min. Now with increasing temperature $K_{II} \rightarrow K_I$ and then $K_I \rightarrow N$. Again the free energy diagram is extremely useful in interpreting experimental results. The reported crystal-nematic temperature of Vorländer here also appears to be for $K_I \rightarrow N$.

4-Ethoxy-4'-n-undecanoyloxyazobenzene (Undecanoate). The nematic isotropic transition temperature agrees to within implied error with literature. Undecanoate exhibits two crystal modifications K_{II} and K_I . For the higher homologs the lower temperature crystal is K_{II} while for the lower homologs K_{III} is the stable low temperature crystal. Experimentally the crystal-crystal transition was undetectable by DSC and the $K_{II} \rightarrow N$ and $K_I \rightarrow N$ transitions are too close to be resolved. The $K_{II} \rightarrow K_I$ transition (both heating and cooling) is observable visually but no distinct temperature could be assigned. The free energy diagram is given by lines K_{II} , K_I , N , and I , and the calorimetric results reported in Table I for the $K_{II} \rightarrow N$ transition undoubtedly contains to some degree the $K_I \rightarrow N$ transition as well.

4-Ethoxy-4'-n-dodecanoyloxyazobenzene (Dodecanoate). The nematic-isotropic transition temperature agrees with the literature value. Dodecanoate exhibits the same solid state polymorphism as undecanoate with the same lack of resolution of the $K_{II} \rightarrow N$, $K_I \rightarrow N$ transitions and the unobserved (DSC) $K_{II} \rightarrow K_I$ transition. The shoulders often observed on the DSC $K_{II} \rightarrow N$ peak strongly suggest the unresolved nature of this transition. The inability to resolve these transitions compared to the hexanoate and the heptanoate cases is explained by the only 0.5° dif-

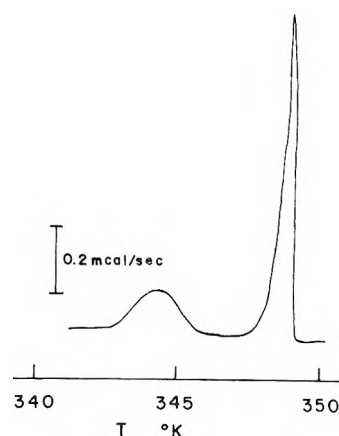


Figure 5. A heating DSC curve obtained at 0.625°/min for 4-ethoxy-4'-*n*-decanoyloxyazobenzene.

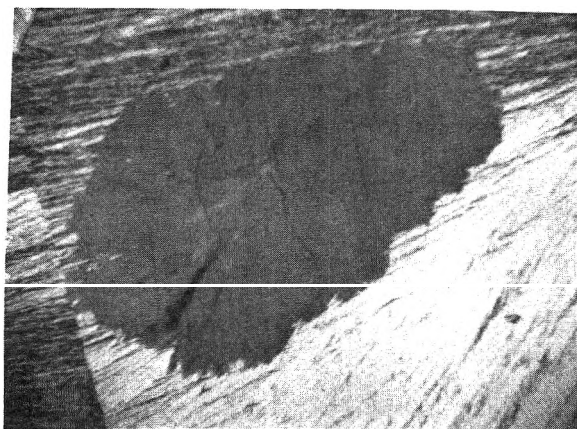


Figure 6. A photomicrograph, 50 \times at film plane, of the K_{II} (sheet) and K_I (spherulite) crystalline modifications of 4-ethoxy-4'-*n*-dodecanoyloxyazobenzene.

ference in the transitions for dodecanoate vs. the 5–6° difference for the previous compounds. Figure 6 is a photomicrograph of the two crystal forms coexisting at 22°. The smooth, sheet-like crystal we have been calling K_{II} , while the spherulite crystal surrounding it has been called K_I .

4-Ethoxy-4'-n-tridecanoyloxyazobenzene (Tridecanoate). The results and discussion are analogous to that of undecanoate and dodecanoate.

4-Ethoxy-4'-n-tetradecanoyloxyazobenzene (Tetradecanoate). The results are the same as those discussed for undecanoate and dodecanoate.

4. Discussion

Crystal-Nematic Transitions. The curious feature of this homologous series of azobenzenes is the extensive solid state polymorphism. There are trends in the types of crystals observed which are detailed in Table II. Since the morphology of the crystals is not known, the various modifications are simply described by names appropriate to their microscopic appearance. These crystal modifications have been previously called K_{III} , K_{II} , and K_I for star, sheet, and spherulite, respectively. The regular change is obvious but unexplained. The octanoate homolog stands out, however, exhibiting only one crystal form, though the nearest homologs, heptanoate and nonanoate, exhibit complex polymorphism. In Figures 7 and 8 are plotted the transition tem-

TABLE II: Trends in the Observed Solid State Polymorphism of 4-Ethoxy-4'-*n*-alkanoyloxyazobenzenes

	Star (K _{III})	Sheet (K _{II})	Sphelite (K _I)
Pentanoate	X		
Hexanoate	X		X
Heptanoate	X		X
Octanoate	X		
Nonanoate	X	X	X
Decanoate	X	X	X
Undecanoate		X	X
Dodecanoate		X	X
Tridecanoate		X	X
Tetradecanoate		X	X

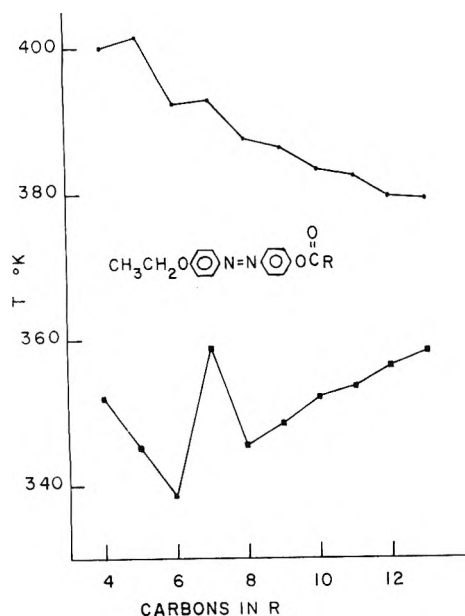


Figure 7. Transition temperatures K_I to N and N to I as a function of carbon number in alkyl chain of 4-ethoxy-4'-*n*-alkanoyloxyazobenzenes.

peratures and calorimetric data and here again the octanoate appears to be out of place. The $K_I \rightarrow N$ transition temperature especially appears anomalously high. Other homologous series based on the normal alkanes also show this anomaly. For example, the amides of the *n*-alkyl carboxylic acids show the greatest variation in melting point around the eight carbon chain.¹¹ Apparently for the eight carbon homolog in many derivatives of these aliphatic acids the crystal packing must give rise to larger intermolecular crystalline forces

Few theoretical studies have been made of the crystal-nematic transition. Chandrasekhar et al. have done a statistical calculation which does predict at least two possible solid state transitions for various values of a parameter measuring the relative barriers to rotation and diffusion in the crystal.¹² Either, a solid-solid rotational transition precedes the melting (to nematic) transition, or some type of positional transition occurs prior to melting. For most of the homologs here two transitions are observed, but it is not known whether the nature of the transition is rotational or positional. Moreover the theory, at least within the model of one parameter, cannot account for the three observed transitions for the nonanoate and decanoate homo-

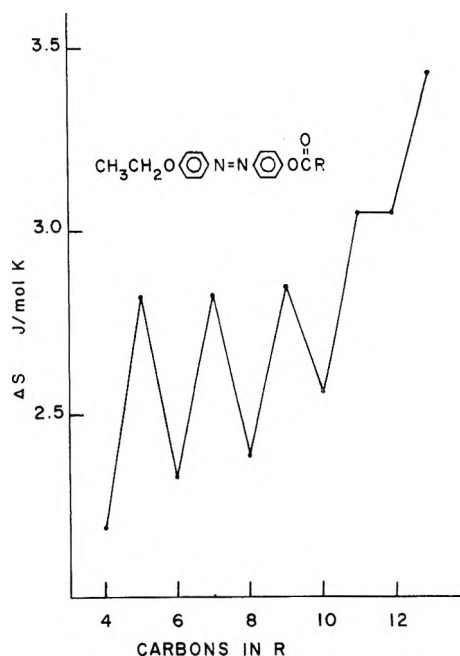


Figure 8. Entropy of N to I transition as a function of carbon number in alkyl chain of 4-ethoxy-4'-*n*-alkanoyloxyazobenzenes.

logs. For the one case where the ΔS for a solid-solid transition could be measured, $K_{III} \rightarrow K_{II}$ for nonanoate, a value of 38 J/mol K was obtained which is very much larger than the values noted by Chandrasekhar et al. Also the $\Delta S/R$ values for the crystal-nematic transition are in the range of 10–12 in rough agreement with other materials but in poor agreement with theory. Hijikuro et al. give a theoretical treatment of the crystal-nematic transition that can predict a solid phase which is orientationally disordered, corresponding to a rotational transition, as well as a melting to the nematic positionally disordered state.¹³ X-Ray studies might better define the nature of the transitions as Wendorff and Price have done for several esters of cholesterol.¹⁴

Nematic-Isotropic Transitions. Only enantiotropic nematic mesophases are observed for this series notwithstanding Vorländer's report of monotropic phases. The lack of smectic phases is surprising since, for essentially all homologous series of liquid crystalline materials reported in the literature, once the alkyl chain length becomes longer than eight carbons, smectic mesophases occur. For this series of azobenzenes McCaffrey and Castellano explain this lack of smectics by the absence of a transverse dipole. However, this suggestion seems doubtful as many new compounds, for example, several cyanobiphenyl derivatives, have no transverse dipole yet often exhibit extensive smectic mesomorphism.¹⁵ The lack of smectic phases for the higher homologs of this series still seems unexplained.

A regular alternation of increasing nematic-isotropic transition temperature, T_{NI} , on going from even to odd is observed in Figure 7 up to C8. Past C8 T_{NI} always decreases but still in an alternate manner. Vorländer's data show a regular increase in T_{NI} going from even to odd until past C13 at which point T_{NI} decreases for even to odd. Several possible explanations for the uniform alternation exist in the literature but none attempt to account for the reversal. Kaplan describes T_{NI} as a function of the intermolecular potential which in turn is a function of molar volume $T_{NI} \propto AV^{-n}$, where V is the molar volume and A is a parameter from Maier-Saupe theory.^{16,17} Since T_{NI} is ob-

served to alternate, either A or the molar volume must alternate. It is unlikely that the molar volume is anything but a smooth function of chain length, and moreover, de Jeu et al. point out that A does alternate with chain length and reflects a change in the anisotropy of the polarizability.¹⁸ Stenschke relates T_{NI} to a characteristic energy, Δ , reflecting the energy difference between alkyl chain *trans* and *gauche* conformations.¹⁹ The alternation of T_{NI} then becomes an alternation of Δ on going from odd to even vs. even to odd when adding carbons to the chain. Marcelja has quantified this approach by calculating all the conformational energies accessible to a zig-zag alkane chain and noting that the alternation is indeed due to the change in anisotropic properties of the molecule engendered on the odd to even vs. the even to odd change.²⁰ Marcelja's work provides a rationale for the previous suggestions in that the Maier-Saupe parameter A does depend on anisotropy differences in polarizability, and the *trans*-*gauche* interaction energy does change alternating down the chain. Further, the temperature drop with increasing chain length observed for this series is explained in Marcelja's calculation by the weakening of the strong forces between the central azobenzene groups caused by the increasing alkyl chains.

The odd-even variation of ΔS_{NI} with chain length depicted in Figure 8 is much more marked than the T_{NI} variation. The marked alternation here has its origin in the fact that ΔH_{NI} alternates markedly and in the same manner as T_{NI} (not surprisingly). With Young et al. we note that the increment of ΔS_{NI} with chain length is much less than $R \ln 3$ which suggests that the nematic phase alkyl chain cannot exist in a single conformation.²¹ This argument is confirmed by Marcelja's results. The prediction by van der Veen et al. that the variation of ΔS_{NI} with chain length reflects the variation in the order parameter is also suggested by Marcelja's calculations but no experimental order parameter data exists to check this. The variation in the order parameter might also simply be a reflection of the variation of the Maier-Saupe A . Work is in progress to test the variation of order parameter with chain length.

Acknowledgments. The authors thank Edward Newton for assistance in the design of the microscope hot stage. Financial support from the National Science Foundation through its Undergraduate Research Participation Program, the Harvey Mudd College Research Committee, and the Cal Biochem Research Foundation is gratefully acknowledged.

References and Notes

- (1) (a) Cal Biochem undergraduate research fellow. (b) NSF undergraduate research participant.
- (2) (a) J. van der Veen, W. H. de Jeu, M. W. M. Wanninkhof, and C. A. M. Teinoven, *J. Phys. Chem.*, **77**, 2153 (1973), and references therein; (b) D. Vorländer, *Z. Phys. Chem. (Liepzig)*, **126**, 449 (1927).
- (3) V. D. Neff, M. K. Chang, and D. L. Fisher, *Mol. Cryst. Liq. Cryst.*, **17**, 369 (1972).
- (4) We will call the individual homologs by their systematic parent acids name. Hence the seven carbon containing C-R homolog will be called heptanoate.
- (5) M. T. McCaffrey and J. A. Castellano, *Mol. Cryst. Liq. Cryst.*, **18**, 209 (1972).
- (6) Chemalytics, Inc., Tempe, Ariz. 85281.
- (7) The Koeffler hot stage was modified with a constant temperature controller capable of holding the temperature to better than $\pm 0.05^\circ$ and built for less than \$40. Details on request.
- (8) G. J. Davis, R. S. Porter, and E. M. Barrall, II, *Mol. Cryst. Liq. Cryst.*, **10**, 1 (1970).
- (9) W. C. McCrone in "Physics and Chemistry of the Organic Solid State", D. Fox, M. M. Labes, and A. Weissberger, Ed., Interscience, New York, N.Y., 1965, Chapter 8.
- (10) L. Verbit, *Mol. Cryst. Liq. Cryst.*, **15**, 89 (1971).
- (11) Data selected from "Handbook of Tables for Organic Compound Identification", 3rd ed, Chemical Rubber Publishing Co., Cleveland, Ohio, 1967.
- (12) S. Chandrasekhar, R. Shashidhar, and N. Tara, *Mol. Cryst. Liq. Cryst.*, **10**, 337 (1970); **12**, 245 (1971).
- (13) N. Hijikuro, K. Miyakawa, and H. Mori, *Phys. Lett.*, **45A**, 257 (1973), and references therein.
- (14) J. H. Wendorff and F. P. Price, *Mol. Cryst. Liq. Cryst.*, **25**, 71 (1974).
- (15) G. W. Gray, paper given at the Vth International Liquid Crystal Conference, Stockholm, Sweden, 1974.
- (16) J. I. Kaplan, *J. Chem. Phys.*, **57**, 3015 (1972).
- (17) W. Maier and A. Saupe, *Z. Naturforsch. A*, **14**, 882 (1959); **15**, 287 (1960).
- (18) W. H. de Jeu, J. van der Veen, and W. J. A. Goossens, *Solid State Commun.*, **12**, 405 (1973).
- (19) H. Stenschke, *Solid State Commun.*, **10**, 653 (1972).
- (20) S. Marcelja, *J. Chem. Phys.*, **60**, 3599 (1974).
- (21) W. R. Young, I. Haller, and A. Aviram, *IBM J. Res. Develop.*, **15**, 41 (1971).

Isocyanate Formation from Adsorbed Carbon Monoxide and Ammonia or Hydrazine on Vanadium, Iron, and Nickel

R. W. Sheets

Department of Chemistry, Southwest Missouri State University, Springfield, Missouri 65802

and G. Blyholder*

Department of Chemistry, University of Arkansas, Fayetteville, Arkansas 72701 (Received January 27, 1975)

Adsorption of NH_3 on V or Fe at 25° followed by exposure to 30 Torr of CO produces infrared bands for CO, NH_3 , and an isocyanate complex on the surface. Assignments are confirmed by isotope shifts using $^{15}\text{NH}_3$, ND_3 , and C^{18}O . The reverse order of addition of CO and NH_3 does not give the isocyanate complex. Use of N_2H_4 in place of NH_3 produces identical results and no evidence of a surface species containing N-N bonds. On Ni adsorption of CO and NH_3 or N_2H_4 does not give an isocyanate complex. Exposure of Ni with preadsorbed N_2H_4 to CO produces adsorbed NH_3 which is not given by N_2H_4 alone while the reverse order of addition gives a chemisorbed hydrazine complex containing a N-N bond.

Isocyanate has been reported by London and Bell¹ on CuO and by Unland^{2,3} as surface species formed during the reaction of CO with NO over Pt, Pd, Rh, and Ir and proposed as a possible intermediate in NH_3 formation in automobile exhaust catalysts. Little is known about the conditions under which it may be formed and its stability. On CuO it was noted at 135 to 200° while Unland only reported its formation above 200° . Here we wish to report on the formation of an isocyanate surface species from the interaction of CO with NH_3 or N_2H_4 on V and Fe at 25° . We have previously discussed⁴ the structure of adsorbed species formed by NH_3 on V, Fe, and Ni under similar conditions and structures due to adsorbed N_2H_4 will be described here as only one other work on the infrared spectra of N_2H_4 adsorbed on Fe has appeared.⁵

The experimental technique, which has been described in detail elsewhere,⁶ consists of evaporating a metal from an electrically heated tungsten filament in the presence of a small pressure of helium. The metal particles formed in the gas phase deposit in a hydrocarbon oil film on the salt windows of an infrared cell. These dispersed particles are referred to hereafter as films both for convenience and because their behavior is similar to that of vacuum evaporated films. The gas to be studied is then admitted to the cell, and the spectrum of the chemisorbed species obtained. Spectra are recorded before and after admission of the gas to the cell. Five minutes of pumping has been found sufficient to remove all spectra due to gas phase molecules.

The spectra were obtained using a Perkin-Elmer Model 337 spectrophotometer. This is a grating instrument which scans the region from 4000 to 400 cm^{-1} . No unusual spectrometer settings were used. The adsorbates were obtained as reagent grade chemicals from commercial sources. They were degassed by repeated freeze-thaw cycles in the vacuum system.

This technique has the advantage that a wide infrared spectral region is available for study. It has the disadvantage that the metal surface is covered with oil. This oil is apparently only weakly adsorbed since many gases have been found to chemisorb readily on the metal. Essentially, the oil is regarded as a solvent which has weak interactions with the system of interest. Having a wide spectral range available aids greatly in determining structure.

When NH_3 gas is admitted over evaporated V or Fe at 25° and evacuated, infrared bands near 3340, 1590, and 1140 cm^{-1} indicate the presence of undissociated NH_3 groups adsorbed on the surface.⁴ Addition of 30 Torr of CO for 30 min results in small shifts in some of the surface NH_3 bands and in the appearance of a weak band at 2180 cm^{-1} on V and 2170 cm^{-1} on Fe. No band appears in this region with Ni and Pd. On the basis of comparison with metal isocyanate complexes⁷ which have bands near 2200 (strong), 1300 (weak), and 600 cm^{-1} (weak), the 2180-cm^{-1} band may be tentatively assigned to a surface isocyanate structure. In view of the weakness of the 2180-cm^{-1} band and the relative intensities of the NCO complex bands, and the existence of interfering background bands, it was not expected that surface bands corresponding to the 1300- and 600-cm^{-1} absorptions of the complex would be observable. The assignment of the 2180-cm^{-1} band to a surface NCO structure is reasonably well confirmed by comparing the isotope shifts for $^{15}\text{NH}_3$ ($\Delta\nu = 15\text{ cm}^{-1}$) and C^{18}O ($\Delta\nu = 10\text{ cm}^{-1}$) with those of 17 and 8 cm^{-1} observed⁸ for ^{15}N and ^{18}O substitution in cyanate ion in a KBr matrix. Using ND_3 produced no shift in the surface band. Addition of NH_3 to a cell with CO preadsorbed (gas phase CO evacuated) on Fe or V does not produce the band near 2180 cm^{-1} .

Exposure of evaporated V, Fe, or Ni to 10 Torr of N_2H_4 gave spectra indicative of a rapid decomposition of N_2H_4 to NH_3 . Spectra of the V and Fe films taken after removal of the gas phase were identical with those published⁴ for exposure of Fe and V to NH_3 . Subsequent CO chemisorption resulted in the formation of the weak isocyanate band near 2180 cm^{-1} as well as chemisorbed CO. Spectra of Ni films exposed to N_2H_4 showed no bands due to chemisorbed species and subsequent exposure to CO gave bands identical with those reported⁴ previously for NH_3 and CO indicating the presence of undissociated NH_3 on the surface.

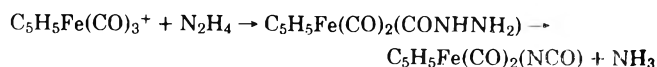
Chemisorption of CO first on V and Fe, followed by N_2H_4 treatment, produced the same results as indicated above for the reverse order of addition. On Ni films containing preadsorbed CO the results of adding N_2H_4 are quite different in that only traces of gas phase NH_3 appear and the spectra indicate a surface species that contains an N-N bond and is similar to a hydrazine complex. The chemisorbed CO bands are shifted to 1940(m) and 1790(s)

cm^{-1} which is in accord with CO being coadsorbed with an electron-donating species.⁹ The infrared bands for the surface species are at 3330(sh), 3260(m), 1590(m), 1160(m), 1100(m), and 920(m) cm^{-1} . The 920- cm^{-1} band is assigned to the N-N stretch and the other bands to NH_2 stretching and bending motions by direct analogy with spectra for N_2H_4 vapor¹⁰ and hydrazine complexes.¹¹ The N-N stretch in liquid N_2H_4 is found at 873 cm^{-1} . An extensive study of hydrazine derivatives and complexes¹¹ reported the N-N stretch at 931 to 936 cm^{-1} for unidentate complexes and at 948 to 980 cm^{-1} for bridging complexes. On this basis the complex on the Ni surface is probably chemisorbed through only one nitrogen atom.

Whereas an isocyanate surface species has previously been found only on CuO and noble metals,¹⁻³ we have found it also on Fe and V. It was reported only to be formed above 135° on CuO and above 200° on the noble metals, but on Fe and V it is formed at 25°. Its formation from the reaction of NO and CO is of interest because of its possible role in NH_3 formation. Since we have found that the isocyanate surface complex can be formed from NH_3 and CO at 25°, there clearly must exist low energy pathways connecting NH_3 and the isocyanate complex.

Since the NCO complex is formed on V and Fe when NH_3 is adsorbed first and then CO added but is not in the reverse order, the mechanism probably involves addition of CO to an adsorbed N atom or complex. While the infrared spectra indicate that undissociated NH_3 groups are the predominant surface species produced by adsorbing NH_3 gas, there may be small amounts of nitrogen surface species containing fewer hydrogen atoms. However, in the case of hydrazine and CO, the NCO surface species is produced

with both orders of addition. Since N_2H_4 readily dissociates to give NH_3 the mechanism of NCO formation when N_2H_4 is added first is likely to be the same as when NH_3 is used. When CO is added first the mechanism may be similar to the reaction proposed by Angelici and Busetto¹² on the basis of infrared spectra:



There is considerable interest in the existence of N-N bonds in surface species because of applications in nitrogen fixation. Adsorption of NH_3 on V, Fe, and Ni produced no evidence of any species containing N-N bonds at 25°. In hydrazine adsorption at 25° cleavage of the N-N bond occurred in all cases except on a Ni surface with preadsorbed CO. The same electronic factors previously found⁴ to stabilize undissociated NH_3 adsorption when coadsorbed with CO would also be important in N_2H_4 adsorption.

References and Notes

- (1) J. W. London and A. T. Bell, *J. Catal.*, **31**, 96 (1973).
- (2) (a) M. L. Unland, *Science*, **179**, 567 (1973); (b) *J. Phys. Chem.*, **77**, 1952 (1973).
- (3) M. L. Unland, *J. Catal.*, **31**, 459 (1973).
- (4) G. Blyholder and R. Sheets, *J. Catal.*, **27**, 301 (1972).
- (5) R. Brill, P. Jiru, and G. Schulz, *Z. Phys. Chem. (Frankfurt am Main)*, **64**, 215 (1969).
- (6) G. Blyholder, *J. Chem. Phys.*, **36**, 2036 (1962).
- (7) D. Nicholls and R. Swindells, *J. Inorg. Nucl. Chem.*, **30**, 2211 (1968).
- (8) A. Maki and J. C. Decius, *J. Chem. Phys.*, **31**, 772 (1959).
- (9) G. Blyholder, *J. Phys. Chem.*, **68**, 2772 (1964).
- (10) P. A. Giguere and I. D. Liu, *J. Chem. Phys.*, **20**, 136 (1952).
- (11) A. Braibanti, F. Dallavalle, M. A. Pellinghelli, and E. Loporati, *Inorg. Chem.*, **7**, 1430 (1968).
- (12) R. J. Angelici and L. Busetto, *J. Am. Chem. Soc.*, **91**, 3197 (1969).

Relation between Amounts of Chemisorbed Water and Carbon Dioxide on Zinc Oxide

Tetsuo Morimoto* and Kunimitsu Morishige

Department of Chemistry, Faculty of Science, Okayama University, Okayama, Japan

(Received February 15, 1974; Revised Manuscript Received March 3, 1975)

The desorbability of chemisorbed CO_2 on ZnO is investigated by measuring adsorption isotherms of CO_2 on the samples which have been fully precovered with CO_2 and then outgassed at different temperatures. The result shows that chemisorbed CO_2 can be removed from the surface almost completely by heating at temperatures higher than 300° in vacuo. Next, the relation between the amounts of chemisorbed water and CO_2 is examined by measuring adsorption isotherms of water at 25° and of CO_2 at -78° on the ZnO surfaces controlled with the amount of surface hydroxyl groups. It is found that the number of chemisorbed molecules of both adsorbates is approximately equal to each other, which suggests that the chemisorption of CO_2 does not take place on the surface hydroxyl groups, but occurs on dehydroxylated surfaces. The substitution adsorption of water for CO_2 is tested on the ZnO surfaces fully covered with chemisorbed CO_2 ; the results indicate that chemisorbed CO_2 can be displaced almost completely by water at a partial pressure of 0.46 cmHg at 25°.

Introduction

It has been known that ZnO surfaces chemisorb water and CO_2 simultaneously in the atmosphere;¹⁻³ recently, such properties of chemisorbed water, i.e., of surface hy-

droxyl groups, on ZnO as desorbability,⁴ heat of formation,² and effect on physisorption of water,^{5,6} have been investigated by means of various approaches, but those of chemisorbed CO_2 seem to remain unsolved. A number of

papers on the adsorption state of CO_2 on metal oxides have been published, some of them indicating that CO_2 molecules are bonded to surface hydroxyl groups to produce surface bicarbonate species.⁷⁻¹¹ On the other hand, Atherton et al. reported that the chemisorption of CO_2 leading to the formation of carbonate ions occurs on a partially dehydroxylated ZnO surface, but the chemisorption is much reduced if the surface is in the fully hydroxylated state.¹² If surface bicarbonate formation is a principal mode also in the chemisorption of CO_2 on ZnO, the amount of chemisorbed CO_2 on ZnO surfaces controlled by the population of surface hydroxyl groups will increase with increasing surface hydroxyl concentration. Experiments carried out along this line give the reverse result: the amount of irreversibly adsorbed CO_2 decreases almost linearly with increase in the amount of surface hydroxyl groups.¹³ This indicates that the formation of bicarbonate species does not play a major part in the chemisorption of CO_2 on ZnO. Infrared studies may not be applied for the identification of the formation of bicarbonate species because the perturbation of surface hydroxyl groups due to the formation of bicarbonates is very weak.^{12,14}

In a previous investigation,¹³ the irreversibly adsorbed CO_2 measured at 25° was assumed tentatively to be equal to the maximum amount of chemisorbed CO_2 . We have, however, no evidence that the removal of chemisorbed CO_2 did not occur on evacuating the CO_2 -covered sample at 25°; it appears that the adsorption and the succeeding desorption procedure at a lower temperature is appropriate for the quantitative measurement of chemisorbed CO_2 on ZnO.

The purpose of the present work is to investigate quantitatively the fundamental properties of the ZnO surfaces in connection with the adsorption of CO_2 , such as the desorbability of CO_2 , the character of the sites chemisorbing CO_2 , and the relation between the amounts of chemisorbed CO_2 and H_2O . The same approach as used for the investigation of the desorbability of surface hydroxyl groups is first applied:⁴ adsorption isotherms of CO_2 on ZnO are measured repeatedly after evacuating the CO_2 -covered surfaces at increasingly elevated temperatures. Next, the amounts of chemisorbed CO_2 and H_2O are determined by adsorption measurements on differently dehydroxylated surfaces of ZnO, and the relation between them is discussed. Additionally, substitutional chemisorption of water for CO_2 is attempted in order to compare the adsorption forces of the two adsorbates on ZnO, which will confirm the result from infrared study that carbonate ions formed on ZnO are readily displaced by exposure of the carbonated surface to an excess of water.¹²

Experimental Section

Materials. The ZnO sample used in this study was the same as that described in the preceding paper, obtained by burning Zn metal in air.¹³ The impurity of the Zn metal was, according to the manufacturer, 0.01% Pb, 0.002% Cu, 0.005% Cd and Fe, 0.00005% As, and traces of S and P. X-Ray analysis showed that ZnO thus prepared was highly crystalline. The specific surface area of the sample, which was measured by the BET method with nitrogen as an adsorbate, was 3.5 m²/g after treating at 600° for 30 hr in vacuo. The CO_2 gas obtained from Dry Ice was purified by repeating the condensation at liquid nitrogen temperature and the sublimation at the Dry Ice-ethanol temperature.

Adsorption of CO_2 and Water. Adsorption measurements were carried out volumetrically by using a conven-

tional apparatus equipped with an oil and with a mercury manometer. Prior to the adsorption of CO_2 or water, an appropriate pretreatment of the sample was accomplished. Since it has been found that ZnO kept in the atmosphere has both chemisorbed CO_2 and water, the sample was first evacuated at 600° for 30 hr under a vacuum of 10^{-5} Torr in order to remove most of them. Then the sample was subjected to the investigation of desorbability of adsorbed CO_2 , to which the same approach as used for the observation of the desorbability of surface hydroxyl groups on metal oxides was applied: on the 600° treated sample the adsorption isotherm of CO_2 was measured at -78°, and the second adsorption isotherm of CO_2 was measured at -78° after outgassing at -78°. The pretreatment at increasingly elevated temperatures and the adsorption of CO_2 at -78° were practiced repeatedly, giving a series of isotherms. Similar procedures were carried out at higher adsorption temperatures.

In order to examine the relation between the amounts of chemisorbed CO_2 and water, samples having different amounts of surface hydroxyl groups were prepared. The population of surface hydroxyl groups was controlled in the following way: a sample of about 10 m² was treated at 600° for 30 hr in vacuo (ZnO-600), exposed to saturated water vapor at room temperature overnight, and outgassed for 4 hr at different temperatures of 30, 300, and 400° (ZnO-30, ZnO-300, and ZnO-400), which left different amounts of hydroxyl groups on the ZnO surfaces. The amount of surface hydroxyl groups remaining on ZnO was determined by the successive ignition-loss method,^{15,16} which gave the data V_h listed in Table I. These samples were subjected to the measurement of the adsorption isotherm of CO_2 at -78°, the succeeding evacuation at -78°, and then the measurement of the second adsorption isotherm at the same temperature; the adsorption equilibrium was attained within 20 min after every dose of CO_2 . On the other hand, the same samples were also used for the determination of the chemisorbed amount of water at 25°.^{17,18} The time required for the attainment of adsorption equilibrium after every dose of water was about 2 hr in the measurement of the first adsorption isotherm, and about 1 hr in that of the second.

Substitutional Chemisorption of Water for CO_2 . For this purpose, the sample pretreated at 450° for 30 hr in vacuo was exposed to CO_2 of 5.0 cmHg for 2 hr at 25°, followed by degassing at 25° for 2 hr. This procedure resulted in the surface having 3.3 CO_2 /100 Å², according to the determination by the successive ignition-loss method.¹ The sample thus controlled with the content of chemisorbed CO_2 was employed for the experiment of the substitutional adsorption of water: the sample was exposed to the water vapor of 0.46 cmHg at 25° for a given time, followed by the evacuation at the same temperature to remove physisorbed molecules, and then the amounts of chemisorbed water and CO_2 on the surfaces were analyzed volumetrically by the ignition-loss method.

Results and Discussion

Desorbability of Chemisorbed CO_2 on ZnO. Adsorption isotherms of CO_2 obtained at -78° on the 600° treated sample of ZnO are shown in Figure 1a. The uppermost curve is the first adsorption isotherm obtained immediately after 600° treatment, the lowest curve refers to the second adsorption which was measured on the same sample evacuated at -78° for 4 hr after the accomplishment of the first

TABLE I: Amount of Adsorbed Water and CO₂ on ZnO (Molecules/100 Å²)

Sample	Water adsorption					CO ₂ adsorption				
	V _h	V _m	V _p	V _c ^a	2(V _h + V _c) ^b	V _m	V _p	V _c ^a	V _c ^{H₂O} / V _c ^{CO₂}	V _p ^{CO₂} / (V _c ^{CO₂} + V _h)
ZnO-30	4.57	2.50	2.50	0	9.14	3.98	3.90	0.08		0.84
ZnO-300	3.50	3.17	2.50	0.67	8.34	4.82	4.01	0.80	0.84	0.93
ZnO-400	1.29	5.43	2.50	2.93	8.44	6.56	3.82	2.74	1.07	0.95
ZnO-600	0.16	6.16	2.50	3.66	7.64	7.13	3.44	3.69	0.98	0.89

^a V_c is equal to the difference between V_m and V_p. ^b 2(V_h + V_c) is equal to the total quantity of surface hydroxyl groups on ZnO.

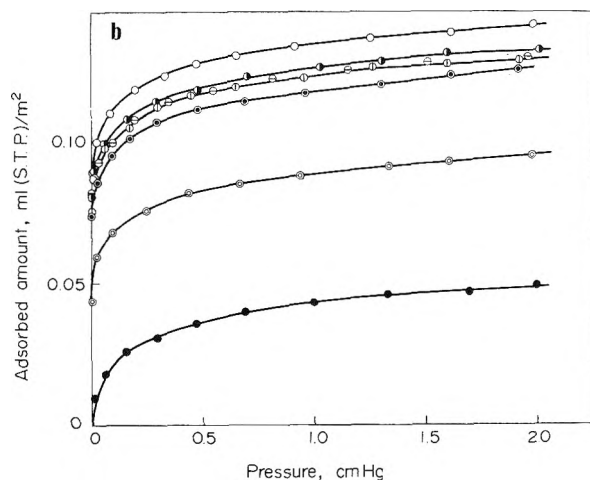
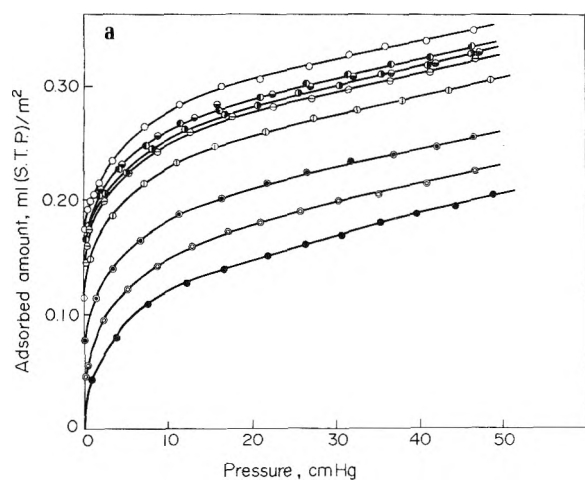


Figure 1. (a) Adsorption isotherms of CO₂ at -78° on ZnO pretreated at various degassing temperatures of (○) 600°, (●) -78°, (⊙) 25°, (⊖) 100°, (⊕) 200°, (⊗) 300°, (⊘) 400°, (⊚) 500°, (⊛) 600°. (b) Adsorption isotherms of CO₂ at 100° on ZnO pretreated at various degassing temperatures of (○) 600°, (●) 100°, (⊙) 200°, (⊖) 300°, (⊕) 400°, (⊗) 500°, (⊘) 600°.

adsorption, it can be seen from Figure 1a that, when the pretreatment temperature is elevated, the amount of adsorbed CO₂ increases progressively and approaches that of the first adsorption after treatment at 300°. The adsorption experiments carried out after pretreating in irregular order of temperature also gave reproducible isotherms. As another example, the adsorption isotherms of CO₂ obtained at 100° are illustrated in Figure 1b. It is found from Figure 1b that the amount of adsorbed CO₂ at 100° increases with increasing pretreatment temperature and approaches the first adsorption when treated at 300°, as in the case of adsorption at -78°, and that the type of the isotherm at 100°

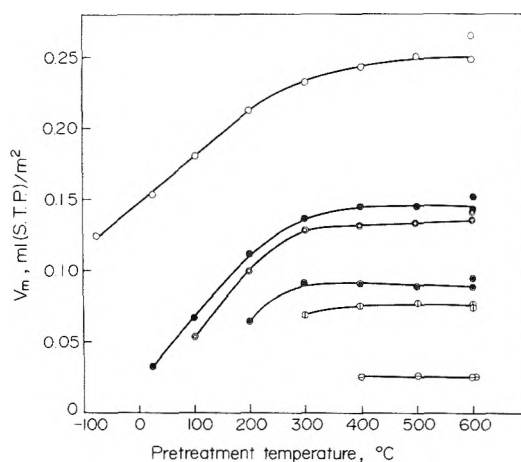


Figure 2. Relation between monolayer capacity of CO₂ and pretreatment temperature of ZnO.

is different from that obtained at -78°: the adsorption isotherms at 100° reach a saturated value even at rather lower pressures, representing the Langmuir type, contrary to the fact that the isotherms at -78° are of the multilayer type. When the adsorption was performed at temperatures higher than 25°, all the isotherms obtained were found to be of the Langmuir type; this enables us to estimate the saturation value of adsorbed CO₂ in each isotherm by applying the Langmuir equation.

The capacity of monolayer adsorption computed from the data in Figure 1 is plotted against the pretreatment temperature, along with the adsorption data at various temperatures, as shown in Figure 2. Here, the values for the adsorption at -78° are those calculated by applying the BET equation to the data in Figure 1a. It can be seen clearly from Figure 2 that the amount of post-adsorbed CO₂ increases with the rise in the pretreatment temperature of the sample and reaches, when pretreated at temperatures higher than 300°, a limiting value characteristic of each adsorption temperature; this indicates that the degassing of the sample at 300° results in an almost complete desorption of chemisorbed CO₂. This result thus leads to a conclusion that the desorbability of chemisorbed CO₂ on ZnO is higher than that of chemisorbed water, i.e., surface hydroxyl groups, on ZnO, since surface hydroxyl groups can be mostly removed at 300–400° in vacuo, the rest being desorbed gradually by heating to temperatures higher than 400° in vacuo.⁴ It may be reasonable to consider that adsorbed CO₂ remaining on the surface after degassing at 300° is chemisorbed, taking also into account the fact that the isotherms of CO₂ at temperatures higher than 25° are of the Langmuir type. The limiting value of chemisorbed CO₂ is replotted against adsorption temperature as shown

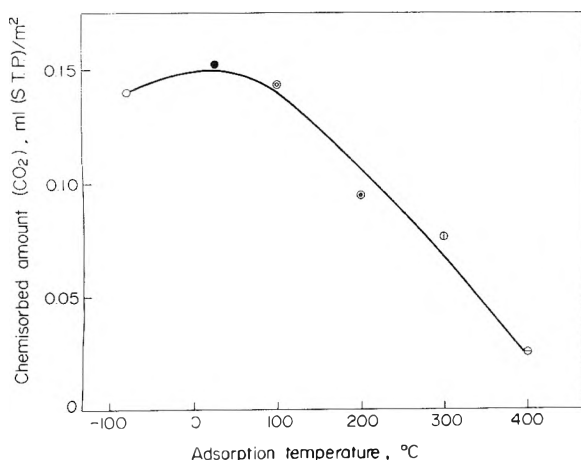


Figure 3. Relation between the saturation amount of chemisorbed CO_2 on ZnO and adsorption temperature.

in Figure 3. Since, in the case of adsorption at -78° , both physisorbed and chemisorbed CO_2 may reasonably be included in the monolayer capacity computed by the BET method, the chemisorbed amount can be obtained by subtracting the physisorbed monolayer capacity, which is deduced from the second adsorption isotherm at -78° , from the monolayer capacity calculated from the first adsorption isotherm.

Figure 3 demonstrates the change in the saturation amount of chemisorbed CO_2 on ZnO as a function of adsorption temperature. Thus, we can see from Figure 3 that the chemisorption of CO_2 increases with decreasing adsorption temperature and attains a maximum value around 25° .

Relation between Amounts of Chemisorbed Water and CO_2 on ZnO. Adsorption isotherms of water at 25° are obtained on the surfaces of ZnO with different amounts of surface hydroxyl groups, as plotted in Figure 4. The uppermost curve is the first adsorption isotherm measured on the 600° treated sample, the lower curve referring to the second adsorption obtained on the same sample which was degassed at 25° for 4 hr after the first adsorption measurement. All the adsorption isotherms of water observed in Figure 4 exhibit a similar shape to those obtained previously on the same system in this laboratory: the isotherms have a step in the relative pressure range of 0.2–0.3.^{1,4,6,19} The second adsorption isotherms, measured on different samples, all coincide with one another, despite that the first ones show different amounts of adsorption depending on the content of surface hydroxyl groups. These results are evidently due to the additional chemisorption of water in the first adsorption on the dehydroxylated sites on ZnO, and consequently the difference between the adsorbed amounts in the first and second adsorptions will give the amount of chemisorbed water as in the cases of various metal oxides.^{1,17,20–22}

The adsorption isotherms of CO_2 at -78° on the same samples are given in Figure 5. It is interesting to note that, as in the case of water adsorption, the amount of adsorbed CO_2 in the first adsorption is always greater than that in the second one, the former being reduced with increasing amounts of surface hydroxyl groups.

In Table I, the amounts of physisorbed and chemisorbed molecules of the two adsorbates on differently hydroxylated ZnO samples are summarized. V_h is the surface water content expressed in the number of water molecules per 100 \AA^2 , twice the number of this value being the amount of

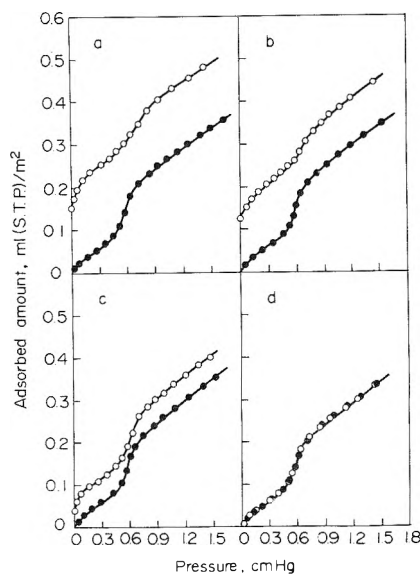


Figure 4. Adsorption isotherms of H_2O at 25° on ZnO pretreated at (a) 600° , (b) 400° , (c) 300° , (d) 30° ; (O) first adsorption, (●) second adsorption.

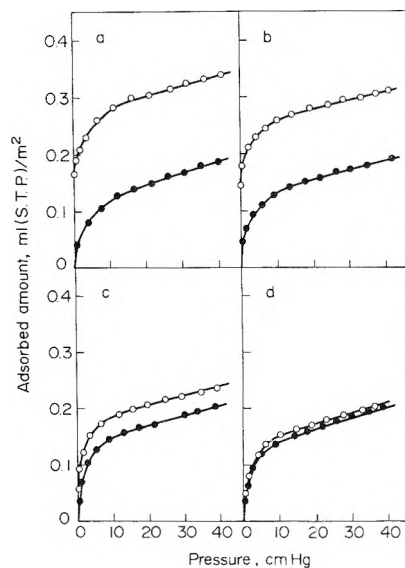


Figure 5. Adsorption isotherms of CO_2 at -78° on ZnO pretreated at (a) 600° , (b) 400° , (c) 300° , (d) 30° ; (O) first adsorption, (●) second adsorption.

surface hydroxyl groups present on the samples pretreated at the temperatures indicated. V_m is the monolayer capacity of each adsorbate as obtained by applying the BET method to the first adsorption isotherms in Figures 4 and 5, including both physisorbed and chemisorbed portions. On the other hand, V_p is the monolayer capacity calculated by applying the BET method to the second isotherms in Figures 4 and 5, which involves only the physisorbed molecules. Thus, the difference V_c between V_m and V_p implies the chemisorption amount.

A linear relationship is observed between the amounts of chemisorbed water and CO_2 as is shown in Figure 6. Moreover, it is interesting to note that the ratio of the two is 1:1; this suggests that the irreversible chemisorption of CO_2 takes place on the dehydroxylated surfaces, but not on the surface hydroxyl groups.

The cleavage of the ZnO crystal, which belongs to the

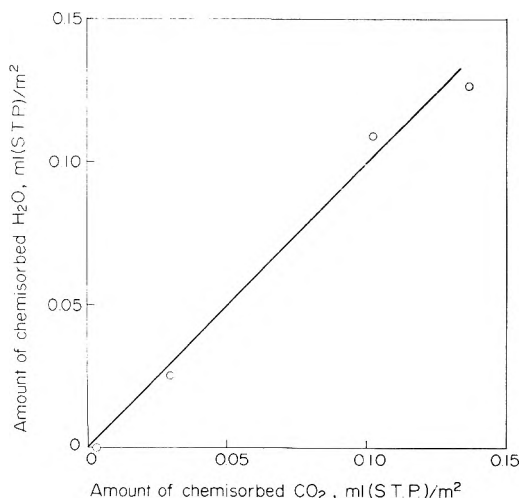


Figure 6. Relation between amounts of chemisorbed H₂O and CO₂.

wurtzite type, is known to be perfect on the planes of (0001) and (10 $\bar{1}$ 0), on which the population of Zn atoms can be calculated crystallographically to be 11 and 6/100 Å², respectively.²³ If we assume that the actual surface of ZnO exhibits the two kinds of planes in equal quantity, and that one hydroxyl group is bonded to each Zn atom, the average population of surface hydroxyl groups will amount to 8.5/100 Å².¹

The experimental results indicate that the sample treated at 600°, having a small amount of residual hydroxyl groups of 0.32/100 Å², chemisorbs water molecules to produce 7.32 OH/100 Å², which is almost equal to the population calculated above. The similarly treated surfaces chemisorb 3.69 CO₂/100 Å², i.e., numerically, one molecule of CO₂ is bonded to two Zn atoms. In this case, the CO₂ molecules may react with surface O atoms, e.g., to form carbonate species, though the chemisorption state of CO₂ is still a problem to be clarified.

Table I further indicates that the first physisorption layer of CO₂ completes on the chemisorbed CO₂ with the ratio of about 1:1 (sample treated at 600°). Moreover, this ratio is true in all cases where the substrate layer is composed of chemisorbed water and/or CO₂. These facts lead to a conclusion that the first layer physisorption of CO₂ on the various surface species of ZnO at -78° is not localized and consequently of nonpolar character, giving a relatively large molecular area of about 26 Å².

Substitutional Chemisorption of Water for CO₂. The result of substitution experiment of water for CO₂ at 25° is shown in Figure 7, where the ordinate is expressed in the number of molecules of chemisorbed water and/or CO₂ per 100 Å². In accord with the result from infrared study,¹² Figure 7 demonstrates the ready displacement of chemisorbed CO₂ by an excess of water: the amount of chemisorbed water increases exponentially with time, accompanied by a simultaneous decrease in the amount of chemisorbed CO₂. Here, it is interesting to note that during the substitution process the sum of the chemisorbed portions of the two ad-

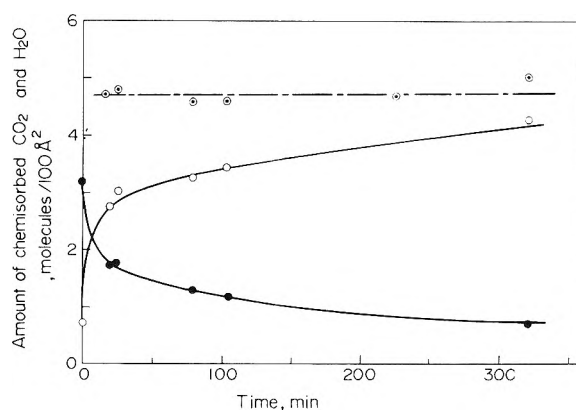


Figure 7. Substitution adsorption of H₂O for CO₂ at 25° on ZnO: (O) H₂O, (●) CO₂, (⊙) sum of H₂O and CO₂.

sorbates remains unchanged as shown by the broken line in Figure 7, which proves the exact exchange of one molecule of water for one molecule of CO₂. Since it is clear that chemisorbed water is in the state of surface hydroxyl groups on ZnO, this fact verifies the above-mentioned supposition: the chemisorption sites for CO₂ are the same as the dehydroxylated sites on ZnO. In addition, it can be reasonably concluded that the chemisorption force of the ZnO surface for water is greater than that for CO₂, though the energetics of this substitution reaction remains unsolved.

Acknowledgment. The authors wish to express their gratitude to Dr. Mahiko Nagao for his helpful advice during this study.

References and Notes

- (1) T. Morimoto and M. Nagao, *Bull. Chem. Soc. Jpn.*, **43**, 3746 (1970).
- (2) T. Morimoto, M. Nagao, and M. Hirata, *Kolloid-Z. Z. Polym.*, **225**, 29 (1968).
- (3) M. Nagao, K. Morishige, T. Takeshita, and T. Morimoto, *Bull. Chem. Soc. Jpn.*, **47**, 2107 (1974).
- (4) T. Morimoto, M. Nagao, and F. Tokuda, *Bull. Chem. Soc. Jpn.*, **41**, 1533 (1968).
- (5) M. Nagao and T. Morimoto, *J. Phys. Chem.*, **73**, 3809 (1969).
- (6) M. Nagao, *J. Phys. Chem.*, **75**, 3822 (1971).
- (7) J. V. Evans and T. L. Whateley, *Trans. Faraday Soc.*, **63**, 2679 (1967).
- (8) H. P. Boehm, *Discuss. Faraday Soc.*, **52**, 264 (1971).
- (9) N. N. Parkyns, *J. Phys. Chem.*, **75**, 526 (1971).
- (10) Ya. M. Grigor'ev, D. V. Pozdnyakov, and V. N. Fillimonov, *Zh. Fiz. Khim.*, **46**, 316 (1972).
- (11) A. Zecchina, S. Coluccia, E. Guglielminotti, and G. Ghiotti, *J. Phys. Chem.*, **75**, 2790 (1971).
- (12) K. Atherton, G. Newbold, and J. A. Hockey, *Discuss. Faraday Soc.*, **52**, 33 (1971).
- (13) T. Morimoto and K. Morishige, *Bull. Chem. Soc. Jpn.*, **47**, 92 (1974).
- (14) J. H. Taylor and C. H. Amberg, *Can. J. Chem.*, **39**, 535 (1961).
- (15) T. Morimoto, K. Shiomi, and H. Tanaka, *Bull. Chem. Soc. Jpn.*, **37**, 392 (1964).
- (16) T. Morimoto and H. Naono, *Bull. Chem. Soc. Jpn.*, **46**, 2000 (1973).
- (17) T. Morimoto, M. Nagao, and F. Tokuda, *J. Phys. Chem.*, **73**, 243 (1969).
- (18) T. Morimoto, M. Nagao, and J. Imai, *Bull. Chem. Soc. Jpn.*, **44**, 1282 (1971).
- (19) T. Morimoto and M. Nagao, *J. Phys. Chem.*, **78**, 1116 (1974).
- (20) F. H. Healey, J. J. Chessick, and A. V. Fraioli, *J. Phys. Chem.*, **60**, 1001 (1956).
- (21) C. M. Hollabaugh and J. J. Chessick, *J. Phys. Chem.*, **65**, 109 (1961).
- (22) J. J. Jurinak, *J. Colloid Sci.*, **19**, 477 (1964).
- (23) S. Dana and W. E. Ford, "A Textbook of Mineralogy", Wiley, New York, N.Y., 1960, p 480.

Zeolite Crystallization Kinetics Related to Dissolution Rates of Quartz Reactant

R. A. Cournoyer, W. L. Kranich, and L. B. Sand*

Department of Chemical Engineering, Worcester Polytechnic Institute, Worcester, Massachusetts 01609 (Received December 17, 1974)

Publication costs assisted by the Department of Chemical Engineering, Worcester Polytechnic Institute

In this study quartz is used as the only source of silica in the synthesis of several zeolitic phases at low temperatures. The study is concerned primarily with the kinetics of crystallization of zeolite HS (a hydroxy-sodalite) as related to the rate of dissolution of the quartz reactant. The two rates are found to be essentially equal. The crystals nucleate and grow on the surface of the quartz reactant. The results support the theory of zeolite crystallization from solution (rather than solid-solid transformation). The activation energy for the process is 21.7 kcal/mol. The rate-limiting step in the dissolution of the quartz reactant is believed to occur as bonds are broken on the surface of the dissolving crystals; this is consistent with the surface-diffusion and step-growth theory of crystal growth. An interesting side result of the study was the synthesis for the first time using quartz as the only source of silica of the molecular sieve zeolites, zeolite A and zeolite X.

Introduction

One purpose of this study was to help resolve the question as to whether zeolite crystallization proceeds by a solid-solid transformation of amorphous gel into crystalline zeolite or by crystallization from solution. Quartz was selected as the only source of silica for two reasons. First, as the rate of solution of quartz is slow at low temperature, it is possible to determine if a correlation exists between the rate of solution of the quartz reactant selected for the study and the rate of formation of crystalline product. Second, since it has not been reported in the literature, the synthesis of molecular sieve zeolites at low temperature using quartz as the only source of silica is of interest. Although zeolite HS is not regarded currently as a molecular sieve zeolite it was chosen for this study, since with quartz as a reactant zeolite HS was found to crystallize as the only crystalline phase at three different low temperatures from the same batch composition.

Sodalite is the most sodium-rich member of the sodalite group of minerals and has the idealized formula, $\text{Na}_8\text{-Al}_6\text{Si}_6\text{O}_{24}\text{Cl}_2$. A phase having the sodalite structure but with no Cl and synthesized in the $\text{Na}_2\text{O-Al}_2\text{O}_3\text{-SiO}_2\text{-H}_2\text{O}$ system has been given several designations: basic sodalite,¹ hydrosodalite,² hydroxysodalite,³ hydrated sodalite,^{4,5} sodalite hydrate,⁶ and hydrated hydroxysodalite (zeolite HS).⁷ This paper will use the designation zeolite HS.

Two mechanisms have been proposed for the crystallization of zeolitic phases. Breck and Flanigen⁸ and McNicol et al.^{9,10} support the theory of a solid-solid transformation of amorphous gel into crystalline zeolite. Kerr,^{11,12} Ciric,¹³ and Culfaz and Sand¹⁴ support the theory of zeolite crystallization from solution. Others also have attempted to determine the mechanism of zeolite crystallization.¹⁵⁻¹⁸

Experimental Section

Synthesis. The reactants used for the quartz synthesis were distilled water, silicic acid (J. T. Baker), sodium silicate solution (N-brand, Phila. Quartz), and amorphous silica (Degussa aerosil). The reactants used for zeolite synthesis were distilled water, sodium hydroxide, sodium aluminate (Nalco), and quartz. The quartz used was either syn-

thesized or flint of 99.5% purity (lot no. C3713 obtained from Norton Co.).

Reactants were mixed with a mortar and pestle until they become homogeneous in consistency. Synthesis runs producing quartz as a single crystalline phase were made in modified Morey-type autoclaves of 15-ml capacity at autogenous pressure. When a larger amount of product was needed, a 400-ml Type 304, low carbon stainless steel autoclave was used for synthesis. For synthesis of zeolite phases at temperatures below 100°, 250-ml capacity polypropylene bottles were used. The sealed reactant vessels were placed in mechanically convected ovens for the required period of time. The vessels were quenched in cold water and the contents then were transferred with distilled water to a mortar and milled to disaggregate the solids. The slurry of solids was filtered in a Buchner funnel and washed with distilled water until the pH of the wash water approached neutral. The solid product then was dried at 90°.

Quartz Solubility Determination. The quartz to be used for the solubility determination was weighed on an analytical balance either in a Teflon liner to be inserted in a steel autoclave or in a 15-ml polypropylene centrifuge tube. The sodium hydroxide solution then was added and the mixture stirred with a small spatula. Alumina necessarily was omitted from the batch to avoid zeolite crystallization which would preclude determination (by weighing solids) of the rate of dissolution of the quartz. The mixture was sealed and allowed to react at the appropriate temperature. At the completion of the run, the sample was removed and quenched with cold water. The sample contained in the Teflon liner then was transferred quantitatively to a centrifuge tube of known weight. The tube was centrifuged and the clear solution discarded. Distilled water was added to remove the remaining hydroxide solution from the wet solids and the centrifuging carried out again. The same procedure was followed with the polypropylene tubes but without the initial transfer to another tube. The samples were then dried at 90°. The dried samples were reweighed on an analytical balance and the amount of quartz in solution was calculated.

Phase Determination. Synthesized samples were analyzed by X-ray powder diffraction using monochromatic Cu

$K\alpha_1$ radiation with a Philips-Norelco Model 3000 X-ray diffractometer.

Quantitative determination of the phases present in a sample was made by summation of selected peak heights referred to a standard. From the extent of crystallization, the kinetics of the process was determined.

Results and Discussion

Synthesis. The synthesis of quartz for use as a reactant in zeolite crystallization was carried out in the $\text{Na}_2\text{O}-\text{SiO}_2-\text{H}_2\text{O}$ system using various sources of soda and silica and from batch compositions selected from the work of Tuttle and Friedman.¹⁹ The morphology and yield of crystals proved to be dependent on the batch composition, the reactants used, and the duration of synthesis. The predominant morphology was determined to be euhedral prismatic with the size of the crystals increasing from 5×15 to $15 \times 50 \mu\text{m}$ with increasing duration of synthesis. The temperature chosen for synthesis was 280° which resulted in crystallization rates that were adequate for this work. The most favorable conditions for synthesis resulted from the use of sodium hydroxide, "aerosil", and distilled water with an overall batch composition of $\text{Na}_2\text{O}-7\text{SiO}_2-79\text{H}_2\text{O}$. Crystallization was achieved in 6 hr at 280° under these conditions.

Synthesis of zeolites in the $\text{Na}_2\text{O}-\text{Al}_2\text{O}_3-\text{SiO}_2-\text{H}_2\text{O}$ system was attempted initially at 175 and 220° . The $\text{SiO}_2/\text{Al}_2\text{O}_3$ ratio was varied between 6 and 36. All of these syntheses yielded analcime in varying amounts. Some products also contained either hydroxycancrinite or gismondine. The phases synthesized were all zeolitic in nature.

Since quartz was almost always a coexisting phase under the above conditions as well as being a reactant it was decided to attempt synthesis with much lower silica to alumina ratios in the overall batch. In addition, it was decided to use lower temperatures in the belief that the metastable molecular sieve zeolites would be more likely to form under less severe conditions.

At 123° zeolite HS was synthesized using overall batch compositions with $\text{SiO}_2/\text{Al}_2\text{O}_3$ ratios of 0.6 to 3.33. In some cases the crystallization of zeolite HS was followed by a recrystallization to hydroxycancrinite. No molecular sieve zeolites were synthesized in this system at 123° .

The batch compositions used for the synthesis of zeolites at 92° were similar to those used at 123° . As was the case at 123° , zeolite HS was readily synthesized. However, at this temperature the synthesis of zeolite A also was achieved from two different batch compositions ($2.33\text{Na}_2\text{O}-\text{Al}_2\text{O}_3-3.33\text{SiO}_2-124\text{H}_2\text{O}$ and $1.89\text{Na}_2\text{O}-\text{Al}_2\text{O}_3-1.56\text{SiO}_2-100\text{H}_2\text{O}$). The yield of zeolite A was very low (10% after 14 hr) but this is believed to be the first report of a molecular sieve zeolite synthesized using quartz as the only source of silica.

At all temperatures and batch compositions used, silica was the only species which was not initially present in the solution phase. At 123 and 92° the phases synthesized were zeolite A and zeolite HS. These results are consistent with the results of Schwochow and Heinze²⁰ who studied the change of concentration with time in the liquid phase before crystallization begins. Their experiments showed that zeolite A and sodalite, which are poorer in silica, are obtained from the liquid phase if the solutions remain on the aluminate side of the concentration diagram.

From an overall batch composition of $6.21\text{Na}_2\text{O}-\text{Al}_2\text{O}_3-1.63\text{SiO}_2-88.4\text{H}_2\text{O}$ at room temperature, zeolite X was synthesized (15% in 22 days) with $a_0 = 25.00(2) \text{ \AA}$, giving a

Si/Al ratio of 1.06 as determined from the correlation of Breck and Flanigen.⁸ This is believed to be the first report of a faujasite-type zeolite synthesized using quartz as the only source of silica. From this same batch composition at the higher temperatures of 64 and 92° the only crystalline phase synthesized was zeolite HS. The formation of zeolite X at room temperature probably is due to more favorable conditions for nucleation of the phase. At higher temperatures the conditions may be too severe and the less stable molecular sieve zeolites are unable to achieve conditions necessary for nucleation and crystal growth. This is consistent with many observations that the more open structures nucleate at lower temperatures.

Kinetics. In studying the kinetics of zeolite crystallization a single batch composition was used. The batch composition chosen was $6.21\text{Na}_2\text{O}-\text{Al}_2\text{O}_3-1.63\text{SiO}_2-88.4\text{H}_2\text{O}$ because initial data indicated that zeolite HS was the only phase to crystallize at the temperatures of interest which were 64 , 92 , and 123° , even though further study showed that at 123° zeolite HS eventually reacted to form hydroxycancrinite.

The percentage of quartz dissolved (in the absence of sodium aluminate) from a single size fraction of reactant was determined as a function of time at each of three temperatures. Typical results (for $4.6\text{-}\mu\text{m}$ quartz) are shown by the solid symbols in Figure 1. On the same graph are plotted open points representing the transformation of the same size quartz into zeolite HS when aluminate is present.

Similar experiments (not shown) were conducted on two other sizes of quartz reactant. Within the limits of experimental error, the two sets of points (quartz dissolution and conversion to zeolite) can be represented by a single curve for each size at each temperature. The rate of formation of zeolite is therefore approximately equal to the rate of dissolution of quartz. In other words the rate-controlling step appears to be the rate of supply of silica in solution rather than its diffusion to nucleation sites or zeolite crystal growth.

In those few cases where the drawing of separate curves for solution and transformation might be justified, the rate of solution is slightly higher than the rate of crystal growth. This may indicate minor secondary influence of diffusion on the transformation rate. For most of the data, however, separate curves cannot be justified; therefore, a single averaged line is drawn through both sets of data.

The effect of crystal size on solution and conversion is shown graphically in Figure 2, the collected data at 92° . As would be expected, the rate of solution (or conversion) is greater for the smaller sizes of reactant.

The rate of crystallization of zeolite HS and the rate of solution of the quartz reactant increase with increasing temperature and decreasing size of the quartz reactant. An activation energy for the overall process was calculated assuming Arrhenius type dependence on temperature. The Arrhenius plots are presented in Figure 3. The average activation energy was calculated to be 21.7 kcal/mol which compares closely with the 20 kcal/mol observed by Bergman²¹ for the solution of quartz.

From scanning electron micrographs it was determined that the zeolite HS crystals were uniform and about $1 \mu\text{m}$ in length regardless of the amount synthesized. This is probably due to crystals nucleating on or in the vicinity of dissolving quartz particles (see Figure 4) and then growing rapidly until the nutrients immediately surrounding them are exhausted. The results indicate that nucleation and

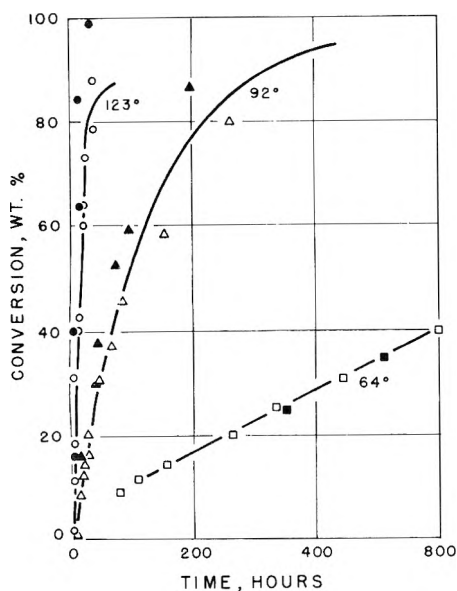


Figure 1. Rates of crystallization of zeolite HS (open symbols) and rates of dissolution of 4.6- μm size quartz reactant (solid symbols) at 64, 92, and 123 $^{\circ}$.

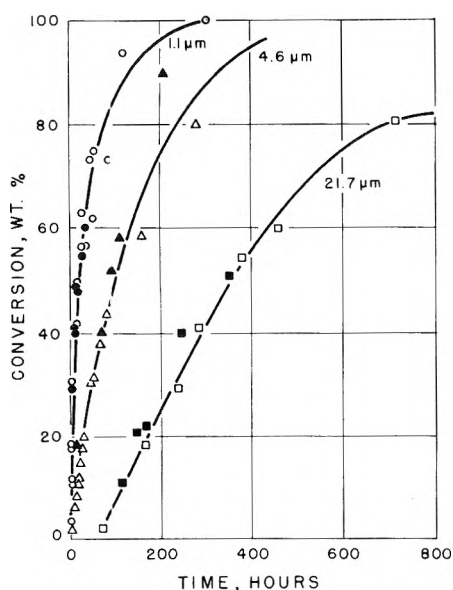


Figure 2. Rates of crystallization of zeolite HS (open symbols) and rates of dissolution of quartz reactant (solid symbols) at 92 $^{\circ}$ as a function of particle size of quartz.

crystal growth are relatively rapid processes and the limiting process is the dissolving of the quartz nutrient.

Mechanism. An attempt was made to interpret the data in terms of the various crystallization theories reviewed by Ohara and Reid.²² Many of the concepts which they cite for crystallization can be extended to the process of dissolution.

The high activation energy observed for the controlling process (the dissolution of quartz) suggests that an activated bond breaking process is limiting. If a bulk diffusion process were controlling (either near the dissolving surface or in the bulk solution) much lower apparent activation energies would be anticipated.

Further insight can be obtained by examining the linear dissolving rate in a direction perpendicular to the dissolv-

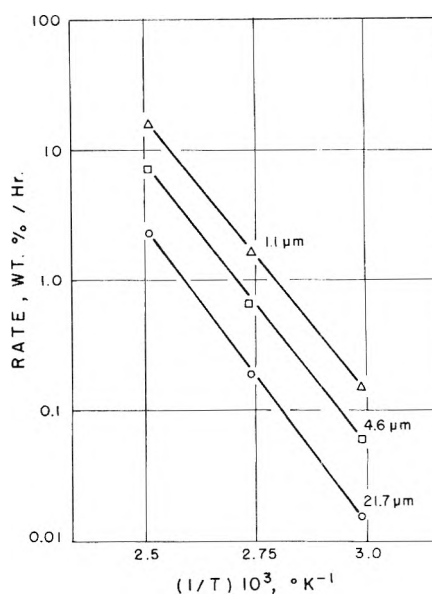


Figure 3. Arrhenius plots of crystallization rates for three particle sizes of quartz.

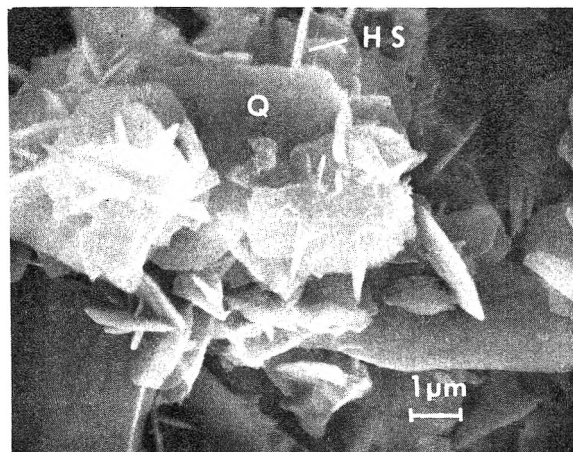


Figure 4. Scanning electron micrograph showing zeolite HS crystal growth on the surface of the quartz (Q) reactant. Synthesized from batch composition $6.21\text{Na}_2\text{O}-\text{Al}_2\text{O}_3-1.63\text{S O}_2-88.4\text{H}_2\text{O}$ at 92 $^{\circ}$ for 40.5 hr: F. Kudarauskas, microcopist, Nortcn Co., using AMR Model 1000.

ing surface. To obtain this, several approximations are necessary.

Up to this point, although the data have been segregated into three size classifications, only a qualitative use has been made of the stated dimensions. If the rate of change of crystal length (or diameter) is to be examined quantitatively, the basis for the stated size must be considered critically.

The effective average size was based on the diameter of a sphere having the same ratio of surface to volume as the observed particles. For each size fraction a characteristic dimension of each particle was measured using a scanning electron microscope. Then using a shape factor of 1.5 obtained from Perry²³ (for crushed glass) the equivalent diameter of the related sphere was calculated. Since for each size fraction there was a distribution of particle sizes, the characteristic diameter was calculated as the diameter of a sphere having the same average area as the particles.

Based on this average initial diameter for each size fraction, the mass rate of solution observed can be interpreted in terms of the corresponding rate of change in diameter of the average equivalent sphere. The calculated results are shown in Table I.

If (as the rate-controlling process) molecules are being stripped by an activated bond breaking from the exposed crystal planes in successive stepped layers, the rate of shrinkage of linear dimension (diameter) would be expected to be nearly independent of diameter. On the other hand, if diffusional phenomena were controlling, mass transfer theory would predict for stagnant (unstirred) solutions that the rate would be inversely proportional to diameter.

The data of Table I show only a weak dependence on diameter. A nearly 20-fold change in effective average diameter is accompanied by only a two- or three-fold change in shrinkage rate. Furthermore the direction of the apparent effect of diameter is opposite to that predicted by diffusion theory.

Both the high activation energy and the small influence of diameter on linear shrinkage rate are consistent with a controlling process involving a surface bond-breaking step rather than diffusion in solution.

Conclusions

Crystallization rates of zeolite HS using quartz reactant and solubility rates of the quartz reactant used were determined independently. Results showed that there was direct agreement between the rate of crystallization of zeolite HS and the rate of dissolution of the quartz reactant.

Scanning electron micrographs showed zeolite HS crystals to be all submicron in size. This indicates that there are very many sites for nucleation and growth. No gel particles were observed. Only quartz and zeolite HS crystals were present in the product. Although it is theoretically possible for a transitional gel phase to have formed when the dissolved silica reacted with the solution containing sodium and aluminum ions, none was detected. Large particles of gel aggregate would have had to be formed to make probable the zeolite's growing in the gel matrix by a solid-solid transformation mechanism. The dissolution and crystallization data and the SEM observations support the hypothesis of crystallization from solution.

For this system it is believed that the rate of dissolution of the quartz reactant by an activated bond-breaking process is the rate-limiting step in the growth of zeolite HS crystals. Using sources of silica which have higher rates of solution should lead to higher crystallization rates. However, using another source of silica which has a greater rate of solution may cause a greater supersaturation of species in solution, and other metastable phases may crystallize first.

In the solution of the quartz reactant it is believed that the rate-limiting step occurs on the surface of the dissolving crystal and that the process is not mass transfer limited. This is in agreement with the calculated activation energy which is much higher than would be expected for a mass transfer limited case. The activation energy is that expected for making or breaking chemical bonds.

The least accurate of the calculations made is believed to be the calculation of the equivalent diameter of the various size fractions of quartz used. In each size fraction there was a variety of particle sizes and shapes. The selection of an

TABLE I: Calculated Rates of Decrease in the Size of Quartz Reactant

Temp, °C	Effective av size of quartz reactant, μm	Calcd shrinkage rate, $\mu\text{m/hr}$
123	1.1	0.085
123	4.6	0.18
123	21.7	0.252
92	1.1	0.0083
92	4.6	0.0091
92	21.7	0.016
64	1.1	0.00069
64	4.6	0.0011
64	21.7	0.0014

appropriate diameter to assign to each particle is difficult, and because of the varying shapes no single characteristic dimension can be measured. The equivalent diameter assigned to each size fraction, however, does lead approximately to the relationship predicted for surface-controlled, bond-breaking kinetics. Quartz crystals of uniform morphology are needed to improve the accuracy.

Quartz usually is regarded as an unreactive source of silica in the synthesis of zeolites. This study has shown, however, that under certain conditions quartz may be used as a source of silica in the synthesis of a variety of zeolitic phases. Most of the phases synthesized are not characterized as possessing commercially valuable molecular sieve properties and are regarded as being some of the most stable denser zeolites. However, in the course of this study two molecular sieve zeolites were synthesized using quartz for the first time as the only source of silica.

References and Notes

- (1) R. M. Barrer and E. A. White, *J. Chem. Soc.*, 1561 (1952).
- (2) J. Wyart and C. M. Levy, *Bull. Soc. Fr. Mineral. Cristallogr.*, **78**, 577 (1955).
- (3) A. Regis, L. B. Sand, C. Calmon, and M. E. Gilwood, *J. Phys. Chem.*, **64**, 1567 (1960).
- (4) S. P. Zhdanov and N. N. Buntar, *Dokl. Akad. Nauk SSR*, **147**, 1118 (1962).
- (5) S. P. Zhdanov, N. N. Buntar, and E. N. Egarova, *Dokl. Akad. Nauk SSR*, **154**, 419 (1964).
- (6) W. M. Meier, "Molecular Sieves", Society of Chemical Industry, London, 1968, p 10.
- (7) D. W. Breck, "Zeolite Molecular Sieves", Wiley, New York, N.Y., 1974, p 77.
- (8) D. W. Breck and E. M. Flanigen, "Molecular Sieves", Society of Chemical Industry, London, 1968, p 47.
- (9) B. D. McNicol, G. T. Pott, and R. K. Loos, *J. Phys. Chem.*, **76**, 3388 (1972).
- (10) B. D. McNicol, G. T. Pott, R. K. Loos, and N. Mulder, *Adv. Chem. Ser.*, **No. 121**, 152 (1973).
- (11) G. T. Kerr, *J. Phys. Chem.*, **70**, 1047 (1966).
- (12) G. T. Kerr, *J. Phys. Chem.*, **72**, 1385 (1968).
- (13) J. Ciric, *J. Colloid Interface Sci.*, **28**, 315 (1968).
- (14) A. Culfaz and L. B. Sand, *Adv. Chem. Ser.*, **No. 121**, 140 (1973).
- (15) R. Aiello, R. M. Barrer, and I. S. Kerr, *Adv. Chem. Ser.*, **No. 101**, 44 (1971).
- (16) R. Aiello, C. Collela, and R. Sersale, *Adv. Chem. Ser.*, **No. 101**, 51 (1971).
- (17) W. Meise and F. E. Schwochow, *Adv. Chem. Ser.*, **No. 121**, 169 (1973).
- (18) F. Polak and A. Cichocki, *Adv. Chem. Ser.*, **No. 121**, 209 (1973).
- (19) O. F. Tuttle and I. Friedman, *J. Am. Chem. Soc.*, **70**, 923 (1948).
- (20) F. E. Schwochow and G. W. Heinze, *Adv. Chem. Ser.*, **No. 101**, 102 (1971).
- (21) E. Bergman, *J. Appl. Chem.*, **13**, 319 (1963).
- (22) M. Ohara and R. C. Reid, "Modeling Crystal Growth Rates from Solution", Prentice Hall, Englewood Cliffs, N.J., 1973.
- (23) J. H. Perry, "Chemical Engineers' Handbook", 4th ed, McGraw-Hill, New York, N.Y., 1963, pp 5-50.

Oxygen Exchange between $C^{18}O_2$ and "Acidic" Oxide and Zeolite Catalysts¹

J. B. Peri

Research and Development Department, Amoco Oil Company, Amoco Research Center,
Naperville, Illinois 60540 (Received November 25, 1974)

Publication costs assisted by Amoco Oil Company

The exchange of oxygen between $C^{18}O_2$ and several high-area oxides, including silica, γ -alumina, silica-alumina, and zeolite catalysts, was studied. Infrared spectra of adsorbed CO_2 and of surface "carbonates" were used to follow the rate of oxygen exchange and investigate the nature of unusually exchangeable surface oxide ions, present at low concentrations. Interaction of CO_2 with the surface typically produced initial exchange of one oxygen atom, as expected from interaction with a single oxide ion ($CO_2 + O^{2-} \rightleftharpoons CO_3^{2-}$), and the number of exchangeable ions increased with increasing temperature. The rate of oxygen exchange did not correlate with chemisorption to form stable surface carbonates or with the extent of strong physical adsorption of CO_2 . With dry silica, exchange was insignificant below 600°; with catalytically active zeolites and dry γ -alumina, it was detectable at 200° and fairly rapid at 300–400°. Silica-alumina required 100–150° higher temperature for exchange than did an active zeolite. Activity for cracking and other hydrocarbon reactions may be related to the ease of exchange of some surface oxide ions with CO_2 . Active zeolites have reactive oxide sites resembling those on dry γ -alumina, but such sites on zeolites are probably less-readily eliminated by chemisorption of H_2O or other compounds.

Introduction

Substantial evidence shows that the catalytic properties of "acidic" oxides such as γ -alumina and silica-alumina cannot be explained solely in terms of surface acidity, whether Lewis, Brønsted, or a mixture of both. The surface sites which catalyze many reactions of hydrocarbons and H_2 on acidic oxides are apparently "acid-base" or ion pair sites in which a reactive oxide ion (or ions) closely adjoins an "exposed", or incompletely coordinated metal ion.^{2–14} Adsorption of cocatalysts such as H_2O or hydrocarbons on such sites may be essential for some reactions. In contrast with the extensive research reported on the nature of surface acid sites, little attention has been given to the oxide base sites, which apparently show just as much variability.

Certain strong acid-base sites are created at low concentrations, typically 3×10^{12} to 9×10^{12} sites/cm², on surfaces of γ -alumina and silica-aluminas by removal at high temperatures of surface hydroxyl groups which characteristically cover these surfaces after exposure to atmospheric humidity. These sites can be eliminated by chemisorption of H_2O or NH_3 .³ Such sites, called α sites,⁴ show a characteristic ability to physically adsorb CO_2 strongly at room temperature. The CO_2 is held with a heat of adsorption ranging up to 15 kcal/mol,⁴ but can be readily displaced by olefins or on mild heating. These sites show some activity for olefin isomerization and polymerization, but are probably not the most active sites for many hydrocarbon reactions.^{4,5}

Other catalytically active sites on γ -alumina, however, can be poisoned by strong chemisorption of CO_2 .^{8–13} Exchange of H between benzene molecules¹¹ or between butene¹² and D_2 over dry γ -alumina is eliminated by chemisorption of CO_2 on a small number of surface sites ($<1.6 \times 10^{13}$ /cm²) without major effect on the selectivity or rate of 1-butene isomerization.¹² The sites that are poisoned by CO_2 , but not by NH_3 or by pyridine, are apparently base sites, presumably oxide ions. They are possibly the same as

those responsible for a band at 1780 cm⁻¹ produced by adsorption of CO_2 on dry γ -alumina.^{12,13}

The nature of the active sites on zeolite catalysts has also been the subject of much research and speculation.^{15,16} These catalysts are highly active for hydrocarbon cracking and isomerization, in some cases possibly over 100 times more active than conventional silica-alumina catalysts. As measured by usual tests, however, the number and types of acid sites on the zeolites normally seem roughly comparable to those on silica-aluminas. Both Lewis and Brønsted acid sites exist on both types of catalysts, but neither appears to completely explain the extraordinarily high activity of zeolites. Unusually strong Brønsted acid sites exist on at least some zeolites (e.g., H-Y and H-Zeolon) and are widely believed to be essential for their catalytic activity, but maximum activity apparently does not coincide with maximum Brønsted acidity.¹⁶ The catalytic activity of zeolites also probably reflects, in part, greater adsorption of hydrocarbon at reaction temperatures, but it remains possible that certain active sites, not yet properly identified, may be far more numerous and/or effective on active zeolites than on silica-alumina catalysts. Infrared studies of adsorbed CO_2 on cation-exchanged zeolites^{17,18} can, as on alumina, provide information about the exposed cations and reactive oxide ions.

Isotopic exchange of ^{18}O has been used to characterize the reactivity of oxide ions in catalyst surfaces.^{19,20} Water vapor readily exchanges O with silica, alumina, or silica-alumina.^{21,22} Exchange of O between $C^{18}O_2$ and the surface occurs readily with some catalysts,¹⁹ probably through carbonate formation. In general, however, O exchange between H_2O and the surface involves the surface OH groups and many more surface oxide ions than can be catalytically important. Exchange of O between $C^{18}O_2$ and oxide surfaces seemed to offer a better prospect for studying unusually reactive oxide ions present at low concentrations in oxide and zeolite surfaces.

Infrared spectroscopic study of ¹⁸O labeled C¹⁸O₂ physically adsorbed on the catalysts permitted, in most cases, concurrent evaluation of changes in catalyst surface chemistry and in the isotopic composition of the adsorbed CO₂. The study was intended as a preliminary survey for significant effects rather than for quantitative measurement of exchange rates.

Experimental Section

Apparatus and Procedures. The infrared cell and associated equipment have been described.²³ A Beckman IR-9 spectrometer was used in single beam operation. The spectrometer background was freed from CO₂ bands by flushing the spectrometer with dry air passed over Ascarite. Procedures were generally similar to those used before. Disks of zeolites were prepared for infrared study by pressing 0.15 g of zeolite powder in a steel die, 1.25 in. in diameter, usually at 5 tons/in.². Weights of pressed disk samples, trimmed for mounting in the cell, averaged about 0.065 g, ranging from 0.061 (Ca-Y) to 0.082 (H-Zeolon), and sample "thicknesses" were typically 20–25 mg/cm². Aerogel plate samples of SiO₂ (0.092 g) and γ -Al₂O₃ (0.14 g) were also studied.

Unless otherwise specified, samples were calcined for 1 hr in O₂ and predried by evacuation for 1 hr at 600°. A dose of roughly 1.5×10^{-5} mol of C¹⁸O₂ was then admitted to the cell, giving a cell pressure of 0.20–0.36 Torr (typically about 0.25 Torr) depending on the extent of adsorption. This dose added ¹⁸O equal to about 1.5 atom % of the O content of the sample. In the case of SiO₂ aerogel, owing to greater sample weight and increased addition of CO₂, the added ¹⁸O was about 7 atom % of the catalyst oxygen. Spectra were recorded before and after this CO₂ addition. The furnace section of the cell was preheated to a selected temperature, and the sample was raised into this heated zone for 15 min to 1 hr. The sample was cooled to 40° and a spectrum was again recorded. Circulation of CO₂ over the catalyst was by convection only. Exchange was normally evaluated by comparison of the relative intensities of the bands due to physically adsorbed C¹⁸O₂, C¹⁸O¹⁶O, and C¹⁶O₂. This was simple for most of the catalysts since they reversibly adsorbed sufficient CO₂ to give fairly strong bands in the 2330–2380-cm⁻¹ region. Silica presented a greater problem owing to weaker adsorption of CO₂.

Materials. The Ca- and La-Y zeolites were, as described elsewhere,¹⁶ made from a sample of Na-Y with a Si/Al ratio of 2.4. Ultrastable (US) faujasite (in "soda" form) holding 2.5% Na was used as supplied by the Davison Division of W. R. Grace & Co. Hydrogen Zeolon ultrapure powder (H-Zeolon), a synthetic mordenite, was used as supplied by the Norton Co. It had a Na content of 0.13%. Nalco HA-1 silica-alumina (26% Al₂O₃, 495 m²/g) was used as supplied and previously described.⁴ Aerogel plate samples of γ -Al₂O₃²⁴ and silica²⁵ were also as previously described.

C¹⁸O₂ was used as supplied by Miles Laboratories, whose analyses showed 93.7 and 97.4% atom % ¹⁸O for two samples. Oxygen-18 enriched H₂O (10 atom % ¹⁸O) from International Chemical and Nuclear Co. was also used in a few experiments.

Calculations. The number of surface oxide ions exchangeable at a given temperature was typically calculated as follows. The fraction x of the ¹⁸O left in the adsorbed CO₂ after heating the sample for 1 hr in the known dose of C¹⁸O₂ added originally was estimated from the relative intensities of the CO₂ bands in the 2330–2380-cm⁻¹ region.

Isotopic equilibration was assumed to have occurred between the N_0 oxygen atoms in the CO₂ and N_{ex} exchangeable oxide ions on the catalyst surface. A standard isotopic dilution calculation then gave $N_{ex} = N_0[(1/x) - 1]$. Calculation of N_{ex}/g or N_{ex}/cm^2 was then made from the sample weight or surface area.

Results

H₂¹⁸O Exchange. Preliminary study was made of ¹⁸O exchange between H₂O and oxide catalyst surfaces. In these experiments 0.25 ml of H₂O was heated at 100° with ~0.38 g of Nalco HA silica-alumina and with Davison US faujasite. Mass spectrometric analysis of separated H₂O showed that 21% of the oxygen atoms in the Nalco HA and 31% of those in the Davison US faujasite had exchanged in 1 hr. These results are probably indicative mainly of the relative accessibility of the oxide ions in the structure and confirm previous findings showing rapid exchange and lack of selectivity.

Silica. Adsorption of CO₂ on silica aerogel was very slight at 40° and 0.36 Torr so that no conclusions as to exchange could be reached from study of infrared bands due to physically adsorbed CO₂. When the pressure was increased to 2.6 Torr, however, bands in the 2310–2365-cm⁻¹ range, principally gaseous CO₂, were intense enough (~0.03 absorbance unit) to show that exchange was negligible after heating at 500 or 600° for up to 1 hr but substantially complete after 0.5 hr at 800°.

Alumina. As shown in Figure 1, addition of C¹⁸O₂ to dry γ -alumina aerogel produced prominent bands at 2338 cm⁻¹ (C¹⁸O₂ on α sites) and below 1900 cm⁻¹ showing various carbonate or carboxylate structures. (The band at ~2350 cm⁻¹ in the background spectrum may arise from CO₂ trapped in closed pores in the alumina²⁶.) No exchange occurred at 40°, but after heating for 15 min at 400°, essentially complete exchange was evidenced by the spectrum of adsorbed CO₂ which now showed a band at 2372 cm⁻¹ representing C¹⁶O₂ as well as shifts in the positions of bands in the 1750–1900-cm⁻¹ region.

The alumina sample was then rehydrated in 15 Torr of H₂O vapor at 200° (three changes of H₂O vapor) and redried by evacuation at 600°. Figure 2 shows the spectra obtained after subsequent addition of C¹⁸O₂ to the alumina and heating at 200 and 300°. After 15 min heating at 200°, the formation of new bands near 2350, 2360, and 2370 cm⁻¹ showed exchange of surface oxide to form adsorbed C¹⁸O¹⁶O and C¹⁶O₂. Further heating at 200° for up to 1 hr did not significantly increase the apparent extent of exchange, but heating at 300° for 15 min gave substantial further exchange. Here again, longer heating, up to 1 hr, did not significantly increase the extent of exchange. Heating at 400° subsequently gave essentially complete exchange, as seen previously; most of the catalyst oxygen was, of course, still ¹⁶O.

It can be safely assumed that the weakly adsorbed CO₂ responsible for the bands in the 2338–2372- and 1825–1865-cm⁻¹ regions is in equilibrium with gaseous CO₂. No significant shifts were evident in the positions of the stable carbonate or bicarbonate bands at 1640 cm⁻¹ and lower frequencies although changes to be expected in these bands are 10–20 cm⁻¹ at most,²⁷ and the bands are not sharp. The band initially at 1770 cm⁻¹ does show a definite shift of about 30 cm⁻¹ to 1800 cm⁻¹ (final), however, and corresponds at least in part to a form of CO₂ apparently held slightly more strongly than that responsible for the 2338–

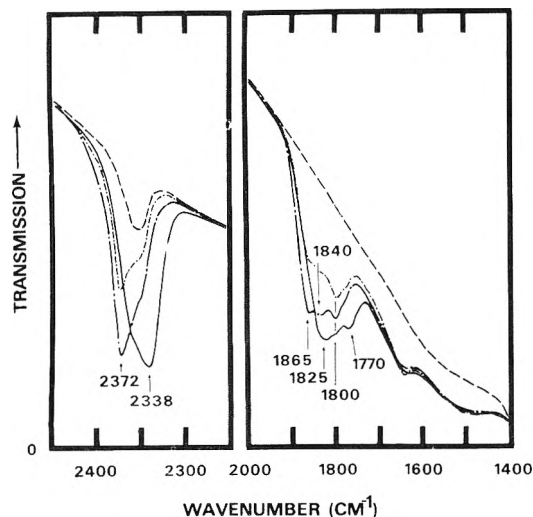


Figure 1. Spectra of adsorbed CO_2 on $\gamma\text{-Al}_2\text{O}_3$: (---) original alumina; (—) after addition of C^{18}O_2 ; (- · -) after 15 min at 400° ; (- - -) after 5-min evacuation.

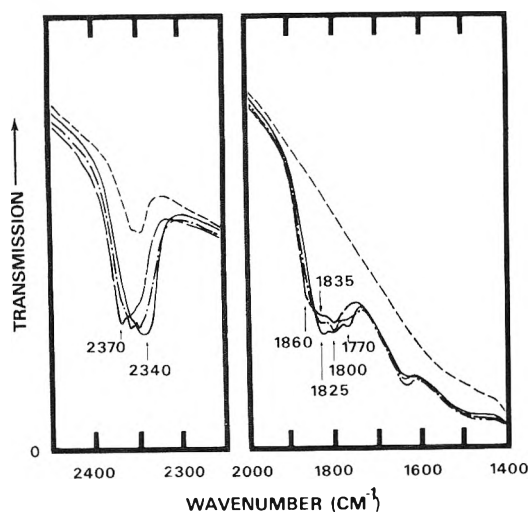


Figure 2. Spectra of adsorbed CO_2 on $\gamma\text{-Al}_2\text{O}_3$: (---) original; (—) after addition of C^{18}O_2 ; (- · -) after 15 min at 200° ; (- -) after 15 min at 300° .

2372-cm^{-1} bands.⁵ Apparently this form is also in equilibrium with gas phase CO_2 .

Bands near 1820 and 1775 cm^{-1} , as well as bands near 3605 , 1475 , and 1225 cm^{-1} assigned by Parkyns²⁷ to surface bicarbonate groups, were subsequently observed for CO_2 on a similar, but more-conventional γ -alumina, in pressed disk form, predried at 600° . Except for the 1820-cm^{-1} band, these bands remained in the spectrum after 5-min evacuation at 115° , but all were almost completely removed by 15-min evacuation at 200° . They thus represent fairly unstable structures which probably contribute to O exchange on γ -alumina at 200° . In addition to these bands, two bands near 1480 and 1530 cm^{-1} , apparently representing stable unidentate carbonates, were produced by heating the alumina in CO_2 at 300° . These two bands were largely removed by 15-min evacuation at 300° , and completely removed at 400° , suggesting that they represent carbonates which contribute to O exchange at 300 to 400° .

Figure 3 shows spectra of the adsorbed CO_2 in the $2300\text{-}2400\text{-cm}^{-1}$ region after 15-min exchange at 200° re-

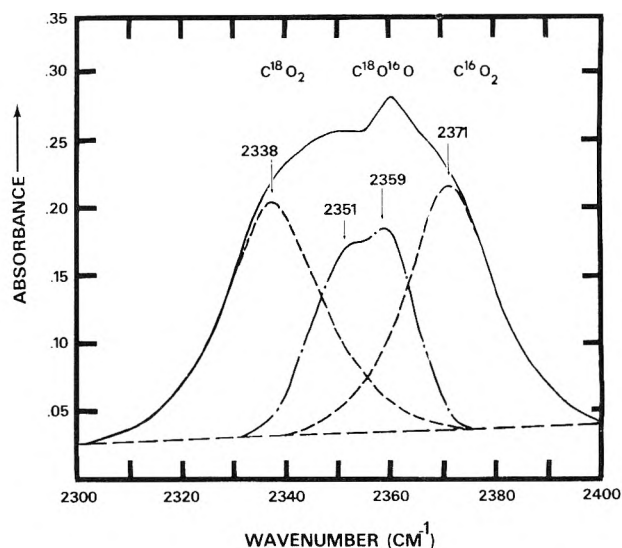


Figure 3. Replotted spectrum of CO_2 on $\gamma\text{-Al}_2\text{O}_3$ after 15 min at 200° .

plotted from original spectra for Figure 1 after subtraction of the "entrapped CO_2 " band in the background. (This band does not show exchange in these experiments.) Graphical resolution of these bands was made by assuming symmetrical bands for C^{18}O_2 and C^{16}O_2 and subtracting these from the observed band contour to produce the incompletely resolved doublet shown for $\text{C}^{18}\text{O}^{16}\text{O}$. The added C^{18}O_2 is about 50% exchanged. Calculation shows that this corresponds to equilibration with approximately 4.3×10^{13} oxide ions/ cm^2 of Al_2O_3 surface, comparable to the maximum number of "triplet" oxide defects ($\sim 4.8 \times 10^{13}/\text{cm}^2$) postulated previously on the surface of dry alumina,²⁸ but roughly ten times the maximum number of α sites developed on dry γ -alumina. After heating at 300° , the exchange appears to involve equilibration with at least 1×10^{14} oxide ions/ cm^2 ($3 \times 10^{20}/\text{g}$), comparable to the postulated maximum sum of pair + triplet oxide defects ($\sim 1.1 \times 10^{14}/\text{cm}^2$). To produce the estimated 90%+ exchange seen after heating at 400° , at least 4×10^{14} oxide ions/ cm^2 would have to equilibrate with the added CO_2 , comparable to the total number of oxide ions/ cm^2 previously postulated in the outermost layer on the dry γ -alumina.

Silica-Alumina. The results of addition of C^{18}O_2 to silica-alumina, predried at 600° , are shown in Figure 4. No exchange was seen at 40° and very little after 1 hr at 200° . Estimation of the maximum exchange at 200° ($\sim 12\%$) shows that equilibration could not have been with more than 8×10^{12} oxide ions/ cm^2 ($3.8 \times 10^{14}/\text{g}$). This is about the upper limit for the expected number of α sites.⁴ After 1 hr at 300° further exchange (estimated $\sim 35\%$) had led to equilibration with roughly 3×10^{13} oxide ions/ cm^2 ($1.4 \times 10^{20}/\text{g}$). The sample was then repeatedly reexchanged with C^{16}O_2 and redried by evacuation at 600° . Subsequent readdition of C^{18}O_2 and heating at 400 and 500° gave spectra as shown in the last panel of Figure 4. The number of exchangeable oxide ions appeared only slightly greater at 400 than at 300° , but heating at 500° for 15 min gave nearly complete exchange with surface oxide, equilibration with at least 2×10^{14} oxide ions/ cm^2 (roughly twice the number of acid sites which can strongly hold NH_3).

The spectra on silica-alumina, as on γ -alumina, showed evidence for two bands (2365 and 2353 cm^{-1}) arising from adsorbed $\text{C}^{18}\text{O}^{16}\text{O}$ in addition to the bands for adsorbed

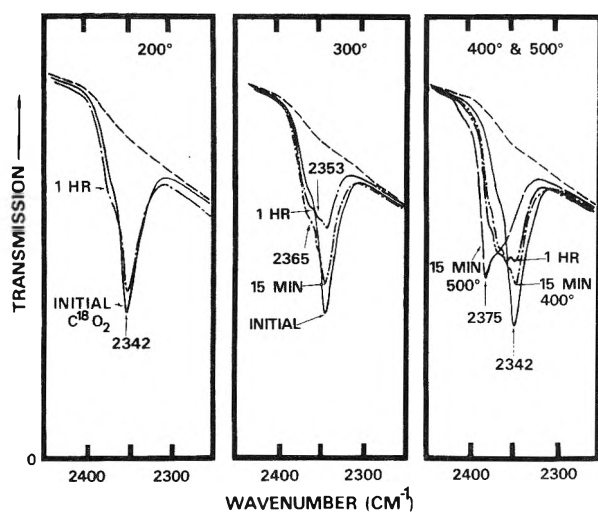


Figure 4. Spectra of CO_2 on silica-alumina.

$C^{18}O_2$ (2342 cm^{-1}) and $C^{16}O_2$ (2375 cm^{-1}). The apparent separation of the doublet peaks for $C^{18}O^{16}O$ of 12 cm^{-1} is slightly larger than that on alumina ($\sim 8\text{ cm}^{-1}$), as are also the corresponding frequencies for adsorbed CO_2 ($\sim 4\text{ cm}^{-1}$ increase). No bands were seen at lower frequencies in the $1200\text{--}2300\text{-cm}^{-1}$ range to indicate formation of carbonates or other forms of chemisorbed CO_2 . The slight decrease in total band intensities around 2350 cm^{-1} on heating at 300° may, however, indicate that some of the α sites were blocked by CO_2 or H_2O during exchange.

Na-Y Zeolite. Figure 5 illustrates the exchange of $C^{18}O_2$ with Na-Y zeolite. A slight exchange is seen in 1 hr at 200° , and this increases at 300 and 400° but still does not involve a very large number of oxide ions. Allowing for differences in the number and frequencies of the bands for adsorbed CO_2 ($C^{18}O_2$, 2323 cm^{-1} ; $C^{18}O^{16}O$, 2341 ; and $C^{16}O_2$, 2358 cm^{-1}), the degree of exchange seems to be approximately the same as that observed on silica-alumina after similar heating. The existence of one, rather than two, bands for adsorbed $C^{18}O^{16}O$ may be related to the apparently weakened adsorption of CO_2 ($C^{16}O_2$ band at 2358 cm^{-1} as compared with 2375 cm^{-1} on silica-alumina), which would minimize the splitting arising from adsorption of $C^{18}O^{16}O$ with one end or the other down.

At lower frequencies (not shown) the only significant band resulting from CO_2 adsorption and exchange was at 1640 cm^{-1} this was relatively large after 500° exchange. No other bands were noted from 1200 to 2300 cm^{-1} .

Ca-Y Zeolite. Figure 6 shows the exchange of $C^{18}O_2$ on Ca-Y zeolite. Experiments were run at each temperature after the samples had been rehydrated by heating in 15 Torr of H_2O vapor at 200° and predried by evacuation for 1 hr at 600° . The spectra of adsorbed CO_2 show that while exchange is relatively slight at 200° , it is substantially greater at 300° than on silica-alumina or Na-Y zeolite. Assuming 50% exchange of the added CO_2 in 1 hr at 300° , calculation shows about 3×10^{20} exchangeable oxide ions/g. This is much less than the number of Na ions/g in the original Na-Y ($2.4 \times 10^{21}/g$), or than the number of Ca ions after 72% ion exchange with calcium ($\sim 9 \times 10^{20}$), and far less than the total number of oxide ions/g (2×10^{22}). At 400° the number of oxide ions exchangeable in 1 hr rose to an estimated $7 \times 10^{20}/g$, and at 500° to at least 3×10^{21} .

The frequencies of the bands caused by adsorbed CO_2 ($C^{16}O_2$, 2368 cm^{-1} ; $C^{18}O^{16}O$, 2348 and 2355 cm^{-1} ; $C^{18}O_2$,

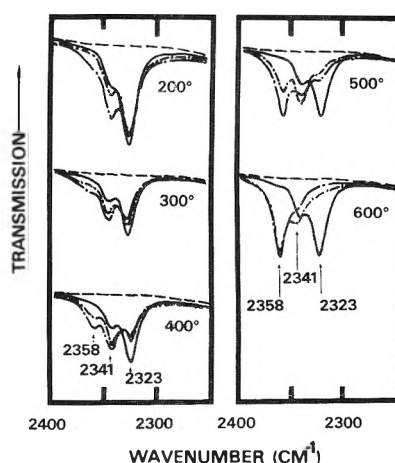


Figure 5. Spectra of CO_2 on Na-Y Zeolite: (---) original; (—) after addition of $C^{18}O_2$; (- · - · -) after 15 min at indicated temperature; (- —) after 1 hr at temperature.

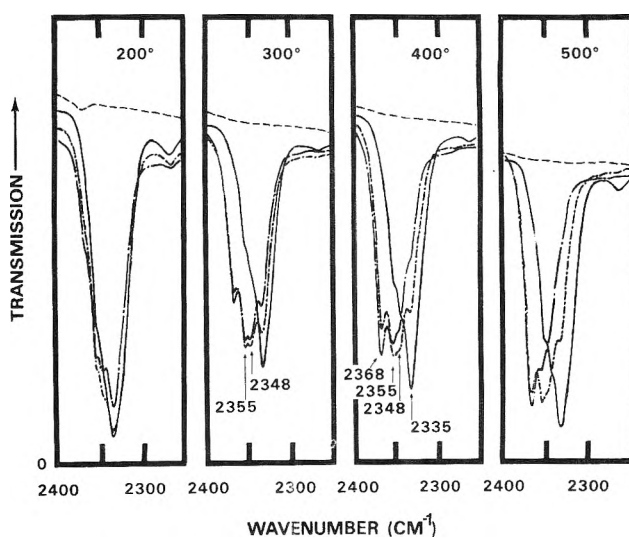


Figure 6. Spectra of CO_2 on Ca-Y zeolite predried at 600° : (---) original; (—) after addition of $C^{18}O_2$; (- · - · -) after 15 min at indicated temperature; (- —) after 1 hr at temperature.

2335 cm^{-1}) and the apparent 7-cm^{-1} splitting of the $C^{18}O^{16}O$ doublet are about like those seen for alumina.

Figure 7 shows the carbonate bands produced at lower frequencies during exchange of Ca-Y with $C^{18}O_2$ at the same temperatures. The Ca-Y was rehydrated and redried at 600° and fresh $C^{18}O_2$ was added before obtaining the spectra for 400 and 500° exchange. Three principal bands are evident (1632 , 1480 , and 1425 cm^{-1}). No other bands resulting from adsorption of CO_2 were detected in the $1200\text{--}2250\text{-cm}^{-1}$ region. The $1632\text{--}1638\text{-cm}^{-1}$ band, typically present after 600° preevacuation, but increased by initial CO_2 addition, corresponds in frequency to bands reported for CO_2 on a number of oxides and zeolites.²⁹ This band is usually attributed to the asymmetric stretching of bidentate carbonate or bicarbonate, the symmetrical stretching band presumably falling slightly below 1300 cm^{-1} where poor transmission and low spectral sensitivity preclude its observation. The bands at 1480 and near 1425 cm^{-1} , which develop slowly on heating at 300 or 400° in CO_2 , resemble bands reported¹⁷ for CO_2 on Na-X zeolite, where they appeared immediately after CO_2 addition.

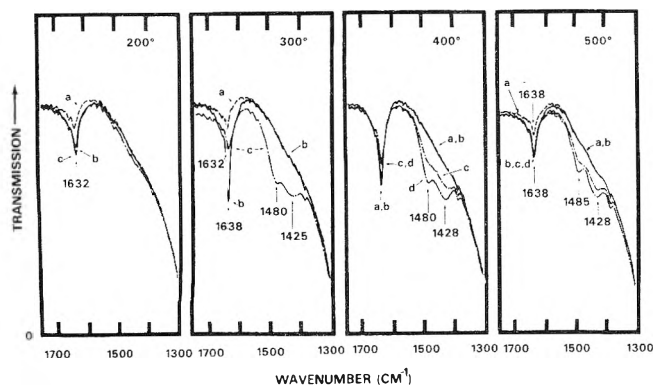


Figure 7. Spectra of chemisorbed CO_2 on Ca-Y zeolite predried at 600° : (a) original; (b) after addition of C^{18}O_2 ; (c) after 1 hr at indicated temperature; (d) after 1 hr at temperature.

These interesting bands, attributed to CO_3^{2-} in an almost symmetrical environment, appear to represent the most stable configuration for small amounts of adsorbed CO_2 . Alternatively, they can be regarded as the asymmetric and symmetric stretches of a unidentate carbonate.²⁹

None of these carbonate bands appears to represent an obvious intermediate in the exchange with CO_2 below 400° . The 1480- and 1425-cm^{-1} bands increase in intensity during heating in CO_2 at 300 and 400° while the activity for O exchange decreases. The 1638-cm^{-1} band might represent an intermediate, especially for exchange at 300° . Fairly prominent at 200° , it increased after redrying at 600° and readdition of C^{18}O_2 . Subsequent heating at 300° decreased its intensity (while the 1480- and 1425-cm^{-1} bands were increasing) as might occur if it represented an intermediate present in decreasing amounts owing to progressive blocking of sites by formation of stable carbonate. The spectra obtained during exchange at 400 and 500° cast some doubt on the possible role of bidentate carbonate as an intermediate at lower temperatures, however. The intensity of the 1632-cm^{-1} band does not decrease greatly during exchange at 400° , and not at all during exchange at 500° . The initial intensity of this band, moreover, seems to vary erratically after predrying and initial addition of C^{18}O_2 (where presumably the surface should be the same in all cases) without any consistent effect on the subsequent rate of exchange. The shift of the 1632-cm^{-1} band during exchange was only about 6 cm^{-1} . The intensities of the bands at 1480 and 1425 cm^{-1} , although increasing progressively with time of heating in CO_2 at all temperatures, are less after heating at 500° than at 300 or 400° . This suggests that formation and decomposition of unidentate carbonates may contribute significantly to the greatly increased exchange observed on heating at 500° .

To further investigate this subject the Ca-Y was rehydrated as before but then dried at 400° instead of 600° . If bicarbonate formation, involving catalyst OH groups or H_2O held in some other way, was involved in the exchange, drying at 400° might give more rapid exchange. Exchange was, in fact, slightly more rapid at 200° , but showed almost identically the same rate at 300 and 400° as that previously seen on 600° predried Ca-Y.

Figure 8 shows the carbonate spectra during exchange with 400° predried Ca-Y. Corresponding to the higher exchange rate at 200° , we see both a larger band at 1635 cm^{-1} and somewhat greater development of the 1480- and 1435-cm^{-1} bands. These bands had remained in the background

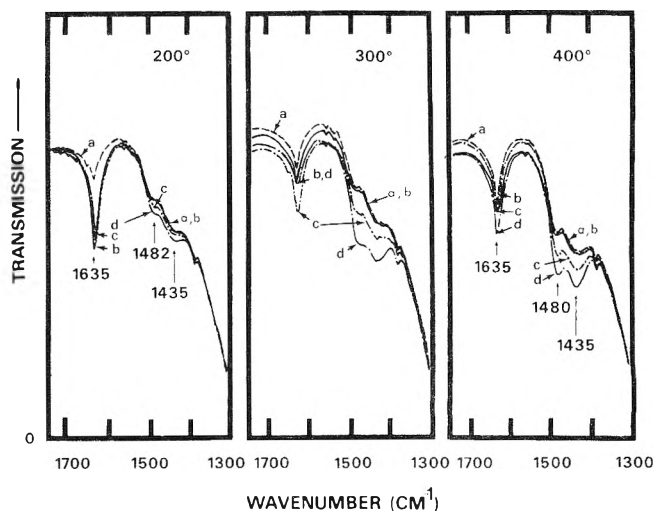


Figure 8. Spectra of chemisorbed CO_2 on Ca-Y zeolite predried at 400° : (a) original; (b) after addition of C^{18}O_2 ; (c) after 15 min at indicated temperature; (d) after 1 hr at temperature.

spectrum to a considerable extent after preevacuation at 400° . The original band at 1635 cm^{-1} prior to exchange at 300° was smaller than that prior to 200° exchange and than that seen previously on 600° predried Ca-Y before and during exchange at 300° , but the rates of exchange at 300° were similar on the two samples.

La-Y. Figure 9 shows spectra obtained during exchange of O between C^{18}O_2 and La-Y zeolite. The extent of exchange at 200 and 300° appears somewhat greater than for Ca-Y, although still not so great as on alumina. The exchange at 400° in 1 hr is evidently slightly less than at 300° . The maximum number of oxide ions exchanged at 300° appears to be about $4 \times 10^{20}/\text{g}$, only slightly higher than that seen on Ca-Y at this temperature. The development of the unidentate carbonate bands at 1460 and 1480 cm^{-1} with time is greater at 400 than at 300° , but there is no evidence for a carbonate or bicarbonate band near 1635 cm^{-1} .

H-Zeolon. Figure 10 shows exchange with H-Zeolon. The spectra are poorer than in the other figures, owing to low transmission of the H-Zeolon in this spectral region, but H-Zeolon clearly exchanges O at 200° and apparently gives essentially complete exchange with the added CO_2 after 1 hr at 300° . The number of oxide ions exchanged at 300° ($\geq 1 \times 10^{21}/\text{g}$) appears substantially greater than on Ca-Y or La-Y. No evidence was seen in spectra at lower frequencies for formation of carbonate or bicarbonate bands.

US Faujasite. Figure 11 shows exchange with US faujasite. Although, at first sight, some exchange appears to occur immediately on addition of C^{18}O_2 at room temperature, the 2340-cm^{-1} band probably does not reflect $\text{C}^{18}\text{O}^{16}\text{O}$. Instead, this band evidently arises from adsorption of C^{18}O_2 on sites like those on silica-alumina, while the 2325-cm^{-1} band shows adsorbed C^{18}O_2 on sites like those on Na-Y or La-Y. Such interpretation is supported by the spectra after 400 and 500° exchange, which show bands at 2375 and 2360 cm^{-1} as expected for C^{18}O_2 on these two types of sites. The rate of exchange is roughly comparable to that on La-Y or H-Zeolon, but apparently fewer oxide ions exchange at 300° than with H-Zeolon, whereas more exchange at 300 and 400° than with La-Y. The reversal, after exchange, of the ratio of the relative intensities of the bands attributed to CO_2 on two types of sites probably shows preferential

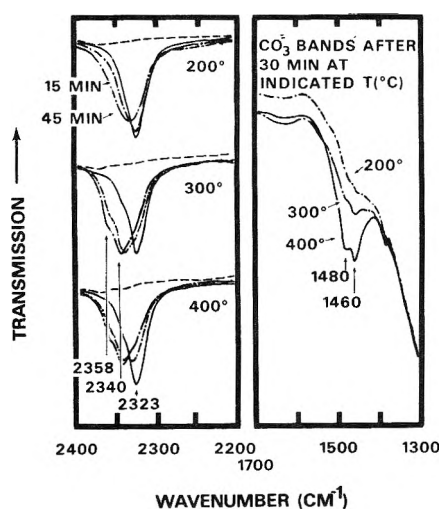


Figure 9. Spectra of CO₂ on La-Y zeolite: (---) original; other spectra are after addition of C¹⁸O₂ and after heating as indicated at the temperature shown.

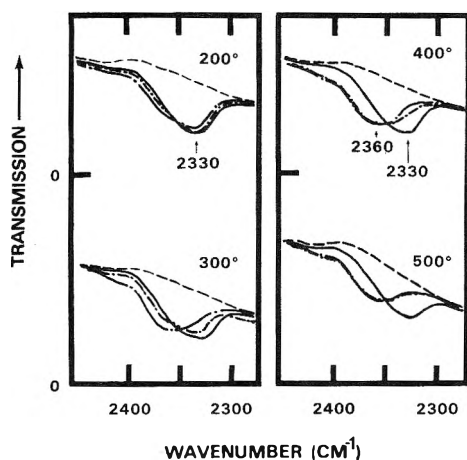


Figure 10. Spectra of CO₂ on H-Zeolon: (---) original; (—) after addition of C¹⁸O₂; (-·-·-) after 15 min at indicated temperature; (- -) after 1 hr at temperature.

blocking of the "silica-alumina" type sites (bands at 2375 and 2340 cm⁻¹).

Discussion

From the spectra, a rough estimate can be made of the temperature required for 50% exchange of the added C¹⁸O₂ after 1 hr contact, as shown in Table I. Table I also ranks the catalysts in order of the estimated number of oxide ions/g exchangeable in 1 hr at 300° and shows an activity ranking of some of the same catalysts studied previously for cracking of *n*-heptane.¹⁶ Relative catalytic activities depend on the particular reaction, catalyst pretreatment, and reaction conditions. Nevertheless, general agreement probably exists that for catalytic cracking of normal hydrocarbons pure silica is essentially inactive and H-Zeolon is quite active, with the other catalysts falling somewhere between.

Although the data are hardly conclusive, the catalysts can apparently often be correctly ranked for catalytic activity on the basis of their O-exchange activity. Dry γ -alumina has been reported by others to show relatively high cracking activity. It was also found to show high activity for

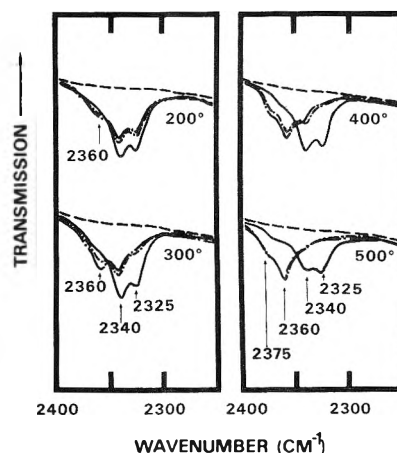


Figure 11. Spectra of CO₂ on US faujasite: (---) original; (—) after addition of C¹⁸O₂; (-·-·-) after 15 min at indicated temperature; (- -) after 1 hr at temperature.

TABLE I: O Exchange and Cracking Activity

Catalyst	T, °C (for 50% exchange) ^a	N _{ex} /g × 10 ⁻²⁰ (300°) ^b	<i>n</i> -C ₇ cracking activity rank ^c
γ -Al ₂ O ₃	200	3	
La-Y	250	4	2
H-Zeolon	250	10	1
US-Faujasite	250	5	
Ca-Y	300	3	3
Silica-alumina } Na-Y	400	1.4	4-5
Silica	600?	0	6

^a of 1.5 × 10⁻⁵ mol of C¹⁸O₂ in 1 hr. ^b Oxide ions/g exchangeable in 1 hr at 300°. ^c Reference 16.

hydrocracking of *n*-butane at 550° in unpublished pulse microreactor studies by R. L. Mieville of this laboratory, ranking between H-Zeolon and La-Y. The major problem with this catalyst seems to be that it is easily poisoned by readsorption of H₂O, CO₂, and/or by formation of coke. The high catalytic activity of H-Zeolon may arise from the greater number of exchangeable oxide ions at 300°, but other explanations can also be advanced. The very high protonic acidity of this catalyst is probably catalytically important, and the smaller pore diameters characteristic of H-Zeolon could cause greater adsorption of normal hydrocarbons near cracking temperatures. H-Zeolon may also be less readily poisoned at cracking temperatures by H₂O or other compounds than alumina or La-Y.

The nature of the oxide sites most easily exchanged is not completely clear. Exchange with CO₂ obviously requires activated formation and decomposition of some type of surface carbonate, bicarbonate, or carboxylate structure. This characteristically involves exchange of adsorbed CO₂ with a single reactive oxide ion, rather than multiple exchange with two or more oxide ions before desorption. Adsorbed H₂O molecules could produce similar exchange with CO₂, but experiments (not described) showed that the role of adsorbed water was minor under the conditions of this study. In nearly all cases, exchange of a relatively small number of unusually reactive surface oxide ions occurs at

lower temperatures. The number of exchangeable ions typically increases very rapidly above 500° and, at 600° all surface oxide ions are probably exchangeable.

The formation of stable unidentate or "symmetrical" carbonate bands near 1480 and 1430–1460 cm^{-1} often seems to accompany a marked decrease in the rate of exchange at a given temperature. Such behavior is most evident on Ca–Y, but apparently also occurs on La–Y. A similar process may also occur on alumina, but the spectra were too poor in this region to establish this.

Exchange with, and site blocking by, C^{18}O_2 may be represented as in Figure 12. Here reaction of CO_2 with an oxide ion forms an unstable bridged carbonate or bidentate carbonate. This can either decompose, to give exchange as indicated, or rearrange to form a more stable unidentate carbonate, which temporarily blocks the site. At higher temperatures the stable carbonate can decompose, contributing to the exchange. We are apparently dealing with a broad range of oxide sites, varying in reactivity and tendency to form stable unidentate carbonates. The type of "bridged" or bidentate carbonates responsible for exchange may differ from catalyst to catalyst, or even from point to point on the surface of a given catalyst. Less reactive oxide ions neither exchange oxygen nor give stable carbonates until heated with CO_2 at higher temperatures.

None of the bands for weakly held CO_2 appears to represent sites containing the most readily exchangeable oxide ions. The α sites on γ -alumina and silica–alumina are present at similar concentrations, but alumina shows much greater exchange with C^{18}O_2 . Ca–Y has many more α sites than alumina but gives less exchange. The strength of the binding of CO_2 on α sites, as evidenced by the frequency of adsorb CO_2 , and the splitting of the $\text{C}^{18}\text{O}^{16}\text{O}$ doublet, likewise appears to bear no relation to the ease of oxygen exchange. Probably oxide ions in α sites are not sufficiently reactive toward CO_2 , or are improperly positioned to permit formation of bridged or bidentate carbonate. Rapid exchange of α site oxide on alumina might, however, escape detection because of the low concentration of such sites. The bands below 1500 cm^{-1} usually represent carbonate species too stable to contribute significantly to oxide exchange at temperatures below 400°.

The unstable carbonates important in exchange are probably those which would be expected to give bands in the 1600–1900- cm^{-1} region, but there is no consistent evidence for such bands on catalysts which show ready exchange. The band around 1630 cm^{-1} for CO_2 on Ca–Y could show a possible intermediate, but the band size does not seem to correlate with exchange rate. In the case of γ -alumina, the bands around 1800 and 1640 cm^{-1} probably reflect bridged and bidentate carbonate structures of various types, sufficiently unstable to be effective exchange intermediates. Other catalysts, such as, La–Y or H-Zeolon, which show active exchange with C^{18}O_2 , show no bands in the 1600–1900- cm^{-1} region, however. At this point, it appears impossible to demonstrate a single type of active exchange site for all acidic oxide catalysts.

The sites effective for exchange apparently must permit two-point attachment of carbonate to one or two metal ions and desorption of CO to leave a vacant site containing one or two exposed metal ions which adjoin a reactive oxide ion. Such sites could also be expected to catalyze hydrocarbon reactions, as previously postulated. Reactive oxide ions are, however, apparently neither necessary nor sufficient for all the hydrocarbon reactions characteristic of acidic

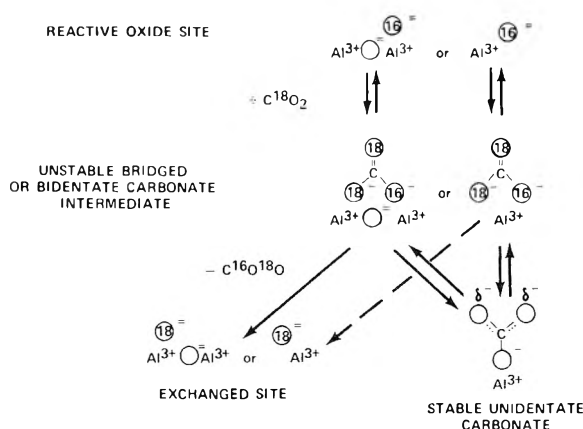


Figure 12. Mechanism for exchange of O.

oxides. Fluoride can apparently replace all the reactive oxide ions which form carbonates of all types on the surface of dry alumina.⁵ This does not eliminate activity for dimerization and polymerization of butene (α sites are not eliminated by fluoride treatment) and probably does not eliminate cracking activity. Likewise the ease of O exchange with CO_2 is not always a dependable indication of activity for "acid-catalyzed" hydrocarbon reactions. Many oxide oxidation catalysts, such as nickel oxide and cuprous oxide, exchange O very readily with CO_2 ¹⁹ and yet are ineffective for cracking or isomerization of hydrocarbons, apparently because they are too easily reduced.

The oxide ions easily exchanged with CO_2 probably normally play an important role in catalytic cracking and in other reactions of hydrocarbons on acidic oxide catalysts. Further study is needed, however, before all details of the structure of the sites on which they are held and of their catalytic role are fully understood.

References and Notes

- (1) Presented at the 167th National Meeting of the American Chemical Society, Los Angeles, Calif., April, 1974.
- (2) J. B. Peri, *Proc. Int. Congr. Catal.*, 3rd, 1964, 2, 1100 (1965).
- (3) J. B. Peri, *J. Phys. Chem.*, 69, 231 (1965).
- (4) J. B. Peri, *J. Phys. Chem.*, 70, 3168 (1966).
- (5) J. B. Peri, *J. Phys. Chem.*, 72, 2917 (1968).
- (6) J. B. Peri, *Discuss. Faraday Soc.*, 52, 55 (1971).
- (7) B. D. Flockhart, J. A. N. Scott, and R. C. Pink, *Trans. Faraday Soc.*, 62, 730 (1966).
- (8) J. G. Larson and W. K. Hall, *J. Phys. Chem.*, 69, 3080 (1965).
- (9) F. H. Van Cauwelaert and W. K. Hall, *Trans. Faraday Soc.*, 66, 454 (1970).
- (10) J. W. Hightower and W. K. Hall, *Trans. Faraday Soc.*, 66, 477 (1970).
- (11) P. C. Saunders and J. W. Hightower, *J. Phys. Chem.*, 74, 4323 (1970).
- (12) M. P. Rosynek, W. D. Smith, and J. W. Hightower, *J. Catal.*, 23, 204 (1971).
- (13) M. P. Rosynek and J. W. Hightower, *Proc. Int. Congr. Catal.*, 5th, 1972, 2, 851 (1973).
- (14) R. J. Kokes, *Proc. Int. Congr. Catal.*, 5th, 1972, 1, 1 (1973).
- (15) J. W. Ward, *Prepr., Div. Pet. Chem., Am. Chem. Soc.*, 16, No. 2, B6–B23 (1971).
- (16) P. D. Hopkins, *J. Catal.*, 12, 325 (1968).
- (17) L. Bertsch and H. W. Habgood, *J. Phys. Chem.*, 67, 1621 (1963).
- (18) J. W. Ward and H. W. Habgood, *J. Phys. Chem.*, 70, 1178 (1966).
- (19) E. R. S. Winter, *Adv. Catal.*, X, 196 (1958).
- (20) J. Nováková, *Catal. Rev.*, 4, 77 (1970).
- (21) G. A. Mills and S. G. Hindin, *J. Am. Chem. Soc.*, 72, 5549 (1950).
- (22) A. G. Oblad, S. G. Hindin, and G. A. Mills, *J. Am. Chem. Soc.*, 75, 4096 (1953).
- (23) J. B. Peri, *Discuss. Faraday Soc.*, 41, 121 (1966).
- (24) J. B. Peri, *J. Phys. Chem.*, 69, 211 (1965).
- (25) J. B. Peri, *J. Phys. Chem.*, 70, 2937 (1966).
- (26) N. D. Parkyn, *J. Catal.*, 27, 34 (1972).
- (27) N. D. Parkyn, *J. Chem. Soc. A*, 410 (1969).
- (28) J. B. Peri, *J. Phys. Chem.*, 69, 220 (1965).
- (29) L. H. Little, "Infrared Spectra of Adsorbed Species", Academic Press, New York, N.Y., 1966, pp 76–84.

Investigations on the Growth of the Zeolite Type NaY

Hartmut Kacirek and Hans Lechert*

Institute of Physical Chemistry of the University of Hamburg, 2 Hamburg 13, West Germany (Received December 13, 1974)

Publication costs assisted by the Institute of Physical Chemistry of the University of Hamburg

In the hydrothermal system $\text{Na}_2\text{O}/\text{Al}_2\text{O}_3/\text{SiO}_2/\text{H}_2\text{O}$ we have studied the growth of faujasite crystals with varying Si/Al ratios using seed crystals of the zeolite NaX and a water glass solution as the silica source. The kinetics of the process of growth of the faujasite from amorphous aluminosilicate gel has been investigated and procedures for the synthesis of faujasites with varying but definite silicon contents are described. It can be shown that the growing of faujasite crystals from nuclei is possible in concentration ranges where nucleation of this or other species is negligible. In a wide range of crystallization, the growth obeys a kinetic law of the order $2/3$.

Introduction

Until now kinetic studies of zeolite growth have been carried out mostly for A-type zeolites. Kerr^{1,2} and Ciric³ found that the growing of A- and X-type zeolites has to be regarded as an autocatalytic process which is in agreement with results received by Breck and Flanigen⁴ and Mirskii and Pirozhkov¹² showing that the formation of zeolites is accelerated by nuclei already present. Detailed studies of Zhdanov⁵ deal with the influence of liquid and solid phases of the hydrothermal system taking also into account the crystal size in his kinetic considerations. Following the arguments of Zhdanov,⁵ Meise and Schwchow⁶ were able to study nucleation and growth of the crystals of A-type zeolites separately, analyzing distribution curves of the particle size and the crystallization curves. Using nuclei for their experiments, they were able to show that the growth can be regarded as a reaction of first order, whereas the nucleation is a reaction of higher order.

Investigations of Culfaz and Sand⁷ deal with the influence of nuclei on the formation of mordenite. In their experiments, nuclei showed only slight influence on the crystallization of A-type and no influence on the crystallization of X-type zeolites.

Besides the composition of the batch, formation of the zeolites are influenced by a number of parameters, e.g., the kind of starting material, the age of the gel, stirring, etc., which have been investigated in various papers.^{4-6,8,9} In order to keep these influences low, studies on the growth of the zeolites were carried out after a concentration equilibrium had been established between the solid and the liquid phases.

Experimental Section

The aluminosilicate gels were prepared from sodium aluminate, sodium hydroxide, and a technical water glass solution ($d = 1.37$). As nuclei we used zeolites of the type NaX of different particle size. We obtained the nuclei from starting solutions of the composition $\text{NaAlO}_2 \cdot n\text{SiO}_2 \cdot m\text{Na}_2\text{O} \cdot p\text{H}_2\text{O}$ ($n = 2 \dots 5$; $m = 1,4 \dots 2,4$; $p = 180 \dots 450$). After formation of the gel, the reaction mixture was stored for a period of a few hours to a few days, sometimes it was stirred or shaken during the reaction time. Crystallization was carried out in polyethylene vessels in a water bath. The course of crystallization was followed by taking small samples from the reaction mixture which were fil-

tered, washed, dried, and analyzed quantitatively by X-ray phase analysis.

The Si/Al ratio was determined by X-ray fluorescence analysis. For some samples, we have carried out an analysis of the particle size distribution. This analysis proved to be necessary for the investigation of the kinetics but also for an exact X-ray phase analysis. To obtain the particle size electron micrographs were produced. The distribution curve was derived by counting the particles of different size. For this procedure, one obtains the curve of the distribution density representing the number $q_0(r)$ of particles with radii between r and $r + dr$ present in the sample. For $q_0(r)$ holds

$$\int_{r_{\min}}^{r_{\max}} q_0(r) dr = 1 \quad (1)$$

The average particle radius is given by

$$\bar{r} = \int_{r_{\min}}^{r_{\max}} r q_0(r) dr \quad (2)$$

For X-ray phase analysis, the average mass of the particles is needed. The distribution density $q_3(r)$ for the mass can be calculated from the above-mentioned distribution density of the radii by

$$q_3(r) = \frac{r^3 q_0(r)}{\int_{r_{\min}}^{r_{\max}} r^3 q_0(r) dr} \quad (3)$$

Now $q_3(r)$ gives the mass of the particles in an interval r to $r + dr$. The average mass can be calculated by

$$\bar{m} = \int_{r_{\min}}^{r_{\max}} r q_3(r) dr \quad (4)$$

Quantitative analysis is performed as follows. From the mixtures of pure faujasite and amorphous aluminosilicate of the same composition, the intensity (peak height \times width at half-peak height) of the (555) peak is obtained by diffraction measurements with the Guinier method with Cu $K\alpha$ radiation and compared with the noise level of the measurements. The noise level has been defined as the connection of lowest intensities between the (551) and the (642) peaks. The measured relative intensities have been plotted against the composition of the dehydrated part of the sample.

The lines in the diffraction pattern are very close together, so that for powders with a low average particle size (because of the broadening of the diffraction lines) a noise level is observed which is too high. Therefore the content of faujasite is obtained as too low. For this reason a correction of the calibration curve has been carried out, measuring the (555) peak for products with $\bar{m} = 0.3 \dots 4.5 \mu\text{m}$ and plotting the relative deviations of the intensity against the average particle size. This procedure will prove to be correct because in the crystallization curves each degree of crystallization can be correlated with an average particle size which can be calculated. Systematic errors of measurement because of different widths of the distribution curves or because of the fact that the particles are mostly polycrystalline are comparatively low and can be neglected.

Results and Discussion

From gels of the composition $\text{NaAlO}_2 \cdot (3 \dots 10)\text{SiO}_2 \cdot m\text{Na}_2\text{O} \cdot 400\text{H}_2\text{O}$ with m in the range $m = 0.33$ to 1.33 at 88° , mainly zeolite of the type NaP1 crystallizes with compositions $\text{NaAlO}_2 \cdot x\text{SiO}_2$ with $x = 1.4$ to 3.5 . Faujasite is only observed as a by-product or in quantities undetectable by X-ray analysis.

Preliminary experiments show that the yield of faujasite can be increased by adding nuclei of NaX to the reaction mixture. Table I shows some examples for different compositions of the products and varying times for complete crystallization with and without additional faujasite nuclei.

The molar ratio $\text{SiO}_2/\text{NaAlO}_2$ of the reaction mixture has been chosen to be 5, the ratio $\text{H}_2\text{O}/\text{AlO}_2 = 400$, and the temperature of crystallization was 88° . NaAl/SiO_2 was varied between 2.6 and 1.2. The amount of the added faujasite nuclei with respect to the whole amount of the crystalline products is 2.5 to 3.0%.

These results show that the addition of faujasite particles accelerates the transition of the amorphous aluminosilicate in crystalline faujasite considerably. Starting with the conception that the increase of the volume of the particles is proportional to the free surface $\bar{O}(x)$ of the NaX or NaY particles being available for the members of the solution, one obtains from

$$V = \frac{xM\sum n_i}{D}$$

a formulation of the kinetic equation

$$\frac{dx}{dt} = K\bar{O}(x) \frac{D}{M\sum n_i} \quad (5)$$

where D represents the density of the faujasite of the composition $\text{NaAlO}_2 \cdot n\text{SiO}_2$; M is the formal molecular weight of a formula unit $\text{NaAlO}_2 \cdot n\text{SiO}_2$; $\sum n_i = [\text{NaAlO}_2 \cdot n\text{SiO}_2]_{\text{faujasite}} + [\text{NaAlO}_2 \cdot n\text{SiO}_2]_{\text{amorphous}} + [\text{NaAlO}_2 \cdot n\text{SiO}_2]_{\text{cryst by-products}}$; x represents the mole fraction of the amount of faujasite

$$x = \frac{[\text{NaAlO}_2 \cdot n\text{SiO}_2]_{\text{faujasite}}}{\sum n_i}$$

The above formulation of the kinetic equation starts with the assumption that the compositions of the different components in the solid phase does not differ considerably. This can be shown to be the case after aging the gel for a suitable time if one starts with water glass as a silica source.

At equilibrium, the Si/Al ratio in the solid phase is determined by the pH and the $\text{SiO}_2/\text{AlO}_2^-$ ratio of the solution. From eq 5 follows

TABLE I: Comparison of the Quantities of Synthetic Faujasite Grown from Different Batches^a

Samples	Na-Al/ Si	$\frac{a}{\%}$ NaY	\bar{c} NaP1	Si/Al	Time, hr	Add. of seeds
1/11	2.6	98	2	1.52	17	+
1/12	2.6	99		1.54	11	+
0/53	2.6	5	95	1.48	20	-
0/61	2.6	75	25	1.49	18	-
1/21	2.2	90	6	1.63	16	+
1/22	2.2	95	5	1.65	12	+
0/55	2.2	2	98	1.60	25	-
0/71	2.2	70	30	1.63	22	-
1/31	1.8	85	2	1.85	22	+
1/32	1.8	99		1.87	19	+
0/56	1.8	7	90	1.73	28	-
0/73	1.8	15	85	1.71	28	-
1/41	1.6	96	4	1.90	20	+
1/42	1.6	85	3	1.37	16	+
0/57	1.6	20	80	1.78	35	-
0/74	1.6	25	75	1.76	33	-
1/51	1.4	96	2	1.97	24	+
1/52	1.4	88	2	1.91	24	+
0/63	1.4	7	93	2.01	48	-
0/75	1.4	3	95	2.00		-
1/61	1.2	82	4	2.14	30	+
1/62	1.2	80	3	2.11	30	+
0/64	1.2	15	85	2.09	48	-

^a (+) With addition of seed crystals, (-) without addition of seed crystals.

$$\frac{dx}{dt} = k\bar{O}(x)Z \frac{D}{M\sum n_i} \quad (6)$$

in case the particle number Z is constant in the course of the crystallization. Later this assumption will prove to be correct. Now $\bar{O}(x)$ represents the average surface of a particle. Because of

$$\bar{O}(x) = (\bar{m}(x))^{2/3}(4\pi)^{1/3}3^{2/3}D^{-2/3}$$

and

$$x = \frac{\bar{m}(x)Z}{M\sum n_i}$$

holds

$$\frac{dx}{dt} = kx^{2/3}D^{1/3}(M\sum n_i)^{-1/3}(4\pi)^{1/3}3^{2/3} \quad (7)$$

and because of

$$\frac{D}{M\sum n_i} = \frac{x_0}{\sqrt[3]{3\pi}\bar{r}_0 Z}$$

$$\frac{dx}{dt} = 3kx^{2/3}x_0^{1/3}\bar{r}_0^{-1} \quad (8)$$

By rearrangement and integration follows from the starting conditions

$$\int_{x_0}^x x^{2/3} dx = 3kx_0^{1/3}\bar{r}_0 \int_0^t dt \quad (9)$$

$$3(x^{1/3} - x_0^{1/3}) = 3kx_0^{1/3}\bar{r}_0^{-1}t \quad (10)$$

for x follows

$$x = x_0 + 3k\frac{x_0}{\bar{r}_0}t + 3k^2\frac{x_0}{\bar{r}_0^2}t^2 + k^3\frac{x_0}{\bar{r}_0^3}t^3 \quad (11)$$

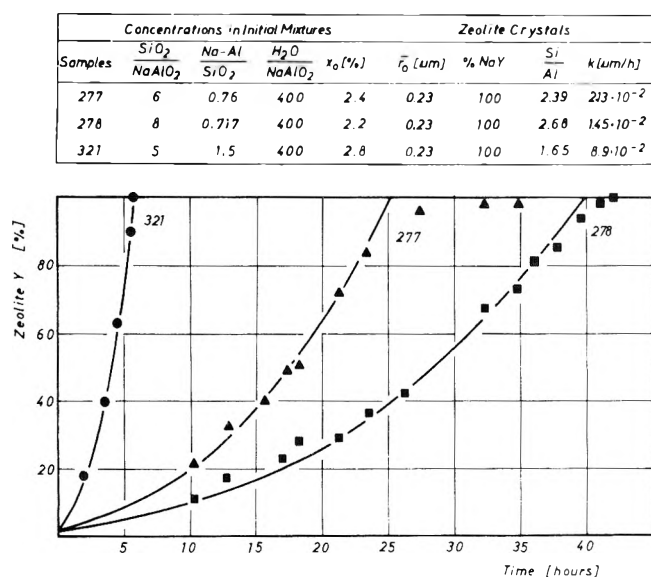


Figure 1. Growth of faujasite crystals as a function of time for different gel compositions using seeds with $\bar{r}_0 = 0.23 \mu\text{m}$.

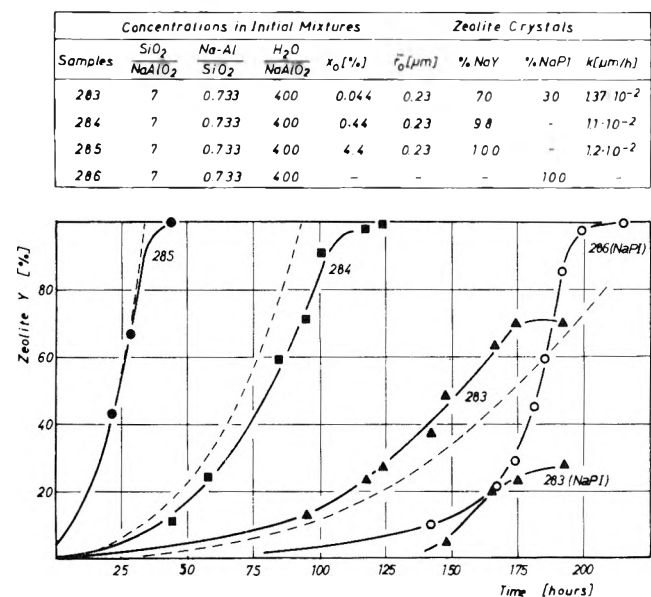


Figure 2. Growth of faujasite crystals as a function of time for one gel composition using different quantities of seeds with $\bar{r}_0 = 0.23 \mu\text{m}$.

For the reaction constant k follows

$$\bar{k} = \left(3 \sqrt{\frac{\bar{x}}{x_0}} - 1 \right) \frac{\bar{r}_0}{t} \quad (12)$$

k has the dimension (length/time), therefore it describes the linear growth of a particle in a time unit. Figure 1 shows the validity of eq 11 for some examples. The curves demonstrate the calculated course of the crystallization. In further experiments with starting mixtures of the same composition, the mole fraction x_0 of the nuclei has been varied. The temperature of crystallization has been 83° . The velocity constants k of eq 11 should be equal for the experiments 283 to 285. The dotted curves in Figure 2 show the calculated curve with $k = 1.22 \times 10^{-2} \mu\text{m}/\text{hr}$. The agreement with the measured values proves to be very

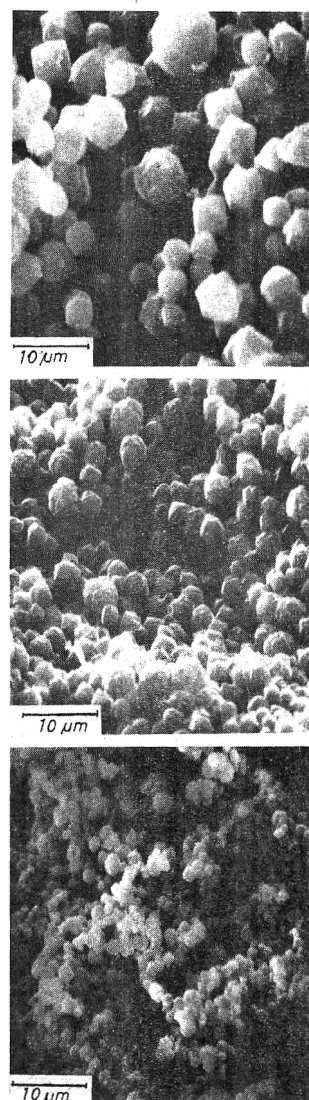


Figure 3. Raster scan micrographs of NaY particles grown from different quantities of seed crystals.

good. For samples 283 and 286 the crystallization curves for the growth of NaP1 have been drawn. For the derivation of eq 11, the assumption has been made that the number of particles Z in the course of the crystallization is constant.

In samples 283, 284, and 285 with the initial concentrations of faujasite nuclei 1:10:100, the average volumes \bar{V}_E of the crystalline products $\bar{V}_E(283): \bar{V}_E(284): \bar{V}_E(285): V_0$ should be 100:10:1:0.044 when only faujasite growth occurs. For the measured amounts of NaY the ratios should be 70:9.8:1:0.044 corresponding to the ratios of the average radii \bar{r}_E of 4.12:2.14:1:0.353. In Figure 3, the raster scan micrographs show the crystals of the products 283, 284, and 285 at the same magnification. Figure 4 shows the distribution density curves. Because of the considerable degree of inexactness in the calculation of the particle size distribution, the counting of the weighted mean particle size $\bar{r}_{1,3}$ has no advantage. Taking simply the maxima of the distribution curve instead of $\bar{r}_{1,3}$, the resulting average radii of samples 283, 284, and 285 are 27, 1.25, and $0.6 \mu\text{m}$, respectively. For the seed crystals, a value of $0.225 \mu\text{m}$ is obtained. The resulting ratios of the average radii of 4.3:2.1:1:0.37 are in good agreement with the above calculated ratios for $Z =$

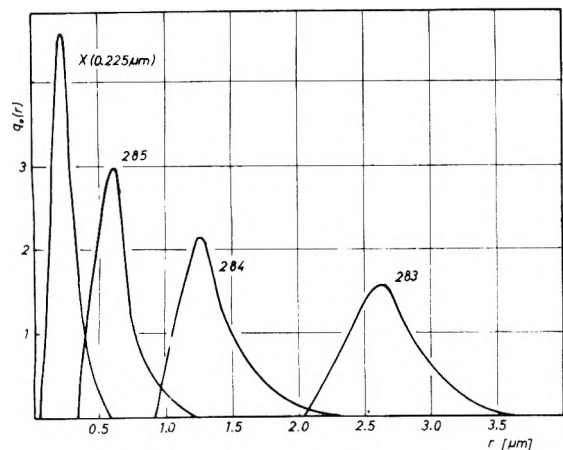


Figure 4. Distribution density curve of NaY particles grown from different quantities of seed crystals.

Concentrations in Initial Mixtures										
Samples	SiO ₂	Na-Al	H ₂ O	x ₀ [%]	r ₀ [μm]	Si	k [μm/h]	τ _{1/2} [h]	τ _{1/2} [h] (calc.)	
	NaAlO ₂	SiO ₂	NaAlO ₂			Al				
255	5	1	400	2.6	0.23	2.00	5.0 · 10 ⁻²	8.45	extr.	87.5
256	5	1	400	2.6	0.45	2.02	4.6 · 10 ⁻²	16.5		15.8
257	5	1	400	2.6	2.5	1.95	4.9 · 10 ⁻²	7.7		7.9

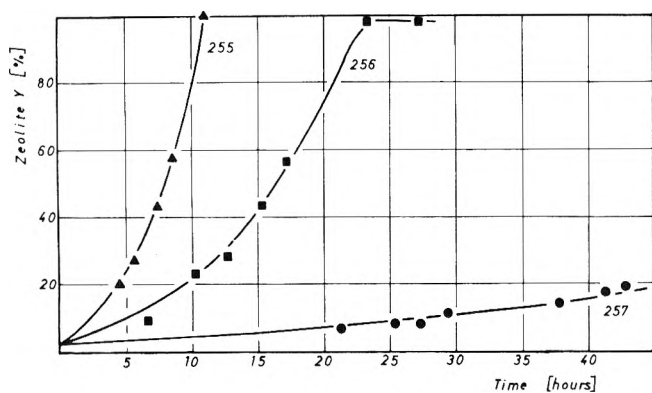


Figure 5. Growth of faujasite as a function of time from one gel composition using the same quantities of seeds with different radii.

constant of 4.12:2.14:1:0.353. (In the course of the counting procedure, only NaY particles have been considered which can be distinguished from NaP1 particles by their shape.) Because of the heterogeneous distribution of the seeds, not all particles grow with the same rate, as can be observed from the broadening of the distribution density in Figure 4. Therefore, the rate constant *k* describes an average rate.

In the course of the synthesis of samples 255, 256, and 257, *x*₀ was kept constant and *r*₀ was varied. For different starting mixtures it can be concluded from eq 11 that *r*₀ ~ *t*(*x*) referring to the same degree of crystallization.

The times *t* = τ_{1/2} = *f*(*x* = 0.5) in which half of the material has crystallized should have the ratios 11.1:2:1 for mixtures 255, 256, and 257. The table accompanying Figure 5 shows good agreement with the predicted values of the half reaction time using *k* = 4.8 × 10⁻² μm/hr. Figure 6 shows the stereo scan of the seed crystals used. In Figure 7 the corresponding particle size distributions are demonstrated.

The experiments described until now show the following. The amount of nuclei and also their size are of central importance in the synthesis of faujasite. Under wide ranges of

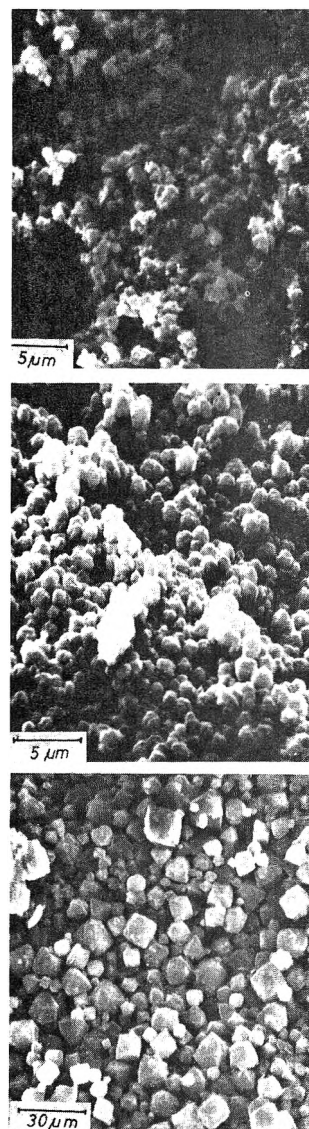


Figure 6. Raster scan micrographs of NaX crystals with *r*₀ = 0.23, 0.45, and 2.5 μm used as seed crystals.

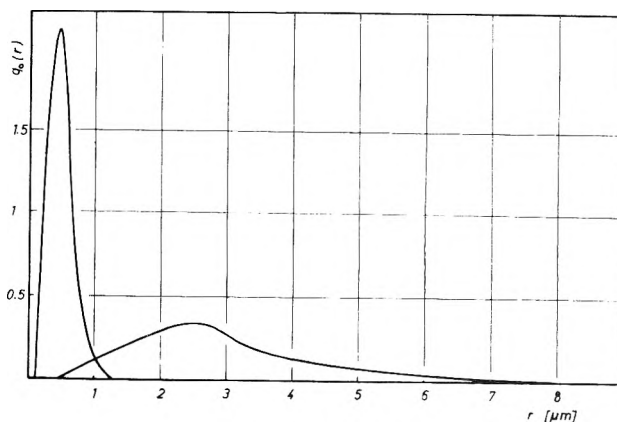


Figure 7. Distribution density of NaX particles used as seed crystals.

crystallization conditions, the growth of faujasite is independent of the concentration of the gel. Only at the end of the crystallization process, the rate of dissolution of the amorphous aluminosilicate gel can become the rate-deter-

TABLE II: Quantities of NaY Grown from Different Batches where Seed Crystals Were Added before Gelling

Samples	SiO ₂ / NaAlO ₂	Na-Al/ SiO ₂	% NaY	Time, hr (at 88°)
222	4	0.835	8	120
223	5	0.780	6	120
224	6	0.760	4	168
225	7	0.733	3	168
226	8	0.717	5	430
230	10	1.00	11	66
232	10	0.80	6	161
236	10	1.00	4	50
238	10	0.80	3	135

mining step which has the consequence of the concentration in the solution. Equation 11 then is no longer valid.

The validity of eq 11 is extended, the more the better the seed crystals dispersed in the gel. The crystallization can be followed by X-ray phase analysis until all amorphous aluminosilicate has vanished from the reaction mixture. Slight progress takes place until a concentration equilibrium between the faujasite and the solution has been established. The rate of transition of faujasite in NaP1 is comparatively low and can be neglected herein. Further parameters influencing the rate constant k shall be treated in another paper.

A further impressive proof of the fact that growth of the crystals only occurs at the interface of the crystals and the solution, and a direct transition of the gel into the crystalline state must be excluded, is evident from the following experiments. In the mixtures of Table II, the nuclei have not been introduced into the gel after some aging but were suspended in the solution before gelling. In this case gelling takes place at the surface of the nuclei preventing the development of the interface crystal solution. In the course of the preparation of the samples 222 to 226 and 230 to 232, the nuclei have been suspended in a diluted water glass solution, in the preparation of the samples 236 to 238, the suspension of the nuclei was done in the sodium aluminate solution. The amount of faujasite nuclei was between 2.1 and 2.6%, their average radius $\bar{r}_0 = 0.45 \mu\text{m}$. Table II shows the contents of faujasite. The rest of the samples consisted of NaP1 and some percent of amorphous aluminosilicate. It can be observed that the catalytic activity of the nuclei is lost completely. Even after long periods of crystallization, products are obtained as in the case of a reaction without nuclei. Therefore, in agreement with the papers of Kerr,^{1,2}

TABLE III: Quantities of NaY and NaP1 Grown from Different Batches where Seed Crystals Were Added after Gelling

Sam- ples	SiO ₂ / NaAlO ₂	Na-Al/ SiO ₂	% NaY	% NaP1	Si/Al	Time, hr
233	10	0.76	96		2.78	90
241	10	0.72	100		2.97	190
243	10	0.71	95	5	3.00	312
245	10	0.70	95	3	3.24	330

we state that a direct solid-solid transformation of amorphous substrate to crystalline product does not occur.

In Table III some mixtures are described which are set up under the same conditions, but the nuclei are added some hours after the formation of the gel. The autocatalytic effect is fully active.

The investigations described show that it is possible to obtain faujasite of any desired purity in a wide range of composition taking a small amount of nuclei to start the crystallization. The particle size distribution can be adjusted in wide ranges, too.¹¹ The faujasite can be brought to complete crystallization before nucleation of any other species of zeolites takes place.

The synthesis can be carried out with use of solutions of sodium silicate only. Because the kind of solution has no influence on this method of preparation, the mother liquor can be used directly for a new run of crystallization.

Detailed studies on the influences on the rate constant and energetical aspects of the nucleation and the growth of the nuclei (in preparation) give a deeper insight into the mechanism of zeolite growth which can be extended to other hydrothermal systems.

References and Notes

- (1) G. T. Kerr, *J. Phys. Chem.*, **72**, 1385 (1968).
- (2) G. T. Kerr, *J. Phys. Chem.*, **70**, 1047 (1966).
- (3) J. Ciric, *J. Colloid. Interface Sci.*, **28**, 315 (1968).
- (4) E. W. Breck and E. M. Flanigen, "Molecular Sieves", Society of Chemical Industry, London, 1968, p 47.
- (5) S. P. Zhdanov, *Adv. Chem. Ser.*, **No. 101**, 20 (1971).
- (6) F. E. Schwochow and F. Meise, *Adv. Chem. Ser.*, **No. 121**, 152 (1973).
- (7) A. Culfaz and L. B. Sand, *Adv. Chem. Ser.*, **No. 121**, 152 (1973).
- (8) F. Polak and A. Cichocki, *Adv. Chem. Ser.*, **No. 121**, 209 (1973).
- (9) S. P. Zhdanov, "Molecular Sieves", Society of Chemical Industry, London, 1968, p 12.
- (10) K. Leschonski, W. Alex, and B. Koglin, *Chem. Ing. Tech.*, **46** 1, 23 (1974).
- (11) H. Lechert and H. Kacirek, application of patent, No. P 2324 235 5 (1973).
- (12) Y. V. Mirskii and V. V. Pirozhkov, *Russ. J. Phys. Chem.*, **44**, 1508 (1970).

Crystallographic Evidence for Hydrolysis in Zeolites. The Structure of Hydrated Partially Cobalt(II)-Exchanged Zeolite A

Paul E. Riley and Karl Seff*

Chemistry Department, University of Hawaii, Honolulu, Hawaii 96822
(Received May 13, 1974; Revised Manuscript Received March 7, 1975)

Publication costs assisted by the National Science Foundation

The crystal structure of a fully hydrated, partially Co(II)-exchanged form of the synthetic molecular sieve zeolite A, $\text{Co}_{0.33}\text{Na}_{0.33}[\text{AlSiO}_4]\text{-A}$, stoichiometry $\text{Co}_4\text{Na}_4\text{Al}_{12}\text{Si}_{12}\text{O}_{48}\cdot x\text{H}_2\text{O}$ (x ca. 35) per unit cell, has been determined from three-dimensional X-ray diffraction data gathered by counter methods. The structure was solved and refined in the cubic space group $Pm\bar{3}m$: $a = 12.267(5)$ Å at $19(1)^\circ$. Cobalt(II) ions are located at two distinct crystallographic sites. One Co(II) ion (Co(1)) resides in the sodalite unit where it is coordinated by a regular octahedron of water molecules (Co(1) to $\text{H}_2\text{O} = 2.11(3)$ Å); the other three Co(II) ions (Co(2)) are distributed about equivalent sites on unit cell threefold axes. These Co(2) ions apparently promote an extensive hydrolysis of the aluminosilicate framework, and stoichiometrically produce Brønsted acid sites. Structural evidence suggests that each Co(2) ion is responsible for the addition of three water molecules to the zeolite framework, probably with the dissociation of one proton per water molecule, to form three Co(2)-O-(Si,Al) bridges to each Co(2). To achieve each Co(2)-O-(Si,Al) linkage, one (Si,Al) atom, probably Al, has increased its coordination number from four to five. The Co(2)-O bonds of the resultant Co(2)-O-(Si,Al) bridges are long ($2.36(3)$ Å), probably a virtual result due to Co(2) disorder about the threefold axis position, but the (Si,Al)-O bonds, probably Al-O bonds, are normal ($1.74(3)$ Å). Each Co(2) ion is coordinated at a fourth position by a water molecule which projects well into the large cage. Three of the four Na^+ ions per unit cell are located at two sites of threefold symmetry, close to triads of framework oxygen atoms. A fourth Na^+ ion apparently has selected a position in the large cage, at a site of fourfold symmetry. Altogether, the positions of 35 water molecules per unit cell have been determined. Full-matrix least-squares refinement using 291 reflections for which $I_0 > 3\sigma(I_0)$ has converged to a conventional R index (on F) of 0.072.

Introduction

Successful exploitation of the well-known selective sorptive and catalytic properties¹ of crystalline aluminosilicate zeolites relies heavily upon an appreciation of the structural features of these molecular sieves; i.e., the dimensions of zeolitic channels and cages, the locations of the exchangeable cations and their interactions with the zeolitic framework at those locations, and the nature of the active sites that may have been formed by modification of the aluminosilicate framework. To this end, a number of first row transition-metal-exchanged zeolite A systems (zeolite nomenclature and structure are described in ref 2) of stoichiometry $\text{M}_z\text{Na}_{12-2z}\text{Al}_{12}\text{Si}_{12}\text{O}_{48}\cdot x\text{H}_2\text{O}$ per unit cell, where $\text{M} = \text{Mn(II)}$, Co(II) , Ni(II) , or Zn(II) and $2.5 \leq z \leq 5.5$, have been examined by single-crystal X-ray diffraction techniques in our laboratory. Diffraction experiments have been carried out with these materials in both their hydrated and dehydrated forms,³⁻⁷ as well as following sorption of a variety of small molecules (principally with the Mn(II)- and Co(II)-containing zeolites^{4,7-9}).

The results attained from the hydrated work alone suggest a diverse zeolite "aqueous" chemistry that varies as the exchangeable cation. For example, Mn(II) and Zn(II) ions adopt quite different coordination environments within the zeolite; the Mn(II) ions³ favor trigonal bipyramidal coordination, but the two crystallographically distinct kinds of Zn(II) ions⁵ select tetrahedral coordination. In both of these structures, however, these ions share a common feature—they are tightly bound to zeolite framework

oxygen atoms. (Actually, this is true for 4.5 of the 5.5 Zn(II) ions per unit cell; the remaining Zn(II) ion, at the unit cell origin, is far from the framework.) By coordinating directly with framework oxygen atoms, the Mn(II) and Zn(II) ions act much like the Na^+ ions of unexchanged zeolite 4A¹⁰ and the T1(I) ions of fully T1(I)-exchanged zeolite A.¹¹

However, preliminary studies quickly revealed that the Co(II) and Ni(II) ions of their respective zeolite systems depart radically from this behavior. These ions are too far (2.8 to 2.9 Å) from the framework oxygen atoms, as usually located, to coordinate to them. To explain this anomaly, the crystal structure of the Co(II) system, $\text{Co}_4\text{Na}_4\text{Al}_{12}\text{Si}_{12}\text{O}_{48}\cdot x\text{H}_2\text{O}$ (x ca. 35) per unit cell, or $\text{Co}_{0.33}\text{Na}_{0.33}[\text{AlSiO}_4]\text{-A}$ (exclusive of water molecules) in conventional nomenclature,^{2b} was studied. (The structure of the Ni(II)-exchanged form of zeolite A, $\text{Ni}_{2.5}\text{Na}_7\text{Al}_{12}\text{Si}_{12}\text{O}_{48}\cdot y\text{H}_2\text{O}$, is available elsewhere.⁶)

Experimental Section

Single crystals of zeolite 4A, $\text{Na}[\text{AlSiO}_4]\text{-A}$ (exclusive of water molecules), or $\text{Na}_{12}\text{Al}_{12}\text{Si}_{12}\text{O}_{48}\cdot 27\text{H}_2\text{O}$ per unit cell, were grown as colorless cubes by the method of Charnell.¹² Ion exchange with aqueous 0.1 M $\text{Co}(\text{NO}_3)_2$ as previously described⁴ yielded pink-tan colored cubes of appropriate composition as established by elemental analysis. A relatively large single crystal, about 0.08 mm along an edge, was selected for X-ray diffraction studies. It was mounted at the tip of a glass fiber and maintained at $19(1)^\circ$ and 30% relative humidity during the X-ray experiments.

Previous crystallographic studies in this laboratory^{2a,11} have indicated that the space group $Pm\bar{3}m$ (cubic system; no reflections systematically absent) is suitable for our crystals, although it cannot distinguish between ordered Si and Al atoms, and is therefore only approximately correct. Gramlich and Meier¹⁰ have reported that for the hydrated unexchanged form of sodium zeolite 4A, the cubic space group $Fm\bar{3}c$ is appropriate. However, only a few very weak superlattice reflections (indicative of an F -centered unit cell with a doubled lattice constant) were noted in our work with this Co(II)-containing material, and most of these violated the systematic absence rules of $Fm\bar{3}c$.

All diffraction experiments were performed with an automated, four-circle Syntex $P\bar{1}$ diffractometer, equipped with a graphite monochromator and a pulse-height analyzer. Molybdenum radiation ($K\alpha_1$, λ 0.70926 Å; $K\alpha_2$, λ 0.71354 Å) was employed for preliminary experiments and for data collection as well. The cubic unit cell constant at 19 (1)°, as determined by least-squares refinement of 15 intense reflections for which $20^\circ < 2\theta < 24^\circ$, is 12.267 (5) Å.

Reflections were examined by the $\theta - 2\theta$ technique at a constant scan speed of 0.5 deg min⁻¹. Initially each reflection was scanned symmetrically, i.e., from 1.0° (in 2θ) below the calculated $K\alpha_1$ peak to 1.0° above the calculated $K\alpha_2$ peak. However, after about two-thirds of the data had been gathered, an asymmetric scan (1.0° below the $K\alpha_1$ peak to 1.3° above the $K\alpha_2$ peak) was utilized to compensate for a minor misorientation of the crystal. Background intensity was examined at each end of the scan range for a time equal to half the time necessary to measure the reflection. As a check on crystal and instrument stability, the intensities of three reflections in diverse regions of reciprocal space were recorded after every 100 reflections initially; when the asymmetric scan was used, these check reflections were remeasured after every 25 reflections. No systematic variations in intensity were observed for the check reflections.

All reciprocal lattice points within the sphere defined by $2\theta < 70^\circ$ were examined. Although few reflections are significantly greater than background for high 2θ values, this limit was chosen to maximize the size of the relatively small data set.

Standard deviations were assigned in accordance with the expression

$$\sigma(I_0) = [\omega^2(CT + B_1 + B_2) + (\rho I_0)^2]^{1/2}$$

where ω is the scan rate, CT is the total integrated count, B_1 and B_2 are the background counts, and the intensity I_0 is computed as $I_0 = \omega(CT - B_1 - B_2)$. A value of 0.02 has been found satisfactory for the empirical parameter p .^{11,13} The data were corrected for Lorentz and polarization effects,¹⁴ including that due to reflection from the monochromator crystal, which was assumed to be half perfect and half mosaic in character. An absorption correction was not made; the linear absorption coefficient is 14.0 cm⁻¹, and the transmission factors varied only slightly, from 0.855 to 0.870. Of the 883 reflections measured, the 291 with intensities I_0 for which $I_0 > 3.0\sigma(I_0)$ ¹⁵ were used in subsequent structural analysis.

Structure Determination and Solution

Full-matrix least-squares refinement was commenced using the zeolite framework ((Si,Al), O(1), O(2), and O(3); see Figure 1) atomic parameters of hydrated Tl(I)-exchanged¹¹ zeolite A. (Because of the indistinguishability of

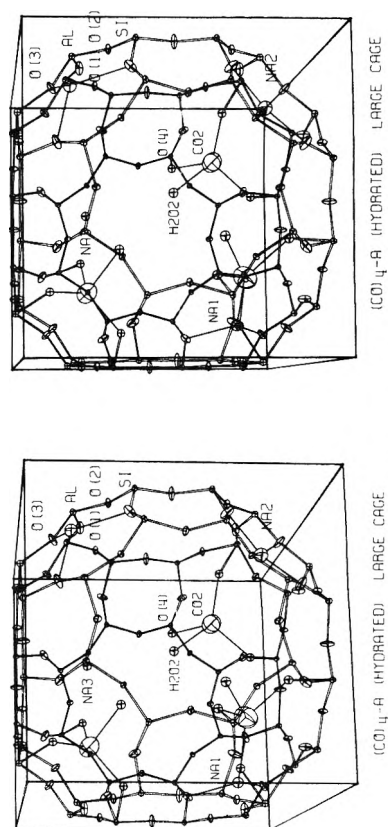


Figure 1. A stereoview of the unit cell. Heavy bonds indicate coordination about the Co(II) ion. Ellipsoids of 20% probability are used.

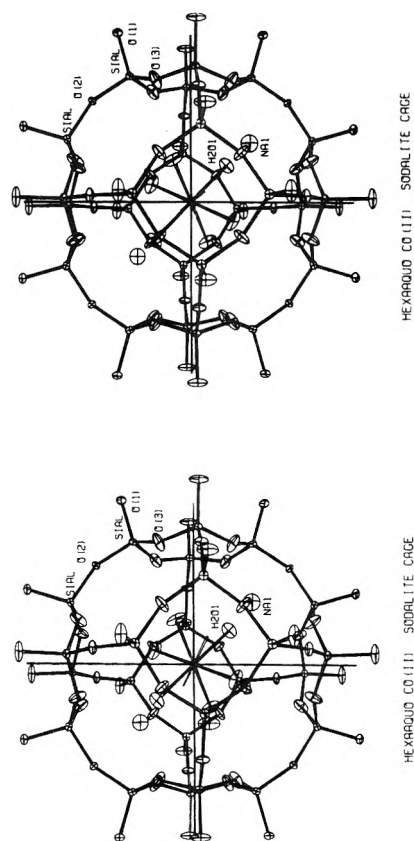


Figure 2. A stereoview of the octahedral coordination about the Co(II) ion in the small cage. Ellipsoids of 30% probability are used. To produce a physically meaningful drawing, the thermal parameter β_{23} for H₂O(1) is reduced by 1.0 σ .

SiO₄ and AlO₄ tetrahedra (vide supra), only the average species, (Si,Al), is considered in this work.) From a subsequent difference Fourier function, the four Co(II) ions were located; one at the unit cell origin (Co(1)) and the remaining three (Co(2)) in the large central cage on the unit cell threefold axes at $x = y = z = 0.25$ (equipoint Wyckoff 8(*g*)). Inclusion of these positions in isotropic least-squares refinement led to convergence with error indices $R_1 = \sum |F_o - |F_c|| / \sum F_o = 0.16$ and $R_2 = (\sum w(F_o - |F_d|)^2 / \sum w F_o^2)^{1/2} = 0.15$.

In the least-squares treatment, the quantity minimized is $(\sum w(F_o - |F_d|)^2)^{1/2}$ and the weights (w) are the reciprocal squares of $\sigma(F_o)$, the estimated standard deviation of each observation. Atomic scattering factors for O⁻ and (Si,Al)^{1.75+} for the zeolite framework, Co²⁺ and Na⁺ for the exchangeable cations, and O⁰ for water oxygen atoms were used.¹⁶ (The function describing (Si,Al)^{1.75+} is the mean of the Si⁰, Si⁴⁺, Al⁰, and Al³⁺ scattering functions.) The scattering factors for (Si,Al)^{1.75+} and Co²⁺ were modified to account for the real parts ($\Delta f'$) of the anomalous dispersion correction.¹⁷

A difference Fourier synthesis using framework atomic and Co(II) positions indicated a variety of positions which could be attributed to Na⁺ ions and H₂O molecules. The most significant of these had densities between 1.0 and 3.0 e Å⁻³. Several criteria were to be fulfilled before the conclusions suggested by the subsequent least-squares treatment were accepted. First, the peaks were to refine close to their initially estimated positions; also the occupancies of these sites should be chemically meaningful and the corresponding thermal parameters should be realistic; finally, the resultant positions should make suitable approaches to well-established parts of the structure (e.g., framework atoms, exchangeable ions, or water molecules).

Application of these conditions resulted in the acceptance of a few positions. Six water molecules (H₂O(1)'s, see Table I) which describe a regular octahedron about the Co(1) ion were located in the small cage (see Figure 2). Two Na⁺ ions (Na(1)'s) were located at the surface of the small cage, along threefold axes near the centers of the oxygen six-windows, a position selected by Na⁺ ions in the dehydrated form of this Co(II)-containing zeolite.⁴ (An oxygen six-window, as shown in Figure 3, is composed of six alternating (Si,Al) atoms and six oxygen atoms conjoined so as to form a puckered twelve-membered aluminosilicate ring.) A third Na⁺ ion (Na(2)) was also observed at a threefold axis site, but in the large cage. The remaining Na⁺ ion (Na(3)) apparently occupies a position in the large cage, along a fourfold axis passing through the center of a unit cell face.

The closest approaches to the three equivalent Co(II) ions (Co(2)'s) in the large cage are made by three sets of three equivalent oxygen atoms (O(4)'s), located at general positions. These O(4) atoms act as bridges and are in turn bonded to (Si,Al) cations (probably to Al) of the framework. Although some water molecules in the large cage may coordinate the Co(2) ions so that more complete coordination spheres are achieved, only one other position (H₂O(2)) refined at a satisfactory distance from the Co(2) ions, indicating that the Co(2) ions are only four coordinate.

Of the remaining Fourier peaks (all with densities between 1 and 2 e Å⁻³), only those designated as water molecules H₂O(3), -(4), -(5), and -(6) in Table I behaved properly in least-squares refinement, and also fulfilled the conditions listed above. From consideration of thermal param-

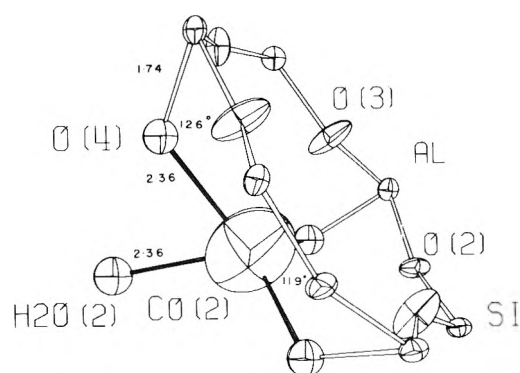


Figure 3. Coordination of a Co(2) ion in the large cage. Ellipsoids of 50% probability are used.

eters (Table I) and spatial limitations, we conclude that altogether these peaks correspond to approximately 17 water molecules.

In the last cycle of least-squares refinement, the framework atoms, the three threefold axis Co(2) ions, and the H₂O(1) molecules were treated anisotropically, and all remaining species of Table I were treated isotropically. Convergence was attained with $R_1 = 0.072$, $R_2 = 0.073$, and a goodness-of-fit, $(\sum w(F_o - |F_d|)^2 / (m - s))^{1/2}$ of 1.33, where m (291) is the number of observations and s (60) is the number of variables in least-squares refinement. In this final cycle of refinement, shifts in positional and thermal parameters were all less than 1% of their corresponding estimated standard deviations except for some H₂O(5) and H₂O(6) parameters; for these all shifts were less than 2% of their corresponding esd's.

A subsequent difference Fourier function revealed five peaks of densities 0.7–1.7 e Å⁻³. Upon least-squares refinement, the three shallowest peaks shifted greatly in position, and therefore were not regarded as meaningful features of the structure. The two remaining, more significant positions (1.0 and 1.7 e Å⁻³), located near the center of the large cage and separated from one another by about 1.8 Å, diverged in least-squares refinement, requiring thermal parameters of 20–40 Å² for low occupancies. These two peaks are reasonably far from other parts of the structure, and perhaps as suggested by Gramlich and Meier¹⁰ who observed similar residual electron density in their work with sodium zeolite A, this may be due to a small number of unresolvable water molecules. Accordingly, these two peaks along with the three mentioned above were not included in final structural calculations. On this final difference Fourier map the standard deviation of the electron density was calculated to be 0.10 e Å⁻³.

Final position, thermal, and occupancy parameters are presented in Table I; bond lengths and bond angles in Table II. A listing of $10F_o$ and $10F_c$ is available.¹⁸

Discussion

The four Co(II) ions per unit cell are located at two sites (see Figures 1 and 2, and Table I): one cation, Co(1), is at the unit cell origin (at the center of the sodalite unit), and the remaining three, Co(2)'s, are on the unit cell body diagonals (sites of threefold symmetry) in the large cavity. The Co(1) ion is coordinated by a regular octahedron of water molecules, H₂O(1)'s, at distances of 2.11 (3) Å (see Table II), in agreement with the mean bond length reported for CoSO₄·6H₂O (2.11 Å).¹⁹ Each H₂O(1) oxygen atom lies on a

TABLE I: Positional, Thermal, and Occupancy Parameters for Hydrated $\text{Co}_{0.33}\text{Na}_{0.33}[\text{AlSiO}_4]\text{-A}^a$

Wyckoff position	x	y	z	β_{11} or B_{iso}	β_{22}	β_{33}	β_{12}	β_{13}	β_{23}	Occ - occupancy factor	
(Si, Al)	24(k)	0	1833(2)	3706(2)	23(2)	23(1)	14(1)	0	0	6(2)	1 ^b
O(1)	12(h)	0	2204(10)	1/2	110(14)	31(8)	15(6)	0	0	0	1
O(2)	12(i)	0	2963(5)	2963(5)	54(9)	17(4)	17(4)	0	0	11(9)	1
O(3)	24(m)	1106(6)	1106(6)	3418(8)	45(4)	45(4)	77(9)	55(10)	57(9)	57(9)	1
Co(2)	8(g)	2665(24)	2665(24)	2665(24)	262(20)	262(20)	262(20)	85(56)	85(56)	85(56)	3/8
H ₂ O(1)	24(m)	595(29)	1144(16)	1144(16)	92(34)	55(19)	55(19)	-73(29)	-73(29)	-91(41)	1/4
Co(1)	1(a)	0	0	0	0.8(1)						1
Na(1)	8(g)	1575(29)	1575(29)	1575(29)	5(1)						1/4
Na(2)	8(g)	2106(75)	2106(75)	2106(75)	6(3)						1/8
Na(3)	6(f)	2361(81)	1/2	1/2	5(2)						1/6
O(4)	48(n)	1195(26)	2566(23)	3897(24)	2.3(5)						3/16
H ₂ O(2)	48(n)	3006(77)	3804(78)	4173(75)	3(2)						1/16
H ₂ O(3)	48(n)	2387(56)	2898(63)	4710(68)	10(3)						3/16
H ₂ O(4)	24(m)	382(151)	4544(99)	4544(99)	8(7)						1/12
H ₂ O(5)	48(n)	1909(158)	3594(171)	4797(254)	9(6)						1/16
H ₂ O(6)	48(n)	1468(111)	4021(130)	4317(133)	6(4)						1/16

^a Positional and anisotropic thermal parameters are given $\times 10^4$; isotropic thermal parameters are given in (ångström)². Numbers in parentheses are the estimated standard deviations in the last significant digits. See Figure 1 for the identities of the atoms. The anisotropic temperature factor = $\exp[-(\beta_{11}h^2 + \beta_{22}k^2 + \beta_{33}l^2 + \beta_{12}hk + \beta_{13}hl + \beta_{23}kl)]$. ^b Occupancy for (Si) = 1/2; occupancy for (Al) = 1/2.

TABLE II: Selected Interatomic Distances (Å) and Angles (deg)^a

(Si, Al)-O(1)	1.652(4)	O(1)-(Si, Al)-O(2)	107.3(4)
(Si, Al)-O(2)	1.658(3)	O(1)-(Si, Al)-O(3)	110.6(4)
(Si, Al)-O(3)	1.661(3)	O(1)-(Si, Al)-O(4)	74(1)
(Si, Al)-O(4)	1.736(31)	O(2)-(Si, Al)-O(3)	109.4(5)
		O(2)-(Si, Al)-O(4)	69(1)
Na(1)-O(2)	3.09(2)	O(3)-(Si, Al)-O(3)	109.5(7)
Na(1)-O(3)	2.40(2)	O(3)-(Si, Al)-O(4)	68(1)
Na(2)-O(2)	2.98(2)	O(3)-(Si, Al)-O(4)	175(1)
Na(2)-O(3)	2.37(3)	(Si, Al)-O(1)-(Si, Al)	148.0(4)
Co(2)-O(2)	3.31(2)	(Si, Al)-O(2)-(Si, Al)	156.7(7)
Co(2)-O(3)	2.86(3)	(Si, Al)-O(3)-(Si, Al)	146.3(7)
Co(2)-O(4)	2.36(3)	(Si, Al)-O(4)-Co(2)	126(2)
Co(2)-H ₂ O	2.36(10)	H ₂ O(1)-Co(1)-H ₂ O(1)	90
(2)		O(2)-Co(2)-O(2)	102(1)
Co(1)-H ₂ O	2.11(3)	O(3)-Co(2)-O(3)	89(1)
(1)		O(4)-Co(2)-O(4)	119(2)
Na(1)-H ₂ O	2.77(4)	O(4)-Co(2)-H ₂ O(2)	70(3)
(1)		O(4)-Co(2)-H ₂ O(2)	103(2)
Na(2)-H ₂ O	2.49(16)	O(4)-Co(2)-H ₂ O(2)	112(2)
(1)		O(2)-Na(1)-O(2)	113(1)
		O(3)-Na(1)-O(3)	113(2)
		O(2)-Na(2)-O(2)	119(5)
		O(3)-Na(2)-O(3)	116(7)
		O(3)-H ₂ O(1)-Co(1)	135(1)

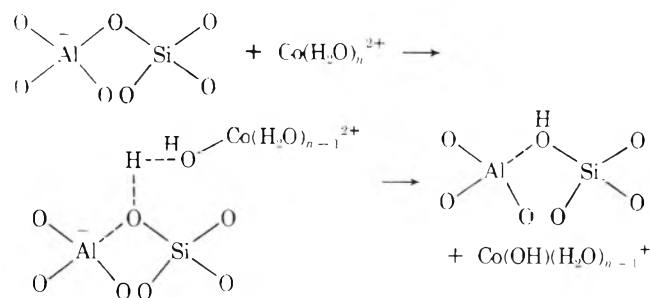
^a Numbers in parentheses are the estimated standard deviations in the last significant digits.

diagonal mirror plane which allows each H₂O(1) molecule to form two equivalent hydrogen bonds, 2.86 (2) Å in length, to framework O(3) atoms.

The three Co(2) ions have unusual zeolitic cation coordi-

nation environments. Like the Mn(II) and Zn(II) ions mentioned earlier, the Co(2) ions reside on (or very near) the unit cell body diagonals; but unlike the Mn(II) and Zn(II) ions, these Co(II) ions are displaced far into the central cavity of the zeolite (see Figure 1) so that conventional contact with framework oxygen atoms, specifically the O(3)'s, is precluded (Co(2) to O(3) = 2.86 (3) Å). It has been shown that Mn(II)³ and Zn(II)⁵ ions coordinate strongly with the framework: Mn(II) to O(3) = 2.28 (1) Å and Zn(II) to O(3) = 2.24 (1) Å. Clearly, then, the Co(2) ions must fulfill their coordination requirements in another way. The results to be presented indicate that the Co(2) ions attain suitable coordination and, at the same time, satisfy the nucleophilic demands of the zeolite framework by hydrolyzing portions of the framework.

The strong electrostatic fields of the Co(2) ions tend to enhance the polarity of the water molecules that constitute its coordination sphere, an enhancement that is further augmented in the presence of the anionic zeolite framework. Conceivably then, the magnitude of these interactions may be sufficient to promote abstraction of some H⁺ ions from the hydration sphere of the Co(2) ions,²⁰ and thereby produce framework hydroxyl groups (probably Si-OH). Such a process is summarized by the following equations:



That the formation of framework hydroxyl ions can be induced by the strong electrostatic fields of polyvalent cat-

ions is generally accepted.²¹ Uytterhoeven et al.²² have suggested that production of framework hydroxyl groups may be initiated by dissociation of water molecules coordinated to divalent ions. This yields $[M^{m+}(H_2O)_{n-1}(OH)]^{(m-1)+}$ ions and the powerful Brønsted acids H^+ , which then can attack the anionic framework to give Si-OH groups. Furthermore from infrared studies of Cu(II)-containing Y-type zeolites (see ref 1 for a description of zeolite Y), Naccache and Taarit²³ have proposed the formation of framework hydroxyl groups, and tricoordinated aluminum atoms as well.

In accordance with the above equation, the apparent weakening of the bonds between the (Si,Al) atoms and the hydrolyzed framework oxygen atoms (possibly accompanied by small changes in framework geometry) suggest that some ligands of the Co(2) coordination sphere (probably OH groups resulting from hydrolysis, and designated as O(4)) may approach the positively charged (Si,Al) ions sufficiently closely to form bridged Co(2)-O(4)-(Si,Al) moieties. This possibility is now confirmed and extended. Structural analysis (i.e., refinement of the occupancy and thermal parameters of the O(4) species) shows that each Co(2) ion is responsible for the formation of three such bridges at the oxygen six-window with which it is associated, resulting in $Co(OH)_3(H_2O)_{n-3}^-$ ions, where n appears to be 4 (see Figure 3). Thus there should be nine O(4) species per unit cell.

It should be noted in support of this unusual result, that the least-squares treatment strongly supports these O(4) atoms. When the O(4) atoms are omitted from least-squares refinement, the R_1 and R_2 values reported above rise to 0.099 and 0.095, respectively. If the number of O(3) atoms (the only reasonable and most abundant source of framework oxygen atoms) is reduced by nine per unit cell, so that the nine newly determined framework species may be accounted for, a similar effect is observed after refinement; R_1 increases to 0.102, and R_2 to 0.097.

Additional oxygen atoms may be incorporated into the zeolite framework in one of (at least) two ways: by expansion of the valence of some (Si,Al) ions from four to five; or by cleavage of some (Si,Al)-O-(Si,Al) linkages to give tricoordinated framework cations (see the work of Naccache and Taarit²³ referenced above) which then react with hydrated Co(2) ions to restore four coordination to all (Si,Al) ions and to achieve an oxygen-bridged structure.

The possibility of valence expansion for either silicon or aluminum ions is considered first. Five-coordinated silicon derivatives, although rare, can be prepared.²⁴ Crystallographic studies have shown that in pentameric dimethylsilylamine $(H_3SiN(CH_3)_2)$ ²⁵ the silicon atoms are coordinated in a trigonal bipyramidal manner, and that the anions of $(C_6H_5)_4AsSiF_5$ ²⁶ are discrete SiF_5^- ions (of highly distorted geometry). Similarly, aluminum, although favoring four or six coordination, exhibits five coordination in a few instances. For example, both bis(trimethylamine)alane $AlH_3 \cdot 2N(CH_3)_2$ ²⁷ and the dinuclear bridged species μ -oxo-di[bis(2-methyl-8-quinolinolato)aluminum(III)]²⁸ possess aluminum atoms with trigonal bipyramidal geometry. Also, in the mineral andalusite, Al_2SiO_5 , half the aluminum ions are coordinated octahedrally, and half in a distorted trigonal bipyramidal arrangement. All silicon ions are coordinated tetrahedrally.²⁹ Hence from the limited structural evidence available in the literature it would appear that aluminum is more likely to form five-coordinate complexes with oxygen ligands (see Figure 4) than is silicon. It should

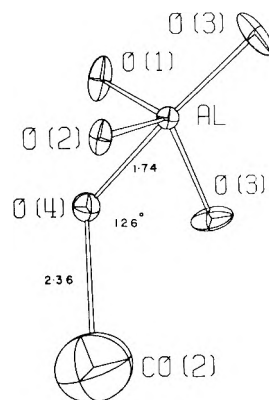


Figure 4. Five coordination of a framework (Si,Al) atom. Ellipsoids of 30% probability are used. The reader should note, as paragraphs 9 and 10 of the Discussion section outline, that all oxygens shown here, except for O(4), are average positions very much more like those of four-coordinate (Si,Al) than five-coordinate Al. The Discussion argues that these two environments of Si and Al framework atoms average to give the figure shown. As is stated in paragraph 9 of the Discussion, the angles involving O(4) (see Table II) in the above figure are unrealistic, as would be the distances from O(4) to adjacent oxygens. However, these features are *virtual*; they are found only in this average (Si,Al) structure; they are not features of the component (Si,Al) sites into which this figure is resolved—the tetrahedral (Si,Al) for 12 Si and 3 Al atoms, and a five-coordinate Al site involving 9 Al atoms per unit cell. The geometric details of this latter coordination are obscured by the predominant (four-coordinate) coordination sphere, so a comparison with the distorted Al trigonal bipyramid in andalusite²⁹ is not possible.

be emphasized that, if valence expansion has indeed occurred, a distinction as to which cation, Al or Si, has increased its valency cannot be made by a purely crystallographic argument due to the equivalence of these ions in $Pm\bar{3}m$.

If approximately 9 of the 24 (Si,Al) species per unit cell are five coordinate, then small changes in the average coordination geometry about the (Si,Al) atoms might be expected. However, the framework geometry reported in Table II and shown in Figure 4 agrees well with the corresponding values determined for other unhydrolyzed zeolite structures (ref 11 provides a tabulation of framework bond angles for three other zeolite structures). Nevertheless, from a consideration of the bond angles at (Si,Al) in this structure, a highly distorted trigonal bipyramid can be constructed by placing an O(3) atom and the O(4) atom at axial positions $O(3)-(Si,Al)-O(4) = 175(1)^\circ$, and O(1), O(2), and the second O(3) at equatorial positions. The three O-(Si,Al)-O angles of the "equatorial oxygens" range from 107 to 111° , values which are clearly tetrahedral but at the same time not so different from the trigonal value of 120° . The angles between the "axial" O(4) atom and the "equatorial" atoms are less than 90° (they are 68 , 69 , and 74° (see Table II)), while the corresponding angles with the "axial" O(3) atom as reported are, of course, tetrahedral.

It must be remembered that even if 9 (Si,Al) tetrahedra per unit cell are hydrolyzed, the 15 unhydrolyzed tetrahedra would be expected to dominate in the final "average" framework geometry, so that the small changes in atomic positions due to possible valence expansion are likely to be concealed. Note, however, that the thermal motions of the oxygen atoms equatorial to aluminum (see Figure 4) are elongated along the (Si,Al)-O(4) axial direction, an effect consistent with an averaging of tetrahedrally and trigonally placed oxygen atoms in disorder in the proportion proposed. Perhaps then, to achieve the observed Co(2)-O(4)-

(Si,Al) linkages, nine framework tetrahedral faces, prompted by hydrolysis of the hydrated Co(II) ions, open sufficiently to allow the formation of an additional (Si,Al)-O bond, with a resulting geometry about (Si,Al), exclusive of O(4), that resembles a somewhat flattened tetrahedron. (It will soon be argued that (Si,Al) as used in this paragraph should be replaced by Al.)

Another description that may account for the presence of nine additional framework oxygen atoms requires an initial rupture of some Si-O-Al linkages (promoted by strong framework hydrolysis) followed by the formation of corresponding numbers of Si-OH groups and tricoordinated aluminum atoms. These aluminum atoms, then functioning as Lewis acids, would coordinate the electron-donating O(4) atoms to complete the observed Co(2)-O(4)-(Si,Al) linkages, and thereby restore tetrahedral coordination about all framework cations.

Such a mechanism should lead to three different (Si,Al) positions—one for the majority of unhydrolyzed (Si,Al) atoms, and two more for the (Si,Al) atoms involved in bond cleavage (i.e., one Si-OH and one Al-O(4)-Co(2) for each broken Si-O-Al link). In addition, large concomitant changes in some framework oxygen positions, resulting from the movement of adjacent hydrolyzed framework tetrahedra away from one another to minimize a very close oxygen-oxygen approach, would be expected. However, scrutiny of the final difference Fourier map revealed no new positions close to "principal" framework positions (in Table I) that might be ascribed to shifted framework atoms. (Indeed, the residual electron density at the (Si,Al) position given in Table I is quite small, $0.3 \text{ e } \text{Å}^{-3}$, indicating that full occupancy of this position is warranted.) Furthermore, the anisotropic temperature factor coefficients for all of the framework atoms in this structure agree well with the corresponding coefficients determined for two other hydrated but unhydrolyzed zeolite A structures (those of fully K⁺-exchanged^{30a} and of $7/12$ Cs⁺-exchanged^{30b} zeolite A), suggesting that each framework atom is restricted (or nearly so, considering the (Si,Al) disorder) to one firm position in this structure, and that none of the framework positions refined to an average of two distant (by at least 2.4 Å for two oxides) ions. In addition, if four coordination were maintained, as the mechanism proposes, a possible new position for a framework oxygen should not be axial with respect to a (Si,Al)O₄ tetrahedron, as is observed for O(4). Finally, the occupancy parameters for the original framework oxygen atoms should have decreased but, as has been stated earlier, refined oxygen thermal parameters do not suggest such a change. When these occupancy parameters are lowered, the thermal parameters become unreasonably small and the *R* values rise sharply (vide supra). This, then, argues conclusively against a bond cleavage mechanism.

Closer examination of the structure reveals that the (Si,Al)-O(4) distances (1.74 (3) Å) are slightly longer than any of the (Si,Al)-O(1), -O(2), and -O(3) distances, whose mean is 1.66 (2) Å. Interestingly, the former value agrees with the average Al-O framework distance of 1.73 (3) Å, reported by Gramlich and Meier¹⁰ in unexchanged sodium zeolite 4A, and is close to an average value of 1.757 Å suggested by Smith.³¹ Furthermore, the mean Al(III)-O distance in μ -oxo-di[bis(2-methyl-8-quinolinolato)aluminum(III)]²⁸ is 1.68 (1) Å. These Al-O bond lengths, then, provide some further support for the argument that only Al, and not Si, has become five coordinate.

Each Co(2) ion lies essentially in the plane formed by the three O(4) atoms to which it is bound. The deviation of the Co(2) ions from these planes is 0.2 (1) Å, and so the angles at the Co(2) ions (119 (2)°) are nearly trigonal planar. The Co(2)-O(4) bonds are long, 2.36 (3) Å, probably a virtual result due to Co(2) disorder about the threefold axis position reported. However, this value compares somewhat favorably with the mean Co(II)-O distance of 2.24 (3) Å determined for the bridging oxygen atoms of tetrameric bis(acetylacetonato)cobalt(II).²² In this latter complex the Co(II) to nonbridging oxygen distance is 2.06 (3) Å, clearly demonstrating by contrast the appreciable bond elongation for the bridging species. A similar variation in Co(II)-O bond length is observed in dimeric bis(acetylacetonato)aquocobalt(II).³³ Co(II)-O (nonbridging) = 2.02 (2) Å, Co(II)-O (bridging) = 2.16 (3) Å, and Co(II)-O (water) = 2.20 (3) Å.

One water molecule (H₂O(2)), located well into the central cavity, coordinates each Co(2) ion at a fourth position. The Co(2) to H₂O(2) bond is again long (2.36 (10) Å); and the wide range of values for the O(4)-Co(2)-H₂O(2) angles (Table II) indicates the unconventional coordination about the Co(2) ions. It is likely that the H₂O(2) molecules are hydrogen bonded to other water molecules of the structure which in turn hydrogen bond with the aluminosilicate framework. Such linkages might account for the unusual orientation of the H₂O(2) molecules with respect to the other members of the Co(2) coordination sphere. However, because no water molecules located in this structure form plausible geometric arrangements with the Co(2)-H₂O(2) groups, this model could not be established.

Clearly, the coordination about the Co(2) ions thus far presented is unusual and may represent only a partial description of the Co(2) environment. However, since no other water molecules were located near the Co(2) ions, it was hoped that examination of the electronic spectrum of this material could provide a better understanding of the nature of the Co(2) coordination sphere. Hence, samples were prepared as Nujol mulls and were supported on strips of filter paper. Spectra were obtained with a Cary 14 recording spectrophotometer from 5000 to 20,000 cm⁻¹. Only one band due to Co(II) ions appeared, a very intense shoulder at 19,000-20,000 cm⁻¹, which, however, is common to octahedral,³⁴ trigonal bipyramidal,³⁵ and square pyramidal Co(II).³⁶ (Indeed, the octahedral Co(1) ion at the unit cell origin, although lower in concentration than the Co(2) ions, may be wholly or partially responsible for this shoulder.) Because of the absence of other spectral features, conclusions about the nature of these Co(2) ions could not be reached by this method. This may be due to the low concentration of the Co(2) species, and to the probable weak ligand fields at the Co(2) ions, resulting from the weak interactions between Co(2) ions and its rather distant oxygen ligand atoms. Note that these crystals are pink-tan in color, implying octahedral Co(II) ions.³⁴ It has been shown that zeolite crystals containing trigonal or tetrahedral Co(II) ions are, as expected, deep blue in color.⁴

Of the four Na⁺ ions of this structure, three have been located, and a location for the fourth ion seems secure. Two Na(1) ions have selected sites in the zeolite six-windows, recessed into the sodalite unit, along the two remaining threefold axial sites which allow satisfactory displacement from H₂O(1) molecules (see Figure 2 and Table II). (To avoid severe electrostatic repulsions with Co(2) ions, those axes chosen by the Co(2) ions must be avoided also.) Each

Na(1) is coordinated to that triad of O(3) atoms related by the threefold axis on which it lies. In both the hydrated and vacuum-dehydrated sodium zeolite 4A system, the Na⁺ ions occupy similar positions close to the framework, and accordingly the Na⁺-O(3) distances are comparable: 2.36 (4), 2.32 (1), and 2.40 (2) Å in the hydrated 4A,¹⁰ dehydrated 4A,^{2a} and hydrated Co_{0.33}Na_{0.33}[AlSiO₄]-A forms, respectively. For reasons discussed in ref 4, the Na(1)-O(3) distances for hydrated Co_{0.33}Na_{0.33}[AlSiO₄]-A are likely to be somewhat longer than reported, due to minor disorder considerations. Tables II and III supply other features of Na(1) coordination geometry.

A third sodium ion, Na(2), is located near the principal Na⁺ site in Na[AlSiO₄]-A,^{2a,10} (on a threefold axis, protruding into the large cage). The Na(2)-O(3) distances are 2.37 (3) Å, in good agreement with the values listed above. To diminish electrostatic repulsions, the Na(2) and Co(2) ions are probably arranged "tetrahedrally" in the large cage. There is no indication of the coordination of water molecules to the Na(1) and Na(2) ions.

The remaining sodium ion, Na(3), has been assigned to the scattering matter located on the axis of fourfold symmetry. (A similar position was ascribed to the three Na⁺ ions of Mn_{0.375}Na_{0.25}[AlSiO₄]-A.³) At this location the Na(3) ion is far from the framework, the Na(3) to O(1) distance of ca. 4.5 Å being the closest approach. However, Na(3) may interact with large cage water molecules: Na(3) to H₂O(3) = 2.60 (8) Å, and Na(3) to H₂O(4) = 2.55 (20) Å. As shown in Table IV, these water molecules are very likely hydrogen bonded to framework oxygen atoms. However, the possible coordination angles (based on hydrogen bonding arrangements) H₂O(3)-Na(3)-H₂O(3) and H₂O(3)-Na(3)-H₂O(4) are calculated to be about 90 and 76°, respectively, values which are clearly far from acceptable tetrahedral values. In contrast though, the angles Na(3)-H₂O(3)-O(1) (104 (3)°), Na(3)-H₂O(4)-O(2) (117 (5)°), and Na(3)-H₂O(4)-O(1) (109 (4)°) are close to tetrahedral.

The zeolite samples were initially prepared⁴ by exchange with Co(II) to give 4.5 Co(II) and 3 Na⁺ per primitive unit cell, an apparent limit, followed by back-exchange with a small amount of unexchanged zeolite. The final structure suggests that it is Na(3) which was introduced in the back-exchange step, and that at our observed kinetic limit of exchange (see ref 37) all Na⁺ ions are at Na(1) and Na(2), and are associated with the six-ring oxygens.

The two ions at Na(1) recessed into the sodalite unit fill that position in a noncrystallographic sense; they occupy the two of the eight six-windows which are not partially occluded by the six H₂O(1)'s coordinated to Co(II). Similarly the one ion at Na(2) apparently fills its site, presumably either by completing the large tetrahedron in the large cavity which has the three Co(2) ions as its other members, or (less likely) by occupying the six-window surrounded by those occupied by the three Co(2) ions. (Na(2) is not equivalent to Na(1) because Na(2) shares its six-window with an H₂O(1) in the sodalite unit.) Finally, the fourth Na⁺ is located at a new and more loosely bound site at Na(3), far from the negatively charged zeolite framework. Two of the eight six-windows, then, are associated with neither a Co(II) nor a Na⁺ ion. Of course, the very acid protons on O(4) could not be located by X-ray diffraction methods; some of these are likely to have dissociated and may occupy those remaining six-windows.

Although several large cage water molecules could be close enough to the ligands that coordinate to Co(2) ions

TABLE III: Deviations of Atoms (Å) from the (111) Plane at O(3)^a

Co _{0.33} Na _{0.33} [AlSiO ₄]-A	(hydrated)	Co _{0.33} Na _{0.33} [AlSiO ₄]-A	(dehydrated) ^b
Co(2)	1.66(5)	Co	0.34(5)
Na(1)	-0.66(5)	Na	-0.56(4)
Na(2)	0.50(11)	O(2)	0.29(4)
O(2)	0.19(3)		
O(4)	1.42(11)		

^a A negative deviation indicates that the atom lies on the same side of the plane as the origin. Numbers in parentheses are the estimated standard deviations in the last significant digits. ^b See ref 4.

TABLE IV: Some (Possible)^a Nonbonded Interactions (Å)

(x, y, z) ^b	O(1)···H ₂ O(3)	3.07(7) ^c	
	O(1)···H ₂ O(6)	2.99(15)	
	O(1)···H ₂ O(4)	2.96(10)	
	O(1)···H ₂ O(5)	2.91(20)	
	O(2)···H ₂ O(4)	2.78(17)	
	O(2)···H ₂ O(6)	2.77(15)	
	O(2)···H ₂ O(1)	3.24(2)	
	O(3)···H ₂ O(1)	2.86(2)	
	O(3)···H ₂ O(3)	3.13(8)	
	H ₂ O(3)···H ₂ O(4)	3.19(17)	
(x, z, y)	H ₂ O(4)···H ₂ O(5)	2.23(26)	
	H ₂ O(3)···Na(3)	2.60(8)	
	H ₂ O(4)···Na(3)	2.55(21)	
	H ₂ O(3)···H ₂ O(3)	3.14(11)	
	H ₂ O(3)···H ₂ O(6)	2.24(17)	
	H ₂ O(3)···H ₂ O(5)	2.76(30)	
	(y, x, z)	H ₂ O(2)···H ₂ O(5)	2.55(23)
		H ₂ O(2)···H ₂ O(6)	3.13(17)
		H ₂ O(3)···H ₂ O(6)	2.71(17)
	(y, z, x)	H ₂ O(2)···H ₂ O(3)	2.46(12)
H ₂ O(2)···H ₂ O(5)		3.12(24)	
(z, x, y)	H ₂ O(3)···H ₂ O(6)	3.06(17)	

^a Due to partial occupancies of all nonframework sites, these contacts are speculative. ^b The first atom of each pair has coordinates as given in Table I; and the second atom is related to the one in Table I by the symmetry operation given in the subheading. ^c Numbers in parentheses are the estimated standard deviations in the last significant digits.

(i.e., O(4)'s and H₂O(2)'s) to form hydrogen bonds, the resultant bond angles would be extremely acute. Furthermore a network of hydrogen bonded water molecules and framework atoms, as observed in the hydrated forms of Na-[AlSiO₄]-A,¹⁰ Mn_{0.375}Na_{0.25}[AlSiO₄]-A,³ and Zn_{0.458}Na_{0.083}[AlSiO₄]-A,⁵ is not apparent here. The large cavity of the unit cell has been interpreted here as being quite unsymmetrically filled by Co(2), O(4), Na(1), Na(2), Na(3), and H₂O(2); this has made a single unique assignment of water positions within the sites H₂O(3), -(4), -(5), and -(6) difficult to discuss and justify. In Table IV, then, is a listing of possible water-framework interactions.

As a final note of caution, the reader should be aware that only the average three-dimensional electron density of one octant of the unit cell has been determined crystallo-

graphically. (The asymmetric unit is actually only one-sixth of an octant; however, since most atoms occupy special positions that fraction is misleading.) The four different kinds of occupation of these octants, which can be considered to mean the six-windows and their environments, as have been discussed in this work, have been deduced using basic chemical considerations. These have allowed a relatively detailed interpretation of the crystallographic result.

The Co(II) ions and Ni(II) ions occupy similar positions in hydrated zeolite A which are quite different from those occupied by Mn(II) and Zn(II) ions. Perhaps this may be understood in terms of relative crystal field stabilization energies (cfse). Presumably all these cations are high spin (maximum electron multiplicity). The d^7 Co(II) ions and the d^8 Ni(II) ions may achieve greater cfse by coordinating with intrazeolitic H_2O molecules than with framework oxygen atoms. The d^5 Mn(II) ions and the d^{10} Zn(II) ions, on the other hand, are unable to benefit from such effects³⁸ (i.e., csfe), and respond more prosaically to the electrostatic attractions of the anionic framework.

It is noteworthy that small amounts of water in some transition-metal-exchanged zeolites may be stoichiometrically hydrolyzed as they are in this structure, giving rise to Brønsted acid sites which are active sites in many catalytic processes.¹

Acknowledgment. This work was supported by the National Science Foundation (Grant No. GP-38639X). We are also indebted to Kevin B. Kunz for performing the ion-exchange experiments, to Larry G. Warner for assistance in gathering and in interpreting the electronic spectral data and for his useful comments on the coordination chemistry of this system, and to the University of Hawaii Computing Center.

Supplementary Material Available. Listings of $10F_o$ and $10F_c$ for this structure will appear following these pages in the microfilm edition of this volume of the journal. Photocopies of the supplementary material from this paper only or microfiche (105 × 148 mm, 24× reduction, negatives) containing all of the supplementary material for the papers in this issue may be obtained from the Journals Department, American Chemical Society, 1155 16th St., N.W., Washington, D.C. 20036. Remit check or money order for \$4.00 for photocopy or \$2.50 for microfiche, referring to code number JPC-75-1594.

References and Notes

- (1) Accounts of reactions catalyzed by zeolite systems are available: R. F. Gould, *Adv. Chem. Ser.*, No. 101, 102 (1971); No. 121 (1973).
- (2) (a) R. Y. Yanagida, A. A. Amaro, and K. Seff, *J. Phys. Chem.*, **77**, 805 (1973); (b) R. M. Barrer, Third International Conference on Molecular Sieves, Zürich, 1973.
- (3) R. Y. Yanagida, T. B. Vance, Jr., and K. Seff, *J. Chem. Soc., Chem. Commun.*, 382 (1973); R. Y. Yanagida, T. B. Vance, Jr., and K. Seff, *Inorg. Chem.*, **13**, 723 (1974).
- (4) P. E. Riley and K. Seff, *Inorg. Chem.*, **13**, 1355 (1974).
- (5) A. A. Amaro, C. L. Kovaciny, K. B. Kunz, P. E. Riley, T. B. Vance, Jr., R. Y. Yanagida, and K. Seff in "Proceedings of the Third International Conference on Molecular Sieves", J. B. Uytterhoeven, Ed., Leuven University Press, Belgium, 1973, p 113.
- (6) C. L. Kovaciny, M.S. Thesis, University of Hawaii, 1973.
- (7) P. E. Riley, Ph.D. Dissertation, University of Hawaii, 1974.
- (8) P. E. Riley and K. Seff, *J. Am. Chem. Soc.*, **95**, 8180 (1973).
- (9) P. E. Riley, K. B. Kunz, and K. Seff, *J. Am. Chem. Soc.*, **97**, 537 (1975).
- (10) V. Gramlich and W. M. Meier, *Z. Kristallogr.*, **133**, 134 (1971).
- (11) P. E. Riley, K. Seff, and D. P. Shoemaker, *J. Phys. Chem.*, **76**, 2593 (1972).
- (12) J. F. Charnell, *J. Cryst. Growth*, **8**, 291 (1971).
- (13) S. W. Peterson and H. A. Levy, *Acta Crystallogr.*, **10**, 70 (1957).
- (14) Principal computer programs used in this study were: data reduction program, A. Christensen, LPCOR, Syntex Analytical Instruments, 1970; full-matrix least squares, P. K. Gantzel, R. A. Sparks, and K. N. Trueblood, UCLALS4, American Crystallographic Association Program Library (old) No. 317 (modified); Fourier program, C. R. Hubbard, C. O. Quicksall and R. A. Jacobson, Ames Laboratory Fast Fourier, Iowa State University, 1971; C. K. Johnson, ORTEP, Report No. ORNL-3794, Oak Ridge National Laboratory, Oak Ridge, Tenn., 1965.
- (15) A recent discussion of the selection of this quality of data is available: A. J. C. Wilson, *Acta Crystallogr., Sect. B*, **29**, 1488 (1973).
- (16) "International Tables for X-Ray Crystallography", Vol. III, Kynoch Press, Birmingham, England, 1962, p 212.
- (17) C. H. Dauben and D. H. Templeton, *Acta Crystallogr.*, **8**, 841 (1955).
- (18) See paragraph at end of text regarding supplementary material.
- (19) A. Zalkin, H. Ruben, and D. H. Templeton, *Acta Crystallogr.*, **15**, 1219 (1962).
- (20) J. A. Rabo and P. H. Kasai, *Prog. Solid State Chem.*, **9**, 1219 (1974).
- (21) J. W. Ward, *J. Colloid Interface Sci.*, **28**, 269 (1968).
- (22) J. B. Uytterhoeven, R. Schoonheydt, B. V. Liengme, and W. K. Hall, *J. Catal.*, **13**, 425 (1969).
- (23) C. Naccache and Y. B. Taarit, *J. Catal.*, **22**, 171 (1971).
- (24) H. C. Clark, K. R. Dixon, and J. G. Nicolson, *Inorg. Chem.*, **8**, 450 (1969).
- (25) R. Rudman, W. C. Hamilton, S. Novick, and T. D. Goldfarb, *J. Am. Chem. Soc.*, **89**, 5157 (1967).
- (26) P. W. R. Corfield and J. A. Ibers, American Crystallographic Association Abstract Papers, Summer Meeting, No. 52, 1968.
- (27) C. W. Heitsch, C. E. Nordman, and R. W. Parry, *Inorg. Chem.*, **2**, 508 (1963).
- (28) Y. Kushi and Q. Fernando, *J. Chem. Soc., Chem. Commun.*, 555 (1969).
- (29) C. W. Burnham and M. J. Buerger, *Z. Kristallogr.*, **115**, 269 (1961).
- (30) (a) P. C. W. Leung, K. B. Kunz, I. E. Maxwell, and K. Seff, *J. Phys. Chem.*, in press; (b) T. B. Vance, Jr., and K. Seff, *ibid.*, in press.
- (31) J. V. Smith, *Adv. Chem. Ser.*, No. 101, 171 (1971).
- (32) F. A. Cotton and R. C. Elder, *Inorg. Chem.*, **4**, 1145 (1965).
- (33) F. A. Cotton and R. C. Elder, *Inorg. Chem.*, **5**, 423 (1966).
- (34) A. B. P. Lever, "Inorganic Electronic Spectroscopy", Elsevier, New York, N.Y., 1968, p 318.
- (35) M. Ciampolini and N. Nardi, *Inorg. Chem.*, **5**, 41 (1966).
- (36) F. Lions, I. G. Dance, and J. Lewis, *J. Chem. Soc. A*, 565 (1967).
- (37) I. J. Gal, O. Jankovic, S. Malčić, P. Radovanov, and M. Todrović, *Trans. Faraday Soc.*, **67**, 999 (1971).
- (38) R. S. Drago, "Physical Methods in Inorganic Chemistry", Reinhold, New York, N.Y., 1965, p 79.

The Insignificance of Second Coordination Sphere Interactions in Cobalt-59 Nuclear Magnetic Resonance Relaxation

K. L. Craighead and R. G. Bryant*¹

Department of Chemistry, University of Minnesota, Minneapolis, Minnesota 55455 (Received October 28, 1974; Revised Manuscript Received March 24, 1975)

Publication costs assisted by the National Institutes of Health

Nuclear magnetic resonance relaxation time measurements are reported which permit evaluation of the electrostatic contribution to field gradients from ions external to the first coordination sphere of the observed nucleus. It is concluded that for the tris(ethylenediamine)cobalt(III) ion the presence of phosphate ion in the second coordination sphere makes little if any contribution to the electric field gradient at the cobalt nucleus.

Considerable attention has been focused on the origins of NMR relaxation in aqueous electrolyte solutions.² For many nuclei the nuclear electric quadrupole interaction dominates; but definitive evidence that any of the theoretical approaches to this problem is correct is lacking. A theory developed by Hertz focuses on electrostatic contributions to the electric field gradient at the observed nucleus and is able to obtain approximate agreement with experimental observations.^{3,4} In spite of this result some discussions of NMR data for quadrupole relaxed nuclei have ignored electrostatic contributions to relaxation originating external to the first sphere of interaction and focused only on that part which results from molecules or ions in the first coordination sphere of the observed ion. The present experiment is directed at assessing the validity of this approach.

Tris(ethylenediamine)cobalt(III) chloride is a very well-characterized chemically inert coordination complex in which the ⁵⁹Co NMR signal is readily observed. The ⁵⁹Co nuclear electric quadrupole moment⁵ is 0.40 in units of 10⁻²⁴e cm² which is sufficiently large that the resonance is not detected in some unsymmetrical complexes.⁶ In alkaline aqueous solutions phosphate ion forms an ion pair with Co(en)₃³⁺ in high yield which has been investigated by several methods.⁷⁻¹³ The ⁵⁹Co NMR signal from this complex is both shifted and broadened by the formation of the ion pair.^{14,15} This system therefore provides a direct means of assessing electrostatic contributions to quadrupole relaxation which originate in ionic charges placed external to the first coordination sphere of the ion.

The ⁵⁹Co NMR relaxation is dominated by the nuclear electric quadrupole relaxation mechanism. In the present case the cobalt nucleus experiences approximately spherical symmetry and the relaxation equation may then take the form²

$$\frac{1}{T_1} \propto \frac{2I + 3}{I^2(2I - 1)} \left(\frac{eQ}{h} \right)^2 J$$

where T_1 is the longitudinal relaxation time, I the nuclear spin quantum number, e the unit charge, Q the nuclear electric quadrupole moment, and J the Fourier transform of the time correlation function describing the fluctuations of the components of the electric field gradient tensor. In the limit of extreme narrowing and where a covalent bond is formed this expression becomes¹⁶

$$\frac{1}{\pi T_1} = \frac{2\pi}{49} \left(\frac{e^2 q Q}{h} \right)^2 \tau$$

where τ is the correlation time for the reorientation of the electric field gradient, q . Usually τ may be identified with a rotational correlation time. In either description changes in the relaxation time may reflect changes in either the magnitudes of the field gradient tensor components or in their time dependence.

In the present case the magnitude of the electric field gradient at the cobalt nucleus originating from negative charge on the phosphate ion is to be estimated. An accurate theoretical prediction of the field gradient would require sufficiently precise wave functions for the system to accurately include antishielding effects. The metal system is too large for this approach. A very crude estimate may be made based on electrostatic ideas where the electric field gradient is approximately q'/r^3 where q' is the charge and r is the distance from the phosphate ion to the cobalt nucleus. This estimate is expected to be low because antishielding effects are ignored. If the ligand system about cobalt were absent the antishielding correction to the field gradient would be about a factor of 10.¹⁷ Calculations of this correction for a metal complex have not been reported. Substitution of a reasonable distance into the above expression suggests that the field gradient originating from the phosphate ion will have a negligible effect on the ⁵⁹Co relaxation time unless the antishielding factor is on the order of or larger than 10.

Although the basis for the estimate of the field gradient may be questioned, the suggestion that the effects observable at the cobalt nucleus are small or even negligible is supported by the data in Table I. These data show that the ⁵⁹Co relaxation rate changes by a factor of about 2.5 upon ion pair formation. This may come about from changes in either the magnitude or time dependence of the field gradient tensor elements. The ¹³C T_1 provides a good measure of the change in the rotational correlation time suffered by the metal complex on formation of the ion pair.¹⁸ The ¹³C data show that the change in the correlation time describing reorientation of the C-H vectors in the complex exceeds a factor of 4 when the ion pair is formed. This result is also consistent with proton and deuterium measurements made on the same complex.¹⁹ There is a possibility that the correlation time change monitored at the carbon

TABLE I: NMR Relaxation Times in Co(en)_3^{3+} Ion

^{59}Co line width, Hz ^a	^{13}C relaxation rate, $1/T_1$, sec ⁻¹ ^b
310 ± 27 pH 13.5, $[\text{PO}_4^{3-}] = 0.7 M$ $[\text{Co(III)}] = 0.1 M$	1.34 ± 0.1 pH 13.5, $[\text{PO}_4^{3-}] = 0.5 M$ $[\text{Co(III)}] = 0.3 M$
127 ± 12 pH 13.5, $[\text{Co(III)}] = 0.1 M$	5.8 ± 0.5 pH 13.5, $[\text{Co(III)}] = 0.3 M$

^a Recorded at 14.1 MHz as previously reported.²⁰ ^b Recorded on a Varian XL-100 NMR spectrometer using the inversion recovery method.

atoms is larger than that experienced at the cobalt ion because of changes in ligand motion upon formation of the ion pair. Nevertheless it is clear that the correlation time for rotational motion of the complex is altered by at least a factor of 2. To the extent that rotation dominates the field gradient time dependence, the measured correlation time change accounts for the observed changes in the ^{59}Co relaxation rate on ion pair formation. Therefore contributions to the cobalt relaxation rate arising from the electric field of the phosphate ion are small in this instance and the previous neglect of field gradient contributions from ions external to a first coordination sphere appears to be justified.

NOTE ADDED IN PROOF: Alder and Loewenstein have previously approached this problem somewhat differently using an anionic cobalt complex. Their data and interpre-

tation also suggest that in the present case such a field gradient contribution should be small. (R. Alder and A. Loewenstein, *J. Mag. Resonance*, **5**, 248 (1971).)

Acknowledgment. This work was supported by the National Institutes of Health, GM-18719, the Research Corporation, and the Chemistry Department and the Graduate School, The University of Minnesota.

References and Notes

- (1) Camille and Henry Dreyfus Teacher Scholar.
- (2) H. G. Hertz in "Water, A Comprehensive Treatise", F. Franks, Ed., Plenum Press, New York, N.Y., 1973, Chapter 7.
- (3) (a) H. G. Hertz, *Ber. Bunsenges. Phys. Chem.*, **77**, 531 (1973); (b) **77**, 688 (1973).
- (4) H. G. Hertz, et al., *Ber. Bunsenges. Phys. Chem.*, **78**, 24 (1974).
- (5) Varian NMR Table, Varian Associates, Palo Alto, Calif., 1963.
- (6) A. Yamasaki, F. Yajima, and S. Fujiwara, *Inorg. Chim. Acta.*, **2**, 39 (1968).
- (7) H. L. Smith and B. E. Douglas, *Inorg. Chem.*, **5**, 784 (1966).
- (8) R. Larsson, S. F. Masson, and B. J. Norman, *J. Chem. Soc. A*, 301 (1966).
- (9) S. F. Masson and B. J. Norman, *Proc. Chem. Soc., London*, 339 (1964).
- (10) S. F. Masson and B. J. Norman, *J. Chem. Soc. A*, 307 (1966).
- (11) J. L. Sudmeier and G. L. Blackmer, *J. Am. Chem. Soc.*, **92**, 5238 (1970).
- (12) J. L. Sudmeier, G. L. Blackmer, C. H. Bradley, and F. A. L. Anet, *J. Am. Chem. Soc.*, **94**, 757 (1972).
- (13) L. R. Froebe and B. E. Douglas, *Inorg. Chem.*, **9**, 513 (1970).
- (14) T. H. Martin and B. M. Fung, *J. Phys. Chem.*, **77**, 637 (1973).
- (15) K. L. Craighead, Ph.D. Thesis, University of Minnesota, 1973.
- (16) A. Abragam, "The Principles of Nuclear Magnetism", The Clarendon Press, Oxford, 1961, p 314.
- (17) E. A. C. Lucken, "Nuclear Quadrupole Coupling Constants", Academic Press, New York, N.Y., 1969.
- (18) A. Allerhand, D. Doddrell, and R. Komoroski, *J. Chem. Phys.*, **55**, 189 (1971).
- (19) K. L. Craighead, P. Jones, and R. G. Bryant, unpublished data.
- (20) K. L. Craighead, *J. Am. Chem. Soc.*, **95**, 4434 (1973).

Conductance of the Alkali Halides. XIII. Cesium Bromide, Lithium-7 Chloride, and Lithium-7 Iodide in Dioxane–Water Mixtures at 25°

Charles F. Mattina¹ and Raymond M. Fuoss*

Department of Chemistry, Yale University, New Haven, Connecticut 06520 (Received January 20, 1975)

Publication costs assisted by the Office of Water Research and Technology

Conductance data for cesium bromide, lithium-7 chloride, and lithium-7 iodide in dioxane–water mixtures covering the range $78.35 \geq D \geq 10$ in dielectric constant are presented. Values of limiting conductance Λ_0 , association constant K_A , and pairing distance R are computed, using the three-parameter conductance equation $\Lambda = \Lambda(c; \Lambda_0, K_A, R)$. The model on which the equation is based defines ion pairs as those which are uniquely partnered with center to center distances r in the range $a \leq r \leq R$, where a is the contact distance. Ion pairs are formed by the diffusion of partner anions into spheres of radius R centered on the cations of the pairs (Debye–Eigen model) and dissociate by outward diffusion. For the systems of higher dielectric constant, R is somewhat larger than the sum of the lattice radii, corresponding to an average over a population consisting of contact pairs and solvent separated pairs; as D decreases, R increases, corresponding to the increasing range of electrostatic attraction. For the lower range of dielectric constant, the ion pairs are predominantly contact pairs, as shown by the relative insensitivity of the association constant to the numerical value of R .

In previous papers of this series^{2–6} the conductances of a number of the alkali halides in dioxane–water mixtures covering the approximate range $78.35 \geq D \geq 10$ in dielectric constant have been reported. The data have been analyzed by several variations of a three-parameter conductance equation of the general form

$$\Lambda = \gamma[\Lambda_0 - L(c\gamma)] \quad (1)$$

where Λ is equivalent conductance, c is stoichiometric concentration, $c\gamma$ is the free ion concentration, and $L(c\gamma)$ represents the decrease in conductance with increasing concentration produced by the long-range interionic forces. The function $L(c\gamma)$ contains a distance parameter whose physical significance depends on the model chosen to represent the electrolytic solution; for the primitive model (rigid charged spheres in a continuum), this parameter is the center-to-center distance a of ions in contact. An equilibrium is assumed between free ions and nonconducting ion pairs, such that the fraction $(1 - \gamma)$ of solute present as pairs is given by the mass action equation

$$1 - \gamma = K_A c \gamma^2 f^2 \quad (2)$$

where K_A is the association constant. For the primitive model⁷

$$K_A = (4\pi N a^3 / 3000) \exp(\epsilon^2 / a D k T) \quad (3)$$

if the pair population is defined to consist solely of pairs in contact. According to (3), a plot of $\log K_A$ against reciprocal dielectric constant should be linear. For all of the systems which have been studied over a wide range of dielectric constants, the $\log K_A - D^{-1}$ plots are not linear but concave down for the water-rich mixtures, and approach linearity only in the range of dielectric constants below about 25. The various equations of type (1) fit the data well within experimental error; assuming that no blunders have been made in the theoretical derivation of $L(c\gamma)$, the discrepancy between theory and observation can only mean that the primitive model inadequately represents real physical systems, especially in the higher range of dielectric

constants. It is also in this range where the Bjerrum model fails; although it leads to the observed shape of the $\log K_A - D^{-1}$ curve, it incorrectly predicts that the association constant drops to zero at a critical value of dielectric constant, above which association abruptly ceases. The virtue of the Bjerrum definition of ion pairs is the counting as pairs not only cation–anion pairs in contact but also those which are relatively near to each other; by definition, the interaction of unpaired ions then is weak enough to justify the classical time average treatment of Debye and Hückel. The false prediction just mentioned is merely the consequence of Bjerrum's choice of the pairing distance: he defined as pairs those ions for which the center-to-center distance r lies in the range

$$a \leq r \leq \epsilon^2 / 2 D k T = \beta / 2 \quad (4)$$

If this artificial restraint is removed by defining⁸ as pairs those ions for which $a \leq r \leq R$, where R is a distance parameter to be determined from the data, the problem of a "critical" dielectric constant vanishes. Furthermore, this definition avoids the unrealistic property of the primitive model for which r can vary continuously. In real solutions, ion pairs are pairs in contact and solvent-separated pairs; R is to be considered as the average radius of the spheres containing the partner ion for paired ions and the diameter of the spheres around free ions outside of which the solvent may be approximated by a continuum (Gurney's co-spheres).

The purpose of this paper is to present conductance data for cesium bromide, lithium-7 chloride, and lithium-7 iodide in dioxane–water mixtures covering the range $78.35 \geq D \geq 10$ in dielectric constant and to derive the conductance parameters Λ_0 , K_A , and R for the model described above. It will be shown that the model approaches two limiting forms: for solvents of higher dielectric constant, R appears as the radius of the Debye–Eigen diffusion sphere while for solvents of lower dielectric constant, most of the pairs are contact pairs, corresponding to the primitive model.

Experimental Section

Materials. Cesium bromide was used as received from the Harshaw Chemical Co.; the material was random cuttings from single crystals grown from melts of purified salt. Lithium chloride was obtained from the Isotopes Division of the Oak Ridge National Laboratory; certification reported 99.9926% ^7Li . The salt was used as received to make master solutions as described below. Lithium iodide (99.93 ^7Li , 0.007 ^6Li) was also from Oak Ridge; the sample was pinkish tan in color and contained a small amount of unidentified organic material. The certificate reported 0.0448% carbon and 0.0291% nitrogen in the lithium from which the iodide was prepared. The salt was purified by recrystallization as the trihydrate, $\text{LiI}\cdot 3\text{H}_2\text{O}$, from water which had been thoroughly deoxygenated by boiling and then sparging with nitrogen while cooling; 10 g of salt as received was dissolved in 30 ml of water, and after filtration under nitrogen to remove some insoluble material, the solution was evaporated under vacuum to about 12 ml and cooled. Long glass-clear crystals formed; these were filtered out under nitrogen and washed on the filter with several portions of ice-cold peroxide-free diethyl ether. The crystals were stored in an evacuated desiccator, where they gradually lost some water of crystallization; this change in composition was unimportant, because the material was used to prepare master solutions which were then standardized. Lithium iodide, either in solution or as trihydrate, oxidizes in air very readily; it is therefore essential to handle it under nitrogen. The conductance of solutions in water or in dioxane-water mixtures remains constant within 0.01% for days if air is carefully excluded; after even a few minutes exposure to air, however, the yellow color of the triiodide begins to develop. Dioxane was first refluxed over potassium hydroxide to condense aldol impurities; it was stored over sodium-lead alloy under nitrogen, and distilled as needed, with a gentle flow of nitrogen through the still, condenser, and receiver during distillation. It is, of course, essential to avoid formation of peroxide in the dioxane.

Methods. All solutions were made up by weight and volume concentrations (c equivalents/liter) were calculated using the appropriate densities. Cesium bromide was dried overnight at 80° ; samples weighed on the microbalance in platinum cups were dropped into solvent in the conductance cells (after determination of solvent conductance) to give the initial solution for a conductance run. Other points were obtained by successive dilutions, by adding solvent by nitrogen pressure from the solvent storage flask. In some runs, in order to cover a wide concentration range, solution was removed after four or five dilutions from the cell using an evacuated pipet, and the (weighed) solution remaining in the cell was then further diluted. Since the lithium salts are extremely hygroscopic, direct weighing was not practical. Instead, master solutions in water were prepared, and standardized by potentiometric titration against silver nitrate solutions which had in turn been standardized against pure potassium chloride for the lithium chloride work and against pure potassium iodide for the lithium iodide work. The titrations were made with chilled solutions, with minimum light in the room, using a silver wire as the measuring electrode and a Corning glass electrode as reference. Solutions were acidified by a few drops of halogen-free nitric acid. Approximately 0.1 N solutions from weight burets were used to reach about 98–99% of complete titer; the titration was then carried through the endpoint using three-

drop portions of 0.01 N solutions from an ordinary buret. Concentrations of master solutions were frequently checked; they held constant within $\pm 0.01\%$.

For the conductance runs, secondary master solutions were made up by weight by adding aqueous master solution to a mixture of dioxane and water in a weight buret, amounts of solution, dioxane, and water chosen to give the desired dioxane-water ratio, and a salt concentration such that the concentration for the initial point would be approximately $2 \times 10^{-7} D^3$ (D = dielectric constant of solvent). This upper limit is set by the range of validity of the conductance-concentration equation used to analyze the data. Then, knowing the composition of the solution in the weight buret, water was added to dioxane in the solvent storage flask (or vice versa) until the mixture in the latter had within $\pm 0.02\%$ the same dioxane-water ratio as the solution in the weight buret. The various compositions are listed in Table I (see paragraph at end of text regarding miniprint material), where w is weight percent dioxane in the mixture, D is the dielectric constant (measured at 25° and 1 MHz^2), and 100η is viscosity (centipoises; measured in an Ubbelohde viscometer with 470.8 sec water-flow time). Conductance parameters are summarized in Tables IV and V.

Electrical equipment and general measuring technique have already been described.² Several conductance cells were used: three with cell constants $8.3234 \pm 0.00008 \text{ cm}^{-1}$, 5.1331 ± 0.0005 , and $1.7602_5 \pm 0.0001_3$ were calibrated by comparison with the 1.76 cell, using dilute aqueous solutions of sodium bicarbonate. Calibrations were, of course, checked at intervals during the work. All conductance measurements were made at $25.000 \pm 0.003^\circ$. Resistances were measured at 0.5, 1, 2, and 5 kHz and extrapolated to infinite frequency. The conductance data are summarized in Tables II and III (see paragraph at end of text regarding miniprint material), where c is concentration (equivalents/liter) and Λ is equivalent conductance ($\text{cm}^2 \text{ equiv}^{-1} \text{ ohm}^{-1}$).

Discussion

As preface, a critical examination of conductance theory appears appropriate. The original statement of the problem about a century ago was deceptively simple: why does equivalent conductance Λ decrease with increasing concentration c ? Arrhenius provided a partial answer by his hypothesis that free current-carrying ions were in mass action equilibrium with nonconducting entities; the relative concentration of the latter increased with increasing concentration and therefore Λ decreased with increasing c . The other part of the answer was given by Debye and Hückel in 1923 when they showed that the long-range effects of electrostatic forces between ions produced a relaxation field ΔX and an electrophoretic countercurrent $\Delta \Lambda_e$, both of which led to a decrease in Λ , initially proportional to the square root of ionic strength. The Arrhenius theory gave a good account of the conductance of weak electrolytes where ionic concentrations were low and where, therefore, the long-range effects could be practically neglected; the Debye-Hückel theory was equally successful in predicting the conductimetric behavior of strong electrolytes at low concentrations in solvents of high dielectric constant. A general theory, rather than two special theories, was finally made possible by Bjerrum's proposal in 1926 that short-range ion pairs would play the same role in solutions of strong electrolytes as did the neutral molecules of the Arrhenius theory in solutions of weak electrolytes.

Table I. Solvent Properties

μ	β	100°	μ	β	100°
For cesium bromide					
4.5	78.75	0.976	0.0	78.35	0.890
7.8	71.90	1.045	19.8	62.25	1.290
10.0	70.28	1.086	33.7	49.99	1.608
18.8	67.42	1.268	44.9	40.47	1.848
21.8	57.91	1.353	52.2	33.84	1.933
36.0	47.56	1.626	60.3	27.18	2.015
37.6	46.17	1.716	66.7	21.97	1.989
38.2	45.91	1.722	70.4	18.88	1.944
40.8	43.70	1.771	71.3	18.13	1.931
43.0	41.76	1.820	71.6	18.07	1.929
46.8	38.59	1.883	73.9	16.23	1.888
56.2	30.48	1.997	76.3	14.45	1.836
63.8	24.17	2.042	77.8	13.48	1.803
69.0	20.11	1.951	80.5	11.69	1.732
73.2	16.73	1.898			
73.4	16.54	1.891			
76.2	15.57	1.839	40.8	44.21	1.763
76.6	15.08	1.820	58.0	29.30	1.999
77.2	13.81	1.811	70.1	19.35	1.936
78.8	13.44	1.787	74.2	16.15	1.869
79.0	11.56	1.767			
80.8	11.22	1.729			
81.8	10.76	1.695			
82.6	10.29	1.670			
88.1	9.36	1.629			

Table II. Conductance of Cesium Bromide in Dioxane-Water at 25°

$10^3 \Sigma$	γ	$10^3 \Sigma$	γ	$10^3 \Sigma$	γ	$10^3 \Sigma$	γ
$D = 74.75$							
509.50	135.77	371.28	88.81	136.02	67.18	38.970	50.12
399.07	127.26	286.76	90.01	86.06	68.84	30.023	51.03
297.87	128.96	182.68	91.97	56.90	70.15	18.495	52.47
196.81	131.13	101.85	96.18	29.28	71.80	9.963	56.05
85.45	134.80	76.55	99.12	17.68	72.97	8.085	56.46
$D = 71.90$							
460.73	117.56	202.20	82.81	63.70	7.088	56.39	
318.67	119.31	133.12	83.92	59.99	66.78	18.578	44.22
218.42	121.59	104.81	85.31	43.43	67.56	13.573	45.32
99.17	135.01	81.55	86.12	27.92	68.68	10.056	46.41
80.23	125.78	60.53	87.02	16.34	69.80	7.378	47.31
$D = 70.28$							
533.67	112.23	33.00	88.56	41.74	5.759	67.89	
453.05	113.19	49.20	87.60	4.953	68.85		
353.17	116.54	115.62	72.47	58.87	63.80	0 = 20.11	
233.77	116.61	123.83	71.76	40.12	64.91	15.807	38.45
160.16	120.20	92.66	74.75	26.57	65.79	12.837	39.58
78.26	121.01	63.01	75.95	17.505	66.85	9.467	40.85
65.03	121.66	53.00	76.46	10.319	67.76	6.362	42.37
56.23	122.21	39.39	77.90	8 = 38.59		4.317	43.29
$D = 62.42$							
276.30	96.46	9 = 46.37		99.59	37.68	0 = 16.12	
190.99	98.17	86.11	69.10	85.48	32.27	9.519	35.13
106.72	100.46	78.56	69.81	63.80	34.29	7.339	35.16
86.70	101.26	52.26	71.05	44.41	60.57	6.360	35.83
63.39	102.18	28.68	72.76	36.40	61.20	5.129	37.07
42.49	103.26	15.78	73.80	20.334	62.21	0.808	42.92
$D = 16.56$							
6.431	35.72	4.572	30.50	12.270	63.51	0 = 10.19	
3.296	36.64	3.734	31.63	15.724	18.99	1.049	25.00
4.203	37.67	3.162	32.51	13.270	19.88	0.657	27.60
3.074	38.96	2.674	33.76	9.876	21.44	0.460	29.43
2.1176	40.30	2.1251	34.69	4.063	26.56	0.2168	31.31
1.1500	42.18	1.5960	35.96	1.969	30.53	0.232	32.96
$D = 13.43$							
18.035	25.09	7.344	26.56	0.1955	33.47	0 = 9.36	
15.778	25.83	6.302	27.66	2.7512	33.07	1.928	16.50
12.933	26.95	5.283	28.43	2.2247	26.26	1.6576	17.18
9.396	28.76	4.295	29.58	1.9840	28.17	1.3731	18.09
6.808	32.62	3.086	31.73	1.1000	30.14	1.0264	19.82
2.925	36.72	1.628	35.16	0.4983	32.93	0.6862	21.71
$D = 10.76$							
3.0835	33.30	3.1276	28.27	2.4509	22.43	0 = 10.76	
2.4876	35.36	2.3508	29.80	2.0573	23.48		
1.9714	35.39	1.6485	32.26	1.1887	26.71		
1.4676	36.27	0.9693	34.03	0.8935	27.66		
0.9146	38.27	0.6981	35.31	0.7716	28.98		
0.6793	39.15	0.5272	36.25	0.7274	30.83		
0.4264	40.26	0.4561	36.68	0.7274	30.83		

Table III. Conductance of Lithium (7) Chloride and Iodide

Chloride		Iodide	
$10^3 \Sigma$	γ	$10^3 \Sigma$	γ
$D = 78.35$			
78.35	0.81	78.35	0.81
62.25	1.63	62.25	1.63
49.99	2.98	49.99	2.98
33.84	4.91	33.84	4.91
27.18	7.50	27.18	7.50
21.97	11.56	21.97	11.56
18.88	15.56	18.88	15.56
18.13	20.08	18.13	20.08
18.07	25.00	18.07	25.00
16.23	30.45	16.23	30.45
14.45	34.45	14.45	34.45
13.48	40.09	13.48	40.09
11.69	40.09	11.69	40.09
$D = 71.90$			
71.90	0.81	71.90	0.81
62.25	1.63	62.25	1.63
49.99	2.98	49.99	2.98
33.84	4.91	33.84	4.91
27.18	7.50	27.18	7.50
21.97	11.56	21.97	11.56
18.88	15.56	18.88	15.56
18.13	20.08	18.13	20.08
18.07	25.00	18.07	25.00
16.23	30.45	16.23	30.45
14.45	34.45	14.45	34.45
13.48	40.09	13.48	40.09
11.69	40.09	11.69	40.09
$D = 70.28$			
70.28	0.81	70.28	0.81
62.25	1.63	62.25	1.63
49.99	2.98	49.99	2.98
33.84	4.91	33.84	4.91
27.18	7.50	27.18	7.50
21.97	11.56	21.97	11.56
18.88	15.56	18.88	15.56
18.13	20.08	18.13	20.08
18.07	25.00	18.07	25.00
16.23	30.45	16.23	30.45
14.45	34.45	14.45	34.45
13.48	40.09	13.48	40.09
11.69	40.09	11.69	40.09
$D = 62.25$			
62.25	0.81	62.25	0.81
49.99	2.98	49.99	2.98
33.84	4.91	33.84	4.91
27.18	7.50	27.18	7.50
21.97	11.56	21.97	11.56
18.88	15.56	18.88	15.56
18.13	20.08	18.13	20.08
18.07	25.00	18.07	25.00
16.23	30.45	16.23	30.45
14.45	34.45	14.45	34.45
13.48	40.09	13.48	40.09
11.69	40.09	11.69	40.09
$D = 49.99$			
49.99	0.81	49.99	0.81
33.84	4.91	33.84	4.91
27.18	7.50	27.18	7.50
21.97	11.56	21.97	11.56
18.88	15.56	18.88	15.56
18.13	20.08	18.13	20.08
18.07	25.00	18.07	25.00
16.23	30.45	16.23	30.45
14.45	34.45	14.45	34.45
13.48	40.09	13.48	40.09
11.69	40.09	11.69	40.09
$D = 33.84$			
33.84	0.81	33.84	0.81
27.18	7.50	27.18	7.50
21.97	11.56	21.97	11.56
18.88	15.56	18.88	15.56
18.13	20.08	18.13	20.08
18.07	25.00	18.07	25.00
16.23	30.45	16.23	30.45
14.45	34.45	14.45	34.45
13.48	40.09	13.48	40.09
11.69	40.09	11.69	40.09
$D = 27.18$			
27.18	0.81	27.18	0.81
21.97	11.56	21.97	11.56
18.88	15.56	18.88	15.56
18.13	20.08	18.13	20.08
18.07	25.00	18.07	25.00
16.23	30.45	16.23	30.45
14.45	34.45	14.45	34.45
13.48	40.09	13.48	40.09
11.69	40.09	11.69	40.09
$D = 21.97$			
21.97	0.81	21.97	0.81
18.88	15.56	18.88	15.56
18.13	20.08	18.13	20.08
18.07	25.00	18.07	25.00
16.23	30.45	16.23	30.45
14.45	34.45	14.45	34.45
13.48	40.09	13.48	40.09
11.69	40.09	11.69	40.09
$D = 18.88$			
18.88	0.81	18.88	0.81
18.13	20.08	18.13	20.08
18.07	25.00	18.07	25.00
16.23	30.45	16.23	30.45
14.45	34.45	14.45	34.45
13.48	40.09	13.48	40.09
11.69	40.09	11.69	40.09
$D = 18.13$			
18.13	0.81	18.13	0.81
18.07	25.00	18.07	25.00
16.23	30.45	16.23	30.45
14.45	34.45	14.45	34.45
13.48	40.09	13.48	40.09
11.69	40.09	11.69	40.09
$D = 18.07$			
18.07	0.81	18.07	0.81
16.23	30.45	16.23	30.45
14.45	34.45	14.45	34.45
13.48	40.09	13.48	40.09
11.69	40.09	11.69	40.09
$D = 16.23$			
16.23	0.81	16.23	0.81

basis of a model. The situation thus poses two new problems: first, what shall the model be? Obviously, it must be simple enough to be amenable to theoretical treatment; ideally, it should correspond as closely as possible to a real physical system. However, the latter desideratum would involve a multiplicity of system-specific parameters such as ionic size, shape, polarizability, and charge distribution, and analogous parameters characteristic of the solvent. This catalog leads to the second problem, a practical one: how many parameters can be obtained from conductance data? The answer is three, and no more than three. It has been shown⁸ that the following semiempirical equation will reproduce conductance data for 1-1 salts in water up to about $0.1N$

$$\Lambda = \Lambda_0 - Sc^{1/2} + Ec \ln c + Ac + Bc^{3/2} \quad (7)$$

where S and E are theoretically predictable coefficients. In principle, the empirical coefficients A and B are determined by the second and third derivatives of $\Lambda(c^{1/2})$. To determine a fourth parameter would require data of sufficient precision to guarantee a reliable value for the fourth derivative of the Λ - $c^{1/2}$ curve, an inaccessible goal. Therefore the explicit function must be a three-parameter equation; two, Λ_0 and K_A , are already present. The net result is that we must choose a model which can be described by one more parameter; dimensional arguments show that this parameter must be a distance R . The conductance function therefore will be $\Lambda = \Lambda(c; \Lambda_0, K_A, R)$ and all system-specific parameters must be contained in the conductimetric parameters Λ_0, K_A , and R .

Based on the above arguments, the following model has been proposed:⁸ surround each ion by a sphere of diameter R , outside of which the solvent is describable by its macroscopic dielectric constant and viscosity. If the sphere for a given cation overlaps an anionic sphere, the two ions are counted as a nonconducting pair, and their electrostatic interaction with unpaired ions is approximated by zero. The spheres for the unpaired ions are by hypothesis immersed in a charged continuum, such that the integral of the space charge is equal and opposite to that of the central ion

$$-\epsilon_j = 4\pi \int_R^\infty \rho_j r^2 dr \quad (8)$$

where ρ_j is the Debye-Hückel charge density. The relaxation field and electrophoresis have been calculated¹⁰ for this model and given as explicit functions of the variables t and τ , where

$$t = \kappa R \quad (9)$$

$$\tau = \beta\kappa/2 = (\epsilon^2/DkT)(\kappa/2) \quad (10)$$

These equations are summarized in the Appendix. The Debye-Hückel parameter is calculated using the concentration of unpaired ions

$$\kappa^2 = (4\pi/DkT) \sum_i n_i \gamma_i \epsilon_i^2 \quad (11)$$

The activity coefficient is given by

$$-\ln f = \tau/(1 + \kappa R) \quad (12)$$

The boundary conditions used in the theoretical development are nonspecific and valid for electrolytes in general: electroneutrality, continuity of all functions at $r = R$ and nonsingularity of functions for $\kappa R = 0$.

Given a set of N conductance data points ($c_j, \Lambda_j; j = 1, \dots, N$) and eq 5, 6, and 12, values for the three parameters

Λ_0, K_A , and R must be found by the method of successive approximations, because eq 5 is nonlinear in two of the parameters. The conductance can be expanded as a truncated Taylor's series in $\Delta\Lambda_0, \Delta K$, and ΔR around preliminary estimated values $\Lambda_0', K_A',$ and R' to give

$$\Lambda_j = \Lambda_j(c_j; \Lambda_0', K_A', R') + (\partial\Lambda_j/\partial\Delta\Lambda_0)\Delta\Lambda_0 + (\partial\Lambda_j/\partial\Delta K)\Delta K + (\partial\Lambda_j/\partial\Delta R)\Delta R \quad (13)$$

which is linear in the increments $\Delta\Lambda_0, \Delta K$, and ΔR . This set of equations is then solved to find the values which minimize

$$\Sigma^2 = \sum_j [\Lambda_j(\text{calcd}) - \Lambda_j(\text{obsd})]^2 \quad (14)$$

In effect, the procedure is to locate the minimum in the four-space ($\Sigma; \Lambda_0, K_A, R$), as illustrated in Figure 1 which shows two-dimensional cross sections of the surface for the data for a typical example (cesium bromide in the dioxane-water mixture with $D = 74.75$). The ordinate is the standard deviation

$$\sigma = [\Sigma^2/(N - 3)]^{1/2}(100/\Lambda_0) \quad (15)$$

expressed as percentage of limiting conductance. Curve 1 shows the values of σ corresponding to a sequence of values $0.8 \leq \beta/R \leq 1.3$ and curve 2 the corresponding values of Λ_0 ; minimum σ appears at $\beta/R = 1.12$. Curve 3 shows values of σ for the perpendicular cross section for the sequence $0.0 \leq K_A \leq 1.0$ and curve 4 the corresponding values of Λ_0 ; here, minimum σ comes at $K_A = 0.75$. Projecting up from the minima to curves 2 and 4 gives the value $\Lambda_0 = 142.84$ corresponding to the minimizing values of K_A and β/R ; minimum σ is 0.004%. The dashed line in the lower part of the figure is drawn at $\sigma = 0.010\%$; it shows that values of β/R between 1.05 and 1.20 and values of K_A between 0.70 and 0.80 would still give a pretty good fit to the data, but the fit with the actual minimizing values is, of course, much better. The significant feature of curves 1 and 3 is the sharpness of the minima. This pattern is common to all the systems with solvents in the higher range of dielectric constant. A computer program¹⁴ designed to determine the three parameters simultaneously usually converges within three or four cycles (i.e., reaches a value of Λ_0 which is changed by less than 0.01% by one more cycle of approximations) for such systems.

However as the dielectric constant decreases, the minima lose their sharpness, and the computer futilely hunts through the shallow trough in the four-space without finding the lowest point. For these systems, a two-parameter program is used: the values of Λ_0 and K_A are determined which will minimize σ for a sequence of values of β/R . Examples of this type of calculation are shown in Figure 2 for eight of the cesium bromide-dioxane-water systems which are identified in the figure by rounded values of the dielectric constants. The vertical scale ($0.0 \leq \sigma \leq 0.10$) is the same for the eight curves; the horizontal scale is compressed to one half for the mixtures at lower dielectric constants. Down to a dielectric constant of about 20, the minimizing value of β/R can be located without ambiguity, but it will be noted that the minima become steadily more shallow as D decreases from 75 to 20, in the sense that a wider range of values of β/R would fit the data within an acceptable precision. In other words, for the lower range of dielectric constants, the goodness of fit becomes quite insensitive to the value of R . The explanation lies in the form of the mass action eq 6 and in the fact that, at lower dielectric constants, the change of Λ with c due to ion pairing domi-

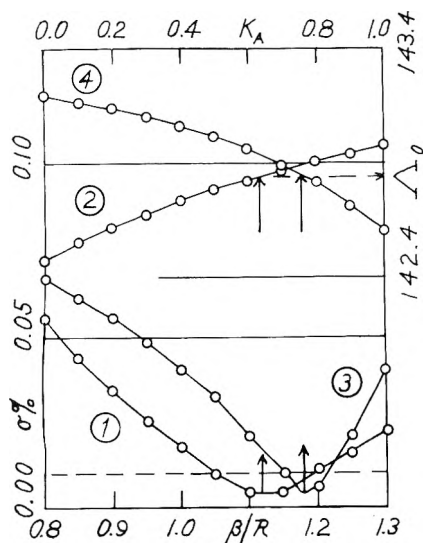


Figure 1. Determination of conductance parameters for cesium bromide-dioxane-water at $D = 74.75$.

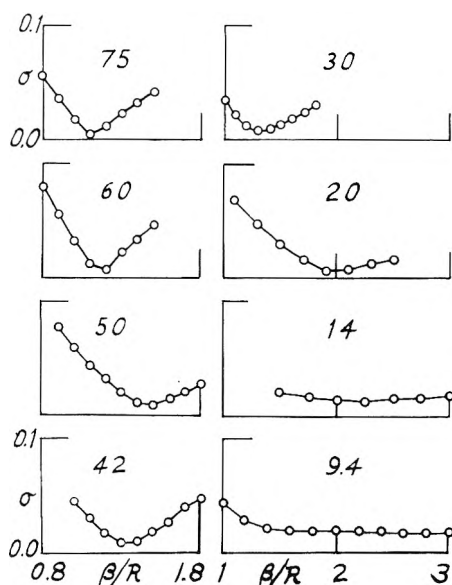


Figure 2. Variation of σ with β/R ratio for cesium bromide-dioxane-water at $D = 74.75, 59.91, 49.58, 41.74, 30.48, 20.11, 13.83,$ and 9.36 .

nates, the long-range ΔX and $\Delta \Lambda_e$ terms becoming relatively insignificant. The product $f\gamma$ appears in (6); if R is increased, more solute is counted as pairs, and γ decreases. However more ions paired means fewer free ions and therefore f increases, and in such a way that the product $f\gamma$ remains nearly constant. Of course the values of R and K_A are coupled in the sense that a change in R at (nearly) constant σ around the minimum produces changes in K_A . The coupling, however, is not tight at lower dielectric constants: for example, at $D = 13.83$, and β/R varies by a factor of 2 from 1.5 to 3.0, K_A decreases by only about 20%, from 1340 to 1090; at $D = 9.36$, K_A decreases from 13,500 to 12,400 for the same twofold change in β/R .

The ion pairs of the present model include both contact pairs⁷ and solvent separated pairs, because they are defined as those two-ion configurations in which the center-to-center distance r lies in the range $a \leq r \leq R$, subject to the condition^{8,11} that the pairing is statistically unique.

(Here a is the contact distance.) The model has two advantages over previous models. The first is a practical one: removing the paired ions from the total ionic population guarantees that the mutual Coulomb energy $\epsilon_i \epsilon_j / Dr_{ij}$ of all pairs of unpaired ions will be small compared to the thermal energy kT , with the consequence that the exponential Boltzmann factor in the charge density

$$\rho_j = \sum_i n_i \epsilon_i \exp(-\epsilon_i \psi_j / kT) \quad (16)$$

may be approximated by the first three terms of its series expansion, thereby enormously simplifying the mathematical treatment of the long-range interactions. The second is the implicit inclusion in the model of the particulate structure of real solutions as contrasted to the long-recognized artificiality of the primitive model which represents the ions as rigid charged spheres moving in a continuum. For the primitive model, all interionic distances $r_{ij} > a$ are permissible. In real solutions, ions are either in contact, or separated by one or more solvent molecules; that is, interionic distances clustering around $(a + md_s)$ are much more probable than intermediate distances. (Here, $m = 0, 1, 2, \dots$ and d_s is the diameter of a sphere which contains a solvent molecule plus the corresponding free volume.) From this point of view, R may be considered as the average radius of spheres surrounding the cations of the pairs and containing both the partner anions and the solvent in the immediate vicinity.

In Figure 3, the values of R for the three salts are plotted against the Bjerrum distance $\beta/2$, which is inversely proportional to dielectric constant ($\beta = 560.4 \times 10^{-8} / D_{25} \text{ cm}$). The parameter R appears to be a characteristic of the solvent rather than of the individual salts because the differences between points for different salts at the same solvent composition is no greater than the scatter of the points for a given salt. The averaging curve extrapolates to about 4 \AA at $\beta/2 = 0$; this would correspond to the pairing radius in a hypothetical solvent of infinite dielectric constant where, due to chance collisions, the probability of finding pairs is not zero. As the dielectric constant decreases, the probability is enhanced by electrostatic attraction, corresponding to the increasing range of Coulomb forces; as expected, R is seen to increase. It becomes equal to the Bjerrum radius around a dielectric constant of 20, and then increases at a lower rate. It should be mentioned that, with this model, association is possible at all dielectric constants, in contrast to the original Bjerrum model which led to the unrealistic requirement that association abruptly cease when the parameter $b = \beta/a$ is less than two.

Unlike the R parameter, which (for these examples at least) depends primarily on the solvent, the association constants are salt dependent, as shown in Figure 4. At a given dielectric constant, lithium iodide has a lower association constant than the chloride, which in turn is somewhat less associated than cesium bromide. This is a reasonable sequence, if we assume that the lithium ion is hydrated and that the association constant contains the factor $\exp(\epsilon^2 / aDkT)$ or its asymptotic equivalent. The shape of the $\log K_A - D^{-1}$ curve suggests that the model may be approximated by one of two limiting descriptions, one valid for the range of higher dielectric constants and the other for lower. Debye¹² and Eigen¹³ calculated theoretical association constants for a model closely similar to the present one: cations are surrounded by spheres of volume Δv and pair formation and dissociation is treated as the diffusion of anions into and out of the volumes Δv . If we identify Δv with $4\pi R^3/3$, Eigen's equation becomes

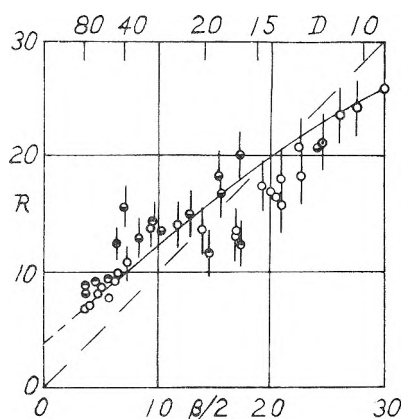


Figure 3. Dependence of pairing radius R on solvent composition: upper abscissa scale, dielectric constant; lower abscissa scale, $\beta/2$, proportional to reciprocal dielectric constant; dashed line, $R =$ Bjerrum radius; O, CsBr; ◐, LiCl; ◑, LiI.

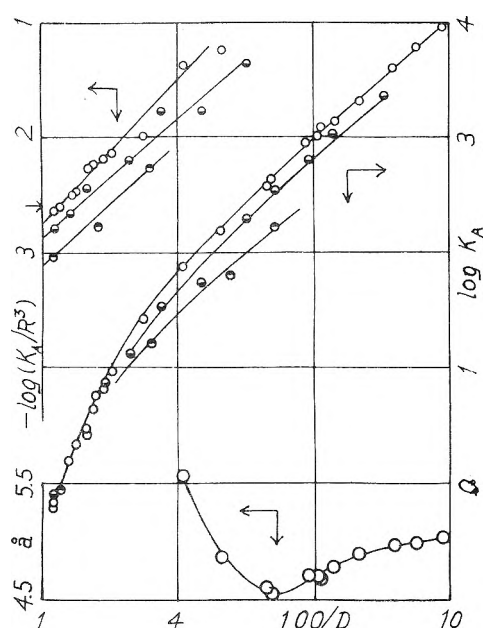


Figure 4. Dependence of parameters on dielectric constant: upper curves, $\log(K_A/R^3)$; central curves, $\log K_A$; lower curve, \AA for cesium bromide; O, CsBr; ◐, LiCl; ◑, LiI.

$$K_A = (4\pi NR^3/3000) \exp(\beta/a) \quad (17)$$

At the upper left in Figure 4 are shown plots of $\log(K_A/R^3)$ against D^{-1} . If the data conformed to (17), the plots would be linear, with a common intercept of $\log(4\pi N/3000)$ at $D^{-1} = 0$, at the point indicated by the arrow on the vertical scale of Figure 4. The plots are linear, and give a values of 6–7 Å; they have, however, different intercepts. This discrepancy can be covered by an ad hoc hypothesis, of course. The factor $\exp(\beta/a)$ in the Eigen equation describes rigid charged spheres in a continuum, for which the potential energy at contact equals β/a . If the Eigen equation is rewritten

$$K_A = (4\pi NR^3/3000) \exp[\beta/a - u(a)/kT] \quad (18)$$

where $u(a)$ is the potential of all the short-range forces, real and virtual, other than coulombic, which are involved in ion pair formation, the desired multiplicative factor can be included. This approach can account for the behavior at high dielectric constants; in the lower range, the $\log(K_A/R^3)$

plots become nonlinear. In this range, the dominant term in the probability function which describes ion pairing is the exponential $\exp(\beta/r)$. If other terms are neglected, the association constant is

$$K_A = (4\pi N/1000) \int_a^R r^2 \exp(\beta/r) dr \quad (19)$$

Using the values of K_A and R derived from the data for cesium bromide, values of the lower limit in the above integral were calculated. The results are shown by the curve at the lower right in Figure 4. Over the range $10 \leq D \leq 20$, the values of a lie in the range $4.52 \leq a \leq 4.75$, which is reasonably constant. For higher dielectric constants, unrealistically large values of a are found; not unexpected behavior, because the integrand in (19) is no longer a good approximation to the probability function appropriate for ion pairing in such solvents. For any dielectric constant, the total pair population consists of statistically paired ions (solvent separated pairs) and contact pairs; at higher dielectric constants, the former species is a significant fraction of the total, while at lower dielectric constants, the latter predominates.

Acknowledgment. This work was supported by Grant No. 14-01-0001-1308 from the Office Water Research and Technology.

Appendix

The conductance equation¹⁰ used to obtain the parameters given in Tables IV and V is

$$\Lambda(c) = \gamma[\Lambda_0(1 + RX) + HY] \quad (A1)$$

where the relaxation field is given by

$$RX = -\beta[\exp(1 - qt) - 1]/3R(1 + t) + (\tau^2/3\mu^2) \ln t + 4\tau^2(\text{FB2}) + (4\beta\tau^2/R)(\text{FB3}) \quad (A2)$$

and the hydrodynamic terms by

$$HY = -\beta_0 c^{1/2} \gamma^{1/2} [(1/(1 + t) + (\tau/2\mu^2) \ln t + H1 + H2)] \quad (A3)$$

The symbols are defined as follows:

$$\beta = e^2/DkT \quad (A4)$$

$$q = 2^{1/2} = 0.70711 \quad (A5)$$

$$t = \kappa R, \tau = \beta\kappa/2 \quad (A6)$$

$$\kappa^2 = \pi N\beta c \gamma/125 \quad (A7)$$

$$1/\mu = e^t/(1 + t) \quad (A8)$$

$$\beta_0 = 82.5/\eta(DT)^{1/2} \quad (A9)$$

The terms given explicitly in (A2) and (A3) are the leading square root and $c \log c$ terms; the higher terms are summarized by the following interpolation formulas:

$$\text{FB2} = 0.0755 - 0.1089t + 0.0705t^2 - 0.0569t^3 \quad 0 < t < 0.8 \quad (A10)$$

$$\text{FB3} = -0.08038 + 0.4760t - 1.232t^2 + 1.505t^3 \quad 0 < t < 0.22 \quad (A11)$$

$$= -0.07101 + 0.3388t - 0.5533t^2 + 0.3752t^3 \quad 0.22 < t < 0.4 \quad (A12)$$

$$= -0.05110 + 0.1940t - 0.1962t^2 + 0.0766t^3$$

$$0.4 < t < 0.8 \quad (\text{A13})$$

$$H1 = t(0.1248 - 0.10295t + 0.07925t^2 - 0.03031t^3)$$

$$0 < t < 0.8 \quad (\text{A14})$$

$$H2 = 2\tau(-0.0944 + 0.1174t - 0.2155t^2)$$

$$0 < t < 0.4 \quad (\text{A15})$$

$$= 2\tau(-0.08885 + 0.08461t - 0.16796t^2)$$

$$0.4 < t < 0.8 \quad (\text{A16})$$

A Fortran IV program has been written¹⁴ for obtaining values of Λ_0 , K_A , and R from conductance data using eq A1–A16, 6, and 12.

Miniprint Material Available. Full-sized photocopies of the miniprinted material from this paper only [Tables I (solvent properties), II (conductance of CsBr in dioxane-water), and III (conductance of ⁷LiBr and ⁷LiI)] or microfiche (105 × 148 mm, 24× reduction, negatives) containing all of the miniprinted and supplementary material for the

papers in this issue may be obtained from the Journals Department, American Chemical Society, 1155 16th St., N.W., Washington, D.C. 20036. Remit check or money order for \$4.00 for photocopy or \$2.50 for microfiche, referring to code number JPC-75-1604.

References and Notes

- (1) The results for cesium bromide and lithium chloride are included in a thesis presented by C. F. Mattina to the Graduate School of Yale University in partial fulfillment of the requirements for the degree of Doctor of Philosophy. The work on lithium iodide was done during the tenure of a post-doctoral research fellowship, 1969–1970.
- (2) J. E. Lind, Jr., and R. M. Fuoss, *J. Phys. Chem.*, **65**, 999 (1961).
- (3) J. E. Lind, Jr., and R. M. Fuoss, *J. Phys. Chem.*, **65**, 1414, 1727 (1961).
- (4) R. W. Kunze and R. M. Fuoss, *J. Phys. Chem.*, **67**, 911, 914 (1963).
- (5) J. C. Justice and R. M. Fuoss, *J. Phys. Chem.*, **67**, 1707 (1963).
- (6) T. L. Fabry and R. M. Fuoss, *J. Phys. Chem.*, **68**, 971, 974 (1964).
- (7) R. M. Fuoss, *J. Am. Chem. Soc.*, **80**, 5059 (1958).
- (8) R. M. Fuoss, *Proc. Natl. Acad. Sci. USA*, **71**, 4491 (1974).
- (9) J. E. Lind, Jr., J. J. Zwolenik, and R. M. Fuoss, *J. Am. Chem. Soc.*, **81**, 1557 (1959).
- (10) R. M. Fuoss, *J. Phys. Chem.*, **79**, 525 (1975).
- (11) R. M. Fuoss, *Trans. Faraday Soc.*, **30**, 967 (1934).
- (12) P. Debye, *Trans. Electrochem. Soc.*, **82**, 265 (1942).
- (13) M. Eigen, *Z. Phys. Chem. (Frankfurt am Main)*, **1**, 176 (1954).
- (14) R. M. Fuoss in "Computer Programs for Chemistry", Vol. 5, K. W. Wiberg, Ed., Academic Press, New York, N.Y., in press.

Electrical Conductivity of the Molten Bismuth Chloride–Aluminum Chloride, Tellurium Chloride–Aluminum Chloride, and Potassium Chloride–Tellurium Chloride Systems

Finn W. Poulsen and Niels J. Bjerrum*

Technical University of Denmark, Chemistry Department A, DK-2800 Lyngby, Denmark (Received December 3, 1974)

Specific conductivities have been measured in the binary molten systems BiCl₃–AlCl₃, TeCl₄–AlCl₃, and KCl–TeCl₄ in the composition ranges 0–100, 0–100 mol % AlCl₃ and 0–50 mol % KCl, respectively. The high equivalent conductivities for these systems can be explained tentatively by a Grotthaus-type chloride transfer mechanism involving bimolecular reactions of the type 2BiCl₃ ⇌ BiCl₂⁺ + BiCl₄[−] and 2TeCl₄ ⇌ TeCl₃⁺ + TeCl₅[−].

Introduction

The possibility of Grotthaus-type ionic conduction in molten salts has been suggested by Spedding¹ to explain the fact that molten salts such as the bismuth trihalides,² CuCl₃,³ and SnCl₂³ exhibit maxima in the electrical conductivity isotherms. The Grotthaus mechanism can be visualized as transfer of ions between polyatomic agglomerates present in the melt. It is generally assumed that the acceptor and donor species involved in the transfer reaction have already been brought sufficiently close together by diffusion for the transfer to take place. It can be anticipated that suitable conditions under which the Grotthaus mechanism may operate can be found in melts containing labile acceptor and donor units simultaneously.

Anomalous ionic conduction behavior has been demonstrated in molten AsCl₃ and SbCl₃. Klemensiewicz in 1908 reported abnormally high equivalent conductivities of various metal chlorides in molten SbCl₃.⁴ This was later on

confirmed by Baugham,⁵ who suggested that the Grotthaus-type chloride transfer mechanism SbCl₄[−] + SbCl₃ ⇌ SbCl₃ + SbCl₄[−] was responsible for the phenomenon. The measurements by Frycz and Tolloczko give an unusually high value (ca. 0.9) for the transference number of Cl[−] (t_{Cl^-}) of dilute solutions of KCl and NH₄Cl in molten SbCl₃.⁶ The Cl[−] is presumably present as SbCl₄[−]. Gutmann likewise found that t_{Cl^-} lies in the range 0.88–0.97 for solutions of (CH₃)₄N⁺Cl[−] in liquid AsCl₃.⁷

The possible contribution of chloride transfer mechanisms to the electrical conductivity observed in the binary melts BiCl₃–AlCl₃, TeCl₄–AlCl₃, and KCl–TeCl₄ is discussed in this paper.

Experimental Section

AlCl₃ was made from pure metal (99.999%) and HCl gas (electronic grade from Matheson). TeCl₄ and BiCl₃ were made by reaction between the metals (99.999%) and chlo-

rine (Fluka >99.95%). KCl (analytical reagent from Riedel-de Haën) was purified by first passing HCl gas over the solid and then through the melt, flushing with pure N₂, and finally filtering the melt.

The outer shape of the electrode cells was similar to that of cells used in a previous potentiometric work.⁸ The sintered disks, however, have been replaced by capillaries. The electrodes were 3 × 30 mm vitreous carbon rods (Carbone Lorraine, Type V10), which in contrast to platinum foil were not attacked by molten TeCl₄. The carbon electrodes could be sealed vacuum tight into the two electrode compartments. Cell constants (~200 cm⁻¹) were determined at room temperature with aqueous solutions of KCl made in accordance with Jones and Bradshaw.⁹ All measurements were corrected for the temperature dependence of the cell constant. The material that made up a melt was weighed in a nitrogen filled glove box and added to the cells.

Conductivity was measured in two different types of furnaces. One of the furnaces was an aluminum block furnace described previously.⁸ For convenience this furnace is denoted furnace 1. The other furnace (furnace 2) consisted of a Kanthal wire wound quartz tube surrounded by a water-cooled glass jacket. This furnace had two separate heating zones controlled by two Eurotherm Type LP-PID-FC regulators. With this arrangement a temperature higher than the melt temperature could be maintained above the melt to prevent condensation in the upper part of cells. Temperatures were measured at the capillaries of the cells with a calibrated chromel-alumel thermocouple, connected through a cold-junction compensation to a Type DM 2022S digital voltmeter from Digital Measurement Ltd. The temperature variation close to the capillary was ±0.1° in furnace 1 and ca. ±0.5° in furnace 2.

The relatively small temperature ranges within which the conductivities have been measured were a result of the high vapor pressure of the measured systems. In several experiments high vapor pressure caused leaks at the electrodes. The cells were connected through silver contacts and gold wires to a Wheatstone bridge consisting of two 10-kΩ (±0.1%) standard resistances and a Danbridge type PDR5/BCDEF decade resistance box in parallel with a compensation decade capacitance box. The bridge was balanced with a Tektronix oscilloscope Type 5103N connected to a Type 5AN amplifier in the x channel (connected to the generator) and a Type 5A20N differential amplifier in the y channel. All measurements were performed at 2000 Hz ac current from a Grundig Type TG 20 generator.

Results and Discussion

The specific conductivities as a function of the composition are shown in Figure 1 for the molten system BiCl₃-AlCl₃ at 225° and in Figure 2 for the molten system TeCl₄-AlCl₃ at 215°. These temperatures were chosen so that the smallest number of extrapolations were required. The conductance data for the two systems are summarized in Tables I and II. The temperature dependence of the specific conductivity are given in terms of the coefficients A, B, and C in the computer-fitted quadratic equations $\kappa(t) = A + Bt + Ct^2$ (t in °C).

Phase studies¹⁰ and vapor pressure measurements¹¹ of the BiCl₃-AlCl₃ system indicate the presence of a 1:1 compound both in the solid and in the vapor phase. Korshunov et al.¹² have measured conductivities of BiCl₃-AlCl₃ melts containing between 100 and 36 mol % BiCl₃. They claim a

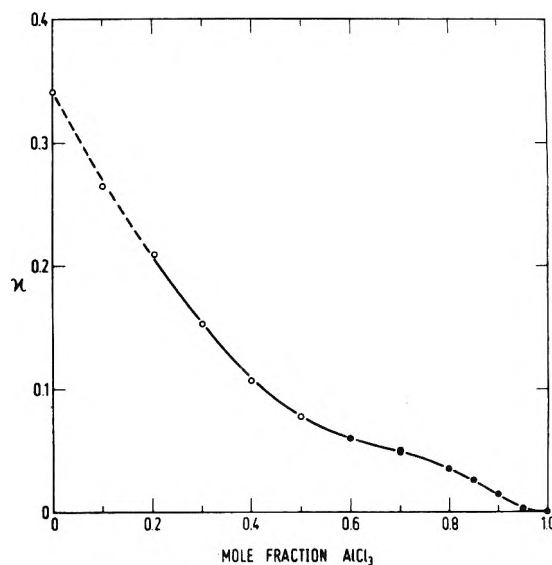


Figure 1. Specific conductivities ($\Omega^{-1} \text{ cm}^{-1}$) at 225° of BiCl₃-AlCl₃ melts. The dashed line indicates values calculated for temperatures outside the range of measurements: open circles, measurements made in furnace 2; filled circles, measurements made in furnace 1 (see Experimental Section).

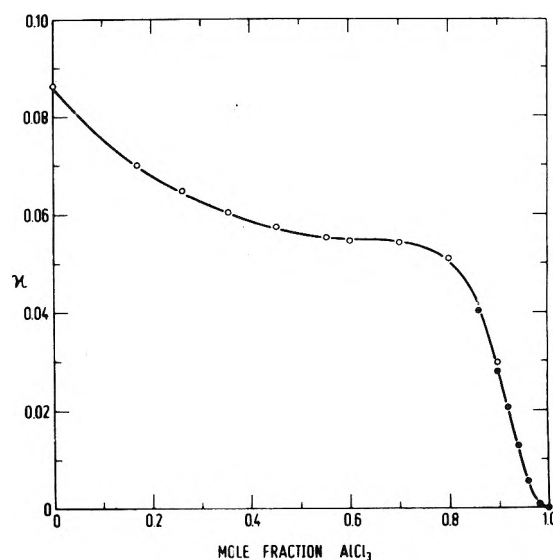


Figure 2. Specific conductivities ($\Omega^{-1} \text{ cm}^{-1}$) at 215° of TeCl₄-AlCl₃ melts: open circles, measurements made in furnace 2; filled circles, measurements made in furnace 1 (see Experimental Section).

local minimum in the conductivity isotherms around 50 mol % BiCl₃ to be indicative of the formation of BiCl₃·AlCl₃ in the melt. We found, however, no minimum. This may be explained by the fact that they used open cells instead of sealed cells. Mamantov et al. were unable to detect any complex formation between BiCl₃ and AlCl₃ in the molten state from the Raman spectrum of the molten 1:1 mixture.¹³

In analogy with the other trichlorides in group 5 molten BiCl₃ is postulated to be slightly dissociated according to



A value of about 10⁻⁴ for the molar equilibrium constant of reaction 1 at 234° has been calculated by Lumsden¹⁴ from cryoscopic data of Topol et al.¹⁵ As well as the short liqui-

TABLE I: Specific Conductivity of BiCl₃-AlCl₃ Melts

$$\kappa = A + Bt + Ct^2 \quad (t \text{ in } ^\circ\text{C})$$

Composition, mol % AlCl ₃	A	10 ³ B	10 ⁶ C	Std dev ×10 ⁴	t range, °C	No. of obser- vations
0.00 ^a	-0.5668	5.6073	-6.970	11.8	243-381	8
10.10 ^a	-0.3368	3.5675	-3.958	1.9	245-388	6
20.60 ^a	-0.2623	2.6762	-2.576	2.7	223-381	6
30.03 ^a	-0.1959	1.8759	-1.447	2.3	212-358	5
40.02 ^a	-0.1223	1.1115	-0.400	2.1	188-310	7
50.01 ^a	-0.0904	0.7659	-0.079	2.9	202-322	5
60.06 ^a	-0.0270	0.2106	0.796	5.4	205-295	5
70.02 ^a	0.0847	-0.8196	2.963	3.2	199-253	4
80.01 ^a	0.0257	-0.3830	1.865	5.3	203-248	9
59.96 ^b	-0.05870	0.47718	0.2271	0.72	200-250	5
69.99 ^b	-0.2492	2.0203	-3.087	5.3	210-250	5
79.96 ^b	0.0117	-0.1574	1.173	1.4	210-230	4
85.01 ^b	-0.7380	6.1890	-12.409	20.9	209-230	4
89.93 ^b	-0.00497	-0.06449	0.6750	0.84	210-230	4
94.96 ^b	-0.01477	0.11273	0.1389	0.17	210-225	4

^a Measured in furnace 2 (see Experimental Section). ^b Measured in furnace 1 (see Experimental Section).

TABLE II: Specific Conductivity of TeCl₄-AlCl₃ Melts

$$\kappa = A + Bt + Ct^2 \quad (t \text{ in } ^\circ\text{C})$$

Composition, mol % AlCl ₃	A	10 ³ B	10 ⁶ C	Std dev ×10 ⁴	t range, °C	No. of obser- vations
0.00 ^a	-0.1928	1.5190	-0.904	4.9	214-300	7
17.15 ^a	-0.0841	0.6971	0.176	4.1	198-317	6
26.19 ^a	-0.0716	0.6330	0.079	5.3	181-299	5
35.57 ^a	-0.0363	0.3612	0.474	2.8	170-302	5
45.23 ^a	-0.0202	0.2697	0.476	2.9	147-300	6
55.36 ^a	-0.0145	0.2373	0.455	2.1	152-307	6
59.99 ^a	-0.01740	0.27052	0.3462	0.47	187-301	5
70.06 ^a	-0.00812	0.21551	0.3893	0.78	191-304	5
79.96 ^a	0.0007	0.1346	0.502	4.3	178-301	11
89.99 ^a	0.0160	-0.0816	-0.702	5.2	194-237	5
85.98 ^b	0.0173	-0.0785	0.893	1.2	186-254	10
89.95 ^b	-0.0132	0.1548	0.198	5.1	200-235	5
91.99 ^b	0.0329	-0.2937	1.120	1.8	205-223	5
93.98 ^b	0.0068	-0.0660	0.449	2.1	202-215	4
95.97 ^b	-0.00568	0.03448	0.0925		202-210	3

^a Measured in furnace 2 (see Experimental Section). ^b Measured in furnace 1 (see Experimental Section).

range (234-440°) another indication that molten BiCl₃ is only slightly dissociated is given by the observation that BiCl₃ acts as a molecular liquid near its critical point.¹⁶ The true equivalent conductivity of BiCl₃, Λ_{BiCl_3} ($\lambda_{\text{BiCl}_2^+} + \lambda_{\text{BiCl}_4^-}$), can then be calculated from the relationship

$$\kappa = 1/1000 \sum \lambda_i c_i \quad (2)$$

where c_i is the equivalent concentration of the i th ion (the molar concentration times the charge on the ion). Λ_{BiCl_3} is ca. $2.9 \times 10^3 \text{ cm}^2/\Omega \text{ mol}$ at the melting point (234°). A conduction mechanism superior to migration must evidently be responsible for an equivalent conductivity of such a magnitude. By comparison the equivalent conductance for a LiNO₃-NaNO₃ melt (60 mol % NaNO₃) at the same temperature can be calculated by interpolation to be ca. 27

$\text{cm}^2/\Omega \text{ mol}$.¹⁷ The density is here calculated assuming ideal mixtures of LiNO₃ and NaNO₃.

As can be seen from Figure 1 a decrease is obtained in the specific conductivity by addition of AlCl₃ to BiCl₃. Since it is to be expected that AlCl₃ is a stronger chloride acceptor than BiCl₃ one would assume more ions to be formed by addition of AlCl₃ and hence the conductivity to increase rather than decrease if migration alone were responsible for the conductivity. Unfortunately we see no way by which the present measurements can be used to make more detailed calculations relating to this phenomena. The main problem is that the ionic strength of the melt is changed considerably as more and more AlCl₃ is added thus changing the activity coefficient for the bismuth ions in an unknown way. An interesting phenomenon is that a

TABLE III: Specific Conductivity of TeCl₄-KCl Melts

$$\kappa = A + Bt + Ct^2 \quad (t \text{ in } ^\circ\text{C})$$

Composition, mol % KCl	A	10 ³ B	10 ⁶ C	Std dev $\times 10^4$	t range, $^\circ\text{C}$	No. of obser- vations
0.00 ^a	-0.3733	2.8125	-3.229	6.5	251-395	7
2.28 ^a	-0.3400	2.6180	-2.884	8.7	245-397	7
7.03 ^a	-0.3779	2.7583	-2.852	4.9	294-392	5
12.84 ^a	-0.2489	1.9952	-1.590	4.9	295-395	5
19.43 ^a	-0.2577	1.9869	-1.350	6.7	234-394	13
24.86 ^a	-0.2676	2.0154	-1.234	22.0	271-395	7
30.87 ^a	-0.3451	2.4346	-1.706	19.8	296-392	6
38.57 ^a	-0.1814	1.4572	-0.144	7.34	342-418	4
50.01 ^a	0.0681	0.2649	1.406	12.9	442-474	5

^a Measured in furnace 2 (see Experimental Section).

very low specific conductivity is obtained for the BiCl₃-AlCl₃ system in the range 95-100 mol % AlCl₃. A similar phenomenon is found in the TeCl₄-AlCl₃ system. This can probably be explained by the formation of uncharged complexes. Uncharged complexes formed in molten AlCl₃ have previously been suggested by Oye and Gruen¹⁸ for the elements Ti, V, Cr, Mn, Fe, Co, Ni, and Cu in the oxidation state +2 in small concentrations.

Raman spectra¹⁹ of the molten TeCl₄-AlCl₃ system indicate at the 1:1 composition the existence of TeCl₃⁺ and AlCl₄⁻ ions. Potentiometric²⁰ and Raman spectroscopic¹⁹ measurements on the dilute system AlCl₃-TeCl₄-KCl in a KAlCl₄ solvent indicate the stepwise formation of the tellurium complexes, TeCl₃⁺, TeCl₄, TeCl₅⁻, and TeCl₆²⁻, as the chloride ion concentration is increased. The Raman spectroscopic measurements also indicate that no polymeric units are present in molten TeCl₄. Furthermore the concentration of free Cl⁻ ions was found by a potentiometric method to be less than 10⁻² M.¹⁹ From this information it is reasonable to expect the dissociation in molten TeCl₄ to be



The problem, however, is to what extent TeCl₄ is dissociated according to equilibrium 3. From the previous mentioned Raman spectra the molar equilibrium constant for reaction 3 could be calculated to be about 0.5×10^{-2} at 250°. This value is based on the assumption that (3) is the only equilibrium in the melt, that the Raman intensities are proportional to the concentrations, and that the scattering intensities of the symmetrical stretching vibration for each of the complexes are the same (this seems to be the case for the complexes dissolved in KAlCl₄). The value obtained for the equilibrium constant in this way is not so different from the value one can calculate from the previously mentioned potentiometric data of dilute solutions of TeCl₄ in KAlCl₄ at 300°. The value of the molar equilibrium constant of reaction 3 can here be calculated as 2.69×10^{-2} and the chloride concentration in molten TeCl₄ can be calculated as ca. 1.1×10^{-3} M. Of course one has to take into consideration different activity coefficients for the two systems. The true equivalent conductance Λ_{TeCl_4} ($\lambda_{\text{TeCl}_3^+} + \lambda_{\text{TeCl}_5^-}$) can now be calculated as about 2.2×10^2 cm²/Ω mol of ion at 250°. This value is higher than the values usually encountered in molten salt systems at this temperature. By comparison the equivalent conductivity for a LiNO₃-NaNO₃ (60 mol % NaNO₃) melt at 250° can be calculated

as ca. 31 cm²/Ω mol and the equivalent conductance for NaAlCl₄ (49.7 mol % NaCl-50.3 mol % AlCl₃) 61 cm²/Ω mol at the same temperature.²¹ Based on this it seems difficult to explain the conductivity in TeCl₄ by migration alone. That another mechanism other than migration is present is in accordance with the observed decrease in the specific conductivity of the melt by addition of AlCl₃. It has previously¹⁹ been pointed out that at the 1:1 composition the reaction must be TeCl₄ + AlCl₃ → TeCl₃⁺ + AlCl₄⁻ with almost complete reaction. What is observed is that the conductivity decreases even if the concentrations of the conducting ions increase. The probability that the acceptor and donor species are brought sufficiently close together for the transfer to take place is probably reduced considerably by dilution. At the 1:1 composition at 215° the equivalent conductance can be calculated by interpolation as about 11 cm²/Ω mol. The uncertainty in this value is due to the lack of density measurements. It is, however, possible to make a good guess of the densities based on comparison with chloroaluminate melts such as NaCl-AlCl₃ and BiCl₃-AlCl₃.²² A value around 11 cm²/Ω mol of ions seems reasonable if only migration is responsible for the conductivity. It is lower than the values obtained for the LiNO₃-NaNO₃ system and for NaAlCl₄²¹ at the same temperature, but this can be explained by the greater size of the cation in the present system.

As can be calculated from Table III addition of KCl to molten TeCl₄ causes a steady increase in the specific conductivity. At 450° the equivalent conductivity of the 1:1 mixture (of KCl and TeCl₄), where one would expect formation of K⁺ and TeCl₅⁻, amounts to ca. 77 cm²/Ω mol of ions. The density is computed on the basis of an ideal mixture. This can be compared with 54.0 cm²/Ω mol calculated for molten KNO₃ at the same temperature.²³ These figures are typical of ionic melts and can in the present cases be ascribed mainly to the high mobility of the potassium ions.

Since we have observed in the TeCl₄ case that neither the formation of more TeCl₃⁺ (upon addition of AlCl₃) nor formation of more TeCl₅⁻ (addition of KCl) cause inexplicable changes in the conductivity, the Grotthaus mechanism in molten TeCl₄ may be of the same type as the self-dissociation reaction involving both TeCl₃⁺ and TeCl₅⁻. The conduction mechanism type could thus be of the asymmetrical dissociation type described by Wyatt for H₂O and H₂SO₄.²⁴ The chloride transfer mechanism postulated for molten BiCl₃ may also be essentially of this type.

The final conclusion of the present work is that we are

dealing with some kind of chloride transfer mechanism in the $\text{BiCl}_3\text{-AlCl}_3$, $\text{TeCl}_4\text{-AlCl}_3$, and KCl-TeCl_4 systems, but with the present knowledge it is impossible to treat this problem more than semiquantitatively. Other methods are needed to determine exactly the magnitude of self-dissociation of concentrated molten salt systems.

References and Notes

- (1) P. L. Spedding, *J. Phys. Chem.*, **76**, 1348 (1972).
- (2) L. F. Grantham and S. J. Yosim, *J. Phys. Chem.*, **67**, 2506 (1963).
- (3) L. F. Grantham and S. J. Yosim, *J. Chem. Phys.*, **45**, 1192 (1966).
- (4) Z. Klemensiewicz, *Bull. Int. Acad. Sci. Cracovie*, **6**, 485 (1908).
- (5) G. B. Porter and E. C. Baugham, *J. Chem. Soc.*, 744 (1958).
- (6) K. Frycz and S. Tolloczko, *Festschr. Univ. Lwow*, **1**, 1 (1912); *Chem. Zentralbl.*, **1**, 91 (1913).
- (7) V. Gutmann, *Sven. Kern. Tidskr.*, **68**, 1 (1956).
- (8) J. H. von Barner and N. J. Bjerrum, *Inorg. Chem.*, **12**, 1891 (1973).
- (9) G. Jones and B. C. Bradshaw, *J. Am. Chem. Soc.*, **55**, 1780 (1933).
- (10) B. G. Korshunov, N. I. Kaloev, L. A. Nisel'son, and O. R. Gavrilov, *Russ. J. Inorg. Chem.*, **13**, 1017 (1968).
- (11) E. S. Komova, A. L. Kuz'menkov, and G. I. Novikov, *Zh. Fiz. Khim.*, **46**, 2690 (1972).
- (12) B. G. Koshunov and N. I. Kaloev, *Izv. Vyssh. Uchebny. Zaved., Chem. Metal.*, **11**, 6, 73 (1968).
- (13) K. W. Fung, G. M. Begun, and G. Mamantov, *Inorg. Chem.*, **12**, 53 (1973).
- (14) J. Lumsden, "Thermodynamics of Molten Salt Mixtures", Academic Press, London, 1966, pp 285-287.
- (15) L. E. Topol, S. M. Mayer, and L. D. Ransom, *J. Phys. Chem.*, **64**, 862 (1960).
- (16) J. W. Johnson and D. Cubicciotti, *J. Phys. Chem.*, **68**, 2235 (1964).
- (17) Y. Doucet and M. Bizouard, *Bull. Soc. Chim. Fr.*, 1570 (1959).
- (18) H. A. Oye and D. M. Gruen, *Inorg. Chem.*, **6**, 836 (1964).
- (19) F. W. Poulsen, N. J. Bjerrum, and O. F. Nielsen, *Inorg. Chem.*, **13**, 2693 (1974).
- (20) J. H. von Barner, N. J. Bjerrum, and K. Kiens, *Inorg. Chem.*, **13**, 1708 (1974).
- (21) A. I. Kryagova, *Zh. Obshch. Khim.*, **9**, 2061 (1939).
- (22) C. R. Boston, *J. Chem. Eng. Data*, **11**, 262 (1966); **13**, 117 (1968).
- (23) H. Bloom, I. W. Knaggs, J. J. Molloy, and D. Welch, *Trans. Faraday Soc.*, **49**, 1458 (1953).
- (24) P. A. H. Wyatt, *Trans. Faraday Soc.*, **57**, 773 (1961).

Temperature Dependence of the Diffusion Coefficient of $^{14}\text{CO}_2$ in Dilute HCl

J. G. Hawke* and I. White

Chemistry School, Macquarie University, Sydney 2113, Australia and the Department of Pharmaceutical Chemistry, University of Sydney, Sydney 2006, Australia (Received December 10, 1973; Revised Manuscript Received March 19, 1975)

The temperature dependence of the diffusion coefficients for ^{14}C labeled carbon dioxide gas diffusing in dilute HCl solutions has been measured. The radioactively labeled gas was trapped as it diffused out of unstirred aqueous solutions. The diffusion curves were analyzed according to the mathematical model proposed by Hawke and Parts. The data obtained are from 10 to 20% higher than the literature values measured by a variety of techniques. The wide variations in these quoted values may well be due to uncontrolled variations in the pH of the solutions used. It is proposed that our results refer to the diffusion of free CO_2 in water whereas almost all other workers have measured the diffusion coefficients in solutions, having a pH >4.0 which are a weighted mean of D_{CO_2} , $D_{\text{HCO}_3^-}$, and $D_{\text{CO}_3^{2-}}$. Values of E_D and ΔS^* calculated from Eyring's transition-state theory support the decreased interaction between CO_2 and water in acid solutions.

Introduction

This work has arisen from earlier studies by Hawke and coworkers^{1,2} on the permeability of monolayers at the gas-liquid interface to CO_2 and H_2S in which a mass transfer coefficient across the interface was derived assuming a literature value for the diffusion coefficient in the liquid phase. However substantial variation exists in literature values²⁰ and as yet diffusivities cannot be predicted from molecular descriptions without the aid of experimentally derived parameters. This paper deals with the dependence of the diffusion coefficient of $^{14}\text{CO}_2$ upon acid concentration and also temperature over the temperature range 1-20°.

Since a number of workers have found immeasurably low interfacial resistances for water (Harvey and Smith³), we have here applied the model developed by Hawke and

Parts⁴ for the loss of CO_2 from quiescent aqueous solutions having a clean surface.

A general solution of the equations proposed has been given by McKay⁵ in connection with the drying of porous solids initially saturated with water.

$$\frac{M_t}{M_\infty} = 1 - \sum_{n=1}^{\infty} \frac{2N^2 \exp(-\beta_n^2 Dt/a^2)}{\beta_n^2(\beta_n^2 + N^2 + N)} \quad (1)$$

Here M_t/M_∞ expresses the fraction of the diffusing gas which has left the liquid after time t , $N = aK_S/D$, and the β 's are the positive roots of $\beta \tan \beta = N$. Here a = depth of solution, K_S = surface mass-transfer coefficient for the gas-liquid interface, and D = diffusion coefficient in liquid. For the case of a clean interface K_S is infinite and therefore:

$$\frac{M_t}{M_\infty} = 1 - \sum_{n=1}^{\infty} \frac{2 \exp(-\beta_n^2 \tau)}{\beta_n^2} \quad (2)$$

$$\beta_n = (2n - 1)(\pi/2)$$

$$\tau = D_1 t/a^2$$

* Address correspondence to this author at The University, Chemical Laboratory, Lensfield Rd., Cambridge CB2 1EW, England

Since depth and time are readily measured, eq 2 can be used to measure D for gases in liquids.

Experimental Section

The apparatus used for the determination of the diffusion coefficient has been described by Hawke and White.^{6,7} In addition a heavy gas-tight cap attached to an O ring was introduced through port F to ensure uniform concentration and thermal equilibrium of the solution at time $t = 0$ in conformity with the assumptions used by Hawke and Parts⁴ in their model.

Also to minimize meniscus formation, the inside top edge of cell C was machined out to a depth of 1 mm, in each direction. Cells used had a depth of 0.27–0.30 cm and an internal cross-sectional area of $\approx 14 \text{ cm}^2$.

A number of rigorous tests has been applied to ensure that further assumptions of the model have been obeyed.

(i) The diffusion in the gas phase is fast and nonlimiting.

90 runs were carried out using an Ar–He–N₂O atmosphere instead of nitrogen at various gas thicknesses (0.05–0.59 cm), achieved by inserting close fitting brass extension rings over the cell.

The diffusivities observed were in agreement with those obtained using nitrogen. Most other workers have used CO₂ solely in their determinations.

(ii) Fick's laws of diffusion assume no convection in the liquid, further that the diffusion coefficient is independent of concentration and that the gas does not react with the liquid.

Plevan and Quinn⁸ have shown that buoyancy-driven convection is eliminated when carbon dioxide is desorbed from solution. Also in this work the concentration of CO₂ was very low ($\approx 10^{-7} M$) and the cell was always held below ambient temperature.⁹ Regression analysis of 17 determinations of the diffusion coefficient at 20° in agar-agar gels varying from 0.5 to 2.5% (W/V) showed no significant correlation with gel concentration but agreement with the data in water.

Surface-tension driven convection was tested by performing six runs at 20° in which 0.5 ml of "puriss" grade oleic acid was added to the surface.⁸ Again agreement with the diffusion coefficients obtained on water at pH 2.0 was obtained. In order to demonstrate whether convection caused by stirring could be measured, a Teflon-coated needle 0.076 cm diameter, was rotated in the cell at 30 rpm by means of a magnetic stirrer. Now the overall mass transfer coefficient K_T is given by

$$\frac{1}{K_T} = \frac{1}{K_L} + \frac{1}{K_S} + \frac{1}{K_G} \text{ cm sec}^{-1}$$

and since $K_G(\text{gas}), K_S(\text{interface}) \gg K_L(\text{liquid})$ then $K_T = K_L$. Therefore in a stirred solution:

$$\frac{M_t}{M_\infty} = 1 - \exp(-K_L t/a)$$

or

$$\ln(1 - M_t/M_\infty) = -K_L t/a \quad (3)$$

Figure 1 indicates the marked enhancement of mass transport due to stirring. All results fitted an equation of the form below with a correlation coefficient of 0.997.

$$(1 - M_t/M_\infty) = 1 - A \exp(-Bt) \quad (4)$$

The unstirred case of course required different coefficients. It is not surprising that stirred and unstirred both follow eq 4 since eq 2 for long times becomes:

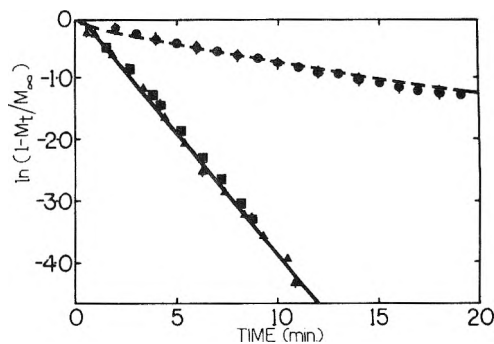


Figure 1. Mass transport enhanced by stirring: stirred run 749 (■), run 751 (▲), unstirred run 750 (●). Predicted behavior for diffusion, from eq 2 (---); line of best fit for runs 749 and 751 (—).

$$\frac{M_t}{M_\infty} = 1 - \frac{8 \exp(-\pi/2)^2 \tau}{\pi^2} \quad (5)$$

D (calculated from τ) can be expressed as an explicit function of time, depth, and fraction of gas absorbed, viz.

$$D = -\frac{4a^2}{\pi^2 t} \ln \left[\frac{\pi^2}{8} (1 - M_t/M_\infty) \right] \quad (6)$$

which has again the same functional form as (4).

The long term approximation agrees with the series solution to sufficient accuracy (differ by <1 in 1000) for $\tau > 0.23$ or a diffusion time greater than 15 min.

Effect of CO₂ Concentration

The lack of dependence of the diffusion coefficient upon CO₂ concentration is seen from Table I over a range of 10⁵.

The dependence of the diffusion coefficient on acid concentration at 9.6° may be seen in Table II.

The diffusion coefficient at pH 6.8 is much lower owing to the reaction of CO₂ with water. Hence all measurements were carried out at pH 2.0.

Results and Discussion

The diffusion coefficients of CO₂ in water found in this work (Table III) are about 12% higher than most of the previously published values (see Figure 2). All diffusion data are quoted with the appropriate standard deviation.

The constancy of the expression $D\eta/T$ conforms with the Stokes–Einstein equation. Unlike most techniques used, the present method does not require a knowledge of the CO₂ concentration in solution. The final constant count rate is assumed to be directly proportional to the initial quantity of CO₂ present. Extensive tests showed that no ¹⁴CO₂ escaped from the cell, reacted with the cell materials, or remained in solution (detectable to <1%).

It does not appear likely that the isotopic difference between ¹⁴CO₂ and ¹²CO₂ could give rise to a 12% difference. The self-diffusion coefficient of H₂¹⁶O lies between 2.13 and $2.51 \times 10^{-5} \text{ cm}^2 \text{ sec}^{-1}$ whereas H₂¹⁸O lies between 2.57 and $2.66 \times 10^{-5} \text{ cm}^2 \text{ sec}^{-1}$.¹¹

Considerations of mass would suggest an isotope effect in the opposite direction. In the literature by Kigoshi and Hashitani,¹² however, the only reported values for ¹⁴CO₂ diffusion coefficients are in close agreement with the values for ¹²CO₂.

It is therefore unlikely that the higher values in this work can be ascribed satisfactorily to an isotope effect.

Longmuir et al.¹³ measured CO₂ diffusing through a filter paper saturated with 0.01 N HCl of unknown path

TABLE I: Effect of CO₂ Concentration on the "Integral" Diffusion Coefficient

Temp, °C	No. of runs	Initial CO ₂ concn, <i>M</i>	10 ⁵ <i>D</i> , cm ² sec ⁻¹
9.6	6	(2.1 ± 0.1) × 10 ^{-2a}	1.45 ± 0.10
	22	(2.0 ± 0.2) × 10 ⁻⁷	1.45 ± 0.10
20.0	5	(9 ± 1) × 10 ^{-7b}	2.05 ± 0.12
	21	(1 ± 0.1) × 10 ⁻⁷	2.05 ± 0.12

^a Concentration increased by the addition of ¹²CO₂. ^b Concentration increased by the addition of ¹⁴CO₂.

TABLE II: Dependence of Diffusion Coefficient on Acid Concentration at 9.6 ± 0.1°

Concn, <i>M</i>	Acid	No. of runs	10 ⁵ <i>D</i> , cm ² sec ⁻¹
0 ^a		9	1.02 ± 0.23
0.01 ^b	HCl	22	1.45 ± 0.10
0.1	HCl	5	1.37 ± 0.04
0.32	HCl	6	1.40 ± 0.08
1.0	HCl	6	1.54 ± 0.12
3.0	HCl	6	1.51 ± 0.09
0.89	H ₂ SO ₄	3	1.50 ± 0.05

^a pH 6.8 ± 0.1. ^b Value from Table I.

TABLE III: Summary of the Diffusion Coefficients of CO₂ in Water at pH 2.0

Temp, °C	No. of Runs	10 ⁵ <i>D</i> , cm ² sec ⁻¹ (this work)	<i>D</i> _η / <i>T</i> (10 ¹⁰), dyn/deg
1.0 ± 0.15	14	1.08 ± 0.05	6.8 ± 0.5
5.0 ± 0.1	24	1.24 ± 0.05	6.8 ± 0.5
9.6 ± 0.1	34	1.45 ± 0.10	6.8 ± 0.7
14.8 ± 0.1	74	1.66 ± 0.10	6.6 ± 0.6
20.0 ± 0.05	113	2.05 ± 0.12	6.9 ± 0.8

length at 37° and found a value for the diffusion coefficient 11% higher than for water (pH unspecified). Their value agrees closely with a value calculated from the Arrhenius-type law found in this work to fit our data. Hashitani and Kigoshi¹⁴ concluded that the diffusion coefficient, \bar{D} , of total "CO₂" at any pH is the weighted mean of the diffusion coefficients of CO₂, HCO₃⁻ and CO₃²⁻, i.e.

$$\bar{D} = (xD)_{\text{CO}_2} + (xD)_{\text{HCO}_3^-} + (xD)_{\text{CO}_3^{2-}} \quad (7)$$

where $(xD)_{\text{CO}_2}$ is the mole fraction of CO₂ multiplied by the diffusion coefficient of CO₂, etc. Wise and Houghton¹⁵ found a similar weighted mean could predict the diffusion coefficient of air in water and it may well be that a relationship of the form of eq 7 is a reasonable description for the total diffusion of dilute mixtures in water.

In Table II it can be seen that increasing the acid concentration beyond 0.01 *M*, where [HCO₃⁻] is negligible, had only a minor effect on the diffusion coefficient whereas at pH 6.8 a substantially lower value for the diffusion coefficient was observed. At pH 6.8 and 25° the ratio [HCO₃⁻]/[CO₂] is 2.8 and thus the observed diffusion coefficient is the "mean" diffusion coefficient of CO₂ and HCO₃⁻. These experiments were only possible in the very low CO₂ concentrations used in this radiochemical technique. In order to

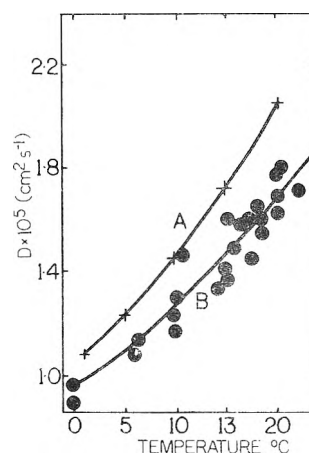


Figure 2. The diffusion coefficient of CO₂ in water in the range 0 to 23°. Curve A is plotted from the best polynomial fitting the data from Table III and curve B the published data from Himmelblau.²⁰

calculate the "mean" diffusion coefficient, D_{CO_2} and $D_{\text{HCO}_3^-}$, must be known. $(xD)_{\text{CO}_3^{2-}}$ in eq 7 is negligibly small at pH 6.8. In order that the value of D_{CO_2} found in this work could be used in the calculation, a value for $D_{\text{HCO}_3^-}$ must be estimated. A value of $D_{\text{HCO}_3^-}/D_{\text{CO}_2}$ at 9.6° of 0.552 was interpolated from Kigoshi's results.¹² Thus using D_{CO_2} equal to 1.45×10^{-5} cm² sec⁻¹ gives a value of 0.80×10^{-5} cm² sec⁻¹ for $D_{\text{HCO}_3^-}$. Published values for the temperature dependence of the first ionization constant of carbonic acid provide a value of 2.15 for the ratio [HCO₃⁻]/[CO₂] at 9.6° which together with the above diffusion coefficients were substituted into eq 7. The calculated value of \bar{D} at 9.6° and pH 6.8 obtained was 1.01×10^{-5} cm² sec⁻¹ which is in excellent agreement with the measured value of 1.02×10^{-5} cm² sec⁻¹ (Table II).

It appears therefore that the high values obtained in this work arise from the pH of the solution.

Indirect supporting evidence comes from a comparison of the diffusivities of CO₂ and N₂O. Gases with similar solubilities, molecular size, and molecular weight, such as N₂O and CO₂, might be expected to have similar diffusion coefficients. Thomas and Adams¹⁷ report a value of 1.92×10^{-5} cm² sec⁻¹ for the diffusion coefficient of N₂O at 20° which is in agreement with the value found in this work for the diffusion coefficient of CO₂ in water at pH 2. However a value for D_{CO_2} taken from their results is about 11% lower. Also the diffusivity of CO₂ measured in this work at 14.8° is close to that for N₂O, at 15°, found by Davidson and Cullen.¹⁸

At low pH the hydration reaction between CO₂ and H₂O becomes negligible and the diffusivity of CO₂ is, as expected, very close to that of N₂O.

The higher values found here are probably the true values for the diffusivity of free CO₂ in water.

Although most workers have used saturated solutions of CO₂ to begin with, at the point of observation the concentration is much less and consequently the pH changes through the system. Such a pH gradient for example would apply in the agar-agar gels used by Tamman and Jessen.¹⁹

Activation Energies

Activation energies calculated from the Arrhenius equation are 5.35 ± 0.5 kcal/mol and are in agreement with the literature^{10,18} values reported here but about 10% higher

than the values calculated from eq 8 which summarizes the literature values, viz. 4.90 kcal/mol at 0° to 4.56 kcal/mol at 20°

$$E_D = -R(35.57 - 6.82 \times 10^5/T) \quad (8)$$

This may be accounted for by the influence of temperature upon the CO₂-H₂O equilibrium in pure water. The transition state for diffusion at pH 2.0 may more nearly approximate the transition state for diffusion at 30° in pure water.

Entropy of Activation

The entropy of activation for the diffusion of CO₂ in water using the usual Eyring expression

$$D = Kd^2(kT/\hbar) \exp(\Delta S^*/R) \exp(-\Delta H^*/RT) \quad (9)$$

was found to be $5.1 \pm 0.2 \text{ cal mol}^{-1} \text{ deg}^{-1}$ compared with a mean value of $1.65 \pm 0.15 \text{ cal mol}^{-1} \text{ deg}^{-1}$ calculated from the results of other workers.¹² In this expression a value of $d = 2.83 \text{ \AA}$ was adopted for the diameter of a water molecule and ΔH^* was calculated from the usual equation $E_D = \Delta H^* + RT$ where T is the mean temperature of the range.

The higher value found in this work again reflects the free state of CO₂ in acid solutions. The entropies of activation found for the self-diffusion of water lie in between. If an increase in entropy of activation is caused by a gain in rotational freedom in the transition state over the initial state then the positive entropy of activation for the diffusion of CO₂ in water may be attributed to the breaking of hydrogen bonds in the water surrounding the CO₂ molecules or the breaking of CO₂-water associations, in the formation of the transition state.

Conclusion

It does appear then that almost all values quoted in the literature for the diffusivity of CO₂ in water are in fact the weighted mean of the diffusion coefficients of CO₂, HCO₃⁻, and CO₃²⁻. The wide variation in these quoted values may well be due to uncontrolled variations in the pH of the solutions used. The diffusivity of "free" CO₂ requires the suppression of the CO₂ hydration reaction by carrying out the measurements below pH 4.

Acknowledgment. This project has been supported and financed, in part, by the Federal Water Pollution Control Administration, U.S. Department of the Interior, pursuant to the Federal Water Pollution Control Act.

References and Notes

- (1) J. G. Hawke and A. E. Alexander, "Retardation of Evaporation by Monolayers", V. K. La Mer, Ed., Academic Press, New York, N.Y., 1962, p 9.
- (2) J. G. Hawke and I. White, *J. Phys. Chem.*, **70**, 3369 (1966).
- (3) E. A. Harvey and W. Smith, *Chem. Eng. Sci.*, **10**, 274 (1959).
- (4) J. G. Hawke and A. G. Parts, *J. Colloid Sci.*, **20**, 253 (1964).
- (5) A. T. McKay, *Proc. Phys. Soc. (London)*, **42**, 547 (1930).
- (6) J. G. Hawke and I. White, *J. Phys. Chem.*, **74**, 14 (1970).
- (7) I. White, Ph.D. Thesis, University of Sydney, 1970.
- (8) R. E. Plevan and J. A. Quinn *AIChE J.*, **12**, 894 (1966).
- (9) H. J. V. Tyrrell in "Diffusion and Heat Flow in Liquids", Butterworths, London, 1961, p 141.
- (10) Y. P. Tang and D. M. Himmelblau, *Chem. Eng. Sci.*, **20**, 7 (1965).
- (11) D. Eisenberg and W. Kauzmann in "The Structure and Properties of Water", Oxford University Press, London, 1969, p 218.
- (12) K. Kigoshi and T. Hashitani, *Bull. Chem. Soc. Jpn.*, **36**, 1372 (1963).
- (13) I. S. Longmuir, R. E. Forster, and C. Y. Woo, *Nature (London)*, **209**, 383 (1966).
- (14) K. Hashitani and K. Kigoshi, *Bull. Chem. Soc. Jpn.*, **48**, 1395 (1965).
- (15) D. L. Wise and G. Houghton, *Chem. Eng. Sci.*, **23**, 1211 (1968).
- (16) R. Nasanen, *Acta Chem. Scand.*, **1**, 204 (1947).
- (17) W. J. Thomas and M. J. Adams, *Trans. Faraday Soc.*, **61**, 668 (1965).
- (18) J. F. Davidson and E. J. Cullen, *Trans. Inst. Chem. Eng.*, **35**, 51 (1957).
- (19) H. G. Tamman and V. Jessen, *Z. Anorg. Allg. Chem.*, **179**, 125 (1929).
- (20) D. M. Himmelblau, *Chem. Rev.*, **64**, 527 (1964).

Photodissociation of Ketene at 313 nm¹

Vaclav Zabransky and Robert W. Carr, Jr.*

Department of Chemical Engineering and Materials Science, University of Minnesota,
Minneapolis, Minnesota 55455 (Received January 14, 1975)

Publication costs assisted by the University of Minnesota

The yields of products resulting from reactions of $\text{CH}_2(^1\text{A}_1)$ and $\text{CH}_2(^3\text{B}_1)$ in 313-nm photolysis of ketene-propane mixtures, and ketene-*n*-pentane mixtures, were determined at pressures between 1 and 709 Torr. Products resulting from $\text{CH}_2(^3\text{B}_1)$ reactions account for $30 \pm 3\%$ of the methylenes, with the balance attributed to $\text{CH}_2(^1\text{A}_1)$ reactions. The relative singlet and triplet methylene yields are independent of pressure in the range investigated. About 85% of the $\text{CH}_2(^3\text{B}_1)$ is formed directly in the ketene primary process, and the remaining 15% is produced by collisional deactivation of $\text{CH}_2(^1\text{A}_1)$. A model for electronic relaxation and photodissociation of ketene at 313 nm in which the initially excited $\text{CH}_2\text{CO}(^1\text{A}'')$ state rapidly internally converts to the ground state, $\text{CH}_2\text{CO}(^1\text{A}_1)$, is shown to be consistent with the data, and to also explain other features of ketene photochemistry and spectroscopy.

Introduction

Although the photodissociation of ketene to methylene and carbon monoxide is well known, there is little information about the details of electronic relaxation processes occurring after excitation. At least part of the difficulty in understanding the primary process lies in the fact that light emission from ketene has never been observed. Although it has been possible to study excited state behavior by luminescence methods, there is an alternative possibility which can be applied to this relatively small and intrinsically interesting molecule. At 300 nm and longer wavelengths both $\text{CH}_2(^3\text{B}_1)$ and $\text{CH}_2(^1\text{A}_1)$, the ground and first excited states of methylene, respectively, are the only two states energetically accessible, and both are present in ketene photolysis in this range. Moreover, these two spin states undergo distinguishably different reactions with hydrocarbons. Measurements of products arising through $\text{CH}_2(^1\text{A}_1)$ reactions, and those arising through $\text{CH}_2(^3\text{B}_1)$ reactions, were undertaken to determine if information on the excited states of ketene which dissociate to these methylene states could be obtained.

Several investigations have differed on the pressure dependence of the relative proportions of products resulting from $\text{CH}_2(^3\text{B}_1)$ and $\text{CH}_2(^1\text{A}_1)$ reactions in the vicinity of 313 nm. Rabinovitch and Simons^{2a} reported that the products resulting from $\text{CH}_2(^3\text{B}_1)$ reactions increased with increasing pressure, relative to products of $\text{CH}_2(^1\text{A}_1)$ reactions, in the 1 Torr to 1 atm range, and Rabinovitch, Watkins, and Ring^{2b} reported that the proportion of products attributable to $\text{CH}_2(^3\text{B}_1)$ reactions went through a maximum near 1 atm, but Ring and Rabinovitch suggested that the maximum may have been due to a pressure effect on the 1,2-dimethyltrimethylene biradical.^{2c} Both investigations used ketene photolysis at ~ 320 nm in the presence of *cis*-2-butene. In contrast, Voisey³ reported that the proportion of triplet products from photolysis of ketene in the presence of methyl ethyl ether at wavelengths ≥ 320 nm decreased with increasing pressure. Finally, Carr and Kistiakowsky⁴ found no evidence for a pressure dependence of relative singlet and triplet product yields from 313-nm photolysis of ketene in the presence of *trans*-2-butene between 162 and 532 Torr, and Rowland, McKnight, and Lee⁵

reported that of the methylenes produced during photolysis of $\text{CH}_2\text{CO}-\text{C}_2\text{H}_4$ mixtures between 10 and 300 Torr, 29% (independent of pressure) triplet CHT addition to the double bond occurred.

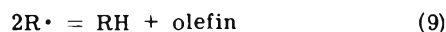
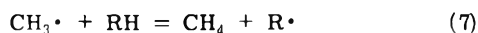
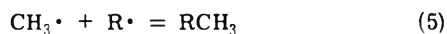
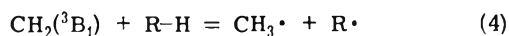
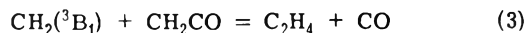
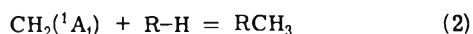
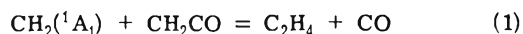
Since the pressure dependence of singlet and triplet products is diagnostic of whether or not $\text{CH}_2(^1\text{A}_1)$ and $\text{CH}_2(^3\text{B}_1)$ are formed by competing first-order and second-order processes, and hence to the details of excited state behavior, we have reinvestigated this aspect of ketene photolysis at 313 nm. In all of the above mentioned work, the yields of singlet and triplet products were obtained from relative product yields. Since many of the reactions and products may be difficult to determine. In this work we have used a pairwise photolysis technique, which we have previously demonstrated to be reliable, to obtain relative have used a pairwise photolysis technique, which we have previously demonstrated to be reliable, to obtain relative *total* singlet and triplet product yields without having to separate individual products into the singlet and triplet components.⁶

Experimental Section

Steady photolysis experiments were done on a conventional vacuum apparatus routinely evacuated to approximately 10^{-5} Torr or better. The optical train consisted of an Osram HBO 500 high-pressure Hg arc, quartz lens, light stop, chemical filter for the 321.6–313.2-nm region,⁷ 2-cm i.d. (141.6 cm³) cylindrical reactor, and an RCA 935 phototube. Ketene was prepared and stored as previously described.⁸ Mixtures of ketene ($\sim 6\%$) with either propane and 0.48 mol % *n*-pentane (internal standard), or *n*-pentane and 0.32 mol % propane (internal standard), were photolyzed both with and without oxygen ($\sim 5\%$) by a pairwise technique.⁶ Product yields were measured relative to the accurately known amount of internal standard. Gas chromatographic analyses were done on a Barber-Colman Series 5000 chromatograph using either 3% squalane on firebrick or Porapak Q columns, and a flame ionization detector. Phillips research grade propane, *n*-pentane, or *n*-heptane were used after degassing and gas chromatography impurity check, and Airco O₂ was used without treatment.

Results

Method of Determining Methylene Yields. It is well known that in ketene photolysis at 313 nm both $\text{CH}_2(^1\text{A}_1)$ and $\text{CH}_2(^3\text{B}_1)$ (the only two accessible states of CH_2 at this energy) are both formed. Furthermore, it is generally agreed that these two states react with alkanes (R-H) via two different mechanisms, as outlined in reactions 1–10.



Since $\text{CH}_2(^1\text{A}_1)$ and $\text{CH}_2(^3\text{B}_1)$ each react with R-H to form products that are in many cases identical, we rely upon the selective removal of $\text{CH}_2(^3\text{B}_1)$ by O_2^9 to determine the amounts of $\text{CH}_2(^1\text{A}_1)$ and $\text{CH}_2(^3\text{B}_1)$ formed during photolysis. That is, in ketene-alkane mixtures *without* O_2 , the stoichiometry of (1–10) shows that measurements of CH_4 , C_2H_4 , C_2H_6 , and those alkanes one CH_2 group larger than the reactant counts the total yields of $\text{CH}_2(^1\text{A}_1)$ and $\text{CH}_2(^3\text{B}_1)$. Also, since 5% O_2 is sufficient to scavenge $\text{CH}_2(^3\text{B}_1)$ (but not $\text{CH}_2(^1\text{A}_1)$), in an experiment identical in every respect except that 5% O_2 is included, measurement of C_2H_4 and those alkanes one CH_2 group larger than the reactant counts the $\text{CH}_2(^1\text{A}_1)$ produced. The $\text{CH}_2(^3\text{B}_1)$ - O_2 reaction yields CO , CO_2 , H , and probably H_2O and OH .⁹ These products will not change the stated stoichiometry of the $\text{CH}_2(^1\text{A}_1)$ reactions. We have previously shown that a small amount of O_2 does not change the relative amounts of $\text{CH}_2(^1\text{A}_1)$ and $\text{CH}_2(^3\text{B}_1)$ in the ketene primary process.¹⁰ Also, accuracy of gas chromatography analysis dictated measurement of methane and ethane, rather than R_2 and olefin to monitor the radical-radical reactions.

Equation 11 follows from the stoichiometry of reactions

$$\frac{[\text{C}_2\text{H}_4] + [\text{R-CH}_3]}{[\text{C}_2\text{H}_4] + [\text{CH}_4] + 2[\text{C}_2\text{H}_6] + [\text{R-CH}_3]} = \alpha_s \quad (11)$$

1–10, where α_s is the fractional yield of singlet methylene, the numerator results from O_2 -containing experiments, and the denominator results from O_2 -free experiments. The concentrations in eq 11 were calculated from product peak areas relative to the peak area of an internal standard, which was deliberately added in small (<1%), accurately measured amounts. Corrections were made for differences in gas chromatography sensitivity among all of the peaks measured, and individual product yields for each photolysis pair were put on an equal percent conversion (of ketene) by making small corrections for differences in reaction time and light intensity.

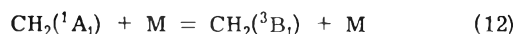
Propane was the reactant (R-H) at higher pressures, 200 to 700 Torr, but was replaced by *n*-pentane in experiments from 1 to 370 Torr because of appreciable decomposition of

chemically activated butanes formed in reaction 2, which is more than 100 kcal/mol exothermic. Several photolyses of ketene in mixtures of *n*-pentane and *n*-heptane (O_2 scavenged) were done at pressures from 1.0 to 100 Torr. The ratio of the sum of the hexanes, which were formed *via* reaction 2, to the sum of the octanes, also produced by (2), remained constant over this pressure range. If chemically activated hexanes were dissociating at the lower pressures, the hexane to octane ratio would be expected to decrease since the octane dissociation would occur to a substantially lesser extent at an arbitrary pressure. Thus "loss" of pentanes by a hot dissociation path did not occur.

Table I contains selected data from runs with *n*-pentane and propane. The yields of CH_4 , C_2H_4 , C_2H_6 , and either $\Sigma\text{C}_6\text{H}_{14}$ (*n*-hexane, 2-methylpentane, and 3-methylpentane) or $\Sigma\text{C}_4\text{H}_{10}$ (*n*-butane and isobutane) are given, along with α_T , the fractional yield of $\text{CH}_2(^3\text{B}_1)$, where $\alpha_T = 1 - \alpha_s$. Oxygen suppresses C_2H_6 , reduces CH_4 by about 90%, and substantially reduces the yields of C_2H_4 , $\Sigma\text{C}_6\text{H}_{14}$, and $\Sigma\text{C}_4\text{H}_{10}$, as expected.

The experimentally determined values of α_T are plotted in Figure 1. These are independent of pressure from 1.0 to 700 Torr, and have an average value of 0.30 ± 0.03 . A linear regression analysis of the data in Figure 1, fitted by $y = a + bx$ yielded $a = 0.29 \pm 0.05$ (standard deviation) and $b = 0.00$ with a standard deviation of 0.00. The HP 65 program used rounded off to two significant figures.

Mechanism of Methylene Formation. Although $\text{CH}_2(^1\text{A}_1)$ must be formed only in the ketene primary process, there are two possible mechanisms for $\text{CH}_2(^3\text{B}_1)$ production. These are (1) the primary process *vi* dissociation of electronically excited, presumably triplet CH_2CO , and (2) collision-induced intersystem crossing, reaction 12. As-



suming that all of the $\text{CH}_2(^1\text{A}_1)$ produced in the primary process either reacts with CH_2CO and R-H, or is deactivated to $\text{CH}_2(^3\text{B}_1)$, and that all of the $\text{CH}_2(^3\text{B}_1)$ produced in O_2 -free experiments reacts with either CH_2CO or R-H, the rates of formation of $\text{CH}_2(^1\text{A}_1)$ and $\text{CH}_2(^3\text{B}_1)$ in the primary process, Y_s and Y_t , respectively, are given by (13) and (14), where R_s and R_t are the overall rates at which singlet

$$Y_s = R_s + k_{12}(^1\text{CH}_2)(\text{M}) \quad (13)$$

$$Y_t = R_t - k_{12}(^1\text{CH}_2)(\text{M}) \quad (14)$$

and triplet methylene react with CH_2CO and R-H, and $(^1\text{CH}_2) \equiv [\text{CH}_2(^1\text{A}_1)]$

$$R_s = k_1(^1\text{CH}_2)(\text{CH}_2\text{CO}) + k_2(^1\text{CH}_2)(\text{R-H}) \quad (15)$$

$$\frac{R_t}{R_s} = \frac{k_{12}}{k_2(1 + gf)} \left\{ \frac{(\text{M})}{(\text{R-H})} + \frac{Y_t}{k_{12}(^1\text{CH}_2)(\text{R-H})} \right\} \quad (16)$$

$$k_1/k_2 = g \quad (\text{CH}_2\text{CO})/(\text{R-H}) = f$$

The quantity $Y_t/k_{12}(^1\text{CH}_2)(\text{R-H})$ in eq 16 is the ratio of the rate of primary process $\text{CH}_2(^3\text{B}_1)$ production to the rate of $\text{CH}_2(^3\text{B}_1)$ production by (12). To evaluate this quantity values of $k_1/k_2 = (\text{C}_2\text{H}_4)(\text{R-H})/(\text{CH}_2\text{CO})\Sigma(\text{RCH}_3)$ were computed from the data for O_2 -scavenged experiments, and $R_t/R_s = \alpha_t/\alpha_s$, which holds for small conversions. Finally k_{12}/k_2 was computed from a previously published correlation of this quantity with polarizability of the collision partner, M,¹⁰ yielding $k_{12}/k_2 = 0.06$ for propane and $k_{12}/k_2 = 0.09$ for pentane. Data for computation of k_{12}/k_2

TABLE I: Product Yields Relative to Internal Standard for 313-nm Photolysis of Ketene-Alkane Mixtures

Pressure, Torr	CH ₄	C ₂ H ₄	C ₂ H ₆	ΣC ₃ H ₁₁	α _t
		n-C ₅ H ₁₂			
6.5	0.090	0.29	0.41	3.69	0.30
6.7 ^b	0.009	0.14		3.28	
253	0.077	0.090	0.17	1.98	0.31
253 ^b	0.003	0.064		1.67	

Pressure, Torr	CH ₄	C ₂ H ₄	C ₂ H ₆	ΣC ₃ H ₁₀	α _t
		C ₃ H ₈			
198	0.098	0.289	0.341	3.72	0.32
211 ^b	0.004	0.218	0.02	3.04	
706	0.073	0.166	0.161	1.72	0.32
709 ^b	0.004	0.125	0.03	1.37	

^a 0.32 mol % C₃H₈ in n-C₅H₁₂-CH₂CO photolyses; 0.48 mol % C₅H₁₂ in C₃H₈-CH₂CO photolyses. ^b Experiments with 5 mol % O₂.

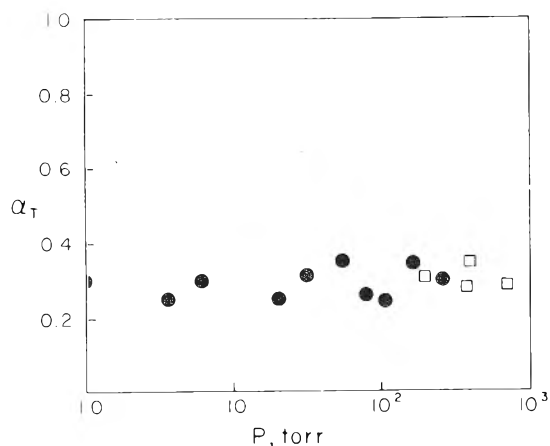


Figure 1. Fraction of total methylenes which are triplet from 1 to 709 Torr: (O) CH₂CO-*n*-C₅H₁₀ photolyses; (□) CH₂CO-C₃H₈ photolyses.

was restricted to that obtained from ketene photolysis in the middle uv absorption band, that is, restricted to conditions commensurate with the present experiments. Using $R_t/R_s = 0.48$ for propane and 0.42 for *n*-pentane yielded $Y_t/k_{12}(^1\text{CH}_2)(\text{R-H}) = 7.5$ and 3.7 for propane and *n*-pentane systems, respectively, or ~ 12 to $\sim 20\%$ of the total CH₂(³B₁) results from (12), the remaining 88 to 80% being formed in the primary process. The value of k_{12}/k_2 would have to be a factor of 6 larger if $Y_t = 0$, which seems highly unlikely. Thus significant amounts of CH₂(³B₁) are produced in the ketene primary process. Substituting the stationary state (¹CH₂) into (16) yields eq 17. Since R_t/R_s is

$$\frac{k_2(1 + gf)}{k_{12}} \frac{R_t}{R_s} = \frac{(M)}{(\text{RH})} + \frac{Y_t}{Y_s} \left\{ \frac{(M)}{(\text{R-H})} + \frac{k_2(1 + gf)}{k_{12}} \right\} \quad (17)$$

independent of pressure (Figure 1), and $(\text{RH})/(M)$ and $(\text{CH}_2\text{CO})/(\text{R-H})$ were constant in these experiments Y_t/Y_s is pressure independent. As a consequence Y_t and Y_s are either both pressure independent or both have the same pressure dependence, which cancels in the ratio Y_t/Y_s . It

should be emphasized that although (12) is bimolecular it does not put any pressure dependence into R_t/R_s since the "branching ratio", k_2/k_{12} , is pressure independent.

Discussion

The electronic absorption spectrum of ketene in the middle and near-uv consists of a series of diffuse bands between 473.5 and about 240 nm.^{11,12} Although there is disagreement whether the bands belong to one electronic state¹² or to two electronic states,^{11,13,14} with the second starting near 370 nm, there is general agreement that the transition in the 370-240-nm region is ¹A₂ ← ¹A₁ if the upper state is described in C_{2v} symmetry, or ¹A'' ← ¹A₁ if the upper state is in-plane bent (C_s symmetry) as indicated by Del Bene's¹³ calculations. The diffuse spectrum is interesting since a molecule of the size and rigidity of ketene would be expected to have detectable rotational structure if the excited states were unperturbed, but no evidence of structure was found at high resolution, even at -78°.¹¹ Another feature of ketene is the failure to detect emission following excitation to ¹A''. A recent attempt to detect emission with a sensitive apparatus has permitted the limit $\phi_f < 10^{-5}$ to be placed on the fluorescence quantum yield.¹⁵ From the integrated intensity of the 380-240-nm interval, the radiative lifetime of the ¹A'' state, $\tau_0 = 4 \times 10^{-5}$ sec, can be calculated and a limit placed on the excited state lifetime, $\tau = \phi_f \tau_0$. This yields $\tau < 4 \times 10^{-10}$ sec, which is consistent with the lack of rotational structure. However since the bands are completely diffuse even at energies considerably below the dissociation limit, which is in the vicinity of 350 nm,¹⁶ true predissociation is not the cause. Thus electronic relaxation, as described by Byrne and Ross,¹⁷ must be invoked as the reason for diffuseness, at least below the dissociation limit. Near the dissociation limit, and at shorter wavelengths dissociation to CO and CH₂ occurs, and dissociative quantum yields are pressure dependent up to about 300 nm. The primary dissociative quantum yield extrapolated to $p = 0$ is unity at 313 nm^{18,19} and slightly less than 1 at 334 nm,¹⁸ but at 366 nm^{18,19} ϕ_d extrapolates to considerably less than 1 at $p = 0$. Values of the overall first-order photodissociation lifetimes, $\tau_d \equiv k_d^{-1}$, where k_d is the overall photodissociation rate coefficient, obtained from the Stern-Volmer plots, are considerably longer than the computed limit of the ¹A'' lifetime, 4×10^{-10} sec, at 366^{18,19} and 334 nm.¹⁸ At 313 nm τ_d values spanning the range from 5×10^{-10} ¹⁸ to 0.9×10^{-10} sec¹⁹ have been reported. Thus at 366 and 334 nm the state that is collisionally deactivated is not ¹A'', but some other state reached by rapid electronic relaxation. At 313 nm the situation is not as clear. Although τ_d is either about equal to or shorter than 4×10^{-10} sec, this figure is a lower limit and τ_d may in fact be longer than the actual lifetime of ¹A''. Also, there is no evidence for a change in ¹A'' behavior between 334 and 313 nm, and it is most likely that rapid electronic relaxation to another longer-lived state occurs at 313 nm as well as at longer wavelengths. The electronic relaxation cannot be photodissociation because ¹A'' correlates with higher excited states of the CH₂ and CO photofragments,²⁰ which are not accessible at 313 nm.

Photodissociation mechanisms can be most easily visualized with reference to Figure 2, in which potential energy is plotted as a function of $r(\text{C-C})$. It should be noted at the outset that the locations of the minima of these curves are only approximate with respect to both energy and $r(\text{C-C})$, since these (particularly the energies) are either poorly

known or in dispute. This deficiency will in no way affect the arguments presented below.

The curves in Figure 2 were deduced from the following information. The ketene ground state, $\text{CH}_2\text{CO}(^1\text{A}_1)$, correlates with $\text{CH}_2(^1\text{A}_1)$ through an avoided crossing,²⁰ the highest point of which cannot be greater than about 85 kcal mol⁻¹ for consistency with the observations at 334 nm that Stern-Volmer plots extrapolate to a value for ϕ_d slightly less than unity at $p = 0$,^{18,21} and at 360–370 nm ϕ_d extrapolates to values appreciably less than unity at $p = 0$.^{18,19} The enthalpy of dissociation to CO and $\text{CH}_2(^3\text{B}_1)$ is 78 ± 1 kcal mol⁻¹ at 298°K, which we have used to place the CH_2 ground state on Figure 2. The cross-hatched region reflects the uncertainty in the excitation energy of $\text{CH}_2(^1\text{A}_1)$.^{16,22,23} Two triplet states are predicted to lie in the energy region of interest.^{13,20,24} The $^3\text{A}'$ state leads to $\text{CO}(^1\Sigma^+) + \text{CH}_2(^3\text{B}_1)$, and although this is completely repulsive in a least-motion path,²⁰ geometry optimization¹³ has shown it to have a minimum at large $r(\text{C}-\text{C})$. The fragmentation products from $^3\text{A}''$ are not established, but do lie at a higher energy than the methylene ground state. Finally, Basch²⁰ shows the $^1\text{A}_2$ state, which is the state of C_{2v} symmetry corresponding to $^1\text{A}''$, correlating with higher energy fragments in a least-motion dissociation, while Del Bene's geometry optimized calculation suggests that $^1\text{A}''$ leads to $\text{CO}(^1\Sigma^+) + \text{CH}_2(^1\text{B}_1)$. Thus the products resulting from $^1\text{A}''$ and $^3\text{A}''$ dissociation are left unspecified in Figure 2. This uncertainty has no effect on arguments presented below since the methylene states involved are energetically inaccessible at 313 nm.

The following three mechanisms for production of $\text{CH}_2(^1\text{A}_1)$ and $\text{CH}_2(^3\text{B}_1)$ after excitation to $\text{CH}_2\text{CO}(^1\text{A}'')$ can be postulated. (1) The $^1\text{A}''$ state undergoes intersystem crossing to $^3\text{A}'$, either with or without the intermediacy of $^3\text{A}''$,²⁵ yielding $\text{CH}_2(^3\text{B}_1)$, and concurrently undergoes internal conversion to the ground state, followed by dissociation to $\text{CH}_2(^1\text{A}_1)$. (2) The $^1\text{A}''$ state undergoes intersystem crossing to $^3\text{A}'$, either with or without the intermediacy of $^3\text{A}''$, and can then either dissociate to $\text{CH}_2(^3\text{B}_1)$, or cross to $^1\text{A}_1$ and from there yield $\text{CH}_2(^1\text{A}_1)$. (3) All the $^1\text{A}''$ undergoes internal conversion to the ground state, followed by dissociation to $\text{CH}_2(^1\text{A}_1)$, and competitive crossing to $^3\text{A}'$, followed by dissociation to $\text{CH}_2(^3\text{B}_1)$.

Assuming that the $\text{CH}_2\text{CO}(^1\text{A}'')$ state does not live long enough to be deactivated, mechanism 1 can be ruled out. The triplet states, $^3\text{A}''$ and $^3\text{A}'$, which would be populated by intersystem crossing in (1) are presumably short-lived because of the failure of ketene to sensitize emission from biacetyl.²⁶ Thus the state which is collisionally deactivated would be $\text{CH}_2\text{CO}(^1\text{A}_1)$. However formation of $\text{CH}_2(^3\text{B}_1)$ by a pressure-independent process via the ketene triplet states, and pressure-dependent formation of $\text{CH}_2(^1\text{A}_1)$ from dissociation of $\text{CH}_2\text{CO}(^1\text{A}_1)$, predicts that α_s should decrease with increasing pressure, contrary to the experiments reported here. Even if the ketene triplet state(s) is long-lived enough to be collisionally deactivated, its lifetime would have to match the $^1\text{A}_1$ lifetime, a highly unlikely situation, in order for α_s to be pressure independent.

Mechanism 2 seems unlikely for the same reasons. If both $^1\text{A}''$ and the triplet state(s) are too short-lived to be collisionally deactivated, the pressure sensitive state must be $^1\text{A}_1$, and again a pressure dependence of α_s is predicted. Alternatively, if $^3\text{A}'$ and $^1\text{A}_1$ can both be collisionally deactivated, α_s would be pressure dependent unless their lifetimes are the same.

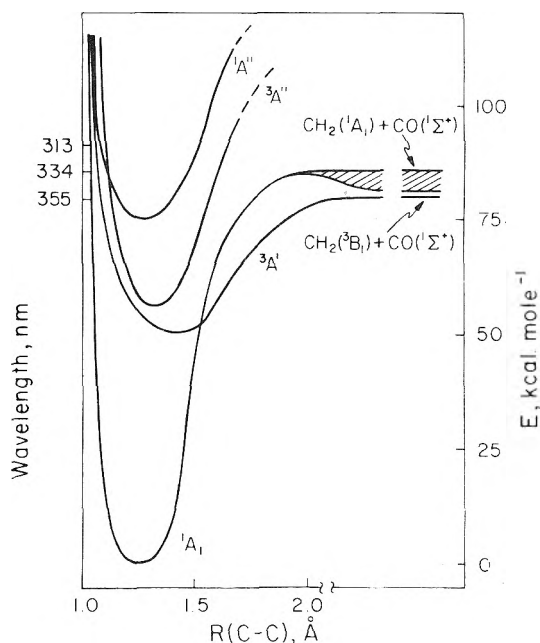
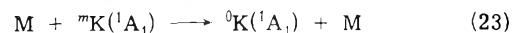
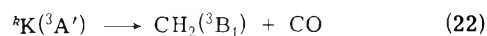
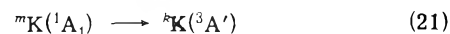
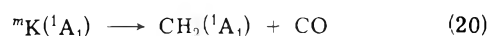
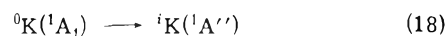


Figure 2. Approximate potential energy curves for $r(\text{C}-\text{C})$ in CH_2CO .

Mechanism 3 can be kinetically represented by (18–23),



where ${}^0\text{K}$, ${}^i\text{K}$, ${}^m\text{K}$, ${}^k\text{K}$ represent ketene molecules in 0, i , m , k vibrational levels of corresponding electronic states. The photoexcitation into ${}^i\text{K}(^1\text{A}'')$ is followed by an internal conversion (19) into the ground state (${}^1\text{A}_1$) in the m th vibrational level. The vibrationally excited ground state can decompose into $\text{CH}_2(^1\text{A}_1)$, (20), or intersystem cross into the (${}^3\text{A}'$) state, (21), or can undergo the collisional deactivation, (23).

A steady-state analysis of the proposed mechanism yields pressure-dependent primary rates, $Y_s = k_{20}I/(k_{20} + k_{21} + k_{23}[\text{M}])$ and $Y_t = k_{21}I/(k_{20} + k_{21} + k_{23}[\text{M}])$, so the constant ratio $Y_t/Y_s = k_{21}/k_{20}$ is consistent with experimental data and (17). (I is absorbed light intensity.) The mechanism predicts a Stern-Volmer type expression for $2/\phi_{\text{CO}}$, with unit value at $p = 0$. In order to account for $\phi_{\text{CO}} = 1$ up to 250 Torr at 313 nm, as found by Strachan and Thornton,¹⁹ additional decomposition and intersystem crossing steps from at least one lower vibrational level of the ${}^1\text{A}_1$ state would have to be included in the model. Such intermediate vibrational levels are reached by the stepwise collisional deactivation of the ground state.

The mechanism is also capable of explaining the decrease of α_s with increasing wavelength, and the effect of wavelength on ϕ_d . As wavelength is increased from 313 nm the observed decrease of $\text{CH}_2(^1\text{A}_1)$ relative to $\text{CH}_2(^3\text{B}_1)$ is predicted because dissociation along $\text{CH}_2\text{CO}(^1\text{A}_1)$ and over

the maximum corresponding to the avoided crossing becomes slower as it becomes energetically less favored, while crossing to $^3A'$, which occurs at lower energy, would not be retarded, but would become relatively faster as the classical velocity in the crossing region becomes slower. At high photon energies ($\lambda \leq 280$ nm), where $\phi_d = 1$, independent of pressure, the $\text{CH}_2\text{CO}(^1A_1)$ lifetime must be very short. However as the $\text{CH}_2\text{CO}(^1A_1)$ energy approaches the top of the "barrier", its lifetime is sufficiently long that it can be collisionally deactivated at pressures below 1 atm. However, at 92 kcal/mol (313 nm), which must be above the "barrier", the lifetime of $\text{CH}_2\text{CO}(^1A_1)$ obtained from Stern-Volmer plots is about 0.1 nsec, and a large number of vibrations occur before dissociation. Thus crossing to $^3A'$ does not have to be very efficient to account for about 25% $\text{CH}_2(^3B_1)$ from the primary process. Finally, at 360 nm only a fraction of the excited molecules dissociate even at zero pressure, consistent with the dissociation limit at about 350 nm. The small activation energy for dissociation at this wavelength,^{19,28} and the large amount of $\text{CH}_2(^3B_1)$ relative to $\text{CH}_2(^1A_1)$, are also explained by the "barrier" in Figure 2.

Russell and Rowland²⁹ have recently suggested that ^{14}CO formation in photolysis of $^{14}\text{CH}_2\text{CO}$ results from rearrangement of an electronically excited singlet state, probably via the intermediacy of oxirene. While the present discussion has implicitly assumed that internal conversion from the $^1A''$ state to the ground state is a physical process, isomerization, as suggested by Lamola, Hammond, and Mallory,³⁰ and discussed by Phillips, Lemaire, Burton, and Noyes³¹ may also provide a route for the radiationless transition. The amount of scrambling, however, is less than 10% at 313 nm, implying that isomerization via oxirene is the lesser route for the radiationless transition.

Acknowledgment. This research was supported by the

U.S. Atomic Energy Commission under Contract No. AT(11-1)2026.

References and Notes

- (1) AEC Document No. COO-2026-18
- (2) (a) J. W. Simons and B. S. Rabinovitch, *J. Phys. Chem.*, **68**, 1322 (1964); (b) B. S. Rabinovitch, K. W. Watkins, and D. F. Ring, *J. Am. Chem. Soc.*, **87**, 4960 (1965); (c) D. F. Ring and B. S. Rabinovitch, *J. Phys. Chem.*, **72**, 191 (1968).
- (3) M. A. Voisey, *Trans. Faraday Soc.*, **64**, 3058 (1968).
- (4) R. W. Carr, Jr., and G. B. Kistiakowsky, *J. Phys. Chem.*, **70**, 118 (1966).
- (5) F. S. Rowland, C. McKnight, and E. K. C. Lee, *Ber. Bunsenges. Phys. Chem.*, **72**, 236 (1968).
- (6) T. W. Eder and R. W. Carr, Jr., *J. Phys. Chem.*, **73**, 2074 (1969).
- (7) J. G. Calvert and J. N. Pitts, Jr., "Photochemistry", Wiley, New York, N. Y., 1966, p 732.
- (8) M. G. Topor and R. W. Carr, Jr., *J. Chem. Phys.*, **58**, 757 (1973).
- (9) R. L. Russell and F. S. Rowland, *J. Am. Chem. Soc.*, **90**, 1671 (1968).
- (10) T. W. Eder and R. W. Carr, Jr., *J. Chem. Phys.*, **53**, 2258 (1970).
- (11) R. N. Dixon and G. H. Kirby, *Trans. Faraday Soc.*, **62**, 1406 (1966).
- (12) A. H. Laufer and R. A. Keller, *J. Am. Chem. Soc.*, **93**, 61 (1971).
- (13) J. E. Del Bene, *J. Am. Chem. Soc.*, **94**, 3713 (1972).
- (14) J. S. E. McIntosh and G. B. Porter, *Can. J. Chem.*, **50**, 2313 (1972).
- (15) J. R. McDonald, private communication.
- (16) R. W. Carr, Jr., T. W. Eder, and M. G. Topor, *J. Chem. Phys.*, **53**, 4716 (1970).
- (17) J. P. Byrne and I. G. Ross, *Aust. J. Chem.*, **24**, 1107 (1971).
- (18) G. A. Taylor and G. B. Porter, *J. Chem. Phys.*, **36**, 1353 (1962).
- (19) A. N. Strachan and D. E. Thornton, *Can. J. Chem.*, **46**, 2353 (1968).
- (20) H. Basch, *Theor. Chim. Acta*, **28**, 151 (1973).
- (21) B. T. Connelly and G. B. Porter, *Can. J. Chem.*, **36**, 1640 (1958).
- (22) C. F. Bender, H. F. Schaefer, III, D. R. Francschetti, and L. C. Allen, *J. Am. Chem. Soc.*, **94**, 6888 (1972).
- (23) V. Staemmler, *Theor. Chim. Acta*, **31**, 49 (1973).
- (24) J. W. Rabalais, J. M. McDonald, V. Scherr, and S. P. McGlynn, *Chem. Rev.*, **71**, 73 (1971).
- (25) Whether or not $\text{CH}_2\text{CO}(^3A'')$ is involved in intersystem crossing to $\text{CH}_2\text{CO}(^3A')$ is unimportant here. However, the density of states is so low in ($^3A''$) at the energy of interest that it is an unlikely intermediate.
- (26) M. Grossman, G. P. Semeluk, and I. Unger, *Can. J. Chem.*, **47**, 3079 (1969).
- (27) S. Y. Ho and W. A. Noyes, Jr., *J. Am. Chem. Soc.*, **89**, 5091 (1967).
- (28) A. N. Strachan and W. A. Noyes, Jr., *J. Am. Chem. Soc.*, **76**, 3258 (1954).
- (29) R. L. Russell and F. S. Rowland, *J. Am. Chem. Soc.*, **92**, 7508 (1970).
- (30) A. A. Lamola, G. S. Hammond, and F. B. Mallory, *Photochem. Photobiol.*, **4**, 259 (1965).
- (31) D. Phillips, J. Lemaire, C. Burton, and W. A. Noyes, Jr., *Adv. Photochem.*, **5**, 329 (1968).

COMMUNICATIONS TO THE EDITOR

Influence of Lower Alcohols on the Pfeiffer Effect of Tris(1,10-phenanthroline)zinc(II) Sulfate-Cinchonine Hydrochloride and *-l*-Strychnine Hydrosulfate Systems in Water

Sir: When a racemic mixture of a certain labile complex is added to a solution containing an optically active substance (often called an environment compound), additional optical activity is developed. To this phenomenon was applied the term "Pfeiffer effect" by Dwyer and Brasted in 1954 and some excellent reviews on it have already appeared.¹⁻⁴

Some authors attributed the Pfeiffer effect to any differential interaction of the dextro and levo enantiomers of the complex with the environment compound and to the resulting "displacement" of an equilibrium between the dextro and levo enantiomers (in favor of one of them).⁵ In fact, Kirschner and Ahmad⁶ succeeded in partial resolution of $[\text{Ni}(\text{phen})_3]^{2+}$ and $[\text{Ni}(\text{bpy})_3]^{2+}$ (phen = 1,10-phenanthroline and bpy = 2,2'-bipyridine) through the Pfeiffer effect. However, little is known yet on the nature of the interaction.

In our preceding papers,^{7,8} we proposed the hydrophobic bonding⁹ between the racemic complex and the environ-

TABLE I: Observed Optical Rotations of the Pfeiffer-Active Systems without Additives^a

Racemic complex	Environment compd	Rotation of environment compd, α_e , deg	Obsd rotation, α_{obsd} , deg	Pfeiffer rotation, ^b α_p , deg
$[Zn(phen)_3]SO_4$	Stry· $\frac{1}{2}H_2SO_4$	-0.160	-0.394	-0.234
$[Zn(phen)_3]SO_4$	Cincho·HCl	+0.725	+0.348	-0.377

^a In a 5-cm cell at 405 nm at 25°. All compounds in the table are of 0.01 M concentration. ^b Defined as $\alpha_{obsd} - \alpha_e$.

ment compound as one of the essential driving forces to the development of the Pfeiffer effect in $[Zn(phen)_3]^{2+}$ -*l*-StryH⁺ and -*d*-BCS⁻ systems in water (StryH⁺ = strychninium ion and BCS⁻ = α -bromocamphor- π -sulfonate ion). It was also pointed out that the former system bears a close resemblance to cationic surfactant solutions in that its Pfeiffer rotation α_p ,¹⁻⁴ defined as the rotation of the Pfeiffer system minus that of the environment compound, is surprisingly affected by the addition of anions⁷ like the critical micelle concentration (cmc) of cationic surfactants. We report here further evidence for the resemblance to surfactant solutions by examining the influence of lower alcohols on the Pfeiffer effect in $[Zn(phen)_3]^{2+}$ -CinchoH⁺ and -*l*-StryH⁺ systems in water (CinchoH⁺ = cinchoninium ion).

Sample solutions containing $[Zn(phen)_3]SO_4$ and cinchon hydrochloride or *l*-strychnine hydrosulfate, both in 0.01 M concentration, were prepared by diluting respective stock solutions in volumetric flasks (25 ml). Nonelectrolytes added to these solutions were methanol, ethanol, 1-propanol, 2-propanol, 1-butanol, *sec*-butyl alcohol, isobutyl alcohol, *tert*-butyl alcohol, dioxane, and urea, all of which were of reagent grade. The stock solution of $[Zn(phen)_3]SO_4$ was prepared by directly dissolving $ZnSO_4 \cdot 7H_2O$ and phen- H_2O in a mole ratio of 1:3 in water. Purity of commercially available Cincho-HCl·2H₂O and Stry·0.5H₂SO₄·2.5H₂O was checked by both elemental analysis and optical rotation measurements. Optical rotation was measured in a 5-cm cell at 405 nm with a Union-Giken PM-71 polarimeter kept at 25 ± 0.1°. The optical activity of the above two environment compounds was not appreciably affected by the additives.

Table I lists the optical rotations at 405 nm of the above two systems without additives. Figures 1 and 2 show the effect of additives on the Pfeiffer rotations α_p of $[Zn(phen)_3]^{2+}$ -CinchoH⁺ and -*l*-StryH⁺ systems in water, respectively, where α_p is plotted against the molar concentration of additives. It is seen that α_p decreases linearly with alcohol concentration C_a in both systems.

It is now well known that ionic surfactant molecules form aggregates called micelles in water through the hydrophobic bonding against their mutual electrostatic repulsion. The concentration of surfactant solutions at which micelles begin to form is termed the critical micelle concentration (cmc). More than 20 years ago, Herzfeld et al.¹⁰ and Shinoda¹¹ found that the cmc decreases linearly with the concentration of added alcohols; i.e., micelle formation is facilitated by the addition of alcohols. Shinoda interpreted the effect of alcohols on the assumption that alcohol molecules penetrate into the micelle,¹² resulting in a decrease in the free energy brought about by both the entropy of mixing and the reduction of charge density on the micelle surface.¹³ It seems appropriate, therefore, to apply his assumption to the Pfeiffer systems since both the environ-

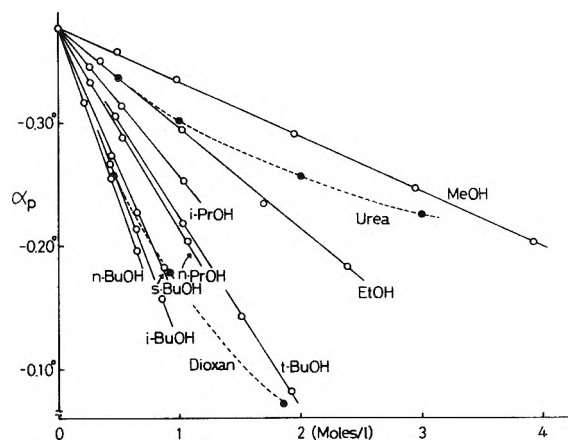


Figure 1. Plots of the Pfeiffer rotations α_p in degrees at 405 nm in a 5-cm cell vs. molar concentration of additives for the $[Zn(phen)_3]^{2+}$ -CinchoH⁺ system in water.

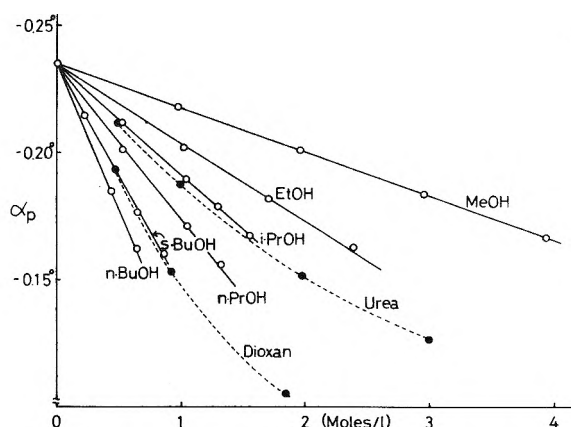


Figure 2. Plots of the Pfeiffer rotations α_p in degrees at 405 nm in a 5-cm cell vs. molar concentration of additives for the $[Zn(phen)_3]^{2+}$ -*l*-StryH⁺ system in water.

ment compounds and the racemic complex appear hydrophobic and carry positive charges like cationic surfactant molecules. As a result, they must interact with each other like ionic surfactant molecules against their mutual repulsion to exhibit additional optical activity.

Table II records $d\alpha_p/dC_a$, i.e., the rate of the decrease of α_p with the molar concentration of added alcohols C_a , and the logarithm of $d\alpha_p/dC_a$ for the two systems. In Figure 3 is plotted the logarithm of $d\alpha_p/dC_a$ vs. the number of carbon atoms in added alcohol molecules, according to the theory¹¹ developed by Shinoda for the interpretation of the effect of alcohols on the cmc. It is seen that a good linear relationship is observed between $\log(d\alpha_p/dC_a)$ and the number of carbon atoms for *n* alcohols and for *i*-PrOH and *s*-BuOH

TABLE II: Rate of the Decrease of α_p in Degrees with Molar Alcohol Concentration C_a ^a

	[Zn(phen) ₃] ²⁺ -CinchoH ⁺ system		[Zn(phen) ₃] ²⁺ -l-StryH ⁺ system		
	$S_c = d\alpha_p/dC_a$	$\log S_c$	$S_s = d\alpha_p/dC_a$	$\log S_s$	$\log (S_c/S_s)$
MeOH	4.45×10^{-2}	-1.35	1.73×10^{-2}	-1.76	0.41
EtOH	8.24×10^{-2}	-1.08	3.12×10^{-2}	-1.51	0.42
n-PrOH	1.64×10^{-1}	-0.785	6.12×10^{-2}	-1.21	0.43
i-PrOH	1.21×10^{-1}	-0.917	4.39×10^{-2}	-1.36	0.44
n-BuOH	2.78×10^{-1}	-0.556	1.13×10^{-1}	-0.947	0.39
i-BuOH	2.56×10^{-1}	-0.592			
s-BuOH	2.26×10^{-1}	-0.646	8.55×10^{-2}	-1.07	0.42
t-BuOH	1.55×10^{-1}	-0.810			

^a Experimental details are the same as those in Table I.

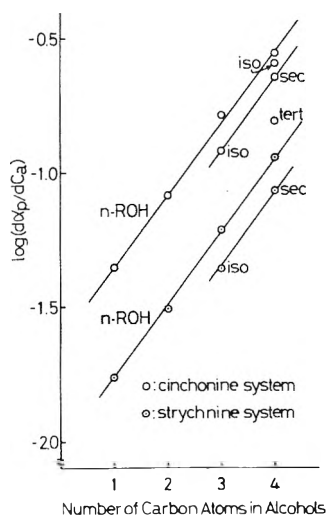


Figure 3. Plots of $\log (d\alpha_p/dC_a)$ vs. the number of carbon atoms in added alcohol molecules.

and that the slopes in Figure 3 are nearly the same for the two systems (see the values of $\log (S_c/S_s)$ in Table II). It should be also noted that the decreasing order of α_p is t -BuOH $>$ s -BuOH $>$ i -BuOH $>$ n -BuOH, which completely agrees with the order of their solubility in water. These phenomena are quite similar to those observed in ionic surfactant solutions¹¹ and indicate that the interaction between the complex and the environment compound resembles that operating between surfactant molecules in water. That is, it is the hydrophobic bonding¹⁴ that leads [Zn(phen)₃]²⁺ and CinchoH⁺ or l -StryH⁺ to associate with each other even at relatively low concentration. Though it is not yet certain whether aggregates like micelles are formed or only dimers composed of [Zn(phen)₃]²⁺ and CinchoH⁺ or l -StryH⁺ are formed in the Pfeiffer systems, added alcohol molecules probably wedge themselves between [Zn(phen)₃]²⁺ and CinchoH⁺ or l -StryH⁺, thereby decreasing α_p . Thus it seems necessary for the complex and the environment compound to come into direct contact with each other in order to exhibit the Pfeiffer effect.

Figures 1 and 2 show the effect of urea and dioxane on α_p . Urea is one of the well-known protein denaturants and its effect on the cmc has been extensively studied.¹⁵ It is true that both additives decrease α_p , but the mechanism by which they diminish the Pfeiffer effect is not clearly elucidated at the present time.

References and Notes

- (1) S. Kirschner and K. R. Magnell, *Adv. Chem. Ser.*, **No. 62**, 366 (1966).
- (2) S. Kirschner, N. Ahmad, and K. R. Magnell, *Coord. Chem. Rev.*, **3**, 201 (1968).
- (3) S. Kirschner and N. Ahmad, "Coordination Chemistry", S. Kirschner, Ed., Plenum Press, New York, N.Y., 1969, p 42; R. C. Brasted, V. J. Landis, E. J. Kuhajek, P. E. R. Nordquist, and L. Mayer, *ibid.*, p 64.
- (4) S. Kirschner, *Rec. Chem. Prog.*, **32**, 29 (1971).
- (5) Even symmetrical complexes sometimes exhibit anomalous optical activity when they are dissolved into or mixed with some optically active substances. This phenomenon is usually attributed to an outer-sphere association of these complexes with optically active substances and has been recently discussed by R. Pollock, Ph.D. Dissertation, Wayne State University, 1972.
- (6) S. Kirschner and N. Ahmad, *J. Am. Chem. Soc.*, **90**, 1910 (1968).
- (7) K. Miyoshi, K. Sakata, and H. Yoneda, *Chem. Lett.*, 1087 (1974).
- (8) K. Miyoshi, K. Sakata, and H. Yoneda, submitted for publication in *J. Am. Chem. Soc.*
- (9) Though the use of the term "hydrophobic bonding" is not appropriate, we dare use it to mean the association between hydrophobic solutes assisted by the water structure: see J. H. Hildebrand, *J. Phys. Chem.*, **72**, 1841 (1968); G. Némethy, H. A. Scheraga, and W. Kauzmann, *ibid.*, **72**, 1842 (1968).
- (10) S. H. Herzfeld, M. L. Corrin, and W. D. Harkins, *J. Phys. Chem.*, **54**, 271 (1950).
- (11) K. Shinoda, *Bull. Chem. Soc. Jpn.*, **26**, 101 (1953); *J. Phys. Chem.*, **58**, 1136 (1954).
- (12) W. D. Harkins, R. W. Mattoon, and R. Mittelmann, *J. Chem. Phys.*, **15**, 763 (1947).
- (13) K. Shirahama and T. Kashiwabara, *J. Colloid Interface Sci.*, **36**, 65 (1971).
- (14) W. Kauzmann, *Adv. Protein Chem.*, **14**, 1 (1959); G. Némethy, *Angew. Chem., Int. Ed. Engl.*, **6**, 195 (1967).
- (15) M. L. Corrin and W. D. Harkins, *J. Am. Chem. Soc.*, **69**, 683 (1947); W. Bruning and A. Holtzer, *ibid.*, **83**, 4865 (1961); P. Mukerjee and A. Ray, *J. Phys. Chem.*, **67**, 190 (1963); M. J. Schick, *ibid.*, **68**, 3585 (1964); M. Abu-Hamdiyyah, *ibid.*, **69**, 2720 (1965); M. F. Emerson and A. Holtzer, *ibid.*, **71**, 3320 (1967); J. M. Corkill, J. F. Goodman, S. P. Harrold, and J. R. Tate, *Trans. Faraday Soc.*, **63**, 240 (1967); J. Piercy, M. Jones, and G. Ibbotson, *J. Colloid Interface Sci.*, **37**, 165 (1971).

Department of Chemistry
Faculty of Science
Hiroshima University
Hiroshima, Japan

Katsuhiko Miyoshi
Koro Sakata
Hayami Yoneda*

Received March 25, 1975

**New concepts
new techniques
new interpretations**

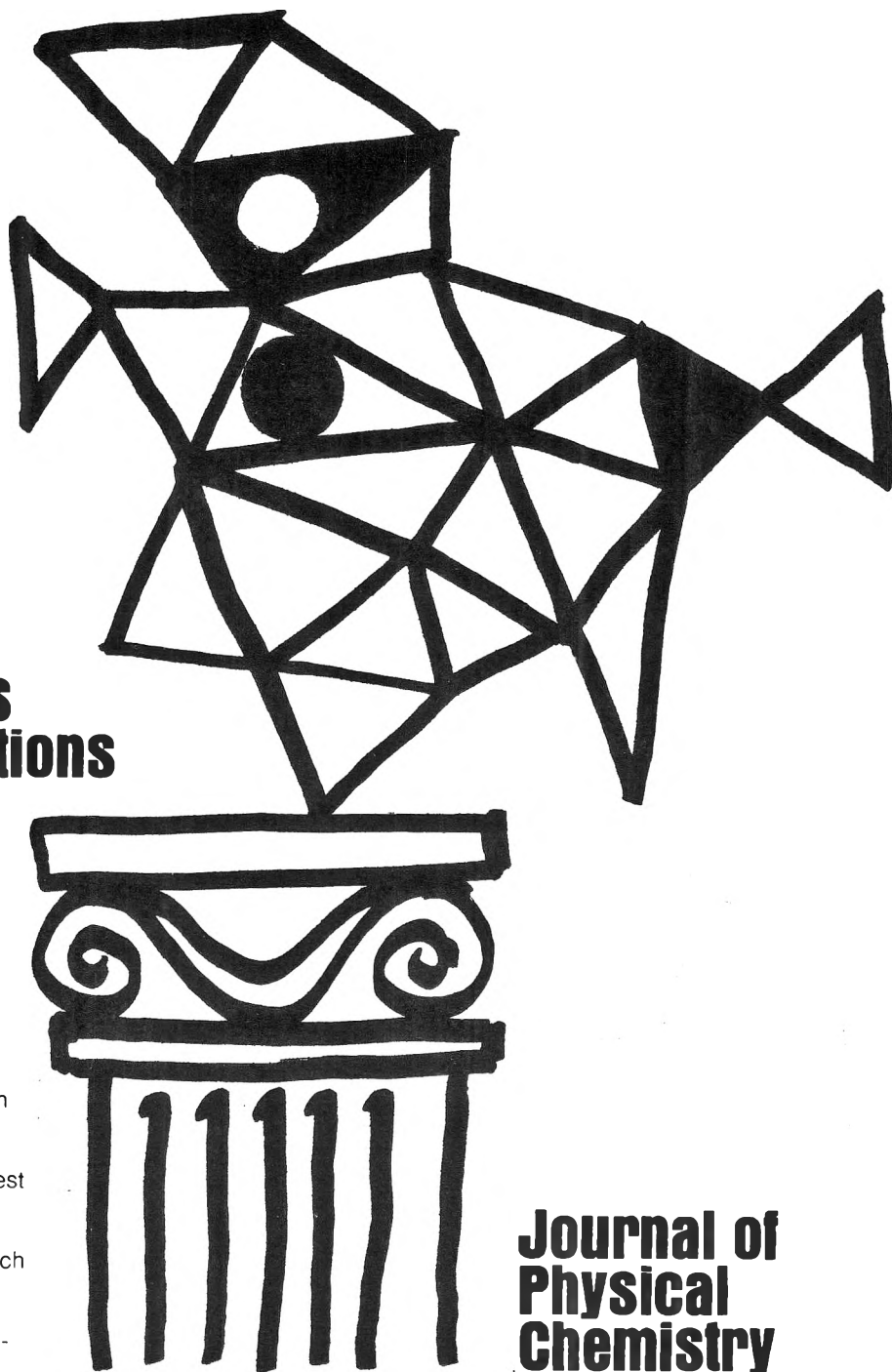
**... together
with valuable reports
on classical areas**

They are all waiting for you between the covers of our well-balanced JOURNAL OF PHYSICAL CHEMISTRY. Whatever your particular interest in physical chemistry, you'll find the JOURNAL's broad range of experimental and theoretical research reports are relevant and beneficial to your work. Each biweekly issue brings you an average of 30 authoritative, comprehensive reports on fundamental aspects of atomic and molecular phenomena, as well as timely notes, communications and reports plus the proceedings of selected symposia.

Join your fellow physical chemists who rely on JPC as an excellent biweekly source of data in both new and classical areas. Just complete and return the form to start your own subscription.



... another ACS service



Journal of Physical Chemistry

**The Journal of Physical Chemistry
American Chemical Society**

1155 Sixteenth Street, N.W.
Washington, D.C. 20036

1975

Yes, I would like to receive the JOURNAL OF PHYSICAL CHEMISTRY at the one-year rate checked below:

	U.S.	Canada**	Latin America**	Other Nations**
ACS Member One-Year Rate*	<input type="checkbox"/> \$20.00	<input type="checkbox"/> \$24.50	<input type="checkbox"/> \$24.50	<input type="checkbox"/> \$25.00
Nonmember	<input type="checkbox"/> \$80.00	<input type="checkbox"/> \$84.50	<input type="checkbox"/> \$84.50	<input type="checkbox"/> \$85.00
Bill me <input type="checkbox"/>	Bill company <input type="checkbox"/>	Payment enclosed <input type="checkbox"/>		

Air freight rates available on request

Name _____

Street _____ Home
Business

City _____ State _____ Zip _____

Journal subscriptions start on January '75

*NOTE: Subscriptions at ACS member rates are for personal use only. **Payment must be made in U.S. currency, by international money order, UNESCO coupons, U.S. bank draft, or order through your book dealer.

Important Additions

TO THE JOURNAL OF PHYSICAL AND CHEMICAL REFERENCE DATA

Two comprehensive reference volumes, each, like the Journal itself, published by The American Institute of Physics, The National Bureau of Standards and The American Chemical Society . . . your triple assurance of their accuracy, immediacy, and usefulness.

SUPPLEMENT NO. 1 TO VOLUME 2

"Physical and Thermodynamic Properties of Aliphatic Alcohols"

by R. C. Wilhoit and B. J. Zwolinski, *Thermodynamics Research Center, Department of Chemistry, Texas A&M University.*

The most exhaustive review and critical analysis of selected physical and thermodynamic properties of aliphatic alcohols that has been published. Coverage of the important properties of the liquid, vapor, and ideal gaseous states as well as pertinent solid state data necessary for equilibrium calculations ordinarily encountered in chemical and chemical engineering applications. All available quantitative data on each property for each aliphatic alcohol are fully documented and critically analyzed providing a "data bank" for the 640 monohydroxy alcohols in the carbon range of C₁ to C₅₀. Internally consistent tables of critical, standard, or selected "best" values are tabulated for each compound. Index included.

SUPPLEMENT NO. 1 TO VOLUME 3

"Thermal Conductivity of the Elements: A Comprehensive Review"

by C. Y. Ho, R. W. Powell, and P. E. Lilly, *1974 Thermophysical Properties Research Center, Purdue University.*

Comprehensive review of the world's thermal conductivity data presents recommended or estimated values for all 105 elements. Reliable thermal conductivity data for those elements which can be used as standard reference materials to calibrate or check apparatus. Original data, specimen characterization and measurement information for 5200 sets of raw data. Detailed discussions for each element, review of the available experimental data and considerations by which the authors arrived at final assessments. Complete biographic citations for 1658 references. Only original sources have been used. All cited documents are available at TPRC in standard microfiche.

Special Issue Sales

American Chemical Society
1155 16th St., N.W., Washington, D. C. 20036

Please send _____ copies of the 420 page supplement to the Journal of Physical and Chemical Reference Data, Volume 2, "Physical and Thermodynamic Properties of Aliphatic Alcohols," at the prices checked below.

Members: Hard cover edition: \$33.00
Nonmembers: Hard cover edition: \$33.00
Members: Soft cover edition: \$10.00
Nonmembers: Soft cover edition: \$30.00

Please send _____ copies of the 796 page supplement to the Journal of Physical and Chemical Reference Data, Volume 3, "Thermal Conductivity of the Elements: A Comprehensive Review," at the prices checked below.

Members: Hard cover edition: \$60.00
Nonmembers: Hard cover edition: \$60.00
Members: Soft cover edition: \$25.00
Nonmembers: Soft cover edition: \$55.00

Check or money order must accompany order. \$1.00 extra for foreign postage and handling.

Name _____

Address _____

City _____ State _____ Zip _____



American Chemical Society

26.02.2019